THE JOURNAL OF PHYSICAL CHEMISTRY

Volume 71

SEPTEMBER—DECEMBER 1967

PAGES 3113—4624

EASTON, PA.
MACK PRINTING COMPANY
1967

THE JOURNAL OF

PHYSICAL CHEMISTRY

AMERICAN CHEMICAL SOCIETY PUBLICATIONS, *1155 Sixteenth St., N.W., Washington, D.C. 20036*

RICHARD L. KENYON, *Director of Publications*

JOSEPH H. KUNEY, *Director of Business Operations and Director of Publications Research*

DAVID E. GUSHEE, *Publication Manager, Journals*

 Published monthly, with symposium issue added in January, by the American Chemical Society at 20th and Northampton Sts., Easton, Pa. 18042. Second-class postage paid at Easton, Pa.

The Journal of Physical Chemistry is devoted to the publication of contributed papers in the broad field of physical chemistry. Preference for publication in *The Journal of Physical Chemistry* is given to papers dealing with fundamental concepts, atomic and molecular phenomena, and systems in which clearly defined models are applicable. Manuscripts containing extensive reviews, reevaluations of existing data, applied chemical data, or measurements on materials of ill-defined nature are, in general, not acceptable for publication. Symposium papers may be published as a group, but only through special arrangement with the Editor.

Except as immediately following, all manuscripts should be sent to *The Journal of Physical Chemistry*, Building 255, Camp Matthews, University of California, San Diego, Post Office Box 109, La Jolla, Calif. 92037. Manuscripts originating in the British Isles, Europe, and Africa should be sent to F. C. TOMPKINS, The Faraday Society, 6 Gray's Inn Square, London, W. C. 1, England.

All manuscripts should be submitted in duplicate, including an original typewritten, double-spaced copy. Original drawings should accompany the manuscript. Lettering at the sides of graphs (black on white or blue) may be pencilled in and will be typeset. Figures and tables should be held to a minimum consistent with adequate presentation of information. All footnotes and references to the literature should be numbered consecutively and placed in the manuscript at the proper places. Initials of authors referred to in citations should be given. Nomenclature should conform to that used in *Chemical Abstracts*, mathematical characters should be marked for italic, Greek letters carefully made or annotated, and subscripts and superscripts clearly shown.

Articles should be written as briefly as possible consistent with clarity, avoiding historical background unnecessary for specialists. They should cover their subjects with reasonable thoroughness and completeness and should not depend for their usefulness on papers to be published later. A brief abstract, generally not exceeding 300 words, should appear at the beginning of each article. All articles are subject to critical reviews by referees.

Notes are similar to Articles, but are shorter and not accompanied by abstracts. The length of a *Note*, including tables, figures, and text, must not exceed 1.5 journal pages (1500 words or the equivalent). A *Note* treats a limited subject with reasonable completeness and should not be considered a preliminary notice. Like Articles, *Notes* are subject to critical review by referees.

Communications to the Editor are divided into two categories, *Letters* and *Comments*. The length of a *Communication*, including tables, figures, and text, must not exceed three-fourths of a page (750 words or the equivalent).

Letters should report preliminary results of immediate interest. It is expected that the material in *Letters* may be republished in *The Journal of Physical Chemistry* at a later date in more complete form. Communications in this category will be treated expeditiously but are subject to review by the Editor and readily available experts.

Comments include significant remarks on the work of others or observations of unusual interest which the authors do not intend to pursue. In the former case, the authors of the work being discussed will, ordinarily, be allowed to reply. *Comments* are not refereed but are published at the discretion of the Editor.

Additions and Corrections are published once yearly in the December issue. See Volume 70, Number 12 for the proper form.

Extensive or unusual alterations in an article after it has been set in type are made at the author's expense, and it is understood that by requesting such alterations the author agrees to defray the cost thereof.

The American Chemical Society and the Editor of *The Journal of Physical Chemistry* assume no responsibility for the statements and opinions advanced by contributors.

Correspondence regarding accepted copy, proofs, and reprints should be directed to Research Journals Production Office, American Chemical Society, 20th and Northampton Sts., Easton, Pa. 18042. Senior Production Editor: CHARLES R. BERTSCH. Assistant Senior Production Editor: MARIANNE C. BROGAN. Assistant Editors: EDWARD A. BORGER and CELIA B. MCFARLAND. Editorial Assistant: BARBARA A. RIEGEL.

Advertising Office: Reinhold Publishing Corporation, 430 Park Ave., New York, N. Y. 10022.

Business and Subscription Information

Remittances and orders for subscriptions and for single copies, notices of changes of address and new professional connections, and claims for missing numbers should be sent to the Subscription Service Department, American Chemical Society, 1155 Sixteenth St., N.W., Washington, D. C. 20036. Allow 4 weeks for changes of address. Please include an old address label with the notification.

Claims for missing numbers will not be allowed (1) if received more than sixty days from date of issue, (2) if loss was due to failure of notice of change of address to be received before the date specified in the preceding paragraph, or (3) if the reason for the claim is "missing from files."

Subscription rates (1967): members of the American Chemical Society, $16.00 for 1 year; to nonmembers, $32.00 for 1 year. Postage to Canada and countries in the Pan-American Union, $2.00; all other countries, $3.00. Single copies for current year: $3.00. Postage, single copies: to Canada and countries in the Pan-American Union, $0.15; all other countries, $0.20. Rates for back issues from Volume 56 to date are available from the Special Issues Sales Department, 1155 Sixteenth St., N.W., Washington, D. C. 20036.

THE JOURNAL OF

PHYSICAL CHEMISTRY

Volume 71, Number 10 September 1967

NOTES

COMMUNICATIONS TO THE EDITOR

THE JOURNAL OF
PHYSICAL CHEMISTRY

VOLUME 71, NUMBER 10 SEPTEMBER 15, 1967

The Acid–Base-Catalyzed Hydration of Acetaldehyde. Buffer and Metal Ion Catalysis[1]

by Y. Pocker[2] and J. E. Meany[3]

Department of Chemistry, University of Washington, Seattle, Washington 98105 *(Received April 17, 1967)*

The capacity of the acid–base components of diethylmalonate, phosphate, and imidazole buffers to catalyze the reversible hydration of acetaldehyde at 0.0° was determined using a spectrophotometric method. It was observed that in imidazole buffers an acetaldehyde–imidazole complex is produced appreciably faster than the hydration, so much so that the rates of hydration are determined after the initial equilibrium between free acetaldehyde, free imidazole, and acetaldehyde–imidazole complex is established: $K = [Ac \cdot Im]/\{[Ac]-[Im]\} \simeq 0.13$ l. mole^{-1}. The hydration data show that although catalysis by imidazole and by the dianion of diethylmalonic acid is moderate, that due to monohydrogen phosphate dianion is significantly larger even though the pK_a values of the respective conjugate acids associated with these bases are similar. Parallel conclusions apply to dihydrogen phosphate, which is a more potent hydration catalyst than either imidazolium ion or the monoanion of diethylmalonic acid. The use of the above-mentioned buffers also enabled the accurate determination of k_{OH^-} as 6.8×10^5 l. mole^{-1} min^{-1}. The catalytic efficiency of HPO_4^{2-} *vs.* imidazole for the hydration of acetaldehyde is shown to parallel that observed for the reversible hydration of carbon dioxide. The solvent deuterium isotope effects associated with several general acids and bases in the reversible hydration of acetaldehyde are shown to be very similar to those observed in the mutarotation of glucose. Zinc ion catalysis was studied in relation to that derived from the zinc metallo enzyme carbonic anhydrase. Thus we have established that while the catalysis afforded by zinc ions in acetate buffers (pH 6.69) or in malonate buffers (pH 7.5) is mild, enhanced catalysis is observed when zinc ions are introduced into imidazole buffers (pH 7.63).

Introduction

We have recently shown that the reversible hydration of acetaldehyde is a useful reaction for mechanistic studies pertaining to the mode of action of the zinc metallo enzyme, erythrocyte carbonic anhydrase.[4–9]

Unlike many enzymes, carbonic anhydrase reversibly promotes the hydrations of reactions which proceed at appreciable rates in the absence of enzyme. Thus, the reversible hydration of CO_2 is very susceptible to general base catalysis[10–13] and that of acetaldehyde to

both general acid and general base catalysis.[14-16]

Since investigations of the enzymatically catalyzed hydration of acetaldehyde are most meaningful around physiological pH, quantitative kinetic studies of buffer catalysis in this region are a prerequisite for evaluation of the accelerative effect of the enzyme and contrasting it with chemical catalysis.

The first part of the present paper describes the capacity of the acid–base components of diethylmalonate, phosphate, and imidazole buffers to catalyze the reversible hydration of acetaldehyde at 0.0° in both H_2O and D_2O. These studies were carried out using a spectrophotometric method.

Earlier work suggests that both protein bound zinc[17,18] and imidazole[4-7] are intimately associated with the active site in erythrocyte carbonic anhydrase. Consequently, we have carried out experiments involving the use of imidazole, its conjugate acid, and zinc ions as hydrating catalysts. These results are also discussed in the present paper.

Experimental Section

Materials. The acetaldehyde used in these experiments was obtained from Baker Analyzed products. The aldehyde has a tendency toward oxidation and it is necessary to fractionate it immediately prior to use. This was done under a stream of dry nitrogen gas using a short Heli-Pak column. The middle fraction (bp 21°) was collected in a receiving flask which was cooled in a Dry Ice–acetone slurry.

Zinc ion solutions were made up in the form of the nitrate which was obtained from Baker and Adamson in reagent grade. The nitrate was chosen as the anion for the solution since the association of the nitrate ion with divalent zinc is small compared with that of halogens and other common anions.[19]

The zinc nitrate concentrations were checked by dithizone determinations as described by Malmstrom.[20]

The phosphate and imidazole buffer solutions employed in these experiments were prepared from the commercially available compounds, analytical or reagent grade, or of comparable purity. The dianion of diethylmalonic acid was prepared by refluxing the ethyl ester in strong alkali. Neutralization of the dianion with HCl produced diethylmalonic acid which was purified by recrystallization from benzene (mp 128–128.5°). Heavy water was obtained from Liquid Carbonic Division of General Dynamics Corp. and contained at least 99.7% D_2O.

In a buffer solution containing general acid A and its conjugate base B, the buffer ratio, $r = [A]/[B]$, is taken as that obtained either by mixing weighed amounts of the components or by appropriate titrations with standardized hydrochloric acid or sodium hydroxide solutions.

Analytical Instruments. The pH and pD values (pD = pH reading +0.41) of all buffer solutions were determined by means of a Beckman 101900 research pH meter, the relative accuracy of which is 0.001 pH unit. A Beckman glass electrode having a low electrical resistance and temperature limits from −5 to 80° was used along with a Beckman Calomel Internal 39071 frit junction reference electrode.

The reactions were followed on a Gilford high-speed recording spectrophotometer, Model 2000. An insulated cell compartment in place of the conventional chamber was attached to the Gilford. The compartment consisted of a bath containing a mixture of water and methanol. An internal coil through which coolant (methanol) flowed lowered the temperature of the bath as required. The temperature of the circulating coolant was kept at about −5° allowing the cell compartment to be thermostated to 0.0 ± 0.02° by means of a Sargent Model SV (S-82060) thermonitor unit.

The phototube housing of the Gilford instrument is neither enclosed in an air-tight fashion nor equipped with desiccant. Consequently, for runs performed at 0.0°, it was necessary to allow a constant stream of dry nitrogen gas to flow into this compartment so that shorting of the phototube by condensation could be

(1) Support of this work by the National Institutes of Health of the Public Health Service is gratefully acknowledged. Data given in this paper are taken in part from a dissertation presented by J. E. Meany to the University of Washington in partial fulfillment of the requirements for the Ph.D. degree, Aug 11, 1966.

(2) Author to whom correspondence should be addressed.

(3) NASA Predoctoral Fellow (1963–1966).

(4) Y. Pocker and J. E. Meany, Abstracts, 6th International Congress of Biochemistry, Vol. IV, 132, New York, N. Y., 1964, p 327.

(5) Y. Pocker and J. E. Meany, *J. Am. Chem. Soc.*, **87**, 1809 (1965).

(6) Y. Pocker and J. E. Meany, *Biochemistry*, **4**, 2535 (1965).

(7) Y. Pocker, J. E. Meany, D. G. Dickerson, and J. T. Stone, *Science*, **150**, 38 (1965).

(8) Y. Pocker and J. E. Meany, *Biochemistry*, **6**, 239 (1967).

(9) Y. Pocker and J. E. Meany, *J. Am. Chem. Soc.*, **89**, 631 (1967).

(10) F. J. W. Roughton and V. H. Booth, *Biochem. J.*, **32**, 2049 (1938).

(11) B. H. Gibbons and J. T. Edsall, *J. Biol. Chem.*, **238**, 3502 (1963).

(12) C. Ho and J. M. Sturtevant, *ibid.*, **238**, 3499 (1963).

(13) J. C. Kernohan, *Biochem. Biophys. Acta*, **81**, 346 (1964).

(14) R. P. Bell, M. H. Rand, and K. M. A. Wynne-Jones, *Trans. Faraday Soc.*, **52**, 1093 (1956), and earlier references quoted therein.

(15) Y. Pocker, *Proc. Chem. Soc.*, 17 (1960).

(16) L. C. Gruen and P. T. McTigue, *J. Chem. Soc.*, 5217 (1963).

(17) D. Keilin and T. Mann, *Biochem. J.*, **34**, 1163 (1940).

(18) S. Lindskog and B. G. Malmstrom, *J. Biol. Chem.*, **237**, 1129 (1962).

(19) J. Bjerrum, *Chem. Rev.*, **46**, 381 (1950).

(20) B. G. Malmstrom, *Arch. Biochem. Biophys.*, **70**, 58 (1957).

avoided. Nitrogen gas was also used to eliminate water vapor condensing on the outside of the windows at the entrance to and the exit from the cell compartment.

Method. Acetaldehyde absorbs at a maximum at 278 mμ (ϵ 16.2 l. mole^{-1} cm^{-1}), and the pseudo-first-order coefficients, k_{obsd}, were obtained by determining the rate of diminution of this peak. First-order plots of log $(A_t - A_\infty)$ *vs.* time (where A_t and A_∞ denote the absorbancies of acetaldehyde at time t and at equilibrium) are linear with $k_{obsd} = -2.3 \times$ slope. The specific rate obtained in this way were reproducible to about 1%.

Since the reaction is reversible, k_{obsd} is actually a sum of first-order rate coefficients for the forward, k_f, and for the reverse, k_r, processes: $k_{obsd} = k_f + k_r$. In diethylmalonate and phosphate buffers, the fraction of hydration, χ, at 0.0° is 0.70 in H_2O and 0.73 in D_2O.[21] These values were obtained from kinetic runs in which the initial optical densities of the substrates were determined by extrapolation to zero time, and the final absorbancies were those observed from the equilibrated reaction solutions. The fraction of hydration for acetaldehyde in water was confirmed by the nmr spectrum associated with the hydrated and unhydrated forms.

Reaction was initiated by introducing acetaldehyde into 3.0 ml of the buffer solution by means of a calibrated Hamilton microsyringe. Since this compound boils at 21°, it was necessary to chill both the syringe and the aldehyde since the high vapor pressure of the substrate at room temperature made it otherwise impossible to draw it into the syringe.

Results

The reversible hydration of acetaldehyde is a general acid, general base-catalyzed reaction in which the acidic and basic components in the reaction medium independently contribute to the over-all reaction rate.[14,22a,b] The over-all pseudo-first-order rate constant, k_{obsd}, can be represented by

$$k_{obsd} = k_0 + k_{L_3O^+}[L_3O^+] + k_{OL^-}[OL^-] + k_A[A] + k_B[B] \quad (1)$$

where k_0 is the spontaneous rate coefficient and L is used to denote the isotopically different hydrogens.

Initially, a series of runs was carried out varying the over-all buffer concentration while maintaining the same buffer ratio and pH. The buffer ratio, r, is defined throughout as the ratio of the concentration of acid to that of the conjugate base; *i.e.*, $r = [A]/[B]$. Rearranging eq 1 leads to

$$k_{obsd} = k_0 + k_{L_3O^+}[L_3O^+] + k_{OL^-}[OL^-] + [k_A + k_B/r][A] \quad (2)$$

Plots of k_{obsd} against (A) were found to be linear for a given buffer ratio. According to eq 2, the slope of the straight line, S_r, is

$$S_r = k_A + k_B/r \quad (3)$$

and the intercept, I_r, is

$$I_r = k_0 + k_{L_3O^+}[L_3O^+] + k_{OL^-}[OL^-] \quad (4)$$

Thus, k_A and k_B were evaluated by deducing values of S_r corresponding to several reciprocal buffer ratios (Table I) and show that S_r is a linear function of $1/r$ for each buffer pair (Figures 1 and 2), indicating the ab-

Table I: Catalysis of Acetaldehyde Hydration by Phosphate, Diethylmalonate, and Imidazole Buffers at 0.0°

Buffer[a]	Concn range of acid, *M*	No. of runs	1/r	*S*, l. mole^{-1} min^{-1}
Phosphate in H_2O; μ = 0.05	0.0016–0.0040	4	0.25	25.2
	0.0010–0.0020	5	1.00	50.6
	0.0007–0.0040	5	2.00	85.8
	0.0004–0.0044	4	3.50	137
	0.0003–0.0020	6	5.00	181
	0.0002–0.0018	14	10.0	367
Phosphate in D_2O; μ = 0.05	0.0056–0.0280	6	0.25	9.89
	0.0007–0.0067	5	2.00	40.1
	0.0004–0.0020	5	5.00	95.5
	0.0005–0.0026	3	6.99	127
	0.0006–0.0031	5	9.62	170
Diethylmalonate in H_2O; μ = 0.15	0.0044–0.0247	5	1.60	6.36
	0.0036–0.0193	5	2.40	8.05
	0.0023–0.0123	5	4.30	13.5
	0.0017–0.0085	4	6.70	21.2
	0.0012–0.0062	5	9.30	29.2
Imidazole in H_2O; μ = 0.10	0.0270–0.0850	4	0.39	1.02
	0.0100–0.0400	5	1.00	4.38
	0.0075–0.0375	5	2.00	7.62
	0.0037–0.0187	5	4.00	16.5
	0.0030–0.0150	5	5.00	19.5
Imidazole in D_2O; μ = 0.10	0.0030–0.0150	5	5.00	7.00

[a] Ionic strengths adjusted using sodium chloride.

(21) Although the freezing point of D_2O is 3.8°, its solutions supercooled with ease and remained so throughout the course of a kinetic run. It was possible to work at 0.0° provided the acetaldehyde was introduced without the syringe needle coming into contact with the walls of the silica cell; shaking the cell to allow proper mixing did not induce crystallization.

(22) (a) R. P. Bell and J. C. Clunie, *Trans. Faraday Soc.*, **48**, 439 (1952); *Proc. Roy. Soc.* (London), **A212**, 33 (1952); (b) R. P. Bell and B. de B. Darwent, *Trans. Faraday Soc.*, **46**, 34 (1950).

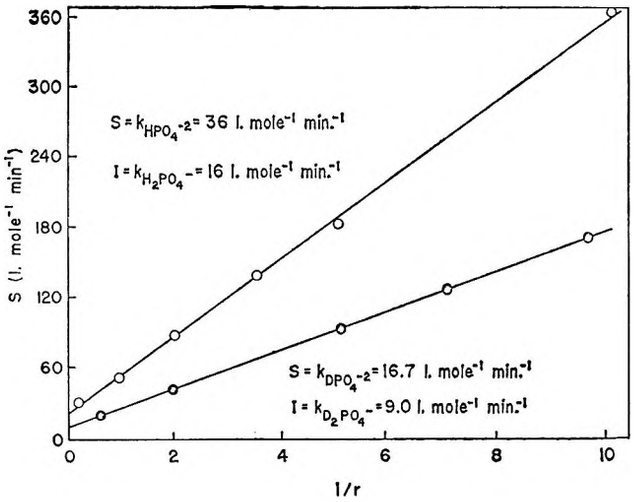

Figure 1. Determination of specific rate coefficients of the components of phosphate buffer in H_2O and D_2O at 0.0°: upper curve, phosphate-catalyzed hydration of acetaldehyde in H_2O; lower curve, phosphate-catalyzed hydration of acetaldehyde in D_2O.

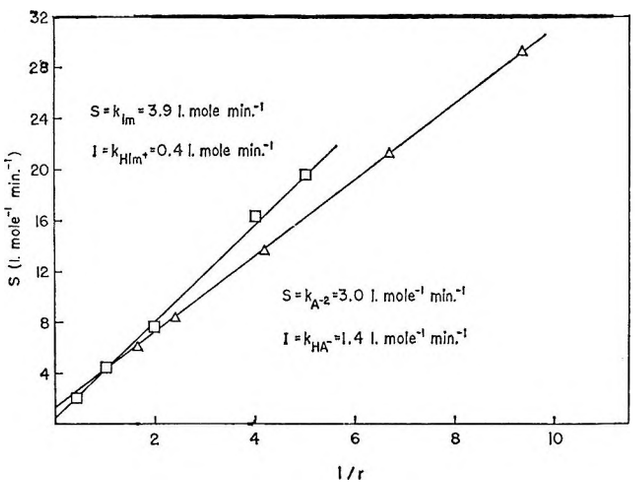

Figure 2. Determination of specific rate coefficients of the components of diethylmalonate and imidazole buffers in H_2O at 0.0°: Δ, diethylmalonate-catalyzed hydration of acetaldehyde in H_2O; A^{2-} represents diethylmalonate dianion; HA^- represents diethylmalonate monoanion; □, imidazole-catalyzed hydration of acetaldehyde in H_2O; Im represents free imidazole; HIm^+ represents the imidazolium ion.

sence of catalytic components arising from the concerted action of both B and A. This sequence of experiments was used to determine the specific rate constants associated with the components of phosphate, diethylmalonate, and imidazole buffers.

The coefficients, k_{OH^-} and k_0 were deduced from data involving phosphate and diethylmalonate buffers. Values of I_r corresponding to the various hydroxide ion concentrations are tabulated in Table II. The intercept I_r is a linear function of hydroxide ion concentration. The catalytic coefficients for water and hydroxide ion were evaluated from Figure 3 as $k_0 = 0.094$ min^{-1} and $k_{OH^-} = 8.9 \times 10^5 \times f_{OH^-} = 8.9 \times 10^5 \times 0.76 = 6.8 \times 10^5$ l. mole min^{-1}. The catalytic coefficients, $k_{D_2PO_4^-}$ and $k_{DPO_4^{2-}}$ were evaluated from a series of parallel measurements in D_2O. It is difficult to deduce k_{OD^-} accurately because under our experimental conditions the catalytic term $k_{OD^-}[OD^-]$ did not vary sufficiently. Our preliminary investigations, however, show that $k_{OD^-} \simeq k_{OH^-}$.

Table II: Catalysis of Acetaldehyde Hydration by Water and Hydroxide Ions

Phosphate buffers		Diethylmalonate buffers	
I, min^{-1}	$a_{OH^-} \times 10^8$, mole $l.^{-1}$ [a]	I, min^{-1}	$a_{OH^-} \times 10^8$, mole $l.^{-1}$ [a]
		0.105	1.62
0.106	0.992	0.117	2.67
0.113	2.01	0.130	4.56
0.126	3.21	0.148	6.63
0.137	3.99	0.173	7.70
0.156	6.95		

[a] Although the buffer ratio was maintained constant throughout each series of runs, small decreases in the experimentally determined pH occurred upon dilution with the NaCl solutions required to maintain constant ionic strength. The extrapolated values of pH corresponding to the intercept, I, were used to deduce a_{OH^-}.

The kinetic rate constant for imidazole in D_2O was deduced from the results obtained from a series of five runs where (Im) = 5(DIm$^+$). A plot of k_{obsd} against $1/(DIm^+)$ gives a straight line the slope of which is given by $S_r = 7.0$ l. mole^{-1} min^{-1} = $k_{DIm} + 5k_{Im}$. If it is assumed that at this buffer ratio catalysis by DIm^+ can be neglected, a k_{Im} value of 1.4 l. mole^{-1} min^{-1} is obtained in D_2O. Such an assumption would appear to be justified since in H_2O, k_{HIm^+} is only about $^1/_{10}$ as large as k_{Im} and at the above buffer ratios the contribution of the $k_{DIm^+}[DIm^+]$ term would be expected to be negligible in comparison to $k_{Im}[Im]$.

The specific rate coefficients in H_2O and D_2O for the various catalytic species present in the above-mentioned buffers are given in Table III.

The catalysis of acetaldehyde hydration by zinc ions was also investigated at 0.0°. Results obtained in acetate and malonate buffers were compared to those obtained in imidazole buffers. The observed rate con-

Table III: Catalytic Rate Coefficients for Acids and Bases in the Hydration of Acetaldehyde

Catalyst	k_c, l. mole^{-1} min^{-1}	pK_a[a]	$k_c^{H_2O}/k_c^{D_2O}$
$H_2PO_4^-$	16.0	7.12	1.8
HPO_4^{2-}	35.9		2.2
$Et_2C(CO_2H)CO_2^-$	1.40	7.22[b]	
$Et_2C(CO_2^-)_2$	3.00		
HIm^+[c]	0.4	7.63	
Im[c]	3.90		2.8
H_2O[d]	0.094	−1.74	
OH^-	6.8×10^5	16.69	*ca.* 1.0[f]
Zn^{2+} in acetate buffer[d,e]	6.5		
Zn^{2+} in imidazole buffer[d]	130		1.7

[a] Refers to the pK_a at 0.0°. [b] The value reported for diethylmalonate monoanion refers to the pH of a solution where [A] = [B] = 0.005 *M*; *cf.* also R. Gane and C. K. Ingold, *J. Chem. Soc.*, 2153 (1931). [c] It was observed that when acetaldehyde (Ac) is dissolved in a buffered system containing free imidazole (Im), the former is partly transformed into a complex consisting of one molecule of imidazole and one molecule of aldehyde (a tetrahedral carbinolamine complex having no C=O or C=N absorption) and partly into acetaldehyde hydrate. These forms of bound acetaldehyde exist in a mobile equilibrium with free acetaldehyde. The rate of formation of the acetaldehyde–imidazole complex is appreciably faster than the hydration, so much so that the rates of hydration are determined after the initial equilibrium between free acetaldehyde and unprotonated imidazole has been established. By taking spectrophotometric readings approximately 10 sec after mixing and extrapolating to zero time, it was found that the apparent initial aldehyde concentration decreased when the hydrations were carried out in the presence of increasing quantities of imidazole. This suggested that a reaction between acetaldehyde and imidazole had taken place prior to the hydration. By calculating the concentration of acetaldehyde involved in this rapid preequilibrium, the following equilibrium constant was evaluated: $K_c = [(Ac)(Im)]/[(Ac\cdot Im)] \simeq 7.6$ moles l.$^{-1}$. The observed catalytic rate constants associated with Im and HIm^+ are consequently apparent constants. [d] See footnote 23. [e] *A priori* one might suspect that the catalytic constant of zinc hydrate might be greater at higher pH and that the behavior in imidazole buffers should not strictly be contrasted with that in acetate buffers but with that obtained in a buffer system of similar pH. Consequently, we have further shown that the catalytic constant of zinc ions dissolved in malonate buffers (pH 7.5) is also low. [f] For a number of reactions involving either slow proton transfer from carbon acid to base (general base catalysis) or a base promoted preequilibrium step (specific base catalysis), k_{OH^-}/k_{OD^-} was found to be *ca.* 0.7; *cf.* Y. Pocker, *Chem. Ind.* (London), 1117 (1958); 17, 599, 1383 (1959). Significantly, this ratio for the hydration of acetaldehyde is higher.

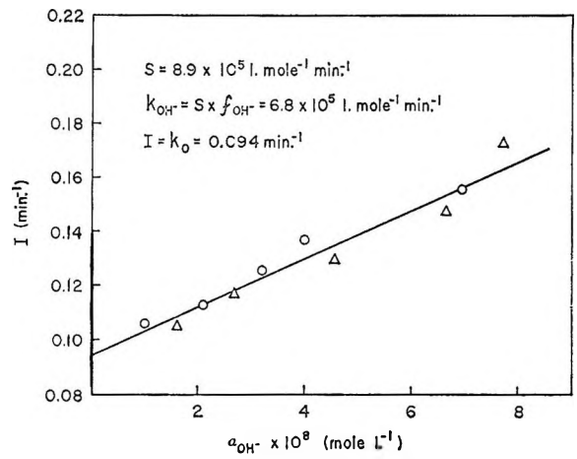

Figure 3. The water and hydroxide ion catalyzed hydration of acetaldehyde at 0.0°: ○, data obtained in phosphate buffers; △, data obtained in diethylmalonate buffers.

stants for these reactions include a catalytic term for the accelerative effect of divalent zinc ions.[23]

$$k_{obsd} = k_0 + k_{L_3O^+}[L_3O^+] + k_{OL^-}[OL^-] + k_A[A] + k_B[B] + k_{Zn^{2+}}[Zn^{2+}] \quad (5)$$

The catalytic coefficient, $k_{Zn^{2+}}$, was determined from a series of runs in which $[Zn^{2+}]$ was the only variant. Thus the catalysis of the hydration reaction by zinc ions in an acetate buffer of pH 6.69 was determined by carrying out several runs in which the concentration of zinc ions was varied from zero to 0.0375 *M*. The graphical representation of these data as given in Figure 4 shows that the catalytic rate constant associated with zinc ions in this medium has a value of 6.5 l. mole^{-1} min^{-1}. To obtain efficient buffering at pH 6.69, the ionic strength had by necessity to be higher in this experiment than that reported below since the concentration of the acetate anion in the buffer was 0.200 *M*. However, control experiments showed that ionic strengths up to 0.35 (using either NaCl or $NaNO_3$) had no measurable effect on the rate of the hydration reaction.

Similar experiments were carried out in imidazole buffers,[24] $r = [HIm^+]/[Im] = 0.048\ M/0.048\ M$, and

(23) (a) In acetate buffers, divalent zinc probably exists in three distinct forms: (i) as the hydrate, $Zn(H_2O)_4^{2+}$; (ii) as an ion pair, $[Zn(H_2O)_4^{2+}OAc^-]$; and (iii) as an innersphere species of zinc acetate, $[Zn(H_2O)_3OAc]^+$: *cf.* M. Eigen and G. Maass, unpublished observations, quoted by M. Eigen and R. G. Wilkins in "Mechanisms of Inorganic Reactions," Advances in Chemistry Series, No. 49, American Chemical Society, Washington, D. C., 1965, p 55. (b) In imidazole buffers, we have determined that each zinc ion binds up to four imidazoles; *cf.* also J. T. Edsall, G. Felsenfeld, D. W. S. Goodman, and F. R. N. Gurd, *J. Am. Chem. Soc.*, **76**, 3054 (1954). Under the conditions employed throughout our kinetic experiments, the most prevalent species in solution is $Zn(Im)_4^{2+}$.

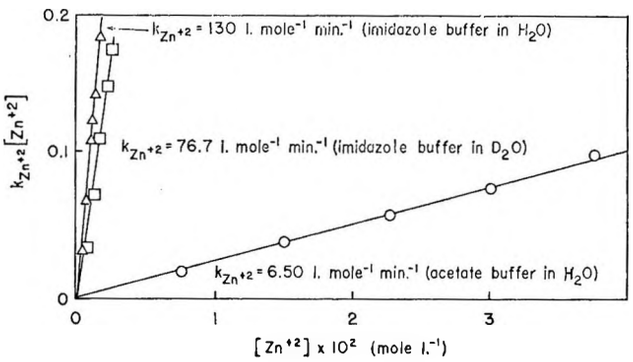

Figure 4. Zinc ion catalysis of the hydration of acetaldehyde at 0.0°. For each point on these plots, the buffer-catalyzed portions of the hydrations have been subtracted from k_{obsd}: *i.e.*, $k_{Zn^{2+}}[Zn^{2+}] = k_{obsd} - k_{buff}$, where $k_{buff} = k_0 + k_{L_3O^+}[L_3O^+] + k_{OL^-}[OL^-] + k_A[A] + k_B[B]$; Δ, catalysis of the hydration of acetaldehyde by divalent zinc in imidazole buffer in H_2O; □, catalysis of the hydration of acetaldehyde by divalent zinc in imidazole buffer in D_2O; ○, catalysis of the hydration of acetaldehyde by divalent zinc in acetate buffer in H_2O.

pH 7.63, where the variation of zinc ion concentration from zero to 0.0015 *M* showed that k_{obsd} was again a linear function of the concentration of the metal ion (Figure 4). The catalytic coefficient of zinc ions in imidazole buffers is 20 times larger than that in acetate buffers (Table III), suggesting that the accelerative effect of zinc ions is greatly enhanced by their coordination to imidazole.

The solvent deuterium isotope effect of zinc ions was determined by carrying out a series of runs in imidazole buffers in D_2O,[24] $r = [DIm^+]/[Im] = 0.048\ M/0.048\ M$ and pD 8.16. The kinetic results obtained from the variation of zinc ion concentration from 0.0000 to 0.0024 *M* shows that $k_{Zn^{2+}} = 76.7$ l. mole^{-1} min^{-1}, so that the solvent deuterium isotope effect is $k_{Zn^{2+}}^{H_2O}/k_{Zn^{2+}}^{D_2O} \simeq 1.7$ (Figure 4).

Discussion

(*a*) *Hydration Mechanisms.* The capacity of the various acidic and basic components of diethylmalonate, phosphate, and imidazole buffers to catalyze the hydration of acetaldehyde substantiates earlier findings pertaining to the general acid and general base catalyzed nature of this reaction.[14-16,a,b] For general acid and general base catalyzed hydration–dehydration, Bell has proposed the following mechanisms. For general acid catalysis

$$Me\cdot CHO + H_2O + HB \underset{slow}{\overset{slow}{\rightleftharpoons}} HO\cdot CHMe\cdot OH_2^+ + B^- \quad (A)$$

$$HO\cdot CHMe\cdot OH_2^+ + B^- \underset{fast}{\overset{fast}{\rightleftharpoons}} Me\cdot CH(OH)_2 + HB \quad (B)$$

For general base catalysis

$$Me\cdot CHO + H_2O + B \underset{slow}{\overset{slow}{\rightleftharpoons}} HO\cdot CHMe\cdot O^- + BH^+ \quad (C)$$

$$HO\cdot CHMe\cdot O^- + BH^+ \underset{fast}{\overset{fast}{\rightleftharpoons}} Me\cdot CH(OH)_2 + B \quad (D)$$

Account being taken of the pK_a and pK_b of acetaldehyde hydrate,[25] the concentration of the conjugate acid of the hydrate in acidic media or of the conjugate base of the hydrate in basic media is exceedingly low. This would require the rate coefficients associated with the reverse of steps A and C in certain cases to be faster than those usually expected for diffusion-controlled processes. Eigen[26] postulates a mechanism involving a cyclic transition state in which protons are transferred to and from the catalyst at a site effectively removed from the substrate by several water molecules. Consequently, one might follow Eigen in writing a cyclic transition state which for the spontaneous process is represented by I.

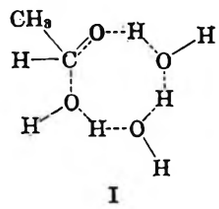

I

Such cyclic transition states have been invoked by Eigen, Kustin, and Strehlow[27] in an attempt to explain the relatively high "spontaneous" rate of hydration of pyruvic acid. The authors ascribed this to the intra-

(24) The pH (or pD) decreases caused by the addition of zinc ions to the imidazole buffer throughout these series of runs were small enough (less than 0.055 pH or pD unit) so that the change in k_{obsd} arising from changes in the catalytic term $k_{OH^-}[OH^-]$ or $k_{OD^-}[OD^-]$ were negligible. Under our experimental conditions each zinc ion removed four imidazole molecules from the buffered solution; consequently, each value of k_{obsd} was corrected to compensate for the corresponding decrease in catalysis by the loss of imidazole. Such corrections amounted to a maximum of *ca.* 3% of the over-all value of k_{obsd}.

(25) R. P. Bell and D. P. Onwood, *Trans. Faraday Soc.*, **58**, 1557 (1962); Y. Pocker, *Chem. Ind.* (London), 968 (1960); for an estimation of the pK_b of acetaldehyde, see M. L. Ahrens and H. Strehlow, *Discussions Faraday Soc.*, **39**, 112 (1965).

(26) M. Eigen, *Angew. Chem.*, **75**, 489 (1963); *Discussions Faraday Soc.*, **39**, 7 (1965).

(27) M. Eigen, K. Kustin, and H. Strehlow, *Z. Physik. Chem.*, **31**, 140 (1962).

molecular catalysis by the carboxyl group in which two water molecules participate in a cyclic transition state.

On the other hand, it is difficult to assess the generality of cyclic transition states involving intramolecular catalysis, for if they were dominant in all hydrations of carbonyl systems one might have expected that the spontaneous hydration of 2-pyridine aldehyde would proceed much more rapidly than that of 4-pyridine aldehyde. Indeed, such assistance is explicitly considered in transition states II and III which differ in the number of water molecules bridging between ring nitrogen and the nearby carbonyl carbon.

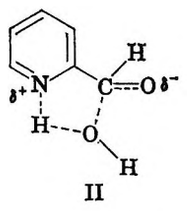

II

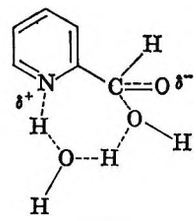

III

The corresponding transition states for the hydration of 4-pyridine aldehyde are prohibited due to the distance separating the ring nitrogen and the aldehydic group. We find,[8,9] however, that the water-catalyzed hydrations of 2- and 4-pyridine aldehyde are of comparable magnitude,[28] so that one cannot ascribe to transition states II and III a significant role in these hydrations.

(*b*) *Buffer Catalysis in H_2O and D_2O.* In determining the rate coefficients for the components of phosphate, diethylmalonate, and imidazole buffers, it was observed that the catalysis of acetaldehyde hydration by monohydrogen phosphate is about 10 times greater than that due to imidazole or diethylmalonate dianion even though the three bases have comparable values of pK_a. Similarly, the catalytic rate coefficient for dihydrogen phosphate was about 10 times greater than the corresponding value for diethylmalonate monoanion and about 40 times as large as the catalytic rate coefficient for the imidazolium ion.

The rate coefficients obtained for kinetic processes involving molecular acids or bases are found to depend on the acid or base strength of these catalysts. Such a relationship has been formulated by Brønsted.[29] Although it is realized that the nature of such linear free energy relationships is approximate, the relatively large catalytic coefficients of both HPO_4^{2-} and $H_2PO_4^-$ may be significant.

One may suggest that HPO_4^{2-} participates in the hydration by a mechanism involving simultaneous general base *and* general acid catalysis, thereby facilitating the transfer of H_2O to the aldehyde.

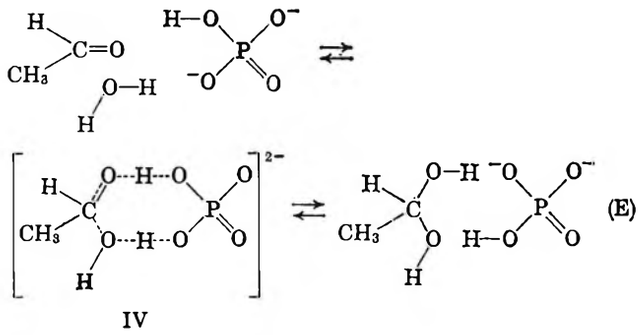

IV (E)

It is interesting to note that Gibbons and Edsall[11,30] have observed strong catalysis by HPO_4^{2-} in the hydration of CO_2. Here too, acceleration by this dianion far exceeded that due to imidazole.[10,31]

A similar interpretation of these results may explain the enhanced catalysis by $H_2PO_4^-$ in the hydration of acetaldehyde.

The solvent deuterium isotope effects observed in the hydration process accord with a mechanism involving a rate-determining proton transfer in H_2O and a deuteron transfer in D_2O.

Kinetics of reversible hydration reactions are closely analogous to the formation of a hemiacetal bond: $>C{=}O + ROH \rightleftarrows >C<^{OH}_{OR}$ which occurs in the mutarotation of glucose[32–34] and in the dimerization of α-hydroxy aldehydes and ketones,[35] well-known examples of general catalysis by acids and bases. Thus, the general acid–base catalysis by the components of diethylmalonate, phosphate, and imidazole buffers, and the magnitude of the deuterium isotope effects determined in the present work further substantiates the similarity in both kinetics and mechanism between acetaldehyde hydration and the mutarotation of glucose (see Table IV).[36,37]

(28) The fractions of hydration, χ, for these aldehydes differ; consequently, comparisons are made in terms of second-order rate coefficients for the forward process, $k_{H_2O}^{f} = k_0\chi/[H_2O]$: $k_{H_2O}^{2-PA} = 0.0043$ l. mole^{-1} min^{-1}; $k_{H_2O}^{4-PA} = 0.0091$ l. mole^{-1} min^{-1}; $k_{H_2O}^{CH_3CHO} = 0.0012$ l. mole^{-1} min^{-1}.

(29) J. N. Brønsted, *Chem. Rev.*, 5, 322 (1928).

(30) On the other hand, Ho and Sturtevant[12] were unable to detect catalysis by HPO_4^{2-} in the hydration of CO_2. In our laboratories we have been able to show (Y. Pocker and R. A. Reaugh, unpublished observations) significant catalysis of the dehydration of HCO_3^- by HPO_4^{2-} using a Durrum–Gibson stopped-flow spectrophotometer.

(31) Personal communication from Dr. J. C. Kernohan to Professor J. T. Edsall, quoted in ref 11.

(32) B. C. Challis, F. A. Long, and Y. Pocker, *J. Chem. Soc.*, 4679 (1957).

(33) Y. Pocker, *Chem. Ind.* (London), 968 (1960).

(34) H. H. Huang, R. R. Robinson, and F. A. Long, *J. Am. Chem. Soc.*, 88, 1866 (1966).

(35) R. P. Bell and E. C. Baughan, *J. Chem. Soc.*, 1947 (1937).

Table IV: Solvent Deuterium Isotope Effects, k_{H_2O}/k_{D_2O} Involved in the Hydration of Acetaldehyde and the Mutarotation of Glucose

Catalyst	Hydration of acetaldehyde	Mutarotation of glucose
$H_2PO_4^-$	1.8	1.9[b]
HPO_4^{2-}	2.2	2.5[b]
Im	2.8	2.3[b]
HOAc	2.5[a]	2.3[c]
OAc^-	2.3[a]	2.4[c]
H_3O^+	1.3[a]	1.4[c]

[a] Reference 15. [b] Reference 36. [c] Reference 37.

(c) *Importance to Enzymatic Catalysis.* (i) Because of general acid–general base catalysis, the reversible hydration of carbonyl systems proceeds at an appreciable rate in the absence of enzyme. Consequently, it is advantageous to find a buffering medium whose threshold of catalysis is low in comparison to the enzymatic catalysis. In most investigations involving the enzymatic hydration of CO_2 by carbonic anhydrase, phosphate buffers were employed[38-40] so that the studies could be conducted at physiological pH. However, analysis of their work[11] shows that the component of nonenzymatic hydration is significant. Indeed, the present work indicates that the catalytic components of phosphate buffers, $H_2PO_4^-$ and HPO_4^{2-}, are at least ten times more efficient than those involved in either imidazole or diethylmalonate. Kernohan[13] has employed imidazole buffers in studying the enzymatic hydration of CO_2. The use of this buffer for similar enzymatic studies involving acetaldehyde is precluded by its facile attack on the carbonyl carbon.[41] Finally, diethylmalonate buffers appear to be best suited for pH control around physiological pH required in enzymatic studies since they neither react with substrate molecules nor do they afford significant acceleration of rate.

(ii) In earlier publications,[4-7] we have shown that the basic form of an ionizable group having a pK_a of 7.0 in bovine carbonic anhydrase[42] and a pK_a of 7.4 in human carbonic anhydrase is important in the enzyme catalyzed hydration of acetaldehyde. These results are consistent with the participation of an imidazole group in the active site. Since it has been demonstrated that the zinc ion associated with the native enzyme is an obligatory component for its hydrase activity,[17,18] we were prompted to test the activity of zinc ions in the presence of imidazole buffers. Our results show that although catalysis by imidazole and its conjugate acid is moderate and that catalysis by zinc ions in acetate buffers (pH 6.69) and malonate buffers (pH 7.5) is also mild, enhanced catalysis is observed when zinc ions are introduced into imidazole buffers (Table III).

Our independent experiments involving pH decreases arising from the addition of zinc nitrate solution to imidazole buffers show that under the experimental conditions prevailing in our kinetic studies, divalent zinc existed predominantly in the form $Zn(Im)_4^{2+}$. Earlier studies[43] concerning the formation of this zinc imidazole complex further substantiates these findings.

Since such a zinc imidazole complex is in mobile equilibrium with V and VI, its catalytic effectiveness[44a,b] could be derived either from an imidazole assisted transfer of H_2O from V or from a transfer of OH^- from VI.

$$Zn(Im)_4^{2+} + H_2O \rightleftharpoons \underset{V}{Zn(Im)_3OH_2^{2+}} + Im \rightleftharpoons \underset{VI}{Zn(Im)_3OH^+} + HIm^+ \quad (F)$$

Other things being equal, the inherent activity of a metal-bound hydroxide should be less than that of a free hydroxide ion. The virtue of a metal ion complex lies, however, in its ability to carry appreciable amounts of potential OH^- at a pH where very little free OH^- could exist.

(36) Y. Pocker, J. W. Long, and D. B. Dahlberg, unpublished results from this laboratory.

(37) W. H. Hamill and V. K. La Mer, *J. Chem. Phys.*, **4**, 3195 (1936); *cf.* also B. C. Challis, F. A. Long, and Y. Pocker, *J. Chem. Soc.*, 4679 (1957).

(38) R. P. Davis, *J. Am. Chem. Soc.*, **80**, 5209 (1958).

(39) H. De Voe and G. B. Kistiakowsky, *ibid.*, **83**, 274 (1961).

(40) B. H. Gibbons and J. T. Edsall, *J. Biol. Chem.*, **239**, 2539 (1964).

(41) See Table III footnote *c*.

(42) This value is shifted to a pK_a of 7.55 in D_2O solvent.

(43) J. T. Edsall, G. Felsenfeld, D. S. Goodman, and F. R. N. Gurd, *J. Am. Chem. Soc.*, **76**, 3054 (1954).

(44) (a) In this connection, it is interesting to note that divalent zinc and cobalt are very effective catalysts for the hydration of 2-pyridine aldehyde, a compound which can simultaneously act as substrate and chelating agent: Y. Pocker and J. E. Meany, *ibid.*, in press. (b) The observed rate enhancement is perhaps reminiscent of the powerful catalysis exhibited by the dipositive ions $[Co(NH_3)_5OH]^{2+}$ and $[Cr(NH_3)_5OH]^{2+}$ in the mutarotation of glucose: J. N. Brønsted and E. A. Guggenheim, *Trans. Faraday Soc.*, **52**, 1093 (1956). Similar observations were made in the decomposition of nitramide: J. N. Brønsted, *Z. Physik. Chem.*, **A155**, 211 (1931); *cf.* also M. L. Bender and B. W. Turnquest, *J. Am. Chem. Soc.*, **79**, 1889 (1957); W. L. Koltun, M. Fried, and F. R. N. Gurd, *ibid.*, **82**, 233 (1960).

Thermodynamics of Complex Dissociation in Aqueous Solution at Elevated Temperatures[1]

by Harold C. Helgeson[2]

Department of Geology, Northwestern University, Evanston, Illinois *(Received May 13, 1966)*

The temperature dependence of the thermodynamics of dissociation for complexes in the temperature range 0–370° is described in terms of functions involving the dielectric constant of water and a power series consistent with nonelectrostatic interaction in the absence of a dielectric medium. Evaluation of the theoretical equations for various reactions yields results in close agreement with published thermodynamic data. Heat capacities of dissociation may vary monotonously with temperature or pass through extrema depending on the relative influence of electrostatic and nonelectrostatic interaction on the stabilities of the complexes as temperature increases. When the dielectric constant of the solvent becomes small at high temperatures, the electrostatic contribution dominates. As a consequence, many complexes become significantly stable at high temperatures, and the enthalpies, entropies, and heat capacities of dissociation become relatively large negative numbers.

Introduction

Integration of the van't Hoff equation permits calculation of dissociation constants at elevated temperatures. The heat capacities of dissociation required for this are usually represented by arbitrary power functions of temperature, limited in each case to the number of terms required to fit experimental data.[3-12] Although this procedure has obvious merit for reproducing experimental results, it is not amenable to theoretical interpretation of the thermodynamic behavior of complexes with changing temperature. A useful approach for this purpose involves separation of the respective thermodynamic variables into hypothetical electrostatic and nonelectrostatic terms.[12-18]

Derivation of Equations

The model adopted here can be discussed conveniently in terms of an isothermal entropy cycle

$$\begin{array}{ccccc} A_{\nu_+}B_{\nu_-(vac)}^{(\nu_+Z_+ - \nu_-|Z_-|)} & \xleftarrow{\Delta S_4^\circ} & \nu_+A_{(vac)}^{Z_+} & + & \nu_-B_{(vac)}^{Z_-} \\ \Delta S_1^\circ \downarrow & & \Delta S_2^\circ \uparrow & & \Delta S_3^\circ \uparrow \\ A_{\nu_+}B_{\nu_-(aq)}^{(\nu_+Z_+ - \nu_-|Z_-|)} & \xrightarrow[\Delta S_r^\circ]{} & \nu_+A_{(aq)}^{Z_+} & + & \nu_-B_{(aq)}^{Z_-} \end{array}$$

in which A and B represent the cation and anion, respectively, ν_+ and ν_- designate the number of ions per mole of complex, and Z_+ and Z_- are the respective charges on the cation and anion.

A. Separation of Variables. Omitting provision

(1) The work reported here was initiated while the writer was employed by Shell Development Co., Houston, Texas.

(2) The author was supported in this investigation by Shell Development Co., the Research Committee of Northwestern University, and the National Science Foundation (NSF Grants G.U. 1700 and G.E. 9758).

(3) K. S. Pitzer, *J. Am. Chem. Soc.*, **59**, 2365 (1937).

(4) H. S. Harned and R. W. Ehlers, *ibid.*, **55**, 652 (1933).

(5) H. S. Harned and R. W. Ehlers, *ibid.*, **55**, 2179 (1933).

(6) H. S. Harned and R. W. Ehlers, *ibid.*, **55**, 2379 (1933).

(7) H. S. Harned and N. D. Embree, *ibid.*, **56**, 1050 (1934).

(8) Th. Ackermann, *Z. Elektrochem.*, **62**, 411 (1958).

(9) Th. Ackermann and F. Schreiner, *ibid.*, **62**, 1143 (1958).

(10) M. Eigen and E. Wicke, *ibid.*, **55**, 354 (1951).

(11) H. S. Harned and R. A. Robinson, *Trans. Faraday Soc.*, **36**, 973 (1940).

(12) D. H. Everett and W. F. Wynne-Jones, *ibid.*, **35**, 1380 (1939).

(13) L. P. Hammett, *J. Chem. Phys.*, **4**, 613 (1936).

(14) L. P. Hammett, "Physical Organic Chemistry," McGraw-Hill Book Co., Inc., New York, N. Y., 1940.

(15) R. W. Gurney, *J. Chem. Phys.*, **6**, 499 (1938).

(16) R. W. Gurney, "Ionic Processes in Solution," McGraw-Hill Book Co., Inc., New York, N. Y., 1953.

(17) G. H. Nancollas, *Discussions Faraday Soc.*, **24**, 108 (1957).

(18) G. H. Nancollas, *Quart. Rev.* (London), **13**, 402 (1959).

for the differences in the usual standard-state conventions adopted for aqueous and gaseous species, the entropy of dissociation, ΔS_r°, for the complex $A_{\nu_+}B_{\nu_-}^{(\nu_+ Z_+ - \nu_- |Z_-|)}$ in an aqueous solution at a given temperature is given by

$$\Delta S_r^\circ = -\Delta S_1^\circ - \Delta S_2^\circ - \Delta S_3^\circ - \Delta S_4^\circ \quad (1)$$

in which ΔS_1°, ΔS_2°, and ΔS_3° represent the entropy changes attending solvation of the complex and its dissociated species, and ΔS_4° is the entropy change for dissociation of the complex in a vacuum. If the total interaction between the ions, complex, and solvent dipoles contributing to the entropy change represented by any part or all of this cycle is regarded as the sum of electrostatic (long range) and nonelectrostatic (short range) interaction, then

$$\Delta S_r^\circ = \Delta S_e^\circ + \Delta S_n^\circ \quad (2)$$

in which the subscripts e and n designate, respectively, the electrostatic and nonelectrostatic contributions to the entropy of dissociation. These two entropies can in turn be represented by

$$\Delta S_e^\circ = -\Delta S_{1,e}^\circ - \Delta S_{2,e}^\circ - \Delta S_{3,e}^\circ - \Delta S_{4,e}^\circ \quad (3)$$

and

$$\Delta S_n^\circ = -\Delta S_{1,n}^\circ - \Delta S_{2,n}^\circ - \Delta S_{3,n}^\circ - \Delta S_{4,n}^\circ \quad (4)$$

Including temperature as a variable, and making the further assumption that $\Delta S_e^\circ(T$, *electrostatic interaction*) and $\Delta S_n^\circ(T$, *nonelectrostatic interaction*) are, respectively, separable in the variables T, *electrostatic interaction* and T, *nonelectrostatic interaction*, we can write

$$\Delta S_r^\circ(T) = \Delta S_e^\circ(T) + \Delta S_n^\circ(T) = \Delta S_e^\circ(T_r) \times f(T) + \Delta S_n^\circ(T_r) \times g(T) \quad (5)$$

where $\Delta S_e^\circ(T_r)$ and $\Delta S_n^\circ(T_r)$ represent the two contributions at the reference temperature, T_r (298.15°K).

The electrostatic free energy of dissociation for a complex in a vacuum is given by

$$\Delta F_{e(vac)} = \sum_i (NZ_i e)^2/2r \quad (6)$$

where Ze is charge, r is distance of separation, and N is Avogadro's number. Because these parameters are temperature independent, $\Delta S_{4,e}^\circ$ is zero. ΔS_e° is thus equal to the net difference in the entropy change attending solvation of the complex and its dissociated species as long as the hydration process is entirely electrostatic.[19-22] The standard state adopted here is based on infinite dilution; consequently ion–ion and ion–complex interaction in the standard state are negligible, and ΔS_e° refers solely to the electrostatic interaction of water dipoles with the complex and its dissociated ions. The nonelectrostatic entropy is dominated by $\Delta S_{4,n}^\circ$ and, in contrast to similar models employed elsewhere,[13-16,18] it is regarded here as a temperature-dependent variable.

B. Electrostatic Temperature Function. The observed relation between log K for various complexes and the reciprocal of the dielectric constant of the solvent at 25° is often (but not always) linear.[23-26] The macroscopic dielectric constant of the solvent is usually employed to fit these data with the Born,[27,28] Bjerrum,[29,30] or Denison–Ramsey[31] equations.[25,32] This approach is obviously open to criticism,[33,34] but it has been successful in closely describing the solvent dependence of many dissociation constants.[25,26] For the present purpose, a general form of the Born or Bjerrum equations will suffice to represent the electrostatic contribution to the free energy of dissociation; that is

$$\Delta F_e^\circ(T) = B + A/\epsilon(T) \quad (7)$$

where A is the slope parameter and B is the integration constant for $-\int \Delta S_e^\circ(T)dt$.

(19) The failure of electrostatic models to describe accurately the thermodynamics of ion hydration[20] has been attributed to the role of covalent interaction in the solvation processes.[21,22]

(20) K. J. Laidler and C. Pegis, *Proc. Roy. Soc.* (London), **A241**, 80 (1957).

(21) J. L. Kavanau, "Water and Solute–Water Interactions," Holden-Day, Inc., San Francisco, Calif., 1964.

(22) L. B. Magnusson, *J. Chem. Phys.*, **39**, 1953 (1963).

(23) R. M. Fuoss and C. A. Kraus, *J. Am. Chem. Soc.*, **79**, 3304 (1957).

(24) C. W. Davies, "Ion Association," Butterworth and Co. Inc., Washington, D. C., 1962.

(25) C. A. Kraus, *J. Phys. Chem.*, **60**, 129 (1956).

(26) Ya. I. Tur'yan, *Russ. J. Inorg. Chem.*, **4**, 369 (1959).

(27) M. Born, *Z. Physik.*, **1**, 45 (1920).

(28) $\Delta F_{i,e}^\circ = [-(Ze)^2N/2r][1 - (1/\epsilon)]$, where N is Avogadro's number and $\Delta F_{i,e}^\circ$ is the change in free energy attending reversible transfer of the ith ionic species of radius r and absolute charge Ze from a vacuum to a medium with a dielectric constant, ϵ.

(29) N. Bjerrum, *Kgl. Danske Videnskab. Selskab, Math. Fys. Medd.*, **7**, 1 (1926).

(30) $K^{-1} = (4\pi N/1000)(|Z_1Z_2|e^2/kT)^3Q(b)$, where K designates the dissociation constant, $|Z_1Z_2|e^2$ represents the product of the absolute charges of the ionic species involved, N is Avogadro's number, k is Boltzmann's constant, ϵ is the dielectric constant, and $Q(b) = 2\int_2^b x^{-4}e^x dx$, in which $x = |Z_1Z_2|e^2/r\epsilon kT$ and $b = |Z_1Z_2|e^2/a\epsilon kT$, where r is the radius and a is the distance of closest approach.

(31) $\Delta F_r^\circ = N\Delta V_2/\epsilon$, where ΔF_r° represents the free energy of dissociation, N is Avogadro's number, ϵ designates the dielectric constant of the solvent, and ΔV_2 is the potential energy of dissociation; J. T. Denison and J. B. Ramsey, *J. Am. Chem. Soc.*, **77**, 2615 (1955).

(32) (a) R. M. Fuoss and C. A. Kraus, *ibid.*, **55**, 1019 (1933). (b) A. M. Sukhotin, *Zh. Fiz. Khim.*, **31**, 792 (1957). (c) L. D. Pettit and S. Bruckenstein, *J. Am. Chem. Soc.*, **88**, 4783, 4790 (1966).

(33) V. P. Vasil'ev, *Russ. J. Inorg. Chem.*, **5**, 1378 (1960).

(34) S. I. Drakin and V. A. Mikhailov, *Russ. J. Phys. Chem.*, **33**, 45 (1959).

The dielectric constant of water from 0 to 370°[35-40] can be represented by

$$\epsilon(T) = \epsilon_0 \exp[-\exp(b + aT) - T/\theta] \quad (8)$$

where $\epsilon_0 = 305.7$, $b = -12.741$, $a = 0.01875$, and $\theta = 219$.[41]

Because $\Delta S_e^\circ(T) = -d\Delta F_e^\circ(T)/dT$, eq 8 and its first derivative can be combined with the first derivative of eq 7 to give

$$\Delta S_e^\circ(T) = -\frac{A \exp[\exp(b + aT) + T/\theta]}{\epsilon_0} \times \left[\frac{1}{\theta} + a \exp(b + aT)\right] \quad (9)$$

However, for the reference temperature, eq 9 can be written as

$$\epsilon_0 = -\frac{A \exp[\exp(b + aT_r) + T_r/\theta]}{\Delta S_e^\circ(T_r)} \times \left[\frac{1}{\theta} + a \exp(b + aT_r)\right] \quad (10)$$

so that

$$\Delta S_e^\circ(T) = \frac{\Delta S_e^\circ(T_r) \exp[\exp(b + aT) - c + (T - T_r)/\theta]}{\omega} \times [1 + a\theta \exp(b + aT)] \quad (11)$$

where $c = \exp(b + aT_r)$ and $\omega = 1 + ac\theta$.

C. Nonelectrostatic Temperature Function. Although calculations of $\Delta S_n^\circ(T)$ could be carried out by characterizing the degrees of freedom contributing to the nonelectrostatic entropy of dissociation,[18] it is sufficient for the present purpose to define this variable in terms of an empirical power series consistent with purely covalent interaction in the absence of a dielectric medium. If we assume for dissociational reactions in aqueous solution that the nonelectrostatic contribution to $\Delta C_{P,r}^\circ(T)$, the heat capacity of dissociation, can be represented by[42-45]

$$\Delta C_{P,n}^\circ(T) = \alpha + \beta T + \lambda T^2 \quad (12)$$

in which α, β, and λ are reaction-dependent coefficients, then eq 12 can be divided by T and integrated to give the following approximation of $\Delta S_n^\circ(T)$

$$\Delta S_n^\circ(T) = \Delta S_n^\circ(T_r) + \int_{T_r}^{T} \Delta C_{P,n}^\circ(T) dT/T = \Delta S_n^\circ(T_r) + \alpha \ln T/T_r + \beta(T - T_r) + \lambda(T^2 - T_r^2)/2 \quad (13)$$

D. Combined Equations. Substitution of eq 11 and 13 in eq 5 yields an expression for the entropy of dissociation as a function of temperature (from 0 to 370°)[46-49]

$$\Delta S_r^\circ(T) = \frac{\Delta S_e^\circ(T_r) \exp[\exp(b + aT) - c + (T - T_r)/\theta]}{\omega} \times [1 + \phi \exp(b + aT)] + \Delta S_n^\circ(T_r) + \alpha \ln T/T_r + \beta(T - T_r) + \lambda(T^2 - T_r^2)/2 \quad (14)$$

in which $\theta = 219$; $a = 0.01875$; $b = -12.741$; $c =$

(35) G. C. Åkerlof and H. I. Oshry, *J. Am. Chem. Soc.*, **72**, 2844 (1950).

(36) F. H. Drake, G. W. Pierce, and M. T. Dow, *Phys. Rev.*, **35**, 613 (1930).

(37) J. Wyman, Jr., *ibid.*, **35**, 623 (1930).

(38) G. C. Åkerlof, *J. Am. Chem. Soc.*, **54**, 4125 (1932).

(39) J. Wyman, Jr., and E. N. Ingalls, *ibid.*, **60**, 1182 (1938).

(40) C. G. Malmberg and A. A Maryott, *J. Res. Natl. Bur. Std.*, **56**, 1 (1956).

(41) This double exponential equation extends Gurney's[16] expression for $\epsilon(T)$ at low temperatures [$\epsilon(T) = \epsilon_0 \exp(-T/\theta)$] to higher temperatures. The maximum deviation of the dielectric constant described by eq 8 from that predicted by the power function proposed by Åkerlof and Oshry [$\epsilon(T) = a/T + b - cT + dT^2 - eT^3$] over the temperature range 100 to 370° is 0.1, but over most of this range it is considerably less. Below 100°, where many more data are available and the scatter is correspondingly large, values calculated from eq 8 are in closest agreement with the data of Malmberg and Maryott.[40] A number of the thermodynamic calculations reported in later discussion were alternately carried out with $\epsilon(T)$ represented by the Åkerlof–Oshry equation to examine the consequences of numerical differences between its derivative and that of eq 8 on calculated thermodynamic variables at elevated temperatures. The effects were found to be insignificant.

(42) The temperature dependence of the heat capacities of hydrocarbon gases for the normal paraffin, monoolefin, acetylene, alkyl benzene, alkyl cyclopentane, and alkyl cyclohexane series from 298.15 to 1500°K takes the form of a simple quadratic or cubic equation in T.[43] Heat capacities of other gases take the form $C_p^\circ(T) = a + bT + c/T^2$, in which the last term or the last two terms may be insignificant.[44,45] Although little is known of the temperature dependence of the heat capacities of dissociation for gases, because the various members of the hydrocarbon series cited above differ from one another by one or more CH_2 groups, the difference in the heat capacities for two members of the series also takes the form of a quadratic or cubic function of T. See B. L. Lewis and G. von Elbe, *J. Am. Chem. Soc.*, 57, 612 (1935).

(43) H. M. Spencer, *Ind. Eng. Chem.*, **40**, 2152 (1948).

(44) K. K. Kelley, U. S. Bureau of Mines Bulletin 584, U. S. Government Printing Office, Washington, D. C., 1960.

(45) G. N. Lewis and M. Randall, "Thermodynamics," 2nd ed, rev by K. S. Pitzer and L. Brewer, McGraw-Hill Book Co. Inc., New York, N. Y., 1961, p 66.

(46) It will be apparent in the later discussion that for certain groups of dissociational reactions, eq 14 is equivalent to that obtained by performing an expansion of $\Delta S_r^\circ(T)$ about a reference $\Delta S_r^\circ(T_r)$ when only the first two terms of the expansion are retained. For such reactions, eq 14 is consistent with the principle of corresponding states employed by Criss and Cobble[47-49] to predict absolute ionic entropies and average ionic heat capacities at elevated temperatures.

(47) C. M. Criss and J. W. Cobble, *J. Am. Chem. Soc.*, **86**, 5385 (1964).

(48) C. M. Criss and J. W. Cobble, *ibid.*, **86**, 5390 (1964).

(49) J. W. Cobble, *Science*, **152**, 1479 (1966).

$\exp(b + aT_r) = 7.84 \times 10^{-4}$; $\omega = 1 + ac\theta = 1.00322$; and $\phi = a\theta = 4.106$. Combining the integral of eq 14 and a statement of eq 5 for T_r along with

$$\Delta F_r^\circ(T) = \Delta F_r^\circ(T_r) - \int_{T_r}^{T} \Delta S_r^\circ(T)\mathrm{d}T \quad (15)$$

and

$$\Delta F_r^\circ(T_r) = \Delta H_r^\circ(T_r) - T_r\Delta S_r^\circ(T_r) \quad (16)$$

results in the equation for the free energy of dissociation

$$\Delta F_r^\circ(T) = -\Delta S_e^\circ(T_r)\left[\frac{\theta}{\omega}\{\exp[\exp(b + aT) - c + (T - T_r)/\theta] - 1\} + T_r - T\right] - T\Delta S_r^\circ(T_r) + \Delta H_r^\circ(T_r) - \alpha(T \ln T/T_r - T + T_r) - \beta(T - T_r)^2/2 - \lambda(T^3/3 - T_r^3/3 - T_r^2T + T_r^3)/2 \quad (17)$$

Combining eq 17 with $\Delta F_r^\circ(T) = -2.303RT \log K(T)$ leads to

$$\log K(T) = \frac{\Delta S_e^\circ(T_r)}{2.303RT}\left[T_r - T - \frac{\theta}{\omega}(1 - \exp[\exp(b + aT) - c + (T - T_r)/\theta])\right] - \frac{\Delta H_r^\circ(T_r)}{2.303RT} + \frac{\Delta S_r^\circ(T_r)}{2.303R} + \frac{\alpha}{2.303R}(\ln T/T_r - 1 + T_r/T) + \frac{\beta(T - T_r)^2}{4.606RT} + \frac{\lambda}{4.606RT} \times (T^3/3 - T_r^3/3 - T_r^2T + T_r^3) \quad (18)$$

Multiplying the first derivative of eq 14 by T yields the following equation for the heat capacity of dissociation.

$$\Delta C^\circ_{P,r}(T) = \frac{T\Delta S_e^\circ(T_r)\exp[\exp(b + aT) - c + (T - T_r)/\theta]}{\omega\theta} \times \{[1 + \phi\exp(b + aT)]^2 + \phi^2\exp(b + aT)\} + \alpha + \beta T + \lambda T^2 \quad (19)$$

Comparison of Calculated and Experimental Data

A. Dissociation Constants. Figures 1 and 2 illustrate fits of eq 18 to dissociation constants taken from the literature sources shown in Table I.[50-52] The calculations were carried out with the aid of a least-squares computer routine. The values of $\Delta H_r^\circ(T_r)$ and $\Delta S_r^\circ(T_r)$ employed in the calculations are given in Table II along with the values of $\Delta S_e^\circ(T_r)$, α, and β obtained from the fits of the data. The least-squares fits depicted in Figures 1 and 2 were calculated with λ set to zero because the dissociation constants are not sufficiently precise in most instances to permit significant values of this parameter to be determined. λ can be defined explicitly only by the second derivative of $\Delta C_{P,n}^\circ(T)$. Also because of uncertainties in the dissocia-

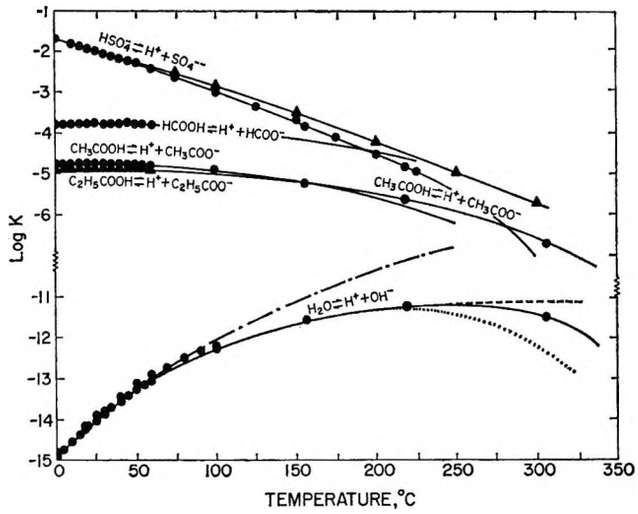

Figure 1. Fit of eq 18 with $\lambda = 0$ (solid curves) to published dissociation constants (represented by the symbols) taken from the sources indicated in Table I. The thermodynamic data employed in the calculations are shown in Table II along with the values of $\Delta S_e^\circ(T_r)$, α, and β obtained from the least-squares fits. In the case of formic and propionic acids, the curves are based on least-squares fits of heat capacity data (Figure 3—see text). Comparative alternate curves based on the assumption that $\Delta C_{P,r}^\circ(T) = 0$ (-·-·-·), $\Delta C_{P,r}^\circ(T)$ = a constant (- - - -), or that $\Delta C_{P,r}^\circ(T)/\Delta C_{P,e}^\circ(T)$ is constant (·····) [see text] are also shown for the dissociation of water. The triangular symbols for log $K_{HSO_4^-}$ represent values calculated by Marshall and Jones [*J. Phys. Chem.*, **70**, 4028 (1966)] from $CaSO_4$ solubilities (see footnote f, Table I, and footnote r, Table II).

(50) All equilibrium constants reported in this paper are consistent with molal units of concentration. Values taken from the literature have been converted from the molar scale where necessary (log K_m = log K_M − n log ρ_{H_2O}, in which ρ_{H_2O} is the density of water and n is one for dissociation constants and two for activity products). The density data for water were taken from Dorsey[51] and Keenan and Keyes.[52] Although the standard state adopted here is a hypothetical 1 m solution at 1 atm, pressure changes up to several hundred atmospheres have a small effect (considered negligible in this discussion) on the thermodynamics of dissociation for most complexes.

(51) N. E. Dorsey, "Properties of Ordinary Water-Substance," Reinhold Publishing Corp., New York, N. Y., 1940.

(52) J. H. Keenan and F. G. Keyes, "Thermodynamic Properties of Steam," John Wiley and Sons, Inc., New York, N. Y., 1936.

Table I: Sources of Experimental Dissociation Constants Plotted in Figures 1, 2, and 10

Dissociational Reaction	Temperature Interval	Dissociational Reaction	Temperature Interval
$H_2O \rightleftarrows H^+ + OH^-$ [a]	0°- 60° [a] 0°-100° [b,c] 100°-306° [c]	$H_3PO_4 \rightleftarrows H^+ + H_2PO_4^-$	0°-156° [r,u]
$HSO_4^- \rightleftarrows H^+ + SO_4^{--}$	0°-225° [d,e] 25°-350° [f]	$NH_4OH \rightleftarrows NH_4^+ + OH^-$	0°- 50° [c,v] 50°-306° [c,r]
$KSO_4^- \rightleftarrows K^+ + SO_4^{--}$	0°- 40° [h] 100°-300° [73]	$NaOH \rightleftarrows Na^+ + OH^-$	5°- 45° [w] 281° [r]
$HCO_3^- \rightleftarrows H^+ + CO_3^{--}$	0°- 50° [j] 60°- 90° [k] 100°-218° [l]	$HCOOH \rightleftarrows H^+ + HCOO^-$	0°- 60° [7]
$H_2CO^m_{3(app)} \rightleftarrows H^+ + HCO_3^-$	0°- 50° [n] 55°- 65° [o] 100°-200° [l]	$CH_3COOH \rightleftarrows H^+ + CH_3COO^-$	0°- 60° [4] 18°-306° [c]
$HCl \rightleftarrows H^+ + Cl^-$	0°- 50° [74] 260°-374° [p,q,r]	$C_2H_5COOH \rightleftarrows H^+ + C_2H_5COO^-$	0°- 60° [6]
$NaCl \rightleftarrows Na^+ + Cl^-$	281°-306° [r] 300°-373° [s] 374° [q,t]	$HNO_3 \rightleftarrows H^+ + NO_3^-$	0°- 70° [x] 218°-306° [e]
$KCl \rightleftarrows K^+ + Cl^-$	281°-306° [r] 374° [q]	$H_2CO^m_{3(app)} \rightleftarrows H_2O + CO_{2(g)}$	0°- 30° [61] 75°-125° [60] 100°-350° [59]
		$H_2S_{(aq)} \rightleftarrows H_2S_{(g)}$	0°-100° [55,56,i] 100°-300° [58]

(a) H. Lunden, J. Chem. Phys., 5, 574 (1907); A. Ölander, Zeit. Physik. Chem., 144, Pt. A., 49 (1929); H. S. Harned and W. J. Hamer, J. Am. Chem. Soc., 55, 2194 (1933); H. S. Harned and W. J. Hamer, ibid., 55, 4496 (1933). (b) A. Heydweiller, Ann. Physik., 28, 503 (1909). (c) A. A. Noyes, Y. Kato, and R. B. Sosman, J. Am. Chem. Soc., 32, 159 (1910). (d) M. H. Lietzke, R. W. Stoughton, and T. F. Young, J. Phys. Chem., 65, 2247 (1961); V. S. K. Nair and G. H. Nancollas, J. Chem. Soc. (London), 4144 (1958); M. Kerker, J. Am. Chem. Soc., 79, 3664 (1956); T. F. Young, L. F. Maranville, and H. M. Smith, in The Structure of Electrolytic Solutions (edited by W. J. Hamer), Wiley, N. Y., 35 (1959); B. N. Ryzhenko, Geochemistry International, No. 1, 8 (1964); I. E. Flis, K. P. Mishchenko, N. V. Pakhomova, Zh. Neorg. Khim., 3, 1772 (1958); C. K. Singleterri, Ph.D. Thesis, Univ. of Chicago (1940). (e) A. A. Noyes, Carnegie Inst. Publ. No. 63 (1907). (f) W. L. Marshall and E. V. Jones, J. Phys. Chem., 70, 4028 (1966). These values were not included in the present analysis of data, but are plotted in Figure 1 for comparison. In addition to the uncertainties introduced by the probable formation of $CaSO_{4(aq)}$ (see footnote r, Table 2), Marshall and Jones' values above 300°C also probably reflect the formation of $H_2SO_{4(aq)}$[g]. (g) A. S. Quist, W. V. Marshall and H. R. Jolley, J. Phys. Chem., 69, 27 (1965). (h) R. P. Bell and J. H. B. George, Trans. Farad. Soc., 49, 619 (1953). (i) J. Kendall and J. C. Andrews, J. Am. Chem. Soc., 43, 1545 (1921). (j) H. S. Harned and S. R. Scholes, Jr., J. Am. Chem. Soc., 63, 1706 (1941). (k) F. Cuta and F. Stráfelda, Chemicke Listy, 48, 1304 (1954). (l) B. N. Ryzhenko, Geochemistry 151 (1963). (m) The subscript "(app)" indicates that the species referred to is the undifferentiated sum of $CO_{2(aq)} + H_2CO_{3(aq)}$. (n) H. S. Harned and R. Davies, Jr., J. Am. Chem. Soc., 65, 2030 (1943). (o) A. J. Ellis, J. Chem. Soc. (London), 3689 (1959). (p) D. Pearson, C. S. Copeland, and S. W. Benson, J. Am. Chem. Soc., 85, 1047 (1963). (q) Extrapolation of supercritical data taken from E. U. Franck, Ang. Chemie, 73, 309 (1961). (r) J. M. Wright, W. J. Lindsay, Jr., and T. R. Druga, U. S. Atomic Energy Comm., WAPD-TM-204 (1961) after Noyes[e]. (s) D. Pearson, C. S. Copeland, and S. W. Benson, J. Am. Chem. Soc., 85, 1044 (1963). (t) Extrapolation of supercritical data taken from J. K. Fogo, S. W. Benson, and C. S. Copeland, J. Chem. Phys., 22, 212 (1954). (u) L. F. Nims, J. Am. Chem. Soc., 56, 1110 (1934); R. G. Bates, J. Res. Nat. Bur. Stds., 47, 127 (1951). (v) R. G. Bates and G. D. Pinching, J. Res. Nat. Bur. Stds., 42, 419 (1949); D. H. Everett and D. A. Landsman, Trans. Farad. Soc., 50, 1221 (1954); E. Arnold, H. Freitag and A. Patterson, Jr., in The Structure of Electrolytic Solutions (edited by W. J. Hamer), Wiley, N. Y., 281 (1959). (w) F. G. R. Gimblett and C. B. Monk, Trans. Farad. Soc., 50, 965 (1954) after H. S. Harned and G. E. Mannweiller, ibid., 57, 1873 (1935). (x) J. F. Young, L. F. Maranville, and H. M. Smith, in The Structure of Electrolytic Solutions (edited by W. J. Hamer), Wiley, N. Y., 35 (1959); A. A. Kraewitz, Ph.D. Thesis, Univ. of Chicago (1955); G. C. Hood and C. A. Reilly, J. Chem. Phys., 32, 127 (1960).

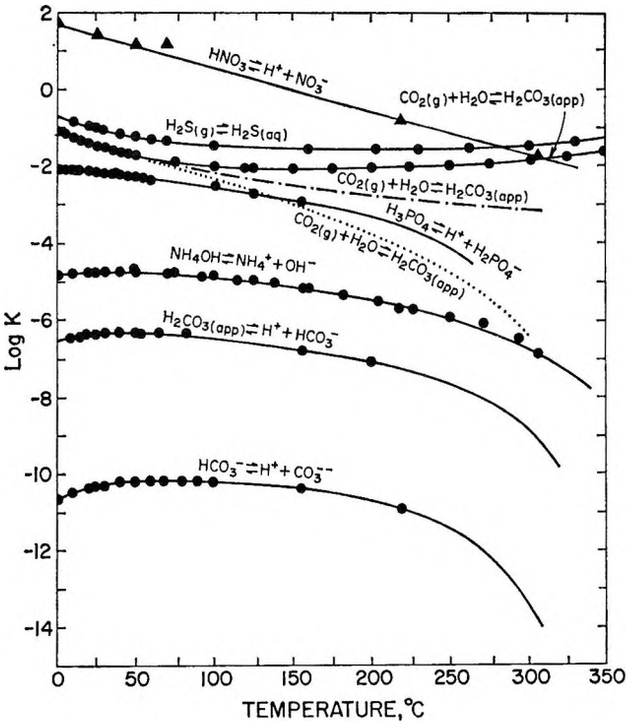

Figure 2. Fit of eq 18 with $\lambda = 0$ (solid curves) to published dissociation constants (represented by the symbols) taken from the sources indicated in Table I. The thermodynamic data employed in the calculations are shown in Table II along with the values of $\Delta S_e^\circ(T_r)$, α and β obtained from the least-squares fits. Comparative alternate curves based on the assumption that $\Delta C_{P,r}^\circ = 0$ (—·—·—) or that $\Delta C_{P,r}^\circ(T)/\Delta C_{P,e}^\circ(T)$ is constant (·····) [see text] are also shown for $CO_2(g) + H_2O \rightleftarrows H_2CO_3(app)$.

tion constants, the numerical values of $\Delta S_n^\circ(T_r)$ defined by a number of the fits cannot be considered thermodynamically significant. The division of $\Delta S_r^\circ(T)$ and $\Delta C_{P,r}^\circ(T)$ into electrostatic and nonelectrostatic portions is numerically reliable only for those species for which precise data are available, but it will be shown later that the general behavior of these quantities with increasing temperature, and the numerical values for the over-all thermodynamic variables defined by the least-squares fits are significant in most instances.

Calculated log $K(T)$ curves based on various assumptions (discussed below) concerning $\Delta C_{P,r}^\circ(T)$ are also shown in Figures 1 and 2. To afford a numerical comparison, dissociation constants taken from the literature for a number of the reactions listed in Table I are presented in Table III along with corresponding values calculated from the fits of the data using eq 18.

The nonelectrostatic contributions to log $K(T)$ arising from $\Delta C_{P,n}^\circ(T)$ for $CO_2(g) + H_2O \rightleftarrows H_2CO_3(app)$ and $H_2S(g) \rightleftarrows H_2S(aq)$[53-61] in Figure 2 dominate the temperature variation of the equilibrium constants for these reactions. The large nonelectrostatic contributions, which are substantially greater than those attending other reactions considered here, result from the participation of a molecular gas in the reactions. The fact that excellent fits of experimental log $K(T)$ values for reactions dominated by nonelectrostatic interaction can be obtained with eq 18 supports the validity of the assumptions inherent in its derivation. A purely electrostatic model fails to render close fits of dissociation constants for such reactions over a large temperature range.

B. Heat Capacities. The temperature dependence of the heat capacities of dissociation for water and formic, acetic, and propionic acids is illustrated in Figure 3. The symbols indicate values derived from calorimetric measurements,[8-10,62,63] and the curves represent least-squares fits of these values using eq 19 with λ set to zero. The $\Delta H_r^\circ(T_r)$ and $\Delta S_r^\circ(T_r)$ values used in the calculations are shown in Table II along with the constants ($\Delta S_e^\circ(T_r)$, α, and β) obtained from the fits of $\Delta C_{P,r}^\circ(T)$ for the dissociation of formic and propionic acids (Figure 3). Although experimental high temperature log $K(T)$ values are not available for formic and propionic acids, those for water and acetic acid up to 218° are consistent with the $\Delta S_e^\circ(T_r)$, α, and β values derived from the experimental heat capacity data plotted in Figure 3.[64] However, at higher temperatures this is no longer true. Heat capacities of dissociation for water and acetic acid, calculated from

(53) Cobble[54] assumed $C_{P,H_2S(aq)}^\circ$ to be 48 cal mole^{-1} deg^{-1} from 25 to 200° on the basis of heats of solution for $H_2S(g)$ from 0 to 104° calculated by Pohl[55] from data presented by Wright and Maass[56] and Selleck, *et al.*[57] Cobble disregarded Pohl's values at 138 and 171° because he considered them to be inconsistent with ideal behavior. Recent data presented by Kozintseva[58] suggest that H_2S solubility in water obeys Henry's law to >200°. Although considerable uncertainty attends the calculation, average heat capacity values for $H_2S(aq)$ of 46, 39, 35, and 32 cal mole^{-1} deg^{-1} at 60, 100, 150, and 200°, respectively, give better fits of the combined heats of solution and high temperature Henry's law coefficients. While the theoretical curve for $H_2S(g) \leftrightarrows H_2S(aq)$ in Figure 2 is based in part on calorimetric data, that for $CO_2(g) + H_2O \leftrightarrows H_2CO_3(app)$ was derived solely from a least-squares fit of Henry's law coefficients.[59-61]

(54) J. W. Cobble, *J. Am. Chem. Soc.*, **86**, 5394 (1964).

(55) H. A. Pohl, *J. Chem. Eng. Data*, **6**, 515 (1961).

(56) R. H. Wright and O. Maass, *Can. J. Res.*, **6**, 94 (1932).

(57) F. T. Selleck, L. T. Carmichael, and B. H. Sage, *Ind. Eng. Chem.*, **44**, 2219 (1952).

(58) T. N. Kozintseva, *Geokhimiya*, No. 8, 758 (1964).

(59) A. J. Ellis and R. M. Golding, *Am. J. Sci.*, **261**, 47 (1963).

(60) E. R. Segnit, H. D. Holland, and C. J. Biscardi, *Geochim. Cosmochim. Acta*, **26**, 1301 (1962).

(61) H. S. Harned and R. Davis, Jr., *J. Am. Chem. Soc.*, **65**, 2030 (1943).

(62) E. Wicke, M. Eigen, and Th. Ackermann, *Z. Physik. Chem.* (Frankfurt), **1**, 340 (1954).

(63) Th. Ackermann, *Discussions Faraday Soc.*, **24**, 180 (1957).

Table II: Thermodynamic Data for the Dissociation of Various Complexes in Aqueous Solution at 25° and 1 Atm[a]

Dissociational Reaction	log $K(T_r)$	$\Delta H^\circ_r(T_r)$ (cal. mole^{-1})	$\Delta S^\circ_r(T_r)$ (cal. mole^{-1} deg.$^{-1}$)	$\Delta S^\circ_e(T_r)$ (cal. mole^{-1} deg.$^{-1}$)	α	β (x 10^2)
$H_2O \rightleftarrows H^+ + OH^-$	-13.997[d,e]	13,335[f]	-19.31[g]	-13.4482	-135.070	34.7941
$H_3PO_4 \rightleftarrows H^+ + H_2PO_4^-$	- 2.15[h]	- 1,840[3]	-16.0[g]	-60.1485	-300.614	116.1389
$H_2CO^i_{3(app)} \rightleftarrows H^+ + HCO_3^-$	- 6.35[61]	1,840[3]	-22.9[g]	-35.1122	-375.081	112.5904
$HCO_3^- \rightleftarrows H^+ + CO_3^{--}$	-10.33[j]	3,600[3]	-35.16[g]	-56.6668	-420.219	138.2404
$NH_4OH \rightleftarrows NH_4^+ + OH^-$	- 4.751[k]	370[3]	-20.5[g]	- 6.7480	26.601	- 14.9602
$HNO_3 \rightleftarrows H^+ + NO_3^-$	1.43[l]	- 4,100[m]	- 7.2[m]	3.7356	10.434	- 18.7598
$HSO_4^- \rightleftarrows H^+ + SO_4^{--}$	- 1.99[n,p,q]	- 3,850[u]	-22.0[48,r]	-39.8978	-424.825	126.5702
$CH_3COOH \rightleftarrows H^+ + CH_3COO^-$	- 4.76[4]	- 112[3]	-22.1[g]	- 3.9504	- 30.199	- 0.8849
$HCOOH \rightleftarrows H^+ + HCOO^-$	- 3.75[7]	- 13[3]	-17.2[g]	-20.5891[v]	-135.086[v]	41.4843[v]
$C_2H_5COOH \rightleftarrows H^+ + C_2H_5COO^-$	- 4.87[6]	- 168[3]	-22.8[g]	-55.2019[v]	-237.867[v]	95.9096[v]
$H_2S_{(aq)} \rightleftarrows H_2S_{(g)}$	0.99[56]	4,100[53]	18.3[g]	- 1.8431	- 87.649	18.1626
$H_2CO^i_{3(app)} \rightleftarrows H_2O + CO_{2(g)}$	1.46[61]	4,650[61]	22.3[g]	- 1.3035	- 54.125	6.7986

(a) With two exceptions (noted below) the values of $\Delta S^\circ_e(T_r)$, α, and β were assigned from least squares analyses of log K(T) data using Equation (18) with $\lambda = 0$. The sources of data listed below are in addition to Latimer[b] and Rossini, et al.[c]. (b) W. H. Latimer, The Oxidation States of the Elements and Their Potentials in Aqueous Solutions, Prentice-Hall, N. J. (1952), 392 pp. (c) R. D. Rossini, D. D. Wagman, W. H. Evans, S. Levine, and I. Jaffe, Nat. Bur. Stds. Circ. 500 (1952). (d) This value is for the activity product constant (K_w) of water. (e) H. S. Harned and W. J. Hamer, J. Am. Chem. Soc., 55, 2194 (1933); H. S. Harned and W. J. Hamer, ibid., 55, 4496 (1933); H. Lunden, J. Chem. Phys., 5, 574 (1907); A. Heydweiller, Ann. Physik., 28, 503 (1909). (f) J. D. Hale, R. M. Izatt and J. J. Christensen, J. Phys. Chem., 67, 2605 (1963); C. E. Vanderzee and J. A. Swanson, ibid., 67, 2608 (1963). (g) Calculated from $\Delta H^\circ_r(T_r)$ and log $K(T_r)$. (h) R. G. Bates, J. Res. Nat. Bur. Stds., 47, 127 (1951). (i) The subscript "(app)" indicates that the species referred to is the undifferentiated sum of $CO_{2(aq)} + H_2CO_{3(aq)}$. (j) H. S. Harned and S. R. Scholes, Jr., J. Am. Chem. Soc., 63, 1706 (1941). (k) E. Arnold, H. Freitag, and A. Patterson, Jr., in The Structure of Electrolytic Solutions (edited by W. J. Hamer), Wiley, N. Y., 281 (1959); R. G. Bates and G. D. Pinching, J. Res. Nat. Bur. Stds., 42, 419 (1949). (l) A. A. Krawitz, Ph.D. Thesis, Univ. of Chicago (1955); G. C. Hood and C. A. Reilly, J. Chem. Phys., 32, 127 (1960). (m) The $\Delta S^\circ_r(T_r)$ and $\Delta H^\circ_r(T_r)$ values shown above are based on a least squares fit of the log K(T) data using Equation (18). The $\Delta H^\circ_r(T_r)$ value is identical with that obtained by Young, et al.[n] from differentiation of a least squares fit of Kraewitz's[l] and Noyes'[o] experimental data (including the value at 306°C) in terms of log K(1/T). The value given by Noyes for log K_{HNO_3} at 306°C was not included in the present analysis because of the apparent disproportionation of the nitrate ion above 250°C (E. U. Franck, personal communication). The value of log K at 70°C given by Hood and Reilly[l], who determined $\Delta H^\circ_r(T_r)$ to be -3300 cal. mole^{-1} and $\Delta S^\circ_r(T_r)$ to be -4.46 cal. mole^{-1} deg.$^{-1}$ from linear interpretation of an R ln K(1/T) plot of their data at 0°, 25°, and 70°C, is not in good agreement with the curve shown in Fig. 2. However, their value of $\Delta H^\circ_r(T_r)$ is fixed largely by the log K value at 70°C. A log K(T) curve consistent with this value of $\Delta H^\circ_r(T_r)$ can be calculated from Equation (18) but it exhibits a double inflection. More high temperature data are required to satisfactorily define $\Delta H^\circ_r(T_r)$ and the log K(T) curve for this reaction. (n) T. F. Young, L. F. Maranville, and H. M. Smith, in The Structure of Electrolytic Solutions (edited by W. J. Hamer), Wiley N. Y., 35 (1959). (o) A. A. Noyes, Carnegie Inst. Pub. No. 63, (1907). (p) T. F. Young and D. E. Irish, Ann. Review Phys. Chem., 13, 435 (1962). (q) V. S. K. Nair and G. H. Nancollas, J. Chem. Soc. (London), 4144 (1958); I. E. Flis, K. P. Mischenko, and N. V. Pakhomova, Zh. Neorg. Khim., 3, 1772 (1958). (r) This value of $\Delta S^\circ_r(T_r)$, which is based on calorimetric data[48], is in agreement with recent log $K_{HSO_4^-}$ values obtained from extrapolation of $CaSO_4$ solubility measurements in H_2SO_4 solutions[t]. However, it forces a value of $\Delta H^\circ_r(T_r)$ that is considerably less negative than the older calorimetric data[p,3]. The $\Delta S^\circ_e(T_r)$, α, and β values shown above for the dissociation of HSO_4^- were derived from least squares fits of various high temperature log K(T) values (Table 1) which include those calculated by Lietzke, et al.[s] from Ag_2SO_4 solubilities in various electrolyte solutions and values obtained by Noyes[o] and Ryzhenko (Table 1) from conductance measurements. The high temperature log K(T) values given by Marshall and Jones[t] do not agree with these data, probably because of the formation of $CaSO_{4(aq)}$ in their solutions. (s) H. H. Lietzke, R. W. Stoughton, and T. F. Young, J. Phys. Chem., 65, 2247 (1961). (t) W. L. Marshall and E. V. Jones, Abstracts of papers, 149th Meeting, Am. Chem. Soc., 225 (1965); W. L. Marshall and E. V. Jones, J. Phys. Chem., 70, 4028 (1966). (u) Calculated from log $K(T_r)$ and $\Delta S^\circ_r(T_r)$. (v) Values obtained from least squares fits of $\Delta C^\beta_{p,r}(T)$ data (Figure 3) using Equation (19) with $\lambda = 0$.

values of $\Delta S_e^\circ(T_r)$, α, and β (Table II) derived from least-squares fits of log $K(T)$ from 0 to 306°, are shown in Figure 4. The fact that the latter curves differ somewhat from those in Figure 3 can be attributed to

Table III: Tabulation of Dissociation Constants at Elevated Temperatures Taken from the Literature[a] with Those Obtained from Least-Squares Fits of the Data Using Eq 18 with $\lambda = 0$—See Table I and Figures 1 and 2

Dissociational Reaction	Temperature C°	Experimental log K(T)	Calculated log K(T)
$H_2O \rightleftarrows H^+ + OH^-$ [b,c]	25	-13.997[d]	-13.995
	50	-13.262[d]	-13.27
	100	-12.28 [e]	-12.27
	156	-11.57 [e]	-11.58
	218	-11.19 [e]	-11.19
	306	-11.46	-11.46
$NH_4OH \rightleftarrows NH_4^+ + OH^-$	25	- 4.75 [f]	- 4.75
	50	- 4.72 [f]	- 4.75
	100	- 4.83 [e]	- 4.86
	156	- 5.16 [e]	- 5.15
	218	- 5.66 [e]	- 5.66
	306	- 6.87 [e]	- 6.87
$CH_3COOH \rightleftarrows H^+ + CH_3COO^-$	25	- 4.756[g]	- 4.75
	50	- 4.787[g]	- 4.78
	100	- 4.93 [e]	- 4.94
	156	- 5.23 [e]	- 5.24
	218	- 5.68 [e]	- 5.68
	306	- 6.70 [e]	- 6.70
$H_2CO_{3(app)}^{h} \rightleftarrows H^+ + HCO_3^-$	25	- 6.352[i]	- 6.35
	50	- 6.285[i]	- 6.31
	100	- 6.45 [j]	- 6.45
	156	- 6.77 [j]	- 6.77
	200	- 7.08 [j]	- 7.08
$HCO_3^- \rightleftarrows H^+ + CO_3^{--}$	25	-10.329[k]	-10.32
	50	-10.172[k]	-10.17
	90	-10.14 [l]	-10.14
	100	-10.12 [j]	-10.16
	156	-10.37 [j]	-10.36
	218	-10.88 [j]	-10.89
$H_2CO_{3(app)}^{h,53} \rightleftarrows H_2O + CO_{2(g)}$	25	1.464[61]	1.465
	50	1.705[61]	1.705
	100	1.99 [59]	1.97
	150	2.07 [59]	2.07
	200	2.05 [59]	2.06
	250	1.97 [59]	1.98
	300	1.84 [59]	1.83
	350	1.57 [59]	1.58
$H_2S_{(aq)} \rightleftarrows H_2S_{(g)}$[53]	25	0.99 [56]	0.99
	50	1.21 [56]	1.20
	100	1.44 [56]	1.43
	160	1.52 [58]	1.53
	202	1.53 [58]	1.54
	262	1.52 [58]	1.51
	301	1.45 [58]	1.45
	330	1.37 [58]	1.37

(a) Log K values shown here are consistent with molal units of concentration. (b) The values shown for the dissociation of water are for K_w, the activity product constant. (c) The calculated values for log K_w up to 250°C reported here are in close agreement with those calculated by Cobble[54] from the correspondence principle. Above that temperature Cobble calculated -11.9 and -11.33 for log K_w at 300° and 350°C from extrapolation of low temperature heat capacity data. The corresponding values computed here are -11.39 and -12.68, which are consistent with the experimental log K(T) data at 218° and 306°C[e]. (d) H. S. Harned and W. J. Hamer, J. Am. Chem. Soc., 55, 2194, 4496 (1933). (e) A. A. Noyes, Y. Kato, and R. B. Sosman, ibid., 32, 159 (1910). (f) R. G. Bates and G. D. Pinching, J. Res. Nat. Bur. Stds., 42, 419 (1949). (g) H. S. Harned and R. W. Ehlers, J. Am. Chem. Soc., 55, 652 (1933). (h) The subscript "(app)" indicates that the species referred to is the undifferentiated sum of $CO_{2(aq)}$ and $H_2CO_{3(aq)}$. (i) H. S. Harned and R. Davis, Jr., J. Am. Chem. Soc., 65, 2030 (1943). (j) B. N. Ryzhenko, Geochemistry, 151 (1963). (k) H. S. Harned and S. R. Scholes, Jr., J. Am. Chem. Soc., 63, 1706 (1941). (l) P. Cuta and P. Strafelda, Chemicke Listy, 48, 1304 (1954).

uncertainties inherent in extrapolating apparent heat capacity measurements to infinite dilution. Ackermann's[8] heat capacities for the dissociation of water were obtained from the equation

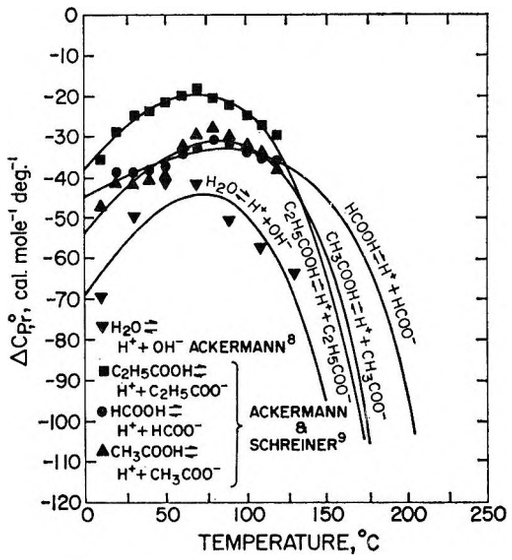

Figure 3. Fit of eq 19 with $\lambda = 0$ (solid curves) to heat capacities of dissociation for water and formic, acetic, and propionic acids taken from the literature.[8,9] The values of $\Delta S_e°(T_r)$, α, and β[64] obtained from the least-squares calculations for the dissociation of formic and propionic acids are shown in Table II, but those for water and acetic acid in Table II were obtained from fits of dissociation constants (Figure 1—see text). $\Delta C_{P,r}°(T)$ curves based on the log $K(T)$ fits for the dissociation of water and acetic acid are shown in Figure 4.

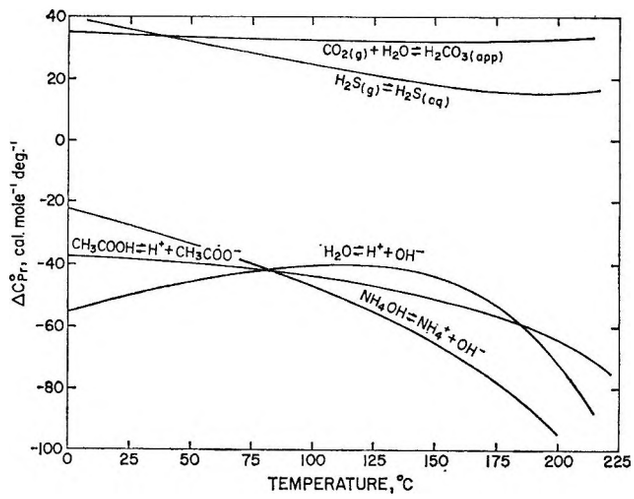

Figure 4. Heat capacities of dissociation calculated from eq 19 and the data shown in Table II.

(64) $H_2O \rightleftarrows H^+ + OH^-$: $\Delta S_e°(T_r) = -71.543$, $\alpha = -332.353$, $\beta = 125.794 \times 10^{-2}$; $CH_3COOH \rightleftarrows H^+ + CH_3COO^-$: $\Delta S_e°(T_r) = -44.772$, $\alpha = -239.667$, $\beta = 86.74903 \times 10^{-2}$; $C_2H_5COOH \rightleftarrows H^+ + C_2H_5COO^-$: $\Delta S_e°(T_r) = -55.202$, $\alpha = -237.867$, $\beta = 95.9096 \times 10^{-2}$; $HCOOH \rightleftarrows H^+ + HCOO^-$: $\Delta S_e°(T_r) = -20.589$, $\alpha = -135.086$, $\beta = 41.48434 \times 10^{-2}$.

$$\Delta C_{P,H_2O}^\circ = C_{P,HCl}^\circ + C_{P,NaOH}^\circ - C_{P,NaCl}^\circ - C_{P,H_2O}^\circ$$

using calorimetrically derived apparent heat capacities extrapolated to infinite dilution.[10,62,63] More recent determinations of $C_{P,NaCl}^\circ$ [65] and $C_{P,HCl}^\circ$ [66] to 100° using the integral heat method fail to agree with the data used by Ackermann.

Figures 4 and 5 illustrate $\Delta C_{P,r}^\circ(T)$ curves calculated from eq 19 and the data shown in Table II for a number of the reactions considered in Figures 1 and 2. Above ~150°, all of the curves in Figures 4 and 5 have relatively large negative slopes, reflecting the increasingly strong influence of the electrostatic contribution to $\Delta C_{P,r}^\circ(T)$ as the dielectric constant of water decreases with increasing temperature. Although the nonelectrostatic contribution to $\Delta C_{P,r}^\circ(T)$ is usually positive and increases with increasing temperature, its primary influence on $d\Delta C_{P,r}(T)/dT$ occurs in the low to intermediate temperature range; at high temperatures, the electrostatic contribution dominates the change in $\Delta C_{P,r}^\circ$ with temperature.

The maxima in the $\Delta C_{P,r}^\circ(T)$ curves (Figures 3, 4, and 5) are caused by $\Delta C_{P,n}^\circ(T)$, which opposes $\Delta C_{P,e}^\circ(T)$. Because $\Delta C_{P,e}^\circ(T)$ and $d\Delta C_{P,e}^\circ(T)/dT$ are almost always negative in the temperature range of interest (*e.g.*, the dashed curve shown for the dissociation of H_2CO_3(app) in Figure 5), and $|\Delta C_{P,e}^\circ(T)| >> |\Delta C_{P,n}^\circ(T)|$ only at high temperatures, the extrema occur in the low to intermediate temperature range. In cases where $\Delta C_{P,n}^\circ(T)$ is negative, maxima may not occur (as in the curves for the dissociation of NH_4OH and CH_3COOH in Figure 4). Although not exhibited by any of the dissociational reactions considered in Figures 3, 4, and 5, it appears likely that $\Delta C_{P,r}(T)$ curves for certain dissociational reactions will prove to be sigmoid in character. This probably occurs when $\Delta H_r^\circ(T_r)$ is a large negative number and the nonelectrostatic contribution to $\Delta C_{P,r}^\circ(T)$ becomes important only at elevated temperatures. Obviously, where $d\Delta C_{P,e}^\circ(T)/dT \approx -d\Delta C_{P,n}^\circ(T)/dT$, $\Delta C_{P,r}^\circ(T)$ is constant. The latter behavior is illustrated by the curve for the CO_2 gas reaction (Figure 4), for which $d\Delta C_{P,e}^\circ(T)/dT \approx -d\Delta C_{P,n}^\circ(T)/dT \approx 0$ and $\Delta C_{P,e}^\circ(T) << \Delta C_{P,n}^\circ(T)$ below 250°. Although all of the curves plotted in Figures 4 and 5 must be regarded as approximations because of their sensitivity to small errors in the log $K(T)$ values from which they were derived, test calculations indicate that the general configurations of the curves do not depend on such uncertainties. Because significant λ values could not be defined from the log $K(T)$ data, the slopes of the curves above 150° in Figures 4 and 5 are maximal approximations.

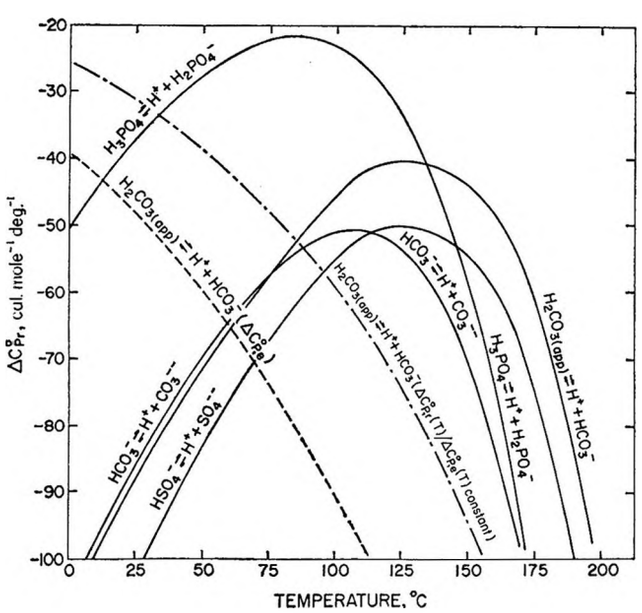

Figure 5. Heat capacities of dissociation calculated from eq 19 and the data shown in Table II. The dashed curve for the dissociation of H_2CO_3(app) represents the electrostatic portion of $\Delta C_{P,r}^\circ(T)$ for that reaction while the dash–dot curve is based on the assumption that $\Delta C_{P,r}^\circ(T)/\Delta C_{P,e}^\circ(T)$ is constant (see text).

C. Entropies. $\Delta S_r^\circ(T)$ curves calculated from eq 14 and the data shown in Table I for a few of the reactions considered in Figures 1 and 2 are depicted in Figure 6.

Dissociational reactions can be grouped according to the relative magnitude of the nonelectrostatic contributions to the thermodynamics of dissociation. For certain groups, eq 14 is analogous to the following entropy correspondence relation for ions,[48] but with the temperature dependence of the parameters for the dissociational reactions defined in terms of the electrostatic-nonelectrostatic model

$$S^\circ_{ion}{}^{abs}(T) = a(T) + b(T)S^\circ_{ion}{}^{abs}(T_r) \qquad (20)$$

The symbols a and b in eq 20 represent temperature-dependent coefficients characteristic of simple cations, simple anions, oxy anions, or acid oxy anions, and the superscript "abs" indicates that the entropy is absolute.[48] It can be seen in the correspondence diagram depicted in Figure 7 that $\Delta S_r^\circ(T_r)$ is linearly related to the corresponding values of $\Delta S_r^\circ(T)$ [calculated from eq 14 and the data in Table II] for the dissociation of a group of neutral species at 100, 150, and 200°. Because small errors in the log $K(T)$ values used to derive the

(65) C. M. Criss and J. W. Cobble, *J. Am. Chem. Soc.*, **83**, 3223 (1961).

(66) J. C. Ahluwalia and J. W. Cobble, *ibid.*, **86**, 5381 (1964).

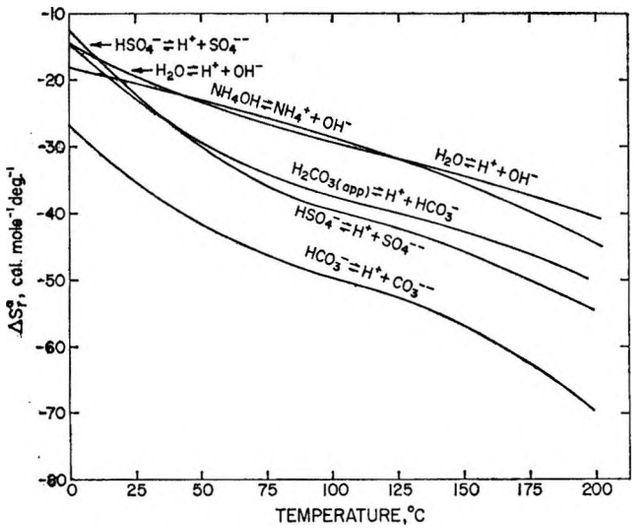

Figure 6. Entropies of dissociation calculated from eq 14 and the data shown in Table II for a few of the reactions considered in Figures 1 and 2.

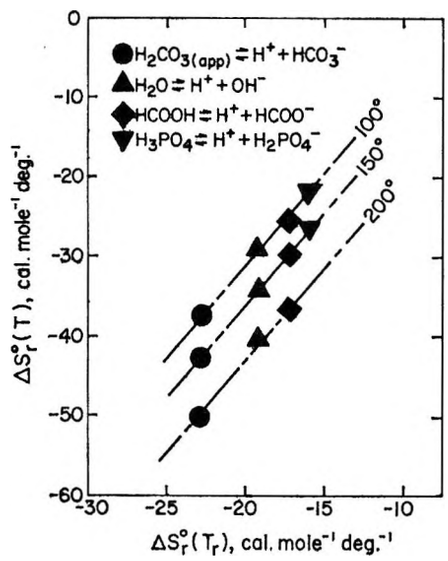

Figure 7. Entropy correspondence diagram illustrating the linear relation between the entropies of dissociation for a group of neutral species at 25, and 100, 150, and 200°. The plotted values were calculated from eq 14 and the data shown in Table II.

constants ($\Delta S_e^\circ(T_r)$, α, and β) preclude calculation of accurate $\Delta S_r^\circ(T)$ curves in many cases, other possible members of the group of reactions considered in Figure 7 could not be determined with confidence.

In terms of electrostatic and nonelectrostatic contributions to the entropy of dissociation, a correspondence relation such as that depicted in Figure 7 occurs when $\Delta S_e^\circ(T)/\Delta S_e^\circ(T_r) - \Delta S_n^\circ(T)/\Delta S_n^\circ(T_r)$ is equal to a constant for all reactions in the group. This results from similarities in the nonelectrostatic behavior of similar chemical species involved in the group of reactions. It would not be unexpected to find groups of dissociational reactions for which $\Delta S_e^\circ(T)/\Delta \cdot S_e^\circ(T_r) \approx \Delta S_n^\circ(T)/\Delta S_n^\circ(T_r)$; the resulting correspondence plot would consist of linear curves fanning out from the origin. It will be shown later that log $K(T)$ for many complexes below ~200° can be closely approximated by assuming such an equality, which is consistent with the statement that $\Delta C_{P,r}^\circ(T)/\Delta C_{P,e}^\circ(T)$ is constant. The effectiveness of the approximation is partly due to the insensitivity of log $K(T)$ to substantial departures from a constant $\Delta C_{P,r}^\circ(T)/\Delta C_{P,e}^\circ(T)$ and partly to the similar behavior of the nonelectrostatic power function of temperature and the electrostatic exponential temperature function at low temperatures.

Approximations of Log $K(T)$

A. Assuming $\Delta C_{P,r}^\circ(T) = 0$. This assumption is invalid for the dissociation of most complexes and it leads to serious errors when used to calculate log $K(T)$ at elevated temperatures. The effect of $\Delta C_{P,r}^\circ(T)$ on log $K(T)$ depends to a large extent on the relative size of $\Delta H_r^\circ(T_r)$ compared to $T_r\Delta S_r^\circ(T_r)$ for the reaction under consideration. Where $\Delta H_r^\circ(T_r)$ is large, as in many polyphase reactions involving solids, the contribution by $\Delta C_{P,r}^\circ(T)$ to log $K(T)$ is usually small and the assumption that $\Delta C_{P,r}^\circ(T) = 0$ renders a fairly close approximation to log $K(T)$. However, for most dissociations, $\Delta H_r^\circ(T_r)$ is relatively small (~±5 kcal mole^{-1}) and $\Delta C_{P,r}^\circ(T)$ cannot be safely ignored. Comparative curves illustrating possible errors attending this assumption are plotted in Figure 1 ($H_2O \rightleftarrows H^+ + OH^-$), Figure 2 ($CO_2(g) + H_2O \rightleftarrows H_2CO_3(app)$) and Figure 9 ($CaSO_4 \rightleftarrows Ca^{2+} + SO_4^{2-}$). Although derivation of $\Delta H_r^\circ(T_r)$ from linear interpretation of R ln $K(1/T)$ plots is still widely practiced, there is little defense for continuing this procedure. A more accurate value of $\Delta H_r^\circ(T_r)$ can be obtained from a least-squares computer routine employing one or the other of the two assumptions discussed below.

B. Assuming $\Delta C_{P,r}^\circ(T)$ *Constant.* This assumption enables accurate calculation of log $K(T)$ for most complexes at low temperatures, but as Cobble[54] recently pointed out, assuming the 25° value for $\Delta C_{P,r}^\circ$ as the constant often leads to serious errors in computed values of log $K(T)$ at higher temperatures. It can be seen in Figures 4 and 5 that $\Delta C_{P,r}^\circ(T_r)$ is not often equivalent to an average value for $\Delta C_{P,r}^\circ(T)$ to 200°. However, because log $K(T)$ is relatively insensitive to small errors in $\Delta C_{P,r}^\circ(T)$ and extrema occur in the $\Delta C_{P,r}^\circ(T)$ curves, assuming $\Delta C_{P,r}^\circ/(T)$ constant but

employing a less negative value than that at 25° will often yield close approximations to log $K(T)$ to about 250°. For most of the $\Delta C_{P,r}^\circ(T)$ curves in Figures 4 and 5, integration of the area above the curves up to ~200° yields values that are not greatly different from those obtained by assuming a constant $\Delta C_{P,r}^\circ(T)$ equal to an average value. A comparative log $K(T)$ curve calculated from such an average $\Delta C_{P,r}^\circ$ value is plotted in Figure 1 ($H_2O \rightleftarrows H^+ + OH^-$) to illustrate the error caused by this assumption at higher temperatures. Although an average $\Delta C_{P,r}^\circ$ value obtained by fitting a few low-temperature log $K(T)$ points assuming $\Delta C_{P,r}^\circ(T)$ constant has a high uncertainty, the value of $\Delta H_r^\circ(T_r)$ resulting from the fit is usually a close approximation to the true value.

C. Assuming $\Delta C_{P,r}^\circ(T)$ Proportional to $\Delta C_{P,c}^\circ(T)$. As might be expected from the relative success of Gurney's[67] equation for proton transfer reactions at low temperatures, many dissociation constants can be closely approximated by assuming $\Delta C_{P,r}^\circ(T)/\Delta C_{P,c}^\circ(T)$ constant. This assumption leads to the following expression for the dissociation constant as a function of temperature

$$\log K(T) = \frac{\Delta S_r^\circ(T_r)}{2.303RT}\left[T_r - \frac{\theta}{\omega}\{1 - \exp[\exp(b + aT) - c + (T - T_r)/\theta]\}\right] - \frac{\Delta H_r^\circ(T_r)}{2.303RT} \quad (21)$$

Log $K(T)$ curves calculated from eq 21 and the $\Delta S_r^\circ(T_r)$ and $\Delta H_r^\circ(T_r)$ values shown in Table II are plotted in Figure 1 ($H_2O \rightleftarrows H^+ + OH^-$), Figure 2 ($CO_2(g) + H_2O \rightleftarrows H_2CO_3(app)$), and Figure 8 to afford comparison with the other calculated curves and the experimental values taken from the literature (Table I). It can be seen in these figures that the log $K(T)$ curves calculated from eq 21 are in close agreement with the experimental dissociation constants for most of the reactions up to 150–250°. As expected, for certain reactions eq 21 is a poor approximation (*e.g.*, $CO_2(g) + H_2O \rightleftarrows H_2CO_3(app)$, Figure 2). In every case, for temperatures greater than 250°, the approximation represented by eq 21 breaks down.

Comparison of the size and sign of $\Delta H_r^\circ(T_r)$ and $\Delta S_r^\circ(T_r)$ for the reactions listed in Table I with the per cent difference in log $K(T)$ calculated from eq 18 and 21 provides a basis for assessing the relative applicability of eq 21 as a general method of approximation for calculating dissociation constants at elevated temperatures. At 200° the error introduced by the assumption that $\Delta C_{P,r}^\circ(T)/\Delta C_{P,c}^\circ(T)$ is constant is 1% for the dissociation of H_2O and HSO_4^-, 1–3% for HCOOH, NH_4OH, H_2CO_3, and HCO_3^-, 3–5% for H_3PO_4 and CH_3COOH, and 9% for C_2H_5COOH. At 300°, the error becomes 2–5% for H_3PO_4, H_2CO_3, and H_2O, 5–10% for HSO_4^-, HCOOH, and HCO_3^-, 13–14% for C_2H_5COOH and NH_4OH, and 22% for CH_3COOH. Although the percentages cited above also reflect uncertainties in the data used in calculating log $K(T)$ from eq 18 and 21, there can be little doubt that eq 21 renders close approximations to log $K(T)$ for many dissociational reactions to >200°. Two generalizations regarding the applicability of eq 21 appear to be justified.

(1) When the heat capacity of dissociation and (or) $\Delta H_r^\circ(T_r)$ and $\Delta S_r^\circ(T_r)$ are positive, the nonelectro-

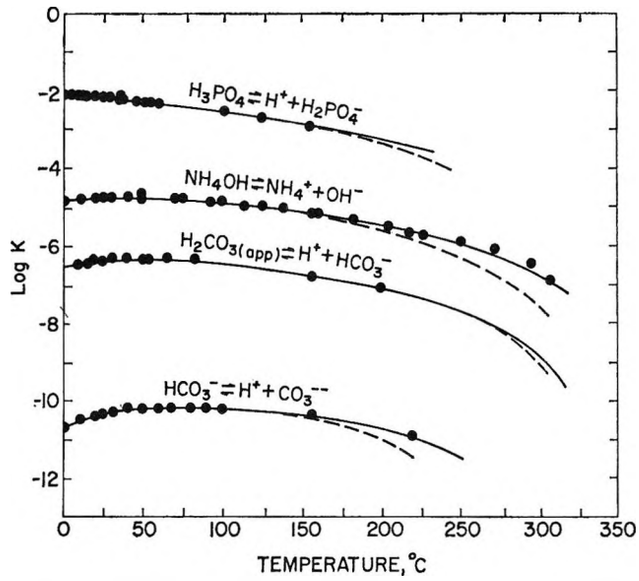

Figure 8. Dissociation constants calculated from eq 21 and the $\Delta S_r^\circ(T_r)$ and $\Delta H_r^\circ(T_r)$ values shown in Table II (——) compared with experimental dissociation constants (represented by the symbols) taken from the literature (Table I). The high-temperature extensions of the curves shown as solid lines are the same as those plotted for the respective reactions in Figure 2.

(67) In considering the thermodynamic behavior of proton transfer reactions at low temperatures. Gurney[15,16] and Hammett[13,14] regarded the free energy of dissociation as the sum of electrostatic and nonelectrostatic contributions, but the nonenvironmental (nonelectrostatic) portion was considered to be independent of temperature. Although this assumption renders results consistent with experimental data for a number of reactions at low temperatures, it is not justified for most dissociations in water at high temperatures. It precludes any nonelectrostatic contribution to the entropy of dissociation and fails to allow for independent changes in the influence of nonelectrostatic interaction on complex stability as the dielectric constant of water decreases with increasing temperature. In the Gurney–Hammett model, $\Delta F_r^\circ(T)$ for proton transfer reactions is considered to be a linear function of $1/\epsilon(T)$ in which $\Delta H_r^\circ(T_r)$ [in the intercept constant for the equation] is entirely nonelectrostatic. In terms of log $K(T)$, the assumption that $\Delta C_{P,r}^\circ(T)$ is proportional to $\Delta C_{P,c}^\circ(T)$ results in an expression [eq 21] that is equivalent to Gurney's log $K(T)$ equation [except for the revised expression for $\epsilon(T)$] for proton transfer reactions where $\Delta C_{P,r}^\circ \neq 0$.

static contribution to $\Delta C_{P,r}^\circ(T)$ is substantial and an approximation to log $K(T)$ using eq 21 is not warranted.

(2) Where the enthalpy and entropy of dissociation at 25° are both negative, close approximations of log $K(T)$ to about 200° can be made assuming $\Delta C_{P,r}^\circ(T)/\Delta C_{P,e}^\circ(T)$ constant. This is also true for certain reactions for which $\Delta H_r^\circ(T_r)$ is a large positive number and $\Delta S_r^\circ(T_r)$ is negative (*e.g.*, $H_2O \rightleftarrows H^+ + OH^-$, Figure 1). However, in such cases the effectiveness of the approximation is due primarily to the fact that log $K(T)$ is dominated by the $\Delta H_r^\circ(T_r)$ term in the log $K(T)$ expression based on this assumption [eq 21]. This term also appears in eq 18.

Of the several methods of approximation that have been advanced for calculating log $K(T)$ where little or no heat capacity data are available, assuming $\Delta C_{P,r}^\circ(T)/\Delta C_{P,e}^\circ(T)$ constant is perhaps the most practical and accurate.[68] It requires only that $\Delta H_r^\circ(T_r)$ and $\Delta S_r^\circ(T_r)$ be known[69-72] and it provides more accurate predictions of log $K(T)$ than those based on assuming $\Delta C_{P,r}^\circ(T)$ to be zero or constant. Equation 21 is consistent with the assumption that

$$\Delta C_{P,r}^\circ(T) = \frac{T\Delta S_r^\circ(T_r)\exp[\exp(b + aT) - c + (T - T_r)/\theta]}{\omega\theta} \times \{[1 + \phi\exp(b + aT)]^2 + \phi^2\exp(b + aT)\} \quad (22)$$

which causes $d\Delta C_{P,r}^\circ(T)/dT$ to take the sign of $\Delta S_r^\circ(T_r)$. Because this is usually negative and because the approximation of $\Delta C_{P,r}^\circ(T)$ in eq 22 is exponential, the area above the $\Delta C_{P,r}^\circ(T)$ curve defined by this expression tends to approximate more closely the integral of the actual $\Delta C_{P,r}^\circ(T)$ curve than either the integral of $\Delta C_{P,e}^\circ(T)$ or that calculated from the assumption that $\Delta C_{P,r}^\circ(T) \approx \Delta C_{P,r}^\circ(T_r)$. This can be seen in Figure 5 where $\Delta C_{P,e}^\circ(T)$, $\Delta C_{P,r}^\circ(T)$, and a curve based on the assumption that $\Delta C_{P,r}^\circ(T)/\Delta C_{P,e}^\circ(T)$ is constant have been plotted for $H_2CO_3(app) \rightleftarrows H^+ + HCO_3^-$ to illustrate the differences in the curves and the behavior of $\Delta C_{P,r}^\circ(T)$ resulting from the various assumptions.

Thermodynamic data for various hydroxide, chloride, and sulfate complexes involving alkaline earth and transition metal ions are presented in Table IV and Figure 9. Table IV affords a comparison of the $\Delta H_r^\circ(T_r)$ and $\Delta S_r^\circ(T_r)$ values taken from the literature with those obtained from least-squares fits of low-temperature dissociation constants for these species, assuming alternately in each case that $\Delta C_{P,r}^\circ(T)$ or $\Delta C_{P,r}^\circ(T)/\Delta C_{P,e}^\circ(T)$ is constant. The literature values were calculated (by the respective authors) from $R \ln K$ *vs.* $1/T$ plots assuming $\Delta C_{P,r}^\circ(T) = 0$. The log $K(T)$ curves computed on the basis of the alternate

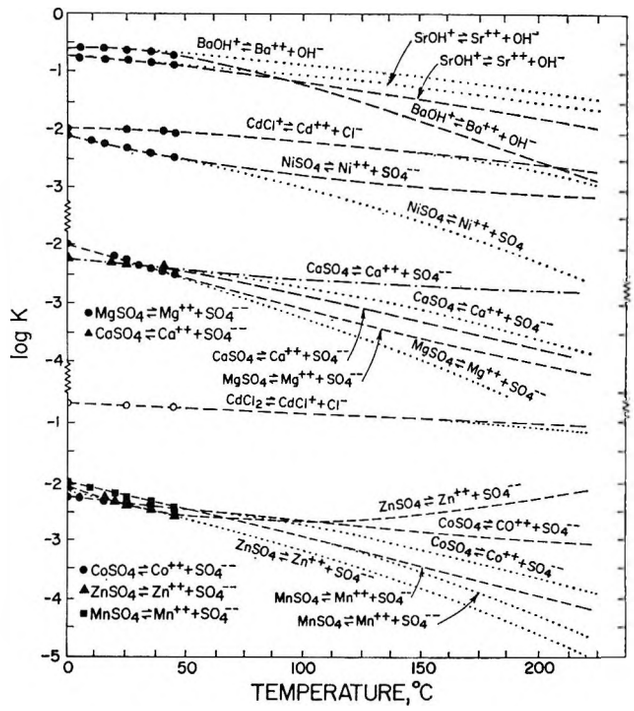

Figure 9. Least-squares fits of experimental low-temperature dissociation constants taken from the literature (represented by the symbols) alternately calculated assuming $\Delta C_{P,r}^\circ(T)/\Delta C_{P,e}^\circ(T)$ constant (· · · · · ·), $\Delta C_{P,r}^\circ(T)$ constant (– – – –), or $\Delta C_{P,r}^\circ(T)$ zero (–·–·–·). The high-temperature extensions of the curves were calculated from the $\Delta H_r^\circ(T_r)$, $\Delta S_r^\circ(T_r)$ and, in the case of the dashed curves, $\Delta C_{P,r}^\circ$ values defined by the low-temperature fits (Table IV). The sources of the experimental log $K(T)$ values plotted above are indicated in Table IV.

assumptions indicated above are plotted in Figure 9 along with the data from which they were derived; the sources of data used in the calculations are indicated in Table IV. It can be seen in Table IV that the $\Delta H_r^\circ(T_r)$ and $\Delta S_r^\circ(T_r)$ values obtained from the alternate interpretations of the low-temperature log $K(T)$ values are not greatly different in most cases. However, either of the two approaches adopted here affords a more accurate analysis of the data than that

(68) Provided that heat capacities or average heat capacities for the complexes involved in dissociational reactions can be estimated with confidence or calculated from equations such as those presented by Criss and Cobble,[48,49] log $K(T)$ can also be calculated up to 200° using the correspondence principle to predict average ionic heat capacities.[54] The principal advantage of the method of approximation advocated above is that no heat capacity data are needed and the thermodynamic quantities involved are for the reactions rather than for the participating species.

(69) If there is no alternative, $\Delta S_r^\circ(T_r)$ can often be estimated with a fair degree of accuracy.[3,70-72]

(70) J. W. Cobble, *J. Chem. Phys.*, **21**, 1443 (1953).

(71) J. W. Cobble, *ibid.*, **21**, 1446 (1953).

(72) J. W. Cobble, *ibid.*, **21**, 1451 (1953).

Table IV: Comparative Summary of Alternate Thermodynamic Data for the Dissociation of Various Complexes in Aqueous Solution at 25° and 1 Atm

Dissociational Reaction	Thermodynamic data based on interpretation of low temperature R ln K(1/T) plots assuming $\Delta C^\circ_{P,r}(T) = 0$.			Thermodynamic data computed from least squares analyses of log K(T) values (Figure 9) taken from the references cited in column 2.				
				Assuming $\Delta C^\circ_{P,r}(T)$ constant			Assuming $\Delta C^\circ_{P,r}(T)/\Delta C^\circ_{P,e}(T)$ constant	
	log $K(T_r)$	$\Delta H^\circ_r(T_r)$ (cal. mole^{-1})	$\Delta S^\circ_r(T_r)$ (cal. mole^{-1} deg.$^{-1}$)	$\Delta H^\circ_r(T_r)$ (cal. mole^{-1})	$\Delta S^\circ_r(T_r)$ (cal. mole^{-1} deg.$^{-1}$)	$\Delta C^\circ_{P,r}(T_r)$[i] (cal. mole^{-1} deg.$^{-1}$)	$\Delta H^\circ_r(T_r)$ (cal. mole^{-1})	$\Delta S^\circ_r(T_r)$ (cal. mole^{-1} deg.$^{-1}$)
$SrOH^+ \rightleftarrows Sr^{++} + OH^-$	-0.82[a]	-1,150[a]	- 7.6[a]	-1,160	- 7.6	-31	-1,140	- 7.6
$BaOH^+ \rightleftarrows Ba^{++} + OH^-$	-0.64[b]	-1,750[b]	- 8.8[b]	-1,230	- 7.1	-74	-1,170	- 6.9
$CdCl_2 \rightleftarrows CdCl^+ + Cl^-$	-0.70[c]	- 600[c]	- 5.2[c]	- 560	- 5.1	- 9	- 550	- 5.0
$CdCl^+ \rightleftarrows Cd^{++} + Cl^-$	-2.00[c,d]	- 600[c]	-11.2[c]	- 680	-11.4	-19	- 660	-11.4
$CaSO_4 \rightleftarrows Ca^{++} + SO_4^{--}$	-2.31[c,f]	-1,650[e,g]	-16.1[e,g]	-1,940	-17.1	-46	-1,760	-16.5
$NiSO_4 \rightleftarrows Ni^{++} + SO_4^{--}$	-2.32[f,g]	-3,310[g]	-21.7[g]	-3,190	-21.3	6	-3,290	-21.6
$CoSO_4 \rightleftarrows Co^{++} + SO_4^{--}$	-2.36[f,g]	-1,740[g]	-16.6[g]	-1,800	-16.8	- 9	-1,840	-16.9
$MnSO_4 \rightleftarrows Mn^{++} + SO_4^{--}$	-2.26[g]	-3,370[g]	-22.6[g]	-3,620	-22.4	-26	-3,700	-22.7
$MgSO_4 \rightleftarrows Mg^{++} + SO_4^{--}$	-2.25[f,h,17]	-4,840[h,17]	-26.5[h,17]	-4,870	-26.7	-19	-4,920	-26.8
$ZnSO_4 \rightleftarrows Zn^{++} + SO_4^{--}$	-2.38[f,h,17]	-4,010[h,17]	-24.4[h,17]	-3,800	-23.7	56	-4,090	-24.5

(a) F. G. R. Gimblett and C. B. Monk, Trans. Farad. Soc., 50, 965 (1954) after H. S. Harned and T. R. Paxton, J. Phys. Chem., 57, 531 (1953). (b) F. G. R. Gimblett and C. B. Monk[a] after H. S. Harned and C. G. Geary, J. Am. Chem. Soc., 59, 2032 (1937). (c) C. E. Vanderzee and H. J. Dawson, Jr., J. Am. Chem. Soc., 75, 5659 (1953). (d) H. S. Harned and M. E. Fitzgerald, ibid., 58, 2924 (1936). (e) R. P. Bell and J. H. B. George, Trans. Farad. Soc., 49, 619 (1953). (f) R. W. Money and C. W. Davies, ibid., 28, 609 (1932). (g) V. S. K. Nair and G. H. Nancollas, J. Chem. Soc. (London), 3934 (1959). (h) V. S. K. Nair and G. H. Nancollas, ibid., 3706 (1958). (i) The values shown in this column have large uncertainties owing to their derivation from least squares fits of the log K(T) data.

assuming $\Delta C_{P,r}^\circ = 0$. Because in each case both $\Delta H_r^\circ(T_r)$ and $\Delta S_r^\circ(T_r)$ are negative, the calculations based on the assumption that $\Delta C_{P,r}^\circ(T)/\Delta C_{P,e}^\circ(T)$ is constant are probably the most reliable. It can be seen in Figure 9 that most of the curves calculated on the basis of this assumption differ considerably from those based on constant values of $\Delta C_{P,r}(T)$ derived from the low-temperature log $K(T)$ data. The log $K(T)$ values predicted by eq 21 up to 200° for the reactions considered in Table IV and Figure 9 are probably close approximations to the true values.

D. Provisional Estimates. Incomplete thermodynamic data are available for a number of dissociations at elevated temperatures that cannot be evaluated completely in terms of the present analysis, yet a few interesting and perhaps significant implications emerge from provisional consideration of these data. Experimental dissociation constants for KSO_4^-, NaOH, KCl, NaCl, and HCl taken from the literature sources indicated in Table I are presented in Figure 10 along with the log $K(T)$ curves calculated from these data on the basis of the various assumptions discussed below.

Because the value of log $K_{KSO_4^-}$ at 300° is suspect,[73] there is considerable ambiguity in the character of the log $K(T)$ curve for this complex at high temperatures. If the 300° value is correct, all of the log $K(T)$ values shown in Figure 10 for this reaction can be represented by eq 18 using $\Delta S_e^\circ(T_r) = 53.902$, $\alpha = 391.583$, $\beta = -1.5907$, and $\lambda = 0.0$ in conjunction with -1000 cal mole^{-1} for $\Delta H_r^\circ(T_r)$ and -7.1 cal mole^{-1} deg^{-1} for $\Delta S_r^\circ(T_r)$. On the other hand, if the 300° value is not included in the least-squares fit of the dissociation constants, a curve consistent with $\Delta S_e^\circ(T_r) = -80.335$, $\alpha = -263.85$, $\beta = 1.1739$, $\lambda = 0.0$, $\Delta H_r^\circ(T_r) = -1250$ cal mole^{-1}, and $\Delta S_r^\circ(T_r) = -7.9$ cal mole^{-1} deg^{-1} provides a slightly better fit of the values up to 200°. However, both alternatives are in substantial agreement below that temperature (Figure 10). If the value of log $K_{KSO_4^-}$ at 300° is correct, the log $K(T)$ curve for this species has an unusual (but not necessarily unreasonable) configuration.

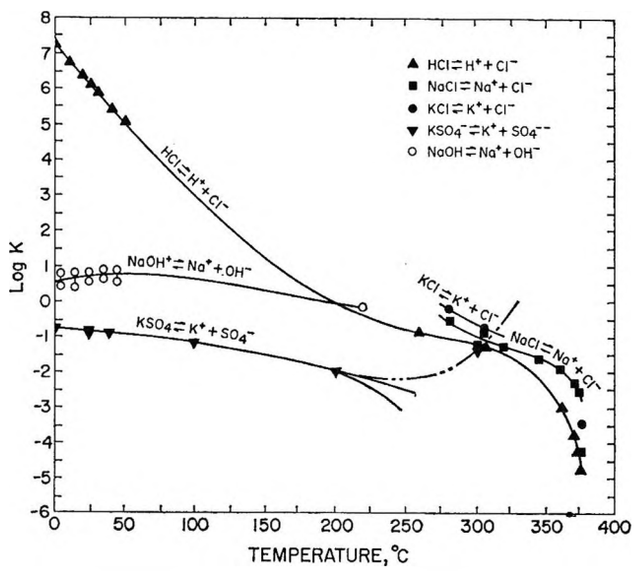

Figure 10. Provisional least-squares fits of dissociation constants for NaOH, KSO_4^-, HCl, NaCl, and KCl taken from various sources (Table I). The assumptions, equations, data obtained from the calculations, and alternate high-temperature curves for the dissociation of KSO_4^- are discussed in the text.

Experimental dissociation constants for NaOH are highly uncertain (Figure 10). Least-squares analysis of the data assuming $\Delta C_{P,r}^\circ(T)$ constant results in $\Delta S_r^\circ(T_r) = 7.6$ cal mole^{-1} deg^{-1}, $\Delta H_r^\circ(T_r) = 1300$ cal mole^{-1}, $\Delta C_{P,r}^\circ(T) = -54$ cal mole^{-1} deg^{-1}, and the curve plotted in Figure 10. The large discrepancies in the low-temperature log $K(T)$ values introduce large uncertainties into the calculation and preclude analysis of the data with the theoretical equations developed here. The positive $\Delta S_r^\circ(T_r)$ obtained from the fit of the log $K(T)$ values is highly suspect and the curve shown in Figure 10 is considered nothing more than a provisional estimate.

It can be seen in Figure 10 that in order for the high-temperature log $K(T)$ values for HCl, which are based on conductivity data, to be consistent with Robinson's[74] low-temperature values (calculated from vapor pressure data),[75,76] the log $K(T)$ curve for HCl must have two inflections. The curve shown in Figure 10 for the dissociation of HCl is based on a least-squares fit of all of these values. The fit coefficients are: $\Delta H_r^\circ(T_r) = -18{,}630$[77,78] cal mole^{-1}, $\Delta S_r^\circ(T_r) = -34.4$ cal mole^{-1} deg^{-1}, $\Delta S_e^\circ(T_r) = -15.525$, $\alpha = -685.562$, $\beta = 1.9054$, and $\lambda = 0.0$. The sigmoid character of the log $K(T)$ curve for HCl in Figure 10 arises from a substantial positive contribution of $\Delta C_{P,n}^\circ(T)$ in the intermediate to high temperature range. At low temperatures, $\Delta C_{P,n}^\circ(T)$ is negative.

(73) A. S. Quist, E. U. Franck, H. R. Jolley, and W. L. Marshall, *J. Phys. Chem.*, **67**, 2453 (1963).

(74) R. A. Robinson, *Trans. Faraday Soc.*, **32**, 743 (1936).

(75) The dissociation constants for HCl calculated by Posner[76] (log $K = 1.25$ at 0, 20, and 50°) from activity coefficients in concentrated HCl solutions were not included here because of the large uncertainty attending extrapolation of the data from which they were computed.

(76) A. M. Posner, *Nature*, **171**, 519 (1953).

(77) This value of $\Delta H_r^\circ(T_r)$ can be compared with $-17{,}900$ cal mole^{-1} calculated by Robinson[74] from an $R \ln K(1/T)$ plot assuming $\Delta C_{P,r}^\circ(T) = 0$, and $-13{,}700$ cal mole^{-1} calculated by McCoubrey[78] from thermodynamic considerations.

(78) J. C. McCoubrey, *Trans. Faraday Soc.*, **51**, 743 (1955).

The sigmoid configuration of the log $K(T)$ curve for HCl plotted in Figure 10 is reflected in the heat capacity of reaction by a maximum of ~100 cal mole^{-1} deg^{-1} in the $\Delta C_{P,r}^\circ(T)$ curve just above 200°. At low temperatures and high temperatures, $\Delta C_{P,r}^\circ(T)$ is negative. Although sigmoid log $K(T)$ curves are not common (perhaps because data are not available for a wide enough variety of dissociations), this behavior may prove characteristic of a number of complexes, especially when $\Delta H_r^\circ(T_r)$ is a large negative number.

Although data are insufficient to define reliable values of log $K(T)$ for NaCl and KCl at low temperatures, least-squares fits of available dissociation constants for these species at elevated temperatures (Figure 10) suggest that the $\Delta H_r^\circ(T_r)$ values for these complexes are large negative numbers. This of course implies inner-sphere complex formation at low temperatures. Although Duncan and Kepert[79] conclude that inner-sphere complex formation for NaCl is "energetically most unlikely," the high-temperature dissociation constants for this species do not appear to be consistent with the value of 0.78 for log K_{NaCl} at 25° proposed by Eigen and Wicke.[80] Least-squares analyses of the high-temperature data suggest a considerably more positive log $K(T_r)$ for this species as well as for KCl.

Discussion

At 25°, ΔH_r° may be positive or negative, but ΔS_r° is negative for most dissociational reactions, reflecting the major contribution of solvent interaction to complex stability. At high temperatures, dissociational equilibria are characterized by large negative heat capacities, entropies, and enthalpies of dissociation, and the first derivative of $\Delta C_{P,r}^\circ(T)$ with respect to temperature is also negative. This behavior appears to be caused by changes in the relative influence of electrostatic and nonelectrostatic interaction on complex stability as temperature increases (and the dielectric constant of the water solvent decreases). At high temperatures, where the dielectric constant of water becomes small, the electrostatic contribution dominates the change in $\Delta C_{P,r}^\circ(T)$ with temperature, causing log $K(T)$ to become increasingly negative.

Although the actual magnitude of $\Delta S_e^\circ(T)$ compared to $\Delta S_n^\circ(T)$ and $\Delta C_{P,e}^\circ(T)$ compared to $\Delta C_{P,n}^\circ(T)$ cannot be defined numerically with confidence from least-squares fits of available experimental log $K(T)$ values for all dissociations (because of uncertainties in the data), a number of provisional conclusions can be drawn about the general thermodynamic consequences of hybrid interaction. The electrostatic contribution to $\Delta C_{P,r}^\circ(T)$ is a monotonous function and the slope, which is determined by the sign of $\Delta S_e^\circ(T_r)$, is usually negative (*e.g.*, $H_2CO_3(app) \rightleftarrows H^+ + HCO_3^-$, Figure 5). On the other hand, the nonelectrostatic portion of $\Delta C_{P,r}^\circ(T)$ is usually positive (or negative only at low temperatures) and it usually becomes increasingly positive with increasing temperature. Because $d\Delta C_{P,n}^\circ(T)/dT$ is greater than $-d\Delta C_{P,e}^\circ(T)/dT$ below 100° for most dissociational reactions, the nonelectrostatic contribution to $\Delta C_{P,r}^\circ(T)$ often causes $\Delta C_{P,r}^\circ(T)$ to become less negative initially as temperature is increased above 25°. However, at higher temperatures, where the dielectric constant of water becomes small, the electrostatic contribution to complex stability becomes increasingly more significant owing to the reciprocal relation of $\Delta F_e^\circ(T)$ to $\epsilon(T)$. This causes the heat capacity of dissociation to maximize in the intermediate temperature range and take on a negative slope with further increase in temperature (Figures 3, 4, and 5). Where $d\Delta C_{P,n}^\circ(T)/dT$ is small (or negative), a maximum may not occur in the $\Delta C_{P,r}^\circ(T)$ curve, which will then have a monotonous negative slope (*e.g.*, $NH_4OH \rightleftarrows NH_4^+ + OH^-$ and $CH_3COOH \rightleftarrows H^+ + CH_3COO^-$, Figure 4). For dissociational reactions having a large negative $\Delta H_r^\circ(T_r)$ and a large positive log $K(T_r)$, the effect of $\Delta C_{P,n}^\circ(T)$ in opposing $\Delta C_{P,e}^\circ(T)$ may become significant only at high temperatures, which will cause $\Delta C_{P,r}^\circ(T)$ to maximize at a high temperature and the log $K(T)$ curve to take on a sigmoid configuration.

It has often been observed that log $K(T)$ curves for complexes that are relatively stable at low temperatures pass through maxima with increasing temperature. However, when log $K(T_r)$ is more positive than approximately -2, the curves do not generally show these maxima. As emphasized by Gurney[15,16] and Nancollas,[17,18] the occurrence of a maximum in the log $K(T)$ curve can be related to the effect of temperature on the relative influence of electrostatic and nonelectrostatic interaction on complex stability. This can be described in terms of the enthalpy and entropy contributions to log $K(T)$. A large positive value for $\Delta H_r^\circ(T_r)$ usually reflects a large nonelectrostatic contribution to complex stability, resulting in a large negative value for log $K(T_r)$. With increasing temperature, an increasingly negative $\Delta S_r^\circ(T)$, which is usually the case, favors a more negative log $K(T)$, but the negative contribution by a positive $\Delta H_r^\circ(T)$ is an inverse function of temperature which continues to dominate in the low-temperature region. This leads initially to a less negative log $K(T)$ as temperature increases. With further increase in temperature, the

(79) J. F. Duncan and D. L. Kepert, "Aquo-Ions and Ion Pairs" in "The Structure of Electrolytic Solutions," W. J. Hamer, Ed., John Wiley and Sons, Inc., New York, N. Y., 1959, p 380.

(80) M. Eigen and E. Wicke, *J. Phys. Chem.*, 58, 702 (1954).

effect of $\Delta H_r°(T)$ [as it becomes less positive with increasing temperature] diminishes and $\Delta S_r°(T)$ begins to dominate, causing log $K(T)$ to maximize (when $\Delta H_r°(T)$ becomes zero) and become more negative.

In the case where $\Delta H_r°(T_r)$ and $\Delta S_r°(T_r)$ are both negative, the log $K(T)$ curve usually has a negative slope over the entire temperature range (*e.g.*, $HSO_4^- \rightleftarrows H^+ + SO_4^{2-}$, Figure 1, and $HNO_3 \rightleftarrows H^+ + NO_3^-$ and $H_3PO_4 \rightleftarrows H^+ + H_2PO_4^-$, Figure 2). On the other hand, a large negative $\Delta H_r°(T)$ may result in a sigmoid log $K(T)$ curve owing to the role played by nonelectrostatic interaction at higher temperatures. In certain cases the contribution by $\Delta C_{P,n}°(T)$ is not significant enough to cause a change in sign in the second derivative of log $K(T)$. However, where log $K(T)$ would otherwise take the form of a monotonous function, $\Delta C_{P,n}°(T)$ may lead to an extremum in the curve (*e.g.*, $CH_3COOH \rightleftarrows H^+ + CH_3COO^-$ and $C_2H_5COOH \rightleftarrows H^+ + C_2H_5COO^-$, Figure 1, and $H_2S(g) \rightleftarrows H_2S(aq)$ and $CO_2(g) + H_2O \rightleftarrows H_2CO_3(app)$, Figure 2). As suggested above, where the opposing effects of hybrid interaction increase substantially at elevated temperatures, $\Delta C_{P,n}°(T)$ may cause the extremum in the log $K(T)$ curve to occur at high temperatures or lead to a log $K(T)$ curve having several inflections.

Acknowledgments. The author is indebted to J. W. Cobble, M. H. Waxman, J. T. Smith, D. A. Chesnut, C. L. Christ, R. M. Garrels, J. J. Hemley, and F. T. Mackenzie for their many helpful suggestions and constructive criticism during the course of this study.

Theoretical Calculation of Kinetic Isotope Effects. Effect of Reaction Coordinate Variations on the Temperature-Independent Factor, TIF

by Warren E. Buddenbaum and Peter E. Yankwich

Noyes Laboratory of Chemistry, University of Illinois, Urbana, Illinois 61801 *(Received October 26, 1966)*

A general method is developed for forcing a model activated complex of arbitrary complexity to have a *preselected* imaginary (or zero) frequency corresponding to a *preselected* vibrational motion. Techniques already available in the literature are shown to be special cases of the method. Comparisons are made between the Slater coordinate and the reaction coordinate of the transition-state theory, and an expression is developed for the mass dependence of the latter. An equation also is given for the *ab initio* calculation in terms of Slater coordinate coefficients of the high-temperature limit (TIF) of the kinetic isotope effect, ν_1/ν_1'.

Introduction

Within the framework of the transition-state theory, the relative rates of reaction of two isotopic reactants can be written as the product of two factors, one temperature dependent and one temperature independent.[1] Provided that the transmission coefficient is unaffected by isotopic substitution

$$k/k' = (\nu_L/\nu_L')(f^0/f^{\pm}) \quad (1)$$

where the f's are ratios of isotopic partition functions for the reactants and activated complexes, and the ν_L terms are the isotopic imaginary (or zero) frequencies resulting from solution of the vibrational problem for the activated complexes. The ratios f differ in that f^0 is determined using the $3N - 6$ ($3N - 5$ for a linear

(1) J. Bigeleisen and M. Wolfsberg, *Advan. Chem. Phys.*, **1**, 15 (1958).

molecule) normal vibration frequencies for the reactant molecules, while $f^{\ddagger}$ depends on the $3N - 7$ (or $3N - 6$) normal frequencies of the activated complexes for motion orthogonal to the normal vibration associated with ν_L.

The f's vary with temperature, and their ratio is often called the temperature-dependent factor (TDF); the ratio ν_L/ν_L' is invariant with temperature, is often called the temperature-independent factor (TIF), and is the high-temperature or classical limit of k/k'. The TIF has been the object of much interest in experimental and theoretical studies of kinetic isotope fractionation because of its relation to motion across the potential barrier for a reaction.[2-6]

The interpretive problem of the chemist involves the achievement of correspondence between experimental values of k/k' observed at various temperatures and similar quantities calculated for some model. The mathematical methods employed impose certain formal limitations on the properties of the successful model; but, to the extent that these restrictions are physically and chemically reasonable, the model represents an approximation to the actual reaction situation. For the purposes of this paper, we asume that the experimenter proceeds by first making intuitive guesses as to the detailed nature of the reaction coordinate (these generating TIF) and then by doing the same thing for the shape of the potential energy surface in the region of the transition state (which supplies the additional information required for calculating TDF). In a cyclic process of successive approximations, these guesses are tested, in terms of the calculated k/k' they yield, against the experimental results.

The vibrational frequencies required for the calculation of k/k' at any temperature can be found by solution of the secular equation derived from the potential energy surface for the reaction.[7] At present, however, the difficulty of such calculations has necessitated an alternate approach. In the latter,[8] the Wilson G matrix[9] is determined by assuming a structure for the activated complex of the reaction. The potential energy surface in the neighborhood of the transition state is then assumed by assigning values to the diagonal and to many of the off-diagonal elements of the **F** matrix, by analogy to stable molecules.[10] Finally, the remaining elements of **F** are adjusted so that an imaginary (or zero) frequency will result.[11-14] The normal vibration corresponding to this frequency is then identified with the reaction coordinate for the reaction.

Definite rules are available for forcing this particular coordinate to approximate bond rupture,[12] asymmetric[13] or symmetric[14] motion in a triatomic system, or, for the special case of $\nu_L = 0$, any motion of a three-particle molecule.[15] However, no general method is available for the generation of a ν_L which corresponds to a *preselected* motion of a polyatomic molecule of arbitrary complexity. The object of this paper is to develop such a general method. The development is carried out for *one* reaction model; then, the results are applied to the case of *two* models related by isotopic substitution at one position.

Development

ν_L, the Reaction Coordinate, and the Potential Function. Heretofore, all published theoretical calculations of kinetic isotope effects have assumed harmonic forces. As a result of this approximation, a useful relation exists among a normal coordinate, the vibrational frequency associated with it, and the potential function.[9,16]

Consider the solution of the vibrational problem *via* the Wilson **F**–**G** matrix technique. This approach involves solution of the secular equation

$$|\mathbf{FG} - \lambda_t\mathbf{I}| = 0 \qquad (\lambda_t = 4\pi^2\nu_t^2) \qquad (2)$$

for the $3N - 6$ normal harmonic frequencies, ν_t, of the molecule; here **I** is the identity matrix. If **F** and **G** are expressed in terms of some complete set of internal displacement coordinates (S_j, n in number), the normal coordinate $\mathbf{Q}_t$ corresponding to any ν_t can be obtained in terms of these S_j by solution of

$$(\mathbf{FG} - \lambda_t\mathbf{I})(\mathbf{L}^{-1})^{\dagger}_t = \mathbf{0} \qquad (3)$$

for the n elements of $(\mathbf{L}^{-1})^{\dagger}_t$. Here **0** is a zero column

(2) J. Bigeleisen and M. Wolfsberg, *J. Chem. Phys.*, 21, 1972 (1953).

(3) J. Bigeleisen and M. Wolfsberg, *ibid.*, 22, 1264 (1954).

(4) P. E. Yankwich and R. M. Ikeda, *J. Am. Chem. Soc.*, 81, 1532 (1959).

(5) M. Wolfsberg, *J. Chem. Phys.*, 33, 21 (1960).

(6) C. R. Gatz, *ibid.*, 44, 1861 (1966).

(7) See, for example, R. E. Weston, Jr., *ibid.*, 31, 892 (1959).

(8) A recent illustration is contained in: A. J. Kresge, N. N. Lichtin, K. N. Rao, and R. E. Weston, Jr., *J. Am. Chem. Soc.*, 87, 437 (1965).

(9) E. B. Wilson, Jr., J. C. Decius, and P. R. Cross, "Molecular Vibrations," McGraw-Hill Book Co., Inc., New York, N. Y., 1955.

(10) *E.g.*, W. Gordy, *J. Chem. Phys.*, 14, 305 (1946).

(11) H. S. Johnston, W. A. Bonner, and D. J. Wilson, *ibid.*, 26, 1002 (1957).

(12) M. Wolfsberg and M. J. Stern, *Pure Appl. Chem.*, 8, 225 (1964).

(13) M. Wolfsberg and A. V. Willi, *Chem. Ind.* (London), 2097 (1964).

(14) P. E. Yankwich and J. L. Copeland, *J. Am. Chem. Soc.*, 79, 2081 (1957).

(15) C. R. Gatz, Ph.D. Thesis, University of Illinois. Urbana, Ill., 1959.

(16) G. Herzberg, "Infrared and Raman Spectra of Polyatomic Molcules," D. Van Nostrand Co., Inc., New York, N. Y., 1945, p 201.

matrix, and $(\mathbf{L}^{-1})^{\dagger}_{i}$ is the ith column of the transpose of $\mathbf{L}^{-1}$, such that for $\mathbf{S}$ written as a column

$$\mathbf{Q} = \mathbf{L}^{-1}\mathbf{S} \tag{4}$$

The reaction coordinate of the transition state formalism is a normal mode of the activated complex. For some arbitrary vibration of this complex

$$\mathbf{X}_1 = \mathbf{R}_1\mathbf{S} \tag{5}$$

to be a normal mode with *preselected* frequency ν_1, it is necessary that $\mathbf{F}$ satisfy the relation

$$\mathbf{FG}(\mathbf{R}_1)^{\dagger} = \lambda_1(\mathbf{R}_1)^{\dagger} \tag{6}$$

Consider the solution of eq 6 for the elements of $\mathbf{F}$. In general, these are not determined uniquely by eq 6. Let r be the number of nonzero elements of $\mathbf{G}(\mathbf{R}_1)^{\dagger}$. Since $\mathbf{G}(\mathbf{R}_1)^{\dagger} = \mathbf{0}$ implies no molecular motion,[17] r will always be >0, and the number of F_{ij}'s appearing in eq 6, s, is given by

$$s = r(2n - r + 1)/2 \tag{7}$$

and will usually be $>n$. Therefore, the s constrained F_{ij}'s are not determined uniquely by eq 6, but n of them will depend in some manner on the remaining $(s - n)$.[18] The characteristics of this dependence will now be developed.

Rules for the Construction of $\mathbf{F}$. Equation 6 can be written

$$\mathbf{HT} = \lambda_1(\mathbf{R}_1)^{\dagger} \tag{8}$$

where $\mathbf{T}$ is a column vector of the constrained F_{ij}'s arranged in some order and $\mathbf{H}$ is a $n \times s$ matrix of the coefficients of these force constants as determined by eq 6. One must now pick $(s - n)$ of these constrained force constants to be the necessary parameters in terms of which the remaining n are to be expressed.[19] Let $\mathbf{F}_p$ be a column vector of the selected parametric F_{ij}'s arranged in some order. Equation 8 then becomes

$$\mathbf{EJ} = \lambda_1(\mathbf{R}_1)^{\dagger} - \mathbf{DF}_p \tag{9}$$

where $\mathbf{J}$ is a column vector of the n remaining F_{ij}'s, and $\mathbf{E}$ and $\mathbf{D}$ are $n \times n$ and $n \times (s - n)$ matrices, respectively, formed from the columns of $\mathbf{H}$. Then, if $\mathbf{E}^{-1}$ exists

$$\mathbf{J} = \mathbf{E}^{-1}[\lambda_1(\mathbf{R}_1)^{\dagger} - \mathbf{DF}_p] \tag{10}$$

This solution of eq 9 depends on the assumption that the force constants chosen for $\mathbf{F}_p$ are independent; if this is not true, $\mathbf{E}^{-1}$ will not exist. Two alternatives are possible: one can continue making choices for $\mathbf{F}_p$ until an independent set is found, guaranteeing the existence of $\mathbf{E}^{-1}$, or one can continue with the original choice of $\mathbf{F}_p$ as follows. If $\mathbf{E}^{-1}$ does not exist, $\mathbf{E}$ will be a singular matrix of rank $t < n$[20] and there will exist an $n \times n$ nonsingular matrix $\mathbf{K}$ such that

$$\mathbf{K}_1\mathbf{E} = \mathbf{P}; \quad \mathbf{K}_2\mathbf{E} = \mathbf{0} \tag{11}$$

where $\mathbf{K}_1$ is the first t and $\mathbf{K}_2$ the last $(n - t)$ rows of $\mathbf{K}$, with $\mathbf{P}$ a $t \times n$ matrix. Therefore

$$\mathbf{PJ} = \mathbf{K}_1[\lambda_1(\mathbf{R}_1)^{\dagger} - \mathbf{DF}_p] \tag{12}$$

and

$$\mathbf{K}_2[\lambda_1(\mathbf{R}_1)^{\dagger} - \mathbf{DF}_p] = \mathbf{0} \tag{13}$$

Thus, for eq 9 to have a solution for a given $\mathbf{F}_p$, the elements of $\mathbf{F}_p$ must first satisfy eq 13; then, one need only solve eq 12 for $\mathbf{J}$. Since it will be possible to construct an $n \times n$ nonsingular matrix $\mathbf{V}$ such that

$$\mathbf{PV}_1 = \mathbf{M}; \quad \mathbf{PV}_2 = \mathbf{0} \tag{14}$$

where $\mathbf{V}_1$ is the first t and $\mathbf{V}_2$ the last $(n - t)$ columns of $\mathbf{V}$, with $\mathbf{M}$ a $t \times t$ nonsingular matrix, eq 12 can then be written

$$\mathbf{PJ} = \mathbf{PVV}^{-1}\mathbf{J} = (\mathbf{M0})\mathbf{Y} \tag{15}$$

or

$$\mathbf{MY}_1 = \mathbf{K}_1[\lambda_1(\mathbf{R}_1)^{\dagger} - \mathbf{DF}_p] \tag{16}$$

where $\mathbf{Y}_1$ is the first t elements of $\mathbf{Y}$, and $\mathbf{Y}_2$, the last $(n - t)$ elements of $\mathbf{Y}$, can have any value which, along with some of the $\mathbf{F}_p$, make up the $(s - n)$ parameters of the solution. Thus, the final form of the parametric solution of eq 9 is

$$\mathbf{J} = \mathbf{VY} = \mathbf{V}_1\mathbf{Y}_1 + \mathbf{V}_2\mathbf{Y}_2 \tag{17}$$

or

$$\mathbf{J} = \mathbf{V}_1\mathbf{M}^{-1}\mathbf{K}_1[\lambda_1(\mathbf{R}_1)^{\dagger} - \mathbf{DF}_p] + \mathbf{V}_2\mathbf{Y}_2 \tag{18}$$

with the condition that the $\mathbf{F}_p$ satisfy eq 13.

A Brute-Force Computer Approach. A computer program has been written to solve eq 18 where $\mathbf{F}_p$ contains only the r diagonal force constants. Clearly, if not all of these F_{ii} are independent, there will exist a $\mathbf{K}_2$ (see eq 11) such that

$$\mathbf{K}_2[\lambda_1(\mathbf{R}_1)^{\dagger} - \mathbf{DF}_p] = \mathbf{0} \tag{19}$$

(17) Except for the trivial case of $\mathbf{R}_1 = \mathbf{0}$, $\mathbf{G}(\mathbf{R}_1)^{\dagger} = \mathbf{0}$ implies $\mathbf{R}_1\mathbf{S} = \mathbf{0}$ (ref 9, p 142). This means that $\mathbf{R}_1$ is a redundancy condition for the internal coordinates and not a molecular vibration. Clearly, $\mathbf{R}_1$ should satisfy any redundancy conditions that do exist.

(18) The one exception is for $r = 1$; then $s = n$ and the s force constants involved are determined uniquely by eq 6.

(19) As will be seen below, this choice is not completely arbitrary, but one possible set might be those diagonal and off-diagonal force constants to be assigned values by analogy to stable molecules, plus those interaction constants between widely separated bonds which are usually set equal to zero in most vibrational analyses.

(20) S. Naragan, "A Text Book of Matrices," 4th ed, S. Chand and Co., New Delhi, India, 1962, p 128.

Solution of this set of simultaneous equations will yield the interdependence of the F_{tt}'s independent of the interaction force constants. While determining $\mathbf{V}_2$ and the matrix $[\mathbf{V}_1\mathbf{M}^{-1}\mathbf{K}_1]$, each column of $\mathbf{E}$ is examined in turn, starting at the left, to see if it is linearly dependent on the columns already examined. If a column is linearly dependent, the force constant associated with it becomes one of the $(s - n)$ parameters (*i.e.*, an element of $\mathbf{Y}_2$). This approach tends to make parameters of the lower elements of $\mathbf{J}$; therefore, the force constants are ordered arbitrarily so that the $(r^2 - r)/2$ interaction constants between the r constrained bonds comprise the first elements of $\mathbf{J}$. In this way each of these force constants tends to depend first on the F_{tt}'s of the constrained bonds and then on the interaction force constants between the constrained and unconstrained bonds.

Properties of $\mathbf{F}$. Once $\mathbf{F}$ satisfies eq 6, there will exist an eigenvector of $\mathbf{F}$ which is closedly related to $\mathbf{R}_1$; let this column vector be $(\mathbf{A}_1)^\dagger$. Then, by definition

$$\mathbf{F}(\mathbf{A}_1)^\dagger = (F^0)_{11}(\mathbf{A}_1)^\dagger \tag{20}$$

where $(F^0)_{11}$ is determined from the potential energy surface at the activated complex *via*

$$(F^0)_{11} = \mathbf{A}_1\mathbf{F}(\mathbf{A}_1)^\dagger \tag{21}$$

Since

$$\mathbf{A}_1\mathbf{F}\mathbf{G}(\mathbf{R}_1)^\dagger = (F^0)_{11}\mathbf{A}_1\mathbf{G}(\mathbf{R}_1)^\dagger \tag{22}$$

implies that

$$\lambda_1 = (F^0)_{11}\frac{\mathbf{A}_1\mathbf{G}(\mathbf{R}_1)^\dagger}{\mathbf{A}_1(\mathbf{R}_1)^\dagger} \tag{23}$$

$(F^0)_{11}$ can be regarded as the force constant for the motion $\mathbf{Q}_1$, which for ν_1 imaginary (or zero), we identify as the reaction coordinate. Although $(F^0)_{11}$ and $\mathbf{A}_1$, like $\mathbf{F}$, are independent of isotopic substitution, to the accuracy of the Born–Oppenheimer approximation, they differ in their dependence on the values of the F_{tj}'s, $\mathbf{A}_1$ being independent of the F_{tj}'s and uniquely determined by the choices of ν_1 and $\mathbf{R}_1$ used in the construction of $\mathbf{F}$. Furthermore, $\mathbf{A}_1$ can be identified with the *Slater coordinate*[21-23] which was developed for the case of simple bond rupture in investigation of a classical theory of unimolecular reaction rates at high pressure. Application of this coordinate to three- and four-center reactions has been made by Bigeleisen and Wolfsberg[2,3] and by Yankwich and Ikeda[4] as a technique for calculation of the mass dependence of ν_L, a matter to be examined in detail below.

Because of this previous use, one would like to be able to determine $\mathbf{A}_1$ without resorting to the construction of $\mathbf{F}$; this can be done for the situation where one employs the approximation $\nu_1 = 0$.

A Special Case, $\nu_1 = 0$. When ν_1 is made zero, $\mathbf{F}(\mathbf{A}_1)^\dagger$ and $\mathbf{F}\mathbf{G}(\mathbf{R}_1)^\dagger$ are zero also. Thus

$$\mathbf{G}(\mathbf{R}_1)^\dagger = c(\mathbf{A}_1)^\dagger \tag{24}$$

where c is a constant, and the reaction coordinate will be[24]

$$\mathbf{R}_1 = c\mathbf{A}_1\mathbf{G}^{-1} \tag{25}$$

In Table I are listed several potential functions which have been employed[11-14] to generate a zero frequency in the activated complex; the descriptions are in terms of eq 20 and 25, and the corresponding eigenvectors $\mathbf{A}$ are shown.[25]

Analysis of an approach used by Gatz[15] for the construction of a potential function which forces a zero frequency has not been made in Table I. This method makes use of Slater coordinates and was the first attempt to employ such coordinates in construction of the potential function for an activated complex. It should

Table I: Eigenvectors of Potential Functions Used for Generation of Zero Frequencies

Approximate molecular motion[a]	Conditions on the potential function[b]	Eigenvector[c]
Bond breaking (or formation)[12]	$F_{ii} = 0$	$A_{ii} = 1$
Asymmetric motion, three centers[13]	$F_{12} = \sqrt{F_{11}F_{22}}$	$A_{11} = 1;\ A_{12} = -\sqrt{F_{11}/F_{22}}$
Symmetric motion, three centers[14]	$F_{12} = -\sqrt{F_{11}F_{22}}$	$A_{11} = 1;\ A_{12} = \sqrt{F_{11}/F_{22}}$

[a] The normal coordinate corresponding to the zero frequency depends on the individual molecules and is given by eq 25. [b] All other interaction constants between these and the remaining internal coordinates are assumed equal to zero. [c] Only nonzero elements of $\mathbf{A}_1$ are listed.

(21) N. B. Slater, *Proc. Roy. Soc.* (London), **A194**, 112 (1948).

(22) N. B. Slater, *Proc. Leeds Phil. Lit. Soc., Sci. Sect.*, **5**, 75 (1949).

(23) N. B. Slater, *J. Chem. Phys.*, **35**, 445 (1961).

(24) When redundancy conditions exist among the internal coordinates, $\mathbf{G}^{-1}$ cannot be obtained by the usual methods of matrix inversion. However, the matrix $\mathbf{G}^{-1}$, such that

$$\mathbf{G}^{-1}\mathbf{G} = \begin{pmatrix} \mathbf{I} & 0 \\ 0 & 0 \end{pmatrix}$$

where $\mathbf{I}$ is an identity matrix $(3N - 6)$ in size, can always be found in terms of the eigenvector matrix, $\mathbf{D}$, and the diagonal eigenvalue matrix, Γ, or $\mathbf{G}$: $\mathbf{G}^{-1} = \mathbf{D}\Gamma^{-1}\mathbf{D}^\dagger$.

(25) When $\nu_1 = 0$, $(\mathbf{A}_1)^\dagger$ is an eigenvector both of $\mathbf{F}$ and of the matrix $\mathbf{GF}$, since $\mathbf{G}(\mathbf{L}^{-1})\dagger_i = \mathbf{L}_i$ (eq 3 and 4).

be considered to be a special case of the general problem since it was solved only for a zero frequency in a triatomic molecule.

A Special Case: The Triatomic Molecule. First, one selects a Slater coordinate, $\mathbf{Z}_1$, some linear combination of the internal coordinates[15]

$$\mathbf{Z}_1 = B_{11}S_1 + B_{12}S_2 + B_{13}S_3 \tag{26}$$

and then constructs[26] an orthonormal matrix $\mathbf{B}$ which has $\mathbf{B}_1$ as its first row. An orthonormal transformation is made to the coordinates $\mathbf{Z} = \mathbf{BS}$, and the first row and the first column of the potential energy matrix in this new coordinate system, $\mathbf{F}^0 = \mathbf{BFB}^\dagger$, are set equal to zero. This ensures that a zero frequency will be obtained and provides, once the diagonal force constants are assigned values by analogy to stable structures, a set of three equations for the three unknown interaction constants in terms of the elements of $\mathbf{B}$ and of the diagonal elements of $\mathbf{F}$.

This method for obtaining the interaction constants is equivalent to solving the matrix equation

$$(\mathbf{F}^0)_1 = \mathbf{BF}(\mathbf{B}_1)^\dagger = \mathbf{0} \tag{27}$$

where $(\mathbf{F}^0)_1$ is the first column of $\mathbf{F}^0$ and $\mathbf{0}$ is a zero-column matrix; thus the method is a special case of eq 20 $(F^0)_{11} = 0$ (i.e., $\mathbf{B}_1 = \mathbf{A}_1$). It is clear that $\mathbf{A}_1$ can be identified with the Slater coordinate for all values of ν_1. Indeed, the construction of an $\mathbf{F}$ *via* $\mathbf{A}_1$ (eq 20) rather than *via* $\mathbf{R}_1$ (eq 6) has the principal advantage that the results obtained for each choice of $\mathbf{A}_1$ are transferable from one molecule to another, since no molecular parameters are employed in the construction of eq 8. However, except in two special cases, there is the disadvantage that identification of the reaction coordinate (the normal mode $\mathbf{Q}_1$ of the activated complex) in terms of $\mathbf{A}_1$ becomes difficult. The special case for $\nu_1 = 0$ has been examined above; another arises when $(\mathbf{R}_1)^\dagger$ is an eigenvector of the $\mathbf{G}$ matrix for the molecule in question.

Conditions for Equivalence of a Slater Coordinate and $\mathbf{Q}_1$. When $\mathbf{R}_1$ is an eigenvector of $\mathbf{G}$, eq 6 becomes

$$\mathbf{F}(\mathbf{R}_1)^\dagger = \frac{\lambda_1(\mathbf{R}_1)^\dagger}{(G^*)_{11}} \tag{28}$$

where

$$(G^*)_{11} = \mathbf{R}_1\mathbf{G}(\mathbf{R}_1)^\dagger \tag{29}$$

is the eigenvalue corresponding to $(\mathbf{R}_1)^\dagger$.

It follows from eq 8 and 28 that $(\mathbf{R}_1)^\dagger$ will then also be made the eigenvector of $\mathbf{F}$, $(\mathbf{A}_1)^\dagger$. Thus, this special case contains the necessary condition for the equivalence of a Slater coordinate and the normal mode reaction coordinate $\mathbf{Q}_1$. Because of this "uniqueness of the reaction coordinate of transition state theory,"[23] it is not surprising that a frequency ν_1 calculated by Slater theory[6] may differ from that obtained from an exact calculation.

General Expression Relating ν_1, $\mathbf{R}_1$, *and* $\mathbf{A}_1$. If one knows the Slater coordinate, $\mathbf{A}_1$, a general expression for ν_1 and $\mathbf{R}_1$ in terms of $\mathbf{A}_1$, can be obtained from consideration of the matrix

$$\mathbf{F}_0 = [\mathbf{F} - (F^0)_{11}\mathbf{I}] \tag{30}$$

of which $(\mathbf{A}_1)^\dagger$ is an eigenvector. Since the rank of $\mathbf{F}_0$ is $(n - 1)$,[20] the matrix equation

$$\mathbf{F}_0\mathbf{X} = [\lambda_1(\mathbf{R}_1)^\dagger - (F^0)_{11}\mathbf{G}(\mathbf{R}_1)^\dagger] \tag{31}$$

can be solved for the column vector $\mathbf{X}$ in a manner similar to that employed for solution of eq 6; *i.e.*, the solution can be put into the form of eq 17

$$\mathbf{X} = \mathbf{V}_1Y_1 + \mathbf{V}_2Y_2 \tag{32}$$

Then, since $\mathbf{X}$ is $\mathbf{G}(\mathbf{R}_1)^\dagger$

$$\mathbf{G}(\mathbf{R}_1)^\dagger = (\mathbf{A}_2)^\dagger(\mathbf{F}_z)^{-1}\mathbf{A}_2[\lambda_1(\mathbf{R}_1)^\dagger - (F^0)_{11}\mathbf{G}(\mathbf{R}_1)^\dagger] + \alpha(\mathbf{A}_1)^\dagger \tag{33}$$

where $\mathbf{A}_1$ is the last row and $\mathbf{A}_2$ the first $(n - 1)$ rows of an orthogonal matrix $\mathbf{A}$, and

$$\mathbf{F}_z = \mathbf{A}_2\mathbf{F}(\mathbf{A}_2)^\dagger \tag{34}$$

α will be a nonzero constant, since multiplication of eq 33 by $\mathbf{A}_1$ yields

$$\alpha = \frac{\mathbf{A}_1\mathbf{G}(\mathbf{R}_1)^\dagger}{\mathbf{A}_1(\mathbf{A}_1)^\dagger} = \frac{\lambda_1}{(F^0)_{11}} \tag{35}$$

Rearrangement of eq 33 yields an expression for $\mathbf{R}_1$

$$(\mathbf{R}_1)^\dagger = \alpha\mathbf{G}^{-1}[\mathbf{I} - (F^0)_{11}\mathbf{W}]^{-1}(\mathbf{A}_1)^\dagger \tag{36}$$

where

$$\mathbf{W} = (\mathbf{A}_2)^\dagger(\mathbf{F}_z)^{-1}\mathbf{A}_2[\alpha\mathbf{G}^{-1} - \mathbf{I}] \tag{37}$$

and the nonsingularity of the matrix $[\mathbf{I} - (F^0)_{11}\mathbf{W}]$ is assumed. The limit of eq 36 for $\lambda_1 = 0$ is eq 24.

Although the quantities necessary for the calculation of $\mathbf{R}_1$ are known and can be determined from a knowledge of ν_1 and $\mathbf{A}_1$, the complexity of eq 36 limits its usefulness. In most isotope-effect calculations ν_1 is either zero or very close to it. We have carried out a limited investigation (*vide infra*) of the differences between the $\mathbf{R}_1$'s predicted by eq 24 and 36 for a number of isotopic molecules and various choices of ν_1 and $\mathbf{A}_1$. Since the eigenvectors of the $\mathbf{FG}$ matrix[9,25] are part of

(26) H. Margenau and G. M. Murphy, "Mathematics of Physics and Chemistry," D. Van Nostrand Co., Inc., New York, N. Y., 1943, p 273.

Table II: Comparison of Methods for Calculation of ν_L and Intermolecular TIF for the Unsymmetrical A–B–C Transition State[a]

	1 Eigenvector of F			2	3	4	5	6	7
	A_{11}	A_{12}	A_{13}[b]	ν_S	$(F^0)_{11}$	ν_{calcd}	ν_{39}	TIF = ν_L/ν_L'	
I. $m_A = m_B = m_C = 12$	1	0	0	0	0	0	0	1.0253	1.0198
$m_A' = 13$				$100i$	−0.037	$92i$	$92i$	1.0250	
$m_B' = m_C' = 12$				$300i$	−0.331	$284i$	$289i$	1.0234	
	1	−2	0.5	0	0	0	0	1.0023	1.0034
				$101i$	−0.030	$104i$	$104i$	1.0023	
				$301i$	−0.268	$312i$	$311i$	1.0027	
II. $m_A = m_B = m_C = 1$	1	0	0	0	0	0	0	1.2128	1.1547
$m_A' = 2$				$306i$	−0.037	$270i$	$268i$	1.2102	
$m_B' = m_C' = 1$				$918i$	−0.331	$846i$	$805i$	1.1936	
	1	−2	0.5	0	0	0	0	1.0201	1.0230
				$341i$	−0.030	$353i$	$327i$	1.0208	
				$1024i$	−0.268	$1060i$	$980i$	1.0231	

[a] $q_1 = r_{AB} = 1.42$ A; $q_2 = r_{BC} = 1.76$ A; $q_3 = \angle ABC = 110°$. $F_{11} = 7.00$ mdynes A^{-1}; $F_{22} = 1.75$ mdynes A^{-1}; $F_{33} = 0.50$ mdynes A^{-1}. [b] Dimensions of all $A_{i,j}$ here are the same, the A_{13} used in the calculation having been distance-weighted.

the output of our and most other[12] computer programs for calculation of isotope effects, the study is made conveniently by comparing with $\mathbf{A}_1$ the eigenvector corresponding to ν_1. As predicted by eq 36, the magnitudes of the differences depended on $(F^0)_{11}$, $\mathbf{A}_1$, and the molecular model, but usually were smaller than 10% for $\nu_1 = 300i$ (cm^{-1}) or less.

The Frequency ν_1 in terms of $\mathbf{A}_1$. The general expression for ν_1 in terms of $\mathbf{A}_1$ is

$$\lambda_1 = (F^0)_{11} \frac{\mathbf{A}_1(\mathbf{A}_1)^\dagger}{\mathbf{A}_1\mathbf{G}^{-1}[\mathbf{I} - (F^0)_{11}\mathbf{W}]^{-1}(\mathbf{A}_1)^\dagger} \qquad (38)$$

which computer calculations indicate can be approximated well by

$$\lambda_1 = (F^0)_{11} \frac{\mathbf{A}_1(\mathbf{A}_1)^\dagger}{\mathbf{A}_1\mathbf{G}^{-1}(\mathbf{A}_1)^\dagger} \qquad (39)$$

for ν_1 near zero.[27]

Application

Comparison was made, in the computational experiments mentioned above, of values of ν_1 obtained from exact calculations (ν_{calcd}) with those predicted by eq 39 (ν_{39}); the results for two models, two reaction coordinates, and three preselected ν_1's (ν_S) are collected in columns 1–5 of Table II. The tabulated values of ν_S, ν_{calcd}, and ν_{39} are for the *light*-molecule skeleton in each case. The ν_S and the G-matrix elements were used to calculate $(F^0)_{11}$ *via* eq 28; the potential function was then constructed using the rules determined from solution of eq 21 in the manner described for eq 6. Agreement among the various ν_1's is quite satisfactory; the largest discrepancies are of the order of 10% and are associated with hydrogen. Similarly close correspondence has been obtained in calculations made with a variety of other molecules and Slater coordinates; as a result, we conclude that, for preselected frequencies not too different from zero, eq 39 provides an excellent approximation in obtaining $(F^0)_{11}$ for given choices of ν_1 and $\mathbf{A}_1$.

Illustration of the Construction of **F**. The advantage of transferability in the construction of **F** *via* $\mathbf{A}_1$ rather than *via* $\mathbf{R}_1$ has been discussed above. Another advantage of the former approach is that the matrices are smaller for a problem of given complexity. For example, in the case of simple bond rupture (or formation) $\mathbf{R}_1$ will have one nonzero element, but the number r of nonzero elements in $\mathbf{G}(\mathbf{R}_1)^\dagger$, and therefore in $\mathbf{A}_1$, generally will be near n.[28] If, however, one starts with an $\mathbf{A}_1$ having one nonzero element, the problem is immediately smaller by the factor $1/r$ and experience indicates that the resulting molecular motion is closely approximate to simple bond rupture (or formation).

To illustrate the convenience of an approach to **F**

(27) If **A** is an orthogonal matrix with $\mathbf{A}_1$ as its first row, eq 38 can be shown to be equivalent to the expression obtained when the polynomial of degree n formed by the expansion of the secular equation for the coordinate system $\mathbf{Z} = \mathbf{AS}$ is solved for λ_1.[9] Assuming that second and higher order terms in λ_1 can be neglected, $\lambda_1 = C_n/C_{n-1}$, where the C_i's are the coefficients of the polynomial. Since $\mathbf{A}_1$ is an eigenvector of **F**

$$\lambda_1 = (F^0)_{11} \frac{|\mathbf{G}^0|}{|[\mathbf{G}^0]_{11}|}$$

where $|\mathbf{G}^0|$ is the determinant of $\mathbf{G}^0 = \mathbf{AG}(\mathbf{A})^\dagger$ and $|[\mathbf{G}^0]_{11}|$ is the cofactor of $(G^0)_{11}$. The latter is equivalent to eq 39.

(28) This assumes, of course, that the G matrix is not factored for reasons of symmetry, etc.

via $\mathbf{A}_1$, we consider the case where $\mathbf{A}_1$ has two nonadjacent nonzero elements. Equation 20 for this problem is

$$\mathbf{F}\begin{bmatrix} A_{11} \\ 0 \\ A_{13} \\ 0 \\ \cdot \\ \cdot \\ \cdot \\ 0 \end{bmatrix} = \begin{bmatrix} A_{11}F_{11} + A_{13}F_{13} \\ A_{11}F_{12} + A_{13}F_{23} \\ A_{11}F_{13} + A_{13}F_{33} \\ A_{11}F_{14} + A_{13}F_{34} \\ \cdot \\ \cdot \\ \cdot \\ A_{11}F_{1n} + A_{13}F_{3n} \end{bmatrix} = (F^0)_{11}\begin{bmatrix} A_{11} \\ 0 \\ A_{13} \\ 0 \\ \cdot \\ \cdot \\ \cdot \\ 0 \end{bmatrix} \quad (40)$$

The force constants between constrained bonds (here coordinates 1 and 3) and unconstrained are related by

$$F_{1k} = \rho F_{3k} = -(A_{13}/A_{11})F_{3k}; \qquad k = 2, 4, 5, \ldots, n \quad (41)$$

The quantity ρ has been associated with the relative amounts of bond rupture and bond formation occurring in such a reaction coordinate.[2,3] The interaction constant between the constrained bonds is

$$F_{13} = [F_{11} - (F^0)_{11}]/\rho = \rho[F_{33} - (F^0)_{11}] \quad (42)$$

of which an alternate form is

$$F_{13} = \pm\sqrt{[F_{11} - (F^0)_{11}][F_{33} - (F^0)_{11}]} \quad (43)$$

where the plus sign denotes approximate asymmetric stretching and the minus sign symmetric (compare with Table I). It is apparent from eq 42 that the diagonal force constants are not independent but are related through

$$[F_{11} = (F^0)_{11}]/[F_{33} - (F^0)_{11}] = \rho^2 \quad (44)$$

That is, the values of the force constants determine the ratio of bond rupture to bond formation. A method often used to calculate F_{11}, F_{33}, and F_{13} is[13]

$$\begin{gathered} F_{11} = (1 - x)(F_{11})^0 \\ F_{33} = x(F_{33})^0 \\ (F_{13})^2 - F_{11}F_{33} = d \leq 0 \end{gathered} \quad (45)$$

where the parameter x is a measure of the degree of bond formation or rupture, and $(F_{11})^0$ and $(F_{33})^0$ are the force constants when x equals 0 and 1, respectively. The *curvature parameter* d can be expressed as

$$d = -(F^0)_{11}[F_{11} + F_{33} - (F^0)_{11}] \quad (46)$$

which shows that it also is a function of x; this relation can be employed to obtain $(F^0)_{11}$ for a given value of d. Clearly, x is not equivalent to the ρ defined above, and care must be exercised in interpreting changes in an isotope effect with x in terms of the *relative* amounts of bond rupture and formation.

Isotope Effects on the Reaction Coordinate. To the accuracy of the Born–Oppenheimer approximation, $\mathbf{F}$ is independent of isotopic substitution. Upon isotopic substitution, eq 6 becomes

$$\mathbf{FG}'(\mathbf{R}_1')^\dagger = \lambda_1'(\mathbf{R}_1')^\dagger \quad (6)$$

The effect of isotopic substitution on $\mathbf{R}_1$ could be calculated using eq 36 if that on the frequency were known, since α is mass dependent. The agreement between columns 4 and 5 of Table II suggests that a good approximation of ν_1' to use in this correction term would be that obtained from the primed form of eq 39. For the case of $\nu_1 = 0$, an exact calculation of $\mathbf{R}_1'$ can be made using eq 25, which has been seen to be a good approximation for $\mathbf{R}_1$ when ν_1 is small. When $\mathbf{R}_1$ is an eigenvector of both $\mathbf{G}$ and $\mathbf{F}$ (eq 28), the identity

$$\mathbf{R}_1 = b\mathbf{A}_1 \quad (47)$$

where b is a normalizing constant, should not be used to calculate $\mathbf{R}_1'$ simply by discovering the appropriate b', since that would imply that $\mathbf{A}_1$ is also an eigenvector of $\mathbf{G}'$, which is not true in general. That is, an $\mathbf{A}_1$ which is an eigenvector of a $\mathbf{G}$ matrix is not necessarily an eigenvector of the related $\mathbf{G}'$ matrix. For example, in a triatomic molecule having C_{2v} symmetry the vector $(-1, 1, 0)$ is an eigenvector of the $\mathbf{G}$ matrices for all isotopic forms which retain that symmetry (*e.g.*, HOH, DOD, HO^{18}H, etc.), but is not for those forms in which C_{2v} symmetry has been destroyed (*e.g.*, HOD, TOH, etc.).

TIF. The isotope effect on the imaginary frequency associated with the reaction coordinate follows from eq 38

$$\nu_1/\nu_1' = \left[\frac{\mathbf{A}_1(\mathbf{G}')^{-1}[\mathbf{I} - (F^0)_{11}\mathbf{W}']^{-1}(\mathbf{A}_1)^\dagger}{\mathbf{A}_1\mathbf{G}^{-1}[\mathbf{I} - (F^0)_{11}\mathbf{W}]^{-1}(\mathbf{A}_1)^\dagger}\right]^{1/2} \quad (48)$$

This is the desired expression for TIF within the framework of the transition-state theory, and it can be used to calculate TIF if α' is approximated by combination of the primed forms of eq 35 and 39.

In the case of a zero frequency, the expression

$$\nu_1/\nu_1' = \left[\frac{\mathbf{A}_1(\mathbf{G}')^{-1}(\mathbf{A}_1)^\dagger}{\mathbf{A}_1\mathbf{G}^{-1}(\mathbf{A}_1)^\dagger}\right]^{1/2} \quad (49)$$

is exact; further, it is an excellent approximation to TIF for small values of ν_1, as indicated in column 6 of Table II. The figures listed there are exact values of TIF; their drift with changing ν_s for each $\mathbf{A}_1$ is a measure of the error involved in the use of eq 49 rather than eq 48,[29] since TIF from eq 49 is independent of ν_s.

(29) These expressions for TIF can be obtained also from consideration of the characteristic polynomial of the secular equation.[11,27]

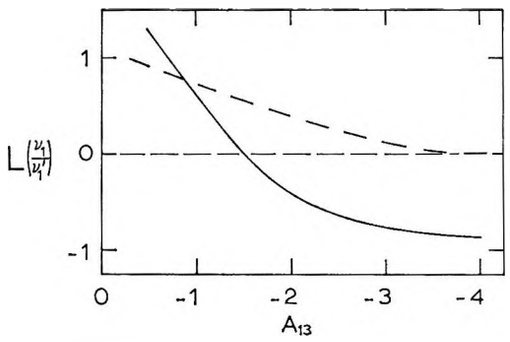

Figure 1. Influence of bending motion in the reaction coordinate on TIF for the intramolecular isotope effect in the reaction C–C–C → C + C–C. $q_1 = r_{AB} = 1.76$ A; $q_2 = r_{BC} = 1.42$ A; $q_3 = \angle ABC = 110°$. $F_{11} = 1.75$ mdynes A^{-1}; $F_{22} = 7.00$ mdynes A^{-1}; $F_{33} = 0.50$ mdynes A^{-1}. $m_A = m_B = m_B' = m_C' = 12$; $m_A' = m_C = 13$. $A_{11} = 2$; $A_{12} = -1$. $\nu_1 = 0$. (See footnote *a*, Table II): ———, exact calculation,[15] eq 49; – – – –, approximate calculation, eq 50.

The figures in column 7 of Table II are obtained from the expression

$$\nu_1/\nu_1' = \left[\frac{\mathbf{A}_1\mathbf{G}(\mathbf{A}_1)^\dagger}{\mathbf{A}_1\mathbf{G}'(\mathbf{A}_1)^\dagger}\right]^{1/2} \qquad (50)$$

given by Gatz[6] for calculation of the TIF associated with the Slater coordinate, $\mathbf{A}_1$, and was used by her to study the effects of bending motions in the Slater coordinate on TIF. The expressions used by Bigeleisen and Wolfsberg[2,3] and by Yankwich and Ikeda[4] are special cases of eq 50. As indicated earlier, the accuracy of eq 50 depends on how closely $\mathbf{A}_1$ is an eigenvector of *both* **G** and **G′**. For the molecules and eigenvectors considered in Table II, eq 50 yields the correct order of magnitude for L(TIF),[30] but this is not always the case. An example can be found in some computer experiments on the effect of inclusion of bending motion in the $\mathbf{A}_1$ used for the construction of **F**.[15] It was found that the intramolecular C^{13} isotope effect in the reaction C–C–C → C + C–C inverted as the amount of bending was increased; these results are shown as the solid curve in Figure 1 (eq 49). The dashed curve is that obtained *via* eq 50. For values of A_{13} near −1, similar values of TIF are obtained, but as A_{13} becomes larger, the difference between the two increases, and, further, eq 50 fails to yield the inversion.

It is interesting to note that eq 50 applied to simple C–C bond rupture in an 11-atom model for the malonic acid decarboxylation predicts TIF = 1.0198 (as obtained for the simple three-atom model) for the intramolecular isotope effect, while eq 49 yields TIF = 1.0020, the same value obtained by Wolfsberg and Stern[12] from the ratio ν_L/ν_L'. That is, the use of $\mathbf{G}^{-1}$ instead of **G** correctly involves in TIF the masses of the other than disjunct atoms in the molecule. The attempt to reduce this discrepancy by use of "molecular fragment" masses involves an insufficiently detailed approximation.

Although the elements of the **F** matrix are not determined uniquely by eq 18, TIF is independent of **F** for values of ν_1 near zero; such is not the case for TDF. In selecting values for the elements of **F**, one must be guided by comparisons with stable molecules and by considerations of chemical and physical reasonableness. Any set of choices will be arbitrary to a degree, just as it always has been.

Acknowledgment. The research upon which this article is based was supported by the U. S. Atomic Energy Commission (COO-1142-70).

(30) $L(x) = 100 \ln x$.

Ligand Field Theory of d^3 and d^7 Electronic Configurations in Noncubic Fields. I. Wave Functions and Energy Matrices[1]

by Jayarama R. Perumareddi

Mellon Institute, Pittsburgh, Pennsylvania 15213 *(Received November 7, 1966)*

The ligand field theory of cubic fields has been extended to include noncubic fields for d^3 and d^7 electronic configurations. Various coupling schemes applicable to noncubic fields in the limit of zero spin-orbit perturbation have been thoroughly discussed. A complete set of symmetry-adapted strong-field cubic wave functions in quadrate and trigonal orientations have been derived for d^3 configuration. The corresponding energy matrices of quadrate and trigonal fields have been constructed in the limit of zero spin-orbit interaction. Energy matrices of cylindrical fields have also been constructed using the weak-field $|L, S, M_L, M_S\rangle$ functions already derived by Condon–Shortley and Finkelstein–Van Vleck. These latter are included, in addition to their application to linear systems, as checks for the quadrate and trigonal calculations. They also provide energy labels for quadrate and trigonal energy plots at zero cubic ligand field parameter. Some generalizations are drawn from the energy matrices, and their application to the study of the spectra of appropriate transition metal systems is pointed out. Application of the energy matrices to systems of d^7 configuration is shown and extensions of the theory of noncubic fields to systems of other configurations are also suggested.

I. Introduction

The development of the theory of ligand fields in the last decade and a half provides the basis for understanding the magnetic and optical behavior of transition metal compounds.[2] The theory of systems of cubic symmetry is well understood. However, attempts in developing the theory to include symmetries lower than cubic have been very few. Thus, Liehr[3] has carried out complete calculations, including spin-orbit and full configuration interaction, on the one-electron and hole configurations in cylindrical (or linear), quadrate (or tetragonal), and trigonal symmetries; Gladney and Swalen[4] on the same configurations in trigonal fields; Fenske, Martin, and Ruedenberg[5] on the two-electron and hole configurations in square planar geometry; Plato and Racah[6] on the two- and three-electron configurations in trigonal weak fields; and finally, Perumareddi and Liehr[7] on the two- and eight-electron configurations in cylindrical, quadrate, and trigonal fields. In addition to these, there exist some restricted calculations, *i.e.*, without or with limited spin-orbit perturbation and configuration interaction. These latter include the examination of the trigonal two-electron trivalent vanadium with no spin-orbit coupling by Hartmann, Furlani, and Bürger,[8] the treatment of the two-electron trigonal chromium corundum without

(1) Portions of this material have been included in a paper presented at the 151st National Meeting of the American Chemical Society, Pittsburgh, Pa., March 1966.

(2) See, for instance: (a) W. Moffitt and C. J. Ballhausen, *Ann. Rev. Phys. Chem.*, **7**, 107 (1956); (b) C. J. Ballhausen, "Introduction to Ligand Field Theory," McGraw-Hill Book Co., Inc., New York, N. Y., 1962; (c) J. S. Griffith, "The Theory of Transition-Metal Ions," The University Press, Cambridge, England, 1961; (d) C. K. Jørgensen, "Absorption Spectra and Chemical Bonding in Complexes," Addison-Wesley Publishing Co., Inc., Reading, Mass., 1962; (e) B. N. Figgis and J. Lewis, *Progr. Inorg. Chem.*, **6**, 37 (1964); (f) W. Low, "Paramagnetic Resonance in Solids," Academic Press, Inc., New York, N. Y., 1960.

(3) (a) A. D. Liehr, *J. Phys. Chem.*, **64**, 43 (1960); (b) A. D. Liehr, Abstracts, Symposium on Molecular Structure and Spectroscopy, Columbus, Ohio, June 1965.

(4) H. M. Gladney and J. D. Swalen, *J. Chem. Phys.*, **42**, 1999 (1965).

(5) (a) R. F. Fenske, D. S. Martin, Jr., and K. Ruedenberg, *Inorg. Chem.*, **1**, 441 (1962); (b) R. F. Fenske and D. S. Martin, AEC Report IS-342, Ames Laboratory, Iowa State University, Ames, Iowa, May 1961. Available from the Office of Technical Services, Department of Commerce, Washington 25, D. C., price $3.50.

spin-orbit interaction by Pryce and Runciman,[9] and the study of the three-electron trigonal chromium corundum system with limited spin-orbit coupling by Sugano and Tanabe.[10] Such restricted calculations have also been carried out on various other configurations by Piper and Carlin,[11] Macfarlane,[12] Goode,[13] Ōtsuka,[14] and others.

Our interest in the d^3 (and hence the d^7) configuration stems from the fact that chromium(III) complexes in both cubic and noncubic symmetries have been extensively investigated. Many trigonally distorted and quadrately substituted chromium(III) compounds are known and their spectral properties have been measured. Although the optical measurements on trigonal chromium(III) systems have been made using polarized light,[15] this is not true for quadrate systems. However, even the solution absorption studies do show splittings of the cubic bands when the cubic chromium(III) complexes are substituted resulting in quadrate symmetry.[16] Although there have been attempts to explain quantitatively the absorption bands of the trigonal systems,[15] no such attempts have been made for the quadrate compounds.[17] Thus, there exists no systematic development of the theory and its application to noncubic compounds of d^3 and d^7 configurations. We aim to undertake this task in the present paper and in the papers to be published in the near future. The present paper lays the ground work in a detailed fashion for the development of the theory of d^3 and d^7 configurations in cylindrical, quadrate, trigonal, and square planar fields in the limit of zero spin-orbit interaction and future papers will consider the applications of the theory to explain the optical phenomena of appropriate systems of these configurations. Finally, the theory will be extended to include spin-orbit perturbation when more accurate spectral data become available.

II. Theory of Noncubic Fields

Octahedral Orientation. If we treat the ligand fields of quadrate and trigonal symmetries as the sum of cubic and axial potentials, three cases arise in the limit of zero spin-orbit perturbation.

$$\sum_{i\neq j} e^2/r_{ij} > (V_C, V_\infty) \qquad \text{(weak-field scheme)} \qquad \text{(i)}$$

$$V_C > \sum_{i\neq j} e^2/r_{ij} > V_\infty$$

[strong-field scheme (weak axial fields)] (ii)

$$(V_C, V_\infty) > \sum_{i\neq j} e^2/r_{ij}$$

[strong-field scheme (strong axial fields)] (iii)

Cases i and ii correspond to the situation where the axial fields are introduced as additional minor perturbations over the major cubic potential and electron correlations, whereas case iii corresponds to the situation where the axial field perturbations are large and hence are diagonalized along with the cubic field before introducing electron correlations as perturbative additions. In cases i and ii, the weak-field and strong-field cubic wave functions, respectively, portray the role of unperturbed states and decompose on going down in symmetry into lower symmetry representations according to Table I. (For the sake of generality, we have written the representations in the case of quadrate symmetry with no *g* subscripts. Written as they are, they are correct if the symmetry is C_{4v}. For D_{4h} symmetry, they should have a *g* subscript.) The resulting quadrate and trigonal functions are said to be octahedrally oriented. The quadrate and trigonal energy matrices corresponding to these cases would now contain diagonal as well

(6) M. Plato and G. Racah, private communication to A. D. Liehr, 1965.

(7) (a) J. R. Perumareddi and A. D. Liehr, Abstracts, Symposium on Molecular Structure and Spectroscopy, Columbus, Ohio, June 1965; (b) J. R. Perumareddi and A. D. Liehr, Abstracts, 150th National Meeting of the American Chemical Society, Atlantic City, N. J., Sept 1965; to be published.

(8) H. Hartmann, C. Furlani, and A. Bürger, *Z. Physik. Chem.* (Frankfurt), **9**, 62 (1956).

(9) M. H. L. Pryce and W. A. Runciman, *Discussions Faraday Soc.*, **26**, 34 (1958).

(10) S. Sugano and Y. Tanabe, *J. Phys. Soc. Japan*, **13**, 880 (1958).

(11) T. S. Piper and R. L. Carlin, *J. Chem. Phys.*, **33**, 1208 (1960).

(12) (a) R. M. Macfarlane, *ibid.*, **40**, 373 (1964); (b) *ibid.*, **39**, 3118 (1963).

(13) D. H. Goode, *ibid.*, **43**, 2830 (1965).

(14) J. Ōtsuka, *J. Phys. Soc. Japan*, **21**, 596 (1966).

(15) See, for instance: (a) S. Sugano and I. Tsujikawa, *ibid.*, **13**, 899 (1958); (b) W. Low, *J. Chem. Phys.*, **33**, 1162 (1960); (c) D. S. McClure, *ibid.*, **36**, 2757 (1962); (d) D. L. Wood, J. Ferguson, K. Knox, and J. F. Dillon, Jr., *ibid.*, **39**, 890 (1963); (e) D. L. Wood, *ibid.*, **42**, 3404 (1965); (f) S. Yamada and R. Tsuchida, *Bull. Chem. Soc. Japan*, **33**, 98 (1960); (g) T. S. Piper and R. L. Carlin, *J. Chem. Phys.*, **36**, 3330 (1962); (h) *ibid.*, **35**, 1809 (1961).

(16) Such studies have been made by (a) M. Linhard and M. Weigel, *Z. Anorg. Allgem. Chem.*, **266**, 49 (1951); (b) M. Linhard and M. Weigel, *Z. Physik. Chem.* (Frankfurt), **5**, 20 (1955); (C) C. S. Garner and D. J. MacDonald in "Advances in the Chemistry of Coordination Compounds," S. Kirschner, Ed., The Macmillan Co., New York, N. Y., 1961, pp 266–275; (d) L. P. Quinn and C. S. Garner, *Inorg. Chem.*, **3**, 1348 (1964); (e) F. Woldbye, *Acta Chem. Scand.*, **12**, 1079 (1958).

(17) Ballhausen (ref 2b) has given the diagonal elements for the quartets of d^3 configuration in quadrate fields. Based on these matrix elements, a semiquantitative empirical treatment has been proposed for the explanation of the spectral characteristics of tetragonal Cr(III) complexes by others. See for instance, (a) R. A. D. Wentworth and T. S. Piper, *Inorg. Chem.*, **4**, 709 (1965). Excellent attempts have been made, though, to explain the band splittings of substituted octahedral Cr(III) and complexes of other configurations based on bonding and molecular orbital approaches by (b) D. S. McClure in "Advances in the Chemistry of Coordination Compounds," S. Kirchner, Ed., The Macmillan Co., New York, N. Y., 1961, p 498; (c) H. Yamatera, *Bull. Chem. Soc. Japan*, **31**, 95 (1958); (d) C. E. Schäffer and C. K. Jørgensen, *Mat. Fys. Medd. Dan. Vid. Selsk.*, **34**, 13 (1965).

Table I: Decomposition of the Representations of Cubic Symmetry Relative to Quadrate and Trigonal Symmetries

Cubic	Quadrate	Trigonal
$A_{1g}{}^C$	$A_1{}^Q$	$A_1{}^T$
$A_{2g}{}^C$	$B_1{}^Q$	$A_2{}^T$
$E_{ga}{}^C$	$A_1{}^Q$	$E_a{}^T$
$E_{gb}{}^C$	$B_1{}^Q$	$E_b{}^T$
$T_{1ga}{}^C$	$A_2{}^Q$	$A_2{}^T$
$T_{1g(b/c)}{}^C$	$E_{(a/b)}{}^Q$	$E_{(a/b)}{}^T$
$T_{2ga}{}^C$	$B_2{}^Q$	$A_1{}^T$
$T_{2g(b/c)}{}^C$	$E_{(a/b)}{}^Q$	$E_{(a/b)}{}^T$

cases do not seem to be common among d^3 configuration and as most of the existing quadrate and trigonal systems of d^3 configuration exemplify small deviations from cubic symmetry, it is by case ii we choose to carry out calculations in this report. It may be pointed out that calculations starting from cases i and iii would provide a very good check on our treatment from case ii. On the other hand, as we will be describing later, other internal checks of our calculations are used and so we have not included here calculations based on cases i and iii.

Wave Functions. Quadrate. As has already been

Table II: Trigonal Oriented d Orbitals and Their Transformation Properties. (z' Is the Threefold Axis of Symmetry Which Is the Axis of Quantization and x' and y' Are the Orthogonal Coordinates. z Refers to the Fourfold Axis of Symmetry. $\omega = \exp -2\pi i/3$)

$$d_{\sigma'} = d_{3z'^2-r^2};\quad d_{\pi_\pm'} = \sqrt{1/2}(d_{z'x'} \pm i d_{y'z'});\quad d_{\delta_\pm'} = \sqrt{1/2}(d_{x'^2-y'^2} \pm i d_{x'y'})$$

O_h	D_3	$\mathcal{C}_3(z')$	$\mathcal{C}_2(y')$	$\mathcal{C}_4(z)$
t_{2ga}	$a_1(t_2): d_{\sigma'}$	$a_1(t_2)$	$a_1(t_2)$	$-{}^1/_3 a_1(t_2) + {}^2/_3\omega^{-1/2} e_+(t_2) + {}^2/_3\omega^{+1/2} e_-(t_2)$
$t_{2g(a/b)}$	$e_\pm(t_2): \sqrt{1/3}\, d_{\pi_\pm'} - \sqrt{2/3}\, d_{\delta_\mp'}$	$\omega^{\pm 1} e_\pm(t_2)$	$e_\mp(t_2)$	${}^2/_3\omega^{\mp 1/2} a_1(t_2) - {}^1/_3 e_\mp(t_2) - {}^2/_3\omega^{\pm 1/2} e_\pm(t_2)$
$e_{g(a/b)}$	$e_\pm(e): \sqrt{2/3}\, d_{\pi_\pm'} + \sqrt{1/3}\, d_{\delta_\mp'}$	$\omega^{\pm} e_\pm(e)$	$e_\mp(e)$	$e_\mp(e)$
t_{1ua}	$a_2(t_1): p_{\sigma'}$	$a_2(t_1)$	$-a_2(t_1)$	${}^1/_3 a_2(t_1) + {}^2/_3\omega^{-1/2} e_+(t_1) + {}^2/_3\omega^{+1/2} e_-(t_1)$
$t_{1u(b/c)}$	$e_\pm(t_1): p_{\pi_\pm'}$	$\omega^{\pm 1} e_\pm(t_1)$	$-e_\mp(t_1)$	${}^2/_3\omega^{\mp 1/2} a_2(t_1) + {}^1/_3 e_\mp(t_1) + {}^2/_3\omega^{\pm 1/2} e_\pm(t_1)$

as off-diagonal ligand field parameters due to axial fields. On the other hand, in case iii, the one-electron symmetry adapted functions suitable to quadrate and trigonal symmetries don the role of the basis set from which the three-electron functions are manufactured.[18] These initial one-electron functions are $e(d_{zz}, d_{yz})$, $b_2(d_{xy})$, $a_1(d_z2)$, and $b_1(d_{x^2-y^2})$ in quadrate fields and $e_\pm(t_{2g})$, $a_1(t_{2g})$, and $e_\pm(e_g)$ in trigonal fields. If the many electron functions constructed from these one-electron sets are used in energy calculations, in addition to the cubic ligand field parameter, the axial ligand field parameters could also be diagonalized except in the trigonal case where there may be few nonvanishing off-diagonal axial parameters because of the nonzero one-electron element $\langle e_\pm(t_{2g})|V_a|e_\pm(e_g)\rangle$.

The usual trigonally distorted chromium(III) systems such as emerald, ruby, etc. (C_{3v} and D_3 point groups) and the slightly tetragonally distorted cubic as well as monosubstituted (C_{4v}) and *trans*-disubstituted (D_{4h}) hexacoordinate octahedral complexes could be well described by case ii, *i.e.*, weak axial fields of the strong-field scheme, whereas large trigonal and quadrate distortions and pentacoordinate square pyramidal and tetracoordinate square planar systems are more appropriately described by case iii. As these latter pointed out, the starting functions are the strong-field symmetry adapted cubic functions the derivation of which has been described clearly in the literature.[2b,c] The complete set of these functions is listed in Appendix A.[19]

Trigonal. The one-electron orbitals of trigonal orientation used here are as given by Liehr[20] which differ from those of the others[9] by phase factors. These orbitals along with their transformation properties are shown in Table II. The process of building d^3,[7] trigonally disposed cubical determinantal wave functions[21] consists of first writing the nondegenerate (orbitally) trigonal components of a given cubical species and then

(18) A detailed account of building two-electron functions starting from one-electron tetragonal functions has been given in ref 5b. Extension to three-electron functions follows similar procedures. The trigonal determinants of d^3 configuration can also be obtained in the same fashion.

(19) Appendices A and B have been deposited as Document No. 9457 with the ADI Auxiliary Publications Project, Photoduplication Service, Library of Congress, Washington, D. C. 20540. A copy may be secured by citing the document number and remitting $3.75 for photoprints or $2.00 for 35-mm microfilm. Advance payment is required. Make checks or money orders payable to: Chief, Photoduplication Service, Library of Congress. Copies may also be obtained by writing to the author.

(20) See ref 3a and also A. D. Liehr, *J. Phys. Chem.*, 68, 665 (1964).

(21) This procedure has been briefly described in ref 20.

using this component to generate the two doubly degenerate components by means of the $\mathcal{C}_4(z)$ symmetry operation. As cubically doubly degenerate species go over into trigonally doubly degenerate species, no significant effort is involved in their orientation. An alternative way of manufacturing the $d^{3,7}$ wave function is by a direct transformation of their known tetragonal representation to their desired trigonal representation by means of the connections of Table II and the matrix connection between the quadrate and trigonal orbital basis functions of eq 1.

$$\begin{bmatrix} d_{3z'^2-r^2} \\ d_{x'^2-y'^2} \\ d_{x'y'} \\ d_{z'x'} \\ d_{y'z'} \end{bmatrix} = \begin{bmatrix} 0 & 0 & \sqrt{1/3} & \sqrt{1/3} & \sqrt{1/3} \\ \sqrt{1/3} & 0 & 2/3 & -1/3 & -1/3 \\ 0 & -\sqrt{1/3} & 0 & \sqrt{1/3} & -\sqrt{1/3} \\ \sqrt{2/3} & 0 & -\sqrt{2}/3 & \sqrt{2}/6 & \sqrt{2}/6 \\ 0 & \sqrt{2/3} & 0 & \sqrt{1/6} & -\sqrt{1/6} \end{bmatrix} \begin{bmatrix} d_{3z^2-r^2} \\ d_{x^2-y^2} \\ d_{xy} \\ d_{xz} \\ d_{yz} \end{bmatrix} \quad (1)$$

The former method will be described here by deriving the $^4T_{1g}$ and $^4T_{2g}$ terms of $(t_{2g}{}^2e_g)$ configuration. We first note that these quartets (spin) arise from $[t_{2g}{}^2(^3T_{1g})e_g]$. The $^3T_{1g}$ of $(t_{2g}{}^2)$ in turn is given by

$$\begin{aligned} {}^3T_{1ga}&: \ |e_+(t_{2g})e_-(t_{2g})| \longrightarrow a_2(t_1) \\ {}^3T_{1gb}&: \ -|a_1(t_{2g})e_+(t_{2g})| \longrightarrow e_+(t_1) \\ {}^3T_{1gc}&: \ |a_1(t_{2g})e_-(t_{2g})| \longrightarrow e_-(t_1) \end{aligned} \quad (2)$$

Let us now construct a table of transformation properties of various determinants such as $|a_2(t_1)e_\pm(e)|$ and $|e_\pm(t_1)e_\pm(e)|$ as shown in Table III.

Table III: Transformation Properties of Determinantal Trigonal Functions

	Determinantal function	$\mathcal{C}_3(z')$	$\mathcal{C}_2(y')$
Φ_1:	$\lvert a_2(t_1)\ e_+(e)\rvert$	$\omega^{+1}\ \Phi_1$	$-\Phi_2$
Φ_2:	$\lvert a_2(t_1)\ e_-(e)\rvert$	$\omega^{-1}\ \Phi_2$	$-\Phi_1$
Φ_3:	$\lvert e_+(t_1)\ e_+(e)\rvert$	$\omega^{-1}\ \Phi_3$	$-\Phi_4$
Φ_4:	$\lvert e_-(t_1)\ e_-(e)\rvert$	$\omega^{+1}\ \Phi_4$	$-\Phi_3$
Φ_5:	$\lvert e_+(t_1)\ e_-(e)\rvert$	Φ_5	$-\Phi_6$
Φ_6:	$\lvert e_-(t_1)\ e_+(e)\rvert$	Φ_6	$-\Phi_5$
Ψ_1:	$\sqrt{1/2}(\Phi_5 - \Phi_6)$	Ψ_1	Ψ_1
Ψ_2:	$\sqrt{1/2}(\Phi_5 + \Phi_6)$	Ψ_2	$-\Psi_2$

Obviously, a combination of Φ_5 and Φ_6 should give rise to the nondegenerate (orbitally) trigonal components of $^4T_{1g}$ and $^4T_{2g}$. Such combinations are Ψ_1 and Ψ_2 which transform as a_1 and a_2 of trigonal symmetry (see Table IV for the character table of trigonal symmetry) thus providing the $^4T_{2ga}$ and $^4T_{1ga}$ components. Substituting the $^3T_{1g}$ functions of eq 2, we finally have

$$\begin{aligned} {}^4T_{2ga} &= \sqrt{1/2}[|a_1(t_{2g})e_-(t_{2g})e_-(e_g)| + |a_1(t_{2g})e_-(t_{2g})e_+(e_g)|] \\ {}^4T_{1ga} &= \sqrt{1/2}[|a_1(t_{2g})e_+(t_{2g})e_-(e_g)| - |a_1(t_{2g})e_-(t_{2g})e_+(e_g)|] \end{aligned} \quad (3)$$

The remaining components are obtained by $\mathcal{C}_4(z)$ symmetry operation on the above functions. Thus, performing this operation on $^4T_{2ga}$, we obtain

$$\begin{aligned} \mathcal{C}_4(z){}^4T_{2ga} &= \mathcal{C}_4(z)\{\sqrt{1/2}[|a_1(t_{2g})e_+(t_{2g})e_-(e_g)| + |a_1(t_{2g})e_-(t_{2g})e_+(e_g)|]\} \\ &= \sqrt{1/2}\{-1/3[|a_1(t_{2g})e_+(t_{2g})e_-(e_g)| + |a_1(t_{2g})e_-(t_{2g})e_+(e_g)|] + \\ &\quad 2/3\omega^{-1/2}[a_1(t_{2g})e_-(t_{2g})e_-(e_g)| - |e_+(t_{2g})e_-(t_{2g})e_+(e_g)|] + \\ &\quad 2/3\omega^{+1/2}[a_1(t_{2g})e_+(t_{2g})e_+(e_g)| + |e_+(t_{2g})e_-(t_{2g})e_-(e_g)|]\} \end{aligned}$$

which when compared with Table II shows that

$${}^4E^T_{(b)}\{{}^4T^C_{2g(c)}[t_{2g}{}^2(^3T_{1g})e_g]\} = \sqrt{1/2}[|a_1(t_{2g})e_\mp(t_{2g})e_\mp(e_g)| - |e_\pm(t_{2g})e_\mp(t_{2g})e_\pm(e_g)|] \quad (4)$$

Similarly

$$\begin{aligned} \mathcal{C}_4(z){}^4T_{1ga}&: \mathcal{C}_4(z)\{\sqrt{1/2}[|a_1(t_{2g})e_+(t_{2g})e_-(e_g)| - |a_1(t_{2g})e_-(t_{2g})e_+(e_g)|]\} \\ &: \sqrt{1/2}\{1/3[|a_1(t_{2g})e_+(t_{2g})e_-(e_g)| - |a_1(t_{2g})e_-(t_{2g})e_+(e_g)|] + \\ &\quad 2/3\omega^{-1/2}[-|a_1(t_{2g})e_-(t_{2g})e_-(e_g)| - |e_+(t_{2g})e_-(t_{2g})e_+(e_g)|] + \\ &\quad 2/3\omega^{+1/2}[|a_1(t_{2g})e_+(t_{2g})e_+(e_g)| - |e_+(t_{2g})e_-(t_{2g})e_-(e_g)|]\} \end{aligned}$$

hence

$${}^4E^T_{(b)}\{{}^4T^C_{1g(c)}[t_{2g}{}^2(^3T_{1g})e_g]\} = \mp\sqrt{1/2}[|a_1(t_{2g})e_\mp(t_{2g})e_\mp(e_g)| + |e_\pm(t_{2g})e_\mp(t_{2g})e_\pm(e_g)|] \quad (5)$$

Table IV: Character Table of Trigonal Symmetry

Representation	$C_3(z')$	$C_2(y')$
a_1	1	1
a_2	1	−1
e	−1	0

Note that in these doubly degenerate functions combinations of Φ_1, Φ_2, Φ_3, and Φ_4 occur as suggested by their transformation properties. The complete set of symmetry-adapted trigonal functions obtained in this manner is listed in Appendix A.[19]

Cylindrical. Appropriate wave functions for this symmetry are simply those of Russell–Saunders coupling[22] characterized by the quantum number M_L. Thus, the ^4F term gives rise to the M_L values of ± 3, ± 2, ± 1, and 0 which are designated, respectively, as $^4\Phi(^4F)$, $^4\Delta(^4F)$, $^4\Pi(^4F)$, and $^4\Sigma^-(^4F)$. Others are obvious.[23] Some of these functions for the d^3 configuration were given by Condon and Shortley[24] and the remainder by Finkelstein and VanVleck,[25] so are not listed in Appendix A.

Parameters. The most general set of parameters needed in the study of any molecular system can be derived by symmetry considerations alone. The various sets of parameters thus arrived at for symmetries of our interest[26] are given in Table V.

Table V: Most General Set of Parameters in Ligand Field Theory (Numbers Given in Parentheses Are the Number of Parameters Actually Used in Our Present Theory)

Symmetry	Ligand field	Electron correlation	Spin-orbit	Total number
Cubic	2 (1)	10 (3)	2 (1)	14 (5)
Cylindrical	3 (2)	14 (3)	4 (1)	21 (6)
Quadrate	4 (3)	23 (3)	5 (1)	32 (7)
Trigonal	4 (3)	27 (3)	6 (1)	37 (7)

Since we are concerned only with the energy differences, the actual number of ligand field parameters is reduced in each case by one. The observable bands in the optical spectra of systems of our interest are far too few when compared with the required number of electron correlation and spin-orbit parameters by general symmetry arguments, and hence we use only three-electron correlation parameters and one spin-orbit parameter (in the present study we are neglecting spin-orbit coupling also) assuming that the relative differences of these parameters are small. Thus, the restricted number of parameters is included in parentheses in the table. The electron correlation parameters are the familiar A, B, and C of Racah (these are related by $A = F_0 - 49F_4$, $B = F_2 - 5F_4$, and $C = 35F_4$ of Slater–Condon–Shortley parameters) parameters reduced from the free-ion values by proper fitting of the experimental spectroscopic data. The ligand field parameters are obtained in the following way.[3a,26] We take the quadrate (V_Q) and the trigonal potentials (V_T) to be the resultant of a cubic (V_C) and an axial field (V_∞), *i.e.*

$$V_{Q,T} = V_C + V_\infty^{Q,T} \tag{6}$$

where the cubic potential has the alternant forms[27]

$$V_C = \sum_i \{ Y_4^0(\theta_i,\phi_i) + \sqrt{5/14}[Y_4^4(\theta_i,\phi_i) + Y_4^{-4}(\theta_i,\phi_i)]\} R_4(r_i) \qquad \text{(quadrate orientation)} \tag{7a}$$

or

$$V_C = -2/3 \sum_i \{ Y_4^0(\theta_i',\phi_i') + \sqrt{10/7}[Y_4^3(\theta_i',\phi_i') - Y_4^{-3}(\theta_i',\phi_i')]\} R_4(r_i) \qquad \text{(trigonal orientation)} \tag{7b}$$

(22) Note that here we are dealing with weak-field representation The corresponding strong-field functions arise from configurations (δ^3), (π^3), $(\delta^2\pi)$, $(\delta^2\sigma)$, $(\delta\pi^2)$, $(\delta\sigma^2)$, $(\delta\pi\sigma)$, $(\pi^2\sigma)$, $(\pi\sigma^2)$ which serially give rise to the levels $^2\Delta$, $^2\Pi$, $^4\Pi + {}^2H + {}^2\Phi + 2^2\Pi$, $^4\Sigma^- + {}^2\Gamma + {}^2\Sigma^+ + {}^2\Sigma^-$, $^4\Delta + {}^2\Gamma + 2^2\Delta + 2^2\Sigma^+$, $^2\Delta$, $^4\Phi + {}^4\Pi + 2^2\Phi + 2^2\Pi$, $^4\Sigma^- + {}^2\Delta + {}^2\Sigma^+ + {}^2\Sigma^-$, $^2\Pi$, where the δ, π and σ are the one-electron d orbitals in linear symmetry. [These later correspond to the $|l, m_l\rangle$ functions of $|2 \pm 2\rangle$, $|2 \pm 1\rangle$, and $|2, 0\rangle$, respectively.] Identical levels, of course, arise from the weak-field representation also as described in the text.

(23) The ^2H term yields a state with $M_L = \pm 5$ which should be denoted by a corresponding Greek letter. As the upper Greek letter corresponding to H is Roman H itself, we retain this symbol as it is, *i.e.*, ^2H (^2H) in the weak field case and $^2H(\delta^2\pi)$ in the strong-field case. We hope no confusion arises from this notation.

(24) E. U. Condon and G. H. Shortley, "The Theory of Atomic Spectra," Cambridge University Press, Cambridge and New York, N. Y., 1957.

(25) R. Finkelstein and J. H. VanVleck, *J. Chem. Phys.*, **8**, 790 (1940).

(26) Derivation of these parameter numbers by symmetry arguments is shown very nicely in lecture notes by A. D. Liehr, "Geometry, Color, and Magnetism: The Ti(III) and Cu(II) Systems and their Relatives," which also includes such noncubic symmetries as rhomboidal, unidigonal, centro- and asymmetrical, and n-polygonal prismoidal ($n > 4$) systems. These lecture notes are available upon request from A. D. Liehr, Mellon Institute, Pittsburgh, Pa. 15213.

(27) $R_4(r_i)$ in six-coordinate octahedral fields is given by

$$R_4(r_i) = eq\, 7/2 \sqrt{\frac{4\pi}{9}} \frac{r_i^4}{a_i^5}$$

and $R_2(r_i)$ and $R_4'(r_i)$ in two-coordinate cylindrical fields are given, respectively, by

$$R_2(r_i) = eq\, 2\sqrt{\frac{4\pi}{5}} \frac{r_i^2}{a_i^3}; \quad R_4'(r_i) = eq\, 2\sqrt{\frac{4\pi}{9}} \frac{r_i^4}{a_i^5}$$

For such a linear system, it can be seen that $D\mu/D\nu = [1/14\sqrt{5/\pi}\langle R_2(r_i)\rangle]/[1/14\sqrt{1/\pi}\langle R_4'(r_i)\rangle] = 3\langle r_i^2/a_i^3\rangle/\langle r_i^4/a_i^5\rangle = 3\langle \rho_2(r)\rangle/\langle \rho_4(r)\rangle$ where $\rho_2(r) = r_i^2/a_i^3$ and $\rho_4(r) = r_i^4/a_i^5$.

and

$$V_\infty = \sum_i [R_2(r_i) Y_2^0(\bar{\theta}_i,\bar{\phi}_i) + R_4'(r_i) Y_4^0(\bar{\theta}_i,\bar{\phi}_i)] \quad (8)$$

where $(\bar{\theta}_i,\bar{\phi}_i) \equiv (\theta_i,\phi_i)$ for quadrate and (θ_i',ϕ_i') for trigonal. Just as Dq is defined as the matrix element

$$\langle 2, \pm 2|V_C|\pm 2, 2\rangle = (1/14\sqrt{\pi})\langle R_4(r_i)\rangle = Dq \quad (9)$$

we define[28]

$$\langle 2, \pm 2|V_\infty^{(4)}|\pm 2, 2\rangle = (1/14\sqrt{\pi})\langle R_4'(r_i)\rangle = D\nu \quad (10a)$$

$$\langle 2, \pm 1|V_\infty^{(2)}|\pm 1, 2\rangle = (\sqrt{5}/14\sqrt{\pi})\langle R_2(r_i)\rangle = D\mu \quad (10b)$$

where $\mu \equiv s$, σ, and $\mathfrak{f}$, and $\nu \equiv t$, τ, and $\mathfrak{t}$, respectively for quadrate, trigonal, and cylindrical symmetries. With these definitions, the nonvanishing matrix elements may thus be written

Quadrate

$$\begin{aligned}
\langle 2, \pm 2|V_Q|\pm 2, 2\rangle &= Dq - 2Ds + Dt \\
\langle 2, \pm 1|V_Q|\pm 1, 2\rangle &= -4Dq + Ds - 4Dt \\
\langle 2, 0|V_Q|0, 2\rangle &= 6Dq + 2Ds + 6Dt \\
\langle 2, \pm 2|V_Q|\mp 2, 2\rangle &= 5Dq \qquad (11a) \\
\langle (z^2)|V_Q|(z^2)\rangle &= 6Dq + 2Ds + 6Dt \\
\langle (x^2-y^2)|V_Q|(x^2-y^2)\rangle &= 6Dq - 2Ds + Dt \\
\langle (xy)|V_Q|(xy)\rangle &= -4Dq - 2Ds + Dt \\
\langle (zx)|V_Q|(zx)\rangle = \langle (yz)|V_Q|(yz)\rangle &= -4Dq + Ds - 4Dt \qquad (11b)
\end{aligned}$$

Trigonal[29]

$$\begin{aligned}
\langle 2, \pm 2|V_T|\pm 2, 2\rangle &= -{}^2/_3 Dq - 2D\sigma + D\tau \\
\langle 2, \pm 1|V_T|\pm 1, 2\rangle &= {}^8/_3 Dq + D\sigma - 4D\tau \\
\langle 2, 0|V_T|0, 2\rangle &= -4Dq + 2D\sigma + 6D\tau \\
\langle 2, \pm 2|V_T|\mp 1, 2\rangle &= \\
\langle 2, \mp 1|V_T|\pm 2, 2\rangle &= \pm\frac{10\sqrt{2}}{3} Dq \qquad (12a) \\
\langle a_1(t_{2g})|V_T|a_1(t_{2g})\rangle &= -4Dq + 2D\sigma + 6D\tau \\
\langle e_\pm(t_{2g})|V_T|e_\pm(t_{2g})\rangle &= -4Dq - D\sigma - {}^2/_3 D\tau \\
\langle e_\pm(e_g)|V_T|e_\pm(e_g)\rangle &= 6Dq - {}^7/_3 D\tau \\
\langle e_\pm(e_g)|V_T|e_\pm(t_{2g})\rangle &= \frac{\sqrt{2}}{3}(3D\sigma - 5D\tau) \qquad (12b)
\end{aligned}$$

Cylindrical

$$\begin{aligned}
\langle 2, \pm 2|V_\infty|\pm 2, 2\rangle &= -2D\mathfrak{f} + D\mathfrak{t} \\
\langle 2, \pm 1|V_\infty|\pm 1, 2\rangle &= D\mathfrak{f} - 4D\mathfrak{t} \\
\langle 2, 0|V_\infty|0, 2\rangle &= 2D\mathfrak{f} + 6D\mathfrak{t} \qquad (13)
\end{aligned}$$

Energy Matrices. Quadrate. The ligand field matrix elements are calculated in the usual way by using the quadrate wave functions listed in Appendix A and the one-electron elements of eq 11b. The matrix elements due to electron correlations can be obtained by the use of the coulomb (J) and exchange (K) integrals of t_{2g} and e_g electrons listed in literature.[30] It may be noted here that since we are using octahedral orientation, except for the axial ligand field parameters, the matrix elements in Dq, A, B, and C would be exactly the same as those in cubic fields. Now in addition, the diagonal and some off-diagonal elements would contain the axial parameters Ds and Dt. In particular, different cubic representations belonging to the same representations of the quadrate symmetry are connected by nonzero off-diagonal elements containing the axial parameters. The doublet and quartet energy matrices of quadrate fields are listed in the tables of Appendices B[19] and C, respectively.

Trigonal. The ligand field matrix elements can be easily obtained by the application of eq 12b and the wave functions of Appendix A. The electron correlation matrix elements can be calculated either by expanding the wave functions into $|l, m_l\rangle$ functions and then using their J and K integrals given in Condon and Shortley, or by directly using the J and K integrals of $e_\pm(t_{2g})$, $a_1(t_{2g})$, and $e_\pm(e_g)$ which were derived earlier by us.[31] Just as in the quadrate case, here also the matrix elements in Dq, A, B, and C would be exactly the same as those of cubic fields. The axial parameters $D\sigma$ and $D\tau$ occur in the diagonal and some off-diagonal elements and connect different cubic representations belonging to the same trigonal representation. Energy

(28) These revised definitions of axial parameters are due to A. D. Liehr (read ref 26) which differ in signs from those earlier used in literature, *e.g.*, ref 2a and 3a. These new signs of $D\mu$ and $D\nu$ have been chosen to parallel that for octahedral Dq, *i.e.*, positive values of $D\mu$ and $D\nu$ correspond to increased axial fields and negative values of $D\mu$ and $D\nu$ to decreased axial fields.

(29) The $D\sigma$ and $D\tau$ parameters are related to the v and v' of Pryce and Runciman[8] and K and K' of Sugano and Tanabe,[10] according to the formulas

$$v' = K' = \frac{\sqrt{2}}{3}(3D\sigma - 5D\tau)$$

$$v = -3K = {}^1/_3(9D\sigma + 20D\tau)$$

(30) See ref 2b,c, and 17c; also L. E. Orgel, *J. Chem. Phys.*, **23**, 1819 (1955). In ref 2b, the element $\langle (z^2)(zx)|1/r_{12}|(xy)(yz)\rangle$ should be $-2\sqrt{3}F_2 + 10\sqrt{3}F_4$ or $-2\sqrt{3}B$.

(31) The complete set of nonvanishing J and K integrals of $a_1(t_{2g})$, $e_\pm(t_{2g})$ and $e_\pm(e_g)$ which were derived by us in the course of our work on d^2 and d^8 configurations in noncubic fields (ref 7) will be published soon by the author in collaboration with A. D. Liehr.

matrices thus obtained are included in the tables of Appendices B[19] and C.

Cylindrical. With the use of the $|L, S; M_L, M_S\rangle$ functions, it is a simple matter to calculate the ligand field matrix elements from the one-electron elements of eq 13. The electron correlation elements are just those of the Russell–Saunders terms ^4F, ^4P, ^2H, ^2G, ^2F, $_a{}^2D$, $_b{}^2D$, and ^2P, given in Condon and Shortley.[24] Appendices B[19] and C contain also the energy matrices of cylindrical symmetry. It may be noted here that from this weak-field cylindrical representation, it is an easy step to arrive at the weak-field quadrate and trigonal energy matrices if the Dq parameter is also included while doing the cylindrical calculations. It is only necessary to recognize that the nonvanishing elements are those connecting different $|L, M_L\rangle$ and $|L, M_L'\rangle$ functions where M_L and M_L' differ by an angular momentum of 4 in quadrate and by 3 in trigonal fields. If we consider ^2H as an example, the various $|L, M_L\rangle$ functions are $|5, \pm5\rangle$, $|5, \pm4\rangle$, $|5, \pm3\rangle$, $|5, \pm2\rangle$, $|5, \pm1\rangle$, and $|5, 0\rangle$. The pairs of functions which have nonvanishing elements in cubic field parameter Dq (*cf.* eq 11a and 12a) are $|5, +5\rangle$ and $|5, +1\rangle$, $|5, +4\rangle$ and $|5, 0\rangle$, $|5, +3\rangle$ and $|5, -1\rangle$, $|5, +2\rangle$ and $|5, -2\rangle$, $|5, +1\rangle$ and $|5, -3\rangle$, $|5, 0\rangle$ and $|5, -4\rangle$, $|5, -1\rangle$ and $|5, -5\rangle$ in quadrate fields and $|5, +5\rangle$ and $|5, +2\rangle$, $|5, +4\rangle$ and $|5, +1\rangle$, $|5, +3\rangle$ and $|5, 0\rangle$, $|5, +2\rangle$ and $|5, -1\rangle$, $|5, +1\rangle$ and $|5, -2\rangle$, $|5, 0\rangle$ and $|5, -3\rangle$, $|5, -1\rangle$ and $|5, -4\rangle$, $|5, -2\rangle$ and $|5, -5\rangle$ in trigonal fields. The other free-ion terms are similar. Once these are calculated, the weak-field quadrate and trigonal energy matrices (octahedral orientation) can be constructed by using, respectively, the quadrate-oriented[32] and trigonally oriented cubic harmonics. (These latter are given by S. R. Polo, "Studies in Crystal Field Theory," Vol. I and II, in press.)

Internal Checks. Both weak-field and strong-field energy matrices can be constructed independently from the corresponding octahedrally oriented wave functions and can be solved for the same set of parametric values, thus arriving at the same eigenvalues. Even before that, using one set of energy matrices in one scheme and the unitary transformations to the other scheme,[33] energy matrices of the latter scheme can be constructed without recourse to the wave functions by the use of the relation

$$H_S = \tilde{T}(\Gamma_j) H_W T(\Gamma_j)^*$$

where the $T(\Gamma_j)$ are the transformation matrices.[33a]

As an alternate to the above, we have carried out the following checks in this case. First, when the axial parameters are set equal to zero in the quadrate and trigonal energy matrices, both should result in the strong-field cubic matrices of Tanabe and Sugano,[34] *i.e.*, for a given set of A, B, C, and Dq, with $Ds = D\sigma = 0$ and $Dt = D\tau = 0$, identical eigenvalues (cubic) should be obtained from both sets of energy matrices. Secondly, if we set $Dq = 0$ with $Ds = D\sigma = Df$ and $Dt = D\tau = Dt$ and for the same set of A, B, C parameters, the same set of eigenvalues (cylindrical) should result from cylindrical, quadrate, and trigonal energy matrices. The first procedure provides a check on our calculations of the cubic ligand field and electron correlation elements, whereas the second checks the electron correlation and axial ligand field elements. The suggested methods have been applied to the energy matrices listed in Appendices B and C, and no inconsistencies were found.

III. Conclusions

The energy matrices presented in this paper provide the counterpart of the cubic matrices of Tanabe and Sugano for the noncubic fields. For accurate interpretation of the spectral data of quadrate, trigonal, and cylindrical systems of d^3 configuration, these energy matrices which include full configuration interaction should be used. It should be noted that the quadrate and trigonal energy matrices as given are useful for treating tetragonal and trigonal perturbations over octahedral fields of d^3 and tetrahedral fields of d^7 configuration (positive values of Dq with appropriate values for B and C parameters) and also over the tetrahedral fields of d^3 and octahedral fields of d^7 configuration (negative values of Dq with appropriate values of B and C). The cylindrical energy matrices are useful for

(32) (a) H. A. Bethe, *Ann. Physik*, **3**, 133 (1929). A complete English translation of this article is available from Consultants Bureau, New York, N. Y. (b) See also ref 2c.

(33) Derivation of unitary transformations connecting the three descriptive processes outlined above for noncubic fields is shown in Appendix D by considering the quadrate quartets as examples.

(34) (a) Y. Tanabe and S. Sugano, *J. Phys. Soc. Japan*, **9**, 753 (1954); (b) *ibid.*, **9**, 766 (1954).

(35) As the $^4A_2{}^Q$ is a 2×2 matrix, it can be easily solved for the energy equations. These are $^1/_2\{(6Dq + 2Ds + 6Dt - 15B) \pm [(10Dq - 6Ds + 10Dt - 9B)^2 + (12B)^2]^{1/2}\}$ or $^1/_2\{(6Dq + 2Ds + 6Dt - 15B) \pm [(10Dq - 6Ds + 10Dt - 15B)^2 + 12B(10Dq - 6Ds + 10Dt)]^{1/2}\}$.

(36) The same conclusion, namely, that an absorption band in the tetragonal system should be positioned at $10Dq$ of the corresponding octahedral band, could be drawn for other d^n configurations where $n = 1$ ($^2B_2$ ground state), 4 ($^5B_1$ ground state), 6 ($^5B_3$ ground state), 8 ($^3B_1$ ground state), and 9 ($^2B_1$ ground state). Good examples for a verification of this prediction will be to study the optical spectra of octahedral as well as a series of monosubstituted and *trans*-disubstituted complexes of Ti(III), V(IV), Cr(II), Mn(III), Fe(II), Co(III), Ni(II), and Cu(II).

(37) See part II of this series and also (a) W. B. Schaap, R. Krishnamurty, D. K. Wakefield, and J. R. Perumareddi, Abstracts, IXth International Conference on Coordination Chemistry, Switzerland, Sept 1966; (b) R. Krishnamurty, W. B. Schaap, and J. R. Perumareddi, *Inorg. Chem.*, **6**, 1338 (1967).

treating linear systems of d^3 and d^7 configurations. At zero Dq value in both quadrate and trigonal sets, the energy levels are characterized by the cylindrical labels and, hence, the cylindrical energy matrices can be used to deduce the corresponding eigenfunctions. Energy level plots can be obtained in both quadrate and trigonal fields by fixing B, C, $D\nu$ and $D\mu/D\nu$ ($\equiv\kappa$) and varying Dq, over the range of 0 to 4000 cm^{-1}. The resulting plots assume the form of well-known Tanabe–Sugano cubic plots, but now the doubly and triply degenerate (orbitally) cubic levels will be split into two each in quadrate, and in trigonal only the triply degenerate cubic levels will be split into two (*vide infra*). Similar energy plots can be constructed, of course, by varying κ, the ratio of the axial ligand field parameters and likewise, for different values of $D\nu$. Energy levels of cylindrical systems can be derived as functions of Dt by fixing all the other parameters since Dq is zero.

In the case of quadrate symmetry, some interesting conclusions can be drawn from the quartet energy matrices. As we already know, the various quartets in quadrate fields[35] are $^4B_1{}^Q[^4A_{2g}{}^C(t_{2g}{}^3)]$, $^4B_2{}^Q[^4T_{2g}{}^C(t_{2g}{}^2e_g)]$, $^4A_2{}^Q[^4T_{1g}{}^C(t_{2g}{}^2e_g)]$, $^4A_2{}^Q[^4T_{1g}{}^C(t_{2g}e_g{}^2)]$ and three of $^4E^Q$ corresponding to the last three levels. The difference in energy between the $^4B_2{}^Q[^4T_{2g}{}^C(t_{2g}{}^2e_g)]$ and $^4B_1{}^Q[^4A_{2g}{}^C(t_{2g}{}^3)]$ levels is still given by $10Dq$. This result is exact including configuration interaction since these two levels are 1×1 matrices. This means that as long as the ground state is $^4B_1{}^Q[^4A_{2g}{}^C(t_{2g}{}^3)]$ [this is true if $(10Dq + 12B) \gtrsim -(4Ds + 5Dt)$], we still expect in the tetragonally distorted (or substituted) octahedral d^3 systems a band ($^4B_2{}^Q$) positioned at $10Dq$, *i.e.*, at the same energy as the $^4T_{2g}$ band of the corresponding octahedral complex.[36] The $^4E^Q$ component of the $^4T_{2g}$ cubic band will then be placed either on the higher or lower energy side of $^4B_2{}^Q$ depending upon whether the Dt is positive (axial compression or substitution by a higher field ligand) or negative (axial elongation or substitution by a lower field ligand). This interesting conclusion suggests another means of constructing useful energy diagrams. If we fix Dq along with A, B, C and κ for a particular octahedral system of d^3 configuration and vary Dt in an energy diagram, such a plot will be useful in the interpretation of the spectral data of a variety of monosubstituted and *trans*-disubstituted derivatives of that particular octahedral system. Such energy plots will be shown where they are applicable in the future papers on applications of our calculations to experimental situations.[37]

A similar result can be deduced for trigonal fields in a special case when $3D\sigma = 5D\tau$. Under these conditions, the $^4A_2{}^T[^4A_{2g}{}^C(t_{2g}{}^3)]$ level does not interact configurationally with the other two $^4A_2{}^T$ levels (*cf.* quartet trigonal matrices of Appendix C) with the result that the energy separation of this ground level and the excited state $^4A_1{}^T[^4T_{2ga}{}^C(t_{2g}{}^2e_g)]$ is given by $10Dq$. Also, the energy equations of the other $^4A_2{}^T$ states in this special circumstance are found to be

$$\tfrac{1}{2}\{(6Dq - 15B + {}^{28}/_3 D\tau) \pm [(10Dq - 9B)^2 + (12B)^2]^{1/2}\}$$

or

$$\tfrac{1}{2}\{(6Dq - 15B + {}^{28}/_3 D\tau) \pm [(10Dq - 15B)^2 + 12B(10Dq)]^{1/2}\}$$

Acknowledgments. Many valuable conversations and discussions with Dr. Andrew D. Liehr on the theory of noncubic ligand fields in general have given the author the stimulation to carry out the work presented in this report. For this, the author is greatly indebted to him. The author wishes to thank Drs. E. W. Baker, R. Krishnamurty, and S. T. Spees, Jr., respectively, of the Mellon Institute, the Indiana University, and the University of Minnesota, for kindly reading and commenting on the manuscript.

Appendix C[19]

Quartet Energy Matrices of d^3 Configuration

Quadrate Fields

$^4B_1{}^Q$	$^4A_{2g}{}^C(t_{2g}{}^3)$	$^4B_2{}^Q$	$^4T_{2ga}{}^C(t_{2g}{}^2e_g)$
$^4A_2{}^C(t_{2g}{}^3)$	$-12Dq - 7Dt$ $+3A - 15B - E$	$^4T_{2ga}{}^C(t_{2g}{}^2e_g)$	$-2Dq - 7Dt$ $+3A - 15B - E$
$^4A_2{}^Q$	$^4T_{1ga}{}^C(t_{2g}{}^2e_g)$		$^4T_{1ga}{}^C(t_{2g}e_g{}^2)$
$^4T_{1ga}{}^C(t_{2g}{}^2e_g)$	$-2Dq + 4Ds - 2Dt$ $+3A - 3B - E$		$+6B$
$^4T_{1ga}{}^C(t_{2g}e_g{}^2)$			$8Dq - 2Ds + 8Dt$ $+3A - 12B - E$
$^4E^Q$	$^4T_{2gb}{}^C(t_{2g}{}^3e_g)$	$^4T_{1gb}{}^C(t_{2g}{}^2e_g)$	$^4T_{1gb}{}^C(t_{2g}e_g{}^2)$
$^4T_{2gb}{}^C(t_{2g}{}^2e_g)$	$-2Dq + {}^7/_4 Dt$ $+3A - 15B - E$	$-\frac{\sqrt{3}}{4}(4Ds + 5Dt)$	0
$^4T_{1gb}{}^C(t_{2g}{}^2e_g)$		$-2Dq - 2Ds - {}^3/_4 Dt$ $+3A - 3B - E$	$+6B$
$^4T_{1gb}{}^C(t_{2g}e_g{}^2)$			$8Dq + Ds + 3Dt$ $+3A - 12B - E$

Trigonal Fields

	$^4A_1{}^T$	$^4T_{2g}{}^C(t_{2g}{}^2e_g)$	
	$^4T_{2g}{}^C(t_{2g}{}^2e_g)$	$-2Dq + D\sigma + 3D\tau$ $+3A - 15B - E$	

	$^4A_2{}^T$	$^4A_{2g}{}^C(t_{2g}{}^3)$	$^4T_{1g}{}^C(t_{2g}{}^2e_g)$	$^4T_{1g}{}^C(t_{2g}e_g{}^2)$
$^4A_{2g}{}^C(t_{2g}{}^3)$		$^2/_3(-18Dq + 7D\tau)$ $+3A - 15B - E$	$^2/_3(3D\sigma - 5D\tau)$	0
$^4T_{1g}{}^C(t_{2g}{}^2e_g)$			$-2Dq + D\sigma + 3D\tau$ $+3A - 3B - E$	$^2/_3(3D\sigma - 5D\tau)$ $+6B$
$^4T_{1g}{}^C(t_{2g}e_g{}^2)$				$^2/_3(12Dq + 3D\sigma + 2D\tau)$ $+3A - 12B - E$

	$^4E^T$	$^4T_{2g}{}^C(t_{2g}{}^2e_g)$	$^4T_{1g}{}^C(t_{2g}{}^2e_g)$	$^4T_{1g}{}^C(t_{2g}e_g{}^2)$
$^4T_{2g}{}^C(t_{2g}{}^2e_g)$		$-^1/_6(12Dq + 3D\sigma + 2D\tau)$ $+3A - 15B - E$	$-^1/_6(9D\sigma + 20D\tau)$	$-^1/_3(3D\sigma - 5D\tau)$
$^4T_{1g}{}^C(t_{2g}{}^2e_g)$			$-^1/_6(12Dq + 3D\sigma + 2D\tau)$ $+3A - 3B - E$	$-^1/_3(3D\sigma - 5D\tau)$ $+6B$
$^4T_{1g}{}^C(t_{2g}e_g{}^2)$				$^1/_3(24Dq - 3D\sigma - 16D\tau)$ $+3A - 12B - E$

Cylindrical Fields

	$^4\Phi$	^4F	$^4\Delta$	^4F
^4F		$D\mathfrak{f} + 3Dt$ $+3A - 15B - E$	^4F	$-7Dt$ $+3A - 15B - E$

	$^4\Pi$	^4F	^4P
^4F		$-^1/_5(3D\mathfrak{f} - 5Dt)$ $+3A - 15B - E$	$-\frac{\sqrt{6}}{5}(4D\mathfrak{f} + 5Dt)$

	$^4\Pi$	^4F	^4P
^4P			$-^7/_5D\mathfrak{f}$ $+3A - E$

	$^4\Sigma^-$	^4F	^4P
^4F		$^2/_5(-2D\mathfrak{f} + 15Dt)$ $+3A - 15B - E$	$-^4/_5(3D\mathfrak{f} - 5Dt)$
^4P			$^{14}/_5D\mathfrak{f}$ $+3A - E$

Appendix D

Weak-Field, Weak Axial Strong-Field, and Strong Axial Strong-Field Conjunctive Relations. We shall consider only the quartets of d^3 configuration in quadrate fields to show the confluence of the three descriptive processes. The conjugative algebra can be carried out by expanding the separate basis vectors, the one in terms of the other. The derivation of the transformation matrices conjoining the weak-field and weak axial strong-field schemes of quadrate (or trigonal) symmetry is a simple process if the corresponding weak-field, strong-field transformation matrices of cubic fields are known. Since octahedral orientation is kept in weak axial field description, the derivation involves merely combining transformation matrices of those cubic representations belonging to the same quadrate representation. Thus the following matrices connect the weak-field and weak axial strong-field processes.

	$^4B_1{}^Q[^4A_{2g}(^4F)]$	$^4B_1{}^Q[^4A_{2g}(t_{2g}{}^3)]$	$^4B_2[^4T_{2g}(^4F)]$	$^4B_2{}^Q[^4T_{2g}(t_{2g}{}^2e_g)]$
$^4B_1{}^Q[^4A_{2g}(^4F)]$		$+i$		$+i$

	$^4A_2{}^Q[^4T_{1g}(^4F)]$	$^4A_2{}^Q[^4T_{1g}(t_{2g}{}^2e_g)]$	$^4A_2{}^Q[^4T_{1g}(t_{2g}e_g{}^2)]$
$^4A_2{}^Q[^4T_{1g}(^4F)]$	$-i/\sqrt{5}$	$+2i/\sqrt{5}$	
$^4A_2{}^Q[^4T_{1g}(^4P)]$	$+2i/\sqrt{5}$	$+i/\sqrt{5}$	

	$^4E^Q[^4T_{2g}(^4F)]$	$^4E^Q[^4T_{2g}(t_{2g}{}^2e_g)]$	$^4E^Q[^4T_{1g}(t_{2g}{}^2e_g)]$	$^4E^Q[^4T_{1g}(t_{2g}e_g{}^2)]$
$^4E^Q[^4T_{2g}(^4F)]$		$+i$	0	0
$^4E^Q[^4T_{1g}(^4F)]$		0	$-i/\sqrt{5}$	$+2i/\sqrt{5}$
$^4E^Q[^4T_{1g}(^4P)]$		0	$+2i/\sqrt{5}$	$+i/\sqrt{5}$

Corresponding transformation matrices connecting the weak axial strong-field and strong axial strong-field schemes are shown to be {Note that the symmetry adapted basis functions in the latter scheme are

$$^4B_1{}^Q(e_g{}^2b_{2g}) = |(zx)(yz)(xy)| \qquad ^4A_2{}^Q(e_g{}^2a_{1g}) = |(zx)(yz)(z^2)|$$
$$^4B_2{}^Q(e_g{}^2b_{1g}) = |(zx)(yz)(x^2-y^2)| \qquad ^4A_2{}^Q(b_{2g}a_{1g}b_{1g}) = |(xy)(z^2)(x^2-y^2)|$$
$$^4E_a{}^Q(e_gb_{2g}a_{1g}) = |(yz)(xy)(z^2)| \qquad ^4E_b{}^Q(e_gb_{2g}a_{1g}) = |(zx)(xy)(z^2)|$$
$$^4E_a{}^Q(e_gb_{2g}b_{1g}) = |(yz)(xy)(x^2-y^2)| \qquad ^4E_b{}^Q(e_gb_{2g}b_{1g}) = -|(zx)(xy)(x^2-y^2)|$$
$$^4E_a{}^Q(e_ga_{1g}b_{1g}) = |(zx)(z^2)(x^2-y^2)| \qquad ^4E_b{}^Q(e_ga_{1g}b_{1g}) = -|(yz)(z^2)(x^2-y^2)|\}$$

$$\begin{array}{c|c|c|c|c|} & ^4B_1{}^Q(e_g{}^2b_{2g}) & & ^4B_2{}^Q(e_g{}^2b_{1g}) \\ ^4B_1{}^Q[^4A_{2g}(t_{2g}{}^3)] & +1 & ^4B_2{}^Q[^4T_{2g}(t_{2g}{}^2e_g)] & +1 \end{array}$$

$$\begin{array}{c|c|c|} & ^4A_2{}^Q(e_g{}^2a_{1g}) & ^4A_2{}^Q(b_{2g}a_{1g}b_{1g}) \\ ^4A_2{}^Q[^4T_{1g}(t_{2g}{}^2e_g)] & +1 & 0 \\ ^4A_2{}^Q[^4T_{1g}(t_{2g}e_g{}^2)] & 0 & +1 \end{array}$$

$$\begin{array}{c|c|c|c|} & ^4E^Q(e_gb_{2g}a_{1g}) & ^4E^Q(e_gb_{2g}b_{1g}) & ^4E(e_ga_{1g}b_{1g}) \\ ^4E^Q[^4T_{2g}(t_{2g}{}^2e_g)] & \sqrt{3}/2 & -1/2 & 0 \\ ^4E^Q[^4T_{1g}(t_{2g}{}^2e_g)] & -1/2 & -\sqrt{3}/2 & 0 \\ ^4E^Q[^4T_{1g}(t_{2g}e_g{}^2)] & 0 & 0 & 1 \end{array}$$

Similar algebraic procedures yield the following connections between the weak-field and strong axial strong-field coupling schemes. It should be noted that these matrices can be independently gotten by merely multiplying the respective transformation matrices of the above two schemes.

$$\begin{array}{c|c|c|c|c|} & ^4B_1{}^Q(e_g{}^2b_{2g}) & & ^4B_2{}^Q(e_g{}^2b_{1g}) \\ ^4B_1{}^Q[^4A_{2g}(^4F)] & +i & ^4B_2{}^Q[^4T_{2g}(^4F)] & +i \end{array}$$

$$\begin{array}{c|c|c|} & ^4A_2{}^Q(e_g{}^2a_{1g}) & ^4A_2{}^Q(b_{2g}a_{1g}b_{1g}) \\ ^4A_2{}^Q[^4T_{1g}(^4F)] & -i/\sqrt{5} & +2i/\sqrt{5} \\ ^4A_2{}^Q[^4T_{1g}(^4P)] & +2i/\sqrt{5} & +i/\sqrt{5} \end{array}$$

$$\begin{array}{c|c|c|c|} & ^4E^Q(e_gb_{2g}a_{1g}) & ^4E^Q(e_gb_{2g}b_{1g}) & ^4E^Q(e_ga_{1g}b_{1g}) \\ ^4E^Q[^4T_{2g}(^4F)] & +i/\sqrt{3}/2 & -i/2 & 0 \\ ^4E^Q[^4T_{1g}(^4F)] & +i/2\sqrt{5} & +i/2\sqrt{3/5} & +2i/\sqrt{5} \\ ^4E^Q[^4T_{1g}(^4P)] & -i/\sqrt{5} & -i\sqrt{3/5} & +i/\sqrt{5} \end{array}$$

It can be seen in this particular configuration no difference prevails between weak axial strong-field and strong axial strong-field descriptions with respect to the B_1, B_2, and A_2 representations. The case of B_1 and B_2 representations is a general result as these are one by one matrices and hence cannot be different, whatever be the coupling scheme. The case of A_2 representation is obvious from the energy matrix where the off-diagonal matrix element does not contain the axial field parameters in the former scheme also. However, difference does exist for the ^4E matrix as it contains nonvanishing off-diagonal elements in axial field parameters in weak axial strong-field scheme, which are now diagonalized in the strong axial strong-field scheme. This, of course, results in more of nonvanishing off-diagonal elements in electron correlations as can be seen from the following energy matrix.

$^4E^g$	$(e_g b_{2g} a_{1g})$	$(e_g b_{2g} b_{1g})$	$(e_g a_{1g} b_{1g})$
$(e_g b_{2g} a_{1g})$	$-2Dq + Ds + 3Dt$ $+3A - 12B - E$	$3\sqrt{3}B$	$-3B$
$(e_g b_{2g} b_{1g})$		$-2Dq - 3Ds - 2Dt$ $+3A - 6B - E$	$-3\sqrt{3}B$
$(e_g a_{1g} b_{1g})$			$8Dq + Ds + 3Dt$ $+3A - 12B - E$

Both the A_2 and E energy matrices of the weak-field scheme differ from those of the weak axial and strong axial strong-field schemes. They are also listed here for comparison with the ^4E matrix given above and the $^4A_2$ and ^4E matrices given in Appendix C.

$^4A_2{}^g$	$^4T_{1g}(^4F)$	$^4T_{1g}(^4P)$
$^4T_{1g}(^4F)$	$^2/_5(15Dq - 2Ds + 15Dt)$ $+3A - 15B - E$	$^4/_5(5Dq - 3Ds + 5Dt)$
$^4T_{1g}(^4P)$		$^{14}/_5Ds + 3A - E$

$^4E^g$	$^4T_{2g}(^4F)$	$^4T_{1g}(^4F)$	$^4T_{1g}(^4P)$
$^4T_{2g}(^4F)$	$^1/_4(-8Dq + 7Dt)$ $+3A - 15B - E$	$\frac{\sqrt{5}}{20}(4Ds + 5Dt)$	$-^1/_2\sqrt{\frac{3}{5}}(4Ds + 5Dt)$
$^4T_{1g}(^4F)$		$^1/_{20}(120Dq + 8Ds + 45Dt)$ $+3A - 15B - E$	$^1/_{10}(40Dq + 12Ds + 15Dt)$
$^4T_{1g}(^4P)$			$-^7/_5Ds + 3A - E$

Ligand Field Theory of d^3 and d^7 Electronic Configurations in Noncubic Fields. II. Applications to Quadrate Chromium(III) Complexes[1,2]

by Jayarama R. Perumareddi

Mellon Institute, Pittsburgh, Pennsylvania 15213 *(Received November 7, 1966)*

The quadrate energy matrices of d^3 configuration derived by us earlier have been solved for suitable sets of parametric values and appropriate energy diagrams constructed to interpret the spectra of various monosubstituted and *trans*-disubstituted complexes of chromium(III). It has been concluded that at the present time there is no unique way of assigning all the observed bands in the systems considered. In all the complexes discussed, the first spin-allowed cubic band splits into two components which are given the definitive quadrate assignments, and the corresponding Dt values are evaluated. As the second spin-allowed cubic band does not split in most of these systems, alternative quadrate assignments have been found possible for different choices of values of B and κ parameters. It is suggested that further measurements of spectra of these and similar systems be made particularly on single crystals by means of polarized light and at low temperatures to verify our choices of assignations. Use of our calculations and energy diagrams for the study of the quadrate complexes of the d^3 configuration, other than Cr(III), and also of the d^7 configuration has been pointed out. It is emphasized however, that it is necessary to take into account full configuration interaction even at the initial stages of applications of theory without resorting to any approximations.

I. Introduction

In the previous paper,[2] we have presented a detailed account of the theory of d^3 and d^7 electronic configurations in quadrate, trigonal, and cylindrical fields, where the symmetry adapted strong-field wave functions were derived and the energy matrices constructed as functions of Dq, and $D\mu$, $D\nu$, the cubic and axial ligand field parameters, and A, B, C, the Racah electron correlation parameters. Spin-orbit interaction has not been included.[3]

It is the purpose of this paper to apply our quadrate calculations for the interpretation of the optical studies of d^3 systems as exemplified by the substituted chromium(III) complexes belonging to quadrate symmetry. As has been pointed out in part I, these systems will be treated as deviations from cubic symmetry.

II. Theoretical Digression

Parameters. It has been shown that in the quadrate fields all the parameters with the exception of Ds and Dt are the same as those that occur in cubic fields. Although the axial parameters Ds and Dt are used in our present work as empirical parameters just as are the other cubic parameters in ligand field theory, it is instructive to examine these parameters in the limit of crystalline field theory. In quadrate fields, we will be concerned with either a monosubstituted octahedral or a pentacoordinate square pyramidal system both belonging to C_{4v} symmetry, or a *trans*-disubstituted octahedral or a tetracoordinate square planar system both belonging to D_{4h} symmetry. If the quadrate potential V_Q is expressed as a sum of cubic, V_C, and the axial, V_∞, fields, then

$$V_Q = V_C + V_\infty \quad (1)$$

For a six-coordinate octahedral system

(1) Presented at the 151st National Meeting of the American Chemical Society, Pittsburgh, Pa., March 1966.

(2) See preceding paper for part I: J. R. Perumareddi, *J. Phys. Chem.*, **71**, 3144 (1967).

(3) The available data on the spectra of substituted octahedral chromium(III) complexes have been obtained from a study of absorption spectra in solution giving rise to broad bands with low resolution. Hence, inclusion of spin-orbit interaction in our calculations at this stage is not warranted.

$$V_C = V_{Oh} = eqR_4(r)\sqrt{\frac{4\pi}{9}}\left[\frac{7}{2}Y_4^0 + \frac{\sqrt{35}}{2}Y_4^{4c}\right] \quad (2)$$

where the e and q are the electronic charge and the effective charge of the ligand, respectively, $R_4(r) = r_<^4/r_>^5$, $r_<$ and $r_>$ being the lesser and greater of the electronic radius and bond distance, and Y_4^{4c} is the cosine combination of Y_4^4 and Y_4^{-4}, *i.e.*, $Y_4^{4c} = 1/\sqrt{2}\,(Y_4^4 + Y_4^{-4})$.

The generalized axial potential is given by

$$V_\infty = eq'\left[R_2(r)\sqrt{\frac{4\pi}{5}}Y_2^0 + R_4(r)\sqrt{\frac{4\pi}{9}}Y_4^0\right] \quad (3)$$

where $R_2(r) = r_<^2/r_>^3$ and all others are the same as above.

From the definitions[4]

$$Dq = \langle 2, \pm 2|V_{Oh}|\pm 2, 2\rangle = \frac{1}{6}eq\langle R_4(r)\rangle$$

$$Dt = \langle 2, \pm 2|V_\infty(Y_4^0)|\pm 2, 2\rangle = \frac{1}{21}eq'\langle R_4(r)\rangle$$

$$Ds = \langle 2, \pm 1|V_\infty(Y_2^0)|\pm 1, 2\rangle = \frac{1}{7}eq'\langle R_2(r)\rangle \quad (4)$$

it follows that

$$\kappa \equiv Ds/Dt = 3\langle R_2(r)\rangle/\langle R_4(r)\rangle$$

where

$$\langle R_l(r)\rangle = \int_0^\infty R_{kd}(r)^2(r_<^l/r_>^{l+1})r^2dr$$

The radial integrals $\langle R_2(r)\rangle$ and $\langle R_4(r)\rangle$ can be evaluated if the radial wave functions, $R_{kd}(r)$, and the bond distances are known. In a few cases, such an evaluation has been carried out[5] using hydrogenic, Slater, and Hartree–Fock functions with the result that their ratio comes out to be 4 to 5. On the other hand, they can be obtained as empirical parameters by fitting the experimental spectral data where it is possible. This has been attempted in the case of copper(II) complexes where this ratio has been found to be[6] approximately unity. A value of unity can be obtained by a theoretical calculation if a reduced bond distance is used.[5c,d] With this value of unity, κ turns out to be 3. As already noted, we shall adjust these parameters empirically.

Energy Diagrams. We have shown previously[2] that in quadrate fields the transition energy $^4B_1{}^Q$. $[^4A_{2g}{}^C(t_{2g}{}^3)] \rightarrow {}^4B_2{}^Q[^4T_{2g}{}^C(t_{2g}{}^2e_g)]$ is given by $10Dq$ including configuration interaction. This means that the $^4B_2$ component in both mono- and *trans*-disubstituted systems should remain positioned at the frequency of the parent octahedral $^4T_{2g}$ band. The $^4E^Q$ component would then be placed either on the higher or on the lower energy side of the $^4B_2$ band depending upon whether the substituting ligand is of higher or of lower ligand field strength than that of the original ligand. Accordingly, it is possible to fix the value of Dq appropriate to an octahedral complex and to construct an energy diagram as a function of Dt parameter. Such plots are useful for the interpretation of the optical spectra of the substituted tetragonal derivatives of the parent complex. Figures 1 and 2 show the energy level diagrams[7] in the range of Dt, 0 to ± 2000 cm^{-1}. We have chosen a Dq value of 2155 cm^{-1} which corresponds to that of the hexaammine Cr(III) complex so that these diagrams can be employed for the interpretation of the spectra of acidopentaammines and *trans*-diacidobisethylenediammines[8] of Cr(III). Note that these diagrams are also appropriate to describe the energy levels of a quadrately distorted (compressed or elongated) tetrahedral d^7 complex of $Dq = 2155$ cm^{-1}.

Several points may be noted from these energy diagrams. As expected, the $^4B_2{}^Q$ component of $^4T_{2g}$ is a parallel level to the $^4B_1{}^Q(^4A_{2g})$ state separated by $10Dq$. The energy levels at zero Dt value correspond to levels of parent cubic complex (hexaammine); *i.e.*, they correspond to a one-dimensional cross section of Tanabe–Sugano octahedral plot at a Dq value of 2155 cm^{-1}. At both ends of the diagrams are given the quadrate labels with no g subscripts along with their octahedral parentage. These are true as given for C_{4v}, but they are to be supplemented with g subscripts for

(4) From these definitions, some simple relations among these parameters can be derived for C_{4v} and D_{4h} systems in the limit of crystalline field formalism. If the parent octahedral complex is MX_6, for the case of MX_5Y and MX_5 belonging to C_{4v}, we may write the axial field as that due to $(-X + Y)$ and $(-X)$, respectively. Substitution of the corresponding charges in the definitions give rise to $Dt = {}^1/_{21}(-q_x + q_y)e\langle R_4(r)\rangle = -{}^2/_7(Dq_x - Dq_y)$ for monosubstituted and $Dt = {}^1/_{21}(-q_x)e\langle R_4(r)\rangle = -{}^2/_7 \cdot Dq_x$ for pentacoordinate square pyramid. Similar relations for *trans*-disubstituted MX_4Y_2 and square planar MX_4 systems can be found. These are: $Dt = -{}^4/_7(Dq_x - Dq_y)$ and $Dt = -{}^4/_7Dq_x$, respectively. (Note that in the derivation of these formulas, substitution of $eq\langle R_4(r)\rangle = 6Dq$ implies the assumption that the Dq of an octahedral complex is made up of six *equal* contributions from its six ligands.)

(5) (a) D. S. McClure, *J. Chem. Phys.*, **36**, 2757 (1962); (b) H. A. Weakliem, *ibid.*, **36**, 2117 (1962); (c) T. S. Piper and R. L. Carlin, *ibid.*, **33**, 1208 (1960); (d) J. R. Perumareddi, unpublished results.

(6) (a) W. E. Hatfield and T. S. Piper, *Inorg. Chem.*, **3**, 841 (1964); (b) P. Day, *Proc. Chem. Soc.*, 18 (1964).

(7) All of our energy matrices were solved and energy levels were plotted on the IBM 7090 computer at the University of Pittsburgh Computer Center. Energy diagrams have been plotted on a Calcomp Plotter through IBM 1401, which is fed by a magnetic tape from IBM 7090. For the sake of simplicity, only the quartet and the lower energy doublet states are shown in these energy diagrams.

(8) Although the Dq value of trisethylenediammine complex is 2185 cm^{-1}, we have not constructed energy diagrams suitable for this value, since it does not differ much from 2155 cm^{-1}. On the other hand, the energy diagrams of this paper have been used to estimate the transition energies only for the acidopentaammines, whereas special runs have been made for particular sets of parameters for *trans*-diacidobisethylenediammines and other miscellaneous systems.

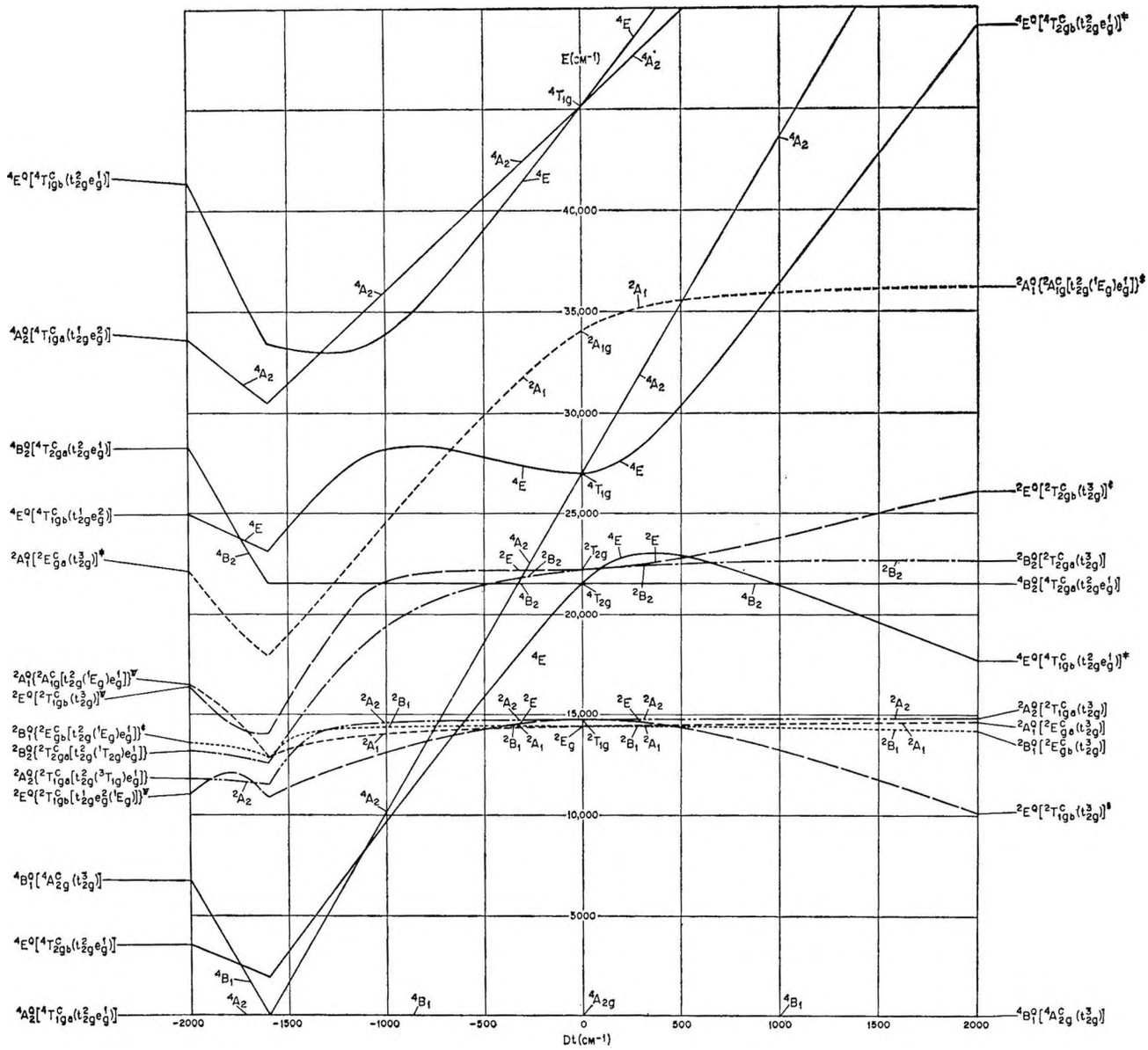

Figure 1. Energy level diagram for d^3 configuration in quadrate fields: $\zeta = 0$, $B = 500$ cm^{-1}, $C/B = 7$, $Dq = 2155$ cm^{-1}, $\kappa = 3$. At both ends of the diagram are given the strong-field configurational labels. At the center of the diagram, $Dt = 0$ refers to octahedral levels. The quadrate designations as given are true for C_{4v} symmetry. They have to be supplemented with g subscripts for D_{4h} symmetry. Quartets are drawn in solid lines and the doublets are distinguished by various kinds of broken lines. The superscripts on the energy labels refer to the per cent of that eigenvector component of the eigenfunction. The various symbols have the following meaning: §, 75 ± 2.5%; ‡, 70 ± 2.5%; ‡, 65 ± 2.5%; $, 60 ± 2.5%; ¢, 55 ± 2.5%; P, 50 ± 2.5%; ¥, 45 ± 2.5%; #, 40 ± 2.5%; V, 35 ± 2.5%.

D_{4h} symmetry. The negative side of these plots is applicable to either an elongated octahedron or to systems derived by substitution of low-field ligands and the positive side to either a compressed octahedron or to systems derived by substitution of high-field ligands.

For low negative values of Dt and Ds, the quadrate components of the first two cubic quartets will be $^4E < {}^4B_2 < {}^4A_2 < {}^4E$, in the order of increasing energy. Since the splitting of the second quartet and the positions of its components depend on the values of B and κ (the splitting of the first band depends only on the value Dt and on the effect of configuration interaction), by a proper adjustment of these parameters, *e.g.*, by decreasing B and increasing κ, it is possible for negative values of Dt to bring down the $^4A_2$ component of $^4T_{1g}$ in energy closer to the $^4B_2$ component of $^4T_{2g}$. Such a

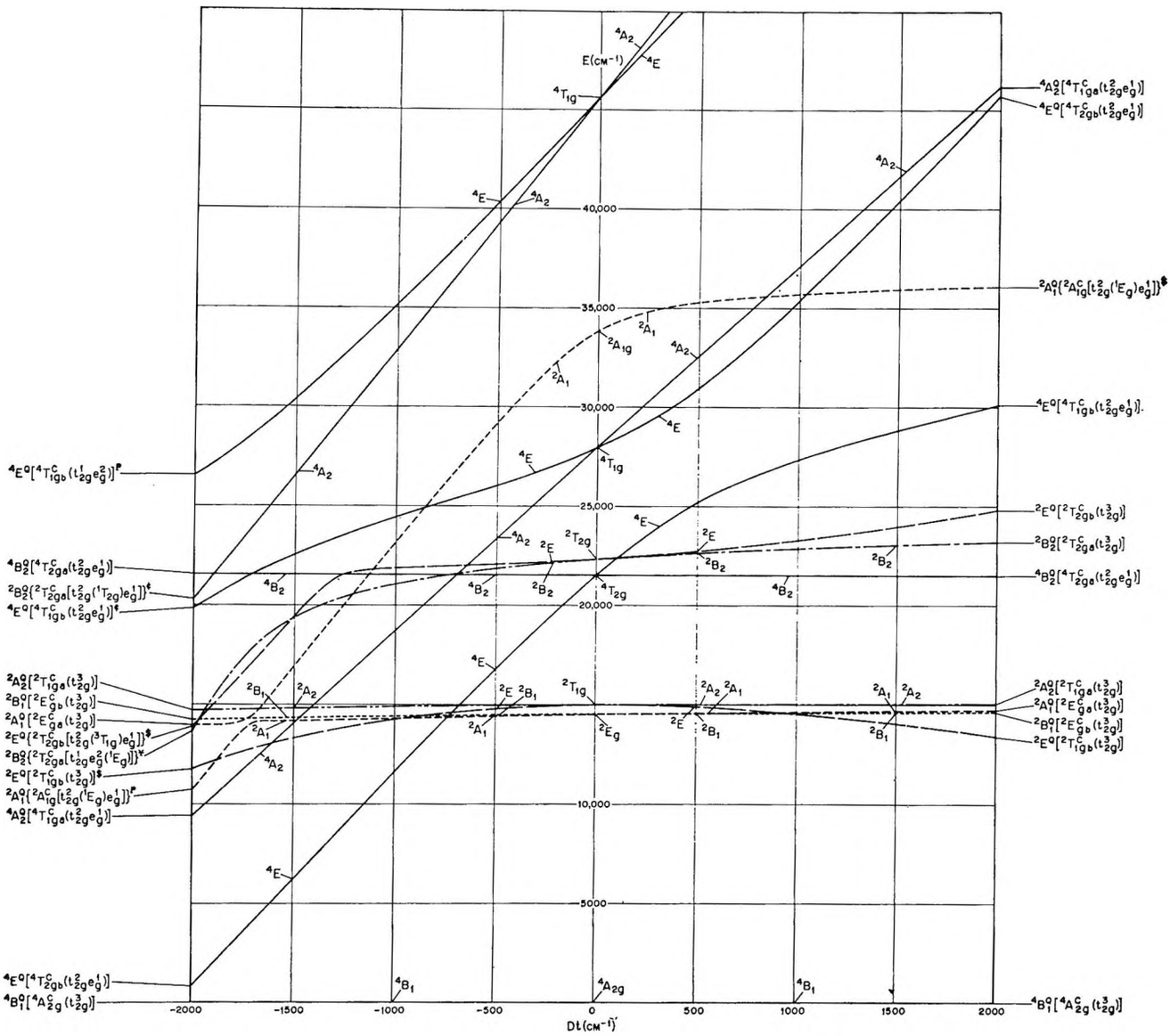

Figure 2. Energy level diagram for d^3 configuration in quadrate fields: $\zeta = 0$, $B = 600$ cm^{-1}, $C/B = 5.5$, $Dq = 2155$ cm^{-1}, $\kappa = 1$. [Read the caption of Figure 1 for further details.]

set of parameters may exist for some systems, thus making the $^4A_2$ and $^4B_2$ levels nearly degenerate with unresolvable separation so that these compounds may show only three spin-allowed transitions in their spectra instead of the usual four components of the two octahedral bands predicted by the theory. Likewise, a lower ratio of κ would not show observable splitting of the second band, thus once again predicting a three-banded spectra. Because of the former possible explanation, it is not safe to assume immediately that the ratio of axial parameters is small whenever splitting of the second quartet in quadrate systems is not observed. Thus, in the energy diagram with $\kappa = 1$ (Figure 2), the energy separation of the split components of the second quartet for all values of Dt between -300 and 2000 cm^{-1} is small and thus may not be observable in solution spectral studies.[9] In the energy diagram with $\kappa = 3$ (Figure 1) for a region of Dt around -300 cm^{-1}, the $^4A_2{}^Q$ component of the second quartet moves closer to the $^4B_2{}^Q$ and thus in systems where this set of parameter applies, one may still observe only a three-band spectra. The sharp reversal of the direction of the energy levels at the

(9) We have chosen unity as an example for a smaller value of κ. It could be less than 1, of course.

extreme end of the negative side of the energy plot with $\kappa = 3$ is due to change in the ground state; *i.e.*, for large negative Dt values, $(10Dq + 12B)$ becomes less than $\sim|(4Ds + 5Dt)|$ so that the $^4A_2{}^Q[^4T_{1g}(t_{2g}{}^2e_g)]$ level assumes the ground state. This situation is similar to the change of the magnetic ground state in cubic compounds of d^4, d^5, d^6, and d^7 configurations.[10]

Another important point to be noted is on the positive side of Dt. Because of the occurrence of levels of same symmetry designation in sequence, namely the ^4E components of the first two quartets, these two levels do not cross (the so-called noncrossing rule) and because of configuration interaction, the lower ^4E is depressed and the upper ^4E is raised in energy. So, for the systems which are represented by this region of the diagrams, one should not use diagonal elements only and conclude that the splitting of the first quartet is given by $^{35}/_4Dt$ and that of the second quartet by $(6Ds - {}^5/_4Dt)$. Indeed, it follows from the above reasoning as an obvious corrollary that for the same negative and positive values of Dt, the same amount of splitting of the first two quartets may not be expected. Because of configuration interaction, larger splittings are expected for a system of negative Dt than for a system of same positive Dt. Finally, for large values of Dt, both positive and negative, the representation used here, *i.e.*, the octahedral orientation, is not pure. For more on this, see part I.[2]

Although the doublets ^2E_g, $^2T_{1g}$, and $^2T_{2g}$ of $(t_{2g}{}^3)$ configuration do not appear to be split (from the diagonal elements of the energy matrices), they do so by a few tens of wavenumbers when configuration interaction is included. It is interesting to note that none of these doublets arising from the strong-field configuration $(t_{2g}{}^3)$ split in the first order as we go to lower symmetry such as quadrate (or trigonal). Thus, the $^2A_1{}^Q$ and $^2B_1{}^Q$ of $^2E_g{}^C(t_{2g}{}^3)$ and the $^2A_2{}^Q$ and $^2E^Q$ of $^2T_{1g}{}^C(t_{2g}{}^3)$ and $^2B_2{}^Q$ and $^2E^Q$ of $^2T_{2g}{}^C(t_{2g}{}^3)$ are all degenerate pairs, just as the $^2E_g{}^C$ and $^2T_{1g}{}^C$ of $(t_{2g}{}^3)$ configuration are in cubic fields. [Indeed because of this latter degeneracy in cubic fields, the $^2A_1{}^Q(^2E_g)$, $^2B_1{}^Q(^2E_g)$, $^2A_2{}^Q(^2T_{1g})$, and $^2E^Q(^2T_{1g})$ states are all degenerate in the first-order, their energy separation from the ground level being $(9B + 3C)$. The transition energy to the $^2B_2{}^Q(^2T_{2g})$ and $^2E^Q(^2T_{2g})$ levels from the ground state is $(15B + 5C)$]. It is the configuration interaction that can lift the otherwise first-order degeneracy of these doublet levels both in cubic and noncubic fields.[11]

III. Applications

Acidopentaammines. The spectra of chloro- and bromopentaammines were studied by diffuse reflectance

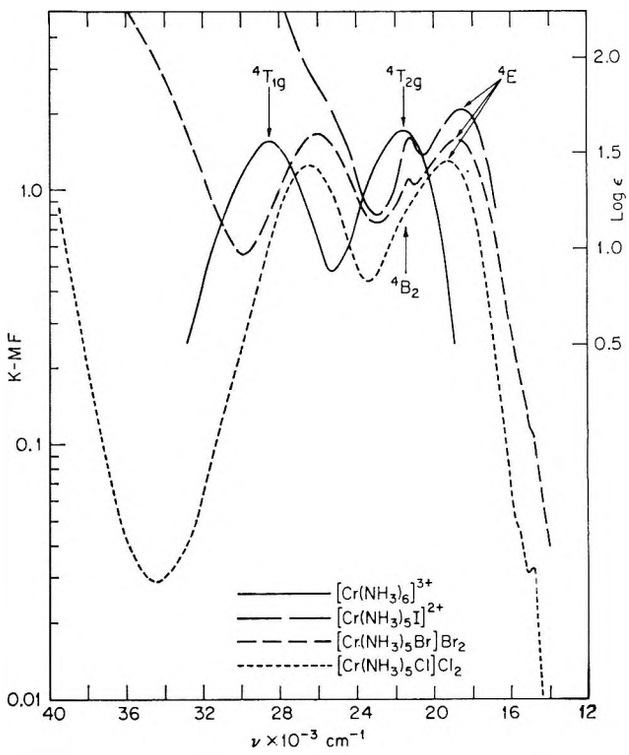

Figure 3. Spectra of hexaammine and acidopentaammines of Cr(III). [Extinction coefficient scale on the right of the figure refers to the hexaammine and iodopentaammine (ref 12). The K-M F on the left is Kubelka–Munk function which is given by a function of reflectance, $f(R) = (1 - R)^2/2R$, where R is the fraction reflectance and is roughly proportional to the extinction coefficient. The K-M F scale refers to the reflectance spectra of bromo- and chloropentaammines measured against LiF as white standard.]

measurements of pressed powders at room temperature against LiF as white standard on a Carl Zeiss PMQ II spectrophotometer. These spectra are given in Figure 3 along with the solution absorption spectra of iodopentaammine and hexaammine obtained by Linhard and Weigel.[12] These workers have also studied the solution absorption spectra of chloro- and bromopentaammines which agree with ours presented in the figure. We have achieved better resolution of the two-component system of the first cubic spin-allowed band in the bromopentaammine complex than that observed in its solution absorption spectrum. Such resolution was not achieved, however, in the spectrum of chloropenta-

(10) See, for instance, the corresponding Tanabe–Sugano plots: Y. Tanabe and S. Sugano, *J. Phys. Soc. Japan*, **9**, 766 (1954).

(11) See also (a) S. Sugano and Y. Tanabe, *Discussions Faraday Soc.*, **26**, 43 (1958); (b) Y. Tanabe and H. Kamimura, *J. Phys. Soc. Japan*, **13**, 394 (1958).

(12) M. Linhard and M. Weigel, *Z. Anorg. Allgem. Chem.*, **266**, 49 (1951).

Table I: Spectral Data of $Cr(NH_3)_5Cl^{2+}$

Obsd		Calcd ν_{max}; assignment	
		Dq = 2155 cm^{-1}, Dt = −225 cm^{-1}	
ν_{max} (log ϵ) (Ref 12)	ν_{max} (This work)	B = 600 cm^{-1}, C/B = 5.5, κ = 1	B = 500 cm^{-1}, C/B = 7, κ = 3
	14,800	14,478; $^2A_1(^2E_g)$ 14,496; $^2B_1(^2E_g)$	14,377; $^2A_1(^2E_g)$ 14,434; $^2B_1(^2E_g)$
	~15,500	14,921; $^2E(^2T_{1g})$ 14,958; $^2A_2(^2T_{1g})$	14,660; $^2E(^2T_{1g})$ 14,749; $^2A_2(^2T_{1g})$
		22,143; $^2B_2(^2T_{2g})$	21,960; $^2B_2(^2T_{2g})$
		22,280; $^2E(^2T_{2g})$	22,152; $^2E(^2T_{2g})$
19,400 (1.58)	19,200	19,482; $^4E(^4T_{2g})$	19,232; $^4E(^4T_{2g})$
(22,100) (0.90)	~21,400	21,550; $^4B_2(^4T_{2g})$	21,550; $^4B_2(^4T_{2g})$ 23,259; $^4A_2(^4T_{1g})$
26,600 (1.64)	26,400	25,918; $^4A_2(^4T_{1g})$ 27,054; $^4E(^4T_{1g})$	27,229; $^4E(^4T_{1g})$
		42,782; $^4A_2(^4T_{1g})$	42,288; $^4E(^4T_{1g})$
		43,264; $^4E(^4T_{1g})$	43,041; $^4A_2(^4T_{1g})$

Table II: Spectral Data of $Cr(NH_3)_5Br^{2+}$

Obsd		Calcd ν_{max}; assignment	
		Dq = 2155 cm^{-1}, Dt = −275 cm^{-1}	
ν_{max} (log ϵ) (Ref 12)	ν_{max} (This work)	B = 600 cm^{-1}, C/B = 5.5, κ = 1	B = 500 cm^{-1}, C/B = 7, κ = 3
	14,800	14,469; $^2A_1(^2E_g)$ 14,491; $^2B_1(^2E_g)$	14,364; $^2A_1(^2E_g)$ 14,435; $^2B_1(^2E_g)$
		14,902; $^2E(^2T_{1g})$ 14,954; $^2A_2(^2T_{1g})$	14,612; $^2E(^2T_{1g})$ 14,745; $^2A_2(^2T_{1g})$
		22,096; $^2B_2(^2T_{2g})$	21,889; $^2B_2(^2T_{2g})$
		22,175; $^2E(^2T_{2g})$	22,150; $^2E(^2T_{2g})$
19,050 (1.58)	18,800	19,000; $^4E(^4T_{2g})$	18,657; $^4E(^4T_{2g})$
21,770 (1.07)	21,300	21,550; $^4B_2(^4T_{2g})$	21,550; $^4B_2(^4T_{2g})$ 22,418; $^4A_2(^4T_{1g})$
26,490 (1.66)	26,000	25,458; $^4A_2(^4T_{1g})$ 26,866; $^4E(^4T_{1g})$	27,325; $^4E(^4T_{1g})$
		42,142; $^4A_2(^4T_{1g})$	41,668; $^4E(^4T_{1g})$
		42,733; $^4E(^4T_{1g})$	42,582; $^4A_2(^4T_{1g})$

ammine complex. Note that the low intensity doublets have also been discovered in both the chloropentaammine and bromopentaammine spectra. The doublet in the chloropentaammine spectrum is actually split into two components.

Tables I and II collect our spectral data on chloro- and bromopentaammines along with those obtained by Linhard and Weigel. The spectral data on iodopentammine are given in Table III. These tables also contain tentative assignments. All the complexes have absorption maxima around ~22,000 cm^{-1}, which is roughly the band maximum (21,550 cm^{-1}) of the $^4T_{2g}$ transition in the parent cubic hexaammine complex. This may be immediately assigned to the $^4B_2$ component so that the component on the low-energy side of this transition is the ^4E. From these two transitions, the Dt value can be derived by an exact fitting. These Dt values are also given in the tables. It may be noted that they are in the expected order.[13] Now the nonsplitting (or nonobservable splitting) of the second band can be explained on the basis of two values; *i.e.*, κ = 1 where the splitting is not observable in solution and κ = 3, where the $^4A_2{}^Q$ component of $^4T_{1g}(t_2{}^2ge_g)$ is placed close to $^4B_2{}^Q$ so that only one spin-allowed transition may still be seen at higher energy in solution spectrum. Both choices of assignments are included in

(13) Because of the similarity of the harmonic terms appearing in the definitions of Dq and Dt (as against Dq and Ds), it may be expected that a smooth relation may exist between Dq and Dt. Such a relation has been shown in the limit of crystalline field model (*cf.* footnote 4). Although this relation may not be exact, it seems to be a very good guideline in an *a priori* estimate of Dt, at least in the case of Cr(III) complexes. (See Addendum.)

Table III: Spectral Data of $Cr(NH_3)_5I^{2+}$

Obsd ν_{max} (log ϵ) (Ref 12)	Calcd ν_{max}; assignment Dq = 2155 cm^{-1}, Dt = −325 cm^{-1}, B = 600 cm^{-1}, C/B = 5.5, κ = 1	Calcd ν_{max}; assignment Dq = 2155 cm^{-1}, Dt = −325 cm^{-1}, B = 500 cm^{-1}, C/B = 7, κ = 3
	14,461; $^2A_1(^2E_g)$	14,349; $^2A_1(^2E_g)$
	14,487; $^2B_1(^2E_g)$	14,435; $^2B_1(^2E_g)$
	14,879; $^2E(^2T_{1g})$	14,556; $^2E(^2T_{1g})$
	14,951; $^2A_2(^2T_{1g})$	14,741; $^2A_2(^2T_{1g})$
	22,047; $^2B_2(^2T_{2g})$	21,811; $^2B_2(^2T_{2g})$
	22,151; $^2E(^2T_{2g})$	22,151; $^2E(^2T_{2g})$
18,500 (1.73)	18,513; $^4E(^4T_{2g})$	18,070; $^4E(^4T_{2g})$
21,250 (1.43)	21,550; $^4B_2(^4T_{2g})$	21,550; $^4B_2(^4T_{2g})$
		21,577; $^4A_2(^4T_{1g})$
~26,000 (1.70)?	24,998; $^4A_2(^4T_{1g})$	27,430; $^4E(^4T_{1g})$
	26,685; $^4E(^4T_{1g})$	
	41,502; $^4A_2(^4T_{1g})$	41,050; $^4E(^4T_{1g})$
	42,203; $^4E(^4T_{1g})$	42,123; $^4A_2(^4T_{1g})$

the tables. The third spin-allowed absorption of weak intensity at still higher energies has not been uncovered in these complexes.

The reflectance spectrum of chloropentaammine shows two weak absorptions at 14,800 and 15,500 cm^{-1}, whereas the bromopentaammine spectrum contains only one at 14,800 cm^{-1}. These are the spin-forbidden doublet transitions. Although the two cubic doublets in this region, namely the ^2E_g and $^2T_{1g}$ of (t_{2g}^3) configuration, split into four quadrate doublets by configuration interaction, it can be seen from Table I that the splitting of the quadrate components of these doublets is only of the order of 20 to 30 cm^{-1} (or 60 to 90 cm^{-1} for alternative assignment) which cannot be resolved in the room temperature reflectance spectra. Thus, in the spectrum of chloropentaammine, the 14,800-cm^{-1} band is assigned to both $^2A_1$ and $^2B_1$ levels, and the 15,500-cm^{-1} band to both $^2A_2$ and ^2E levels. The agreement of the observed transitions with the calculated can be brought still closer than shown in the table if the C value is slightly increased, probably by another 100 cm^{-1}. Since only one band at 14,800 cm^{-1} is observed in the bromopentaammine spectrum, this is assigned to all the four quadrate transitions, *i.e.*, $^2A_1$, $^2B_2$, $^2A_2$, and ^2E. The resolution of these sharp doublets which are only separated by a few hundred wavenumbers in the room temperature spectra of some of the systems, but not in all, seems to depend on how far are they removed in energy from the first broad and more intense spin-allowed band. The farther they are removed, the better they seem to be resolved.

trans-Diacidobisethylenediammines. Since the Dq value of trisethylenediammine complex is almost the same as that of the hexaammine complex, it may be expected that in the case of the *trans*-diacidobisethylenediammine complexes, the Dt values be correspondingly roughly twice that of the acidopentaammines. This is shown in Tables IV–VIII, where the spectral data for these systems are collected from the papers of Linhard and Weigel,[14] Garner and co-workers,[15] and also from the work of Woldbye.[16] Figure 4 summarizes the observed transition energies in all these compounds.

All these complexes show well-resolved splitting of the first cubic band ($^4T_{2g}$), but no such splitting has

Table IV: Spectral Data of *trans*-$Cr(en)_2(H_2O)_2^{3+}$

Obsd ν_{max} (log ϵ) (Ref 15, 16)	Calcd ν_{max}; assignment Dq = 2185 cm^{-1}, Dt = −225 cm^{-1}, B = 650 cm^{-1}, C/B = 5, κ = 1	Calcd ν_{max}; assignment Dq = 2185 cm^{-1}, Dt = −225 cm^{-1}, B = 500 cm^{-1}, C/B = 7, κ = 4
	14,666; $^2A_1(^2E_g)$	14,369; $^2A_1(^2E_g)$
	14,686; $^2B_1(^2E_g)$	14,447; $^2B_1(^2E_g)$
	15,172; $^2E(^2T_{1g})$	14,474; $^2E(^2T_{1g})$
	15,209; $^2A_2(^2T_{1g})$	14,749; $^2A_2(^2T_{1g})$
	22,434; $^2B_2(^2T_{2g})$	21,954; $^2B_2(^2T_{2g})$
	22,489; $^2E(^2T_{2g})$	22,363; $^2E(^2T_{2g})$
19,700 (1.35)	19,788; $^4E(^4T_{2g})$	19,386; $^4E(^4T_{2g})$
22,600 (1.47)	21,850; $^4B_2(^4T_{2g})$	21,850; $^4B_2(^4T_{2g})$
		22,695; $^4A_2(^4T_{1g})$
27,700 (1.59)	26,677; $^4A_2(^4T_{1g})$	28,107; $^4E(^4T_{1g})$
	27,801; $^4E(^4T_{1g})$	
	43,673; $^4E(^4T_{1g})$	42,681; $^4E(^4T_{1g})$
	43,928; $^4A_2(^4T_{1g})$	44,055; $^4A_2(^4T_{1g})$

Table V: Spectral Data of *trans*-$Cr(en)_2Cl_2^+$

Obsd ν_{max} (log ϵ) (Ref 14, 15a)	Calcd ν_{max}; assignment Dq = 2185 cm^{-1}, Dt = −475 cm^{-1}, B = 700 cm^{-1}, C/B = 4.5, κ = 1
	14,635; $^2A_1(^2E_g)$
	14,686; $^2B_1(^2E_g)$
	15,125; $^2E(^2T_{1g})$
	15,282; $^2A_2(^2T_{1g})$
	22,201; $^2B_2(^2T_{2g})$
	22,396; $^2E(^2T_{2g})$
17,301 (1.39)	17,355; $^4E(^4T_{2g})$
22,075 (1.36)	21,850; $^4B_2(^4T_{2g})$
25,252 (1.53)	24,786; $^4A_2(^4T_{1g})$
~27,250 (~1.36)	27,264; $^4E(^4T_{1g})$
	40,814; $^4A_2(^4T_{1g})$
	41,881; $^4E(^4T_{1g})$

(14) M. Linhard and M. Weigel, *Z. Physik. Chem.* (Frankfurt), **5**, 20 (1955).

(15) (a) C. S. Garner and D. J. MacDonald in "Advances in the Chemistry of Coordination Compounds," S. Kirschner, Ed., The Macmillan Co., New York, N. Y., 1961, pp 266–275; (b) L. P. Quinn and C. S. Garner, *Inorg. Chem.*, **3**, 1348 (1964).

(16) F. Woldbye, *Acta Chem. Scand.*, **12**, 1079 (1958).

Table VI: Spectral Data of *trans*-$Cr(en)_2Br_2^+$

Obsd ν_{max} (log ϵ) (Ref 15b)	Calcd ν_{max}; assignment Dq = 2185 cm^{-1}, Dt = −575 cm^{-1} B = 500 cm^{-1} C/B = 7, κ = 1	B = 600 cm^{-1} C/B = 5.5, κ = 1/3
	14,358; $^2A_1(^2E_g)$	14,261; $^2E(^2T_{1g})$
	14,394; $^2B_1(^2E_g)$	14,442; $^2B_1(^2E_g)$
	14,597; $^2E(^2T_{1g})$	14,449; $^2A_1(^2E_g)$
	14,739; $^2A_2(^2T_{1g})$	14,944; $^2A_2(^2T_{1g})$
	21,719; $^2B_2(^2T_{2g})$	21,907; $^2B_2(^2T_{2g})$
	22,004; $^2E(^2T_{2g})$	22,538; $^2E(^2T_{2g})$
16,474 (1.54)	16,246; $^4E(^4T_{2g})$	16,534; $^4E(^4T_{2g})$
~21,739 (~1.38)	21,850; $^4B_2(^4T_{2g})$ 22,099; $^4A_2(^4T_{1g})$	21,850; $^4B_2(^4T_{2g})$
24,630 (1.49)	25,332; $^4E(^4T_{1g})$	24,400; $^4A_2(^4T_{1g})$ 25,231; $^4E(^4T_{1g})$
	38,301; $^4A_2(^4T_{1g})$	38,266; $^4A_2(^4T_{1g})$
	39,523; $^4E(^4T_{1g})$	40,452; $^4E(^4T_{1g})$

Table VII: Spectral Data of *trans*-$Cr(en)_2(H_2O)Cl^{2+}$

Obsd ν_{max} (log ϵ) (Ref 15a)	Calcd ν_{max}; assignment Dq = 2185 cm^{-1}; Dt = −350 cm^{-1} B = 500 cm^{-1} C/B = 7, κ = 2	B = 600 cm^{-1} C/B = 5.5, κ = 1/3
	14,370; $^2A_1(^2E_g)$	14,476; $^2B_1(^2E_g)$
	14,426; $^2B_1(^2E_g)$	14,479; $^2A_1(^2E_g)$
	14,733; $^2E(^2T_{1g})$	14,690; $^2E(^2T_{1g})$
	14,747; $^2A_2(^2T_{1g})$	14,957; $^2A_2(^2T_{1g})$
	21,895; $^2B_2(^2T_{2g})$	22,110; $^2B_2(^2T_{2g})$
	22,044; $^2E(^2T_{2g})$	22,347; $^2E(^2T_{2g})$
18,315 (1.31)	18,322; $^4E(^4T_{2g})$	18,670; $^4E(^4T_{2g})$
22,321 (1.39)	21,850; $^4B_2(^4T_{2g})$ 22,814; $^4A_2(^4T_{1g})$	21,850; $^4B_2(^4T_{2g})$
26,315 (1.68)	26,902; $^4E(^4T_{1g})$	25,942; $^4A_2(^4T_{1g})$ 26,381; $^4E(^4T_{1g})$
	41,625; $^4E(^4T_{1g})$	41,375; $^4A_2(^4T_{1g})$
	41,836; $^4A_2(^4T_{1g})$	42,715; $^4E(^4T_{1g})$

Table VIII: Spectral Data of *trans*-$Cr(en)_2(H_2O)Br^{2+}$

Obsd ν_{max} (log ϵ) (Ref 15b)	Calcd ν_{max}; assignment Dq = 2185 cm^{-1}, Dt = −400 cm^{-1} B = 500 cm^{-1} C/B = 7, κ = 2	B = 600 cm^{-1} C/B = 5.5, κ = 1/3
	14,360; $^2A_1(^2E_g)$	14,469; $^2B_1(^2E_g)$
	14,425; $^2B_1(^2E_g)$	14,473; $^2A_1(^2E_g)$
	14,726; $^2E(^2T_{1g})$	14,609; $^2E(^2T_{1g})$
	14,744; $^2A_2(^2T_{1g})$	14,954; $^2A_2(^2T_{1g})$
	21,830; $^2B_2(^2T_{2g})$	22,068; $^2B_2(^2T_{2g})$
	21,972; $^2E(^2T_{2g})$	22,378; $^2E(^2T_{2g})$
17,825 (1.37)	17,773; $^4E(^4T_{2g})$	18,201; $^4E(^4T_{2g})$
21,978 (1.40)	21,850; $^4B_2(^4T_{2g})$ 22,167; $^4A_2(^4T_{1g})$	21,850; $^4B_2(^4T_{2g})$
26,041 (1.65)	26,879; $^4E(^4T_{1g})$	25,602; $^4A_2(^4T_{1g})$ 26,121; $^4E(^4T_{1g})$
	41,049; $^4E(^4T_{1g})$	40,682; $^4A_2(^4T_{1g})$
	41,283; $^4A_2(^4T_{1g})$	42,211; $^4E(^4T_{1g})$

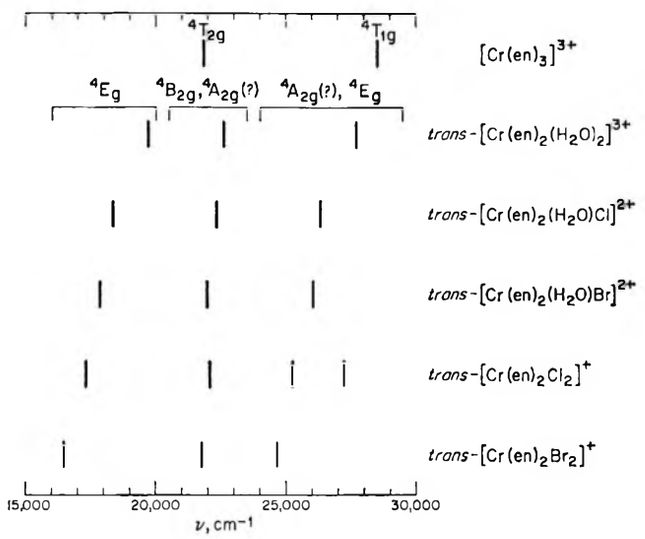

Figure 4. Observed absorption maxima in the spectra of trisethylenediammine and *trans*-diacidobisethylenediamminechromium(III) complex cations.

been observed for the second cubic band ($^4T_{1g}$) in any of these systems except the dichloro, in which there seems to be a well-defined shoulder on the high-energy side of the second band. The two components of the first band were fitted in the way described for the acidopentaammines, and the derived Dt values of all the systems are reported in the respective tables of spectral data. Since in the case of the dichloro spectrum the second band is also split, the ratio of the Ds to Dt parameters can be exactly derived by fitting the two components. This has been found to be unity.

Once again in the case of the diaquo complex, two different values of κ have been used to interpret the spectral data, whereas in the other *trans* systems the Dt values are large enough so that for even a smaller value of 1 or 2 for κ, the $^4A_2$ component of the second cubic band already is positioned in proximity to the $^4B_2$ component of the first band. Thus, if it is supposed that the second band is not split to a considerable extent in these cases, a still smaller value of κ such as 1/3 or less is to be used. The third spin-allowed absorption of weak intensity at high energy has not been found in any of the complexes. The spin-forbidden doublet transitions also have not been observed.

It is to be noted that in the case of aquochloro and aquobromo systems (Tables VII and VIII), the Dt value is found to be the average of the Dt values of the diaquo and dichloro, and, diaquo and dibromo, respectively. In other words, the fields of the two axial ligands are averaged even if these two ligands are not identical. If this argument is extended, the *cis*-disub-

stituted systems can be treated as though belonging to quadrate fields in the sense that they are derived from the *cis*-symmetrically trisubstituted parent compound. This situation is more fully explained elsewhere.[17]

Miscellaneous Systems. Finally, Tables IX, X, and XI have spectral data of three different complexes. The *trans*-difluorotetraaquo system of King and coworkers[18] shows no splitting of the first band, which is in agreement with the fact that the fluoro ligand stands very close to the aquo group in spectrochemical series, so that the *Dt* value for the system under consideration is very small. In fact, the *Dt* value of about -100 cm^{-1} predicts a splitting of 1000 cm^{-1} which may not be resolved in the solution absorption spectrum. Interestingly, there is wide splitting of the second band which could be explained by a κ value of 5. It is worthwhile to note that cubic fluoro complexes are examples of where the *B* values are closer to the free-ion *B* values and once again fluoro substitution seems to require a larger value of κ compared to other systems. Another interesting feature of this spectrum is the finding of the third spin-allowed band at 37,000 cm^{-1}, which is one of the few systems in which such a third band has been uncovered. This band has not been found to be split, which is in agreement with the calculated splitting of 530 cm^{-1} (*cf.* Table IX) not being observable in the solution spectrum. This system also has a weak absorption at 14,800 cm^{-1} which has been assigned to all the four quadrate doublets $^2A_1$, $^2B_1$, $^2A_2$, and ^2E of ^2E_g and $^2T_{1g}$ cubic levels. The doublets are not resolved in the room temperature spectrum probably because they are placed close to the first spin-allowed transition at 16,300 cm^{-1}.

The two other complexes that are included in Tables X and XI are of special interest. It may have been noted already that in all the systems that are described above, the *Dt* values are negative. Examples where the *Dt* values are positive seem to be very few. The cyanopentaaquo complex cation which has been recently prepared[17] is one and the other is Reinecke's salt[19] which is a *trans*-diamminotetraisothiocyanatochromium(III) complex. On the basis of the *Dt* values estimated for the above systems, the *Dt* values of these two complexes may be expected to be around 200 cm^{-1}. As has been pointed out earlier, if the *Dt* is positive,

Table IX: Spectral Data of *trans*-$Cr(H_2O)_4F_2^+$

Obsd ν_{max} (log ϵ) (Ref 18)	Calcd ν_{max}; assignment Dq = 1740, Dt = -100, B = 750 cm^{-1} C/B = 4, κ = 5
14,800	14,403; $^2A_1(^2E_g)$
	14,498; $^2B_1(^2E_g)$
	15,039; $^2E(^2T_{1g})$
	15,147; $^2A_2(^2T_{1g})$
	21,554; $^2B_2(^2T_{2g})$
	21,835; $^2E(^2T_{2g})$
16,300	16,399; $^4E(^4T_{2g})$
	17,400; $^4B_2(^4T_{2g})$
22,700	22,463; $^4A_2(^4T_{1g})$
25,500	24,995; $^4E(^4T_{1g})$
37,000	37,456; $^4E(^4T_{1g})$
	37,987; $^4A_2(^4T_{1g})$

Table X: Spectral Data of *trans*-$Cr(NCS)_4(NH_3)_2^-$

Obsd ν_{max} (log ϵ) (Ref 19)	Obsd ν_{max} (This work)	Calcd ν_{max}; assignment Dq = 1765 cm^{-1}, Dt = 200 cm^{-1}, B = 600 cm^{-1}, C/B = 5, κ = 1
13,400		13,535; $^2B_1(^2E_g)$
13,800		13,553; $^2A_1(^2E_g)$
14,250	~13,800	14,009; $^2E(^2T_{1g})$
14,550		14,026; $^2A_2(^2T_{1g})$
		20,719; $^2B_2(^2T_{2g})$
		20,724; $^2E(^2T_{2g})$
~17,600 (1.78)?		17,650; $^4B_2(^4T_{2g})$
19,230 (2.02)		19,294; $^4E(^4T_{2g})$
~25,000 (1.98)		24,910; $^4E(^4T_{1g})$
		25,723; $^4A_2(^4T_{1g})$
		40,196; $^4E(^4T_{1g})$
		40,627; $^4A_2(^4T_{1g})$

Table XI: Spectral Data of $Cr(H_2O)_5CN^{2+}$

Obsd ν_{max} (log ϵ) (Ref 17)	Calcd ν_{max}; assignment Dq = 1740 cm^{-1}, Dt = 250 cm^{-1} B = 600 cm^{-1}, C/B = 5.5, κ = 1
~14,700	14,446; $^2B_1(^2E_g)$
	14,466; $^2A_1(^2E_g)$
	14,899; $^2E(^2T_{1g})$
	14,925; $^2A_2(^2T_{1g})$
	21,955; $^2E(^2T_{2g})$
	21,988; $^2B_2(^2T_{2g})$
~17,500 (~0.70)	17,400; $^4B_2(^4T_{2g})$
19,200 (1.42)	19,418; $^4E(^4T_{2g})$
25,500 (1.32)	24,940; $^4E(^4T_{1g})$
	25,920; $^4A_2(^4T_{1g})$
	40,242; $^4E(^4T_{1g})$
	40,780; $^4A_2(^4T_{1g})$

(17) (a) W. B. Schaap, R. Krishnamurty, D. K. Wakefield, and J. R. Perumareddi, Abstracts, IXth International Conference on Coordination Chemistry, Switzerland, Sept 1966; (b) R. Krishnamurty, W. B. Schaap, and J. R. Perumareddi, *Inorg. Chem.*, **6**, 1338 (1967).

(18) T. Y. Chia and E. L. King, *Discussions Faraday Soc.*, **29**, 109 (1960).

(19) The spectral data of this system can be found in (a) E. E. Wegner and A. W. Adamson, *J. Am. Chem. Soc.*, **88**, 394 (1966); (b) A. W. Adamson, *ibid.*, **80**, 3183 (1958).

the splittings of the first two quartets may not be the same as is expected for systems of same negative *Dt*. For this reason, no well-resolved splitting of the first band is observed in either system. Since it is the $^4B_2$ component which is not resolved, *Dt* values could still be evaluated by fitting the corresponding ^4E components and the energies of the $^4T_{2g}$ transitions in the parent octahedral complexes, namely the hexaaquo[20] and hexaisothiocyanato[21] complex ions. For the second band, only the lower ratio of κ resulting in nonobservable splitting is reasonable in these systems because it is never possible to bring down the ^4E component of the second quartet close to that of the first quartet for any reasonable value of *B*. Thus the data of these two systems are best interpreted by assigning κ a value of unity.

The third spin-allowed band has not been uncovered in either of these systems, probably because it is buried under charge-transfer absorption. Both complexes show the weak intensity transitions in the low energy region. Only one such transition is observed at 14,700 cm^{-1} in the spectrum of the cyanopentaaquo complex cation which has been ascribed once again to the four quadrate doublets expected at this energy. However, in the case of the Reinecke salt, although only one weak intensity absorption has been found in the reflectance spectrum, four well-defined weak intensity absorptions, in the form of humps, have been observed in its room temperature solution absorption spectrum.[19a] It is rather difficult to evaluate exactly the absorption maxima of these humps from the published spectrum. Our estimate as given in Table X shows that all four are almost equally separated, although the calculated values show that they should occur as two pairs separated by about 450 cm^{-1}, each pair in turn splitting into 20 cm^{-1}. If our estimate of equal separation of these four doublets from the published spectrum is correct, in order to obtain better agreement of the calculated levels with the observed, either a completely different set of all parameters must be used or spin-orbit interaction should be included in the calculations.

IV. Conclusions

We have made an attempt to apply our calculations on d^3 configuration in quadrate fields for the interpretation of the spectra of substituted octahedral chromium(III) compounds. Although the two components of the first cubic quartet band can be definitely assigned, it is clear that, at the present time, the two components of the second cubic quartet band cannot be uniquely assigned because of the low resolution and large band widths of the spectra. Many of the spectral data can be interpreted by a consistent set of parameters[22] of *B*, *C*/*B*, *Dq*, *Dt*, and two different values[23] of κ. In the case of the spectra of *trans*-difluorotetraaquochromium(III), *trans*-dichlorobisethylenediamminechromium(III) and of systems of positive *Dt* even one value of κ is sufficient. The exact choice of the κ value can only be decided by making further spectral measurements on single crystals by means of polarized light and at low temperatures, hoping to narrow the widths of the absorption bands and to attain greater resolution, which in turn would permit the choice of the assignments of the absorption bands proposed in this paper. Further studies on solution absorption spectra at room temperature of the same systems discussed in this work are not likely to provide any better understanding than is already presented here.

It should be added that similar energy diagrams applicable to tetragonally distorted tetrahedral chromium(III) and other compounds of d^3 configuration and octahedral and tetrahedral cobalt(II) and other compounds of d^7 configuration can be constructed with an appropriate set of parametric values from the energy matrices given in part I.[2]

Finally, we have attempted to show that within the limits of ligand field or crystalline field theory, a complete theory with full configuration interaction can be

(20) R. Tsuchida and M. Kobayashi, *Bull. Chem. Soc. Japan*, **13**, 471 (1938). See also ref 17b.

(21) J. Bjerrum, A. W. Adamson, and O. Bostrup, *Acta Chem. Scand.*, **10**, 329 (1956); see also ref 19a.

(22) The *B*, *C* values used for all the systems discussed in this report are very reasonable in the sense that they are below the Cr(III) free-ion values of 920 and 3680 cm^{-1}, respectively [A. D. Liehr, *J. Phys. Chem.*, **67**, 1314 (1963)]. In addition, the *B* value of a quadrate complex has been chosen to be similar to that of the either of the ligands, original or substituting, of the corresponding octahedral complex. As the assignments of some of the bands in the spectra of these quadrate systems are at present not definitive, the *B* values quoted in the assignment tables are only tentative. Exact *B* values can be derived when the assignments are given on a definitive basis by further experiments, such as polarized spectral studies. It is premature to attempt suggesting theories to explain the variational trends of *B* values of the quadrate complexes at this time. It may be pointed out here that in the cubic series, although the *B* value varies from 60% (hexacyanide) to 82.5% (hexafluoride) of the free-ion value, corresponding *C* value varies only from 78% (hexacyanide) to 82% (hexafluoride) of the free-ion value. In other words, the *C* value remains almost constant in a series of cubic complexes. This trend seems to be true in the case of quadrate complexes also.

(23) Strictly speaking, still alternative assignments are possible in terms of ligand field theory, particularly for the components of the second cubic quartet band until further experimental resolution of the spectra is achieved and polarization properties of the bands are measured. The alternative assignments arise from the fact that the ratio of the axial parameters can be negative. If this be so, for positive values of *Dt* and negative values of κ, the present sequence of the two components of the second quartet will be reversed placing $^4A_2$ below in energy to ^4E in which two values of κ smaller or larger result in nonobservable splitting or near coincidence of the $^4A_2$ energy with that of the ^4E component of the $^4T_{2g}$ transition. For negative values of *Dt* and κ, the ^4E will be placed lower in energy to $^4A_2$ so that only one alternative assignment is possible because of configuration interaction (*cf.* the case of positive *Dt* and κ).

developed and applied with ease wherever suitable systems exist, and thus there is no need for applications with any approximations or restricted calculations.

V. Addendum

We wish to make one final remark on the applicability of crystal field model for quadrate chromium(III) complexes insofar as the values of *Dt* are concerned. Since the *Dt* values have been fairly definitely established in this work by fitting the experimental spectral data, it is interesting to compare these values with those that can be calculated on the basis of crystal field model as has been pointed out earlier. The results of such calculations[24] using the formulas of footnote 4 are given in Table XII where the observed *Dt* values as extracted from the spectra[25] are also included for comparison. The predicted values of *Dt* can be seen to be remarkably close to the observed values for all the systems studied in this report, thus suggesting that *Dt* values indeed can be calculated by crystal fields assumptions at least in the case of quadrate chromium(III) complexes. This then should permit one to estimate from the knowledge of *Dq* values of the ligands in a quadrate Cr(III) complex, a rough value of *Dt* and, hence, the extent of splitting of the first cubic quartet band.

Table XII: Comparison of Observed *Dt* Values with Those Calculated by Crystal Field Model

Complex[a]	Obsd *Dt*, cm^{-1} (by spectral fitting)[b]	Calcd *Dt*, cm^{-1} (by crystal field model; see footnote 4)[c]
$Cr(NH_3)_5Cl^{2+}$	−225	−239
$Cr(NH_3)_5Br^{2+}$	−275	−275[c]
$Cr(NH_3)_5I^{2+}$	−325	−325[c]
$Cr(en)_2(H_2O)_2^{3+}$	−225	−254
$Cr(en)_2Cl_2^{+}$	−475	−494
$Cr(en)_2Br_2^{+}$	−575	−567
$Cr(en)_2(H_2O)Cl^{2+}$	−350	−374
$Cr(en)_2(H_2O)Br^{2+}$	−400	−401
$Cr(H_2O)_4F_2^{+}$	−100	−74
$Cr(NCS)_4(NH_3)_2^{-}$	200	223
$Cr(H_2O)_5CN^{2+}$	250	260

[a] All the disubstituted complexes are *trans*-geometrical isomers. [b] See footnote 25. [c] See footnote 24.

Acknowledgments. The author wishes to thank Professor S. T. Spees, Jr., of the University of Minnesota, for kindly supplying the samples of chloro- and bromopentaammines of chromium(III) and for many helpful discussions. Many conversations with Dr. R. Krishnamurty of Indiana University are responsible for clarification of most of the material presented here. This paper, indeed, has greatly benefited by our frequent discussions on the problem. The author also wishes to thank Dr. E. W. Baker of the Mellon Institute for kindly reading and commenting on the manuscript. Finally, thanks are due Mr. R. L. Anderson and his associate, Mr. J. Beasley, of the Mellon Institute for computer programming and Mr. J. F. Benes and E. L. Helgerman, also of the Mellon Institute Research Drafting Department, for expert tracing of the complicated energy diagrams obtained from the computer.

(24) The *Dq* values for six-coordinate bromo and iodo complexes are not known, and hence these *Dt* values are fitted with the observed values. By such a fitting, the $10Dq$ of a bromo complex is 11,925 cm^{-1} and that of an iodo complex is 10,175 cm^{-1}. These values in turn are used to calculate the *Dt* values of the corresponding *trans* systems. The *Dq* values of the other complexes used are as follows: NH_3 = 2155 cm^{-1}, en = 2185 cm^{-1}, H_2O = 1740 cm^{-1}, NCS^- = 1765 cm^{-1}, Cl^- = 1320 cm^{-1}, F^- = 1610 cm^{-1}, CN^- = 2650 cm^{-1}.

(25) These values are subject to minor changes to allow for an exact fitting and configuration interaction effects when the other parameters are also exactly evaluated by definitive assignments.

Application of the Statistical Theory of Mass Spectra to the Decomposition of $C_2H_6^+$ and $C_2D_6^+$ [1a,b]

by Z. Prášil[1c] and W. Forst

Department of Chemistry, Université Laval, Québec 10, Canada *(Received December 16, 1966)*

In an effort to obtain a meaningful test of the statistical theory of mass spectra, breakdown curves are calculated for the decomposition of excited $C_2H_6^+$ and $C_2D_6^+$ and compared with experimental curves obtained in charge-transfer experiments. This procedure obviates any assumption about the energy distribution function which would be necessary for the calculation of actual mass spectra. The Marcus–Rice formulation is used for unimolecular rate constants, and anharmonic vibration–rotation energy sums are calculated on a computer. All important parameters for the molecular ions and their complexes are taken, when available, from their respective neutral counterparts and the corresponding thermal reactions. In the case of the complexes, the average Morse dissociation energy, D, which determines the anharmonic correction, cannot be readily estimated and is used as an adjustable parameter to obtain the best fit between theory and experiment. Good agreement is obtained between the two for reasonable values of D for first-generation fragment ions. Fluctuation of energy is considered in calculating breakdown curves for second-generation ions, and good agreement between theory and experiment is likewise obtained. It is concluded that while this agreement does not furnish proof either for or against the assumption that electronic excitation energy is converted into internal energy of the ground-state ion, it does indicate that at least in the present case the other assumptions made in the theory are successful.

Introduction

The statistical theory of mass spectra[2,3] views the fragmentation of a molecular ion after electron impact as a process consisting of these principal steps: (1) conversion of electronic excitation energy into vibrational–rotational energy of the ground electronic state; (2) statistical distribution of this vibrational–rotational energy among internal degrees of freedom of the molecular ion; and (3) fragmentation of the molecular ion in a series of consecutive and/or competitive unimolecular decompositions. It is then assumed that (4) the first two steps are sufficiently faster than the third so that unimolecular rate theory can be used to describe the individual fragmentations. The Marcus–Rice version of the theory of unimolecular reactions has met with considerable success in the case of unimolecular decompositions of molecules activated thermally[4–10] or chemically[11–16] and can therefore be considered as essentially correct. In this sense, then, a test of the statistical theory of mass spectra is a test of assumptions 1–4 above rather than a test of unimolecular rate theory.

(1) (a) Work done with financial assistance from the National Research Council of Canada. (b) Presented at the 152nd National Meeting of the American Chemical Society, New York, N. Y., Sept 12–16, 1966. (c) Institute for Nuclear Research, Řež near Prague, Czechoslovakia.

(2) H. M. Rosenstock, M. B. Wallenstein, A. L. Wahrhaftig, and H. Eyring, *Proc. Natl. Acad. Sci. U. S.*, **38**, 667 (1952).

(3) (a) H. M. Rosenstock and M. Krauss in "Mass Spectrometry of Organic Ions," F. W. McLafferty, Ed., Academic Press, New York, N. Y., 1963, p 1; (b) "Advances in Mass Spectrometry," R. M. Elliott, Ed., Vol. 2, The Macmillan Co., New York, N. Y., 1963, pp 251–284.

(4) R. A. Marcus, *J. Chem. Phys.*, **20**, 359 (1952).

(5) R. A. Marcus and O. K. Rice, *J. Phys. Colloid Chem.*, **55**, 894 (1951).

(6) G. M. Wieder and R. A. Marcus, *J. Chem. Phys.*, **37**, 1835 (1962).

(7) F. W. Schneider and B. S. Rabinovitch, *J. Am. Chem. Soc.*, **84**, 4215 (1962); **85**, 2365 (1963); **87**, 158 (1965).

(8) W. Forst, *J. Chem. Phys.*, **44**, 2349 (1966).

When applied to the calculations of mass spectra[17-20] and radiation-chemical yields,[21-24] a straightforward test of the statistical theory is not usually possible because little is known about the internal energy distribution function of the excited molecular ion formed by electron impact in the mass spectrometer as well as in radiolysis. In a few cases[25] this function has been roughly determined experimentally, but generally rather crude assumptions about its form must be made. In recent years, however, Lindholm and co-workers[26] have obtained by dissociative charge-transfer experiments breakdown curves for a number of simple molecules, including ethane. These curves offer a more direct test of the statistical theory of mass spectra, since what is calculated and compared with experiment is the decomposition of the molecular ion excited to a (presumably) precisely known energy and not the mass spectrum itself, which is an integral of the breakdown curve over some (doubtful) internal energy distribution function.

The decomposition of the molecular ion of ethane (considered many years ago by Kropf[27] using an early version of the theory, and more recently by Wincel[28] in connection with the radiolysis of methane) was chosen mainly for two reasons. First, the mechanism of the decomposition is well known and not too complicated. The second is a practical consideration dictated by the present general ignorance of the molecular parameters (vibrational frequencies, moments of inertia, and the like) of charged species. Assuming these parameters are the same for ions and the corresponding neutral molecules, all the necessary information of this kind is available for the ethane molecule,[29] including the structure of complexes for decomposition into $2CH_3$ and $C_2H_4 + H_2$ as obtained from the study of the thermal decomposition of the molecule.[16]

Decomposition of the Molecular Ion of Ethane

The mass spectrum of ethane at 50 ev is accounted for almost completely (within 95%) by the following ions:[30] $C_2H_6^+$ (11.9%), $C_2H_5^+$ (9.8%), $C_2H_4^+$ (45.5%), $C_2H_3^+$ (15.1%), $C_2H_2^+$ (10.6%), and CH_3^+ (2.0%). Metastable ions are observed[31] at masses 26.2, 25.2, and 24.2 which correspond to the processes

Mass	Process
26.2	$C_2H_6^+ \rightarrow C_2H_4^+ + H_2$
25.2	$C_2H_5^+ \rightarrow C_2H_3^+ + H_2$
24.2	$C_2H_4^+ \rightarrow C_2H_2^+ + H_2$

The results of charge-transfer experiments[32] are shown in Figure 1. The ion requiring the least amount of energy for its formation is $C_2H_4^+$. The ion formed at the next higher energy is $C_2H_5^+$, and the decrease of its abundance above 29,000 cm^{-1} is almost exactly equal to the increase of the abundance of $C_2H_3^+$, so that the latter must be formed mainly by the process $C_2H_5^+ \rightarrow C_2H_3^+ + H_2$. The appearance of $C_2H_2^+$ causes a decrease of the abundance of $C_2H_4^+$, but the ethylene molecule-ion persists even at very high excitation energies. This can be most easily explained if it is assumed that there are two different structures of $C_2H_4^+$, namely $CH_2CH_2^+$ and CH_3CH^+, of which only the latter predominantly decomposes to yield $C_2H_2^+$. Evidence for this mechanism is provided by von Koch's experiments[32] with CH_3CD_3. Immediately above the $AP(C_2X_4^+)$ he found only CH_2CD_2, while at higher energies CH_3CD and CD_3CH were also present. He also observed that $C_2H_2^+$ was predominantly formed by loss of H_2 from the same carbon atom, *i.e.*, by the reactions $CH_3CD^+ \rightarrow CHCD^+ + H_2$ or $CHCD_3^+ \rightarrow CHCD^+ + D_2$.

On the basis of this information, the most important

(9) W. Forst and P. St-Laurent, *Can. J. Chem.*, **43**, 3052 (1965).

(10) J. H. Yang and D. C. Conway, *J. Chem. Phys.*, **43**, 1296 (1965).

(11) B. S. Rabinovitch and R. W. Diesen, *ibid.*, **30**, 735 (1959).

(12) R. E. Harrington, B. S. Rabinovitch, and R. W. Diesen, *ibid.*, **32**, 1245 (1960).

(13) B. S. Rabinovitch, R. F. Kubin, and R. E. Harrington, *ibid.*, **38**, 405 (1963).

(14) B. S. Rabinovitch, E. Tschuikow-Roux, and E. W. Schlag, *J. Am. Chem. Soc.*, **81**, 1081 (1959).

(15) D. W. Setser and B. S. Rabinovitch, *Can. J. Chem.*, **40**, 1425 (1962).

(16) B. S. Rabinovitch and D. W. Setser in "Advances in Photochemistry," Vol. 3, Interscience Publishers Inc., New York, N. Y., 1964, pp 1–82.

(17) M. Vestal, A. L. Wahrhaftig, and W. H. Johnston, *J. Chem. Phys.*, **37**, 1276 (1962).

(18) M. Vestal, *ibid.*, **43**, 1356 (1965).

(19) Ch. Lifshitz and F. A. Long, *J. Phys. Chem.*, **69**, 3737 (1965).

(20) P. C. Haarhoff, *Mol. Phys.*, **8**, 49 (1964).

(21) M. Vestal, A. L. Wahrhaftig, and W. H. Johnston, "Theoretical Studies in Basic Radiation Chemistry," Report ARL 62-426 (1962).

(22) J. Futrell, *J. Chem. Phys.*, **35**, 353 (1961).

(23) Z. Prášil, *Collection Czech. Chem. Commun.*, **31**, 3252, 3263 (1966).

(24) Z. Prášil, Ph.D. Thesis, Czechoslovak Academy of Sciences, 1965.

(25) W. A. Chupka and M. Kaminsky, *J. Chem. Phys.*, **35**, 1991 (1961).

(26) E. Lindholm, *et al.*: (a) *Arkiv Fysik*, **8**, 257, 433 (1954); (b) *ibid.*, **18**, 219 (1960); (c) *ibid.*, **19**, 123 (1961); (d) *ibid.*, **21**, 97 (1962); **24**, 49 (1963); **25**, 181, 349, 417 (1964); **28**, 529, 559 (1965); **29**, 565 (1965); **31**, 159, 287 (1966); **32**, 275 (1966).

(27) A. Kropf, Ph.D. Thesis, University of Utah, 1954.

(28) H. Wincel, *Nukleonika*, **7**, 25 (1962).

(29) G. E. Hansen and D. M. Dennison, *J. Chem. Phys.*, **20**, 313 (1952).

(30) API Catalog of Mass Spectral Data, Serial No. 2.

(31) J. A. Hipple, R. E. Fox, and E. U. Condon, *Phys. Rev.*, **69**, 347 (1946).

(32) H. von Koch, *Arkiv Fysik*, **28**, 559 (1965).

reactions in the decomposition mechanism of $C_2H_6^+$ can be represented by the sequence

$$C_2H_6^+ \longrightarrow C_2H_5^+ \longrightarrow C_2H_3^+$$
$$\longrightarrow CH_3CH^+ \longrightarrow CHCH^+$$
$$\longrightarrow CH_2CH_2^+$$
$$\longrightarrow CH_3^+$$

Table I summarizes the appearance potentials and enthalpies of reaction for the various processes. In the following, the activation energy of each decomposition will be assumed to be equal to the corresponding difference in the mass spectrometrically measured appearance potentials. The justification is that even if the activation energy so measured does not quite correspond to the energy difference between the ground state of the reactant ion and the top of the potential energy barrier leading to product formation, *e.g.*, because excess energy is required above activation energy to cause a high enough rate of reaction on the time scale of the mass spectrometer (this effect is called kinetic shift by Chupka[33]), the rate constant increases so steeply above threshold (*cf.* Table VI further below) that the error in activation energy as determined from appearance potentials is likely to be small. In any event, such an error, provided it is not too large, would merely cause a shift of the calculated breakdown curves along the energy axis, and would result in a minor change of shape.

The values of ΔH_f in Table I are merely informative and can serve as a check on the values of ΔA.P. only insofar as $\Delta H_f \leqq$ ΔA.P., the inequality indicating that there is some activation energy for the back reaction. Only for the process $C_2H_6^+ \rightarrow C_2H_5^+$ do we have $\Delta H_f > \Delta AP$; however, the difference is still within ±0.2ev, the estimated accuracy of these particular appearance potential measurements, and within the accuracy of the respective ΔH_f.

The only activation energy not available from appearance potential measurements is that for the formation of CH_3CH^+. From von Koch's measurements,[32] it follows that at recombination energy (R.E.) of 12.13 ev (3873 cm^{-1} excitation energy) only $CH_2CH_2^+$ is formed, so that the measured A.P. corresponds to the third reaction in the decomposition scheme. On the other hand, the same measurements show that at R.E. = 13.44 ev (14,442 cm^{-1} excitation energy) the ion CH_3CH^+ is already formed in rather high abundance. This means that the activation energy of this process is somewhere between 3873 and 14,472 cm^{-1}; we have estimated it to be 10,000 cm^{-1}. Conceivably, a very careful measurement of the ionization efficiency curve for $C_2H_4^+$ formed from ethane could reveal a discontinuity which might be identified with the formation of CH_3CH^+ and thus yield a better value for the activation energy of this process.

For the decomposition of $C_2D_6^+$ the same sequence of reactions was assumed. The activation energies used in the calculations were those of the hydrogenated species (*cf.* Table I), increased by 0.2 ev, in accordance with the observation of von Koch.[32] Roughly the same difference in activation energies could be calculated from the frequencies assumed for $C_2H_6^+$ and $C_2D_6^+$ in normal and activated complex configurations.[34]

Table I: Correlation between Differences in Appearance Potentials (ΔA.P.) and Differences in Heats of Formation (ΔH_f)

Process	ΔA.P., ev	Ref	ΔH_f, ev[a]	Ref
$C_2H_6^+ \rightarrow C_2H_5^+ + H$	1.15	38	1.37	*b*
$C_2H_6^+ \rightarrow CH_3CH^+ + H_2$	1.24 (?)[c]	32	?	
$C_2H_6^+ \rightarrow CH_2CH_2^+ + H_2$	0.5	38	0.28	*b*
$C_2H_6^+ \rightarrow CH_3^+ + CH_3$	2.30	38	1.85	*b*
$C_2H_5^+ \rightarrow C_2H_3^+ + H_2$	2.52	38	2.40	*b*
$CH_3CH^+ \rightarrow CHCH^+ + H_2$	2.11 (?)[c]	32	?	

[a] Sources of ΔH_f: $C_2H_4^+$, $C_2H_2^+$, and CH_3^+: spectroscopic data, estimated accuracy ±0.01 ev; $C_2H_6^+$, H, and CH_3: data of good precision not from electron impact studies; $C_2H_5^+$: good quality electron impact data, estimated precision ±0.1 ev. [b] R. R. Bernecker and F. A. Long, *J. Phys. Chem.*, **65**, 1565 (1961). [c] The only certain information available about the two A.P.'s with a question mark is that their sum should be equal to 3.35 ev, which is the difference between the A.P.($C_2H_2^+$) and the I.P.(C_2H_6).

Calculation of the Breakdown Curves

The over-all character of the calculated breakdown curves is determined by competitive unimolecular decompositions producing first-generation fragment ions, *i.e.*, ions formed directly from parent. The fractional amount $F_j(E)$ of the jth first-generation fragment present at time t is given by[35]

$$F_j(E) = \frac{k_j(E)}{k_j'(E) - \sum_i k_i(E)} \left\{ \exp\left[-\sum_i k_i(E)t \right] - \exp[-k_j'(E)t] \right\} \quad (1)$$

where $k_i(E)$ and $k_j(E)$ are the rate constants for the production of the ith and jth fragment, respectively,

(33) W. A. Chupka, *J. Chem. Phys.*, **30**, 19 (1959).

(34) A. Kropf, E. M. Eyring, A. L. Wahrhaftig, and H. Eyring, *ibid.*, **32**, 149 (1960).

(35) N. M. Rodiguin and E. N. Rodiguina, "Consecutive Chemical Reactions," D. van Nostrand Co. Inc., New York, N. Y., 1964, p 51.

E is the internal excitation energy of parent, $k_j'(E)$ is the rate constant for the subsequent decomposition of the jth fragment to a second-generation fragment, and the sum is taken over all i's, *i.e.*, over all decompositions of the parent. If $k_j'(E) = 0$, and if advantage is taken of the fact that at all excitation energies E (except in the very neighborhood of the activation energy), the sum $\sum_i k_i(E)t \gg 1$, then (1) simplifies to

$$F_j(E) = \frac{k_j(E)}{\sum_i k_i(E)}$$

This simplification is permissible if (1) rate constants increase sharply with energy and (2) activation energies for consecutive decompositions are far enough apart compared with the rate of rise with energy of the rate constants. These conditions are satisfied in the present case and as a result a new process sets in only when the rate of the preceding one $[k(E)]$ has reached such a value that $\exp[-k(E)t] \sim 0$, so that it can be effectively ignored in the rate expression.

It will be assumed in the following that each unimolecular rate constant can be adequately represented by the Marcus–Rice model. Their expression for $k(E)$ is[4,5]

$$k(E) = \alpha \times \frac{Q_R^{\neq}\Gamma(t/2)\sum_{E_v=0}^{E_v=E-E_a} P^{\mp}(E_v)(E - E_a - E_v)^{r/2}}{Q_R\Gamma(1 + r/2)h(kT)^{(r-t)/2}\sum_{E_v=0}^{E_v=E} P(E_v)(E - E_v)^{(t/2)-1}}$$

where α is the reaction path degeneracy, Q_R and $Q_R^{\neq}$ are the partition functions for active rotations in the molecule (ion) and activated complex, respectively, Γ is the Γ function, r and t are the number of active rotations in the activated complex and the molecule (ion), respectively, h is Planck's constant, k is the Boltzmann constant, and T is temperature. The sum involving the power $(t/2) - 1$ is proportional to the density of vibrational–rotational states of the molecule (ion) at energy E, the sum involving the power $r/2$ is proportional to the integral of the density of vibrational–rotational states of the activated complex at energy $E - E_a$, where E_a is the critical energy of the process under consideration and E_v is that part of total excitation energy contained in the vibrational degrees of freedom.

The difficult part here is the evaluation of the sums at high energies. Exact counting is possible but requires excessive computer time; therefore, an approximation formula due to Haarhoff[36a] was used which a recent test[36b] has shown to be quite adequate at higher energies. If all vibrations are assumed to be harmonic, we have in Haarhoff's notation

$$\sum_{E_v=0}^{E_v=E} P(E_v)(E - E_v)^{m-1} = \Gamma(m)I_m(E)$$

where

$$I_m = \left\{\left(\frac{2}{\pi n}\right)^{1/2}\left(\frac{n}{n+m}\right)^{n+m-1/2}\left(1 - \frac{1}{12(n+m)}\right)\times \frac{\lambda(h\bar{\nu})^{m-1}}{1+\eta}\right\}\left[\left(1+\frac{\eta}{2}\right)\left(1+\frac{2}{\eta}\right)^{\eta/2}\right]^{n+m}\times \left[1 - \frac{1}{(1+\eta)^2}\right]^{\beta_m} \quad (2)$$

$$\beta_m = \{(n+m-1)(n+m-2)\alpha_2 - n(n+m)\}/6n$$

$$\alpha_2 = \overline{\nu^2}/(\bar{\nu})^2; \quad \eta = E/\epsilon_z^\circ; \quad 1/\lambda = \prod_{i=1}^{n}(\nu_i/\bar{\nu})$$

and n is the number of (harmonic) oscillators, ν_i is the frequency of the ith oscillator, and ϵ_z° is the zero-point energy. Haarhoff also developed a correction factor by means of which the harmonic density of states can be corrected for anharmonicity, on the assumption that a molecule can be considered as an array of Morse oscillators. The correction factor is

$$I_m(\text{anharm}) = I_m(\text{harm})\left\{\left(1+\frac{2}{\eta}\right)^{(\eta/2)[1+\eta/2]}\times \exp\left[-\frac{(\alpha_2-1)}{3(1+\eta)}\right]\right\}^{n\epsilon_z^\circ/(n+m)D}\times \exp\left[M_2(1+\eta)^2\left(\frac{\epsilon_z^\circ}{D}\right)^2 + M_3(1+\eta)^3\left(\frac{\epsilon_z^\circ}{D}\right)^3\right] \quad (3)$$

where $M_2 = n(4n + 5m)/8(n+m)^2(n+m+1)$, $M_3 = n(24n^2 + 59nm + 37m^2)/24(n+m)^3(n+m+1)(n+m+2)$, $1/D = \langle 1/D_i\rangle$, where D_i is the Morse dissociation energy of the ith oscillator, and m and n have the same significance as in the previous formula.

In this work, all densities were corrected for anharmonicity. Each D_i for the molecule ion was calculated from the relation

$$D_i = \omega_i/2x_i \quad (4)$$

where ω_i is the normal frequency of the ith oscillator in ethane and x_i is its anharmonicity constant.[29] In the case of the complexes, where the x_i's cannot be estimated in any straightforward manner, D was used as an adjustable parameter within reasonable limits. All formulas were programmed in FORTRAN IV and

(36) (a) P. C. Haarhoff, *Mol. Phys.*, **7**, 101 (1963); (b) W. Forst Z. Prášil, and P. St-Laurent, *J. Chem. Phys.*, **46**, 3736 (1967).

Table II: Fundamental Frequencies, Anharmonicity Factors, Normal Frequencies, and Frequencies Grouped to Groups of Higher Degeneracy for C_2H_6 and C_2D_6 (All Values in cm^{-1})

Hansen and Dennison[29]			Rabinoviteh and Setser[16]	This work
ν_i	x_i	ω_i	ν_i	ν_i
		C_2H_6		
2915 (1)	0.0420	3042.8 (1)	350 (1)	1 free rotation
1400 (1)	0.0340	1449.3 (1)	822 (2)	820 (2)
993 (1)	0.0225	1015.8 (1)	993 (1)	1000 (1)
275 (1)	0.0933	303.3 (1)	1190 (2)	1200 (2)
2915 (1)	0.0477	3061.0 (1)	1436 (6)	1460 (6)
1379.2 (1)	0.0405	1437.5 (1)	2960 (6)	2950 (6)
2995.5 (2)	0.0460	3139.9 (2)		
1472.2 (2)	0.0350	1525.6 (2)		
821.52 (2)	0.0004	821.8 (2)		
2955 (2)	0.0694	3175.1 (2)		
1460 (2)	0.0590	1551.6 (2)		
1190 (2)	0.0450	1246.0 (2)		
		C_2D_6		
2100 (1)	0.0303[a]	2165.5 (1)		1 free rotation
1158 (1)	0.0281[a]	1191.5 (1)		590 (2)
852 (1)	0.0193[a]	868.8 (1)		850 (1)
200 (1)	0.0678[a]	214.6 (1)		970 (2)
2095 (1)	0.0343[a]	2169.4 (1)		1080 (6)
1077 (1)	0.0316[a]	1112.2 (1)		2190 (6)
2236 (2)	0.0343[a]	2315.5 (2)		
1082 (2)	0.0257[a]	1110.5 (2)		
593.7 (2)	0.0003[a]	593.9 (2)		
2225 (2)	0.0523[a]	2347.8 (2)		
1055 (2)	0.0426[a]	1102.0 (2)		
970 (2)	0.0367[a]	1006.9 (2)		

[a] Calculated from the relation $\nu_i = (1 - x_i)\omega_i$. Degeneracies are given in parentheses.

computations were done on IBM 1410 at 2000-cm^{-1} intervals.

The calculation of $k(E)$ requires the knowledge of the moments of inertia (*i.e.*, of the structure) and of the vibrational assignment for the various ionic species and their decomposition complexes. Very little is known at present about the molecular parameters of polyatomic ions. There are some recent data on potential energy curves for simple diatomic molecules (N_2, O_2, and NO) and their ions[37] which show that at least in these three molecules there is no substantial difference in vibrational frequency of the ground electronic state of the molecule and its ion, and also that the equilibrium interatomic distance is not much different in the molecule and the ion. This suggests that probably no gross error is committed if molecular parameters of the neutral species are assumed to be identical with those of the respective ions. Moreover, the over-all character of the calculated breakdown curves is determined to a considerable degree by the nature of the activated complexes which in many instances can only be guessed at, so that a wrong choice for an activated complex is likely to have more serious repercussions than a wrong choice for the molecular parameters of an ionic species.

All the molecular parameters used in the calculations are summarized in Tables II, III, and IV and are discussed in some detail in the Appendix.

When the decomposition of an ion of the first generation to an ion of the second generation is considered, fluctuation of energy among the fragments of the first generation must be taken into account.[21] As a rule, the value of every $k(E)$ at energies slightly higher than the activation energy is of the order of 10^{12} to 10^{14} sec^{-1}, so that an ion decomposes practically immediately on the time scale of a mass spectrometer (10^{-5} sec^{-1}). The probability $\phi(E)$ that at a given parent energy E an ionic fragment of the first generation will have internal energy $\geq E_a'$ (= activation energy for decomposition to a second-generation ionic fragment), while the acti-

(37) K. E. Shuler, T. Carrington, and J. C. Light, *Appl. Opt.* (Supplement on Chemical Lasers), 81 (1965).

Table III: Parameters Used in the Calculation of Breakdown Curves of $C_2H_6^+$ [a]

	Molecular ion $C_2H_6^+$	Complex $C_2H_6^+\cdots H$	Complex $CH_3CH^+\cdots H_2$	Complex $CH_2CH_2^+\cdots H_2$	Complex $CH_3^+\cdots CH_3$	Fluctuation 1 $C_2H_6^+$	Fluctuation 1 H	Fluctuation 2 CH_3CH^+	Fluctuation 2 H_2
ν_i	820 (2)	300 (2)	500 (3)	600 (1)	950 (2)	820 (2)	...	800 (1)	4400 (1)
	1000 (1)	700 (2)	700 (2)	900 (3)	1460 (4)	1000 (1)		1000 (1)	
	1200 (2)	1000 (1)	1200 (2)	1000 (2)	2950 (6)	1200 (2)		1200 (1)	
	1460 (6)	1200 (2)	1460 (4)	1200 (2)		1460 (4)		1460 (4)	
	2950 (6)	1460 (4)	2950 (4)	1460 (4)		2950 (5)		2950 (4)	
		2950 (5)	3500 (1)	2950 (5)					
n	17.0	16.0	16.0	17.0	12.0	14.0	0.0	11.0	1.0
m	0.5	1.5	1.5	1.0	3.5	0.5	0.0	0.5	0.0
E_a	...	9279	10,000	4034	18,557	$E_a = 9300$		$E_a = 10,000$	
						$E_a' = 20,200$		$E_a' = 17,000$	
D	13,255.8	20,000	20,000	30,000	15,000	25,000	0	25,000	36,114
				...	$I_1 = 5.96$ (1)	...	...	...	...
				...	$I_2 = 2.98$ (2)	...	...	...	...
I_{red}	2.735	3.5	4.10	...	$I_3 = 2.98$ (2)	...	...	...	...
σ_i	3	3	3	...	$\sigma_1 = 3$	...	...	...	...
					$\sigma_2 = 2$				
					$\sigma_3 = 1$				
α_i	...	6	6	9	2	...	...	...	...

[a] Degeneracies are in parentheses. Frequency and energy values are given in cm^{-1}, moments of inertia in units of 10^{-40} g cm^2. The value of α_i means the reaction path degeneracy; σ_f is the symmetry number for rotation. All other symbols are explained in the text; m and n are constants appearing in eq 2.

vation energy for the decomposition of the parent ion is E_a, is[21]

$$\Phi(E) = \frac{\int_{Ea'}^{E-Ea} \rho_1(\epsilon)\rho_2(E - E_a - \epsilon)d\epsilon}{\int_0^{E-Ea} \rho_1(\epsilon)\rho_2(E - E_a - \epsilon)d\epsilon}$$

where ρ_1 and ρ_2 refer to the density of states of the first and second fragments, respectively, of the first generation. The abundance of the second generation is then given by

$$F_j'(E) = \frac{k_j(E)}{\sum_i k_i(E)} \Phi_j(E)$$

The various parameters used in the calculation of fluctuations are summarized in Tables III and IV and are further discussed in Appendix II.

Discussion

In charge-transfer experiments a presumably known amount of energy is transferred to the molecular ion and the ionized fragment formed in its decomposition is then mass-analyzed. The initial process is

$$M + X^+ \longrightarrow M^{+*} + X$$

and the excitation energy of M^{+*} is calculated by taking the difference between the recombination energy (R.E.) of the incident ion (assuming, in effect, that the neutral is not formed in an excited electronic state) and the lowest ionization potential (I.P.) of M. Actually a charge transfer in this collision under Lindholm's experimental conditions[26c] is possible only as essentially a resonance process, *i.e.*, under the condition that there exist some (higher) vertical ionization potential of the molecule M, which is just equal to the R.E. of X^+. The difference between this higher I.P. (= R.E.) and the first I.P. of M will appear as internal excitation energy of the ground electronic state of M^+ only if there is fast conversion of electronic excitation energy into vibrational–rotational energy of the ground electronic state. Thus the basic assumption made in the interpretation of charge-transfer experiments is the same as assumption 1 of the quasi-equilibrium theory of mass spectra (*cf.* Introduction), so that these experiments cannot provide a test of assumption 1. It is well to keep this in mind.

A priori, even under the assumption that the conversion of electronic energy into vibrational–rotational energy of the ground electronic state is complete, there are reasons to believe it unlikely that the excitation energy of M^{+*} could be calculated simply by taking the difference R.E. − I.P.; it seems more probable that this excitation energy will depend on the way the difference between the R.E. of X^+ and the I.P. of M is partitioned between M^{+*} and X. If X is a rare gas

Table IV: Parameters Used in the Calculation of Breakdown Curves of C_2D^+ [a]

	Molecular ion $C_2D_6^+$	Complex $C_2D_6^+\cdots D$	Complex $CD_3CD^+\cdots D_2$	Complex $CD_3CD_2^+\cdots D_3$	Complex $CD_3^+\cdots CD_3$	Fluctuation 1 $C_2D_6^+$	Fluctuation 1 D	Fluctuation 2 CD_3CD^+	Fluctuation 2 D_2
ν_i	590 (2)	220 (2)	300 (3)	400 (1)	720 (2)	500 (2)	...	600 (1)	3120 (1)
	850 (1)	500 (2)	600 (2)	800 (3)	1080 (4)	850 (1)		800 (1)	
	970 (2)	850 (1)	970 (2)	850 (2)	2190 (6)	970 (2)		1000 (1)	
	1080 (6)	970 (2)	1080 (4)	970 (2)		1080 (4)		1080 (4)	
	2190 (6)	1080 (4)	2190 (4)	1080 (4)		2190 (5)		2190 (4)	
		2190 (5)	2690 (1)	2190 (5)					
n	17.0	16.0	16.0	17.0	12.0	14.0	0.0	11.0	1.0
m	0.5	1.5	1.5	1.0	3.5	0.5	0.0	0.5	0.0
E_a	...	10,893	11,614	5648	20,171	E_a = 10,900		E_a = 11,600	
						E_a' = 20,200		E_a' = 17,000	
D	13,012.6	25,000	30,000	30,000	30,000	25,000	0	25,000	36,740
				...	I_1 = 11.92 (1)	...	...	...	...
					I_2 = 5.96 (2)	...	...	...	...
I_{red}	5.47	7.29	8.21	...	I_3 = 5.96 (2)	...	...	...	...
σ_i	3	3	3	...	σ_1 = 3	...	...	...	...
					σ_2 = 2				
					σ_3 = 1				
α_i	...	6	6	9	2	...	...	...	...

[a] Degeneracies are in parentheses. Frequency and energy values are given in cm^{-1}, moments of inertia in units of 10^{-40} g cm^2. The value of α_i means the reaction path degeneracy; σ_i is the symmetry number for rotation. All other symbols are explained in the text; m and n are constants appearing in eq 2.

atom, the amount of energy it can carry away as kinetic energy will be a function of its mass, and so will be the excitation energy of M^{+*}. The experimental arrangement of Lindholm, *et al.*, was such, however, that only fragments without appreciable kinetic energy were measured. Therefore, the assumption that the difference between R.E. (X^+) and I.P. (M) is the actual internal excitation energy of the ion M^{+*} seems quite reasonable for X^+ = rare gas ion.

In charge-transfer experiments with X^+ = molecular ion (N_2O^+, CO_2^+, and CO^+), there is a possibility of transfer of charge as well as of internal energy. For example, von Koch[32] found that N_2O^+ with R.E. = 12.7 ev produced $C_2H_5^+$ with A.P. = 12.8 ev; CO_2^+ with R.E. = 13.8 ev yielded CH_3^+ whose A.P. = 13.95 ev, and COS^+ with R.E. <11.5 ev produced $C_2H_2D_2^+$ having A.P. = 11.65 ev. The discrepancy increases if ions derived from $C_2D_6^+$ are considered. In his paper, von Koch[32] shows only results for $C_2D_6^+$ and states that results for $C_2H_6^+$ are substantially similar, except that all A.P.'s are about 0.2 ev lower in the latter case. This means that N_2O^+ is found to yield $C_2D_5^+$ (A.P. 13.0 ev) and CO_2^+ is found to produce CD_3^+ (A.P. 14.15 ev); *i.e.*, the difference (A.P.) − (R.E.) increases from 0.1–0.15 ev for the hydrogenated species to 0.3–0.35 ev for the deuterated species. This can only mean that (1) the R.E.'s or the A.P.'s, or both, are incorrect, or (2) that the polyatomic ions transfer some internal energy in addition to their R.E. The second alternative seems to be the more likely, since the difference (A.P.) − (R.E.) is almost constant for the ions mentioned, while it would take a very fortuitous coincidence indeed to find an experimental error not only of the same magnitude but also of the same sign for these polyatomic ions, and not find a similar error for the atomic ions. If this second interpretation is correct, all the experimental points in Figures 1 and 2 obtained in collisions with polyatomic ions should be shifted to higher energies. This would not result in any important over-all changes, but would slightly increase the agreement between theory and experiment.

It should also be noted that in drawing his breakdown curves for $C_2D_6^+$, von Koch used appearance potentials of the *hydrogenated* species. For this reason, in Figures 1 and 2 tabulated appearance potentials[38] are used to plot the experimental points for $C_2H_6^+$, and A.P.'s 0.2 ev higher are used in the case of $C_2D_6^+$. The effect is merely a shift of the experimental points lying on the energy axis.

In a general way, the agreement between theory and experiment is rather good, as even a casual glance at Figures 1 and 2 will show. The discrepancies are only minor, at most a 10% difference between the cal-

(38) F. H. Field and J. L. Franklin, "Electron Impact Phenomena," Academic Press, New York, N. Y., 1957.

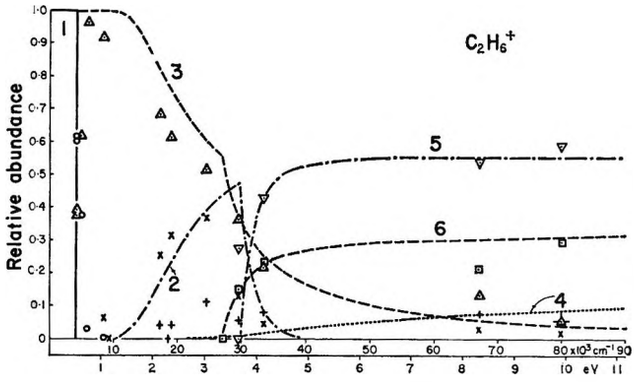

Figure 1. Comparison of calculated breakdown curves for $C_2H_6^+$ with experiment. Calculated curves: 1, $C_2H_6^+$; 2, $C_2H_5^+$; 3, $C_2H_4^+$; 4, CH_3^+; 5, $C_2H_3^+$; 6, $C_2H_2^+$. Experimental points: O, $C_2H_6^+$; ×, $C_2H_5^+$; Δ, $C_2H_4^+$; +, CH_3^+; ∇, $C_2H_3^+$; □, $C_2H_2^+$. Excitation energy is given in both cm^{-1} and ev.

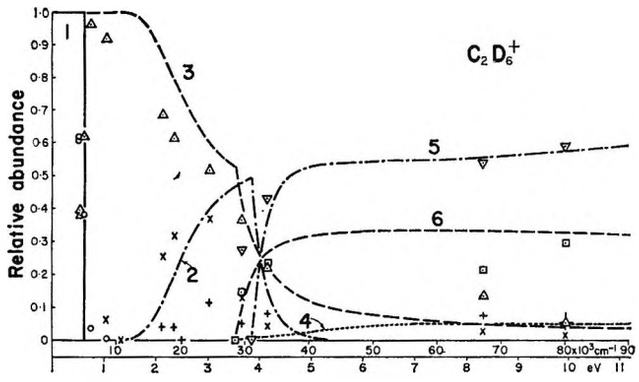

Figure 2. Comparison of calculated breakdown curves for $C_2D_6^+$ with experiment. Calculated curves: 1, $C_2D_6^+$; 2, $C_2D_5^+$; 3, $C_2D_4^+$; 4, CD_3^+; 5, $C_2D_3^+$; 6, $C_2D_2^+$. Experimental points: O, $C_2D_6^+$; ×, $C_2D_5^+$; Δ, $C_2D_4^+$; +, CD_3^+; ∇, $C_2D_3^+$; □, $C_2D_2^+$. Excitation energy is given in both cm^{-1} and ev.

culated and experimentally determined abundance, which is probably better than one has a right to expect, considering the numerous approximations it was necessary to make. This agreement is an indication that assumptions 2, 3, and 4 mentioned in the Introduction are at least approximately fulfilled. However, as shown at the beginning of this Discussion, this agreement does not provide any support, either for or against the validity of assumption 1, so that the results of the present calculations yield only a partial, though reasonably successful, test of the statistical theory of mass spectra. Thus, while there remains some uncertainty about the nature of the electronic state from which M^{+*} decomposes, the theory does appear to provide a useful picture of events following ionization. That the theory does not explain everything becomes obvious if attention is focused on some of the details.

First, there is a difficulty with the breakdown curves of CH_3^+ (and CD_3^+) (curves 4 in Figures 1 and 2). Theory shows no appreciable abundance of these ions just above their A.P., *i.e.*, between 20,000 and 30,000 cm^{-1}, while (one) experiment (with Kr^+) actually shows a small maximum in this region, corresponding to about 10% abundance. This discrepancy is unlikely to be due to a poor performance at low energies of Haarhoff's formula for the density of states of the complex. The activated complex postulated for the decomposition into two methyls involves five active rotations, and a check of the formula at low energies showed[36b] that for several active rotations it gave a count that was on the high side, so that, if anything, the first two or three theoretical points above the A.P. are likely to give an abundance that is actually too high. On the other hand, in order to prevent the abundance of CH_3^+ from becoming too high at high energies (60,000–80,000 cm^{-1}), it was not possible to use a low value for D (*cf.* Tables III and IV). Thus it is impossible to fit the abundance of CH_3^+ at both high and low energies with the same set of parameters. Moreover, the experimentally observed abundance of CH_3^+ near its A.P. is so high that probably no reasonable choice of parameters for the complex would yield a theoretical rate constant that would be high enough. It would thus appear that the ion CH_3^+ (and in fact any first generation ion with high A.P.) produced in charge-transfer experiments is "prepared" in a special way that gives it an abnormally high rate of decomposition at excitation energies slightly above its A.P., but that at higher energies its excitation energy is more nearly randomized in accordance with the assumptions of the theory. This special "preparation" would have to be such that the $C_2H_6^+$ systems are distributed only over a limited portion of energy hypersurface in phase space, resulting in a lower number of effective degrees of freedom, a higher average energy per degree of freedom, and increased specific dissociation probability, or it might involve decomposition by predissociation; however, dissociation from a repulsive state would seem to be excluded since the CH_3^+ fragments would then have appreciable kinetic energy and would not have been detected in Lindholm's experimental arrangement.

A similar difficulty exists with the breakdown curves of $C_2H_5^+$ and $C_2D_5^+$ (curves 2 in Figures 1 and 2), although in a less acute form. The two experimental points representing the relative abundance of 0.07 and 0.25 were obtained in experiments with N_2O^+ and CO_2^+, respectively, and shifting them slightly to higher energies, for reasons discussed above, would decrease the discrepancy between theory and experiment.

On the other hand, if the true appearance potential of CH_3CH^+ is less than the value of 10,000 cm^{-1} used in the calculations, this discrepancy would increase.

The abundance of CH_3CH^+ is not shown, only the sum of the abundance of CH_3CH^+ and $CH_2CH_2^+$ (marked $C_2H_4^+$, curve 3 in Figures 1 and 2), since the experimental data available do not distinguish between the two structures. However, without postulating the existence of the structure CH_3CH^+ it would have been quite impossible to fit the observed abundance of $C_2H_2^+$. Experiment also shows a high-energy tail on the parent-ion breakdown curve; this seems to be a general feature of all experimental breakdown curves. The tail represents ions decomposing at a slower rate than they should, which is difficult to explain on theoretical grounds. However, the abundance of these slow-decomposing ions is less than 3% in the case of $C_2H_6^+$ and $C_2D_6^+$ and hence represents only a very minor difficulty.

The justification for using D as an adjustable parameter in the case of the complexes is the difficulty of making a rational choice for any particular value of D. A low D has the effect of appreciably increasing the density of states with increasing energy compared with the harmonic case, as is shown for one typical complex in Table V. For a D that is not too low, approximately the same increase in the harmonic density could have been accomplished (with a great deal more computational effort) by an appropriate variation of the molecular parameters of the complex, so that a variable D is merely a convenient device for adjusting the density of states of the complex. All of the D's used for the complexes in this work are between 15,000 and 30,000 cm^{-1}, so that the adjustment is modest and no doubt quite within reason.

Table V: Anharmonicity Correction Factor $I_m(\text{anh})/I_m(\text{harm})$ for the Density of States[a]

Excitation energy E, cm^{-1}	Complex $(C_2H_6^+ \cdots H)^{\ddagger}$ D_e = 10,000 cm^{-1}	D_e = 20,000 cm^{-1}	D_e = 86,000 cm^{-1}	Molecule $C_2H_6^+$ D = 13,256 cm^{-1}
10,000	1.046	1.008	1.000	2.136
20,000	2.593	1.534	1.097	3.837
30,000	5.573	2.116	1.172	6.964
40,000	12.680	2.906	1.247	13.21
50,000	31.87	4.037	1.324	26.59
60,000	90.85	5.713	1.406	57.47
70,000	299.6	8.268	1.493	134.50
80,000	1163.1	12.27	1.587	343.71

[a] Excitation energy E is that of the molecule-ion. The excitation energy of the complex is smaller by the activation energy, which in this case is 9279 cm^{-1}.

The D for the molecular ion must be considered as resting on fairly solid grounds, based as it is on the spectroscopically determined anharmonicity coefficients; ultimately, however, it depends on the validity of the Morse potential as a fair representation of the potential energy function of each normal vibration. While it is true that occasionally eq 4 yields a D_t that is different from a D_t obtained calorimetrically or from kinetics experiments, it is unlikely that D, which is an average of the D_t's, should be very much in error. In the case of ethane, this D happens to be quite low, so that the anharmonic correction for the molecule-ion increases rapidly with energy (*cf.* Table V), in fact, more rapidly than the corresponding correction for the complex, so that the value of the rate constant, which is proportional to the ratio of the two, actually shows a maximum as a function of energy that grows more pronounced as the inequality $D(\text{complex}) > D(\text{molecule})$ increases (Figure 3). However, when $D(\text{complex}) < D(\text{molecule})$, the rate constant increases with energy more steeply than in the harmonic case (Figure 3). This somewhat disturbing maximum in the rate constant does not appear to be due to a failure of Haarhoff's anharmonicity correction factor at high energies, since, on the one hand, he appears to have taken into account a cutoff for each individual oscillator, and on

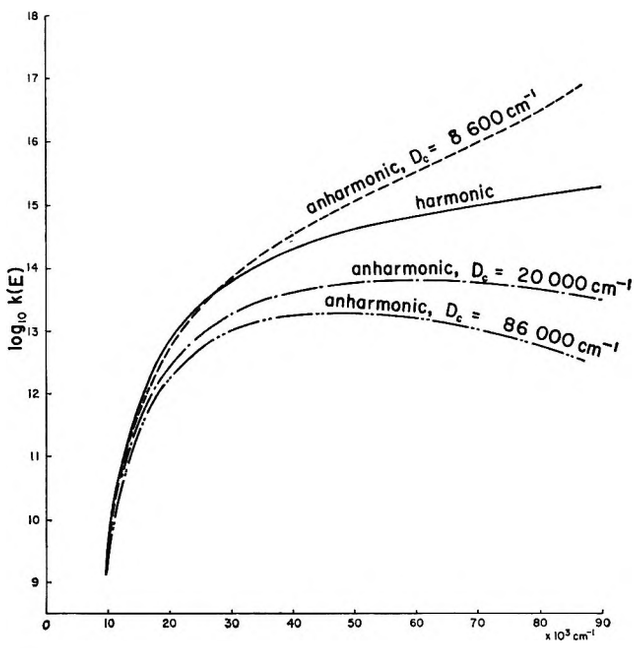

Figure 3. Example of dependence of rate constant on anharmonic correction in complex. D_e is the mean Morse dissocation energy of the complex. The mean Morse dissociation energy of the molecule is 13,256 cm^{-1} in all three anharmonic cases. Calculations done for the decomposition $C_2H_6^+ \rightarrow C_2H_5^+ + H$. Abscissa is excitation energy in cm^{-1}.

the other hand, the energies involved here are well below the energy necessary to dissociate the whole molecule, where one might expect his formula to run into difficulties. It should also be noted that the curves in Figure 3 are quite unlike those obtained by Vestal and Rosenstock[39] for a rate constant based on an array of identical harmonic (or exponential) oscillators with a cutoff. This peculiar behavior of the calculated rate constants is without much practical consequence.

With a D(complex) $\approx$ 30,000 cm^{-1}, a value most frequently used in this work, the decrease at high energies is modest (Figure 3), and the energies at which this decrease occurs are so high (>80,000 cm^{-1}) that most of the breakdown curves are not affected at all. Furthermore, since all the rate constants behave in a similar fashion at these high energies, and since a breakdown curve is given by one particular rate constant divided by a sum of all the rate constants, the effect more or less averages out and the shape of the breakdown curve is little affected. In other words, the breakdown curve in its horizontal portion is insensitive to the behavior of the rate constants as a function of energy, provided all the rate constants follow the same trend.

The maximum values of the calculated rate constants for the various processes are given in Table VI. The lifetimes of the various species are equal to the reciprocal of the respective rate constants, and it is seen that they are all of the order of one period of molecular vibration, which would require the randomization of energy, if assumption 2 holds, to be completed within this time. Bunker[40] has calculated the rate constants for intramolecular relaxation for a number of triatomic molecules and found the usual value to be 10^{11} sec^{-1}, although he found in the case of cyclopropane and H_2O_2 values as high as 10^{14} and 10^{13} sec^{-1}, respectively. The present results would appear to present a borderline case; however, it seems quite likely that some energy randomization already occurs during charge exchange, *i.e.*, during the (assumed) cascading through higher electronic states into the ground state of the ion, so that not all of the randomization is dependent on vibrational anharmonicity as the only mechanism. Therefore, it would seem rather premature, at the present time, to conclude from the high values of the rate constants in Table VI that assumption 2 of the theory does not hold.

The minimum value of each rate constant occurs at threshold, *i.e.*, when excitation energy is equal to activation energy E_a; then

$$k(E_a) = \alpha[h\rho(E_a)]^{-1}$$

where $\rho(E_a)$ is the density of states (obtained by linear interpolation) of the molecule ion at energy E_a, and the other symbols have their usual significance. The values of $k(E_a)$ for the various first-generation processes are listed in Table VI; because of the interpolation procedure, the rate constants are minimum values.

Table VI: Maximum and Minimum Values of Calculated Unimolecular Rate Constants for Various Processes[a]

Process	Max $k(E)$, sec^{-1}, at E, cm^{-1}		$k(E_a)$ sec^{-1}
$C_2H_6^+ \rightarrow C_2H_5^+$	1.14×10^{14}	58,000	2.08×10^8
$\rightarrow CH_3CH^+$	6.23×10^{13}	60,000	1.46×10^8
$\rightarrow CH_2CH_2^+$	2.21×10^{13}	40,000	7.45×10^{10}
$\rightarrow CH_3^+$	1.46×10^{13}	68,000	3.28×10^5
$C_2D_6^+ \rightarrow C_2D_5^+$	4.04×10^{13}	60,000	3.35×10^6
$\rightarrow CD_3CD^+$	2.46×10^{13}	58,000	1.86×10^6
$\rightarrow CD_2CD_2^+$	5.32×10^{12}	46,000	8.68×10^8
$\rightarrow CD_3^+$	3.80×10^{12}	62,000	8.10×10^3

[a] Maximum value of calculated unimolecular rate constant is Max $k(E)$; E is excitation energy of the molecule-ion at which maximum occurs. Minimum value is given by $k(E_a)$, the value of rate constant at threshold (excitation energy equal to activation energy E_a).

Experimentally, there is observed a metastable transition in the decomposition to ethylene ion (without distinction between the two possible structures); Table VI gives for the slower process a rate constant of $\sim 10^8$ sec^{-1} in the case of the hydrogenated species, which is about two orders of magnitude too fast for it to be detected as a metastable transition. In the case of the deuterated species, the rate constant is $\sim 10^6$ sec^{-1}, which would make it just barely detectable as a metastable transition.

On the other hand, calculated rate constants for decomposition to methyl radical ion are low enough so that a metastable transition might be observed at mass $m^* = 7.5$ in the case of $C_2H_6^+ \rightarrow CH_3^+$, and at $m^* = 9.0$ in the case $C_2D_6^+ \rightarrow CD_3^+$. There do not seem to be any experimental data about metastable transitions in ethane below mass 12.

Acknowledgment. Z. P. is grateful to Université Laval for the award of a postdoctoral fellowship.

Appendix I

Assignment of Structural Parameters

Refer to Tables I, II, III, and IV in the text.

Molecular Ions $C_2H_6^+$ and $C_2D_6^+$. Vibrational frequencies used correspond to those known from infra-

(39) M. L. Vestal and H. M. Rosenstock, *J. Chem. Phys.*, **35**, 2008 (1961).

(40) D. L. Bunker, *ibid.*, **40**, 1946 (1964).

red and Raman spectra[29,41] for the neutral molecules. Free internal rotation around the C–C bond is assumed since the hindering potential is likely to be very small in comparison with the excitation energies involved here. The reduced moment of inertia for the internal rotation (I_{red}) is taken equal to that in the neutral molecule.

The Activated Complexes $(C_2H_5^+ \cdots H)^{\ddagger}$ *and* $(C_2D_5^+ \cdots D)^{\ddagger}$. In these complexes one C–H (C–D) stretching vibration at 2950 cm^{-1} (2190 cm^{-1}) becomes the reaction coordinate. By analogy with complex postulated in the thermal decomposition of the neutral molecule,[16] two CH_3 (CD_3) bending frequencies were lowered from 1460 to 300 cm^{-1} (1080 to 220 cm^{-1}) and the doubly degenerate bending vibrations at 820 cm^{-1} (590 cm^{-1}) were lowered to 700 cm^{-1} (500 cm^{-1}). Free internal rotation around the C–C bond is again assumed. The moment of inertia for this rotation (I_{red}) was calculated under the assumption that the distance C $\cdots$ H (C $\cdots$ D) is double the normal distance in the neutral molecules. Direct count shows the reaction path degeneracy to be 6. The activation energy of 9279 cm^{-1} (10,893 cm^{-1}) corresponds to the mass spectrometrically measured appearance potential.[32,38] The mean Morse dissociation energy D was treated as an adjustable parameter and best results were obtained for D = 20,000 cm^{-1} (25,000 cm^{-1}), which would seem to be a reasonable value.

The Activated Complexes $(CH_3CH^+ \cdots H_2)^{\ddagger}$ *and* $(CD_3CD^+ \cdots D_2)^{\ddagger}$. Here two hydrogens come off the same carbon atom and the complexes are assumed to have the cyclic structure

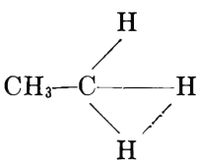

The symmetric C–H (C–D) stretch becomes the reaction coordinate and the H–H stretching vibration is assigned the value 3500 cm^{-1} (2690 cm^{-1}), *i.e.*, about 80% of the frequency of this vibration in H_2 (D_2). The CH_3 (CD_3) bending vibrations are lowered to 500 cm^{-1} (300 cm^{-1}). Direct count again yields 6 as the reaction path degeneracy. Free internal rotation about the C–C axis is assumed and the reduced moment of inertia was calculated assuming double the normal distance for C$\cdots$H (C$\cdots$D). Activation energy was estimated to be 10,000 cm^{-1}, as mentioned in the text (11,614 cm^{-1} for the deuterated species, *i.e.*, 0.2 ev higher). The best value of D was found to be 20,000 cm^{-1} (30,000 cm^{-1}).

Activated Complexes $(CH_2CH_2^+ \cdots H_2)^{\ddagger}$ *and* $(CD_2CD_2^+ \cdots D_2)^{\ddagger}$. Here one hydrogen comes off each carbon atom and the activated complex is assumed to have the structure of a four-membered ring. The symmetric C–H (C–D) stretch transforms into the reaction coordinate and two ring deformation frequencies are taken to be 600 and 900 cm^{-1} (400 and 800 cm^{-1}). This complex is rigid with no internal rotation; reaction path degeneracy is 9, by direct count. The activation energy is the corresponding appearance potential, *i.e.*, 4034 cm^{-1} (5648 cm^{-1}). The best value of D turned out to be 30,000 cm^{-1} for both hydrogenated and deuterated species.

Activated Complexes $(CH_3^+ \cdots CH_3)^{\ddagger}$ *and* $(CD_3^+ \cdots CD_3)^{\ddagger}$. Again by analogy with the thermal study of the neutral species,[16] this complex is assumed to be very loose with both methyls rotating freely, giving a total of five free internal rotations. The methyls are assumed to be planar, the largest moment of inertia representing the mutual rotation about the C–C axis (symmetry number 3), and two smaller moments of inertia belonging to the other two degrees of freedom of rotation per methyl, one of the symmetry number 2, the other of the symmetry number 1. Activation energy is the measured appearance potential,[32,38] 18,557 cm^{-1} (20,171 cm^{-1}). The reaction path degeneracy of two corresponds to two ways of locating the charge in the molecule. The best value of D was found to be 15,000 cm^{-1} (30,000 cm^{-1}).

Appendix II

Calculation of Fluctuations

Fluctuation in the Formation of $C_2H_3^+$ *and* $C_2D_3^+$. The vibrational frequencies of $C_2H_5^+$ ($C_2D_5^+$) were assumed to be those of C_2H_5 (C_2D_5). Activation energies E_a and E_a' were rounded off to the nearest 100 cm^{-1} to simplify the computations. As a modest variation in D affects the results only very slightly, D was arbitrarily set in this case at 25,000 cm^{-1}. Because in this case the neutral counterpart is an atom (H or D), ρ_2 = 1, and $\phi(E)$ depends only on the ratio of densities of $C_2H_5^+$ ($C_2D_5^+$) integrated between different limits.

Fluctuations in the Formation of $C_2H_2^+$ *and* $C_2D_2^+$. Since there are no known neutral species of the structure $CH_3CH(CD_3CD)$, the vibrational frequencies of $CH_3CH^+(CD_3CD^+)$ listed in Tables II and III are little better than an educated guess. Free rotation about the C–C axis is assumed. E_a' = 17,000 cm^{-1} corresponds

(41) G. Herzberg, "The Infrared and Raman Spectra of Polyatomic Molecules," D. van Nostrand Co., Inc., New York, N. Y., 1945.

to the difference of measured appearance potential of $C_2H_2^+(C_2D_2^+)$ and the assumed activation energy for the formation of CH_3CH^+ and CD_3CD^+ (10,000 and 11,614 cm^{-1}, respectively). The vibrational frequencies and Morse dissociation energies of H_2 and D_2 are literature values.[42] The values of D for both CH_3CH^+ and CD_3CD^+ were estimated as 25,000 cm^{-1}.

(42) G. Herzberg, "The Spectra of Diatomic Molecules," D. van Nostrand Co., Inc., New York, N. Y., 1950.

Electron Spin Resonance Spectra of Free Radicals in Irradiated Cyclohexanecarboxylic Acid[1]

by Philip M. K. Leung and John W. Hunt

Department of Medical Biophysics, University of Toronto, and The Ontario Cancer Institute, Toronto, Ontario, Canada *(Received January 16, 1967)*

The esr spectra of irradiated cyclohexanecarboxylic acid (CCA) were observed following irradiation at 4 and 153°K. Following irradiation at 153°K, three free-radical species were detected, two being identified as *c*-$C_6H_{11}\cdot$ and *c*-C_5-$H_{10}\dot{C}$-COOH (CCA radical). The CCA radicals were stable up to the melting point of the compound, with reversible changes in the spectra being observed due to chair–chair interconversion. The cyclohexyl radicals decayed at about 188°K, some of them extracting hydrogen atoms from CCA molecules to give new CCA radicals. At least three transient species were detected in samples irradiated and observed at 4°K, one probably being the ion radical, *c*-C_6H_{11}-$\dot{C}<^{O^-}_{OH}$. The ion radical and another species decayed when the temperature was increased to about 143°K, and the CCA radical grew in their place.

I. Introduction

Cyclohexane is often chosen for radiation chemistry studies because the symmetry of the molecule limits the types of radiation products expected and simplifies the electron spin resonance (esr) spectra. In addition, the effects of the substituted groups on the formation of free radicals may be studied with comparative ease.

The esr spectra of irradiated cyclohexane have been observed by a number of groups at temperatures below 173°K,[2-5] above the phase transition temperature at 186°K, and in the liquid phase using continuous irradiation techniques.[6,7] The spectra were all attributed to the cyclohexyl radical formed by the extraction of a hydrogen atom from the cyclohexane ring. The principal radiolysis products, hydrogen, bicyclo-

(1) Based on work carried out under the auspices of the Ontario Cancer Institute, the National Cancer Institute of Canada, and the National Research Council of Canada.

(2) B. Smaller and M. S. Matheson, *J. Chem. Phys.*, **28**, 1169 (1958).

(3) N. Ya. Cherniak, N. N. Bubnov, L. S. Poliak, Yu. D. Tsvetkov, and V. V. Voevodskii, *Opt. Spectry.*, **6**, 360 (1959).

(4) P. B. Ayscough and C. Thomson, *Trans. Faraday Soc.*, **58**, 1477 (1962).

(5) K. Leibler and H. Szwarc, *J. Chim. Phys.*, **57**, 1109 (1960).

(6) N. Ya, Buben, Yu. N. Molin, A. I. Pristupa, and V. N. Shamshev, *Dokl. Akad. Nauk SSSR*, **152**, 352 (1963).

(7) R. W. Fessenden and R. H. Schuler, *J. Chem. Phys.*, **39**, 2147 (1963).

hexyl, and cyclohexene,[8,9] were formed in the proper proportions and yields to agree with the assignment of the cyclohexyl radical as the most important intermediate radiolysis product. Changes in the esr spectra have been observed at intermediate temperatures which were interpreted in terms of chair–chair interconversion of the cyclohexyl ring.[6,7]

The esr spectra of a number of derivatives of cyclohexane have also been studied.[4,10-13] In general, these esr spectra show the presence of more than one free-radical species. In addition, many of these spectra show puzzling changes with temperatures, some reversible and some irreversible. In one of these derivatives, cyclohexanecarboxylic acid (c-$C_6H_{11}COOH$, abbreviated as CCA), we have been able to identify most of the free radicals which are produced and to understand the changes which take place in the esr spectra as a function of temperature.

Most of the experiments reported here were for irradiations and observations carried out at the intermediate temperature of 153°K. Under these conditions, the reactions of mobile free radicals such as H· and ·OH[14,15] and also ionic reactions should be completed while the less freely diffusing free radicals containing the cyclohexyl ring should be stable. In order to check the conclusions from these experiments, another set of observations was carried out at liquid helium temperature (4°K), and the changes in these esr spectra were also followed as the samples were warmed.

II. Experimental Section

A. Chemicals. Cyclohexanecarboxylic acid (CCA) (Eastman Organic Chemicals) was redistilled three times, the middle 40% being collected in each successive distillation. Deuterium-labeled cyclohexanecarboxylic acid ($C_5H_{10}CDCOOH$, abbreviated as CCA-d_1, Merck and Co. Ltd., Montreal) was used as obtained from the supplier without further purification. Analysis of these samples by gas chromatography showed that the detectable impurities were less than 0.1%.

B. Irradiation and Esr Observations at 153°K. The samples (1 ml) were placed in a special sealed microwave cavity and degassed by three cycles of freezing, evacuation, and thawing. The system was then pressurized to slightly over 1 atm by extra high purity nitrogen (Ohio Chemical Co.), and the samples were irradiated under these conditions.

The 2.6-Mev electron beam from a Van de Graaff generator was directed through an axial hole in the esr magnet and onto the microwave cavity (Figure 1). Using this arrangement, esr spectra could be observed while the sample was being irradiated. This technique also eliminated the problems of extraneous signals from the sample holder and of handling the samples at low temperatures.

The dose absorbed by the sample was estimated by use of a "perspex" solid state dosimeter developed by Boag, *et al.*,[16] and was found to be approximately 50 krads/sec per μa of electron beam. The temperature of the sample was controlled by passing cold N_2 through a brass block attached to the cavity and was held constant to ± 0.5°K by a thermocouple control unit (Thermovolt Co. Ltd., Toronto) which varied the N_2 flow rate (Figure 1).

The esr spectrometer was a conventional instrument operating at about 9.2 GHz at a microwave power level of about 1 mw, and employing magnetic field modulation and phase sensitive detection at 450 kHz. The first derivative of the absorption signal was recorded. The 7-in. magnet (Harvey Wells Corp.) was provided with a $^3/_8$-in. axial hole through the pole face. A pair of 0.005 × 0.5 in. o.d. soft iron shims was used to compensate for the magnetic field distortion due to the axial holes. With these shims in place, the field was homogeneous to better than 0.1 gauss over the sample volume. The spectroscopic splitting factors, g, and the hyperfine splitting constants were determined by making precise measurements of the magnetic field and microwave frequency. The magnetic field was measured by a nuclear magnetic resonance (nmr) probe located beside the esr cavity (Figure 1), and the resonance frequency was determined by a Hewlett-Packard 5245A frequency meter to an accuracy of better than 1 part in 10^5. A small correction (0.18%) was made for the difference between the magnetic field at this position and the sample. This correction factor was obtained by measuring the magnetic field with the nmr probe positioned in an empty cavity. The microwave frequency was measured to the same precision as the magnetic field (1 part in 10^5) using a Dymec (Hewlett-

(8) P. J. Dyne and J. A. Stone, *Can. J. Chem.*, **39**, 2381 (1961).

(9) L. J. Forrestal and W. H. Hamill, *J. Am. Chem. Soc.*, **83**, 1535 (1961).

(10) Yu. D. Tsvetkov, J. R. Rowlands, and D. H. Whiffin, *J. Chem. Soc.*, 810 (1964).

(11) K. Leibler, *J. Chim. Phys.*, **57**, 111 (1960).

(12) T. Ohmae, S. Ohnishe, H. Sakurae, and I. Nitta, *J. Chem. Phys.*, **42**, 4053 (1965).

(13) W. B. Sampson, unpublished Ph.D. Thesis, University of Toronto, 1962.

(14) L. H. Piette, R. C. Rempel, H. E. Weaver, and J. M. Flournoy, *J. Chem. Phys.*, **30**, 1623 (1959).

(15) J. Kroh, B. C. Green, and J. W. T. Spinks, *Can. J. Chem.*, **40**, 413 (1962).

(16) J. W. Boag, G. W. Dolphin, and J. Rotblat, *Radiation Res.*, **9**, 989 (1958).

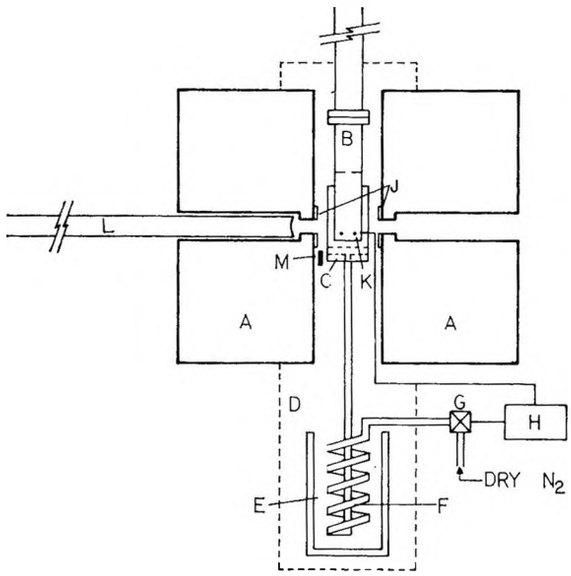

Figure 1. Schematic diagram of the apparatus used to irradiate samples in the esr cavity. Features indicated are: A, esr magnet pole faces; B, sealed esr cavity, H_{012} mode having a 0.010 in. electron entrance window, and accommodating a 1-cm³ sample in the bottom; C, cooling block; D, expanded polystyrene insulation; E, liquid nitrogen reservoir; F, heat-exchange coil; G, gas flow valve; H, thermocouple control unit; J, soft iron shims; K, 450-Hz magnetic modulation wires; L, beam pipe directly connected to Van de Graaff accelerator with a 0.001-in. brass window at exit; M, nmr probe.

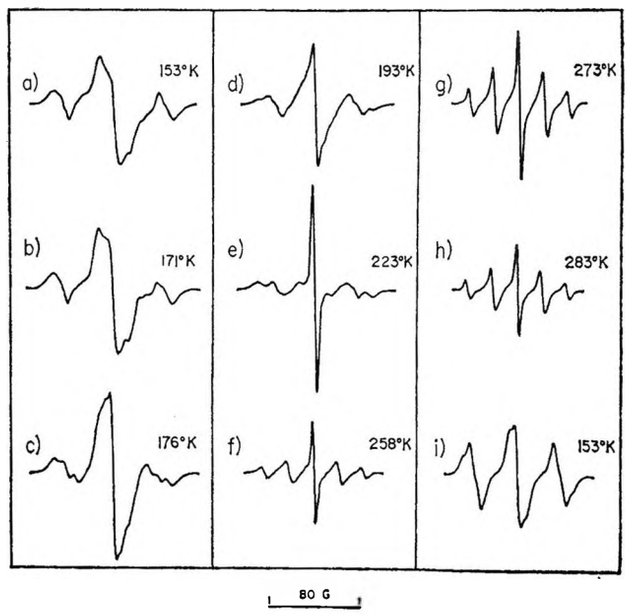

Figure 2. Esr spectra of irradiated cyclohexane-carboxylic acid at various temperatures. The sample was irradiated with a single dose (about 1 Mrad) at 153°K. It should be noted that the relative gains of these spectra were different.

Packard) Dy 2650A oscillator synchronizer modified to lock into the microwave frequency. The frequency of the primary oscillator of the synchronizer (about 100 MHz) was measured with the same frequency meter.

C. Esr Observations at 4°K. These experiments were carried out with a special low-temperature esr spectrometer designed and constructed by H. Box and H. Freund at the Roswell Park Memorial Institute, Buffalo, N. Y. The spectrometer was a superheterodyne instrument operating at a frequency of 24.0 GHz with a 60-Hz sinusoidal magnetic field sweep and using direct detection of the absorption spectrum on an oscilloscope display. The noise level was reduced by repetitive summation of the spectra on a Varian (TMC) computer.

It was not feasible to degas the samples used in these experiments, so that some oxygen was present. Pellets of the sample were frozen, attached to an insertion rod, and lowered into the esr cavity, which was itself immersed in liquid helium. The entire esr cavity was then irradiated at 4°K by unfiltered radiation from a 250-kv X-ray machine to a dose of approximately 0.5 Mrad.

III. Results and Discussion

A. *Esr Spectra of Irradiated Cyclohexanecarboxylic Acid. 1. Esr Spectrum—Irradiation at 153°K.* The esr spectrum in Figure 2a was obtained when cyclohexanecarboxylic acid was irradiated at 153°K to a dose of about 1 Mrad. At this temperature, the complex asymmetrical spectrum observed suggested that a mixture of different radical species was present, but the poor resolution made it very difficult to identify these radicals until experiments had been carried out. A similar spectrum was observed for irradiations at 138°K.

2. *Effect of Temperature.* Both reversible and irreversible changes were observed in the structure of the esr spectrum shown in Figure 2a upon warming and recooling the sample. These changes have been utilized in identifying the free radicals and in studying their possible reaction schemes.

The changes in the spectra when the sample temperature was raised slowly from 153 to 263°K are shown in Figure 2b–h. The initial asymmetrical spectrum observed at 153°K gradually changed into a symmetrical one when the temperature reached about 176°K. On increasing the sample temperature further, some of the lines were observed to broaden and to decay. At 258°K (Figure 2f), two new lines were detected between the broadened lines. The spectra at temperatures above 258°K consisted of five well-resolved lines (Figure 2g and h).

Table I: Summary of Esr Spectra of Cyclohexanecarboxylic Acid

	Compound irradiated	Treatment: T_I, °K[a]	Cycle[b]	Treatment: T_0, °K[c]	Spectrum	Hyperfine splittings, gauss: a_α	Hyperfine splittings, gauss: a_β	Line width, gauss	Intensity distribution, theoret and (measd)[d]	g	Free radicals and (rel intensities)[d]
1	CCA (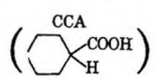)	153	A	153	Asymmetrical, 9 lines +		Unresolved				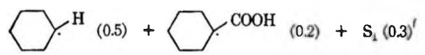 (0.5) + (0.2) + S_1 (0.3)[f]
2	CCA	153	B	153	9 lines		37 ± 0.5, 5 ± 0.5	~5	1:2:1, 2:4:2, 1:2:1	2.0029 ± 0.0001	 (1.0)
		153	B	228	3 lines		42 ± 0.5	~5	1:4:1 (0.94:4.0:0.90)		
		153		303	5 lines		20.9 ± 0.1, 21.3 ± 0.1	~4	1:4:6:4:1 (0.98:3.8:-6:4.0:0.96)		
3	CCA	4.2	A	4.2	Asymmetrical, doublet, singlet, and others		19 ± 2				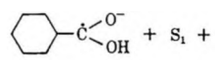 + S_1 + others
4	CCA	4.2	B	4.3	3 lines, each unresolved hfs		37 ± 0.5	~20	1:2:1	2.0029 ± 0.0001	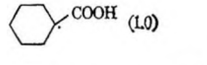 (1.0)
5	CCA-d_1 (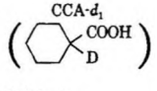)	153	A	153	3 lines, with unresolved hfs		40 ± 0.5				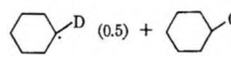 (0.5) + 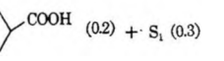 (0.2) + S_1 (0.3)
6	CCA-d_1	153	B	153			Identical with 2				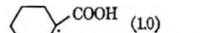 (1.0)
7	CCA-d_1	4.2	A	4.2	Unresolved						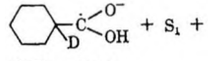 + S_1 + others
8	CCA-d_1	4.2	B	4.2			Similar to 4				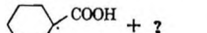 + ?
9	Cyclohexane	153	A	153	6 lines, each an unresolved triplet	21	41 ± 0.5, 5 ± 0.5	~15	2 × (1:2:1; 2:4:2; 1:2:1)	2.0026 ± 0.0001	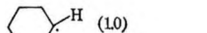 (1.0)
10	Theoretical cyclohexyl-d_1[e]			153	3 lines, with unresolved hfs	3.5	41 ± 0.5	~15	1:2:1	2.0026 ± 0.0001	
11	S_1[f]			153	Singlet			~15		2.0029 ± 0.0002	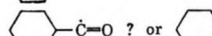 ? or 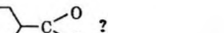 ?

[a] T_I, irradiation temperature. [b] A, initial spectrum at irradiation temperature. B, samples warmed to above 248°K, then recooled to observation temperature, T_0. [c] T_0, observation temperature. [d] Relative intensities determined by first moment integration procedure.[24] [e] Values obtained by reconstruction of spectrum[20] and from the work of Fessenden, *et al.*[7,21] [f] S_1, unidentified singlet.

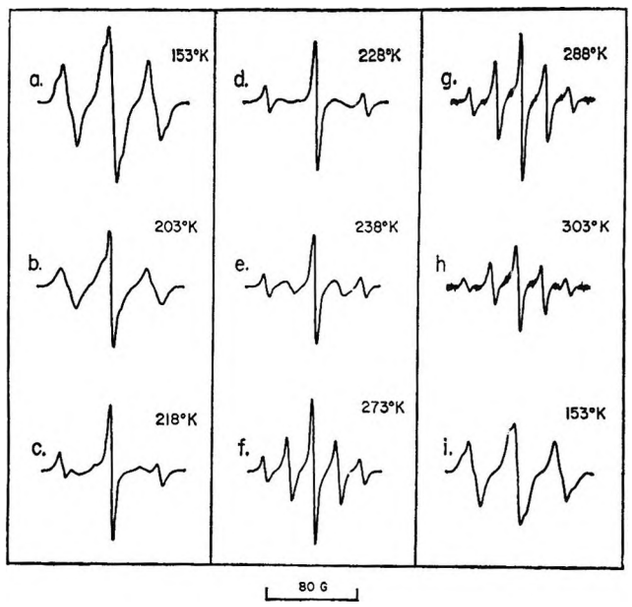

Figure 3. Variation with temperature of the esr spectra of the cyclohexylcarboxylic acid radicals. It should be noted that the relative gains of these spectra were different. These spectra were obtained after the sample had been irradiated at 153°K and annealed at about 253°K.

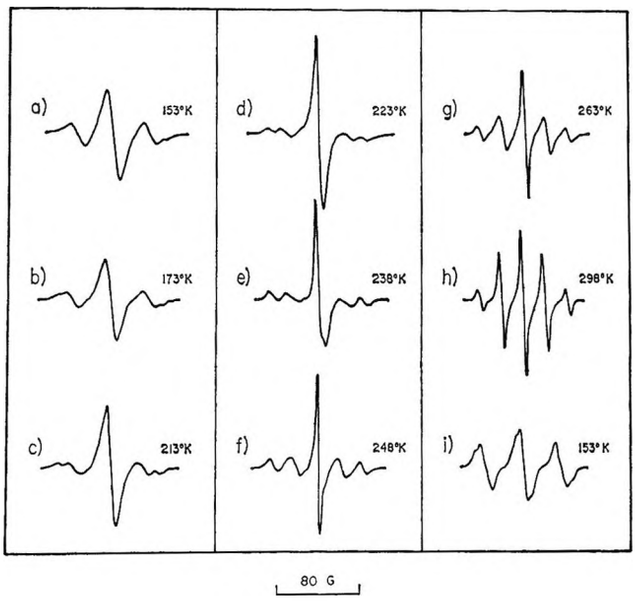

Figure 4. Esr spectra of irradiated cyclohexane-carboxylic acid-d_1 at various temperatures. The sample was irradiated with a single dose (about 1 Mrad) at 153°K.

When the sample was recooled to 153°K, a symmetrical nine-line spectrum was observed (Figure 2i) which had an intensity distribution of approximately 1:2:1; 2:4:2; 1:2:1. It should be noted that this spectrum was very different from the one initially observed (Figure 2a).

When the temperature of this "heat-annealed" sample was again increased gradually up to 188°K, there were no significant changes in the spectrum (Figure 3). Above 188°K, some of the lines broadened and disappeared completely, so that at 228°K only three lines with an intensity distribution of 1:4:1 were seen (Figure 3b–d). As the temperature was increased further, two new lines were detected which sharpened and grew in amplitude (Figure 3e–h). At 303°K, a spectrum containing five narrow lines with an intensity distribution of approximately 1:4:6:4:1 was seen (Figure 3h).

Upon further cycles of warming and cooling, the changes in the spectra were identical with those shown in Figure 3, and there was little decay in the signal amplitude. However, when the temperature approached the melting point of CCA (304°K), the signal decayed very rapidly.

The observed hyperfine splittings, intensity distributions, and spectroscopic splitting factors of these spectra are summarized in Table I.

B. Esr Spectra of Irradiated Deuterium-Labeled Cyclohexanecarboxylic Acid. In order to help identify the radicals which were present initially, a sample was studied in which the hydrogen on the carbon adjacent to the carboxyl group was replaced by deuterium.

1. Esr Spectrum—Irradiation at 153°K. A sample of deuterium-labeled CCA (CCA-d_1) was irradiated at 153°K. The initial esr spectrum observed at this temperature is shown in Figure 4a. It consists of a slightly asymmetric, unresolved triplet which again suggests the presence of a mixture of radicals. This spectrum, however, is different from that of irradiated CCA, both in its over-all hyperfine splitting and structure. This implies that the unpaired electrons in the free radicals initially observed at 153°K interact strongly with the proton (or deuteron in CCA-d_1) on the carbon adjacent to the carboxyl group.

2. Effect of Temperature. When the temperature of the sample was gradually increased, changes in the esr spectra occurred above 193°K which were similar to those observed in irradiated CCA (Figure 4c–i). The spectrum observed at 298°K (Figure 4h) was indistinguishable from that of the CCA at the same temperature, and on the second and subsequent cycles of warming and cooling, the changes were characteristic of those observed in CCA.

C. Analysis of Spectra and Identification of Free Radicals. 1. Stable Radical. After the warming and cooling cycle, the nine-line spectrum observed at 153°K had hyperfine splittings of 37 and 5 gauss which

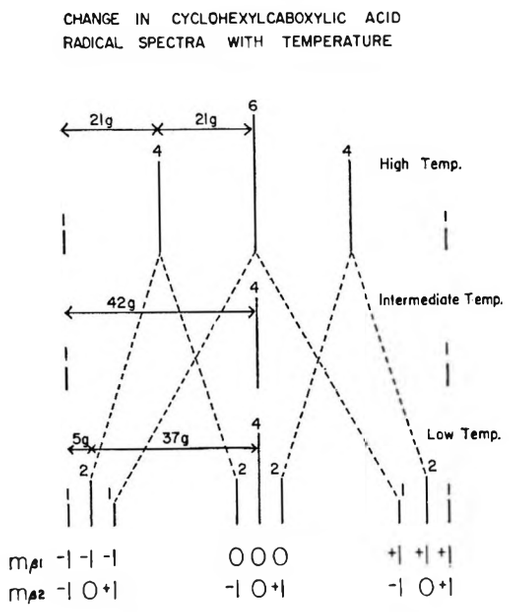

Figure 5. Theoretical changes in the esr spectra of the cyclohexylcarboxylic acid radical as a function of temperature. The symbols $m_{\beta 1}$ and $m_{\beta 2}$ represent the magnetic spin quantum numbers of the strong and weak interacting pair of β protons, respectively. At low rates of inversion, the spectrum consists of nine lines which are due to the interaction of the unpaired electron with the weak and strong interacting pairs of protons (bottom spectrum). When the rate of inversion approaches the hyperfine splitting frequency (middle spectrum), only the lines for which the spin quantum numbers remain unchanged are seen. At inversion rates much higher than the hyperfine splitting frequency, all four β protons appear to be equivalent and five lines in the intensity distribution of 1:4:6:4:1 are observed (upper spectrum).

correspond closely to the β proton splittings of the cyclohexyl radical (Table I). In addition, the intensity distribution of these lines (1:2:1; 2:4:2; 1:2:1) suggests that the unpaired electron in this radical interacts with two pairs of equivalent β protons, and with no α proton. The probable form of this radical is the cyclohexylcarboxylic acid free radical (abbreviated as CCA radical) formed by the removal of the hydrogen on the carbon adjacent to the carboxyl group.

This preliminary identification is confirmed by a detailed examination of the changes in the spectra when the temperature was varied. In Figure 5, the bottom spectrum shows the theoretical hyperfine splittings and intensity distributions for an unpaired electron interacting strongly with two equivalent β protons, and weakly with two others. Upon chair–chair interconversion of the cyclohexyl ring, the two pairs of β protons with spin quantum numbers $m_{\beta 1}$ and $m_{\beta 2}$ would be interchanged. The two outside lines and the central line are invariant on this interchange, while the resonance field of the others would be shifted. At intermediate rates of interconversion, these lines would broaden and move toward their inverse line, so that only three lines with an intensity distribution of 1:4:1 would be observed. At higher temperatures, where the rate of interconversion would be much greater than the hyperfine splitting frequency[17] (>10^8 cs), the broadened lines would then coalesce. If the populations in the two configurations were the same, a five-line spectrum having equal hyperfine splittings and an intensity distribution of 1:4:6:4:1 should be observed.

The behavior of the esr spectra of the free radicals which were stable upon heat annealing completely follows this theoretical variation and supports the initial identification of the CCA radicals. This is also confirmed by the identical spectra observed from annealed samples of CCA and CCA-d_1.

Such an identification of the CCA radical is in agreement with the observations made in other organic acids by a number of workers. Most of these have been discussed in the review by Matheson.[18] One very interesting report has been published by Zhidomirov and Tsvetkov,[19] who discussed similar interconversions in the free radicals formed by the irradiation of a number of sodium salts of alicyclic hydrocarbons. In all cases, the same conclusions were drawn regarding the stable radical species produced, but free radicals from the sodium salt of cyclohexane–carboxylic acid did not show any indication of this rapid interconversion.

2. Synthesis of the Initial Spectra. Although the initial esr spectrum of CCA irradiated at 253°K (Figure 6a) is poorly resolved, a careful examination reveals that some of the lines in this spectrum occupy the same position as some of the lines of the cyclohexyl and CCA radical spectra (Figure 6b, c). It is seen in the initial CCA-d_1 spectrum at 253°K that the lines corresponding to the cyclohexyl radical spectrum are replaced by a broad triplet having a hyperfine splitting of about 40 gauss. This splitting is similar to the β splitting in the cyclohexyl radical. Such a change in the spectrum

(17) The rate of interconversion was calculated from the changes of the width of the noninvariant lines and also from the amplitude of these lines using a procedure similar to that of Ogawa and Fessenden and the basic formulations of J. A. Pople, W. C. Schneider, and H. L. Bernstein, "High-Resolution Nuclear Magnetic Resonance," McGraw-Hill Book Co., Inc., New York, N. Y., 1959. The interconversion rate fitted well to a simple Arrhenius type plot over the range in which it could be determined accurately (230 to 300°K), and showed a variation with temperature of the form $\nu_T = 6.99 \times 10^{11} \exp(-3.4 \times 10^3/RT)$. The enthalpy of activation of 3.4 kcal/mole indicated by these results is much lower than the value of 9.1 kcal/mole for interconversion of cyclohexane, but it is in reasonable agreement with the value of 4.9 kcal/mole observed for the cyclohexyl free radical (see ref 21 in next section).

(18) M. S. Matheson, *Ann. Rev. Phys. Chem.*, 13, 77 (1962).

(19) G. M. Zhidomirov and Yu. D. Tsvetkov, *Opt. i Spectroskopiya*, 8, 67 (1964).

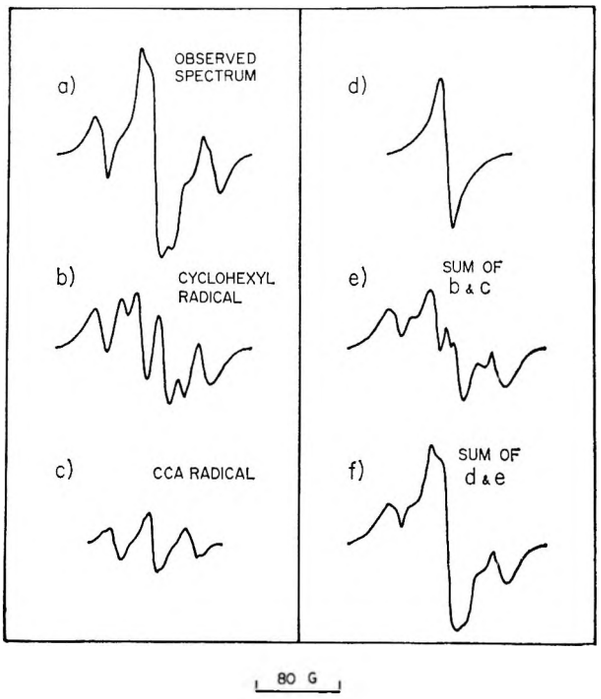

Figure 6. Synthesis of the initial esr spectrum of cyclohexanecarboxylic acid irradiated and observed at 153°K. See text for details.

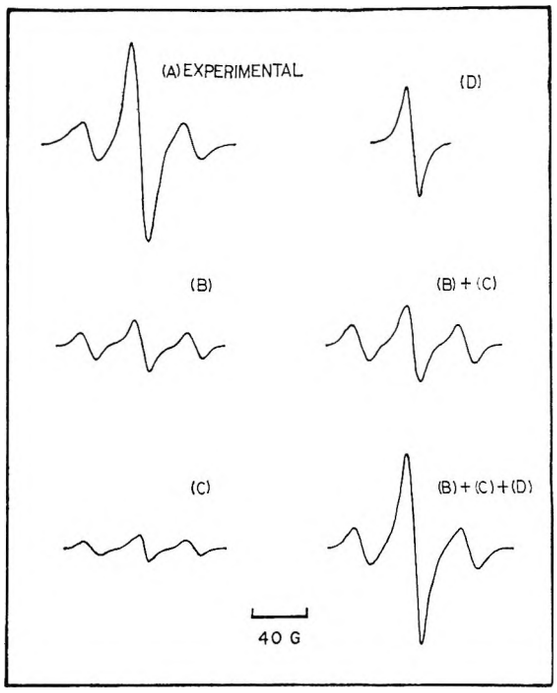

Figure 7. Synthesis of the initial esr spectrum of cyclohexanecarboxylic acid-d_1, irradiated and observed at 153°K (see text). Spectrum (B) is the theoretical spectrum of the $C_6H_{10}CD$ radical, (C) is that of the CCA radical, and (D) is that of the unknown singlet.

could be observed only if the principal species at this temperature was formed by the removal of the carboxyl group, resulting in the free radical $C_5H_{10}\dot{C}D$ which should have a three-line spectrum with a hyperfine splitting of about 41 gauss and intensity distribution of 1:2:1. It would appear, therefore, that the spectrum of free radicals present at 253°K might be that of cyclohexyl radicals upon which the spectra of one or more other radicals were superimposed.

An attempt was made to synthesize the initial CCA spectrum at 253°K by superimposing the spectrum of the CCA radical on that of the cyclohexyl radical with the center of the former shifted about 0.5 gauss toward the high magnetic field (Figure 6e) to allow for the differences in spectroscopic splitting factor (Table I). The calculated spectrum agrees well with the observed one in the outer lines, but did not fit well in the central region. Therefore, a singlet with a line width of 15 gauss (Figure 6d) and the same g value as the CCA radical was added to the composite spectrum. The relative intensity of these spectra (relative yield of the radicals) is about 2 (CCA radicals):3(singlet):5(cyclohexyl radicals). The resulting spectrum (Figure 6f) is very similar to the one originally observed (Figure 6a).

The initial CCA-d_1 spectrum at 253°K could also be synthesized using the same ratio of free-radical yields but by replacing the cyclohexyl radical spectrum with one calculated theoretically for the $C_5H_{10}\dot{C}D$ free radical. The normal cyclohexyl radical spectrum at 253°K may be accurately synthesized using β-proton splitting of 41 and 5 gauss, an α-proton splitting of 21 gauss, and Lorentzian lines having line widths of 15 gauss.[7,20] The spectrum of the $C_5H_{10}\dot{C}D$ radical was synthesized using these values, except that the normal α-hydrogen doublet was replaced by the deuterium triplet which has a splitting of 3.5 gauss[21] (Figure 7B). The synthetic spectrum bears a very close resemblance to the observed one (Figure 7A).

Cyclohexyl radicals could be formed by the removal of the carboxyl group from CCA molecules. A similar spectrum could also be obtained for radicals formed by the extraction of hydrogen atoms from the C-5 and C-4 positions around the cyclohexyl ring. However, since the six-line spectrum characteristic of the normal cyclohexyl radical was absent in the initial CCA-d_1 spectrum observed at 253°K, this possibility may be ruled out.

(20) P. M. K. Leung, unpublished calculation.

(21) S. Ogawa and R. W. Fessenden, *J. Chem. Phys.*, **41**, 994 (1964).

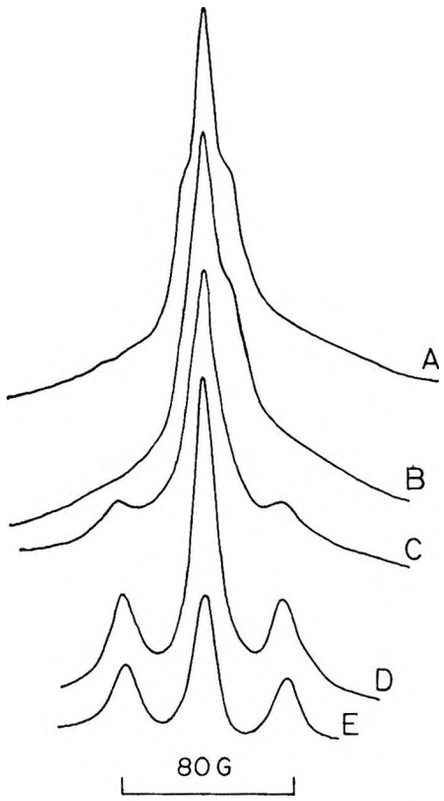

Figure 8. Esr spectra of CCA irradiated at 4°K by 250-kv X-rays to a dose of about 0.5 Mrad. All spectra were observed at 4°K. Spectrum A was obtained without heat annealing. The other spectra were observed by annealing the sample at: B, 50°K; C, 77°K; D, 140°K; and E, 293°K.

It has not been possible to identify the free radicals responsible for the broad singlet esr line, but the absence of any resolvable hyperfine splitting suggests that they might be c-$C_6H_{11}\dot{C}O$ or c-$C_6H_{11}C\lesssim^{O}_{O\cdot}$ radicals. The high yield of H_2O detected[22] suggests that a hydroxyl group might be removed and would tend to implicate the former free radical.

D. Esr Spectra at 4°K. 1. CCA. The esr spectra of CCA irradiated and observed at 4°K are shown in Figure 8. At this temperature the spectrum appears to be produced by at least three species which give an unresolved central line, an asymmetrically positioned doublet with a splitting of 24 gauss, and a very broad line which extends over a width of about 160 gauss and exhibits some unresolved hyperfine structure (Figure 8A). A search was made for the two widely separated lines of the hydrogen atom (about 500 gauss splitting), but they could not be detected. In addition, it should be noted that the characteristic six-line esr spectrum of the cyclohexyl radical was absent.

The sample (Figure 8A) was then annealed at different temperatures and the spectra were observed at 4°K. No change was detected in the spectrum when the temperature was raised to about 50°K, but after annealing at 77°K, the doublet and the broad line disappeared and a triplet was observed which had a hyperfine splitting of 37 gauss (Figure 8C). At temperatures higher than 77°K, it was seen that the singlet decayed, and finally after warming to room temperature (293°K) only the triplet could be detected (Figure 8D, E).

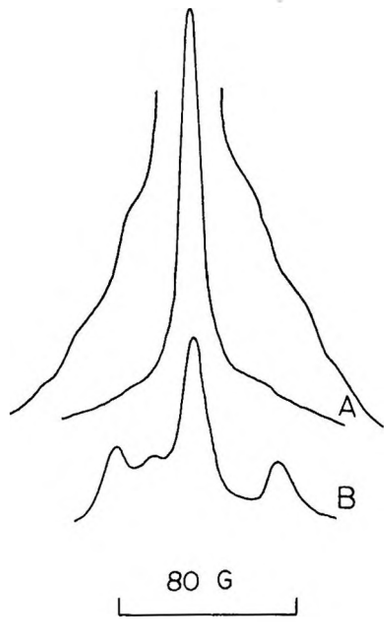

Figure 9. Esr spectra of CCA-d_1 irradiated at 4°K by 250-kv X-rays to a dose of about 0.5 Mrad. All spectra were observed at 4°K. Spectrum A, lower curve, was observed without heat annealing. In the upper curve, this spectrum has been magnified to show the unresolved structures. Spectrum B was obtained after heat annealing to 293°K.

2. CCA-d_1. The esr spectra of CCA-d_1 irradiated at 4°K are shown in Figure 9. At 4°K, the esr spectrum consisted of a single unresolved line and the same broad unresolved structures seen in CCA (Figure 9A). The doublet observed in CCA was not seen in the CCA-d_1 showing that the radical or ion responsible for it had a strong interaction with the hydrogen (or the deuterium in CCA-d_1) at the carbon atom adjacent to the carboxyl group.

In the upper spectrum in Figure 9A, the unresolved structures are shown in a magnified form. It can be seen that these structures contain at least six lines with

(22) P. M. K. Leung and J. W. Hunt, "Free Radical and Radiation Product Yields in Irradiated Cyclohexanecarboxylic Acid," in preparation.

other lines probably being masked by the central lines of the spectrum.

When the irradiated sample was annealed at higher temperature (293°K), a triplet was observed which was identical with the one seen in CCA (Figure 9B). In addition, an unknown line was also detected which was not seen in CCA. This additional spectrum could be due to some impurity such as oxygen which was present in the CCA-d_1 sample.

3. Identification of Intermediate Species. Since the doublet of signal observed in normal CCA was absent in the CCA-d_1 esr spectrum, there was obviously a strong interaction with the hydrogen on the carbon adjacent to the carboxyl group. This suggests that the unpaired electron was located on the carbon of the carboxyl group, and is completely consistent with a radical ion of the form, $c\text{-}C_6H_{11}\text{—}\dot{C}<^{O^-}_{OH}$, which had been identified in irradiated single crystals of succinic acid.[23]

The singlet in this spectrum has the same g value (2.0030 ± 0.0005) and width as the singlet observed when CCA was irradiated at 253°K, and is possibly the $c\text{-}C_6H_{11}\dot{C}{=}O$ radical. However, the hydroxyl radical (·OH), which might be expected if this radical were formed directly, was not observed but might have been responsible for part of the unresolved structures in the original low-temperature esr spectrum.

The triplet observed after the sample had been annealed at higher temperatures (Figure 9E) was that of the CCA radicals. The splitting of 37 gauss agrees with the value previously observed. The 5-gauss β_2 proton splitting could not be resolved at this temperature.

The broad spectrum whose structure was partially resolved in the deuterated compound (Figure 9) could not be identified. Because this spectrum and that of the negative ion both disappeared in the same low-temperature range, it is possible that this is the positive ion initially produced by the ionization of the CCA.

It should be stressed that no cyclohexyl radicals could be seen in the spectra, even after the sample had been warmed to 140°K. When irradiations were carried out at this temperature, a high yield of stable cyclohexyl radicals was observed, as discussed in section C.

E. Intermediate Reactions. The changes of the esr spectra, both as a function of irradiation temperature and during heat annealing, may be used to deduce some tentative schemes for the formation and reaction of the intermediate radiation products.

The spectra observed at 4°K show that the initial reactions at this temperature are probably

$$c\text{-}C_6H_{11}COOH \rightsquigarrow c\text{-}C_6H_{11}COOH^+ + e^- \quad (1)$$

$$e^- + c\text{-}C_6H_{11}COOH \longrightarrow c\text{-}C_6H_{11}\text{—}\dot{C}(O^-)(OH) \quad (2)$$

where the electron capture (reaction 2) gives the negative radical ion and the positive ion may be responsible for the broad esr spectrum which was observed. If these reactions were correct, the single line might be formed by the direct dissociation of a hydroxyl radical from the CCA molecule

$$c\text{-}C_6H_{11}COOH \rightsquigarrow c\text{-}C_6H_{11}\dot{C}O + \cdot OH \quad (3)$$

Alternatively, a proton transfer may take place from the positive ion to a neighboring molecule

$$c\text{-}C_6H_{11}COOH^+ + c\text{-}C_6H_{11}COOH \longrightarrow c\text{-}C_6H_{11}C(=O)(O\cdot) + (c\text{-}C_6H_{11}COOH)H^+ \quad (4)$$

Such a reaction scheme could account for all the species observed at low temperature. The concurrent disappearance of the ions on warming and growth of CCA radical spectra imply that charge neutralization reactions are occurring.

The over-all reaction would appear to be

$$c\text{-}C_6H_{11}\dot{C}(O^-)(OH) + \text{positive ion} \longrightarrow H\cdot + \underline{C_5H_{11}\dot{C}COOH} + \text{neutral molecule} \quad (5)$$

The mechanism of this reaction is obscured by the uncertainty in the initial reactions, but might be formed during the neutralization by the positive ions formed by reactions 1 or 4.

$$c\text{-}C_6H_{11}COOH^+ + e^- \longrightarrow c\text{-}C_6H_{11}COOH^{**} \longrightarrow \underline{C_5H_{10}\dot{C}COOH} + H\cdot \quad (6)$$

and the extraction, by the hydrogen atom, of a hydrogen from a neighboring CCA molecule.

$$H\cdot + c\text{-}C_6H_{11}COOH \longrightarrow \underline{C_5H_{10}\dot{C}COOH} + H_2 \quad (7)$$

(23) H. C. Box, H. G. Freund, and K. T. Lilga, *J. Chem. Phys.*, **42**, 1471 (1965).

Since reaction 7 requires approximately 7 kcal/mole, this reaction would be favored if a "hot" H atom were involved.[24,25]

At intermediate irradiation temperatures (around 153°K), a third temperature-dependent process involved in the formation of cyclohexyl free radicals must be considered. This reaction may be

$$c\text{-}C_6H_{11}COOH \longrightarrow c\text{-}C_6H_{11}COOH^* \longrightarrow c\text{-}C_6H_{11}\cdot + CO_2 + H\cdot \quad (8)$$

While other reaction schemes may be suggested to account for the formation of the cyclohexyl radicals, this mechanism is in good agreement with the observation of a high product yield of CO_2 and H_2 and the low yield of formic acid and CO in the irradiated CCA.[22]

At higher temperatures, the changes in the esr spectrum were due to a combination of free-radical reactions and changes in the configuration of the molecule. In Figure 2, it may be seen that the six-line cyclohexyl radical spectrum decayed as the sample was warmed, disappeared completely at about 193°K, and was not observed on further temperature cycling. The CCA radical spectrum after warming and cooling was found to contain 40 ± 5% (50 ± 5% in CCA-d_1) as many radicals as were present in the initial low-temperature spectrum.[26] However, from the synthesis of temperature spectrum, the CCA radical fraction was not more than 20% of the total yield. The twofold increase of CCA radicals could most likely occur by a radical reaction with the parent CCA molecules. The free radicals which might take part in the reaction could be $c\text{-}C_6H_{11}\cdot$, or the radical responsible for the singlet spectrum. From the changes of the esr spectra, it was observed that the singlet line did not decay appreciably until the temperature reached 243°K. Moreover, the intensity of the CCA radical signal did not seem to increase when the temperature was increased above 198°K. This suggests that about half of the CCA radicals in the annealed spectra were formed by the reaction

$$c\text{-}C_6H_{11}\cdot + CCA \longrightarrow c\text{-}C_6H_{12} + C_5H_{10}\dot{C}COOH \quad (9)$$

This reaction is supported by the observation of cyclohexane as an important radiolysis product.[22,27]

Acknowledgments. The authors wish to thank Drs. H. Box and H. Freund at the Roswell Park Memorial Institute, Buffalo, N. Y., for their assistance in obtaining the low-temperature esr spectra. We also wish to thank Drs. H. E. Johns and A. M. Rauth for their constructive criticism of this article. P. M. K. L. is indebted to the National Research Council for financial assistance.

(24) S. Z. Toma and W. H. Hamill, *J. Am. Chem. Soc.*, **86**, 1478 (1964).

(25) P. J. Dyne and J. Denhartog, *Can. J. Chem.*, **44**, 461 (1966).

(26) In order to compare the relative concentrations of free radicals in a sample following treatments such as heat annealing, the two spectra were observed at the same temperature. The relative concentration was determined from the first moments of the derivative spectra using the method described by A. Muller, *et al.*, *Intern. J. Radiation Biol.*, **7**, 587 (1963).

(27) I. A. Breger and V. L. Burton, *J. Am. Chem. Soc.*, **68**, 1639 (1946).

Solutions of N-Substituted Amino Acids. II. N-Ethyl-N-Phenyl-β-Aminopropionic Acid as a Probe of Hydrogen-Bonding Basicities

by Charles P. Nash, Dennis K. Fujita, and Ernelyne D. Retherford

Department of Chemistry, University of California, Davis, California 95616 *(Received January 23, 1967)*

Relative free energies and enthalpies of formation of 1:1 complexes between N-ethyl-N-phenyl-β-alanine and various acceptor bases have been determined by a spectrophotometric method. Representative ethers, ketones, sulfides, and nitriles have been studied, as well as methanol and ethanol, which here function as H-bond acceptors. A method is indicated by which absolute changes in the thermodynamic functions may also be estimated.

Introduction

Very recently, Drago, *et al.*, have employed methylene chloride as a solvent in nmr studies of hydrogen bonding by phenol[1] and complex formation by iodine.[2] These papers have prompted us to report the results of some hydrogen-bonding studies we have made in this same medium.

The first paper in this series suggested the importance of a study of the effect of solvent on the tautomeric equilibrium between an amino acid and its dipolar-ion isomer.[3] The molecule N-ethyl-N-phenyl-β-alanine (EPBA) seemed a likely prospect for such a study. N-Alkylated aromatic amines display an intense absorption band near 260 mμ which is attributed to an interaction between the lone pair of electrons on nitrogen and the π electrons of the benzene ring.[4] When the nitrogen is protonated, the 260-mμ band disappears.[5] Thus, if tautomerism of EPBA occurred, one would expect the absorbance at 260 mμ to be much higher in carbon tetrachloride solution than in acetonitrile, owing to the highly polar nature of the latter solvent. The experimental facts were precisely the opposite. In carbon tetrachloride the apparent molar absorptivity of this peak was about 10,000, a value compatible with a strongly hydrogen-bonded aromatic amine.[6] In acetonitrile the apparent molar absorptivity was about 17,000, characteristic of "unperturbed" nitrogen.[7]

These results are most easily explained by assuming that in carbon tetrachloride EPBA exists in an intramolecularly hydrogen-bonded form, a proposal made previously by Barrow[8] in a discussion of the nature of N,N-dialkylated amino acids in CCl_4. In acetonitrile, however, the intramolecular hydrogen bond may be replaced by an intermolecular hydrogen bond to the solvent. By applying these concepts in three-component systems we have been able to obtain relative free energies of formation of 1:1 complexes between hydrogen bond acceptors and a carboxylic acid. Values of this kind are presently rather sparse in the literature.

Experimental Section

Materials. All solvents and bases were of the highest commercial purity. Subsequent purifications were carried out by accepted procedures to give materials with the lowest practicable water content. Purities

(1) D. P. Eyman and R. S. Drago, *J. Am. Chem. Soc.*, **88**, 1617 (1966).

(2) R. S. Drago, T. F. Bolles, and R. J. Niedzielski, *ibid.*, **88**, 2717 (1966).

(3) C. P. Nash, E. L. Pye, and D. B. Cook, *J. Phys. Chem.*, **67**, 1642 (1963).

(4) J. N. Murrell, *J. Chem. Soc.*, 3779 (1956).

(5) A. E. Lutskii and V. N. Konel'skaya, *Zh. Obshch. Khim.*, **30**, 3773 (1960).

(6) A. T. Bottini and C. P. Nash, *J. Am. Chem. Soc.*, **84**, 734 (1962).

(7) B. M. Wepster, *Progr. Stereochem.*, **2**, 99 (1958).

(8) G. M. Barrow, *J. Am. Chem. Soc.*, **80**, 86 (1958).

were confirmed by determinations of refractive indices and densities as well as by vpc.

Synthesis. The hydrochloride of EPBA was synthesized by an adaptation of the method of Gresham, *et al.*[9] One mole of β-propiolactone was added to 1 mole of N-ethylaniline in 500 ml of ether and the reaction mixture was allowed to stand for 48 hr. A portion of the reaction mixture was extracted with half its volume of 3 *M* aqueous sodium hydroxide. The basic solution was carefully neutralized with dilute sulfuric acid until an oil separated. The oil was extracted with ether, an equal volume of acetonitrile was added to the extract, and then a small amount of 12 *N* hydrochloric acid was added. Crystalline EBPA hydrochloride formed in a few minutes. The product was recrystallized repeatedly from ether–acetonitrile mixtures. *Anal.* Calcd for $C_{11}H_{16}ClNO_2$: Cl, 15.43. Found: Cl, 15.39.

Preparation of Solutions. We have not succeeded in obtaining EPBA as a crystalline compound. Master solutions were therefore prepared by making a concentrated aqueous solution of the hydrochloride, adding precisely 1 equiv of NaOH, saturating the solution with sodium chloride, and extracting the mixture several times with methylene chloride to yield a 1.0×10^{-2} *M* stock solution of EPBA in methylene chloride. Possible ambiguities due to residual water are negligible, as shown by the fact that the stock solution, when diluted 200-fold with anhydrous methylene chloride, obeyed Beer's law at 260 mμ to within 2%. In addition, the extraction procedure proved to be essentially quantitative, as demonstrated by the fact that the calculated extinction coefficient of the nonhydrogen-bonded aniline function is 17,000 ± 300 in bulk acetonitrile and the other basic media. This figure compares favorably with the value 16,700 quoted by Wepster, *et al.*, for N,-N-diethylaniline in isooctane solution.[10]

The choice of methylene chloride as the principal medium was made on practical grounds. Carbon tetrachloride underwent a light-induced reaction with the amino acid rather rapidly, whereas methylene chloride solutions were reasonably stable when stored in the dark. The extraction was quite clean with methylene chloride; however, ethylene chloride tended to form emulsions.

Spectra were recorded for solutions prepared to be 1.0×10^{-3} *M* in amino acid and from zero to 2.0 *M* in the desired base.

Spectrophotometric Measurements. Ultraviolet spectra were obtained with a Cary Model 14 recording spectrophotometer using matched silica cells. Temperature control was achieved by circulating thermostated water through a hollow cell block attachment.

Infrared spectra were obtained on a Beckman IR-12 infrared spectrophotometer using calibrated sodium chloride cells.

Data Reduction. The formalism used to treat the data is similar to that derived earlier to obtain equilibrium constants in systems in which both an initial and a final species absorb appreciably at the same wavelength.[11] This scheme must be modified, however, since intramolecular hydrogen bonding of the amino acid itself is not necessarily complete, and hence three absorbing species—intramolecularly H-bonded, intermolecularly H-bonded, and non-H-bonded amino acid—may be present in the system. The last two entities, however, should have the same spectrum to a very good approximation. With this assumption, algebra closely parallel to that used previously leads to the linear equation

$$\left[\frac{1}{B}\right] = \left[1 - \frac{A}{A_0}\right]^{-1} [K - \beta] - K \qquad (1)$$

Here B is the molar concentration of added base, A is the absorbance (at fixed wavelength) in the presence of base, and A_0 is the absorbance with no added base. K is a pseudo equilibrium constant. If the two principal equilibria are written

$$\text{closed EPBA} \rightleftharpoons \text{open EPBA}; \quad K_1 = \frac{(\text{open})}{(\text{closed})} \qquad (2)$$

$$\text{closed EPBA} + \text{base} \rightleftharpoons \text{complex};$$

$$K_c = \frac{(\text{complex})}{(\text{closed})(\text{base})} \qquad (3)$$

then $K \equiv K_c/(1 + K_1)$.

If ϵ_c is the molar absorptivity of the closed form of the amino acid and ϵ_e is the molar absorptivity of both extended forms, *i.e.*, the opened ring and the intermolecular complex, then

$$\beta \equiv (K_c\epsilon_e/\epsilon_c) + K_1\epsilon_e \qquad (4)$$

The application of this method of data reduction is quite simple. When the reciprocal of the base concentration is plotted against the reciprocal of $[1 - (A/A_0)]$, a straight line results whose intercept on the ordinate axis is a measure of the free energy of formation of the intermolecular hydrogen bond. Furthermore, if the assumption that the spectra of the two extended forms are identical is valid, all of the lines given

(9) T. L. Gresham, J. E. Jansen, F. W. Shaver, R. A. Bankert, and F. T. Fiedorek, *J. Am. Chem. Soc.*, 73, 3168 (1951).

(10) J. A. C. Browers, S. C. Bijlsma, P. E. Verkade, and B. M. Wepster, *Rec. Trav. Chim.*, 77, 1080 (1958).

(11) C. P. Nash, *J. Phys. Chem.*, 64, 950 (1960).

by the series of bases under investigation should possess a common intercept with the abscissa axis. This criterion is fulfilled by all nine of our systems to within 3%.

Since the intercept K is the product of two factors, one of which depends only on the temperature, differences in the pseudo free energies found by the usual logarithmic recipe will be accurate measures of the differences in the free energies of formation of the several complexes formed according to eq 3. In a similar way, if one differentiates the logarithm of K with respect to inverse temperature and assumes that K_1 is small, it follows that

$$\frac{d \ln K}{d(1/T)} \cong \frac{d \ln K_c}{d(1/T)} - K_1 \frac{d \ln K_1}{d(1/T)} \quad (5)$$

Thus, differences in the "apparent" enthalpies will be accurate measures of the differences in the heats of formation of the several complexes formed according to eq 3.

Results

In Table I are collected values of the constant K and the free energies of formation of the complexes relative to tetrahydrofuran for the nine systems we have studied. The standard deviation in each K, based on both least-squares data reduction of a given experiment and replicate experiments, is about ±4%.

Table I: Equilibrium Parameters and Relative Free Energies of Formation of EPBA–Base Complexes at 25°

Compound	K, M^{-1}	$\Delta G_{rel}°$, kcal/mole
Tetrahydrofuran	3.8	0.00
Tetrahydropyran	3.5	0.05
Trimethylene oxide	3.0	0.14
Methanol	2.3	0.30
Ethanol	2.1	0.35
Diethyl ether	2.1	0.35
Acetone	1.3	0.64
Acetonitrile	0.25	1.60
Pentamethylene sulfide	0.20	1.74

The values of monomeric alcohol concentrations required to determine K for methanol and ethanol were obtained from the integrated intensities of the monomeric hydroxyl stretching bands in the infrared. We assume that in our system the alcohols function as bases, since earlier studies by Gramstad[12] and by Nash and Maciel[13] have shown that diethylaniline is a very poor hydrogen-bond acceptor. In this way we obtain the plausible result that the two aliphatic alcohols and diethyl ether have virtually the same basicities as H-bond acceptors.

We have also measured K for tetrahydrofuran and acetonitrile at 2°, where we obtain values of 7.1 and 0.16, respectively. From these values we calculate apparent enthalpies of formation of the two complexes which differ by 1.2 kcal/mole. Thus the real entropy changes for the several reactions 3 probably do not vary by more than 2 or 3 gibbs over the range of base strengths given here. This behavior is to be expected on the basis of the many existing studies which have used phenol as the H-bond donor (*vide infra*).

Discussion

The only measurements with which the present results may be sensibly compared are infrared spectroscopic determinations of the formation constants of complexes between phenol and bases in carbon tetrachloride solution. Unfortunately, no single investigation has encompassed exactly the same series of bases studied here, and the agreement among the several sets of results on the same compound is often poor. For example, with tetrahydrofuran–phenol, West, *et al.*,[14] and Fritzsche[15] obtain $\Delta G° \approx -1.65$ kcal/mole whereas Gramstad[16] and Lippert and Prigge[17] obtain $\Delta G° \approx -1.47$ kcal/mole.

We are thus constrained to make only qualitative comparisons. There is little doubt that the use of EPBA rather than phenol as the H-bond donor leads to greater differences in the values of the free energies of formation of H-bonded complexes with weak bases. Also, we find a larger equilibrium constant with ether than with acetone. Toward phenol, however, $(-\Delta G°)$ favors acetone (and methyl ethyl ketone) while $(-\Delta H°)$ favors ether.[16,18] Finally, we have been able to study alcohols, a result hitherto impossible to obtain.

Consistency Epilog

We have observed that when a solution of EPBA in methylene chloride is cooled from 25 to 2°, it becomes more absorbing by an amount which, when corrected for thermal contraction of the solvent, implies that about 5% more molecules are now in the closed form. If eq 2 is written as eq 6, then eq 7 or 8 results.

(12) T. Gramstad, *Acta Chem. Scand.*, 16, 807 (1962).

(13) C. P. Nash and G. E. Maciel, *J. Phys. Chem.*, 68, 832 (1964).

(14) R. West, D. L. Powell, M. K. T. Lee, and L. S. Whatley, *J. Am. Chem. Soc.*, 86, 3227 (1964).

(15) H. Fritzsche, *Z. Elektrochem.*, 68, 459 (1964).

(16) T. Gramstad, *Spectrochim. Acta*, 19, 497 (1963).

(17) E. Lippert and H. Prigge, *Ann.*, 659, 81 (1962).

(18) D. L. Powell and R. West, *Spectrochim. Acta*, 20, 983 (1964).

$$K_1 = \frac{(\text{open})}{(\text{closed})} = \frac{X}{1 - X} \quad (6)$$

$$\frac{\mathrm{d} \ln K_1}{\mathrm{d}(1/T)} = -\frac{\Delta H_1^\circ}{R} = -\frac{1}{X}\frac{\mathrm{d} \ln (1 - X)}{\mathrm{d}(1/T)};$$

$$\mathrm{d} \ln (1 - X) \approx 0.05; \ \mathrm{d}(1/T) = 0.28 \times 10^{-3} \quad (7)$$

or

$$X\Delta H_1^\circ \approx 0.35 \times 10^3 \quad (8)$$

It is possible to estimate ΔH_1° in the following way. Infrared spectra of mixtures of acetonitrile and acetic acid in carbon tetrachloride, together with the Barrow and Yerger[19] value for the dimerization constant of acetic acid, lead to an equilibrium constant for the reaction MeCN + HOAc $\rightleftharpoons$ MeCN–HOAc of about 5 M^{-1}. If it is assumed that ΔS° for this reaction is about −13 gibbs (Fritzsche finds −11 gibbs in the MeCN–C_6H_5OH case[15]), then ΔH° is about −5 kcal/mole.

To an approximation good enough for the present purpose, eq 5 may be transformed to

$$\Delta H_{\text{app}} = -R\frac{\mathrm{d} \ln K}{\mathrm{d}(1/T)} =$$

$$\Delta H_c^\circ - K_1\Delta H_1^\circ \approx \Delta H_c^\circ - X\Delta H_1^\circ \quad (9)$$

We have found for MeCN $\Delta H_{\text{app}} \approx -3.2$ kcal/mole and $X\Delta H_1^\circ \approx 0.35$ kcal/mole; hence $\Delta H^\circ \approx -2.8$ kcal/mole. If the estimated 5-kcal/mole enthalpy of complexing of MeCN with acetic acid is representative of its behavior with all aliphatic acids, then the intramolecular hydrogen bond in EPBA is evidently exothermic by some 2.2 kcal/mole. From eq 8 we then find $X \approx 0.16$, $K_1 \approx 0.2$, $\Delta G_1^\circ \approx +1$ kcal/mole, and $\Delta S_1 \approx +4$ gibbs. These estimates, none of which are incompatible with the behavior of intramolecular hydrogen bonds, justify the approximations used in the preceding paragraphs and also permit estimates to be made of the thermodynamic functions for hydrogen bonding to the carboxylic acid function of EPBA in its extended form.

(19) G. M. Barrow and E. A. Yerger, *J. Am. Chem. Soc.*, **76**, 5248 (1954).

Kerr Constant Dispersion. III.[1a,b] The Interaction of Acridine Orange with DNA

by John C. Powers, Jr.,[1c] and Warner L. Peticolas

IBM Research Laboratory, San Jose, California *(Received February 9, 1967)*

The Kerr constant of the complex formed between acridine orange and DNA has been measured throughout the region of dye absorption in the visible spectrum (5500 to 4200 A) at ratios of the number of nucleotide units per dye molecule ranging from 2:1 to 36:1. Complete experimental results are given for ratios of 2:1 and 18:1. A single negative dispersion centered near the dye absorption maximum (5000 A) is found for the latter case; at low ratios two dispersions are found, a negative one at 5000 A and a positive one at 4600 A, indicating a high degree of dye–dye interaction. The intercalated structure is compatible with the results at high ratios; binding to a surface site (phosphate) is necessary to account for the dye–dye interactions present at low ratios.

Recent work in this laboratory has used the Kerr effect as an analytical tool to investigate interactions in various polymeric systems. The aggregation of polybenzyl-L-glutamate in various solvents was studied by changes in the Kerr constant which occur as the solvent is modified[2] and the binding of small dye molecules to polyglutamic acid (PGA) has been examined by measuring the dispersion of the Kerr constant in the wavelength region of absorption of the dye.[1a,b] From these latter results it was possible to assign a structure to the acridine orange–PGA complex which placed the long axis of the dye parallel to the helical axis. These results confirmed a previous structure based on the changes in the circular dichroism spectrum occurring under streaming conditions.[3] The examination of the DNA–acridine orange complex was of immediate interest as the indications are that the dye is bound by DNA in a geometrically different manner than by PGA.[4–6] The dye is bound in a stereospecific manner to DNA as shown by the induced rotation in the dye absorption band.[7–9] The geometry of the complex can be easily determined from the shape of the dispersion of the Kerr constant (*vide infra*).

The DNA–acridine orange complex has been investigated by several workers and two distinct structures have been proposed, the intercalation structure of Lerman[5,6] and the stacked card pack structure of Bradley and Wolf.[4] The intercalation structure places the dye between the DNA strands and sandwiched between two adjacent base pairs while the stack configuration places the dye on the surface of the polymer bound presumably to the phosphate group. In both configurations the dye is oriented perpendicular to the helix axis and this conclusion has been confirmed by measurements of the streaming circular dichroism.[10] The data obtained by our measurements of the Kerr constant dispersion allow the specification, relative to the helical axis of DNA, of the orientation of the transition moment of acridine orange bound both as a single molecule and as an aggregate.

(1) (a) Part I: J. C. Powers, Jr., *J. Am. Chem. Soc.*, **88**, 3679 (1966); (b) part II: J. C. Powers, Jr., *ibid.*, **89**, 1780 (1967); (c) Department of Chemistry, Hunter College, New York, N. Y. 10021.

(2) J. C. Powers, Jr., and W. L. Peticolas in "Advances in Chemistry —Symposium on Ordered Fluids and Liquid Crystals," R. S. Porter and J. F. Johnson, Ed., in press.

(3) R. E. Ballard, A. J. McCaffery, and S. F. Mason, *Biopolymers*, **4**, 97 (1966).

(4) D. F. Bradley and M. K. Wolf, *Proc. Natl. Acad. Sci. U. S.*, **45**, 944 (1959).

(5) L. S. Lerman, *J. Mol. Biol.*, **3**, 18 (1961).

(6) L. S. Lerman, *Proc. Natl. Acad. Sci. U. S.*, **49**, 94 (1963).

(7) D. A. Neville, Jr., and D. F. Bradley, *Biochem. Biophys. Acta*, **50**, 397 (1961).

(8) K. Yamaoka and R. A. Resnik, *J. Phys. Chem.*, **70**, 4051 (1966).

(9) A. Blake and A. R. Peacocke, *Biopolymers*, **4**, 1091 (1966).

(10) S. F. Mason and A. J. McCaffery, *Nature*, **204**, 468 (1964).

Experimental Section

DNA. Highly purified salmon sperm DNA (Cal Biochem.) was stored at 5° and stock solutions (0.1%) were made up by slow addition of a dilute solution of tris buffer (Sigma Chemical Co.); the final concentration was 10^{-3} M in tris. All solutions were stored at low temperatures, and fresh solutions were made up for each run by dilution of the stock solution.

Acridine Orange. Recrystallized zinc-free dye described previously[1b] was used. The apparatus for measuring electrical birefringence is of conventional design and employs a photoelectric method of detecting the induced phase change δ. It has been fully described elsewhere.[1b] Measurements were made using a square-wave dc voltage pulse up to 200 v in magnitude and from 1 to 5 msec duration, the length of the pulse being determined by the time necessary to reach equilibrium. The Kerr constant (B) is obtained from the equation

$$B = \frac{\delta}{2\pi l F^2}$$

(l is the length of the cell) and appropriate corrections were made for the birefringence of the cell. For a given sample only one or two measurements at the same applied voltage were made at each wavelength so as to avoid degradation. Spectra were determined on a Cary Model 14 spectrophotometer.

Theory

The theoretical treatment of the dispersion of the Kerr constant has been reviewed in an earlier contribution[1b] from these laboratories. Briefly, according to the classical theory as summarized by Le Fevre[11] and Labhart,[12] the Kerr constant of a dipolar molecule possessing a permanent moment in the Z direction is given by

$$B = \frac{\pi N}{1115 n \lambda k^2 T^2} \times (n + 2)^2 \times (\epsilon + 2)^2 \mu_z^2 (2\alpha_z - \alpha_x - \alpha_y)$$

where μ_i and α_i are the components of the dipole moment and polarizability along the i axis, n and ϵ are the index of refraction and dielectric constant of the medium, N is the number of molecules per unit volume, and the other symbols have their usual meaning. From the definition of the polarizability,[13] this function varies as $1/(\nu_i - \nu)$ where ν_i is the position of maximum absorption. Buckingham[14] has summarized these results and considered in addition the effect of large applied fields and derived expressions for a nonlinear polarization law. The distortion produced by a high field he termed the hyperpolarizability and this results in an enhancement of the magnitude of the Kerr constant in an absorptive region. The results of these considerations were illustrated graphically in a previous publication (Figure 1 of ref 1b). They can be applied to the experiments described here by replacing the permanent moment μ by an "effective orienting moment" directed along the long axis of the molecule. DNA is oriented with its long axis parallel to the applied field by an ion atmosphere polarization mechanism.[15] Therefore, a positive dispersion in the Kerr constant occurs when the orienting moment and maximum polarizability are parallel, a negative dispersion when they are at right angles.

Results

Measurements of the dispersion of the Kerr constant were made at wavelengths from 5500 to 4200 A on solutions for which the ratio of nucleotide units to dye molecules (PO_4/dye) was varied from 2:1 to 36:1. The solutions contained sufficient tris buffer (*ca.* 10^{-3} M) to maintain the solution pH at 6.80. The complete determinations for ratios of 2:1 and 18:1 are shown in Figure 1 along with the corresponding values for DNA of the same concentration (shown as a dotted line). The birefringence of DNA (negative in sign) was measured in a separate experiment. The small difference in the specific Kerr constants (B/C) for the two illustrated runs is the result of slight degradation of one of the solutions due to aging. The probable errors are not shown; for the low ratio they are quite high, being about 10%; for the high ratio they are about 2%.

The spectrum of the complex is highly dependent on the above ratio. At high ratios there is little evidence for aggregation (stacking) of the dye on the polymer surface (shown by the appearance of an absorption band at 4650 A).[16] In water, the free dye absorbs near 5000 A. The absorption spectra of the two solutions at the same dye concentration are shown as dotted lines in Figures 2 and 3. The difference in magnitude of the dispersions in the two experiments shown in Figure 1 is due to changes in the extinction coefficient of the dye upon binding.

Discussion

The polarizations of the transitions giving rise to the

(11) C. G. Le Fevre and R. J. W. Le Fevre, *Rev. Pure Appl. Chem.*, **5**, 261 (1955).

(12) H. Labhart, *Tetrahedron*, **19**, Suppl. 2, 223 (1963).

(13) H. Eyring, J. Walter, and G. E. Kimball, "Quantum Chemistry," John Wiley and Sons, Inc., New York, N. Y., 1944, p 121.

(14) A. D. Buckingham, *Proc. Roy. Soc.* (London), **A267**, 271 (1962).

(15) C. T. O'Konski, *J. Phys. Chem.*, **64**, 605 (1960).

(16) V. Zanker, *Z. Physik. Chem.* (Leipzig), **199**, 225 (1952).

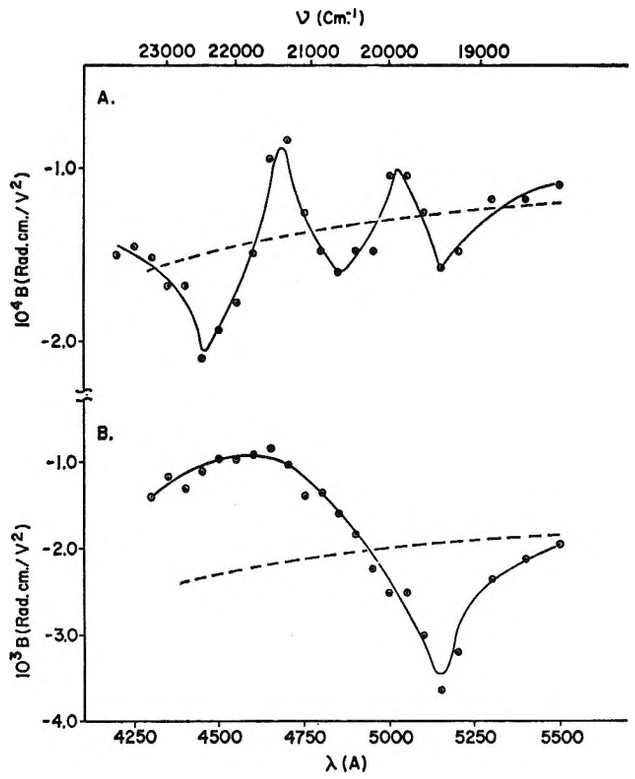

Figure 1. Dispersion of the Kerr constant (B) for the DNA–acridine orange (AO) complex (solid line) and DNA (dotted line): A, DNA = $2 \times 10^{-5}\ M$; AO = $10^{-5}\ M$; B, DNA = $1.8 \times 10^{-4}\ M$; AO = $10^{-5}\ M$.

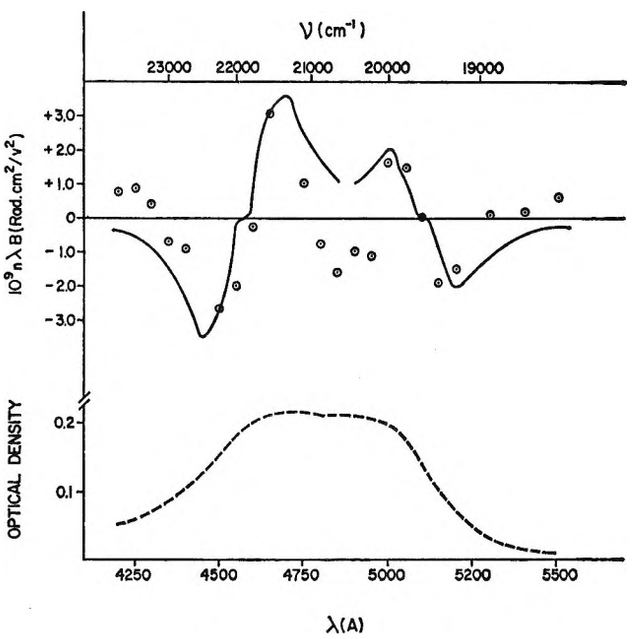

Figure 2. Comparison of the absorption spectrum (dotted line), experimental values of $n\lambda B$ (⊙), and calculated curves (solid lines) of the Kerr constant of the DNA–AO complex. The birefringence of DNA has been subtracted. DNA = $2 \times 10^{-5}\ M$; AO = $10^{-5}\ M$. PO_4/AO = 2:1.

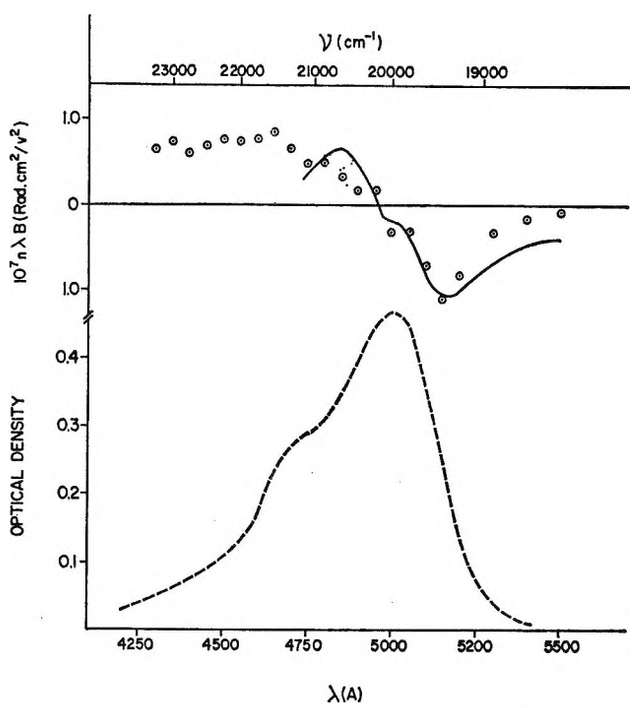

Figure 3. Same as Figure 2 with DNA = $1.8 \times 10^{-4}\ M$; AO = $10^{-5}\ M$; PO_4/AO = 18:1.

dispersion curves shown in Figure 1 can be obtained from a consideration of the absorption spectra and by reference to the theoretical section. To facilitate comparison, the data shown in Figure 1 have been multiplied by $n\lambda$ and the bulk contribution (measured in a separate experiment) of the DNA has been subtracted. The individual points are shown in Figures 2 and 3 along with calculated dispersion curves fit to the data and obtained from Buckingham's formula.[14] Although the fit is only approximate, it is much worse if a simple dispersion curve is used. The absorption spectra of the solutions are shown at the bottom of both figures. For the low ratio case, there are two absorption maxima located at 4950 and 4700 A and corresponding calculated curves are shown in Figure 2 as solid lines. These calculated curves are centered at 4575 and 5100 A with half-widths of 500 and 400 cm^{-1}, respectively. The single strong absorption peak (5000 A) shown in Figure 3 is reflected in the occurrence of a single dispersion. Here the calculated curve was constructed from an absorption centered at 5000 A with a half-width of 600 cm^{-1}. While the indicated dispersions are quite evident, there may be additional absorptions present whose Kerr constant dispersions are not well resolved. Such is certainly the case for the shorter wavelength

region in Figure 3 and probably true also for the 4800-A region in Figure 2. The scatter in the data makes a process of multiple curve fitting unjustified.

The data show that a negative dispersion is present for both high and low ratios of the number of nucleotides per dye molecule for the absorption near 5000 A and an additional negative dispersion in the 4600-A region for the low ratio case. Since DNA is aligned with its helical axis parallel to the applied field, the transition moment for the transition at 5000 A is largely perpendicular to this helical axis. For the unaggregated dye this transition has been shown to be long-axis polarized (X).[3,17] The absorption spectrum of the high ratio case (Figure 3) corresponds to that of essentially free dye and thus the long axis of the dye is perpendicular to the helical axis when there is a large excess of binding sites. The spectrum of the low ratio case (Figure 2) is a superposition of the spectra of free and dimerized acridine orange;[18] part of the long wave-

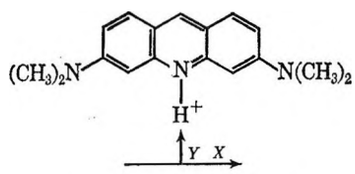

Acridine Orange Cation

length absorption may be due to unbound dye. The transition at 5100 A is again polarized perpendicular to the helical axis, but that near 4600 A is polarized parallel. The dispersion at 5100 A can represent contributions by both unaggregated and aggregated dye, the latter arising from splitting of the aggregate absorption (see below). The general experimental findings are in accord with those of Mason and McCaffery[10] and the pattern of the mutually perpendicular orientation of the transition moments for absorptions in the 4600- and 5000-A regions is similar to that found for the acridine orange-polyglutamic acid system.[1a,b] While the assumption of a simple card pack structure for an aggregate leads to the prediction of a transition moment for the "exciton" parallel to that for the monomer,[19] the card pack to be considered for the DNA–acridine orange system would be skewed due to the helical arrangement of possible binding sites. Thus, it is reasonable to conclude that the aggregate transition moment (being a vector sum of the individual transition moments) could have a large component in a direction perpendicular to the transition moment in the free dye. The splitting of the absorption band of a helical exciton was first discussed by Moffitt[20] for the single-stranded case (polypeptides) and by Rhodes[21] for the double-stranded model (polynucleotides). The absorption of the DNA–AO complex was calculated by Tinoco, Bradley, and Woody[22] to have such a splitting with the perpendicular band lying at longer wavelengths. The results of Lamm and Neville[18] on the dye itself have confirmed this predicted splitting for acridine orange; Rohatgi and Singhal[23] have detected it in other dye aggregates. The position of the long wavelength dispersion in Figure 2 corresponds almost exactly to that obtained by Lamm and Neville[18] for the long wavelength spectrum of acridine orange dimer.

The complex behavior of these dispersions is similar to that observed by Yamaoka and Resnik in the ORD and CD spectra[8] of this same system. They were unable to reproduce the experimental spectra without recourse to at least four separate transitions, even for the high ratio case of Figure 3. Thus, the unresolved portion of the dispersion curve in Figure 3 can be ascribed to such complications. As mentioned above, the relatively high scatter in our data makes a full-scale curve fitting analysis impractical at this time.

Optical measurements of this sort allow the specification of the gross geometrical structure of the dye–polymer complex, but do not directly indicate the method of binding. As mentioned earlier, both proposed structures place the long axis of the dye at right angles to the helical axis. However, binding of the dye to the phosphate groups on the surface allows for direct interaction between the dye molecules at low ratios. Lerman has persuasively stated the arguments for the intercalated structure;[6] while binding of the dye by this method would place it in the same relative orientation each time, the sandwiching of the dye between the aromatic purine–pyrimidine bases would make it impossible for dye–dye interactions to occur. Thus, the changes which occur at low nucleotide:dye ratios must be assigned to binding on a surface site.

The binding of the dye at high ratios can be accommodated by either scheme. All that is required is that the dye molecule be held in the same relative position on separate sites. It is interesting in this connection that the recent work of Yamaoka and Resnik has demonstrated that optical activity of the dye absorption can be caused by asymmetric perturbation and

(17) H. Jakobi and H. Kuhn, *Z. Elektrochem.*, **66**, 46 (1962).

(18) M. E. Lamm and D. M. Neville, Jr., *J. Phys. Chem.*, **69**, 3872 (1965).

(19) M. Kasha, *Rev. Mod. Phys.*, **31**, 162 (1959).

(20) W. Moffitt, *J. Chem. Phys.*, **25**, 467 (1956).

(21) W. Rhodes, *ibid.*, **37**, 2433 (1962).

(22) (a) I. Tinoco, Jr., R. W. Woody, and D. F. Bradley, *ibid.*, **38**, 1317 (1963); (b) D. F. Bradley, I. Tinoco, Jr., and R. W. Woody, *Biopolymers*, **1**, 239 (1963).

(23) K. K. Rohatgi and G. S. Singhal, *J. Phys. Chem.*, **70**, 1695 (1966).

that aggregation of the dye is not necessary. The order of magnitude difference in the Kerr constant dispersions in the 5000-A region suggests that the intercalated structure is transformed into the surface bound structure as the relative amount of dye is increased. The older ORD results of Neville and Bradley[7] also show this same effect as the shorter wavelength dispersion grows at the expense of the longer wavelength one as the amount of dye is increased. It is quite possible that the recent suggestion concerning partial intercalation[24] is correct and that, as the surface sites are filled, the intercalated dye is removed from between the bases to form the dye aggregate.

Acknowledgment. The authors wish to thank Mr. John H. Smith for technical assistance and Professor N. Davidson for helpful discussions and the loan of the thesis of H. Ohlenbusch.

(24) N. J. Pritchard, A. Blake, and A. R. Peacocke, *Nature*, **212**, 1360 (1966).

Coalescence of Mercury Droplets in Aqueous Solutions, with Special Reference to the Examination of Double-Layer Interaction

by Shinnosuke Usui, Taro Yamasaki,

Research Institute of Mineral Dressing and Metallurgy, Tohoku University, Nagamachi, Sendai, Japan

and Junzo Shimoiizaka

Department of Mining and Mineral Engineering, Tohoku University, Aobayama, Sendai, Japan
(Received February 9, 1967)

The coalescence of mercury droplets in aqueous KF solution at concentrations of 10^{-3} to 10^{-2} M was examined by means of twin dropping mercury electrodes. From the critical potentials for the coalescence in the symmetrical case where two mercury droplets were equally charged, 1.2×10^{-12} was obtained as a reliable value of the Hamaker constant for mercury in water. The critical potentials in the asymmetrical case where two mercury droplets were unequally charged were also determined. The agreement between the theoretical and experimental values showed the validity of the Derjaguin–Landau–Verwey–Overbeek theory and the dissimilar double-layer interaction theory. The behavior of the coalescence in the presence of specific adsorption of I^- ions was interpreted qualitatively in terms of the potential of the outer Helmholtz plane at the mercury–solution interface.

Introduction

The coagulation of colloidal dispersion has been discussed by the Derjaguin–Landau–Verwey–Overbeek (DLVO) theory which is based on the electrical repulsion and the long-range London–van der Waals attraction between particles.[1] Experimental verifications of this theory have been attempted on various sols. However, the results have been discussed by using an ambiguous quantity like the electrokinetic ζ potential.

(1) E. J. W. Verwey and J. Th. G. Overbeek, "Theory of the Stability of Lyophobic Colloids," Elsevier Publishing Co., Amsterdam, 1948.

The van der Waals attraction is usually obtained from the coagulation experiments by estimating the residual interaction after allowance has been made for the electrical forces. The Hamaker constants so derived are dependent on the choice of the potential, and reliable values of the Hamaker constant in a simple system have been unavailable. Furthermore, many of the investigations have dealt almost exclusively with the case where particles are equally charged, and few experimental studies have been conducted on the coagulation of unequally charged particles. The theory of the dissimilar double-layer interaction and the theory of heterocoagulation have already been presented by Derjaguin,[2] Bierman,[3] Devereux and de Bruyn,[4] and Hogg, Healy, and Fuerstenau.[5] The difficulty associated with the experimental verification of these theories is believed to lie in the method under such conditions that the interfacial potential of particles and electrolyte concentration can be freely changed, because the interfacial potential of particles is uniquely determined when the system of particle–electrolyte solution is specified.

In connection with these problems, an interesting experiment was undertaken by Watanabe and Gotoh.[6] They studied the coalescence of mercury droplets by means of twin electrodes and demonstrated that the coalescence of mercury droplets was substantially the same as the coagulation of hydrophobic colloid particles and was interpreted quantitatively by the DLVO theory. However, their result lacked in the quantitative treatment of the difference between the rational potential of the electrode and the Stern potential. The twin dropping mercury electrode technique is characterized by the fact that the potential of mercury is controlled to any desired one if a mercury–electrolyte solution interface is in a polarized state.

The purpose of the present study is to examine the DLVO theory in terms of well-defined quantities, *i.e.*, the rational potential of the electrode and the potential of the outer Helmholtz plane of mercury, and to investigate the theory of dissimilar double-layer interaction through the coalescence of mercury droplets by using the twin electrode technique.

Experimental Section

Devices and Materials. The twin electrodes used in this study are shown in Figure 1a and are virtually identical with those used by Watanabe and Gotoh,[6] some modifications being that two potentiometers (P_1 and P_2) were employed to polarize the mercury droplets and a 1 *N* calomel electrode (nce) was used as a reference electrode. Another important improvement was in capillary tip design as shown in Figure 1b,

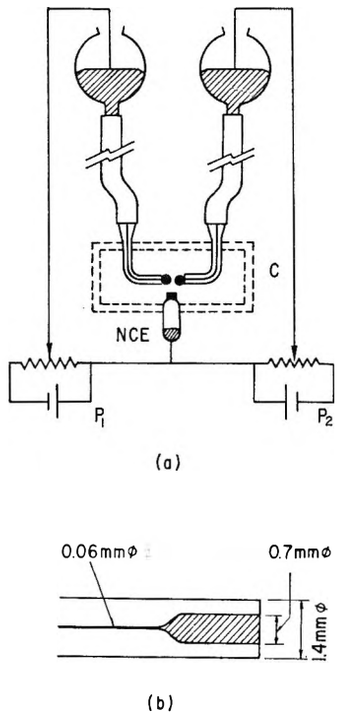

Figure 1. (a) Twin dropping mercury electrodes: P_1, P_2, potentiometer; NCE, 1 *N* calomel electrode; C, plastic cell. (b) Schematic of glass capillary tip in cross-section.

which was indispensable to obtaining reliable and reproducible results. The coalescence experiments were carried out at the flowing rate of mercury of about 1 mg/sec during the course of these investigations.

The plastic cell has a thermostating jacket through which water may circulate from a constant-temperature (25°) source. The capacity of the cell is about 100 ml. Test solutions were deoxygenated by argon bubbling, and measurements were made under the atmospheric condition of an argon stream. The apparatus used for differential capacity measurements was essentially identical with that used by Grahame[7] and is shown in Figure 2. The frequency utilized was 100 cps.

KF was selected as an electrolyte because the specific adsorption of F^- ion at the mercury–solution interface is thought to be negligible. KI was also used for comparison because of the strong tendency of specific ad-

(2) B. V. Derjaguin, *Discussions Faraday Soc.*, **18**, 85 (1954).

(3) A. Bierman, *J. Colloid Sci.*, **10**, 231 (1955).

(4) O. F. Devereux and P. L. de Bruyn, "Interaction of Plane-parallel Double Layers," MIT Press, Cambridge, Mass., 1963.

(5) R. Hogg, T. W. Healy, and D. W. Fuerstenau, *Trans. Faraday Soc.*, **62**, 1638 (1966).

(6) A. Watanabe and R. Gotoh, *Kolloid-Z.*, **191**, 36 (1963).

(7) D. C. Grahame, *J. Am. Chem. Soc.*, **71**, 2975 (1949).

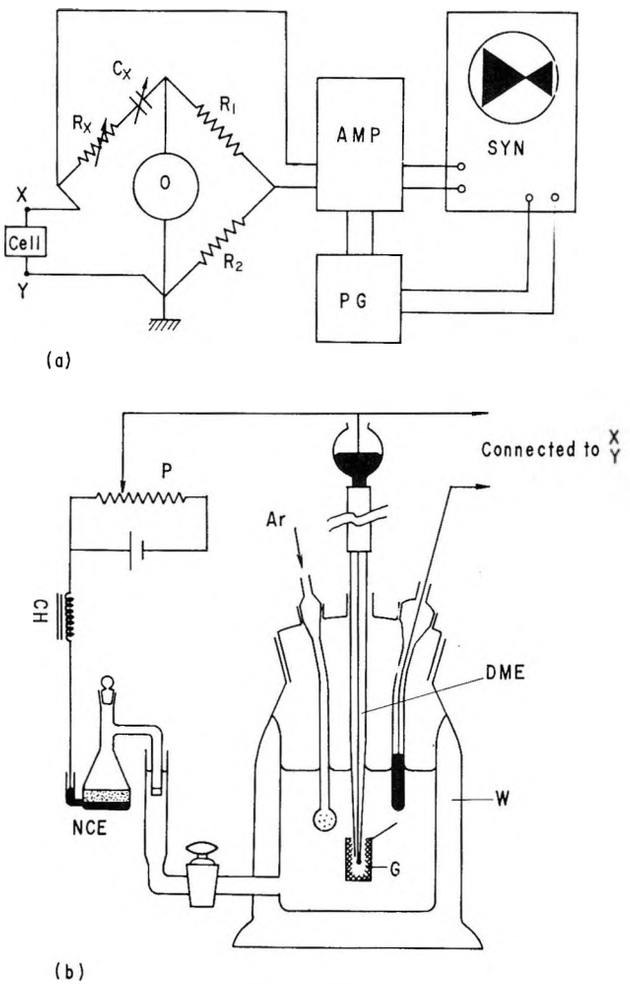

Figure 2. (a) Block diagram of apparatus for differential capacity measurement: R_x, standard variable resistor; C_x, standard variable capacitor; R_1, R_2, resistors; O, twin T oscillator; AMP, twin T differential amplifier; PG, pulse generator; SYN, synchroscope. (b) Schematic of cell for differential capacity measurement: P, potentiometer; CH, choke coil (150 henrys); NCE, 1 *N* calomel electrode; DME, dropping mercury electrode; G, Pt gauze (counterelectrode); W, circulating water jacket.

sorption of I^- ion. Guaranteed grade KF and KI were further recrystallized from conductivity water. The conductivity water was obtained by redistillation from alkali permanganate solution, followed by distillation without the reagent, the specific conductivity of which was less than 1×10^{-6} ohm^{-1} cm^{-1}. The cleaned air was led into high-purity mercury (99.9999%) for 3 days, and then the mercury was washed well with dilute HNO_3 solution and distilled water, dried, and finally distilled twice *in vacuo*.

Procedure. First, critical potentials, E_- and E_+ were determined in the symmetrical case where two mercury droplets are equally charged. Two mercury

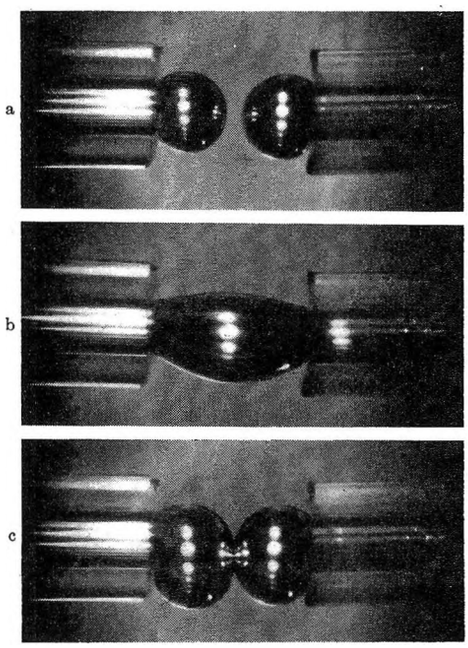

Figure 3. Photographs showing the coalescence and repulsion of mercury droplets: a, growing; b, coalescence; c, repulsion.

droplets were polarized simultaneously by means of potentiometer P_1 against nce after connecting both mercury pools. In the following the polarizing potential E will be given with reference to the rational potential of the electrode; *i.e.*, $E = 0$ when the polarized potential is fixed to the electrocapillary maximum (ecm) potential. The ecm potential (-0.47 v *vs.* nce) was confirmed by measuring the potential at which the differential capacity of mercury in contact with 0.01 *M* KF solution showed a minimum.

If the absolute value of E is small, two droplets coalesce as soon as they grow to the sizes at which their surfaces appear to be in contact with each other. However, if E is increased continuously to the negative or positive direction, a polarization range is obtained over which the twin droplets do not coalesce and continue to grow separately (*i.e.*, repulsion) even if they contact with each other. These behaviors of the mercury droplets were observed *via* the microscope of a cathetometer as shown in Figure 3. After determining the critical potentials, *i.e.*, the upper limit E_+ (>0) and lower limit E_- (<0) of the polarization range of coalescence, the potentiometers P_1 and P_2 were connected as shown in Figure 1a. One of the polarizing potentials, say, E_1 was fixed to any desired value more than E_- or E_+ and then the critical potential of the other side, say E_2, was determined. Below or above the critical potential of E_2 unequally charged mercury droplets coalesced or repelled each other. A set of the

potentials thus obtained provides the critical potential in coalescence of unequally charged mercury droplets (heterocoalescence). Two growing droplets were brought into contact as slowly as possible by regulating three traveling micrometer devices attached to one capillary. It is thought to be necessary to avoid the effect of acting force which results from the nonequilibrium state, such as a resistance in thinning the intervening water layer.[8] In fact, when the contact of the two droplets was not sufficiently slow, the critical potentials showed a tendency to decrease to smaller values. The critical potentials were not so sensitive to the size of the droplets except in the case where the difference in size between the droplets was exceedingly great. The error in the detection of the critical potentials, which depends upon the applied potentials, was estimated to be less than $\pm 6\%$.

Results and Discussion

Interaction between Identical Double Layers. Critical potentials in the symmetrical case, E_- and E_+, are plotted in Figure 4 as functions of KF concentration in molarity. The symmetry between E_- and E_+ with respect to the abscissa is thought to be satisfactory. The Hamaker constant, A, was evaluated in such a way that a maximum in the net potential energy (V_{max}) became zero at the critical potential under the condition of $\kappa D = 2$ (D is the shortest distance between the particle surfaces, and κ is the Debye–Hückel reciprocal length). The values thus obtained from the critical potentials were $(3.10 \pm 0.19) \times 10^{-12}$ and $(1.20 \pm 0.17) \times 10^{-12}$ at a 5% significant level, respectively, where in the former the surface potential referred to E and in the latter the potential of the outer Helmholtz plane, ψ^0, was used in calculating the double-layer interaction. Though the DLVO theory is originally concerned with the diffuse layer potential, it is thought to be interesting to compare the results from the both calculations. In the above calculations the repulsive potential energy of double-layer interaction was evaluated by interpolating the results established by Devereux and de Bruyn,[4] and $A/12\pi D^2$ [1] was used in estimating the van der Waals attraction. That is, the calculation is based on the plane-parallel double-layer model, but this is thought to be a proper choice for our system.

Conversely, we can calculate the critical potential in each concentration if the value of A is known. The dotted curves in Figure 4 represent the theoretical value of the critical potential in the case of $A = 3.10 \times 10^{-12}$. The solid curves show the theoretical value in the case of $A = 1.20 \times 10^{-12}$ where the double-layer interaction energy was calculated in terms of ψ^0. The agreement between theory and experimental results is thought to be satisfactory in each case. The value of ψ^0 (in volts) in KF solutions was calculated at 25° in accordance with the theoretical equation as

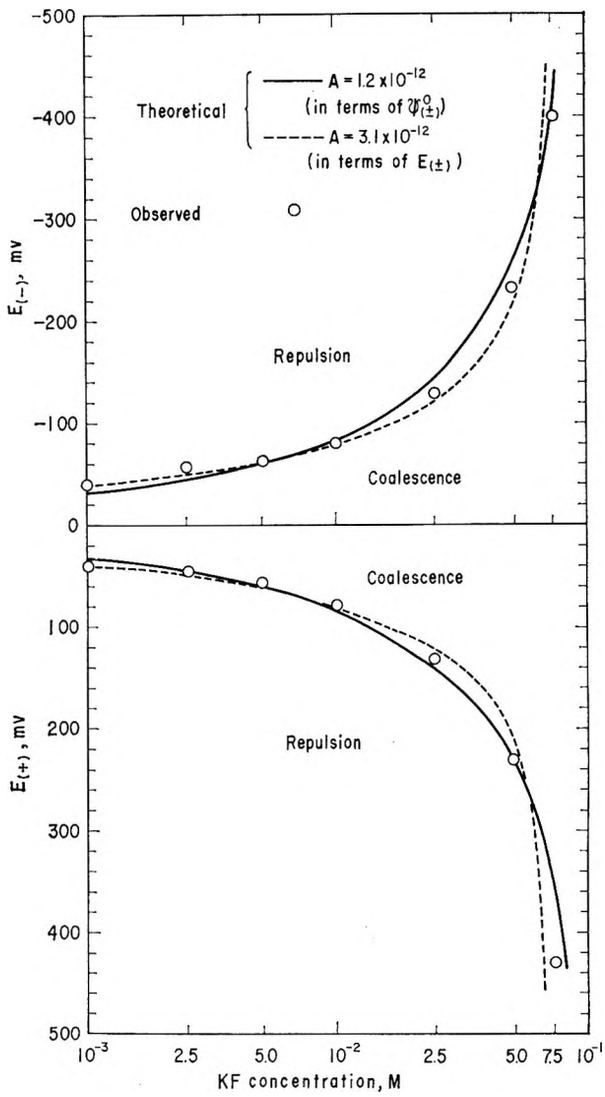

Figure 4. Critical potentials in the symmetrical case as functions of KF concentration.

$$\sigma_S = 11.72C^{1/2} \sinh (19.46\psi^0) \quad (1)$$

where σ_S is the surface charge density in microcoulombs per square centimeter and C is the electrolyte concentration in moles per liter. The surface charge density was obtained by integration of the differential capacity with respect to E except for 0.001 M KF solution. It was difficult in our device to obtain a reliable value of the differential capacity in concentrations less than

(8) B. V. Derjaguin and M. Kussakov, *Acta Physicochim. URSS*, **10**, 25, 154 (1939).

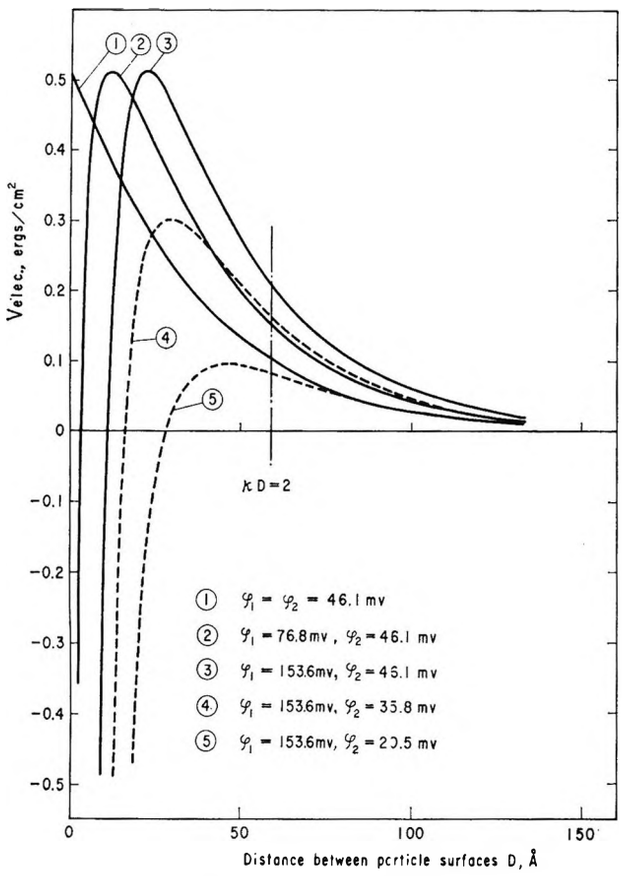

Figure 5. Potential energy due to the double-layer interaction (V_{elec}) as a function of the particle distance in 0.01 M KF solution.

0.0025 M, so that Grahame's data[9] were used for 0.001 M KF solution. The agreement in σ_S between Grahame's and our results was confirmed for 0.01 M and 0.1 M KF solutions. The relation between ψ^0 and E was used for mutual conversion between them.

Interaction between Dissimilar Double Layers in the Absence of Specific Adsorption. Remarkable features demonstrated by Derjaguin[2] are as follows. (a) In contrast to the symmetrical case, a force barrier occurs in the dissimilar double-layer interaction when both potentials are of the same sign. (b) The force barrier depends exclusively on the potential of the more weakly charged surface, say φ_2. (c) The position at which the force barrier appears is shifted to a greater distance as the potential of the more strongly charged surface, say φ_1, increases. The accurate calculation of the potential energy due to the dissimilar double-layer interaction was carried out by Devereux and de Bruyn[4] on the basis of the free energy method. Examples of the potential energy due to the dissimilar double-layer interaction (V_{elec}) in 0.01 M KF solution are illustrated in Figure 5 as functions of the particle distance. Considering that the energy value at $\kappa D = 2$ is a measure of the criterion of the coalescence, it may be seen from this figure that the lower surface potentials, φ_2, must be decreased with increasing higher surface potentials, φ_1, in order to cause the coalescence. The critical potentials determined experimentally in the heterocoalescence are shown in Figure 6. Cross marks along the chain line show the critical potentials (E_- or E_+) in the symmetrical case. The region involving the origin represents the coalescence. In the second and fourth quadrants where two mercury droplets are oppositely charged, the droplets surely coalesce irrespective of the concentration of the solutions under test. In the case of the heterocoalescence, theoretical curves are also given in a way similar to that of the symmetrical case on the assumption that the critical condition corresponds to the point at which $V_{max} = 0$. The Hamaker constant A was evaluated from the experimental value of E_- or E_+ for each concentration. The potential energy due to the dissimilar double-layer interaction was evaluated by a graphical interpolation of Devereux and de Bruyn's table.[4] Solid and dotted curves represent the theoretical values, where the double-layer interaction energies were cal-

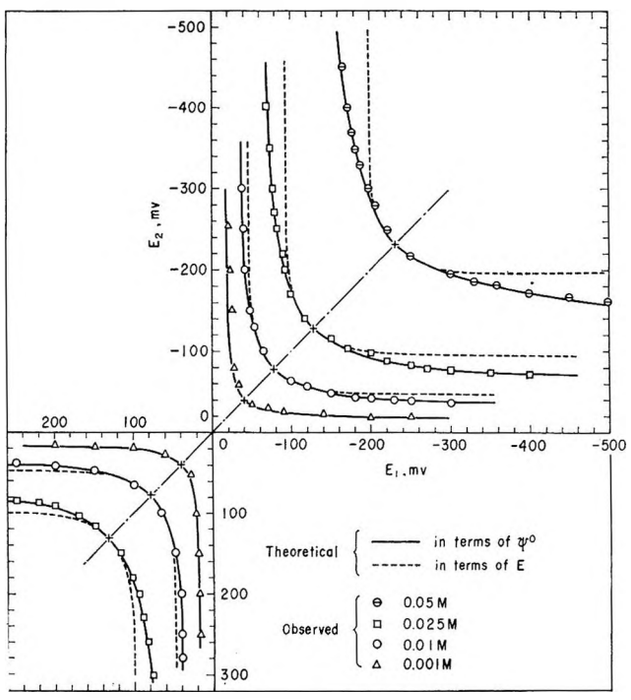

Figure 6. Critical potentials at heterocoalescence in KF solution.

(9) D. C. Grahame, *J. Am. Chem. Soc.*, **76**, 4819 (1954).

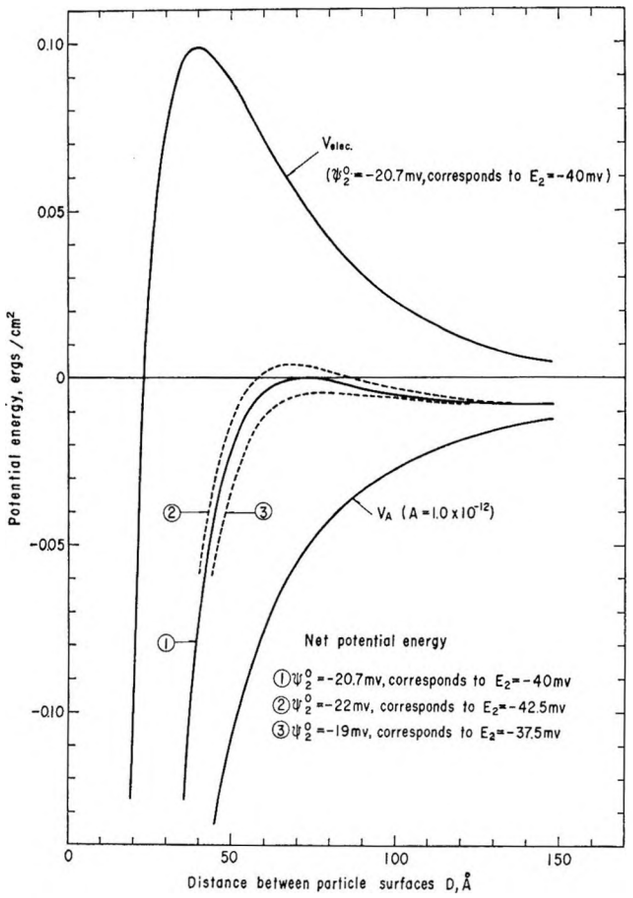

Figure 7. Potential energy curves as functions of the particle distance in 0.01 M KF solution at $\psi^0_1 = -102$ mv (corresponding to $E_1 = -260$ mv).

culated in terms of ψ^0 in the former and in terms of E in the latter, respectively. An example of calculation of the potential energies due to the dissimilar double-layer interaction, V_{elec}, van der Waals attraction, V_A, and total interaction between approaching particles at $\psi_1^0 = -102$ mv (corresponding to $E_1 = -260$ mv) and $\psi_2^0 = -20.7$ mv (corresponding to $E_2 = -40$ mv) is shown in Figure 7 for 0.01 M KF solution. In this figure total potential energy curves at $E_2 = -42.5$ and -37.5 mv are included for comparison. Within the range of these potentials ambiguous results were given to detect the critical potentials.

As is shown in Figure 6, ψ^0 corrections are of significance with higher concentration and less effect appears in dilute solution, especially for 0.001 M solution. The agreement between experimental results and theoretical curves in terms of ψ^0 is thought to be satisfactory. This agreement between theory and experiment proves the validity of the theory of dissimilar double-layer interaction and furthermore indicates that the coalescence of mercury droplets is substantially the same as the coagulation of hydrophobic colloid particles and is interpreted quantitatively by the DLVO theory as has been pointed out by Watanabe and Gotoh.[6] In Figure 4 we obtained the values 3.1×10^{-12} and 1.2×10^{-12} as Hamaker constants, respectively. Confirming the validity of the calculation in terms of ψ^0, it may be concluded that the latter value should be taken as the correct one. This value is very close to the one proposed by Fowkes,[10] 1.3×10^{-12}, which was obtained from a different approach, and this indicates that the interaction between mercury and water molecules consists mainly of molecular forces, because he obtained the value by assuming that the interaction between mercury and water is composed entirely of the London–van der Waals forces and no contribution from electrostatic origin is expected. This may be the reason why the *coalescence* of mercury droplets in water was well interpreted in terms of the *coagulation* theory of hydrophobic colloids.

Interaction between Dissimilar Double Layers in the Presence of Specific Adsorption of Anions. Similar experiments were made on the aqueous solutions of KI with an intention of checking the effect of the specific adsorption of I^- ions. In contrast to KF solutions, no coalescence was observed in 0.001, 0.01, and 0.025 M KI solutions in the whole range of the potential tested. It should be noted that the mercury droplets repel each

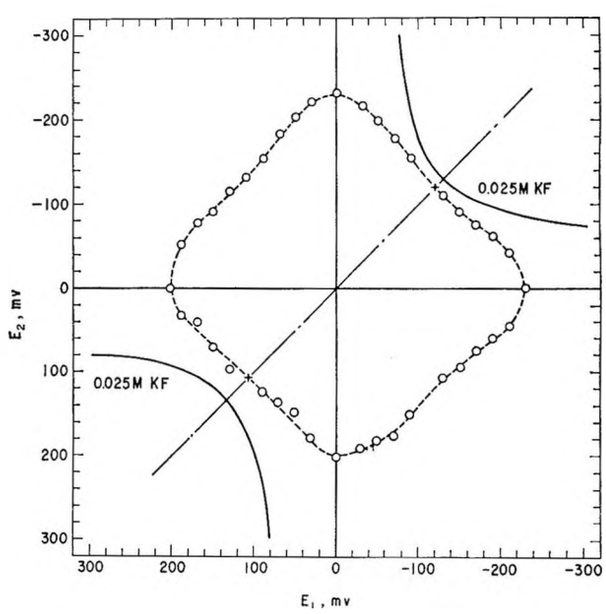

Figure 8. Critical potentials at heterocoalescence in the solution of KI + KF of constant ionic strength, 2.5×10^{-2} M. The concentration of KI is 1×10^{-4} M.

(10) F. M. Fowkes, *Ind. Eng. Chem.*, **56**, 40 (1964).

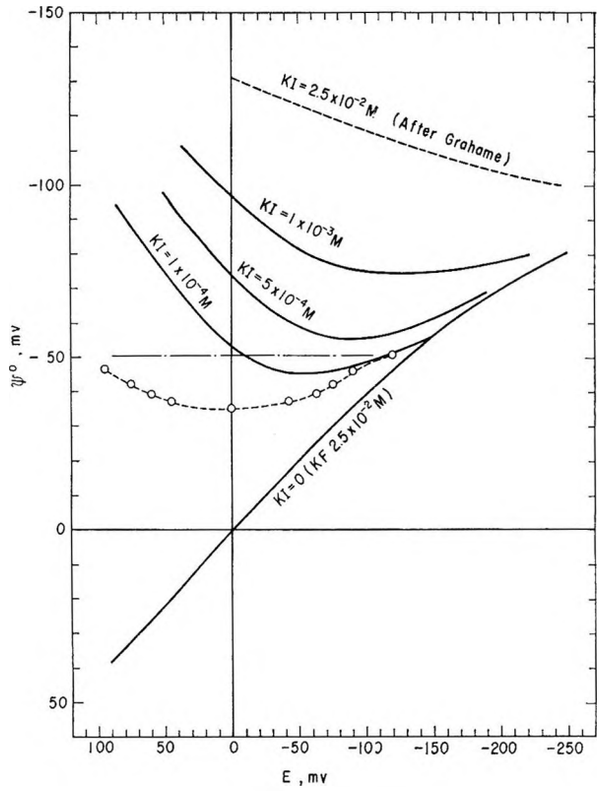

Figure 9. Relation between ψ^0 and E in the solution of KI + KF of constant ionic strength, 2.5×10^{-2} M: --O--, calculated from the coalescence data for [KI] = 1×10^{-4} M.

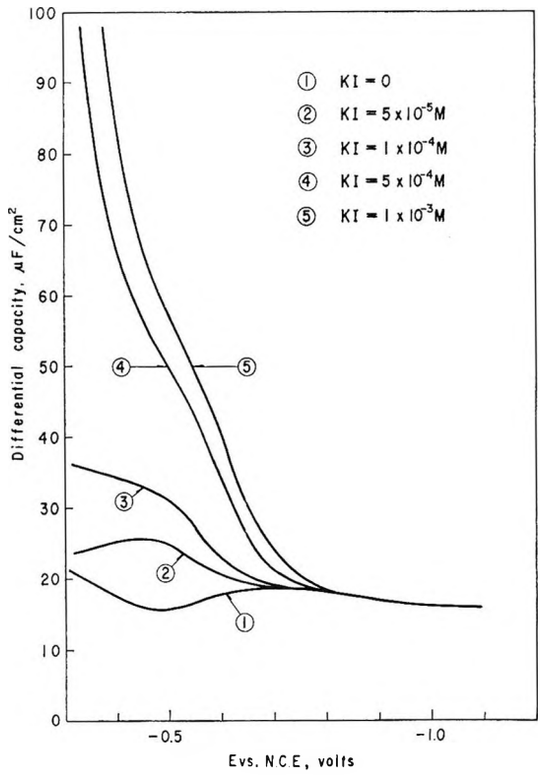

Figure 10. Differential capacities of mercury in contact with the solution of KI + KF of constant ionic strength, 2.5×10^{-2} M.

other even if they are oppositely charged. This fact may be interpreted by assuming that the potential of the outer Helmholtz plane, ψ^0, becomes negative as a result of the specific adsorption of I^- ions, even though the potential of the mercury surface, E, is fixed to the positive side. In order to examine quantitatively the effect of ψ^0 on the coalescence of mercury droplets in the presence of KI, the experiments were undertaken with the solution of KI + KF of constant ionic strength, 2.5×10^{-2} M. In the solutions where [KI] = 5×10^{-5}, 1×10^{-4}, 5×10^{-4}, and 1×10^{-3} M, the coalescence took place only in the first two solutions. In this case, however, the pattern of the critical potentials in the heterocoalescence differs considerably from that in the case of the pure KF solutions. In Figure 8, the critical potentials were plotted for [KI] = 1×10^{-4} M, the range including the origin representing the coalescence. In the same figure the result for the pure KF solution (2.5×10^{-2} M) was included for comparison. From these results we can estimate the ψ^0 for this system as a function of E with the aid of the critical potential data for the pure KF solution of 2.5×10^{-2} M, if we assume that the coalescence of mercury droplets is predominantly determined by ψ^0. In the above calculation it was reasonable to consider from the differential capacity data that the ψ^0 in the range more negative than $E = -150$ mv does not differ from that of the pure KF solution (2.5×10^{-2} M). The results for KI = 1×10^{-4} M are shown in Figure 9 as circles with a dotted line. Solid curves in the figure show the value of ψ^0 calculated from the differential capacity data. Differential capacities as functions of the potential against nce is illustrated in Figure 10. ψ^0 can be calculated by use of the eq 1, but in this case σ_S must be replaced by $\sigma_S + \sigma_{I^-}$ (σ_{I^-} is the amount of specifically adsorbed I^- ions). For our system, σ_{I^-} is obtained by the relation[11]

$$F(\partial\gamma/RT\partial \ln m_{KI})_{Ence} = -\sigma_{I^-} \quad (2)$$

where F is the faraday, γ is the interfacial tension, and m_{KI} is the molal concentration of KI. The value of γ (relative to ecm) was obtained by double integration of the capacity values with respect to E. As is seen in Figure 9, a poor agreement is noted between both approaches for 1×10^{-4} M KI and the discrepancy is much pronounced as the potential becomes positive.

(11) E. Dutkiewicz and R. Parsons, *J. Electroanal. Chem.*, 11, 100 (1966).

A series of measurements of differential capacity at different frequencies (100, 300, 1000, and 3000 cps) was made, and a dependence on the frequency was observed at potentials more positive than −0.7 v (*vs.* nce). Consequently, the above calculation was also carried out by using the differential capacity values extrapolated to zero frequency, but the discrepancy was not diminished at all. The reasonable explanation for this has not yet been given. However, the results in Figure 9 account qualitatively for the behavior of coalescence and repulsion of mercury droplets in KI solution. From the results that the critical potential ψ^0_- in the symmetrical case was −50.5 mv (corresponding to $E_- = -128$ mv), which is marked by the horizontal chain line, for the pure KF solution of 0.025 *M* (in the absence of specific adsorption), it may be expected that no coalescence takes place at any potential E in the KI solutions more concentrated than 5×10^{-4} *M* and coalescence occurs in the KI solutions less dilute than 1×10^{-4} *M*. This expectation is supported by the experimental results as previously described. Thus, the qualitative interpretation of the coalescence of mercury droplets in the presence of specific adsorption of I^- ions is possible in terms of the potential of the outer Helmholtz plane at the mercury–solution interface.

Acknowledgment. This investigation was supported in part by a Grant-in-Aid for Cooperate Research from the Ministry of Education. We are grateful to Professor Akira Watanabe of Kyoto Technical University for his valuable discussions and to Assistant Professor Tsuneo Ikegami of the Chemical Research Institute of Non-Aqueous Solutions of Tohoku University for his help with assembling our devices.

Infrared Spectrum of AlF_3, Al_2F_6, and AlF by Matrix Isolation

by Alan Snelson

IIT Research Institute, Chicago, Illinois 60616 *(Received February 14, 1967)*

The matrix isolation technique has been used to obtain the infrared spectrum of AlF_3, Al_2F_6, and AlF. Orientation effects observed for AlF_3 trapped in an argon matrix aided in the assignment of some absorption bands. The following are the three infrared-active frequencies of AlF_3: $\nu_4(E')$ 270 cm^{-1}, $\nu_3(E')$ 965 cm^{-1}, and $\nu_2(A_2'')$ 300 cm^{-1}. Six frequencies are attributed to the dimer Al_2F_6. Assuming a planar bridge structure, point group D_{2h}, the frequencies are assigned as follows: $\nu_8(B_{1u})$ 995 cm^{-1}, $\nu_9(B_{1u})$ 340 cm^{-1}, $\nu_{13}(B_{2u})$ 660 cm^{-1}, $\nu_{16}(B_{3u})$ 805 cm^{-1}, $\nu_{17}(B_{3u})$ 575 cm^{-1}, $\nu_{18}(B_{3u})$ 300 cm^{-1}.

Introduction

Mass spectroscopic investigations[1,2] have shown aluminum trifluoride vapor at about 1000°K to consist of the molecular species AlF_3 and Al_2F_6, the latter being present to the extent of 1 or 2%. The high-temperature gas-phase infrared spectrum of AlF_3 has been reported by Buchler[3] and Margrave, *et al.*[4] The matrix spectrum has been observed by Linevsky[5] and Snelson[6] but is not reported in the open literature. No data are available on the dimer species. The current investigation by matrix isolation was initiated to fill

(1) R. F. Porter and E. E. Zeller, *J. Chem. Phys.*, **33**, 858 (1960).

(2) A. Buchler, "Study of High Temperature Thermodynamics of Light Metal Compounds," Progress Report No. 3, Arthur D. Little, Inc., Cambridge, Mass., 1962.

(3) A. Buchler, ref 2, Progress Report No. 2.

(4) L. D. McCory, R. C. Paul, and J. L. Margrave, *J. Phys. Chem.*, **67**, 1986 (1963).

this gap, and also supply comparison spectra for a projected study on the mixed species $LiAlF_4$. The spectra obtained initially for AlF_3 were more complex than anticipated and the possibility that the species AlF might be present in the vapor was investigated.

Experimental Section

The matrix isolation cryostat, molecular beam furnace, and experimental procedures used in this investigation were essentially the same as that described by the author in a previous paper.[7] Only those details peculiar to the present experiments will be given.

The aluminum fluoride was reagent grade supplied by Baker and Adamson. It was dehydrated prior to being loaded into Knudsen cells, which were made of either graphite or platinum. The sample was heated at about 875° to observe the spectrum of the saturated vapor, depositions lasting from 1 to 2 hr. To observe the spectrum of the undersaturated vapor, superheating at 1400° was used.

The species AlF was formed by heating spectroscopically pure aluminum metal with AlF_3 at about 800°. A variety of Al:AlF_3 ratios was tried, the only effect on the spectrum being a slight enhancement in the intensity of the AlF_3 absorption bands in mixtures rich in the latter compound.

Most spectra were obtained with M/H >4000 for neon and argon and >2000 for krypton. Under these conditions, good isolation of the species resulted. Typical deposition rates of halide and matrix gas were 8–50 $\times$ 10^{-10} and 5–25 $\times$ 10^{-6} mole/sec, respectively. Spectra were recorded on a Perkin-Elmer 621 spectrophotometer. Frequencies are believed accurate to ± 1 cm^{-1}.

Results

The spectra of saturated aluminum trifluoride vapor in matrices of neon, argon, and krypton are shown in Figure 1a–c, under conditions of good isolation. There are two groups of strong absorption features at approximately 940 and 260 cm^{-1} in all matrices, together with six relatively weak absorption bands at A, C, D, E, F, and G. The spectrum of aluminum trifluoride vapor obtained under poor conditions of isolation is shown in Figure 1d, and the intensity of these six weak absorption features is increased relative to the strong absorptions at 940 and 260 cm^{-1}. The former are attributed to polymeric species. The spectrum of the superheated vapor gives further support to this assignment since only the strong absorption features remained, in addition to implying that the species responsible for the weak absorption bands must be vaporizing from the sample, rather than being formed in the matrix because

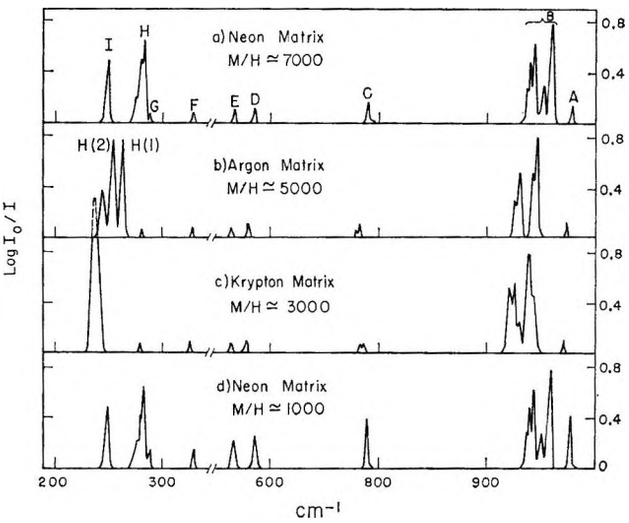

Figure 1. Infrared spectrum of the vapors over AlF_3.

of poor isolation. The absorption features at B, H, and I are assigned to monomeric aluminum trifluoride, and those at A, C, D, E, F, and G to the dimer. Because the intensities of the latter bands were rather weak, relative intensities measurements could not be used to add further support to this assignment.

Vibrational Assignments

1. AlF_3. Aluminum trifluoride vapor has been studied by electron diffraction[8] and infrared spectroscopy[3] at high temperatures. The molecule has a planar configuration of D_{3h} symmetry, analogous to boron trifluoride. The three infrared-active frequencies have been assigned as follows: $\nu_2(A_2'')$ 297 cm^{-1}, $\nu_3(E')$ 935 cm^{-1}, and $\nu_4(E')$ 263 cm^{-1}. In Figure 1, the absorption feature at B is assigned to ν_3. In all matrices, this band shows considerable splitting, some of which may be due to the degeneracy of the mode being removed by the matrix environment, in addition to structure resulting from different trapping sites in the matrix. The bands at H (ν 284 cm^{-1}) and I (ν 256 cm^{-1}) in the neon matrix are assigned to ν_2 and ν_4, respectively, by analogy with the reported gas-phase frequencies. In the krypton matrix only one absorption band occurs in this region and with greater intensity than might be expected for either ν_2 or ν_4 singly. It is assumed that matrix effects have resulted in these two frequencies

(5) M. J. Linevsky, "Spectroscopic Studies of the Vaporization of Refractory Materials," General Electric Space Sciences Laboratory, Contract Report AF33(615)-1150, Nov 1964.

(6) A. Snelson, Report No. IITRI-C6013-6, 1964.

(7) A. Snelson, *J. Phys. Chem.*, **70**, 3208 (1966).

(8) P. A. Akishin, N. G. Rambidi, and E. Z. Zasorin, *Kristallografiya*, **4**, 186 (1959).

becoming coincident, rather than postulating that ν_4 has suffered a particularly large matrix shift resulting in it lying below 200 cm^{-1}, the long wavelength limit of the spectrometer. If the latter were the case, then ν_4(neon) − ν_4(krypton) > 56 cm^{-1}. This is a considerably larger matrix shift than observed for ν_3(neon) − ν_3(krypton) $\simeq$ 20 cm^{-1}. In the alkaline earth fluorides,[4] for which data are available, the maximum difference between matrix shifts in neon and krypton for two frequencies of the same molecule is 12 cm^{-1}. This suggests the above difference of >36 cm^{-1} to be larger than usual, giving support to the initial assumption that the ν_4 and ν_2 bands are accidently degenerate in the krypton matrix.

The absorption bands in the aluminum trifluoride spectrum in an argon matrix at H(1) and I are assigned to ν_2 and ν_4, respectively. An assignment for H(2), resulting presumably from matrix splitting of either ν_2 or ν_4, is not possible owing to the proximity of the three absorption maxima. However, an assignment for this peak may be inferred from a consideration of the orientation effects demonstrated in the spectra shown in Figure 2. In Figure 2a, the matrix surface is perpendicular to the direction of propagation of the incident radiation, while in Figure 2b, it is at an angle of about 40°. The ratios log $(I_0/I)_b$/log $(I_0/I)_a$ for corresponding bands in the two spectra are: 1.15 (l), 1.19 (m), 1.92 (n), 2.02 (o), and 1.63 (p). The cross-sectional area of the analyzing beam in the spectrometer is slightly less than that of the matrix surface when the two are perpendicular to each other and rotation through a small angle results in an increase in the amount of material in the incident beam. This, in part, is responsible for all of the above ratios being >1, but is not the only factor involved since, if it were, the relative increase would be the same for all of the bands. The lack of constancy in the ratios is attributed to the aluminum fluoride molecules having certain preferred orientations in the matrix. The absorption band intensity for a given vibrating mode is proportional to $[(\partial\mu/\partial Q)E]^2$, where $(\partial\mu/\partial Q)$ is the change in dipole moment with respect to the normal coordinate Q, and E is the electric field strength of the incident radiation, both μ and E being vector quantities. The important feature in the present context is the scalar product; radiation with the electric vector perpendicular to the transition moment will not be absorbed. If the planes of all of the AlF_3 molecules are lying parallel to the window surface, a parallel beam of incident radiation perpendicular to the plane of the window would not interact with the ν_2 out-of-plane bending mode of AlF_3 since the electric vector of the radiation would be at right angles to the normal coordinate of

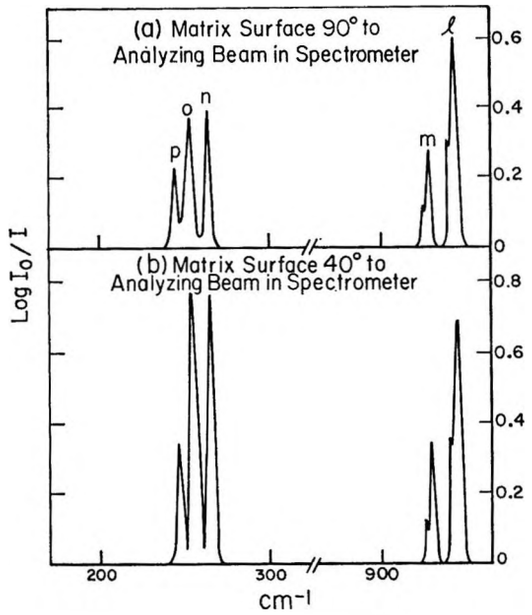

Figure 2. Infrared spectrum of AlF_3 in an argon matrix.

this mode, and the vibration would have zero absorption intensity. The two degenerate E modes, however, will be active since their normal coordinates are parallel to the electric vector of the radiation. Rotation of the plane of the window to make an angle of less than 90° with the analyzing beam would result in ν_2 becoming active, since the above scalar product will not be zero.

In the experimental arrangement used in this work, the analyzing beam in the spectrometer is slightly convergent and polarizing effects occur in the spectrometer which make quantitative deductions from the observed ratios impossible. Qualitatively, the experimental results can be accounted for if it is assumed that trapping sites for AlF_3 are preferred in which the plane of the molecule is more nearly aligned with the matrix surface than perpendicular to it. This is consistent with the relative increases in intensity being smallest for the bands at (l, m) and p, the peaks assigned to the E modes ν_3 and ν_4, respectively, and greatest for the band at n, the out-of-plane bending ν_2 mode. In addition, the similarity in the relative increase for the ratios n = 1.92 and o = 2.02 suggests that both these bands may be assigned to the ν_2 bending mode. Further support for the above interpretation has been obtained in matrix studies on the planar molecules Li_2F_2 and BF_3 in this laboratory, for which intensity increases were found to be much greater for the out-of-plane bending modes than the in-plane stretching modes on rotating the plane of the matrix from an angle of 90° to about 40° with respect to the direction of propagation of the

analyzing radiation. Weltner[9] has also reported orientation effects in neon and argon matrices from electron spin resonance studies on NO_2 and $Cu(NO_3)_2$.

In Table I the observed matrix frequencies of AlF_3 are listed together with their assignment to the symmetry species of the D_{3h} point group. The estimated gas-phase frequencies in the last column were obtained as described in an earlier paper[7] from the values observed in the neon matrix. For the ν_3 mode, which exhibits considerable splitting, the neon matrix frequency was taken as 950 cm^{-1}. Both the observed gas-phase values for ν_2 and ν_4 are in good agreement with the estimated frequencies reported here, which are probably accurate to ± 10 cm^{-1}. The estimated and observed gas-phase frequencies for ν_3 differ by 30 cm^{-1} which is larger than the estimated error of the former value. It is well known that the precise location of band centers in high-temperature infrared gas-phase studies is difficult, and since the frequency shifts in the three matrices show a regular trend toward the red, in the order neon < argon < krypton, it is believed that the estimated frequency, ν_3 965 cm^{-1}, is a consistent assignment for this mode.

Table I: Infrared Frequencies of AlF_3

Symmetry species	Figure designation	Obsd freq, cm^{-1} Neon	Argon	Krypton	Estd gas-phase freq, cm^{-1}
		960			
			945	941	
		951			
			942	938	
$E'(\nu_3)$	B	944			965
			930	925	
		940			
			927	921	
		937			
		284	267		
$A_2''(\nu_2)$	H			244	300
		276	256		
		256			
$E'(\nu_4)$	I		247	244	270
		252			

The estimated gas-phase frequencies were used to calculate the force constants $k_1 = 4.91 \times 10^5$ dynes/cm, $k_\delta/l^2 = 1.85 \times 10^4$ dynes/cm, and $k_\Delta/l^2 = 3.24 \times 10^4$ dynes/cm, using the formulas and nomenclature given by Herzberg.[10] From this value of k_1, the A_1' symmetric stretching frequency was calculated at 660 cm^{-1}.

2. Al_2F_6. No structural information is available on the dimer Al_2F_6 but comparison with the other aluminum halides[11-13] suggests a planar molecule with D_{2h} symmetry. This configuration results in eight infrared-active frequencies belonging to the symmetry species $B_{1u}(\nu_8, \nu_9, \nu_{10})$, $B_{2u}(\nu_{13}, \nu_{14})$, and $B_{3u}(\nu_{16}, \nu_{17}, \nu_{18})$. The frequency numbering is that given by Bell and Longuet-Higgins.[14] In the present investigation, only six absorption bands were recorded; their frequencies are listed in Table II. One of the unobserved frequencies, ν_{10}, an out-of-plane ring-bending mode, almost certainly lies below the long-wavelength limit of the spectrometer (200 cm^{-1}). The same may be true for the second missing frequency, though the possibility that it lies above 200 cm^{-1} and is unobserved owing to either low-absorption intensity or coincidence with other bands cannot be excluded.

Table II: Infrared Frequencies of Al_2F_6

Symmetry species	Figure designation	Obsd freq, cm^{-1} Neon	Argon	Krypton	Estd gas-phase freq, cm^{-1}
	A	979	973	971	995
B_{1u}					
	F	327	326	324	340
B_{2u}	D	586	580	578	600
	C	790	779, 782	785, 781	805
B_{3u}	E	568	563	562	575
	G	290	281	278	300

The vibrational assignment for the observed six infrared-active frequencies was made by comparison with the known spectra of other bridged X_2Y_6 molecules, and also to give the best agreement between the observed and computed values using the equations given by Bell and Longuet-Higgins. In the latter calculations the outer Al–F bond distance was taken as 1.63 A, the same as in AlF_3.[8] The bridge Al–F bond distance was chosen so that the ratio of Al–F(outer)/Al–F (bridge) bond lengths was equal to that in Al_2Cl_6.[15] The F–Al–F outer bond angle θ_2 was reduced slightly from the AlF_3 value of 60° to allow for repulsion from

(9) P. H. Kasai, W. Weltner, and E. B. Whipple, *J. Chem. Phys.*, **42**, 1120 (1965).

(10) G. Herzberg, "Molecular Spectra and Molecular Structure," D. Van Norstrand Co., Inc., New York, N. Y., 1960.

(11) H. Gerding and E. Smit, *Z. Physik. Chem.*, **50B**, 171 (1941).

(12) E. J. Rosenbaum, *J. Chem. Phys.*, **8**, 643 (1940).

(13) W. Klemperer, *ibid.*, **24**, 353 (1956).

(14) R. P. Bell and H. C. Longuet-Higgins, *Proc. Roy. Soc.* (London), **A183**, 357 (1945).

(15) K. J. Palmer and N. Elliot, *J. Am. Chem. Soc.*, **60**, 1852 (1938).

the bridge fluorine atoms. The magnitude of $2\theta_1$, corresponding to the F–Al–F angle in the ring, was chosen so that the two bridge fluorine atoms were just touching at their van der Waals radii. This contrasts with the geometry of Al_2Cl_6[15] in which there appears to be considerable overlap of the bridge halogens. However, it does allay objections to putting the F–F and the Al–Al ring interaction constants equal to zero, data being unavailable for their computation. The terminal Al–F bending (d_2) and stretching (f_2) force constants were assigned by comparison with AlF_3. The remaining force constants were chosen to give the best fit between the observed and calculated frequencies.

The frequency assignments and the results of the calculation are given in Table III. Agreement between the observed and calculated frequencies is about as good as can be expected on the basis of the above assumptions. The quotient $f_2/f_1 = 2.45$ for the nonbridge to bridge Al–F stretching constants is of the same order as in diborane (2.4) and Al_2Cl_6 (1.9). The values of the bending constants d_2, d_3, and d_4 appear reasonable by comparison with those derived for B_2H_6,[14] but d_1 is an order of magnitude larger. In deriving the frequencies corresponding to the A_g mode, only two of the possible four roots of the quartic equation were real. This may be due in part to assuming a zero value for g_1, the interaction constant, since this is the only mode in which this constant is of importance.

Table III: Force Constants (dynes/cm) and Frequencies (cm^{-1}) of Al_2F_6

$f_1 = 2.0 \times 10^5$ $f_2 = 4.90 \times 10^5$ $g_1 = 0$ $g_2 = 0$
$d_1 = 4.5 \times 10^4$ $d_2 = 2.0 \times 10^4$ $d_3 = 0$ $d_4 = 2.85 \times 10^4$
$a = 1.80$ A $b = 1.63$ A $\theta_1 = 49°$ $\theta_2 = 58°$

		Calcd	Obsd
A_g	ν_1	939	
	ν_2	602	
	ν_3		
	ν_4		
A_u	ν_5	191	
B_{1g}	ν_6	874	
	ν_7	326	
B_{1u}	ν_8	980	995
	ν_9	349	340
	ν_{10}		
B_{2g}	ν_{11}	970	
	ν_{12}	259	
B_{2u}	ν_{13}	645	600
	ν_{14}	232	
B_{3g}	ν_{15}	336	
B_{3u}	ν_{16}	860	805
	ν_{17}	550	575
	ν_{18}	315	300

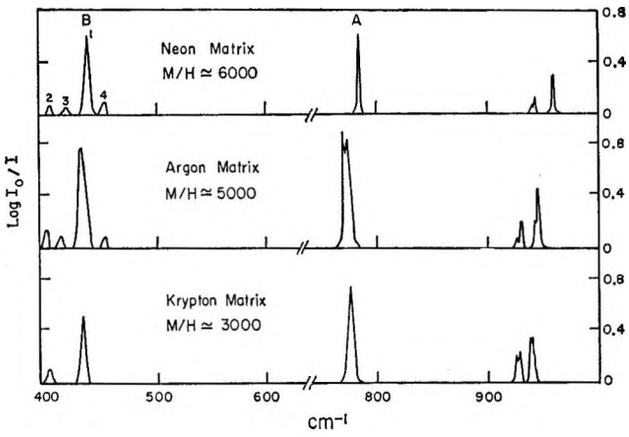

Figure 3. Infrared spectra of the vapors over a mixture of 2Al and AlF_3.

3. AlF. The electronic spectrum of Al–F is well characterized,[16] the $\nu_0 \rightarrow \nu_1$ vibrational transition of the ground state having a frequency of 793 cm^{-1}. In Figure 3 the spectrum of Al–F in neon, argon, and krypton matrices is shown. The position and frequency of the band at A in the three matrices permits an immediate assignment to the monofluoride. Comparison of the matrix frequencies of this band (Table IV), with those of the band at C in the AlF_3 spectra (Figure 1), clearly indicates that different species are responsible for these bands in the two sets of spectra. This eliminates the possibility that the band at C (Figure 1) may be attributed to AlF formed owing to the presence of a metallic impurity in the AlF_3 sample.

Table IV: Infrared Frequencies of Aluminum Monofluoride and Polymers

Molecular species	Point group	Symmetry species	Figure designation	Freq, cm^{-1} Neon	Argon	Krypton
AlF	$C_{\infty v}$	Σ^+	A	785	776	773
			B_1	439	432	426
			B_2	405	404	400
Polymers			B_3	420	415	
			B_4	455	453	

The appearance of the AlF absorption band at A in the neon, argon, and krypton matrices shows the same type of structure as monomeric lithium fluoride in the same matrices.[17,18] This may be attributed to the

(16) S. M. Naude and T. J. Hugo, *Can. J. Phys.*, **35**, 64 (1957).

similar dimensions of the two molecules; for AlF, r_e = 1.65 A and for LiF, r_e = 1.56 A, allowing the same matrix trapping sites to be occupied in both cases. There is, however, a marked difference in frequency shifts for the two molecules; $\nu_{gas} - \nu_{neon\ matrix}$ = 8 and 32 cm^{-1} for AlF and LiF, respectively. In matrix studies, the largest frequency shifts are usually associated with molecules having large dipole moments resulting in strong dipole–induced dipole interactions with the surrounding rare gas atoms. Lithium fluoride (μ = 6.3 D.) is a molecule of this type, compared to AlF(μ = 1.53 D.).[19] Although repulsive and dispersive effects between the trapped molecule and the matrix also result in frequency shifts, for LiF and AlF they are likely to be of the same order of magnitude since the molecular sizes are similar. Hence it is probable that the major factor responsible for the large difference in the frequency shifts of these two molecules is the dipole–induced dipole interaction with the matrix.

The absorption bands at approximately 950 cm^{-1} are assigned to monomeric AlF_3, a small amount vaporizing from the sample, together with the Al–F. The bands at B are assigned to polymeric or agglomerate material since their intensity relative to the monomeric band at A increased markedly under poor conditions of isolation. Under the best conditions of isolation, it was possible to eliminate the peaks at B_3 and B_4 and at the same time reduce the intensities of B_1 and B_2, the maximum decreases occurring for B_2. This behavior implies that none of these bands are attributable to the same chemical species. Mass spectroscopic studies on the AlF_3 + Al system show only the presence of the vapor-phase species AlF and AlF_3. This is fairly strong evidence against the existence of polymers of the type $(AlF)_n$, but the possibility that a species exists whose fragmentation pattern does not lead to its detection cannot be excluded. In the present case it is believed that the polymers are being formed during the deposition of the matrix. However, the available evidence does not permit an assignment of these bands to specific molecular species.

Acknowledgment. The author gratefully acknowledges the support of the Army Office of Research and Air Force Office of Research in funding this research.

(17) A. Snelson and K. S. Pitzer, *J. Phys. Chem.*, **67**, 882 (1963).
(18) R. L. Redington, *J. Chem. Phys.*, **44**, 1238 (1966).
(19) D. R. Lide, *ibid.*, **42**, 1013 (1965).

Hydrogen–Deuterium Equilibration and Ortho–Parahydrogen Conversion on Molecular Sieves

by J. Turkevich and S. Ciborowski

Frick Chemical Laboratory, Princeton University, Princeton, New Jersey 08540 *(Received February 15, 1967)*

An investigation has been made of the ortho–parahydrogen conversion and hydrogen–deuterium equilibration on a number of faujasite-type molecular sieves in order to determine the nature of catalytic centers. For this purpose a simple method of preparing a faujasite material was developed to produce material that would supplement the available commercial product. The conversion of the sodium faujasite to the ammonium, hydrogen, and decationated faujasite was studied. A gas chromatographic analysis was developed for the various hydrogen species. A correlation previously found between extent of sodium replacement and catalytic activity for hydrogen–deuterium equilibration was extended to the degree of conversion of hydrogen faujasite to decationated faujasite. The ortho–parahydrogen conversion was found to be independent of the degree of decationization and must be ascribed to small traces of paramagnetic impurities, or to the effect of the nuclear magnetic moment of aluminum. The effect of γ irradiation was also studied.

Introduction

$H_2 + D_2$ reaction has been investigated for a number of decades. The majority of these investigations were carried out on metal catalysts, particularly on nickel and tungsten. Several authors investigated the $H_2 + D_2$ reaction on oxides, particularly metal oxides. Results of these investigations are presented in several reviews by Trapnell[1] and Brennan.[2]

It was found that the reaction is first order, and the activation energy is very low. There is a wide difference in the views of various authors on the mechanism of this reaction. Three hypotheses have been proposed. The first is the Bonhoeffer and Farkas[3] mechanism according to which both hydrogen and deuterium molecules are chemisorbed and dissociated on the catalyst surface. The reaction takes place between H and D atoms on the surface. The second is the Rideal[4,5] mechanism according to which the reaction proceeds between a chemisorbed atom and a physically adsorbed molecule. The third is the Schwab[6,7] mechanism according to which the reaction takes place between two adsorbed and strongly polarized molecules. The different mechanisms may exist at different reaction conditions: the Bonhoeffer–Farkas mechanism may apply at higher temperatures while the Rideal mechanism may apply at lower temperatures.

Ortho–parahydrogen conversion has also been studied for many years.[1,2] The ortho–parahydrogen conversion may proceed by the same mechanism as the hydrogen–deuterium equilibration reaction. The ortho–parahydrogen conversion may also proceed by a magnetic mechanism on paramagnetic catalytic sites. This mechanism is effective at low temperatures (usually below $-150°$) since physical adsorption of hydrogen molecules is required. The temperature dependence of the ortho–parahydrogen conversion rate is negative in the low-temperature range because of nega-

(1) B. M. W. Trapnell, "Catalysis," Vol. III, P. H. Emmett, Ed., Reinhold Publishing Corp., New York, N. Y., 1955, p 1.

(2) D. Brennan, "Recent Progress in Surface Science," Vol. 2, Academic Press Inc., New York, N. Y., 1964, p 63.

(3) K. F. Bonhoeffer and A. Farkas, *Z. Physik. Chem.* (Leipzig), **B12**, 231 (1931).

(4) E. K. Rideal, *Proc. Cambridge Phil. Soc.*, **35**, 130 (1939).

(5) E. K. Rideal, *J. Soc. Chem. Ind.* (London), **62**, 335 (1943).

(6) G. M. Schwab and E. Killmann, *Bull. Soc. Chim. Belges*, **67**, 305 (1958).

(7) G. M. Schwab and E. Killmann, *Z. Physik. Chem.* (Frankfurt), **24**, 119 (1960).

tive temperature dependence of physical adsorption. At higher temperatures (room temperature) the reaction proceeds again by the same mechanism as that responsible for the hydrogen–deuterium equilibration reaction.

Ortho–parahydrogen conversion has also been found by most authors to be of first order.

Turkevich, *et al.*,[8,9] investigated the hydrogen–deuterium equilibration reaction on molecular sieves. They reached the conclusion that the active sites of catalyst were those sites where sodium ions were replaced by ammonium ions and the latter decomposed by thermal treatment.

It was proposed to investigate more thoroughly the nature of the active site in molecular sieves for the hydrogen–deuterium equilibration reaction and to compare it with the nature of the active site for carrying out the ortho–parahydrogen conversion reaction. Ortho–parahydrogen conversion has not been investigated using molecular sieve catalysts. A laboratory method for preparation of faujasite was developed and the process of conversion of sodium Y sieve into ammonium Y sieve, hydrogen Y sieve, and decationated Y sieve was studied and related to the development of the catalytic centers.

Experimental Section

Materials. Hydrogen (Matheson prepurified grade) and deuterium (Matheson) were purified by contacting with palladium catalyst at 200° and removing any water present by cooling to −196°.

Linde NaY molecular sieve (Research grade) was the main catalyst used (catalyst 0). It has the theoretical composition $Na_{56}(AlO_2)_{56}(SiO_2)_{136}$; however, wet chemical analysis performed by the courtesy of RCA Research Laboratories indicated a somewhat lower aluminum:silicon ratio of 53:139. The water content was 25% corresponding to 250 molecules/unit cell.

A faujasite material with a lower silicon to alumina ratio of 69:124 (catalyst 6) was synthesized from ethyl orthosilicate (Fischer), sodium hydroxide (CP grade), and aluminum metal.

Synthesis of Faujasite. Although synthetic faujasite-type molecular sieves have gained considerable importance in the past decade as catalysts and catalyst carriers, there is little information on their synthesis except in the patent literature.[10–14] It was felt desirable to develop according to the patent literature a simple reproducible way to make in the laboratory a faujasite-type zeolite with the particular view of minimizing paramagnetic impurities.

The molecular sieve was synthesized by allowing sodium silicate and aluminum silicate to react in aqueous alkaline solution at 100°. The sodium silicate was prepared in the following way. Two moles of sodium hydroxide (80 g) was dissolved in 200 ml of distilled water, and 400 ml of ethyl alcohol was added. One mole of ethyl orthosilicate (222 ml or 208 g) was slowly added with vigorous stirring to this solution, and after addition the mixture was stirred for 1 hr. It was allowed to stand overnight and the upper layer was separated off. Nitrogen gas was passed through the vessel to remove the traces of alcohol and the solution was diluted with water to 250 ml. The sodium aluminate solution was prepared by dissolving 1 mole of aluminum metal (27 g) in a sodium hydroxide solution containing 80 g of sodium hydroxide in 250 ml of distilled water. The metal was dissolved slowly and the mixture was allowed to stand overnight; then it was filtered and diluted to the desired volume. The amount of undissolved aluminum was determined and the amount dissolved was calculated. The standard preparation of the faujasite was carried out in the following way. Ten volumes of aluminate solution containing 0.32 mole of sodium aluminate, $NaAlO_2$, and 0.32 mole of sodium hydroxide/l. was slowly added with stirring to eight volumes of sodium silicate solution containing 4 moles of Na_2SiO_3/l. and no excess of sodium hydroxide. A small amount of gel was produced and the stirring was continued for 30 min. The mixture was then transferred from a beaker to a round-bottom flask which was rotated at an angle of 45° in an oil bath. The flask was loosely closed to keep it from contact with the atmosphere. The temperature of the oil bath was kept at 100 ± 1°. Further formation of gel took place at 100° and then it gradually changed into the desired crystalline product. After 7 hr the product was filtered, washed several times with distilled water, and dried at room temperature. The ratio of silicon to aluminum in the product was 1.83. This was determined by wet analysis. Powder X-ray spectra were used to identify the crystalline species present. Thus for faujasite the (111) line at d = 14.3 A and the (555) line at d = 2.87 A and for phillipsite

(8) J. Turkevich, T. Ikawa, F. Nozaki, and D. Stamires, "Industrial Uses of Large Radiation Sources," Vol. II, International Atomic Energy Agency, Vienna, 1963, p 41.

(9) J. Turkevich, F. Nozaki, and D. Stamires, *Proc. Intern. Congr. Catalysis, 3rd, Amsterdam, 1964*, 1, 586 (1965).

(10) D. W. Breck, W. G. Eversole, and R. M. Milton, *J. Am. Chem. Soc.*, **78**, 2338 (1956).

(11) R. M. Barrer, J. W. Baynham, F. W. Baltitude, and W. M. Meier, *J. Chem. Soc.*, 195 (1959).

(12) D. W. Breck, *et al.*, U. S. Patent 3,130,007 (1964).

(13) S. P. Zhdanov and N. N. Buntar, "Sintetitcheskie Zeolity," USSR Academy of Sciences Press, Moscow, 1962, p 105.

(14) S. P. Zhdanov, *Izv. Akad. Nauk SSSR, Ser. Khim.*, 949 (1965).

the (310) line at $d = 3.18$ A were used for estimating the amount of these materials present. X-Ray powder spectra could also be used for determining the silica–alumina ratio in the faujasite since this ratio was related to the size of the unit cell. The position of the (555) line was given by

$$a_0 = d\sqrt{h^2 + k^2 + l^2} = d\sqrt{75} \qquad (1)$$

where a_0 is the size of the unit cell in angstroms. Using values in the literature, a linear relationship was found between the Si/Al ratio and the value of a_0

$$\text{Si/Al} = \frac{25.248 - a_0}{0.245} \qquad (2)$$

which is valid for the Si/Al ratio of 1:3.

The following observations can be made on the synthesis. At times less than 6 hr there was only a partial crystallization of the gel into faujasite. At 6.5, 12.5, and at 26 hr the product was 100% faujasite. At 50 hr 3% phillipsite was formed. At 75 hr 15%, at 96 hr 40%, at 127 hr 50%, and at 151 hr 60% of the product was phillipsite. The other product was faujasite. Thus faujasite is an intermediate in the formation of phillipsite.

Decrease of temperature from 100 to 85° increased the rate of formation of phillipsite, 40% being formed at 22.5 hr, 50% after 35 hr, and 60% after 47 hr.

Decrease in the concentration of all of the components by a factor of 2 favored the formation of phillipsite at 100°. Thus after 18 hr there was very little faujasite formed while after 40 hr the crystalline product was 100% phillipsite.

Increasing the Si/Al ratio in the reacting mixture to 15:1 produced no gel even at 100° and the homogeneous solution slowly produced phillipsite only.

Preliminary investigation was carried out using Raman spectra and nuclear magnetic resonance of Al to determine when in the synthesis the aluminate ion interacts with the silicate ion. The Raman spectrum was measured using a Cary Model 81 spectrophotometer. The exciting line was 4358 A (22,938 cm^{-1}); the slit was 10 cm^{-1} wide and 10 cm long. A standard 7-mm diameter sample tube was used to hold the solution which was centrifuged before use. The concentrations of reactants were chosen so that gel formation was avoided for at least 4 hr. The mixture was allowed to stand for 1 hr before measurement to allow air bubbles to rise from the solution. The Raman spectrum of sodium aluminate is given in Figure 1. The main peak was found at 615 cm^{-1} as reported by Lippincott, *et al.*,[15] who proposed that in the sodium aluminate solution the aluminum species existed as $Al(OH)_4^-$ in tetrahedral configuration and assigned the 615-cm^{-1} peak to the ν_1 vibration. Addition of sodium aluminate to sodium silicate to produce a concentration of 0.8 mole of $NaAlO_2$ gives a spectrum in which the aluminate peak ion is not observed. The resulting spectrum is essentially the same as that of sodium silicate which was present in excess. This is taken as evidence that the interaction between the silicate and aluminate takes place within 1 hr on mixing.

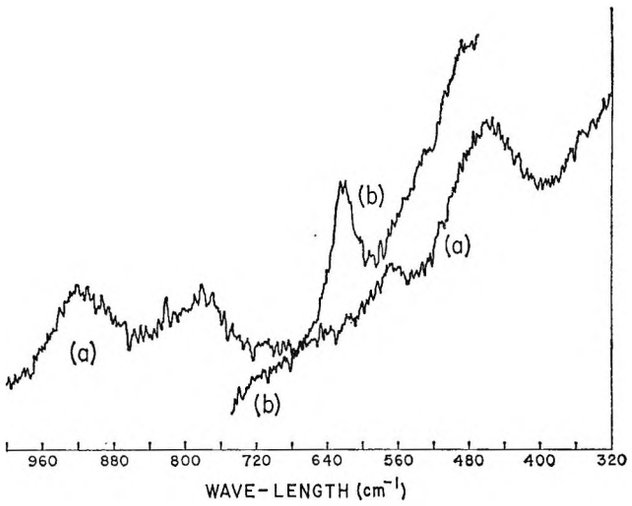

Figure 1. Raman spectra: (a) sodium aluminate and sodium silicate aqueous solution containing 13 *M* Na^+, 2.5 *M* SiO_2, and 0.8 *M* AlO_2; (b) sodium aluminate aqueous solution containing 13 *M* Na^+ and 0.8 *M* AlO_2.

The aluminum nuclear resonance at 11.094 Mc/sec at 10,000 gauss was also measured for a series of aluminate solutions and a sodium aluminate–sodium silicate solution. The intensity of the aluminum resonance line and its width of about 50 mgauss was found to be independent of the sodium hydroxide concentration in the range of 0.4–7.2 g-atoms of sodium/l. of water when the concentration of aluminum was 0.2 g-atom/l. The intensity of the resonance line increases with concentration of aluminum being 800 units for 0.2 g-atom of Al, 4400 units for 1.0 g-atom of Al, and 9100 for 3.6 g-atoms of Al/l., the sodium concentration being kept constant at 7.2 g-atoms/l. However, when the solution contained 0.8 g-atom of Al, 13.0 g-atoms of Na, and 2.5 g-atoms of silicon as silicate in 1 l. of solution, the aluminum resonance intensity was only 9 units instead of the expected 4000. This is taken to indicate that in alkaline solution the silicate ions interact in such a way with the aluminate ion to make the crystalline field asymmetric around the aluminum nucleus. The un-

(15) E. R. Lippincott, J. A. Psellos, and M. C. Tobin, *J. Chem. Phys.*, 20, 536 (1952).

symmetric field interacts with the quadrupole nuclear moment increasing the relaxation time to such an extent that it broadens the resonance line to make its observation difficult.

Synthesis and Analysis of Ammonium, Hydrogen, and Decationized Faujasite. The sodium cations in the Linde Y molecular sieve were replaced by ammonium cations by treatment of the sodium sieve with varying concentrations of aqueous ammonium nitrate for 60 hr with occasional stirring. After filtration and washing several times with distilled water, the solid was dried at room temperature.

Previous workers have determined the extent of replacement of the sodium ions by the ammonium ions by determining the amount of sodium ions in the aqueous solution after the exchange has been completed. We found this method inconvenient and not sufficiently accurate. We used two other methods.

In one method, purified helium was passed over the sample at 480°, then through a standard HCl solution. After at most 5 hr, the ammonia absorbed was determined by titrating excess HCl with sodium hydroxide using methyl orange indicator.

Another method consists in treating for 12 hr a sample which had been previously heated in helium in the above manner with an excess of standard sodium hydroxide solution. Both excess of sodium hydroxide and long treatment are necessary for satisfactory results. The excess sodium hydroxide was determined by titration with HCl using phenolphthalein. The decolorization of the indicator after 1 hr was considered as indicating an end point. The concordance of results was satisfactory (55.8 *vs.* 54.5% and 34.3 *vs.* 33.6% by the first and second method, respectively). The first method, however, was considered as more precise and was applied in all determinations.

The determination of water was carried out in the following way. Helium was passed at 100 cc/min through an empty trap, a trap filled with activated alumina, and a third trap filled with Molecular Sieve Linde 13X. All traps were cooled at −196°. It then passed through one thermal conductivity cell of the gas chromatographic unit, a quartz U tube containing 0.500 g of the sample investigated, an empty U tube cooled to −78°, another thermal conductivity cell, and two wash bottles containing 0.1 *N* hydrochloric acid. Using three-way stopcocks, the helium stream could be made to bypass the solid sample investigated without discontinuing the helium flow. The sample was heated for 5 hr at the desired temperature in the helium flow; the helium flow was then diverted from the sample and used to flush any ammonia in the system into the wash bottles containing acid. The contents of the wash bottles were titrated to determine the amount of ammonia evolved by the sample. Then the U tube containing condensed water vapor was immersed in an ice bath, the water was vaporized by the helium stream, and its amount was determined by the gas chromatographic unit whose output was amplified and recorded by a 12-mv range Brown recorder. The ammonia could be separated in this method from water vapor because at −78° the vapor pressure of ammonia is about 40 mm while that of water is 5.6×10^{-4} mm. The effectiveness of the separation of NH_3 from H_2O was checked by the nature of the gas chromatographic record of the contents of the −78° trap on warming. The sensitivity of this method was 10 μg of water.

Four samples were prepared by exchanging Na^+ cations by NH_4^+ cations for 60 hr at room temperature. The results were the same for 12 hr as for 60 hr indicating equilibrium was reached. The extent of exchange was determined by heating the samples at 480° in a helium stream, absorbing the ammonia evolved in HCl, and titrating excess acid. The results are given in Table I.

Table I: Ion Exchange

Catalyst	NH_4NO_3, g/g of molecular sieve in 17 ml of water	Per cent exchange	No. of cations exchanged per unit cell	Equil const
1	0.0296	10.6	6	1.57
2	0.120	34.3	19	1.45
		33.7		
3	0.362	56.4	31	0.86
		55.5		
		56.7		
		55.8		
4	1.79	67.2	37	0.22
		67.6		

The evolution of ammonia by passing helium over the heated sample was studied as a function of temperature of heating and of time. It was found that ammonium molecular sieve decomposed at 140° and that the decomposition was complete at about 340°. It seems that at a given temperature the decomposition reaches a certain limiting value which on increasing the temperature goes to another higher level. The rate at the lowest temperature studied, 210°, follows the first-order kinetics with a limiting value of 8.8 sites decomposed per unit cell. The kinetics of decomposition at 340° is complex and seems to involve a number of elementary processes.

Table II: Amounts of Water and Ammonia Evolved during Heating Molecular Sieves (per gram)

Temp range, °C	Sample 0 — Water			Sample 3 — Water			Sample 3 — Ammonia	
	mg	mmoles	% of total amount	mg	mmoles	% of total amount	mmoles	% of total amount
25–140	235.8	13.1	97.7	220.4	12.2	91.9	0.174	9.5
140–200	4.54	0.252	1.88	3.60	0.20	1.50	0.552	30.4
200–280	0.64	0.036	0.25	1.12	0.062	0.47	0.970	53.3
280–360	0.14	0.008	0.06	0.26	0.014	0.11	0.084	4.6
360–480	0.14	0.008	0.06	1.30	0.072	0.54	0.040	2.2
480–600	0.12	0.007	0.05	10.62	0.59	4.43	...	...
600–800	...	...		2.52	0.14	1.05	...	...
Total	241.4	13.4	100.0	239.8	13.3	100.0	1.820	100.0

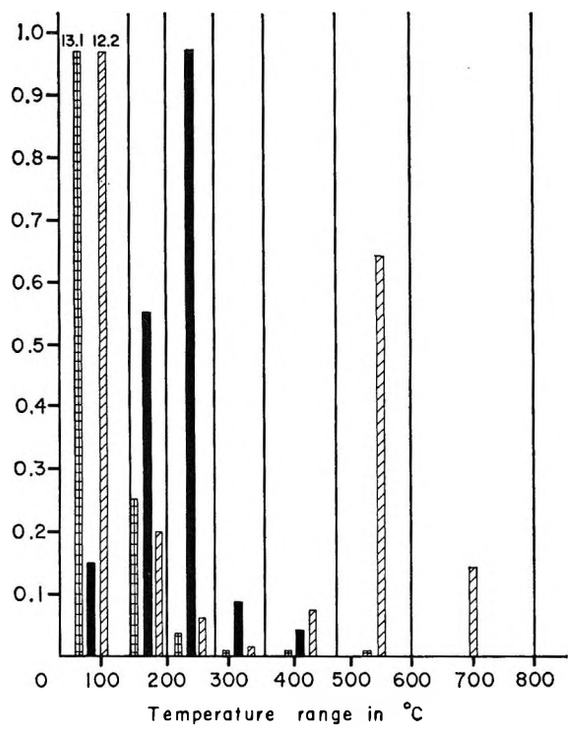

Figure 2. Amounts of water and ammonia evolved per gram of molecular sieve during heating: ⊞, water in sample 0; ■, ammonia in sample 3; ▨, water in sample 3.

The evaluation of water was similarly measured as a function of temperature of the sample. The heating time was 5 hr and the time to reach the next higher temperature from the lower one previously studied was estimated to be about 15 min. The results are presented in Table II and Figure 2 for two samples: no. 0 which was the sodium molecular sieve and no. 3 which was 44% Na and 56% Na_4^+ sieve.

The results of ion exchange permit us to calculate the equilibrium constants for the exchange reaction

$$Na^+Y^- + NH_4^+ \longrightarrow NH_4^+Y^- + Na^+ \qquad (3)$$

as

$$K = \frac{3.25D^2}{(1 - D)(a - 3.25D)} \qquad (4)$$

where 3.25 is the theoretical number of millimoles of Na^+ in 1 g of the NaY sieve whose formula is taken to be $Na_{56}(AlO_2)_{56}(SiO_2)_{136}$ and which contains about 25 wt % of H_2O, a is the number of millimoles of ammonium nitrate which was in contact with 1 g of the sieve, and D is the fraction of Na^+ replaced by NH_4^+. The results of the calculation are shown in Table I. The drop in equilibrium constant with extent of exchange as well as existence of various stages of thermal decomposition at NH_4^+ ions indicates an inhomogeneity of exchangeable sites. Barrer had previously noticed a change in the equilibrium constant for the exchange reaction.[16] Soviet Union workers[17] found that degree of cation exchange depends on the nature of anion associated with ammonium cation.

The inhomogeneity of cation sites was postulated several years ago[18] on the basis of crystal structure and was confirmed later in investigation of electric conductivity.[19] The unit cell has three main classes of cation sites—in the hexagonal drums, in sodalite cages, and in the large cavity. The provisional data on the equilibrium constant for exchange obtained indicate that there is a substantial decrease in equilibrium constants between 19 and 31 exchanged sites.

(16) R. M. Barrer and D. C. Sammon, *J. Chem. Soc.*, 2838 (1955).

(17) G. V. Tsitsishvili, K. A. Bezhashvili, D. N. Barnabishvili, M. S. Shuakrishvili, and G. D. Bagratishvili, *Dokl. Akad. Nauk SSSR*, **152**, 1136 (1963).

(18) D. W. Breck and E. M. Flanigen, Abstract 134, 134th National Meeting of the American Chemical Society, Chicago, Ill., Sept 1958.

(19) D. C. Freeman and D. N. Stamires, *J. Chem. Phys.*, **35**, 799 (1961).

The results of the study of the temperature dependence of the evolution of water and ammonia permitted the evaluation of the nature of acid sites on the decationated molecular sieve. In the case of the sodium sieve, 99.6% of the water is removed below 200° and no appreciable water was produced even at 600°. The behavior of the 56% NH_4^+–44% Na^+ sieve was different. Ammonia was liberated at temperatures below 360°. The water evolution took place in two stages. In the first stage up to 360° the amount of water evolved and its dependence on the temperature was the same as for the 100% Na^+ sieve. This was taken to indicate that water present in both samples (independent of their Na^+ or NH_4^+ ion composition) was removed from the cavities by the same process. In the case of the 56% NH_4^+–44% Na^+ sieve an additional amount of water was evolved in a second stage of dehydration at a temperature of 480–800° with a maximum amount evolved at 600° (Table II).

The decomposition of the 56% NH_4^+–44% Na^+ sieve can be visualized in the following way. At temperatures below 140° essentially all water normally associated with molecular cavity is driven off and in the temperature range 140–360° the ammonia ion is decomposed into NH_3 which is driven off and H^+ which either forms a hydroxyl on the surface or exists as a proton associated with an aluminum ion. This can be considered to produce Brønsted acid sites on the surface. These persist until the material is heated to about 480°. At this temperature a slow process of dehydration takes place converting the Brønsted acid sites into Lewis acid sites. The rate of this process increases with increase in temperature and the number of Lewis acid sites will be a sensitive function of the temperature of heating and the vacuum or flow conditions of the drying gas.

The amount of water formed during decationization was consistent with the view that a molecule of water was produced per two ammonium cation sites. Thus sample no. 3 containing 1.82 mequiv of ammonium ion/g formed 0.80 mequiv of water by heat treatment in the 360–800° range where the theoretical yield should have been 0.91 mequiv. The discrepancy of 0.11 mequiv may be due to the presence of isolated hydroxyl groups (or protons) in a molecular sieve containing as much as 44% sodium cations.

This investigation clearly points out that in high Si/Al ratio, sodium faujasite type of molecular sieves, the ion-exchange treatment with ammonium salts and subsequent heat treatment produces Brønsted-type acid sites at temperatures as low as 140°. Because of the inhomogeneity of cation sites the decomposition of the ammonium ion to Brønsted acid sites is not complete until about 350°. It takes temperatures of over 450° to produce the Lewis acid sites and this process is not complete until above 800°. Thus when there is a partial destruction of the crystal lattice, the usual method of activation of molecular sieves by heating at 450° at a high vacuum produces a mixture of Brønsted and Lewis acids, the exact ratio being dependent on the thermal treatment that is given to the molecular sieve.

Experimental Procedure for Catalyst Studies. Both reactions were studied in static system. Catalyst (grain size 1–2 mm, 0.100 or 0.180 g) was placed on the bottom of the 8-mm tube which was connected to the bulb containing reacting gases. Total volume of the reaction vessel was 330 cc. The catalyst was evacuated *in situ* by heating the tube and pumping off. In most experiments the evacuation was for 17 hr at 10^{-6} mm at 480°. The catalyst was then cooled to reaction temperature, which in most cases was 25° for hydrogen–deuterium equilibration and −196° for ortho–parahydrogen conversion. Then the gas mixture was admitted to the reaction vessel, usually at a pressure 380 mm. For the ortho–parahydrogen conversion study, hydrogen gas equilibrated at room temperature was used and contained 25.1% parahydrogen. For the hydrogen–deuterium equilibration reaction study a hydrogen–deuterium mixture of 1:1 molar ratio was used.

Samples of reacting gas (4 cc each) were taken out of the reaction vessel and analyzed using a gas chromatographic separation method. Activated alumina (Oxy Corp. catalyst) was used at −196° for ortho–parahydrogen separation and Fischer adsorption alumina coated with ferric oxide was used at −196° for the H_2, HD, and D_2 separation.

Analysis of the Different Hydrogen Species. A gas chromatographic method was used to determine the H_2, HD, D_2, ortho- and parahydrogen.[20–32] In our

(20) W. R. Moore and H. R. Ward, *J. Am. Chem. Soc.*, **80**, 2909 (1958).

(21) S. Ohkoshi, Y. Fujita, and T. Kwan, *Bull. Chem. Soc. Japan*, **31**, 770 (1958).

(22) H. A. Smith and P. P. Hunt, *J. Phys. Chem.*, **64**, 383 (1960).

(23) W. A. Van Hook and P. H. Emmett, *ibid.*, **64**, 673 (1960).

(24) W. R. Moore and H. R. Ward, *ibid.*, **64**, 832 (1960).

(25) T. Kwan, *J. Res. Inst. Catalysis, Hokkaido Univ.*, **8**, 18 (1960).

(26) P. P. Hunt and H. A. Smith, *J. Phys. Chem.*, **65**, 87 (1961).

(27) S. Furayama and T. Kwan, *ibid.*, **65**, 190 (1961).

(28) L. Bachmann, E. Bechtold, and E. Cremer, *J. Catalysis*, **1**, 113 (1962).

(29) J. King, Jr., *J. Phys. Chem.*, **67**, 1397 (1963).

(30) E. H. Carter, Jr., and H. A. Smith, *ibid.*, **67**, 1512 (1963).

(31) K. Fujita and T. Kwan, *Bunseki Kagaku*, **12**, 15 (1963).

(32) D. L. West and A. L. Marston, *J. Am. Chem. Soc.*, **86**, 4731 (1964).

method a purified helium stream was passed through an empty trap and an activated alumina trap at liquid nitrogen temperature, through a flowmeter, and then through one thermoconductivity compartment of an Aerograph (Wilkins Instrument and Research Inc.) gas chromatographic unit. The gas stream then entered a sample introduction unit. This consisted of two three-way stopcocks joined together through two of the lead tubes. One of these junctions was a bypass to the sampling section. The other had a lead to the sample container to which it was attached by a stopcock. The sample introduction section had a volume of 4 cc. The helium stream containing the hydrogen sample then passed through four U tubes in series (2-m total length and 4-mm internal diameter) containing the alumina adsorbent.

The helium then passed over copper oxide in a 20 cm long tube of 4-mm diameter heated to 450°. The helium containing water vapor was then passed through the second thermoconductivity compartment of the Aerograph. Under our operating conditions we did not find it necessary to heat the tubing between the copper oxide furnace and the thermal conductivity cell to avoid condensation as recommended by Bachmann, Bechtold, and Cremer.[28]

The output from the thermoconductivity bridge was amplified by a Kintel amplifier (Model 195) and recorded on a Brown potentiometer (range 0–12 mv). The tubing was glass except in a few places where short Tygon connections were used.

The following conditions were found to give best results. The helium flow rate was 140 cc/min. The sample size was 2 cc (STP) of hydrogen. Two different types of aluminas were used. For analysis of H_2, HD, and D_2, complications by overlap of the orthohydrogen on the HD peak and the long-tailing of the deuterium peak must be eliminated. The first complication is avoided by coating the alumina with Fe_2O_3, which catalyzes the ortho–para conversion.

For the H_2, HD, and D_2 determinations Fischer activated alumina was powdered. Fifteen-gram fractions of 40–60 mesh were added to 25 ml of 2 *M* $FeCl_3$ and heated at 100° for 3 min, then cooled. Sixty milliliters of 3 *M* NH_4OH was added; the mixture was stirred occasionally for 1 hr and washed several times with distilled water by shaking. After decanting the supernatant, the alumina was filtered and dried at 110°. It was sieved again, placed in chromatographic column, and activated at 120–130° for 4 hr in an He stream.

H_2–HD–D_2 separation was carried on at −196° at a He flow rate of 140 cc/min. Retention time was about 10 min.

Since the H_2 peak slightly overlaps the HD peak, the latter must be corrected for this overlap. Satisfactory results were obtained for the area of the peaks by using their height and multiplying by the width at half-height. The values for the percentage of H_2, HD, and D_2 were determined within 1%.

Attempts were made to obtain better separation by activation of the column at temperatures up to 300°. The higher the activation temperature, the better was the separation. However, the peaks showed more pronounced "tails" and became "washed out." Satisfactory results were obtained when the column was activated at 300° and then poisoned by passing CO_2 gas at room temperature for 15 min. Helium was then passed for 1 min and the column was cooled to −196°. This complicated procedure was not generally used, but simple activation at 120° gave results shown in Figure 3.

Ortho–parahydrogen separation on Fischer activated alumina and Fischer adsorption alumina (not coated with Fe_2O_3) was not satisfactory since the chromatographic column catalyzed slightly the conversion at −196°. This was probably due to impurities in the pink alumina. Acid washing of the alumina did not decrease this effect. A number of various adsorbents were investigated, and best results were obtained with Oxy catalyst. A 40–60 mesh fraction was placed in the chromatographic column and activated in the same manner as alumina for H_2–D_2 determination.

Since adsorbed oxygen is a very efficient catalyst for

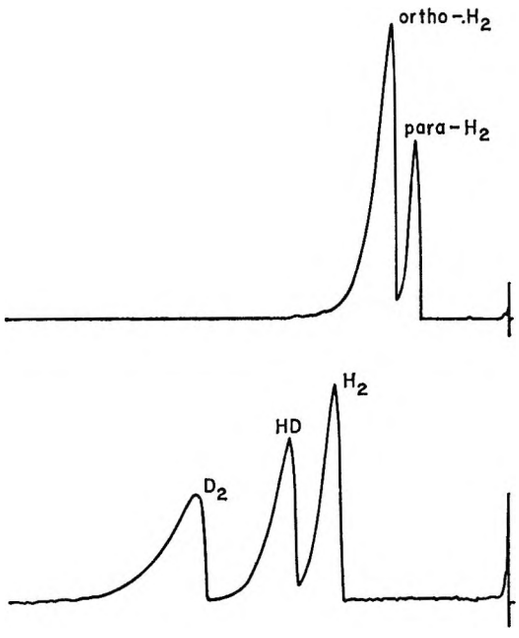

Figure 3. Gas chromatography of H_2–HD–D_2 and para–orthohydrogen.

ortho–parahydrogen conversion at −196°, especial care must be taken to avoid the presence of oxygen in the chromatographic column. Therefore He was passed through an additional trap with Linde 13X Molecular Sieve activated at 450° and cooled at −196°.

Ortho–parahydrogen separation was carried out at −196° at an He flow rate of 140 cc/min. Retention time was about 5 min. The calculation procedure was the same as in the case of H_2–HD–D_2 determination. The alumina grain size was chosen as 40–60 mesh to minimize the pressure drop since we did not find any difference in results with 40–60 and 80–100 mesh. An example of para–orthohydrogen separation is shown in Figure 3.

The per cent of the two species was determined within 0.5% on the Oxy alumina.

Experimental Results. Both ortho–parahydrogen conversion and hydrogen–deuterium equilibration reactions are of first order.[1,2] For the ortho–parahydrogen conversion the kinetic expression is given by

$$k_1 st = \ln \frac{26.7}{51.8 - x}$$

where k_1 is the rate constant at 380 mm with the reaction vessel volume of 330 cc, s is the amount of catalyst in grams, t is the time in hours, and x is the per cent of parahydrogen in the reaction mixture at time t. The number 51.8 is the equilibrium percentage of parahydrogen at −196° and 26.7 is the difference between 51.8 and 25.1 (the percentage of parahydrogen at equilibrium at 25°).[33]

The kinetic expression for the hydrogen–deuterium equilibration was more complicated since there was a poisoning of the catalyst during the course of the reaction. The first-order rate expression valid initially is

$$k_2 st = \ln \frac{47.5}{47.5 - x}$$

where 47.5 is the equilibrium percentage of HD at 25° in a reaction mixture of initial composition of 50 mole % H_2 and 50 mole % D_2.[34,35]

The poisoning effect took place for all catalysts studied and at all temperatures. If the catalytic run was interrupted by pumping off the reaction mixture at room temperature and a new reaction mixture was introduced, the differential rate constant obtained in the initial stages corresponded to the differential rate constant in the last stage of the preceding run. The catalytic activity was therefore characterized by means of a differential rate constant valid for the first 2 hr.

The nature of evacuation treatment affected the catalytic activity as shown in Figure 4. It is seen that there is a marked increase in activity on heating above 480°. This is far above the temperature required to remove the loosely bound water or to decompose the ammonium ion present in the solid (150 and 340°). It is the temperature at which the Brønsted acids on the surface are converted into Lewis acids. The evacuation procedure used for preparing samples was standardized at 17 hr at 480° and high vacuum since X-ray examination showed no evidence of collapse of crystal structure under those conditions. However, evacuation at 600° of sample no. 3 for 17 hr showed more than 50% decomposition of the crystalline zeolite. Times of evacuation of less than 10 hr gave different results while small changes in time at the 17-hr level did not produce noticeable effects. The effect of temperature and time of evacuation on the efficiency of catalysts for the ortho–parahydrogen conversion was not studied. The standard pretreatment of catalysts used for H_2–D_2 reaction was used for this reaction.

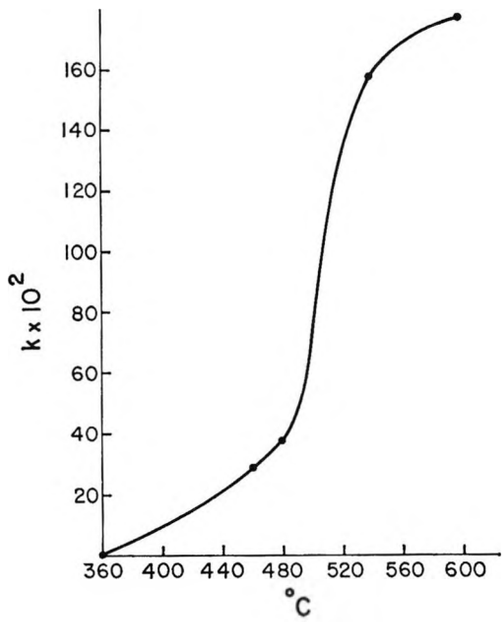

Figure 4. Catalytic activity *vs.* evacuation temperature.

The constant, $10^2 k_2$ for the hydrogen–deuterium reaction at 25° and the ortho–parahydrogen reaction at −196° is given in Table III. The catalytic activity for H_2–D_2 equilibration increases with degree of decationization (Figure 5) and is low both for the sodium

(33) H. W. Wooley, R. B. Scott, and F. G. Brickwedde, *J. Res. Natl. Bur. Std.*, **41**, 379 (1948).

(34) D. Rittenberg, W. Bleakney, and H. C. Urey, *J. Chem. Phys.*, **2**, 48 (1934).

(35) W. Bleakney, *Phys. Rev.*, **45**, 762 (1934).

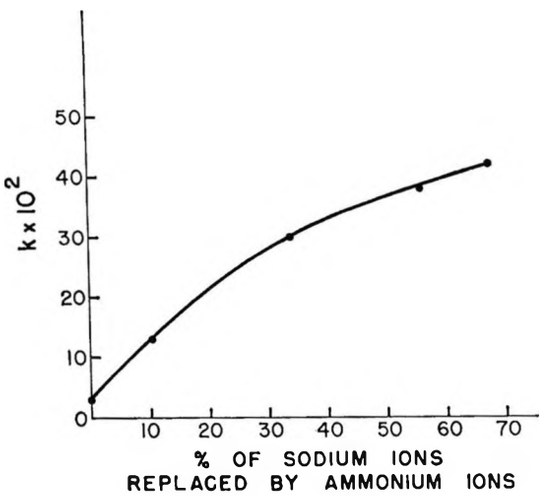

Figure 5. Catalytic activity *vs.* degree of ion exchange.

molecular sieves no. 0 and no. 6 and for the magnesium sieve no. 5, which was obtained by partial replacement of sodium in catalyst 0 by magnesium. The ortho–parahydrogen conversion was independent of the degree of decationization and seemed lower on the sieve that was prepared in our laboratory, no. 6. No poisoning was observed at −196°.

Table III

Catalyst	0	1	2	3	4	5	6
H_2–D_2	3	13	30	38	42	4	0
Ortho–para	140	...	...	140	140	...	46

The activation energy for the hydrogen–deuterium equilibration was 2.0 kcal/mole in the range of −78 to +25°. At −78° the mean rate constant decreased in the course of the reaction, being 6.7 for the first 4 hr, 5.1 in 27 hr, and 4.7 for the period of 50 hr. The rate of decrease of the rate constant was too rapid to determine activation energy for the process at high temperatures.

Hydrogen treatment at room temperature for several days or at 250° for 30 min completely deactivated the catalyst for both reactions at 25°. This activity was restored only by evacuation at temperatures of about 480°. Temperature was an important factor in the poisoning of the catalyst since the hydrogen adsorbed at room temperature at low pressure was sufficient to deactivate the catalyst if the latter were heated at 250°.

The rate of ortho–parahydrogen conversion at room temperature was also studied. It was of the same order of magnitude as the H_2–D_2 equilibration and of course disappeared when the latter reaction was poisoned. However, the rate of ortho–parahydrogen at −196° was not affected in a similar way. This is taken to indicate that the other centers were involved.

Irradiation of Catalysts. Several sets of catalysts 0–4 were γ-irradiated at Industrial Reactor Laboratories in Plainsboro, N. J. The total dose was 1.1×10^7 r. Before irradiation, catalysts were evacuated at high vacuum at 480° for 17 hr in Pyrex tubes and sealed under vacuum. After irradiation these tubes were crushed and catalyst samples were transferred into the reaction vessel. This was accomplished in all-glass equipment under high vacuum. Then the catalytic activity was determined.

No distinct influence of γ irradiation on the ortho–parahydrogen conversion rate was found. In the hydrogen–deuterium equilibration reaction the effect of irradiation was considerable. Values of 10^2k_2 were around 150 for all samples as compared with 3–42 for catalysts which were not irradiated. No indication for decationization degree effect was found.

Adsorption of Hydrogen. Adsorption of hydrogen was measured on catalysts no. 0 and 3 using 2.500-g samples. The amount of hydrogen adsorbed was determined by measuring hydrogen pressure decrease. Helium was used for determining "dead space." Both samples were evacuated at 480° at 10^{-6} mm for 17 hr.

The amount of hydrogen adsorbed at 25° was the same for both catalysts. It was 0.22 cc (STP) or 6×10^{18} molecules/g of catalyst. Adsorption was very fast; more than 80% of hydrogen was adsorbed within 2 min. The adsorption was completed in 30 min. Heating of the catalysts at 100, 200, and 300° for several hours did not cause any additional adsorption. When catalyst no. 3 was evacuated at 600°, the amount of hydrogen adsorbed was the same as for catalyst no. 3 evacuated at 480°.

Influence of Oxygen Adsorption. Adsorption of oxygen at room temperature completely poisoned the catalytic activity of all catalysts for the hydrogen–deuterium equilibration reaction. Evacuation at room temperature did not restore the catalytic activity. Initial activity was restored only after evacuation at 480°.

Adsorption of oxygen increased the catalytic activity at −196° for ortho–para conversion by an order of magnitude.

Esr Measurements. A weak esr signal at $g = 2.0020$, $\Delta H \simeq 2$ gauss, was found for catalysts 0–5 using both 35- and 9.5-Gc Varian esr spectrometers. This signal

was broadened after hydrogen had been adsorbed. It disappeared when oxygen was adsorbed. However, evacuation at room temperature restored the initial signal in both cases.

No esr signal was found for the sodium sieve catalyst no. 6 prepared in our laboratory. The presence or absence of signal is not related to the hydrogen–deuterium equilibration process but may be correlated with the ortho–parahydrogen reaction.

Discussion

The low-temperature catalytic activity for the ortho–parahydrogen conversion is a sensitive test for paramagnetic impurities. We have shown that it is independent of the degree of decationization and is lower in the sample of faujasite prepared in the laboratory where special care was taken to decrease the presence of paramagnetic impurities. Consequently, the formation of either Brønsted acid sites or Lewis sites by dehydration of the former does not produce a paramagnetic species either at the acid site or as a defect in the crystal structure associated with the formation of such acid sites.

The near-linear dependence of the catalytic activity for the hydrogen–deuterium equilibration on the degree of decationization and on the extent of dehydration suggests that the catalytic centers are Lewis acid sites or defects associated with these. However, the reaction is slowly poisoned by hydrogen and this poisoning effect is related in a complicated manner to the adsorption of hydrogen. Thus the amount of hydrogen adsorbed is small compared to the number of Lewis acid sites. Furthermore, the amount irreversibly adsorbed at room temperature is experimentally unobservable. Yet part of this hydrogen slowly poisons the catalyst at room temperature and rapidly at higher temperature. Thus the centers of activity for H_2–D_2 exchange must be orders of magnitude lower than any regular crystallographic position present in the zeolite. They do develop their activity on decationization in a regular manner. We must conclude that the locus of activity is either an impurity such as TiO_2, ZnO_2, or Fe_2O_3 located near an acid center or a combination of Lewis acid sites located close to each other. If the latter is true we would expect molecular sieves with higher Al/Si ratios, such as Linde X sieve, to show higher activity at the same degree of decationization. Some confirmation for this may be found in the variation of catalytic activity of alumina silica gel catalyst which show highest activity in pure alumina and a linear decrease with decrease in alumina concentration in the alumina silica gel.

γ-Irradiation results indicate that the increase of catalytic activity was due to formation of additional adsorption sites. This is consistent with the observation made by Turkevich and Nozaki[36] that γ irradiation increased the hydrogen adsorption ability of molecular sieves.

Acknowledgment. We wish to acknowledge the financial support of the International Atomic Energy Agency in Vienna for a fellowship awarded to S. C. and to the U. S. Atomic Energy Commission for support of the research program of J. T. We wish also to extend our gratitude to Princeton University for furnishing us with the equipment, to Industrial Reactor Laboratories at Plainsboro, N. J., for irradiation of catalysts, and to Mr. E. F. Lyden of Princeton University for cooperation and discussion on X-ray pattern measurements.

(36) J. Turkevich and F. Nozaki, unpublished work.

The Solubilities of Hydrogen Fluoride and Deuterium Fluoride in Molten Fluorides[1a]

by Paul E. Field[1b]

Department of Chemistry, Virginia Polytechnic Institute, Blacksburg, Virginia 24061

and James H. Shaffer

Reactor Chemistry Division, Oak Ridge National Laboratory, Oak Ridge, Tennessee 37830
(Received February 16, 1967)

The solubilities of HF and DF in molten LiF–BeF_2 (66–34 mole %) were determined over the temperature range 500–700° and at solute gas pressures between 1 and 2 atm. Using previously established experimental methods, the solubilities of both gases were found to obey Henry's law. The Henry's law constants, K_H (10^{-4} mole of HF/mole of melt-atm) for HF and DF, respectively, at 500, 600, and 700° were: 3.37 ± 0.13, 2.96 ± 0.07; 2.16 ± 0.05, 1.83 ± 0.03; 1.51 ± 0.06, 1.25 ± 0.03, where the values given were obtained by a linear least-squares fit of the experimental data as ln K_H *vs.* $1/T$ and the uncertainties are at the 95% confidence interval. The heats of solution, ΔH^s, obtained from the least-squares evaluation were −5.98 ± 0.19 and −6.43 ± 0.15 kcal/mole for HF and DF, respectively. The comparison of ΔH^s for HF in this melt composition with those obtained previously in melts ranging from 54 to 89 mole % LiF in BeF_2 reveals linear dependence of ΔH^s on the mole fraction of LiF above and below 67% with a maximum of 67% LiF. Interpretation of the isotope effect is made by comparison of the difference in the entropies of solution between DF and HF with the difference in the calculated values of the entropies of the two gases at 600°.

Introduction

Molten fluoride mixtures are currently in use as the fuel and secondary coolant in a nuclear power reactor experiment at the Oak Ridge National Laboratory.[2] Although these mixtures can be retained, almost indefinitely, at high temperatures in containers of INOR-8 (Hastelloy N), a nickel-base alloy, the presence of HF in the fluoride mixture results in metathetical corrosion of chromium and iron from the alloy. Hydrogen fluoride may be introduced as a dissolved impurity from the fluoride production process or generated by reaction of salt constituents with water vapor in the inert blanket and sweep gases used with these systems. Thus, the behavior of HF in molten fluorides is of interest to the technology of high-temperature fused-salt devices.

Previous studies of the solubility of HF in various molten fluoride mixtures have shown interesting solvent effects which appear as unresolved complex functions of the melt composition.[3,4] Although the solubility of HF in these mixtures may be related to alkali fluoride–hydrogen fluoride compounds, the coordinating effects of other melt constituents with the alkali fluorides have a pronounced influence on the HF solubility. This investigation presents comparative measurements of the solubilities of HF and DF in a mixture of LiF (66 mole %) in BeF_2 as an attempt to elucidate further

(1) (a) Research sponsored by the U. S. Atomic Energy Commission under contract with the Union Carbide Corp. Presented in part at the 152nd National Meeting of the American Chemical Society, New York, N. Y., Sept 1966. (b) ORINS Summer Research Participant, 1965.

(2) H. G. MacPherson, *Power Eng.*, **71**, 56 (1967).

(3) J. H. Shaffer, W. R. Grimes, and G. M. Watson, *J. Phys. Chem.*, **63**, 1999 (1959).

(4) J. H. Shaffer and G. M. Watson, Reactor Chemistry Division Annual Progress Report, April 29, 1960, ORNL-2584, Oak Ridge National Laboratory, p 31.

the solvent characteristics of molten fluoride mixtures. The observed isotope effect also provides a valuable preface to more experimentally difficult measurements of the solubility of tritium fluoride in similar systems.

The solvent composition chosen for this study has been proposed as the fertile blanket for a thermonuclear breeder reactor.[5] Tritium would be produced by neutron irradiation of lithium-6 in the blanket salt mixture and recovered for subsequent injection as the fuel into the core of the fusion reactor. The formation of tritium in the current fission reactor, mentioned above, is minimized by the use of isotopically pure lithium-7 in its molten fluoride mixtures. Despite contrasting interests, the possible generation and dissolution of tritium fluoride in their molten fluoride systems may be common to both machines. Studies of isotope effect with hydrogen and deuterium may provide a basis for estimating some of the physicochemical properties of tritium, a highly radioactive synthetic element, and its compounds.

Experimental Section

Materials. Anhydrous HF was obtained from a cylinder containing 9 lb of liquid hydrogen fluoride supplied by the Matheson Co., Inc., East Rutherford, N. J. The liquid HF had a specified minimum purity of 99.9% and was used without further purification. Anhydrous DF was prepared specifically for this investigation by the Technical Division, Oak Ridge Gaseous Diffusion Plant, by reaction of elemental deuterium and fluorine.[6]

The fluoride mixture of 66 mole % LiF and BeF_2 was a 3.5-kg sample of material prepared by the Oak Ridge National Laboratory for use as the secondary coolant of the molten salt reactor experiment.[7] The removal of oxides, sulfides, and structural metal fluoride impurities from this material was accomplished by treatment at 600° with a gas mixture of 10 mole % HF in H_2 and at 700° with H_2 alone. Results of chemical analyses showed that the fluoride mixture had the following impurities in ppm: Cr, 16; Ni, 39; Fe, 123; S, <5. The hydrofluorination treatment removed 1650 ppm of oxide as water vapor; oxide which remained was believed to be less than 100 ppm in the salt mixture.

Apparatus. The apparatus, shown schematically in Figure 1, essentially duplicated that used for previous HF solubility determinations. All sections of the apparatus in contact with the molten fluoride or at high temperature were of nickel. Pressures were measured on Bourdon pressure indicators of phosphor bronze, known as Ashcroft Laboratory test gauges. The gauges had 4.5-in. diameter faces reading 0–30 psi in 0.1-psi subdivisions and were calibrated by comparison with a mercury U-tube manometer having a scale graduated in 1-mm subdivisions. Temperatures were controlled and recorded from chromel–alumel thermocouples and were checked at least once per day with a platinum—platinum–10% rhodium thermocouple connected to a Leeds and Northrup Type K-2 potentiometer. The temperature of the fluoride melt was probably known to 5°.

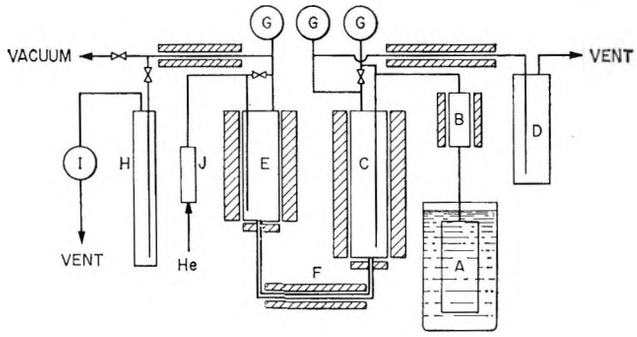

Figure 1. HF solubility apparatus: A, HF cylinder in constant-temperature bath; B, surge tank with filter; C, molten salt saturator; D, KOH scrubber; E, molten salt receiver; F, salt-transfer line with frozen plug; G, pressure gauges; H, standard KOH solution; I, wet-test meter; J, anhydrone–Dry Ice traps; cross-hatched areas, furnaces and heaters.

Procedure. The experimental method has been described in detail in ref 3. Generally, the procedure consisted of sparging the salt mixture in the saturator with HF or DF at constant pressure for approximately 6 hr. The frozen salt plug, which retained all of the salt mixture in the saturator, was thawed, and a portion of the salt mixture was allowed to flow into the receiver section under a constant saturating pressure. The helium pressure in the receiver section was selected so that, at hydrostatic equilibrium, about 1 l. of salt would be isolated for analysis when the frozen salt plug was restored. HF contained in the receiver section was removed by sparging the melt with helium overnight at a flow rate of 8 l./hr. The He–HF gas effluent was passed through a 2.00-l. volume of standard KOH with a bubble path of approximately 80 cm. The HF absorbed in the KOH solution was determined by back titration with standard HCl. The liquid level in the saturator was determined by an electrical resistance

(5) D. J. Rose and M. Clark, Jr., "Plasmas and Controlled Fusion," MIT Press, Cambridge, Mass., 1961, p 296.

(6) S. T. Benton, R. L. Farrar, Jr., and R. M. McGill, "Preparation of Anhydrous Deuterium Fluoride by Direct Combination of the Elements," K-1585, Oak Ridge Gaseous Diffusion Plant, Jan 29, 1964.

(7) J. H. Shaffer, *et al.*, Reactor Chemistry Division Annual Progress Report, Jan 31, 1965, ORNL-3789, Oak Ridge National Laboratory, p 99.

probe before and after salt transfer. The volume of transferred salt was calculated from these measurements and the known geometry of the vessel.

Results

The solubilities of HF and DF in molten LiF–BeF_2 (66 mole % LiF) were determined over the range 500–700° at pressures from about 1 to 2 atm. Measured solubilities had units of moles of HF/ml of melt which are also expressed as moles of HF/mole of melt, in Tables I and II, by use of appropriate partial molal volume data.[8] As in previous investigations, a linear dependence of solubility on HF pressure was observed. Henry's law constants, K_H, were determined by assuming a temperature-independent heat of solution for both solutes and by making linear least-squares calculations of ln K_H *vs.* $1/T$ for all solubility determinations. The uncertainties in the calculated values of K_H were evaluated at the 95% confidence level and are listed in Table III along with respective Henry's law constants.

Table I: Solubility of HF in Molten LiF–BeF_2 (66 Mole % LiF)

Saturating temp, °C	Saturating pressure, atm	Molar vol. of melt, ml/mole	HF solubility: Moles of HF/ml of melt × 10^5	HF solubility: Moles of HF/mole of melt × 10^4
500	1.32	16.54	2.68	4.43
	1.65		3.40	5.62
524	1.99	16.63	3.64	6.05
595	1.24	16.89	1.63	2.75
600	1.33	16.90	1.72	2.90
	1.68		2.06	3.48
	1.97		2.40	4.06
700	1.61	17.29	1.43	2.48
	1.98		1.77	3.07

Table II: Solubility of DF in Molten LiF–BeF_2 (66 Mole % LiF)

Saturating temp, °C	Saturating pressure, atm	Molar vol. of melt, ml/mole	DF solubility: Moles of DF/ml of melt × 10^5	DF solubility: Moles of DF/mole of melt × 10^4
500	1.24	16.54	2.21	3.66
	1.62		2.88	4.76
	1.93		3.52	5.81
600	1.27	16.90	1.37	2.32
	1.61		1.70	2.87
	1.96		2.13	3.60
700	1.70	17.29	1.25	2.15
	1.99		1.48	2.54

Table III: Henry's Law Constants for the Solubilities of HF and DF in Molten LiF–BeF_2 (66 Mole % LiF)[a]

Solute temp, °C	HF	DF
500	3.37 ± 0.13	2.96 ± 0.07
600	2.16 ± 0.05	1.83 ± 0.03
700	1.51 ± 0.06	1.25 ± 0.03

[a] Values of K_H (10^{-4} mole of solute/mole of melt-atm) calculated from linear least-squares fit of ln K_H *vs.* $1/T$ for all solubility determinations shown in Tables I and II.

The maximum uncertainty for K_H is less than 4% in all cases.

As in previous investigations of noble gas solubilities in molten fluorides,[9,10] calculations of the entropies of solution were based on standard states of equal concentrations of gas in solution and in the gas phase. Standard entropies of solution were obtained by considering the two-step solution process

$$HF(g)_P \xrightarrow{I} HF(g)_{P'} \xrightarrow{II} HF(soln)_C$$

where I is the isothermal expansion of the solute gas from the saturation pressure, P, to a pressure, P', corresponding to the concentration, C, of the solute in solution; and II is the dissolution of the gas into the fluoride solvent at constant concentration. If HF and DF behave as ideal gases under the experimental conditions, the standard entropy of solution is the difference between the total entropy change, given by $\Delta S = \Delta H^s/T$ for the equilibrium process and the entropy contribution for the isothermal expansion in step I. This relation can be expressed by the equation

$$\Delta S^s = \frac{\Delta H^s}{T} + R \ln \frac{P'}{P}$$

If Henry's law constants are expressed as moles of solute gas/l. of melt-atm, values for the standard entropy of solution can be calculated from the experimental data according to the equation

$$\Delta S^s = \frac{\Delta H^s}{T} + R \ln K_H RT$$

Values for the heat of solution, ΔH^s, for the two solute gases were calculated from the slope of the least-squares

(8) S. Cantor, Reactor Chemistry Division Annual Progress Report, Dec 31, 1965, ORNL-3913, Oak Ridge National Laboratory, p 27.

(9) M. Blander, W. R. Grimes, N. V. Smith, and G. M. Watson, *J. Phys. Chem.*, **63**, 1164 (1959).

(10) G. M. Watson, R. B. Evans, III, W. R. Grimes, and N. V. Smith, *J. Chem. Eng. Data*, **7**, 285 (1962).

equation according to the van't Hoff relationship. Heats and entropies of solution, with their uncertainties evaluated as one standard deviation, are listed in Table IV.

Table IV: Enthalpies and Entropies of Solution for HF and DF in LiF–BeF_2 (66 Mole % LiF) at 600°[a]

	HF	DF
m	3010	3237
b	−11.838	−12.313
ΔH^s, kcal/mole	−5.98 ± 0.19	−6.43 ± 0.11
ΔS^s, cal/deg mole	−7.07 ± 0.26	−7.92 ± 0.16

[a] The constants in the equation $\ln K_H = (m/T) + b$ were obtained by least squares; the uncertainties listed are taken as one standard deviation.

Discussion

The heats of solution of HF obtained previously in five other LiF–BeF_2 solvent compositions were recalculated by the least-squares method.[3] These are compared to the present results in Figure 2. A sharp maximum in the heat of solution as a function of solvent composition is obtained at 66.6% LiF which corresponds to the stoichiometry of Li_2BeF_4. The corresponding NaF–BeF_2 system shows a less well-defined point of inflection having about a threefold increase in the slope of $-\Delta H^s$ *vs.* X_{NaF} in the region of 0.60–0.70 mole fraction of NaF. It is also interesting to note that the heats of solution in both solvents appear to be equal within experimental error in the BeF_2-rich side of the M_2BeF_4 composition. Unfortunately, the composition range of the solvents extends down to 50% MF only and quantitative comparisons between the alkali metal salts are not justified.

The entropy of solution has been defined previously and can be written as

$$\Delta S^s_{HF} = S^m_{HF} - S^g_{HF}$$

where the superscripts m and g denote the melt phase and gas phase, respectively. The difference in the entropies of the solute isotopes can be written

$$\Delta S^s_{DF} - \Delta S^s_{HF} = (S^m_{DF} - S^m_{HF}) - (S^g_{DF} - S^g_{HF})$$

Therefore it is possible to evaluate the difference in the entropy of the isotopes in the melt since the gas-phase terms can be obtained from the partition functions of the two gases. Table V contains a summary of the various contributions to the entropies of the gases at 1 atm and 600°. These values are based on the Sackur–Tetrode equation for the translational contribution, the rigid rotational contribution, and the harmonic vibrational contribution.[11] The differences in each contribution for the two solutes are listed in the third column.

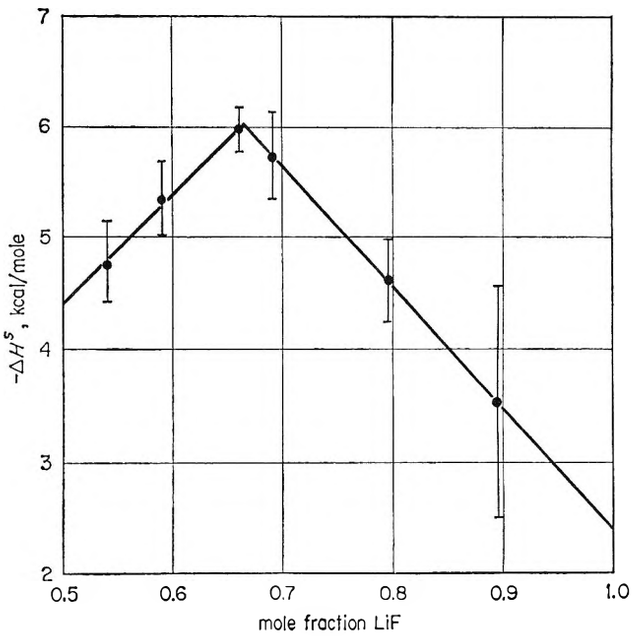

Figure 2. Dependence of the heat of solution of HF on melt composition in LiF–BeF_2.

Table V: Calculated Gas-Phase Molal Entropies of HF and DF at 600° and 1 Atm

	HF	DF	DF–HF
S_{vib}	0.01	0.08	0.07
S_{rot}	8.68	9.96	1.28
S_{trans}	40.28	40.42	0.14
$S°_{873}$	48.97	50.46	1.49

The difference in the entropy of the two solutes in the melt becomes

$$\begin{aligned} S^m_{DF} - S^m_{HF} &= (\Delta S^s_{DF} - \Delta S^s_{HF}) + (S^g_{DF} - S^g_{HF}) \\ &= (-0.9 \pm 0.4) + 1.5 \\ &= 0.6 \pm 0.4 \end{aligned}$$

which indicates approximately zero difference. The significance of this result lies in interpreting the configuration of the solute in the melt phase. Although the molecular partition function is no longer separable into discrete translational, rotational, and vibrational degrees of freedom, the near-zero difference in the

(11) K. K. Kelley and E. G. King, U. S. Bureau of Mines Bulletin 592, U. S. Government Printing Office, Washington, D. C., 1961.

entropies of HF and DF in the melt appears to indicate identical configurations for the isotopes. Since the major entropy difference between the two gases is in the rotational contribution and amounts to 86% of the total difference, a possible explanation for the entropy of solution of the gaseous solute would be a significant loss of rotation of the solute molecule in the melt. Furthermore, this mechanism is consistent with the magnitudes of the rotational contribution to the gases of the order of 9 and 10 eu for HF and DF, respectively, compared to 7 and 8 eu for the respective entropies of solution. It is also interesting to note that this mechanism is in agreement with the solubility model of Blander, *et al.*,[9] where ΔS^{s} for the rare gases in fluoride melts were of the order of -1.0 eu.

Acknowledgment. The authors are especially indebted to Professor D. G. Hill and to Dr. F. F. Blankenship for many interesting and valuable discussions during the course of this work.

The Radiation-Induced Polymerization of Isobutene in the Gas Phase

by Hidemasa Okamoto, Kenji Fueki, and Zen-ichiro Kuri

Department of Synthetic Chemistry, Faculty of Engineering, Nagoya University, Nagoya, Japan
(Received March 2, 1967)

The γ-ray-induced polymerization of isobutene has been investigated at 25° in the gas phase to elucidate its reaction mechanism. The initial rate of polymerization has been found to be directly proportional to dose rate. The polymerization was markedly retarded by the presence of ammonia, indicating a cationic mechanism. Nitric oxide and nitrous oxide also showed considerable retarding effects on the polymerization. The rate of polymerization was enhanced by adding rare gases, Ar, Kr, and Xe. These results indicate that energy transfer from rare gases to isobutene occurs in mixtures of these gases.

Introduction

Recently, much attention has been drawn to the role of ionic processes in radiation chemistry. Considerable evidence has accumulated which indicates that the radiation-induced polymerization of several monomers is caused by ionic intermediates.[1-12] All of these are concerned with the polymerization in the condensed phase. It is expected that the study of polymerization in the gas phase provides additional information about reaction mechanism, because effects of additives on the polymerization can be investigated rather extensively.

The present paper deals with certain aspects of the radiation-induced polymerization of isobutene in the gas phase. Results are presented on the polymerization of pure isobutene and effects of several additives on this polymerization, and the reaction mechanism is discussed on the basis of these results.

(1) W. H. T. Davison, S. H. Pinner, and R. Worrall, *Proc. Roy. Soc.* (London), **A252**, 187 (1959).

(2) E. Collinson, F. S. Dainton, and H. A. Gillis, *J. Phys. Chem.*, **63**, 909 (1959).

(3) J. V. F. Best, T. H. Bates, and F. Williams, *Trans. Faraday Soc.*, **58**, 192 (1962).

(4) T. H. Bates, J. V. F. Best, and F. Williams, *J. Chem. Soc.*, 1531 (1962).

(5) A. Chapiro and V. Stannett, *J. Chim. Phys.*, **56**, 830 (1959).

(6) C. S. H. Chen and R. F. Stamm, *J. Polymer Sci.*, **58**, 369 (1962).

(7) A. Charlesby and J. Morris, *Proc. Roy. Soc.* (London), **A273**, 378 (1963).

(8) S. Okamura, T. Higashimura, and S. Futami, *Intern. J. Appl. Radiation Isotopes*, **8**, 46 (1960).

(9) M. A. Bonin, M. L. Calvert, W. L. Miller, and F. Williams, *Polymer Letters*, **2**, 143 (1964).

Experimental Section

Materials. Research grade isobutene was dried over a freshly prepared sodium mirror at −78°. Samples were degassed by repeating several times the freezing–pumping–thawing cycle. Samples were then further dried several times over freshly prepared sodium mirrors.

Ammonia was prepared by the reaction of ammonium chloride with potassium hydroxide and purified by conventional vacuum-line techniques. The middle fraction from distillation was used for experiments.

Research grade nitric oxide (99.0%) was further purified by distillation under vacuum. Nitrous oxide (99.9%), carbon dioxide (99.99%), argon (99.999%), krypton (99.9%), and xenon (99.9%) were dried prior to use.

Irradiation. Irradiation vessels were spherical glass bulbs approximately 450 cm³ in volume. A mercury manometer was connected with it *via* a capillary tube. After a vessel was baked, sample gases were introduced into it through a tube packed with sodium-coated glass wool. Samples were carefully degassed and sealed off under vacuum.

Irradiations were carried out at 25° with ^{60}Co γ rays at a dose rate of 1.1×10^4 to 1.7×10^5 rads/hr. Total irradiation doses ranged from 1 to 8 Mrads. In evaluating the energy absorbed by gases, it was assumed that the absorbed energy was proportional to the stopping power of materials, and the absolute energy absorption could be determined by means of ferrous sulfate dosimetry.[13]

Analysis of Products. The polymerization yield was determined by measuring the difference in pressure of the sample before and after irradiation, which can be read on a manometer attached to the irradiation vessel. The average molecular weight of polymers produced was determined by measuring the viscosity in benzene at 25° with an Ubbelohde dilution viscometer and applying the equation,[14] $(\eta) = 8.3 \times 10^{-4} Mv^{0.53}$.

The infrared spectrum of liquid products was taken on a Hitachi EPI-S2 infrared spectrometer.

Results

Polymerization of Pure Isobutene. The polymerization of isobutene was reproducible only when isobutene was extremely pure and the irradiation vessel was very clean. The polymer produced was a viscous, colorless, and transparent liquid. The infrared spectrum of the polymer was the same as that of the polymer obtained by conventional cationic polymerization[15,16] over the frequency range from 650 to 4000 cm^{-1}.

The dependence of the polymerization yield on the irradiation dose at a dose rate of 1.7×10^5 rads/hr is shown in Figure 1. At doses less than 1 Mrad, the yield increases linearly with dose and is larger than that obtained in the γ-ray-induced polymerization in the liquid phase at −78°.[1] Figures 2 and 3 show the dependences of the molecular weight of polymers and the polymerization yield on the dose rate at an initial pressure of isobutene of 600 torr and a total dose of 1 Mrad, respectively. It is found that the molecular weight is independent of dose rate and the polymerization yield or the rate of polymerization is directly proportional to dose rate.

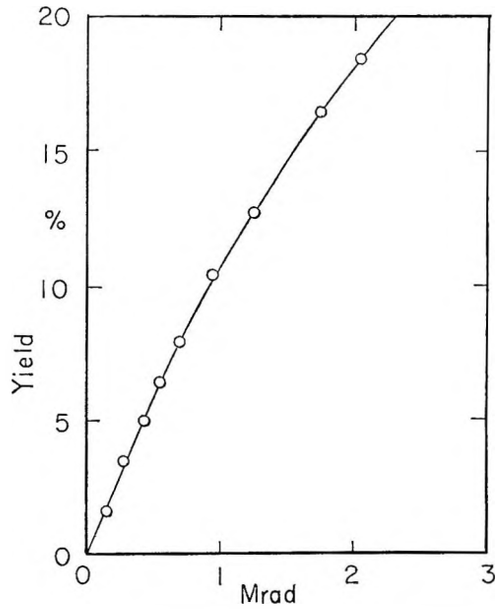

Figure 1. Dependence of polymerization yield on dose. Initial pressure of isobutene, 600 torr; dose rate, 1.7×10^5 rads/hr. The dose and dose rate on the abscissa in figures and described as the experimental conditions in the text are expressed as absorbed in a ferrous sulfate dosimeter and not in the gas sample.

It is of interest to evaluate the G value for the formation of polymer chains, G_i. This is done by dividing the G value for the consumption of monomers by the number-average degree of polymerization. The latter can be calculated from the number-average molecular weight, Mn, which is obtained using the approximate

(10) W. S. Anderson, *J. Phys. Chem.*, **63**, 765 (1959).

(11) M. A. Bonin, W. R. Busler, and F. Williams, *J. Am. Chem. Soc.*, **87**, 199 (1965).

(12) K. Ueno, H. Yamaoka, K. Hayashi, and S. Okamura, *Intern. J. Appl. Radiation Isotopes*, **17**, 595 (1966).

(13) G. R. A. Johnson, *J. Inorg. Nucl. Chem.*, **24**, 461 (1962).

(14) T. G Fox and P. Flory, *J. Phys. Colloid Chem.*, **53**, 197 (1949).

(15) H. L. Dinsmore and D. C. Smith, *Anal. Chem.*, **20**, 11 (1948).

(16) G. M. C. Higgins and D. T. Turner, *J. Polymer Sci.*, **A2**, 1713 (1964).

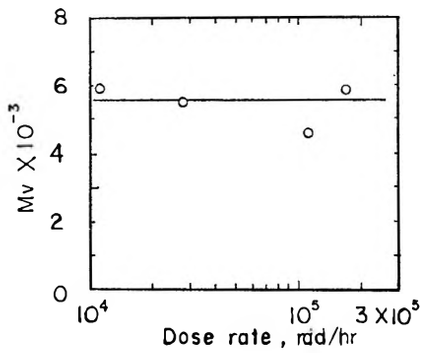

Figure 2. Dependence of molecular weight on dose rate. Initial pressure of isobutene, 600 torr; dose, 1 Mrad.

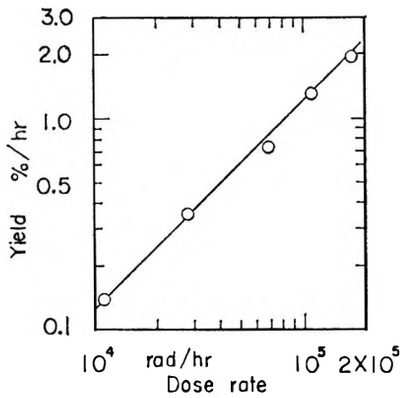

Figure 3. Dependence of polymerization yield on dose rate. Initial pressure of isobutene, 600 torr; dose, 1 Mrad.

formula,[17] $Mv = 1.85Mn$. Thus, we have obtained $G_i = 1750/54 = 32$. Since the 100-ev yield for the formation of primary species is known to be at most 10 in any chemical system, such a high value of G_i implies that chain transfer processes play a part in the polymerization studied here.

Effect of Ammonia. Information about the polymerization mechanism is obtained from observations of the effects of additives. Figure 4 shows the effect of ammonia on the polymerization yield at an initial pressure of isobutene of 500 torr, a dose rate of 1.7×10^5 rads/hr, and doses of 1 to 4 Mrads. The yield is given as the number of consumed monomers per 100 ev absorbed by isobutene only. The G value is calculated from the fractional conversion of isobutene, $c\%$, at a dose of r Mrads using the relation, $G = 145c/rf$, f being the mole fraction of isobutene. In deriving this equation, we have taken the values of stopping power from Lind.[18] It is seen in Figure 4 that ammonia retards the polymerization markedly even at low concentrations.

Effect of Nitric Oxide and Nitrous Oxide. Both nitric oxide and nitrous oxide also retarded the polymerization (Figures 5 and 6), although the retarding effects in these cases is smaller than in the case of ammonia.

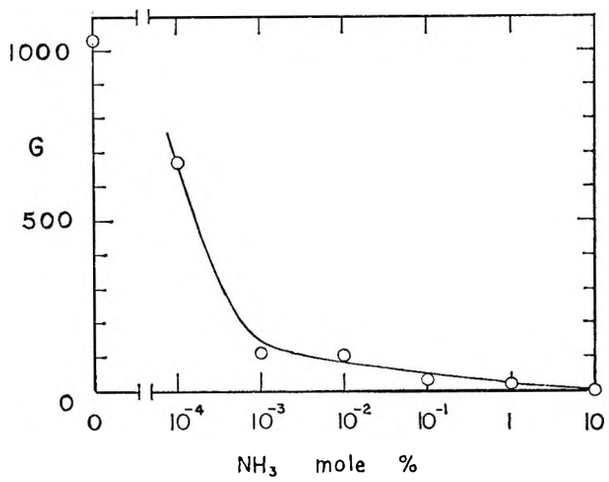

Figure 4. Effects of NH_3 concentration on polymerization yield. Initial pressure of isobutene, 500 torr; dose rate, 1.7×10^5 rads hr; dose, 1 to 4 Mrads.

Effect of Rare Gases. Figure 7 shows the effects of rare gases, Ar, Kr, and Xe, on the polymerization yield at an initial pressure of isobutene of 100 torr, a dose rate of 1.7×10^5 rads/hr, and a dose of 8 Mrads. The increase in yield is seen for all these mixtures of gases, being in the order of Ar, Kr, and Xe. Mechanisms for such sensitization effects will be discussed in the next section.

Discussion

Ionization potentials of various gases and energy levels of optically allowed and metastable states of rare gases are given in Table I. It is well known that ammonia has a large proton affinity and is an efficient proton acceptor.[19] There is no evidence that ammonia is an efficient electron or radical scavenger. Ammonia is, therefore, very useful for determining whether the mechanism for a reaction is cationic or not, because addition of ammonia causes proton transfer from reactive cations to ammonia. The remarkable retarding effect of ammonia observed in the present study is attributed to a proton transfer reaction

$$C_4H_9^+ + NH_3 \longrightarrow C_4H_8 + NH_4^+ \qquad (1)$$

where the *t*-butyl carbonium ion is considered to be

(17) P. Alexander, R. M. Black, and A. Charlesby, *Proc. Roy. Soc.* (London), **A232**, 31 (1955).

(18) S. C. Lind, "Radiation Chemistry of Gases," Reinhold Publishing Corp., New York, N. Y., 1961, p 274.

(19) W. R. Busler, D. H. Martin, and F. Williams, *Discussions Faraday Soc.*, **36**, 102 (1963).

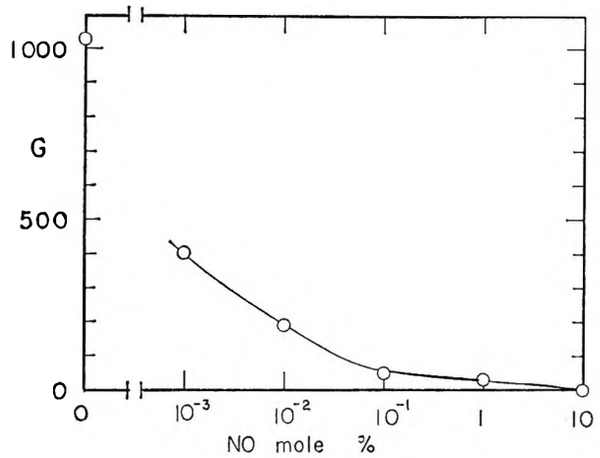

Figure 5. Effects of NO concentration on polymerization yield. Initial pressure of isobutene, 500 torr; dose rate, 1.7×10^5 rads/hr; dose, 4 Mrads.

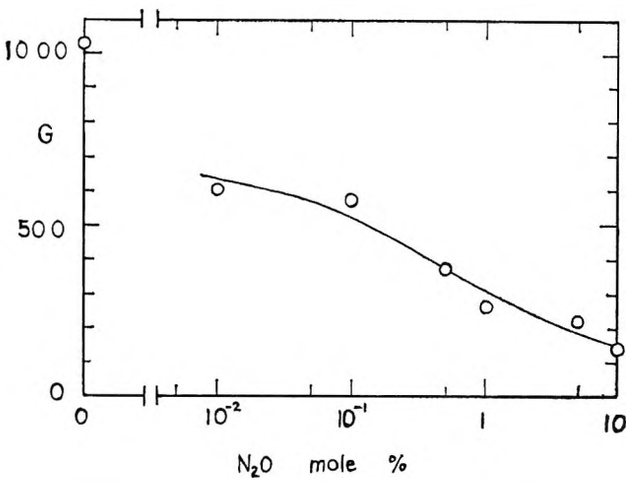

Figure 6. Effects of N_2O concentration on polymerization yield. Initial pressure of isobutene, 500 torr; dose rate, 1.7×10^5 rads/hr; dose, 4 to 8 Mrads.

Table I: Ionization Potentials and Energy Levels of Allowed and Metastable States of Gases

Gas	I.P.,[a] ev	Allowed state,[b] ev	Metastable state,[c] ev
i-C_4H_8	9.23		
Ar	15.8	12.0, 12.2	11.5, 11.7
Kr	14.0	10.4, 11.0	9.9, 10.5
Xe	12.1	8.7, 9.9	8.3, 9.4
NH_3	10.2		
NO	9.25		
N_2O	12.9		
CO_2	13.8		

[a] K. Watanabe, T. Nakayama, and J. Mottl, *J. Quant. Spectry. Radiative Transfer*, **2**, 369 (1962). [b] R. Knox, *Phys. Rev.*, **110**, 375 (1958); J. Geiger, *Z. Physik*, **177**, 138 (1963); D. K. Anderson, *Phys. Rev.*, **137**, A21 (1965). [c] M. M. Shahin and S. R. Lipsky, *Anal. Chem.*, **35**, 1562 (1963).

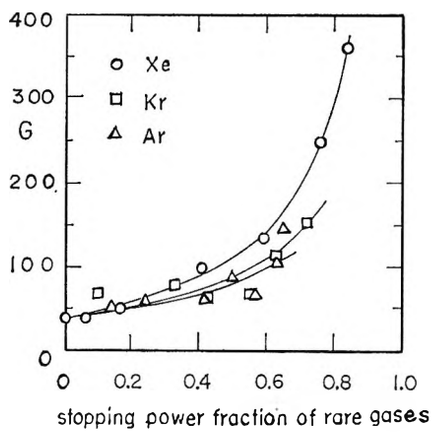

Figure 7. Effects of rare gases on polymerization yield. Initial pressure of isobutene, 100 torr; dose rate, 1.7×10^5; dose, 8 Mrads.

produced from the isobutene parent ion, $C_4H_8^+$, *via* an ion–molecule reaction. This indicates that the polymerization of isobutene in the gase phase is cationic.

The retardation of the polymerization by nitric oxide may be interpreted in terms of charge transfer[20,21]

$$C_4H_8^+ + NO \longrightarrow C_4H_8 + NO^+ \qquad (2)$$

Since the ionization potential of nitric oxide is almost the same as that of isobutene, it is energetically possible for reaction 2 to occur. The reaction of nitric oxide with the *t*-butyl carbonium ion may also be responsible for the retardation of the polymerization, although it has not yet been identified.

The effect of nitrous oxide on the polymerization may be explained in terms of the neutralization of propagating cations and oxygen negative ions, O^- or O_2^-, arising from electron capture by nitrous oxide and a subsequent reaction of O^- with N_2O.[22,23] Otherwise, some slow electrons will reach the wall of the reaction vessel, resulting in a substantial increase of the number of cations. Also, charge transfer (reaction 2) to nitric oxide, a radiolysis product of nitrous oxide, may participate in the retardation of the polymerization.

As plausible mechanisms for the sensitization effects

(20) G. G. Meisels, *J. Chem. Phys.*, **42**, 3237 (1965).
(21) K. Yang and P. J. Manno, *J. Am. Chem. Soc.*, **81**, 3507 (1959).
(22) B. P. Burtt and J. F. Kircher, *Radiation Res.*, **9**, 1 (1958).
(23) F. T. Jones and T. J. Sworski, *J. Phys. Chem.*, **70**, 1546 (1966).

of rare gases, both charge and excitation transfer can be considered.[24] Taking xenon as an illustration, reactions 3 and 4 are likely to occur

$$Xe^+ + C_4H_8 \longrightarrow Xe + C_4H_8^+ \quad (3)$$

$$Xe^* + C_4H_8 \longrightarrow Xe + C_4H_8^+ + e^- \quad (4)$$

Since the rate of polymerization is proportional to the number of isobutene cations, the ratio of polymerization rate in mixtures of isobutene and rare gases to those in pure isobutene, R_m/R_0, is given by eq 5, where n_1 and n_2

$$\frac{R_m}{R_0} = 1 + \frac{n_2\sigma_2}{n_1\sigma_1} \qquad \frac{\sigma_2}{\sigma_1} = \frac{\sigma_i}{\sigma_1} + \frac{\sigma_e}{\sigma_1} \quad (5)$$

are the molarity of isobutene and rare gases, respectively, σ_1 is the ionization cross section of isobutene, and σ_2 is the sum of ionization (σ_i) and excitation (σ_e) cross sections of rare gases. We assume that both charge and excitation transfer from rare gases to isobutene completely take place. The observed values of R_m/R_0 were plotted against n_2/n_1 in Figure 8. It is found that R_m/R_0 is a linear function of n_2/n_1 for each gas. The slope of each line gives rise to σ_2/σ_1. The values obtained are shown in Table II together with the values, $(\sigma_i/\sigma_1)_{calcd}$, calculated from data on total ionization cross sections for 75-ev electrons.[25] Since σ_2/σ_1 is greater than $(\sigma_i/\sigma_1)_{calcd}$, excitation transfer may be involved. The values of σ_e/σ_1 obtained from eq 5 are also given in Table II.

Table II: Relative Cross Sections for Charge and Excitation Transfer

	σ_2/σ_1	σ_i/σ_1 calcd[a]	σ_e/σ_1	σ_i/σ_1
Ar	0.45	0.27	0.18	...
Kr	0.73	0.40	0.33	...
Xe	1.37	0.57	0.80	0.94

[a] Calculated from data given in ref 25.

Since carbon dioxide is known as a quencher of excited rare gas atoms[26] and has an ionization potential higher than that of xenon, it would be expected that information about the role of excitation transfer is obtainable, if the effect of carbon dioxide on the polymerization yield in isobutene–xenon systems is investigated. It is seen in Figure 9 that the yield comes down to a constant value as the concentration of carbon dioxide increases. In the limiting case where the

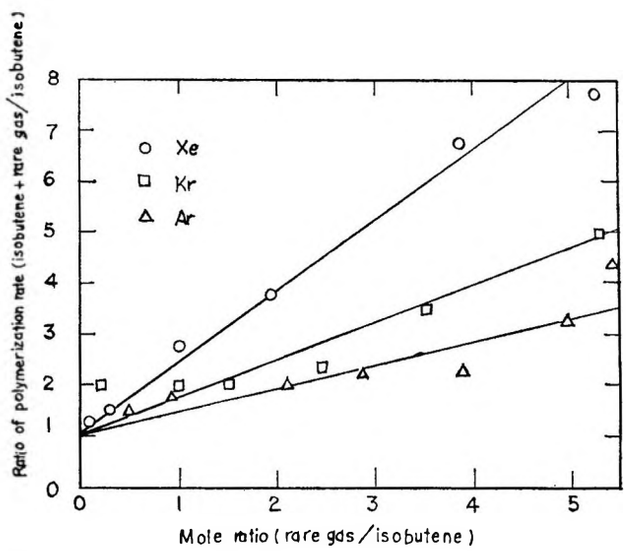

Figure 8. Effects of rare gases on polymerization rate. Initial pressure of isobutene, 100 torr; dose rate, 1.7 × 10^5 rads/hr; dose, 8 Mrads.

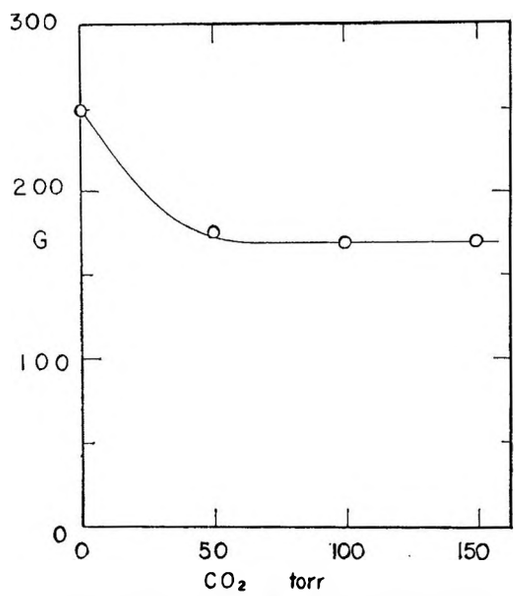

Figure 9. Effects of CO_2 concentration on polymerization yield. Initial pressure of isobutene, 100 torr; Xe, 400 torr; dose rate, 1.7 × 10^5 rads/hr; dose, 8 Mrads.

(24) Ionization of impurity atoms and molecules due to excitation transfer from metastable states of rare gas atoms is a well-known phenomenon, called the Penning or Jesse effect (for example, W. P. Jesse and J. Sadauskis, *Phys. Rev.*, **100**, 1755 (1955)). It has been theoretically predicted that cross sections for ionization of atoms and molecules due to excitation transfer from optically allowed states of excited rare gas atoms are considerably large (K. Katsuura, *J. Chem. Phys.*, **42**, 3771 (1965)). The latter process may be significant for the indirect ionization of isobutene except at very low pressures.

(25) J. L. Franklin and F. H. Field, *J. Am. Chem. Soc.*, **83**, 3555 (1961).

(26) M. M. Shahin and S. R. Lipsky, *J. Chem. Phys.*, **41**, 2021 (1964).

concentration of carbon dioxide is high enough to give a plateau in the yield, the following equation can be applied

$$\frac{R_m'}{R_0} = 1 + \frac{n_2}{n_1}\frac{\sigma_i}{\sigma_1} \quad (6)$$

where R_m' stands for the rate of polymerization corresponding to the limiting value of the yield. The value of σ_i/σ_1[27] obtained from eq 6 is given in the last column of Table II. The agreement between $(\sigma_i/\sigma_1)_{calcd}$ and σ_i/σ_1 is not quantitatively satisfactory, but considering the approximations in the present treatment, it may be said that both charge and excitation transfer take an important part in the polymerization of isobutene in these systems.

We now discuss the kinetics of the γ-ray-induced polymerization of isobutene in the gas phase. The reaction is initiated by the ionization of monomer molecules

$$M \longrightarrow M\cdot^+ + e^-; \quad R_i = \Phi I \quad (7)$$

The parent ion $M\cdot^+$ then reacts rapidly with another monomer molecule to yield the *t*-butyl carbonium ion

$$M\cdot^+ + M \longrightarrow MH^+ + R\cdot \quad (8)$$

Reaction 8 has been observed in a mass spectrometer as a fast reaction.[28,29] Propagation is caused by the *t*-butyl carbonium ion

$$MH^+ + M \xrightarrow{k_p} M_2H^+; \quad R_p = k_p(M_nH^+)(M) \quad (9)$$

Termination is unimolecular with respect to propagating ions, being implied in the dose-rate dependence of the yield, and it may be written as[30]

$$M_nH^+ + X \xrightarrow{k_t = k_t'(X)} M_n + HX^+; \quad R_t = k_t(M_nH^+) \quad (10)$$

where X indicates the wall of the vessel and possibly a trace of impurities. Chain transfer takes place by proton transfer from a polymer ion to a monomer molecule

$$M_nH^+ + M \xrightarrow{k_{tr}} M_n + MH^+; \quad R_{tr} = k_{tr}(M_nH^+)(M) \quad (11)$$

Applying the steady-state treatment to the reaction scheme described above, the rate of polymerization, R, and the number-average degree of polymerization, $\overline{DP}_n$, can be expressed as eq 12 and 13

$$R = \frac{k_p}{k_t}\Phi(M)I \quad (12)$$

$$\overline{DP}_n = \frac{R_p}{R_t + R_{tr}} = \frac{k_p(M)}{k_t + k_{tr}(M)} \quad (13)$$

These equations are compatible with the experimental results that the rate of polymerization is directly proportional to dose rate and the number-average degree of polymerization is independent of dose rate. It is concluded that the cationic mechanism dominates in the polymerization of isobutene in the gas phase.

It should be noted that the polymerization yield under the present experimental conditions is of comparable magnitude to that in the condensed phase reported in the early literature,[1,2] although more recent work on the radiation-induced polymerization of liquid isobutene at $-78°$ indicates that the yield can be much higher.[31] Since it will be expected that the greater polymerization yields are obtained at higher pressures of isobutene, it would be an interesting subject to study the pressure effect on the polymerization in the future work.

(27) This value is taken to be an upper limit of σ_1/σ_i because charge transfer from carbon dioxide to isobutene may enhance the yield of isobutene ions.

(28) I. Koyano, *J. Chem. Phys.*, **45**, 706 (1966).

(29) F. W. Lampe and F. H. Field, *Tetrahedron*, **7**, 189 (1959).

(30) A. Charlesby, S. H. Pinner, and R. Worrall, *Proc. Roy. Soc.* (London), **A259**, 386 (1960).

(31) The authors wish to thank Professor F. Williams for informing them of this result.

Ionization Current Measurements in Mixtures of Organic Vapors[1]

by Linda M. Hunter and Russell H. Johnsen

Department of Chemistry, Florida State University, Tallahassee, Florida 32306 *(Received March 10, 1967)*

Ionization currents have been measured in mixtures of organic vapors such as the cyclohexane–benzene system, by use of a heated ionization chamber. The behavior of the ionization currents in the hydrocarbons was found to deviate from the behavior of that of the molecular gas, nitrogen, and to vary with pressure. The theory of Boag for a parallel plate ionization chamber adequately treated the data from those cases in which negative ionic species are not formed. The mixture W values, the average energy to produce an ion pair, which were determined from these measurements, have been compared on the basis of the electron fraction approximation. The initially absorbed energy was found to be partitioned between the components approximately on the basis of their respective number of electrons. The existence of superexcited states in the hydrocarbon molecules but not in carbon tetrachloride is postulated to explain some deviation in the hydrocarbon–carbon tetrachloride systems. The W values of the pure organic compounds are: cyclohexane, 25.05 ± 0.06; cyclopentane, 25.39 ± 0.06; hexane, 25.30 ± 0.06; cyclohexene, 25.47 ± 0.06; benzene, 26.93 ± 0.06; and carbon tetrachloride, 25.79 ± 0.06 ev/ip.

Introduction

Systems which have long been of interest to radiation chemists are those in which protection occurs; that is, the products resulting from irradiation of an organic mixture indicate some type of interaction, physical and/or chemical, is occurring between the components. This phenomenon was first noted by Schoepfle and Fellows,[2] who irradiated a cyclohexane–benzene mixture and found the gaseous product yield to be much smaller than was anticipated from irradiation studies of the pure components. Since this first experiment, systems of this type have been repeatedly studied and the decrease in product yields has been explained by such interactions as: atom scavenging,[2-6] energy transfer,[7,8] charge transfer,[9-12] preferential energy absorption,[13] electron attachment,[10,12,14] and ion scavenging.[6,15,16]

Measuring the ionization currents produced in irradiated mixtures of gases provides information about physical interactions which lead to ion production. The well-known Jesse effect,[17-22] the abrupt increase in ion production and, therefore, the decrease in the W value, is characteristic of the rare gases when contaminated by a small amount of another gas. In the case of some binary mixtures of molecular gases,[23-27] more gradual changes occur, and the W values follow a smooth curve from the W value characteristic of one pure component to that of the other.

(1) Abstracted from the thesis of L. M. Hunter and supported by U. S. Atomic Energy Commission Contract AT-(40-1)-2001. This is AEC Document ORO-2001-4.

(2) C. S. Schoepfle and C. F. Fellows, *Ind. Eng. Chem.*, **23**, 1396 (1931).

(3) T. J. Hardwick, *J. Phys. Chem.*, **66**, 117 (1962).

(4) J. Y. Yang and I. Marcus, *J. Chem. Phys.*, **42**, 3315 (1965).

(5) J. H. Futrell, *J. Am. Chem. Soc.*, **81**, 5921 (1959).

(6) L. M. Theard, *J. Phys. Chem.*, **69**, 3292 (1965).

(7) J. P. Manion and M. Burton, *ibid.*, **56**, 560 (1952).

(8) J. M. Ramaradhya and G. R. Freeman, *Can. J. Chem.*, **39**, 1769 (1961).

(9) G. R. Freeman, *J. Chem. Phys.*, **33**, 957 (1960).

(10) W. Van Dusen and W. H. Hamill, *J. Am. Chem. Soc.*, **84**, 3648 (1962).

(11) T. J. Hardwick, *J. Phys. Chem.*, **66**, 2132 (1962).

(12) P. J. Dyne, *Can. J. Chem.*, **43**, 1080 (1965).

(13) J. Lamborn and A. J. Swallow, *J. Phys. Chem.*, **65**, 920 (1961).

(14) R. R. Williams and W. H. Hamill, *Radiation Res.*, **1**, 158 (1954).

(15) J. Blachford and P. J. Dyne, *Can. J. Chem.*, **42**, 1165 (1965).

(16) R. P. Borkowski and P. J. Ausloos, *J. Chem. Phys.*, **39**, 818 (1963).

(17) W. P. Jesse and J. Sadauskis, *Phys. Rev.*, **88**, 417 (1952).

(18) W. P. Jesse and J. Sadauskis, *ibid.*, **90**, 1120 (1953).

(19) T. E. Bortner and G. S. Hurst, *ibid.*, **90**, 160 (1953).

(20) J. Sharpe, *Proc. Phys. Soc.* (London), **A65**, 859 (1952).

In order to provide supplemental information about irradiated organic mixtures, in both gaseous and condensed phase, which have shown evidence of physical interactions, the W values have been determined for gaseous binary mixtures of the following hydrocarbons over the full range of composition: cyclohexene, cyclohexane, cyclopentane, hexane, benzene, and carbon tetrachloride. The W value of each binary mixture has been considered as a function of the electron fraction of the mixture (1) to relate ion production in these vapors to previously reported product yields, and (2) to indicate the final partitioning of energy upon some basis other than that expected for a system of given composition, *i.e.*, a "nonideal" behavior. Increased ionization, reflected by a substantial decrease in W value when a small amount of additive, about 5%, is present, may be construed as indicating energy transfer processes leading to "extra" ionization, *i.e.*, the Jesse effect. Deviations from the ideal that encompass the entire concentration range of the mixture suggest preferential energy absorption of one component independent of its electron fraction or some hitherto unconsidered phenomenon.

Experimental Section

Apparatus. The experimental system consisted of an ionization chamber, plumbing necessary to attain a vacuum and fill the chamber with different gases, and electronic equipment to measure the ionization phenomena occurring in the chamber. This system is similar to one used initially by Bortner and Hurst.[23] The chamber, constructed from aluminum, is cylindrical in shape and has two circular, parallel electrodes approximately 12 cm in diameter within it. They are separated by 6 cm. The lower electrode is connected to the positive side of a Fluke No. 408A power supply. The entire chamber is housed within an oven, in which a constant temperature of approximately 80° is maintained by the heat from a resistance coil; all connections which must be outside the oven are heated with heating tapes. The source of radiation in the chamber is Pu^{239} which emits 5.15-Mev α particles. A stainless steel disk, on which the plutonium is plated, is fitted flush into the middle of the bottom plate. The activity of this source was determined to be 2.21×10^7 α particles/min. The experimental parameter determined is the time for a given charge to be collected on the top plate. This electrode is connected to a capacitor that is in series with a potentiometer, which provides a manually variable voltage output which opposes the charging capacitor. The resulting null balance is monitored by a Keithley 600A electrometer. The time for the capacitor to be charged to the predetermined voltage was measured by means of a scale of 256 scalar using the house-main 60-cycle current as an internal standard. Saturation ionization currents were of the order of 5 to 8×10^{-9} amp for the different gases.

Procedure. Preliminary and calibration work was done using Airco prepurified nitrogen (O_2, 0.002%; H_2, 0.002%; H_2O, 0.0012%). The organic compounds used were Fisher benzene, Matheson Coleman and Bell Spectroquality carbon tetrachloride, cyclohexane, cyclopentane, and hexane, and Matheson Coleman and Bell Chromatoquality cyclohexene. These compounds were used as received without further purification.

Experiments with nitrogen were done with the chamber at room temperature. Nitrogen was passed through two liquid air traps before entering the evacuated chamber. Degassed liquid hydrocarbon samples were heated in a glass ampoule and then admitted into the heated, evacuated chamber.

It was necessary to calibrate this experimental system with a gas having a known W value in order to permit the assignment of absolute W values to the organic vapors. The following expression is appropriate for this experimental system.

$$W = \frac{ENq}{CV} \times t$$

where W is the W value of the gas, E is the energy of an α particle, N is the activity of the source, C is the capacitance of the circuit, V is the predetermined maximum voltage, q is the charge of an electron, and t is the experimental time in cycles.

The ratio ENq/CV is not calculable with any degree of precision because of uncertainties associated with the numerical values of the parameters. In practice, this ratio became an experimentally determined factor using a gas having a known W value.

Not only has the W value for nitrogen been very well established at 36.39 ± 0.07 ev/ip,[28-30] but this gas also has those physical properties that make it very accept-

(21) G. Bertolini, M. Bettoni, and A. Bisi, *Phys. Rev.*, **92**, 1586 (1953).

(22) C. E. Melton, G. S. Hurst, and T. E. Bortner, *ibid.*, **96**, 643 (1954).

(23) T. E. Bortner and G. S. Hurst, *ibid.*, **93**, 1236 (1954).

(24) W. Haeberli, P. Huber, and E. Baldinger, *Helv. Phys. Acta*, **26**, 145 (1953).

(25) H. J. Moe, T. E. Bortner, and G. S. Hurst, *J. Phys. Chem.*, **61**, 422 (1957).

(26) T. D. Strickler, *ibid.*, **67**, 825 (1963).

(27) C. Klots, *J. Chem. Phys.*, **44**, 2715 (1966).

(28) G. N. Whyte, *Radiation Res.*, **18**, 265 (1963).

(29) W. P. Jesse, *ibid.*, **13**, 1 (1960).

(30) Z. Bay, P. A. Newman, and H. H. Selinger, *ibid.*, **14**, 551 (1961).

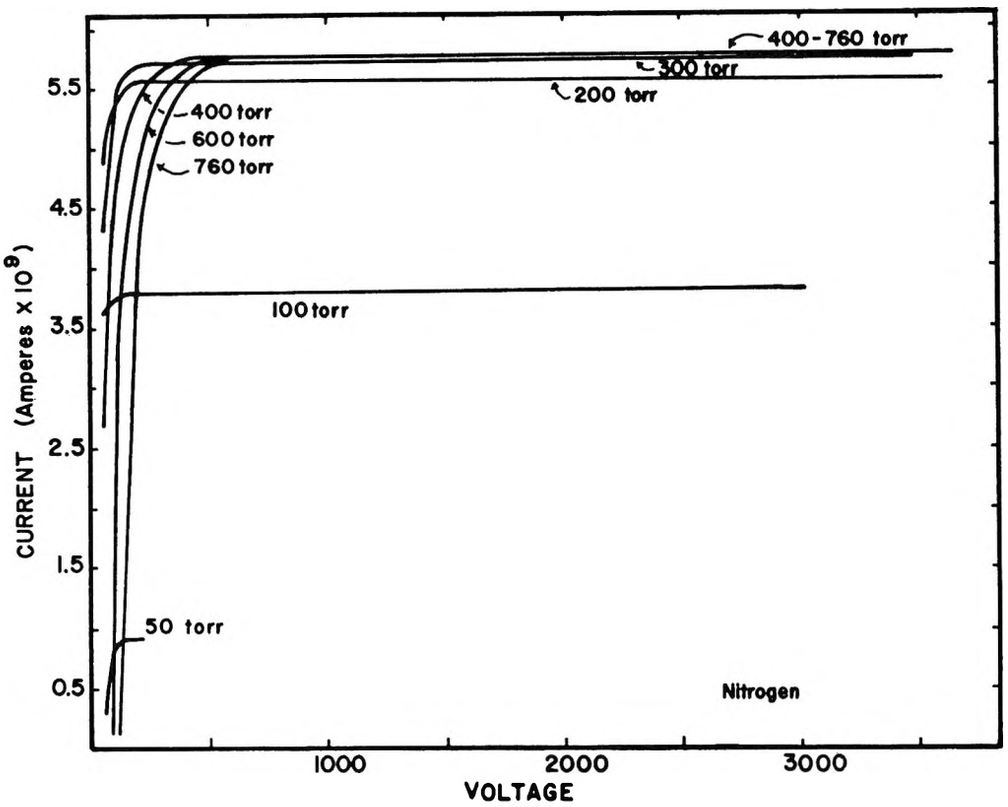

Figure 1. Saturation curves for nitrogen at various pressures.

able for calibration purposes. Because nitrogen does not form negative ions readily, its ionization current saturates at low fields for all pressures. Also, impurity problems, resulting in extreme effects, are not as common in nitrogen as they are in the rare gases.

The ionization currents in nitrogen for varying pressures are indicated in Figure 1, and they are characterized by plateaus above 750 v. Approximately the same saturation currents were measured for pressures from 400 to 760 torr, and with decreasing pressure in this range, saturation occurred at lower voltages. As the pressure decreased below 350 torr, the α particles were not completely stopped in the gas, resulting in erroneous readings.

For conditions of saturation when the α particles are completely stopped in the gas, the saturation currents were consistently lower at higher pressures, as is indicated in Table I. The largest standard deviation for a determination is about 3 cycles ($^1/_{20}$ sec) and this represents an error of about 0.059%. The deviation between the times determined at 700 and 400 torr represents a 0.21% difference, and between those times at 500 and 400 torr the difference represents an increase of 0.073% and is 1.2 times greater than the experimental error. Although the differences are small, there does seem to be a definite trend of decreasing saturation current with increasing pressure. This effect can be explained by columnar recombination, that is, recombination phenomena which occur in the track of the ionizing particle. For α-particle irradiation, the number density of ionic species will be larger near the end of the track and should be larger at higher pressures. Recombination processes would be enhanced, and therefore, the measured saturation current will have an in-

Table I: Experimental Times at Varying Pressures for Nitrogen

Pressure, torr	Exptl time, cycles[a] Average	Std dev
760	5,107.7	2.4
700	5,109.5	1.8
600	5,105.3	2.9
500	5,102.4	2.2
400	5,098.7	2.5
300	5,134	
280	5,168	
200	5,759	
100	11,776	

[a] 1 cycle = $^1/_{60}$ sec.

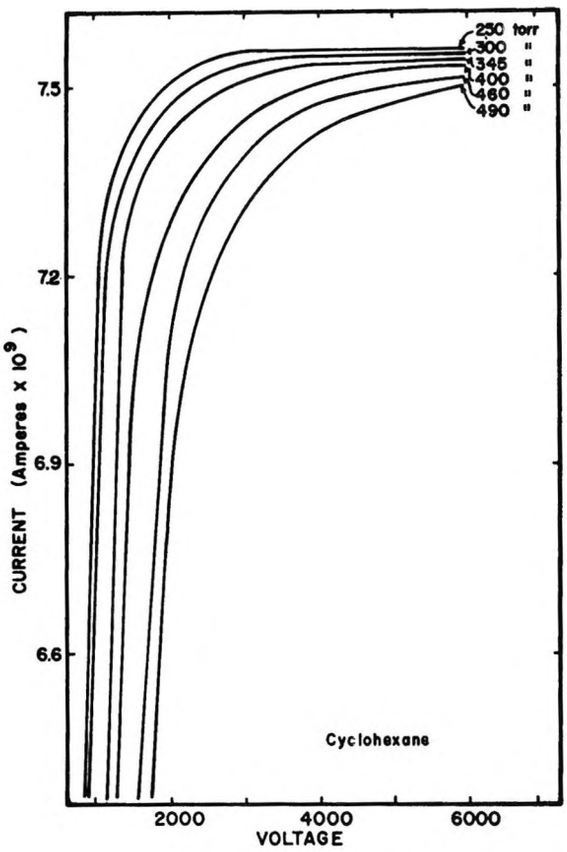

Figure 2. Saturation curves for cyclohexane at various pressures.

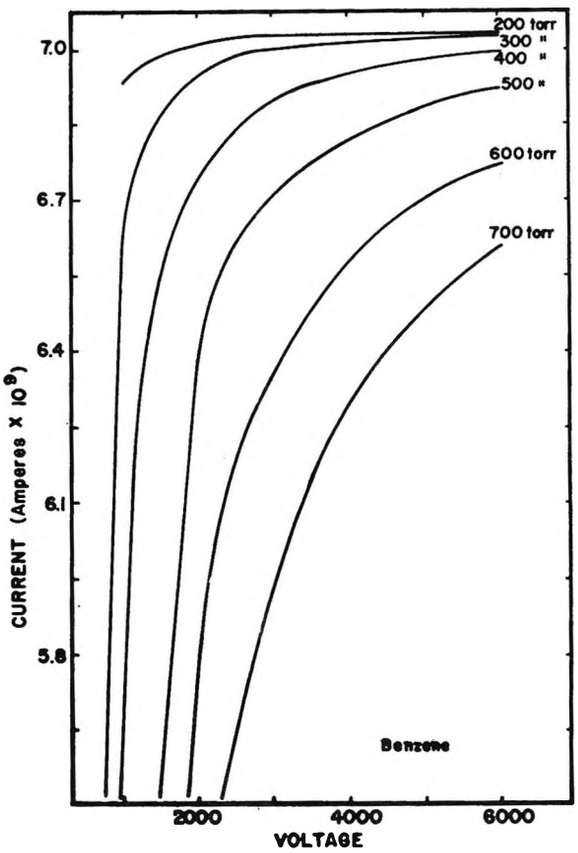

Figure 3. Saturation curves for benzene at various pressures.

verse relationship with pressure. For this reason, calculations were made only with data determined at 400 torr at which pressure it is believed that columnar recombination is negligible. The factor used to convert cycles to electron volts per ion pair is 7.137 ($\pm$0.003) $\times 10^{-3}$ ev/(ip cycle).

In contrast to those of nitrogen under conditions near atmospheric pressure, the ionization currents of the organic vapors did not exhibit saturation phenomena in these voltage and pressure ranges, but appeared to saturate only at lower pressures of about 300 torr and high fields of about 850 v/cm. The ionization currents as a function of pressure for cyclohexane, which are shown in Figure 2, are representative of the other saturated hydrocarbons, cyclopentane and hexane. The effect of pressure is even more pronounced in the case of benzene, represented in Figure 3, and this behavior is also characteristic of cyclohexene. In Figure 4, the behavior of carbon tetrachloride is shown; it should be noted that, although the curves for benzene and carbon tetrachloride appear similar, the ordinate scale of the benzene graph is about one-third that of the carbon tetrachloride.

General recombination phenomena, that is recombination in the bulk of the gas between positive ions and negative ions or electrons as they drift toward their respective electrodes, explain the differences in the behavior of the ionization currents with pressures between the hydrocarbons and nitrogen. This process depends on the number densities of the ionic species and on the probability of their encountering each other. The density of the ionic species, which is proportional to the stopping powers of the compounds, is probably the major consideration for explaining the trends of the saturation currents with the different types of molecular gases.

To a rough first approximation, the stopping power is proportional to the number of electrons in the compound. The electron numbers of nitrogen, the hydrocarbons, and carbon tetrachloride are 14, 40–50, and 74, respectively. The linear density of ions in carbon tetrachloride would be expected to be much larger than in the hydrocarbons and nitrogen. Therefore, the number of ions collected at the same pressure in nitrogen should not be decreased by recombination processes to the extent that recombination affects the

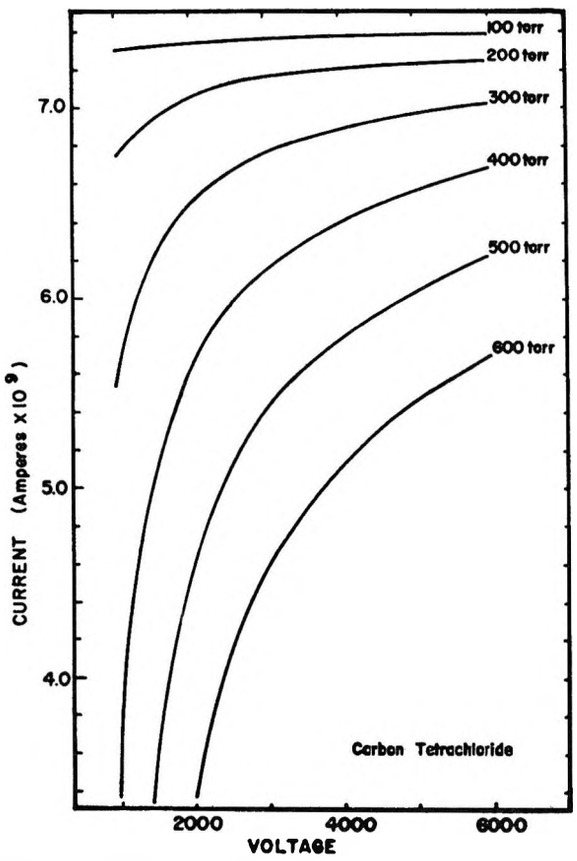

Figure 4. Saturation curves for carbon tetrachloride at various pressures.

number collected in the hydrocarbons. From this consideration alone, one expects recombination to be greatest in CCl_4. However, other important processes affect recombination, and one of these is discussed below.

The mobility is the proportionality constant relating the drift velocity of an ionic species to the field influencing its motion and is an inverse function of the density of the gas and its pressure, when the temperature remains constant. In general, an increased field strength is needed to collect all the ions, when the gas is at a higher pressure. Increased pressure decreases the mobility, and general recombination processes are enhanced. To a first approximation, the mobilities of the charged species can be assumed to be proportional to the inverse of their molecular weights; however, mobilities are also dependent on the nature of the ionic species in the gas and the degree of clustering. Because the electron mobilities are about a factor of 100 greater than the mobilities of the positive ions in the hydrocarbon vapors, the magnitude of the differences between the ionization currents, based on the differences in the mobilities of the positive ions, is small. However, in the case of carbon tetrachloride, the ionization currents are drastically changed, because the electron is attached to the carbon tetrachloride possibly resulting in dissociation into CCl_3 and Cl^-. In any case, an electron attached to a molecule or to an atom has a mobility comparable to a positive ion, and the likelihood for recombination processes is tremendously increased as is evidenced by the ionization currents at varying pressures of carbon tetrachloride in Figure 4.

Therefore, both relative stopping powers and mobilities of positive and negative ions influence the scope of recombination, which accounts for the differences in the ionization currents for nitrogen, the hydrocarbons, and carbon tetrachloride.

In order to study the properties of the ionization current curves at different pressures and to consider the significance of the increasing saturation currents with decreasing pressure, each set of data was analyzed using a number of extrapolation techniques. To find the saturation current using Jaffe's theory of columnar recombination

$$\frac{1}{i} = \frac{1}{i_s} + \frac{f(p)}{E}$$

(where i is the measured current, i_s is the saturation current, $f(p)$ is some function of the pressure, and E is the field strength), extrapolations to infinite field were made for plots of reciprocal current *vs.* reciprocals of both field (referred to as plot A in future discussions) and field divided by pressure (plot B). Boag's theory for a parallel plate ionization chamber, on the other hand, suggests an extrapolation to infinite voltage of a plot of measured current *vs.* current divided by voltage squared (plot C).

$$i = i_s - \frac{ik}{V^2}$$

where k is a constant and V is the voltage applied across the parallel plates.

Table II shows the percentage differences between the extrapolated currents of these various plots at different pressures and the current determined by averaging the data in the range between 5000 and 6000 v at 300 torr for the hydrocarbons and 100 torr for carbon tetrachloride. Generally, plot A and plot B gave identical extrapolations that deviated greatly at higher pressures from the averaged current. This is to be expected if $f(p)$ is some arbitrary function of the pressure. However, results from plot C showed smaller deviations at all pressures with the exceptions of benzene and carbon tetrachloride.

Table II: Percentage Difference between Extrapolated Current Determinations at Varying Pressures and the Saturation Currents

Pressure, torr	Compounds					
	Cyclopentane	Hexane	Cyclohexane	Benzene	Cyclohexene	Carbon tetrachloride
			Plots A and B			
700	2.2	...	...	3.9	...	...
600	0.7	...	2.4	2.3	...	−13.8
580	...	...	...	...	4.4	...
560	...	2.0	...	...	...	...
500	0.2	1.0	0.9	1.0	2.7	−10.2
400	0.25	0.6	0.9	0.7	0.8	−6.6
300	0.3	−0.01	0.1	0.6	0.4	−2.4
200	0.02	0.26	0.8	0.4	0.3	−0.3
100	−0.7	0.42	...	...	...	0.5
			Plot C			
700	0.39	...	...	−2.15	...	...
600	0.11	...	0.21	−1.3	...	−32.0
580	...	...	...	...	0.08	...
560	...	0.31	...	...	...	...
500	−0.08	0.15	0.0	−0.49	0.10	−22.0
400	−0.10	0.16	0.32	0.03	0.01	−16.4
300	0.12	−0.02	0.03	0.31	0.11	−6.5
200	0.01	0.23	0.44	0.32	0.27	−2.0
100	−0.11	0.41	...	...	...	0.29

Boag's theory is valid only near saturation and would not be expected to hold for electronegative gases at pressures where saturation is not possible. It is significant, however, that the extrapolation method from the Jaffe theory does not work either for carbon tetrachloride data. The extrapolated currents are much lower than the saturation currents. It is interesting that benzene behaves as an electronegative gas at high pressures according to plot C.

Plot A and plot B may not provide meaningful extrapolations for these data because too few data points are considered in the least-squares analysis. Since it was possible to consider saturation conditions only for the range between 5000 and 6000 v, eleven points were used. Each of these points was an average of data from six different experiments. It should be mentioned that this type of extrapolation appeared to work satisfactorily for nitrogen in which 20 data points were considered in the range between 3000 and 6000 v.

Boag's theory predicts a relationship which can be utilized as the criterion for saturation in order to interpret these experimental data. Extrapolations to $i/v^2 = 0$ from a plot of current *vs.* current divided by voltage squared indicates the saturation current. This current differs by less than 0.5% from the current determined by averaging data at 300 torr for the hydrocarbons and 100 torr for carbon tetrachloride in the range between 5000 and 6000 v. For the results that follow, the W values of pure compounds have been determined from type C extrapolated data and the W values of mixtures have been determined from data averaged over the range 5000–6000 v at 300 torr.

Results and Discussion

Pure Compounds. The W values determined for the pure organic vapors are indicated in Table III, along with W values determined for other organic gases by other workers. There are few data with which the present W values can be directly compared except those reported by Biber, *et al.*,[31] and Adler and Bothe,[32] who have used heated chambers.

In general, the W values determined here are similar to those for the gaseous hydrocarbons. In a homologous series, the W values decrease and the ratios of W/I increase. The W values increase with unsaturation and since ionization potentials decrease under such circumstances, the ratios of W/I become larger. With increased unsaturation, such as in benzene, the ratio is almost 3. One unsaturated bond in the C_6 ring increased the W/I ratio by about 9%, and a double bond added to the aliphatic C_3 chain increases the ratio approximately 18%; however, the corresponding W values increase by 17 and 34%, respectively.

(31) C. Biber, P. Huber, and A. Muller, *Helv. Phys. Acta*, **28**, 503 (1955).

(32) P. Adler and H. K. Bothe, *Z. Naturforsch.*, **20a**, 1700 (1965).

Table III: Comparison of Pure W Values

Compound	Ionization potential, ev	W Values, ev/ip					
		This work	Irradiation α[a]	Irradiation β[b]	W_α/W_β	W_α/I	W_β/I
CH_4	12.98	...	29.01	27.5	1.05	2.24	2.12
CCl_4	11.47	25.79	25.9[c]	24.3	1.06[e]	2.25[e]	2.12
C_2H_6	11.8	...	26.4	26.0	1.02	2.24	2.21
C_3H_8	11.1	...	26.15	24.3	1.07	2.35	2.18
C_4H_{10}	10.8	...	25.72	23.7	1.08	2.38	2.19
C_5H_{12}	10.6	...	...	23.5	...	...	2.23
C_6H_{14}	10.48	25.30	...	23.4	1.08[e]	2.42[e]	2.24
C_7H_{16}	10.4	...	...	23.2	...	...	2.23
C_2H_2	11.4	...	27.35	25.7	1.06	2.40	2.25
C_2H_4	10.6	...	27.87	26.3	1.06	2.63	2.48
C_3H_6	9.80	...	27.01	...	...	2.76	...
c-C_3H_6	10.2	...	25.82	...	...	2.52	...
c-C_5H_{10}	10.53	25.39	...	...	...	2.41[e]	...
c-C_6H_{12}	9.88	25.05	...	22.7	1.11[e]	2.54[e]	2.30
c-C_6H_{10}	9.24	25.47	...	...	...	2.76[e]	...
C_6H_6	9.24	26.93	27.5[d]	...	...	2.92[e]	...

[a] Klots, ref 27. [b] Adler and Bothe, ref 32. [c] Biber, *et al.*, ref 31. [d] Moe, *et al.*, ref 25. [e] Calculations made with W values determined in this work.

Stevenson[33] has shown that ions from unsaturated molecules have a higher average energy than those corresponding to saturated molecules. This, combined with the presence of low-lying excited states, which are known to exist in particular, in benzene, explains qualitatively the increase in the W values for unsaturates even though their ionization potentials are lower.

Molecules can be classified into groups according to the values of the ratio of the W value to the ionization potential. For β-ray irradiation,[34] the rare gases have a ratio equal to about 1.7 and the ratio for the saturated hydrocarbons is approximately 2.1. Unsaturation increases this ratio 0.3 to 0.4 unit. From the β-ray irradiation of organic gases and organic compounds at elevated temperatures, Adler and Boethe[32] determined the ratios of 2.23 ± 0.5% and 2.54 ± 0.4% for the alkanes and alkenes, respectively. In this research, using α-particle irradiation, the values of the ratio for the saturated hydrocarbons are between 2.4 and 2.5. Unsaturation increases the ratio about 0.25 and 0.4 unit for cyclohexene and benzene, respectively. It is interesting to note that carbon tetrachloride has the same ratio as methane.

The values of W_α/W_β can be calculated for three different molecular gases using these results and those previously published. The value obtained for *n*-hexane is identical with that obtained for the highest hydrocarbon previously reported, *n*-butane. Cyclohexane exhibits a value of 1.11 for this parameter, which is somewhat higher than for the corresponding straight-chain compound. The value for carbon tetrachloride is like that of methane.

Mixtures. Bortner and Hurst[23] have suggested eq 1 to relate the W value of a mixture to the W values of the pure compounds

$$\frac{1}{W_m} = \left(\frac{1}{W_1} - \frac{1}{W_2}\right)\left(\frac{P_1}{P_1 + aP_2}\right) + \frac{1}{W_2} \qquad (1)$$

where W_1 and W_2 are the W values of the first and second component, respectively, and P_1 and P_2 are the respective partial pressures. If it is assumed that the components absorb energy independently of each other, a is the ratio of the true stopping powers.

In considering mixtures in radiation chemistry, the simplifying assumption has frequently been made that the energy is initially absorbed by each component in proportion to its electron fraction. If the parameter a in the above expression is considered as an empirical weighting parameter with regard to energy partitioning, then a can be assumed to equal the ratio of the electron numbers, the second to the first component, and the expression $(P_1/(P_1 + aP_2))$ will be equivalent to the electron fraction. Then a plot of the reciprocal of the W value of the mixture *vs.* the electron fraction should yield a straight line, if energy is indeed partitioned in this manner.

(33) D. P. Stevenson, *Radiation Res.*, **10**, 610 (1959).

(34) R. L. Platzman, *Intern. J. Applied Radiation Isotopes*, **10**, 116 (1961).

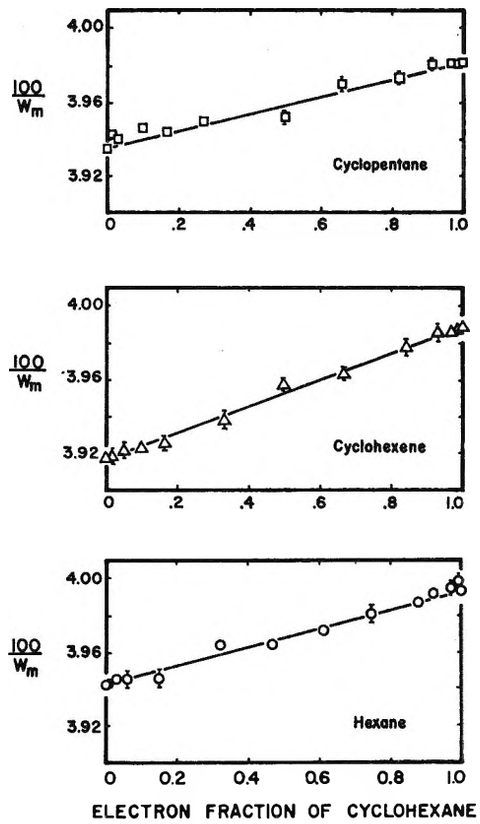

Figure 5. Variation in W value in various mixtures of cyclohexane.

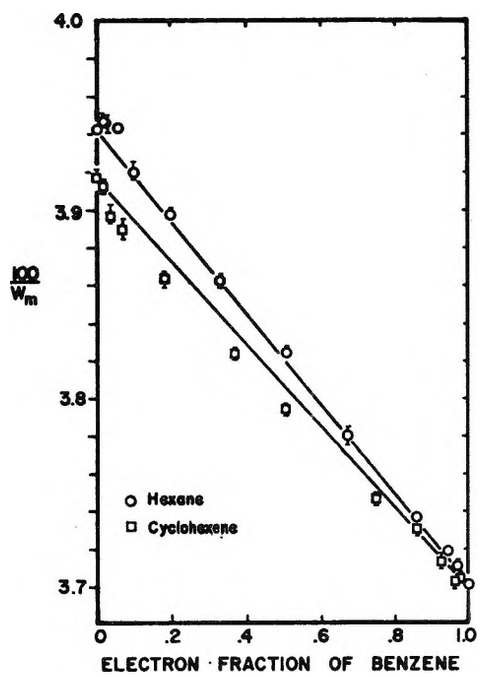

Figure 6. Variation in W value in mixtures of benzene with cyclohexane and n-hexane.

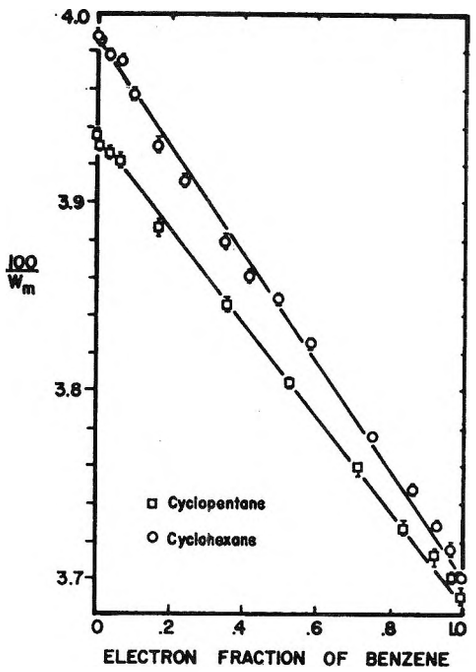

Figure 7. Variation in W value in mixtures of benzene with cyclopentane and cyclohexane.

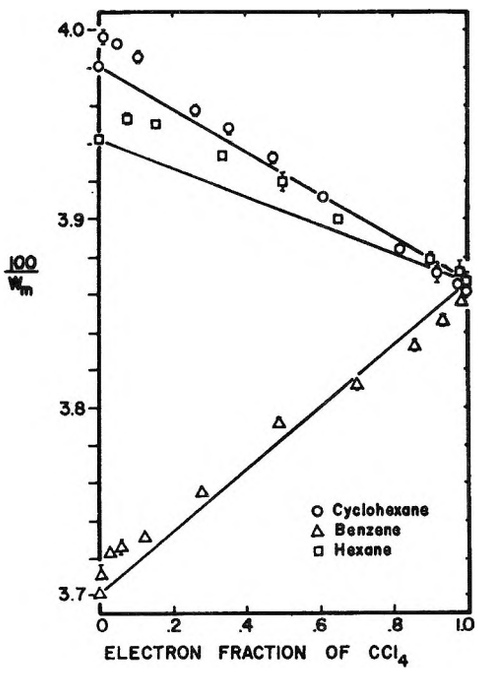

Figure 8. Variation in W value in various mixtures of carbon tetrachloride.

The mixture data, which represent averaged W values with the error bars indicating standard deviation, are present in Figures 5–8. These W values were also determined from plot C. In general, the values

found in this way are in good agreement with the values obtained by averaging.

Mixtures with Cyclohexane. Figure 5 displays the results obtained with mixtures of cyclohexane and the other hydrocarbons: hexane, cyclohexene, and cyclopentane.

Most data points for each mixture fall, within experimental error, on the straight line drawn between the W values of the pure components. Therefore, in mixtures of these hydrocarbons, the energy resulting in ionizing processes is proportional to the respective electron numbers of the components. There is no evidence of any strong physical interactions between the components leading to large amounts of excess ionization.

Mixtures with Benzene. Data for mixtures of benzene are displayed in Figures 6 and 7. In Figure 6, the mixtures of benzene with hexane and cyclohexene are presented. The hexane–benzene mixture data fall close to the predicted line, except for a slight deviation of decreasing W values with a small amount of benzene in hexane. The ionization potential of hexane is higher than that of benzene (10.48 and 9.24 ev, respectively). This small effect could be accounted for by the transfer of excitation energy from hexane to benzene. In the cyclohexene–benzene system in which both components have an ionization potential of about 9.24 ev, there is a more general deviation from the predicted relation. The magnitude of the deviation decreases as the benzene concentration increases. Considering an approximate 50–50 mixture, the percentage experimental error is about 0.08% and the deviation from the expected value is 0.39%. The W values are larger than predicted indicating that fewer ions are being formed. This would be the case if one of the components was absorbing in a disproportionate share of the energy, benzene in this case.

Mixtures of benzene with cyclopentane and cyclohexane are shown in Figure 7. Cyclopentane behaves essentially ideally; however, its ionization potential is larger and an effect similar to that in the benzene–hexane system is expected.

In general, the mixtures of benzene behaved in accordance with the electron fraction approximation. Although definite trends were indicated in some mixtures, a characteristic behavior cannot be assigned to benzene or the hydrocarbons with respect to specific physical interactions.

Mixtures with Carbon Tetrachloride. Figure 8 represents the data for the hydrocarbon–carbon tetrachloride mixtures. The deviations in these mixtures are the largest observed in this series of experiments. At an electron fraction of 0.03 carbon tetrachloride, the percentage deviations from the ideal are 0.36, 0.45, and 0.51% for hexane, cyclohexane, and benzene, respectively. The deviation is one which results in a lowered value of W, indicating an increase in ion production. Since the ionization potential of carbon tetrachloride is higher than those of the hydrocarbons, this enhancement cannot be simply due to transfer of energy from ordinary excited states of the hydrocarbon to the carbon tetrachloride molecule. However, the results can be explained if one assumes that superexcited states of the hydrocarbon are capable of transfering energy to the carbon tetrachloride, which subsequently ionizes. That such states do exist for the hydrocarbons has been suggested by Jesse.[35] In general, for the large hydrocarbons there exists a competition between ionization and dissociation; however, for methane, the predominant mode of energy loss is ionization. The same might be expected to be true for carbon tetrachloride, which shares many similarities[36] both in its spectroscopic properties and radiation chemistry. It is also noted that these two compounds have very similar values of W/I.

This phenomenon will occur if the lifetimes of the superexcited states are sufficiently long to allow transfer of energy. If the lifetime for autoionization of the superexcited states is about 10^{-14} sec, this should be sufficient since this is of the order of the collision frequency in systems at the pressures employed here.

In a preceding section of this paper, some characteristics of the ratio of the W value to the ionization potential were discussed. An explanation for the larger ratio for the higher hydrocarbons compared to methane is now evident. Energy residing in superexcited states that do not necessarily result in ions accounts for the increased ratios with the larger hydrocarbons. Methane's superexcited states preferentially ionize, and therefore, the ratio would be smaller.

There is also a small effect observed when a small per cent of hydrocarbon is added to carbon tetrachloride, in this case an increase in the W value or a decrease in the amount of apparent ionization.

This increase in W value can be explained by the formation of a species that has a smaller mobility than the chloride ion. Any chlorine atom in the system probably abstracts hydrogen.

$$Cl\cdot + RH \longrightarrow HCl + R\cdot$$

If the HCl participates in ion cluster formation similar to a reaction considered by Lee, *et al.*,[37] the mobility

(35) W. P. Jesse, *J. Chem. Phys.*, **41**, 2060 (1964).

(36) T. H. Chen, K. Y. Wong, and P. J. Johnston, *J. Phys. Chem.*, **64**, 1023 (1960).

of the ion cluster should be considerably smaller than that of the ion itself. Recently, mass spectrometer

$$e^-_{(HCl)} + CCl_4 \longrightarrow CCl_3\cdot + Cl^-_{(HCl)}$$

data have shown evidence of ion clustering in C_2H_2,[38] H_2O,[39] and NH_3.[40] The increased size and amount of ion clusters expected with increasing pressure[41] is substantiated in the enhanced deviations of the W values from the expected behavior at higher pressure.

Physical Interaction Related to the Radiation Chemistry of Hydrocarbon Mixtures. Ionization current measurements of organic mixtures should indicate some physical interactions which are important when considering the radiation chemistry of these systems. When a compound (solvent) is contaminated by a small amount of another compound, the solvent molecule may transfer energy to the contaminant resulting in an excessive amount of ionization, as occurs in the Jesse effect. The amount of energy transferred from the excited, metastable, or superexcited states must be larger than the ionization potential of the contaminant to result in excess ionization.

In these experiments, it should be emphasized that all the deviations from ideal behavior are less than 1%. However, contaminants in helium decrease the W value 30%, and hydrocarbons in argon decrease the W value at least 2 to 3%. Therefore, the small deviations observed in these experiments are not of the magnitude of the Jesse effect, although smaller effects would naturally be expected for molecular gases.

In the radiation chemistry of hydrocarbon mixtures, about 5% contamination of cyclohexane with benzene reduces the hydrogen yield approximately 20%. Slight deviations were noted in these mixtures, but they are not of the magnitude that would indicate an abundance of energy transfer processes leading to ionization.

Conclusions

The W values for a number of organic vapors at 80° have been determined.

Binary mixtures of these organic compounds were found to behave, to a first approximation, ideally in an ionization chamber experiment. The electron fraction approximation seems justified for these mixtures; that is, the initially absorbed energy leading to ionization is partitioned between the components on the basis of their electron fraction. Also, except for the case of carbon tetrachloride, no transfer of energy from excited species occurs that results in significant excess ionization. The decrease in product yield of hydrogen, from irradiated cyclohexane with a small amount of added benzene, and likewise from other such systems, cannot be explained by energy transfer from excited cyclohexane species to benzene molecules, which subsequently ionize.

The small increase in the W value when a small amount of the hydrocarbon is present in CCl_4 can be explained by the formation of a species having a small mobility, probably an ion cluster. In order to explain excessive ionization when a small amount of carbon tetrachloride was added to hydrocarbon, superexcited states were posulated to exist for the hydrocarbons.

The ionization currents of benzene exhibited, to a much smaller extent, those traits which were characteristic of the electronegative carbon tetrachloride. Thus, in the radiation chemistry of benzene and mixtures containing benzene, the physical interactions, electron attachment, and possibly dissociative electron attachment, may be important.

Acknowledgments. The authors are greatly indebted to Dr. G. S. Hurst and Mr. T. E. Bortner of the University of Kentucky and Dr. C. E. Klots of the Oak Ridge National Laboratory for advice and assistance in the design of the apparatus and for several stimulating discussions.

(37) R. A. Lee, R. S. Davidow, and D. A. Armstrong, *Can. J. Chem.*, **43**, 1906 (1964).

(38) A. M. Hogg and P. Kebarle, *J. Chem. Phys.*, **42**, 668 (1965).

(39) A. M. Hogg and P. Kebarle, *ibid.*, **42**, 798 (1965).

(40) A. M. Hogg and P. Kebarle, *ibid.*, **43**, 449 (1965).

(41) J. L. Magee and K. Funabashi, *Radiation Res.*, **10**, 622 (1959).

Electron Spin Resonance Studies on the Photolysis of Radicals Produced in Ethyl Mercaptan and Ethyl Disulfide by X-Irradiation[1]

by S. B. Milliken, K. Morgan, and R. H. Johnsen

Department of Chemistry, Florida State University, Tallahassee, Florida 32306 *(Received March 21, 1967)*

The esr spectra and photochemical properties of the radicals generated in ethyl mercaptan and ethyl disulfide by X-irradiation at 77°K have been studied. The initial products are postulated to be ion pairs with the charges localized on the sulfur atoms. Subsequent photolysis in the case of ethyl mercaptan results in the formation of the RS radical whose presence was previously postulated in liquid ethyl mercaptan.

Introduction

This study is concerned with the esr spectrum of irradiated ethyl mercaptan at 77°K before and after photolysis with ultraviolet light.

Evidence from the radiation chemistry of various organic systems appears to establish that ionizing radiation expels electrons in condensed media which are thermalized and migrate through the system by diffusion-like processes.[2] The electrons then may produce a variety of reactions by dissociative or attachment processes at room temperature, and at liquid nitrogen temperatures can be identified by virtue of their paramagnetic properties. After being expelled, they leave behind paramagnetic ions, or neutral radicals resulting from reactions of the parent ion and another molecule. The fate of the electron seems variously to depend on the extent of hydrogen bonding, the accessability of empty orbitals, and the presence of solutes which are able to react with electrons. Typical reactions are summarized below.

(1) Systems without Hydrogen Bonding[3,4]

$$RH \longrightarrow RH^+ + e^- \qquad (1a)$$

$$e^- + RX \longrightarrow R\cdot + X^- \quad \text{(if solute is present)} \qquad (1b)$$

(2) Systems with Hydrogen Bonding[5]

$$ROH \longrightarrow ROH^+ + e^- \qquad (2a)$$

$$e^- + n\text{ROH} \longrightarrow (ROH)_n^- \qquad (2b)$$

$$ROH^+ + ROH \longrightarrow R'\dot{C}HOH + ROH_2^+ \qquad (2c)$$

(3) Systems with Low-Lying Empty Orbitals[6]

$$RSSR \longrightarrow RSSR^+ + RSSR^- \qquad (3)$$

3-Methylpentane, which has been studied extensively by means of optical[3a] and esr[3b] spectroscopy, is representative of organic glasses without hydrogen bonding. The yield of trapped electrons is low in these systems, and unless electron scavengers are present, most of the electrons return promptly to the parent ion. Neutralization occurs and a hydrogen atom and a neutral radical are produced. When the electron is trapped or scavenged, the counterion is most often the paramagnetic parent positive ion as shown in reaction 1a. Dissociative attachment to an electron scavenger (*e.g.*, benzyl chloride) produces a radical and a nonparamagnetic negative ion as suggested by reaction 1b.

When hydrogen bonding is present as in the aliphatic alcohols, the electron is trapped in high yields. The parent positive ion undergoes reaction to produce a nonparamagnetic positive ion and a neutral free radical. Myron and Freeman[7] have suggested that the ion–mole-

(1) This research was supported in part by the U. S. Atomic Energy Commission under Contract AT-(40-1)-2001. This is AEC Document ORO-2001-6.

(2) M. R. Ronayne, J. P. Guarino, and W. H. Hamill, *Radiation Res.*, **17**, 379 (1962).

(3) (a) J. B. Gallivan and W. H. Hamill, *J. Chem. Phys.*, **44**, 1279 (1966); (b) K. Tsuji and F. Williams, *J. Am. Chem. Soc.*, **89**, 1526 (1967).

(4) J. B. Gallivan and W. H. Hamill, *Trans. Faraday Soc.*, **61**, 1 (1965).

(5) (a) R. S. Alger, T. H. Anderson, and L. A. Webb, *J. Chem. Phys.*, **30**, 695 (1959); (b) F. J. Dainton, G. A. Salmon, and J. Tepley, *Proc. Roy. Soc.* (London), **A286**, 27 (1965).

(6) D. C. Wallace, J. E. Hesse, and F. K. Truby, *J. Chem. Phys.*, **42**, 3845 (1965).

cule reaction is assisted by the hydrogen bonding; if so, the RCH–OH radical observed may well be preceded by an alkoxy radical. In any case, the neutral radical has been identified by the $n - 1$ lines characteristic of an electron localized on the hydrocarbon portion of the molecule indicating the detachment of a hydrogen from a carbon.[8] Slight further splitting by the hydroxyl hydrogen and the production of vicinal glycols by radiation suggests the removal of the hydrogen α to the oxygen. Evidence for the ROH_2^+ ion is circumstantial but convincing, resting upon actual observation of the species in high-pressure mass spectrometry,[9] the resistance of aldehydes to scavenging,[7] and thermochemical calculations.[10]

When only first-row elements are present, there are no low-lying vacant orbitals. The ejected electron can thus be expected to be delocalized over several molecules.[11] This should be true for both systems with and without hydrogen bonding, the only difference being that the trap appears deeper for the hydrogen-bonded system.[3,5]

Thus the electron is released from its trap by light of 16,000 A in 3-MP; 12,000 A in methyl tetrahydrofuran,[12] and 7000 A in ethanol.

When atoms are present which have vacant orbitals available which are relatively low in energy, the expelled electron becomes associated with a single molecule. The example shown here is an alkyl disulfide studied by Truby.[6] The spin-orbital interaction is apt not to be quenched, so that there is an anisotropy observed in the spectrum. The electron is usually localized on an atom containing the available orbitals.

In this laboratory some effort has been devoted to the study of alcohol systems with particular attention being paid to the effects of visible and ultraviolet photolysis of the radiation-produced radicals.[13–15] A study of the mercaptans seemed like a natural extension of this line of endeavor. Moreover, the above categorization of the chemical behavior of the electron would predict that the electron would behave more nearly like that in disulfides than in the alcohols, and the product yields should reflect that fact. In a separate study,[16] the yields of the chemical products were investigated.

Experimental Section

The ethyl mercaptan and ethyl disulfide used were the same as in the chemical study, and purification and handling techniques were identical. Samples were sealed in Thermosil tubes 3 mm in diameter for use in the esr spectrometer. Samples for optical studies were placed in ampoules with flattened sides made of the same type of quartz. The esr spectrometery was done in a Varian 4502 spectrometer. Optical spectra were taken on a Cary spectrometer with a special low-temperature sample holder. Irradiations were done using the Florida State 3-Mev Van de Graaff accelerator. Bleaching experiments were carried out with an A-H6 mercury arc lamp. The filters used have been described previously.[15] Doses were of the order of 10^{19} ev/g.

Discussion

The top spectrum of Figure 1 shows ethyl mercaptan immediately after irradiation; the bottom spectrum is the result of subsequent photolysis. The original X-irradiated sample is colored yellow-orange. This color is bleached by near-ultraviolet light but not visible light, and the sample becomes pale yellow or clear. The sample was photolyzed over a range of selected wavelengths from 6000 to 2500 A, and it was found that no change in the radical spectrum occurs above approxi-

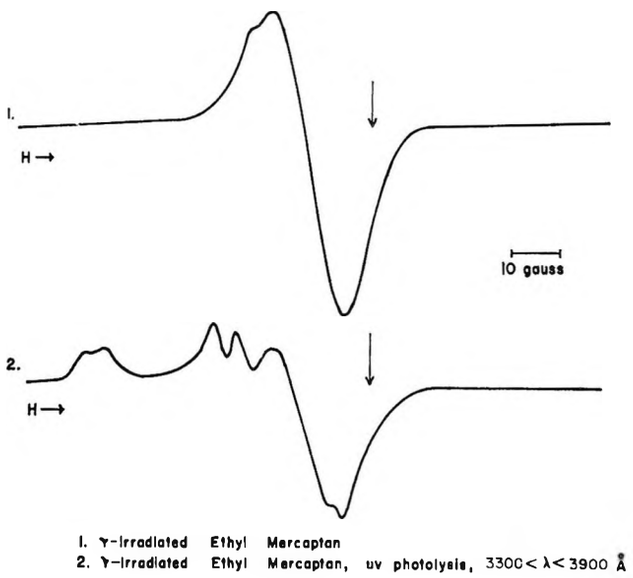

Figure 1. Esr spectra of X-irradiated and photolyzed ethyl mercaptan.

(7) J. J. J. Myron and G. R. Freeman, *Can. J. Chem.*, **43**, 1484 (1965).

(8) B. Smaller and M. Matheson, *J. Chem. Phys.*, **28**, 1169 (1958).

(9) K. R. Ryan, L. W. Sieck, and J. H. Futrell, *ibid.*, **41**, 111 (1964).

(10) J. Tebly, A. Habersbergerovan, and K. Vacek, *Collection Czech. Chem. Commun.*, **30**, 793 (1965).

(11) D. R. Smith and J. J. Pieroni, *Can. J. Chem.*, **43**, 876 (1965).

(12) M. R. Ronayne, J. P. Guarino, and W. H. Hamill, *J. Am. Chem. Soc.*, **85**, 384 (1963).

(13) R. H. Johnsen, *J. Phys. Chem.*, **63**, 2041 (1959).

(14) R. H. Johnsen and D. A. Becker, *ibid.*, **67**, 831 (1963).

(15) S. B. Milliken and R. H. Johnsen, *ibid.*, **71**, 2116 (1967).

(16) J. J. J. Myron and R. H. Johnsen, *ibid.*, **70**, 2951 (1966).

mately 3500 A. The arrow indicates $g = 2.003$, the value for the free electron. The g for the derivative crossover is equal to 2.012. Neither its value nor the concentration of the radical species changes measurably during photolysis. The concentration reflects a yield of 2–3 spins/100 ev. However, this value of the yield is most approximate due to the difficulties of integrating the anisotropic spectra. Both the g value and the estimated yield are based on the known values for these measurements in methanol.

The optical spectrum is shown in Figure 2. X-Irradiation produces the broad band centered around 4500 A. This band disappears with ultraviolet photolysis using light in the 3500-A region. It is noteworthy that light of wavelengths longer than 3500 A, and in particular in the wavelength region around 4500 A, does not affect the optical absorption of the sample. Both optical and esr absorptions disappear rapidly upon warming of the samples.

Because of the lack of structure, the photosensitive species is hard to identify. The bottom esr spectrum, on the other hand, resembles the spectrum of the alkyl sulfide obtained by Kurita and Gordy[17] upon the X-irradiation of cystine dihydrochloride modified as one might expect if its free electron were interacting with two protons instead of one. They irradiated their samples in both powdered and crystalline form. The spectrum of the irradiated crystal revealed three principal axes of the g tensor and a hyperfine doublet characteristic of splitting by a single hydrogen atom. A calculated spectrum consistent with the observed spectra and the nature of this hyperfine splitting suggested to them that the spin was centered on a sulfur atom which was not free to rotate and thus interacted with only one proton on the adjacent carbon atom. They found evidence for this hyperfine splitting in the spectrum of the amorphous solid; it is also apparent here in the glassy mercaptan. This similarity fairly well characterizes the radical produced by ultraviolet photolysis as the ethyl sulfide radical.

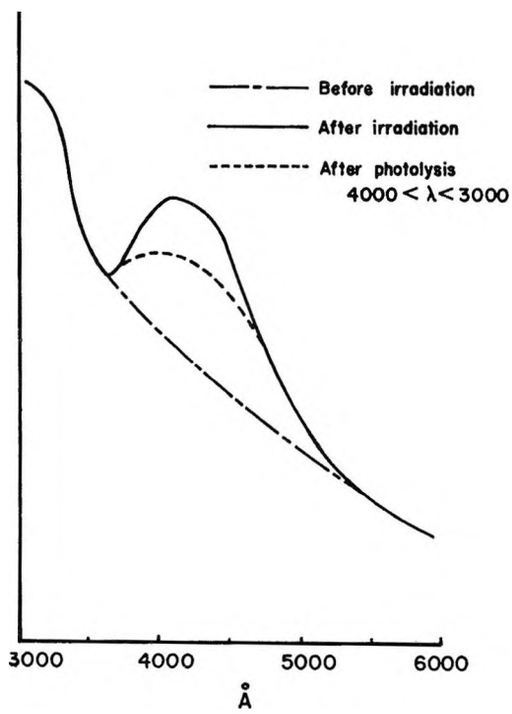

Figure 2. Absorption spectra of ethyl mercaptan before and after X-irradiation and following ultraviolet photolysis.

Characterization of the photosensitive precursor is more difficult. The mercaptan exhibits a limited amount of hydrogen bonding as well as low-lying vacant orbitals on the sulfur so that trapping of the electron can be expected either by reaction 2b or 3. The lack of resolvable hyperfine structure rules out a reaction analogous to (2c). A likely possibility is that the upper spectrum in Figure 1 is the result of the superposition of two signals, one from the positive parent and one from the negative ion formed by attachment of the electron to ethyl mercaptan. The spectra of irradiated ethyl disulfide and ethyl mercaptan are superposed in Figure 3. The similarity is quite marked except for a small shift in g (crossover) toward higher field.

The yields, when corrected for the electron fraction, are about the same for both systems. The g value for the derivative crossover is 2.017, in agreement with the values reported for ethyl disulfide in the literature.[6] Notice that g-(electron) $<$ g(mercaptan crossover) $<$ g(disulfide).

In Figure 4, the effects of photolysis on the esr spectrum of irradiated ethyl disulfide are shown. The wavelengths used are the same as those used for ethyl mercaptan. The solid line represents the spectrum immediately after radiolysis, the dotted curve is what remains after several hours of photolysis, after which there is no further change. The sample is initially dark green in color and is bleached by the action of the ultraviolet light. The arrow again indicates g for the free electron. The presence of the sulfide radical is indicated by the broad line on the low-field side of the spectrum. It is neither increased nor decreased by ultraviolet light. The dashed line spectrum is most probably a mixture of alkyl radicals not containing sulfur. It is unique for alkyl disulfides and is identical with those obtained by Truby,[6] who photolyzed the entire homologous series up through ten carbons. As sug-

(17) Y. Kurita and W. Gordy, *J. Chem. Phys.*, **34**, 282 (1961).

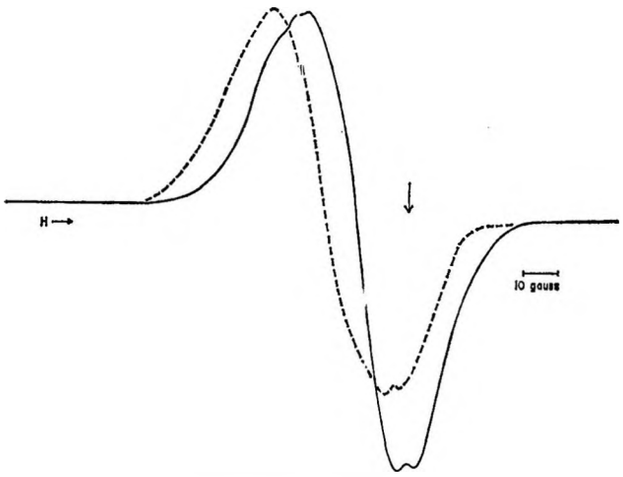

Figure 3. Comparison of X-irradiated ethyl mercaptan an ethyl disulfide spectra: ———, X-irradiated ethyl mercaptan; – – – –, X-irradiated ethyl disulfide.

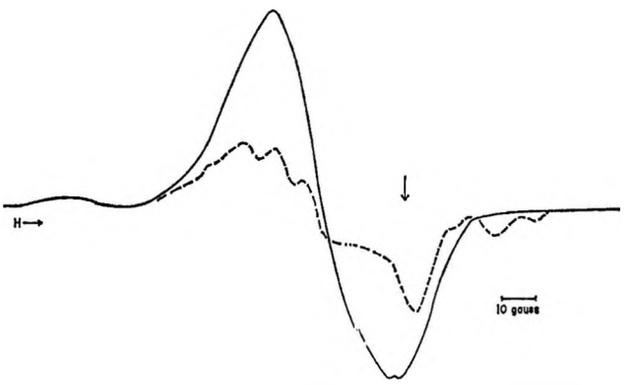

Figure 4. Esr spectra of X-irradiated and photolyzed ethyl disulfide: ———, X-irradiated ethyl disulfide; – – – –, X-irradiated ethyl disulfide, ultraviolet photolysis at 3600 A.

gested before, the initial spectrum is probably due to the presence of an ion pair. In contrast to the mercaptans, the only sulfur-containing radical seen after photolysis is that produced directly by the X-irradiation of the disulfide. The evidence for ion pairs was largely circumstantial. (1) When the solid was warmed slightly, there was no gradual decrease in concentration of the radicals as might be expected in the case of neutral radicals beginning to diffuse and react. (2) The addition of electron scavengers produced spectra characteristic of the reaction of the scavenger with the electron. (3) A change in frequencies from 9 to 35 Gcycles indicated anisotropy. In explaining the *k*-band spectrum, it was necessary to consider a distribution of orientations of the responsible radicals since it is a glass and not a crystal. In doing so, Truby found that an equal mixture of paramagnetic negative and positive ions could account for the line shape observed. His calculation was based on a positive ion with three principal axes in the *g* tensor, and the electron removed from an orbital shared by the two sulfur atoms. The negative ion seemed to be due to an unpaired electron occupying a d orbital on a sulfur atom, and had two principal axes.

At least some of this circumstantial evidence rests upon properties of disulfides sufficiently general to organic sulfur compounds to be true also for mercaptans. Certainly, the initial spectrum and the production of RS· radicals are analogous to phenomena observed in the disulfide case. Therefore, it seems reasonable that the initial spectrum in irradiated ethyl mercaptan results from an ion pair, and the sequence of events that follow is as shown below.

$$C_2H_5SH \rightsquigarrow C_2H_5SH^+ + e^-$$

$$e^- + C_2H_5SH \longrightarrow C_2H_5SH^-$$

$$C_2H_5SH^- \xrightarrow{h\nu} C_2H_5SH + e_m^-$$

$$e_m^- + C_2H_5SH^+ \longrightarrow C_2H_5S\cdot + H\cdot^*$$

$$H\cdot^* + C_2H_5SH \longrightarrow C_2H_5S\cdot + H_2$$

The electron is expelled from the molecule by the ionizing radiation as usual. Mercaptan is its own electron scavenger; the electron attaches to another mercaptan molecule, probably in a d orbital on the sulfur atom. The positive hole is also probably located on the sulfur atom in the parent molecule. Since the mercaptan is less hydrogen bonded than the alcohols, one does not expect the formation of a radical by abstraction of the α hydrogen atom by the positive ion as in reaction 2c. The SH group, furthermore, is rigidly held, leading to the observed anisotropy. Any hyperfine splitting is probably due to the hydrogen atom which is attached to the sulfur. The electron trap is deeper than in alcohol (of the order of 3–4 ev), as indicated by the shorter wavelength necessary to bleach the mercaptan. The effect of photolysis then, is simply to release the electron from its trap, permitting it to return to its parent ion and neutralize it. The resulting energy breaks a sulfur–hydrogen bond. In the case of the disulfide, the fragments are bulky and are caged; in the mercaptan, however, the smaller hydrogen atom escapes, and a significant concentration of RS· radicals is produced. The ultimate fate of the hydrogen atom is not known. However, since the radical concentration apparently does not diminish during photolysis, the hydrogen atom may be hot enough to abstract.

Acknowledgment. The assistance of Mr. D. Pritchett

in carrying out the radiolyses is gratefully acknowledged as well as the assistance received from the Florida State University Institute of Molecular Biophysics in the form of access to the esr spectrometer.

Densities and Apparent Molal Volumes of Molten Phosphoric Acid Solutions

by Ronald A. Munson and Michael E. Lazarus

General Electric Research and Development Center, Schenectady, New York *(Received March 13, 1967)*

The densities of a number of electrolyte solutions in phosphoric acid at 80° and a few at 150° are reported. Most of the 1–1 electrolytes investigated have apparent molal volumes which are quite close to the molar volume of phosphoric acid. This indicates that these electrolytes enter into the solvent structure with very little over-all electrostriction of the phosphoric acid. Apparent molal ionic volumes of a number of ions have been calculated on the basis of the assumption of equality of volumes of the lyonium and the lyate ions. It is suggested that this assumption is of value in comparing electrostrictive influences in different solvents.

The densities of ionic solutions may be used to obtain information concerning ion–solvent interactions. The apparent volume changes observed may result from general influences of the ion on the solvent structure or from the displacement of solvent equilibria. In phosphoric acid, two self-dissociative equilibria are of importance, both of which produce extensive ionization.[1,2]

$$2H_3PO_4 \rightleftharpoons H_4PO_4^+ + H_2PO_4^- \quad (1)$$

$$2H_3PO_4 \rightleftharpoons H_3O^+ + H_3P_2O_7^- \quad (2)$$

Experimental Section

Chemical Preparation. Phosphoric acid was prepared from analytical reagent 85% phosphoric acid by water removal under vacuum.[3] It was adjusted to 100.0% by the crystalline melting point technique used previously.[1] Sulfuric acid (100.0%) was prepared from analytical reagent fuming sulfuric acid and distilled water. A solution 19.0% by weight perchloric acid and 80.8% phosphoric acid was prepared at 120° by stirring analytical reagent phosphorus pentoxide with analytical reagent 70% perchloric acid. Lithium perchlorate was prepared by neutralizing lithium carbonate with analytical reagent perchloric acid. To remove the last trace of water, it was necessary to heat it to 300° just prior to use. It analyzed 92.9% (expected 93.5%) perchlorate. Lithium dihydrogen phosphate (99.0%) was also prepared from lithium carbonate. $Mg(H_2PO_4)_2$, which was prepared from magnesium oxide and phosphoric acid, contained 11.2% (expected 11.1%) magnesium. Reagent potassium bisulfate (100.1%) and potassium dihydrogen phosphate (99.4%), which were analyzed by acid–base titration, as well as the other salts, were stored in a vacuum desiccator at 100°. Solutions were made up by weight and all open manipulations were performed in a drybox furnished with dry N_2 and P_2O_5.

Procedure. The dilatometer (18 cc) was constructed from a small erlenmeyer flask into which was fitted by means of a ground-glass joint a graduated glass tube with a terminal constriction. The volume of the dilatometer was calibrated with doubly distilled water. Temperature in the oven remained constant to ±0.2°.

(1) R. A. Munson, *J. Phys. Chem.*, 68, 3374 (1964).
(2) R. A. Munson, *ibid.*, 69, 1761 (1965).
(3) *Inorg. Syn.*, 1, 101 (1960).

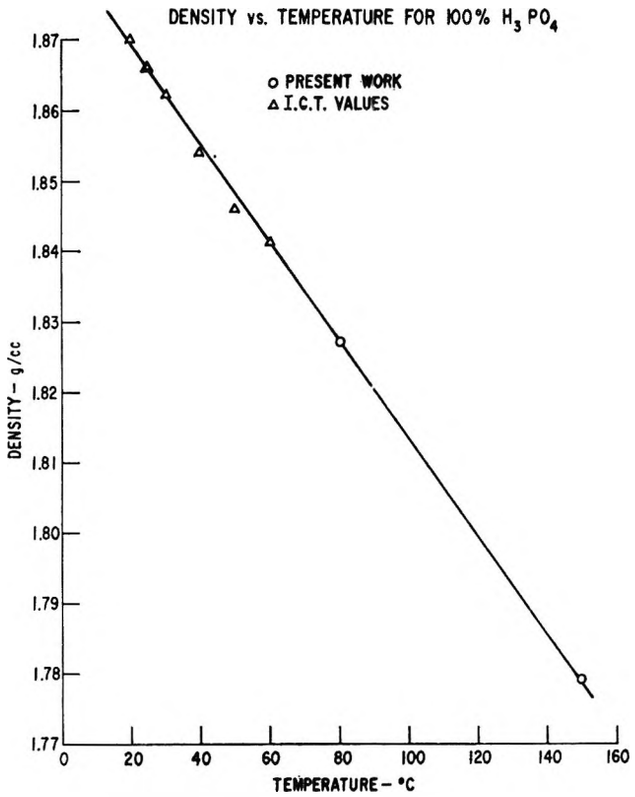

Figure 1. The density of 100.0% phosphoric acid. Data at the lower temperatures are from the "International Critical Tables."

The sample was allowed to reach chemical and temperature equilibrium in 2 hr during which the loss or gain of water was not found to be significant. Measurements were made at 80 and 150° in order to avoid the long wait required for the establishment of equilibrium 2 close to room temperature.

Results and Discussion

The density of phosphoric acid is a linear function of temperature (Figure 1) and may be approximated very closely by

$$\rho_t = \rho_{80} + 6.94 \times 10^{-4}(80 - t) \qquad (3)$$

where $\rho_{80} = 1.827$ is the density at 80° and t is the temperature in degrees centigrade. The densities in phosphoric acid solutions are very nearly linear functions of the solute concentrations to 0.4 m. Freezing point depression measurements indicate these solutes to be essentially fully dissociated.[1] Table I lists the limiting-density–concentration slope for a number of solutes. The apparent molal volumes were calculated by means of the expression

$$\phi_v = -\frac{10^3}{\rho_0^2}\frac{d\rho}{dX} + \frac{M_2}{\rho_0} \qquad (4)$$

Table I: Apparent Molal Volumes of Some Solutes in Phosphoric Acid at 80°

Solute	$d\rho/dX$, g $l.^{-1}$ m^{-1}	ϕ_v, cm^3 $mole^{-1}$
LiH_2PO_4	0.028	48.6
NaH_2PO_4	0.050	50.8
KH_2PO_4	0.054	57.8
$KHSO_4$	0.050	59.1
$LiClO_4$	0.022	51.8
$HClO_4$	0.001	54.7
H_2SO_4	−0.002	54.4
$Mg(H_2PO_4)_2$	0.108	87.1
H_2O	−0.025	17.4

where M_2 is the molecular weight of the solute, ρ_0 is the density of the pure solvent, and X is the molal concentration of the solute. Notice that for most solutes the apparent molal volume is very close to the molar volume of the phosphoric acid (53.6 cc $mole^{-1}$ at 80°) so that these electrolytes must fit into the phosphoric acid structure with very little over-all electrostriction. Figure 2 presents some of the data obtained. The straight lines are not lines of best fit but represent the density changes which would be expected if each mole of solute replaced one mole of phosphoric acid. Self-

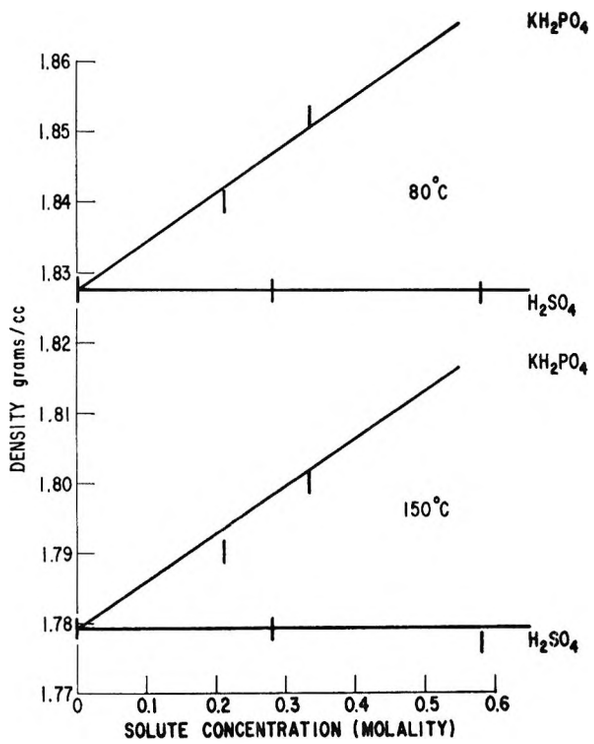

Figure 2. Density dependence on solute concentration for 100.0% phosphoric acid.

dissociation according to eq 1 and 2 is extensive enough so that the electrolyte concentrations used in these solutions are much smaller than the intrinsic ionic concentrations. The addition of 1 mole of base to phosphoric acid shifts the position of equilibrium 1 according to $MH_2PO_4 + {}^1/_2H_4PO_4^+ \rightarrow M^+ + H_3PO_4 + {}^1/_2H_2PO_4^-$. Similar equilibrium shifts occur in phosphoric acid solutions containing acid or water. The volume changes contributing to the apparent molal volume are

$$\phi_v^{(base)} = V_{M^{+n}} + n[V_{H_3PO_4} + {}^1/_2V_{H_2PO_4^-} - {}^1/_2V_{H_4PO_4^+}] \quad (5)$$

$$\phi_v^{(acid)} = V_{X^-} - {}^1/_2V_{H_4PO_4^+} - {}^1/_2V_{H_2PO_4^-} \quad (6)$$

$$\phi_v^{(H_2O)} = {}^1/_2[V_{H_3O^+} - V_{H_3P_2O_7^-}] + V_{H_3PO_4} + {}^1/_2[V_{H_2PO_4^-} - V_{H_4PO_4^+}] \quad (7)$$

Since the $H_2PO_4^-$ and the $H_4PO_4^+$ ions are derived from phosphoric acid by the addition or subtraction of only a proton they must be quite close to the same size, and as their charge magnitude is identical, they should have very similar electrostrictive influences on the solvent. It therefore is reasonable to set $V_{H_2PO_4^-}$ equal to $V_{H_4PO_4^+}$. Table II lists the apparent molal ionic volumes of a number of ions in phosphoric acid and in water[4] calculated using the equality of the apparent molal volumes of the lyonium and lyate ions. The general similarity of the data suggests that the principle of the equality of the volumes of the lyate and lyonium ions provides a rational basis for the comparison of ionic volumes in different solvents. From eq 7 only the difference between ionic volumes of the oxonium and the pyrophosphate ions can be obtained. However, if a reasonable value of -3 cm^3 mole^{-1} is assigned to the oxonium ion, then the volume obtained for the pyrophosphate monoanion (69 cm^3 mole^{-1}) is consistent with the expectation of a somewhat larger volume than that found for the other anions listed in Table II.

Table II: Apparent Molal Ionic Volumes

	Phosphoric acid at 80°, cm^3 mole^{-1}	Water at 25°, cm^3 mole^{-1}
Li^+	−5	−3.6
Na^+	−3	−4.1
K^+	4	6.1
Mg^{2+}	−20	−23.5
ClO_4^-	56	{45}[a]
HSO_4^-	55	
H_3O^+–$H_3P_2O_7^-$	−72	...
H_3O^+	...	−2.6

[a] Estimated.

(4) B. B. Owen and S. R. Brinkley, Jr., *Chem. Rev.*, **29**, 461 (1941)

The Influence of Ionic Solutes upon the Conductivity of Molten Phosphoric Acid

by Ronald A. Munson and Michael E. Lazarus

General Electric Research and Development Center, Schenectady, New York *(Received March 13, 1967)*

The electrical conductivity of phosphoric acid is believed to result from a protonic chain conduction mechanism since the high viscosity of the phosphoric acid effectively hinders the Stokesian or normal conduction. The introduction of an ionizing solute other than water into phosphoric acid results in a linear decrease in the conductivity of the phosphoric acid. The conductivity decrease is ascribed to a breaking of the hydrogen-bonded structure of the phosphoric acid by the ions which inhibits the formation of the structures necessary for proton jumps. A comparison of the conductivity decreases produced by acids and bases in phosphoric acid permits an estimation of the mobilities of the $H_4PO_4^+$ and $H_2PO_4^-$ ions. Activation energies for the proton-jump mobilities in phosphoric acid are very close to those for the proton-jump mechanism in water although the mobilities themselves are about a factor of 4 lower in phosphoric acid. The oxonium ion is anomalous in its influence on the conductivity of phosphoric acid and may itself participate to a limited extent in the protonic conduction.

Owing to the high viscosity (η_{25} = 178 cp) of molten 100% phosphoric acid, ordinary Stokesian migration of its ions is much too small to account for its remarkably high electrical conductivity (σ_{25} = 0.04596 ohm^{-1} cm^{-1}). Greenwood and Thompson[1] interpreted this as evidence for the presence of a protonic chain conduction mechanism utilizing the movement of $H_4PO_4^+$ or $H_2PO_4^-$ ions through the highly hydrogen-bonded structure. Indeed, they found that the transport number for potassium ion (which must conduct by Stokesian migration) was less than 0.002. The equilibria present in phosphoric acid may be represented by

$$2H_3PO_4 \rightleftharpoons H_4PO_4^+ + H_2PO_4^- \quad (1)$$

$$2H_3PO_4 \rightleftharpoons H_3O^+ + H_3P_2O_7^- \quad (2)$$

It is now believed that pyrophosphoric acid is essentially a monoprotic acid behaving as indicated in (2) although some additional protolysis cannot be ruled out. The equilibrium concentrations of these ions can be determined[2,3] from cryoscopic ($[H_3O^+]^\circ = [H_3P_2O_7^-]^\circ$ = 0.28 *m* at 38°) and electromotive force ($[H_4PO_4^+]^\circ = [H_2PO_4^-]^\circ$ = 0.50 *m* at 38°) measurements. From the temperature dependencies[2,3] we estimate $[H_3P_2O_7^-]^\circ$ = 0.39 *m* and $[H_4PO_4^+]^\circ$ = 0.51 *m* at 80° and $[H_4PO_4^+]^\circ$ = 0.58 *m* at 150°.

Experimental Section

The preparation of the phosphoric acid solutions has been described previously.[4] The conductivity of the phosphoric acid solutions was measured in either of two thin, sealable Pyrex conductivity cells of standard design which had been placed in a silicone oil constant-temperature bath. The cell constants, which were determined by standard methods,[5] were 92.23 and 223.56 cm^{-1} at 25° (92.18 and 223.45 cm^{-1} at 150°). Temperatures were established by the use of Beckmann thermometers, which had been standarized to ±0.005° with a National Bureau of Standards calibrated resistance thermometer. After pyrophosphate equilibrium had been reached the conductance was measured with a Jones bridge with Wagner earth at 1000 sec^{-1}.

(1) N. N. Greenwood and A. Thompson, *J. Chem. Soc.*, 3485 (1959).
(2) R. A. Munson, *J. Phys. Chem.*, **68**, 3374 (1964).
(3) R. A. Munson, *ibid.*, **69**, 1761 (1965).
(4) R. A. Munson and M. E. Lazarus, *ibid.*, **71**, 3242 (1967).
(5) G. Jones and B. C. Bradshaw, *J. Am. Chem. Soc.*, **55**, 1780 (1933).

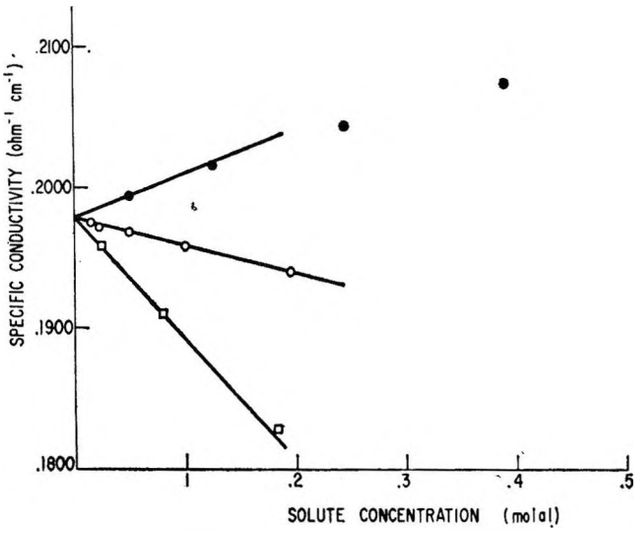

Figure 1. The specific conductivity of phosphoric acid solutions at 80°: ●, H_2O; ○, $HClO_4$; □, NH_4HSO_4.

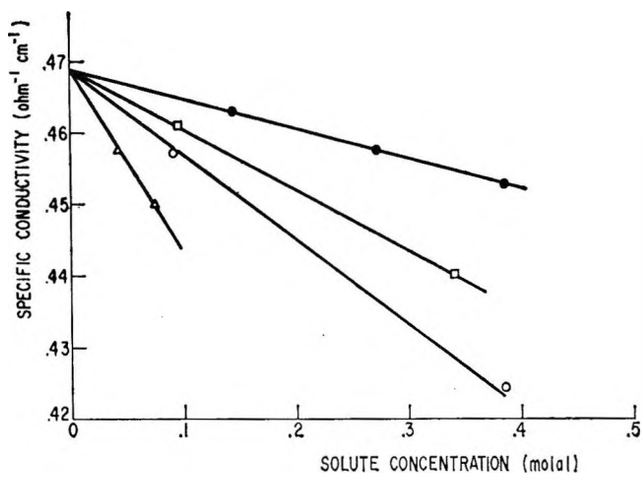

Figure 2. The specific conductivity of phosphoric acid solutions at 150°: ●, H_2SO_4; □, KH_2PO_4; ○, $KHSO_4$; △, $Mg(H_2PO_4)_2$.

Results

Figures 1 and 2 illustrate the effect of several solutes on the conductivity of phosphoric acid. Water is the only solute which has been found to increase the conductivity. The conductivity–concentration plots are all quite linear to at least 0.4 m for the solutes, except water, for which linearity disappears at lower concentrations. Table I lists the initial slopes of these linear plots.

Discussion

The intrinsic ionic concentrations in phosphoric acid are so large that even the extensions of the limiting laws for mobilities in dilute solutions to higher concentrations have limited significance. It seems more productive to concern ourselves with those factors which produce linear changes in the conductivity either by changing the concentrations of the conducting species or by acting on their mobilities by effectively withdrawing solvent molecules from the conduction process. Although higher power terms in the concentrations become predominant above 1 m, we shall not deal with them here. The addition to phosphoric acid of salts which cannot influence equilibria 1 or 2, and which do not effectively contribute to the conductivity themselves because of the high viscosity, can affect the conductivity (σ) by altering the charge carrier mobilities.

$$\sigma_{salt} = C_A^\circ\omega_A^\circ[1 + (s_a + s_c)x] + C_B^\circ\omega_B^\circ[1 + (s_a + s_c)x] \quad (3)$$

C_A°, ω_A°, C_B°, ω_B° are intrinsic charge concentrations and mobilities of $H_4PO_4^+$ and $H_2PO_4^-$, respectively, without solute addition; x is the molal concentration of added solute; and s_a and s_c represent the relative effect of the added anion and cation on the mobilities. In the case of acid or base addition to phosphoric acid, an additional term is required to represent the change in

$$\sigma_{acid} = C_A^\circ\omega_A^\circ\left[1 + \left(S_a + \frac{1}{2A^\circ}\right)x\right] + C_B^\circ\omega_B^\circ\left[1 + \left(S_a - \frac{1}{2A^\circ}\right)x\right] \quad (4)$$

$$\sigma_{base} = C_A^\circ\omega_A^\circ\left[1 + \left(S_c - \frac{1}{2A^\circ}\right)x\right] + C_B^\circ\omega_B^\circ\left[1 + \left(S_c + \frac{1}{2A^\circ}\right)x\right] \quad (5)$$

Table I: The Initial Slope of Conductivity *vs.* Solute Concentration in H_3PO_4

Solute	Slope at 80.00°, ohm^{-1} cm^{-1} m^{-1}	Slope at 150.00°, ohm^{-1} cm^{-1} m^{-1}
H_2SO_4	−0.0169	−0.0416
$HClO_4$	−0.0191	−0.0704
$(NH_4)_2HPO_4$	−0.0628[a]	...
KH_2PO_4	−0.0808	−0.0848
LiH_2PO_4	...	−0.0976
$Mg(H_2PO_4)_2$	...	−0.262
NH_4HSO_4	−0.0814	...
NH_4ClO_4	−0.0838	...
$KHSO_4$	−0.1013	−0.1172
$LiClO_4$	...	−0.1736
H_2O	0.0258	...

[a] Expressed for $NH_4H_2PO_4$.

charge carrier concentrations ($A^\circ = [H_4PO_4^+]^\circ = [H_2PO_4^-]^\circ$). When a and b are the relative effects of changes in $(H_4PO_4^+]$ and $[H_2PO_4^-]$ upon the charge carrier mobilities, then S_a [$= s_a + {}^1/_2(a - b)$] and S_c[$= s_c - {}^1/_2(a - b)$] are the relative changes in mobility per molal produced by acid and base addition. In eq 4 and 5, the cross quadratic terms with coefficients $S_a/2A^\circ$), etc., have been neglected since at low solute concentration these terms will be very small compared with the linear terms. The factor x/A° is halved in eq 4 and 5 since so long as x/A° is small, half the added acid will react with phosphoric acid to produce $H_4PO_4^+$ and half will react with $H_2PO_4^-$ to form phosphoric acid. If base is added, the reverse occurs.

From eq 3, 4, and 5, we find

$$\frac{d\sigma_{acid}}{dx} + \frac{d\sigma_{base}}{dx} = \sigma^\circ(S_a + S_c) = \sigma^\circ(s_a + s_c) = \frac{d\sigma_{salt}}{dx} \quad (6)$$

If the postulated linear influences on the phosphoric acid conductivity are independent of each other, then eq 6 requires that the sum of the conductivity slopes from acid and base addition must equal that obtained from the addition of their salt. Table II contains a comparison of such data, and the equality of eq 6 is verified within experimental error. The mechanism of proton-jump conduction consists of two steps.[6] The first is the orientation of the solvent molecules so that hydrogen bonds are formed through which a proton jump may occur. The second step, which is generally considered to be the fast process in water and is probably the fast one in phosphoric acid also since both processes involve a proton transfer between oxygen atoms, is the proton movement within the hydrogen bridge. The effect of the presence of ions on the mobility of the proton can be ascribed to a modification of the solvent structure so that the protons find themselves in an environment in which the hydrogen-bond orientations are, on the average, less conducive to proton transfer. It is not possible to separate the values given in Table II into anion (s_a) and cation (s_c) components. For the purposes of this paper, we will assume that the s_c's are very nearly equal to the s_a's for monovalent ions, which is quite reasonable if for a first approximation these effects are largely determined by the magnitude of the charge on the ion. It is of interest to compare the conductivity decreases with those expected from the presence of nonconducting spheres of volume v in a total volume V[7]

$$\sigma = \sigma^\circ\left(1 - \frac{3v}{2V}\right); \quad v = \frac{2 \times 10^3(s_a + s_c)}{3\rho^\circ N} \quad (7)$$

Table II: The Effect of the Addition of Acid and Base Compared with the Effect of the Addition of the Salt of the Acid and Base on the Conductivity of Phosphoric Acid

Salt added	Temp, °C	$\frac{1}{\sigma^\circ}\left(\frac{d\sigma_{acid}}{dx} + \frac{d\sigma_{base}}{dx}\right)$, m^{-1}	$\frac{1}{\sigma^\circ}\left(\frac{d\sigma_{salt}}{dx}\right)$, m^{-1}	v (eq 7), cm^3 $mole^{-1}$	Number of moles of H_3PO_4 excluded from conduction/mole of solute
$KHSO_4$	80	−0.494	−0.512	179	2.2
NH_4ClO_4	80	−0.414	−0.424	149	1.8
NH_4HSO_4	80	−0.403	−0.412	145	1.7
$KHSO_4$	150	−0.270	−0.250	97	0.7
$LiClO_4$	150	−0.358	−0.370	136	1.5

where ρ° is the phosphoric acid density and N is Avogadro's number. It has been suggested[4] that the addition of electrolytes to phosphoric acid does not result in appreciable electrostriction; nevertheless, on the average (Table II) 1 mole (at 150°) to 2 (at 80°) moles of phosphoric acid, in addition to the volume taken up by the electrolyte, are effectively removed from the conduction process by the presence of 1 mole of electrolyte. In sulfuric acid,[8] "solvation numbers" of the order of ten times larger were needed to account for the observed protonic mobility decreases. Since the intrinsic ionic concentration in sulfuric acid is some 30-fold smaller than it is in phosphoric acid, there is considerably less shielding of each ion by nearby ions which means that each ion in sulfuric acid has a much more sizeable volume of solvent molecules whose structure it can affect. To the extent that one may speak of ion atmospheres in these intrinsically concentrated ionic solutions, one may say that the radius of the ion atmosphere in sulfuric acid is relatively large, which gives each ion a sizeable sphere of influence on the average, whereas in phosphoric acid this radius is indeed small and correspondingly the number of solvent molecules whose orientation can be affected is much reduced.

By subtracting the slope of eq 5 from that of eq 4, we find

$$\frac{d\sigma_{acid}}{dx} - \frac{d\sigma_{base}}{dx} = \sigma^\circ\,(S_a - S_c) + C_A^\circ\omega_A^\circ\left(\frac{1}{A^\circ}\right) - C_B^\circ\omega_B^\circ\left(\frac{1}{A^\circ}\right) \quad (8)$$

(6) G. J. Hills, P. J. Ovenden, and D. R. Whitehouse, *Discussions Faraday Soc.*, **39**, 207 (1965), and references therein.

(7) J. W. Rayleigh, *Phil. Mag.*, **34**, 481 (1892).

(8) R. H. Flowers, R. J. Gillespie, E. A. Robinson, and C. Solomons, *J. Chem. Soc.*, 4327 (1960).

Since we are assuming that an ion's influence on the mobility is related only to the magnitude of its charge, then ($S_a \cong S_c$), the first term on the right-hand side of eq 8 can be neglected. In that case, eq 8 and 9 can be

$$\sigma^\circ = C_A^\circ \omega_A^\circ + C_B^\circ \omega_B^\circ \qquad (9)$$

solved simultaneously to determine the $H_4PO_4^+$ and $_2PO_4^-$ mobilities. The values so obtained, which are listed in Table III, are just about a factor of 4 lower than is found for hydroxyl and hydronium ion chain conduction mobilities in water at 80°. The lower protonic mobilities in phosphoric acid may result from the disruption of its hydrogen-bonded structure caused by its substantial self-ionization. The apparent "activation energy" for protonic mobility in phosphoric acid is 1.2 kcal mole^{-1} for $H_4PO_4^+$ and 1.6 kcal mole^{-1} for $H_2PO_4^-$. These values are close to those found in liquid water.[9] As in other protonic conductors, the movement of positive charge takes place with greater ease than that of negative charge (*i.e.*, $\omega_A^\circ > \omega_B^\circ$).

Table III: Protonic Mobilities in Phosphoric Acid

Electrolytes employed	Temp, °C	ω_A°, cm^2 v^{-1} sec^{-1}	ω_B°, cm^2 v^{-1} sec^{-1}
H_2SO_4, KH_2PO_4	80	1.28×10^{-3}	0.92×10^{-3}
$HClO_4$, $NH_4H_2PO_4$	80	1.23×10^{-3}	0.98×10^{-3}
H_2SO_4, KH_2PO_4	150	2.48×10^{-3}	2.23×10^{-3}
$HClO_4$, LiH_2PO_4	150	2.46×10^{-3}	2.25×10^{-3}

In the exceptional case of the $H_3P_2O_7^-$ and the oxonium ion, it turns out that separate s_a and s_c values can be obtained. From the decrease in conductivity which occurs when orthophosphoric acid, which initially contains no pyrophosphate, self-dissociates to establish equilibrium 2, we find[3] $s_{H_3P_2O_7^-} + s_{H_3O^+} = -0.235$; from the addition of water to equilibrated phosphoric acid (Table I) we find $^1/_2(-s_{H_3P_2O_7^-} + s_{H_3O^+}) = 0.0258/0.198 = 0.130\ m^{-1}$. At 80° then, $s_{H_3P_2O_7^-} = -0.248$ and $s_{H_3O^+} = 0.013$. The s value for the pyrophosphate is about half the ($S_a + S_c$) values listed in Table II, so that its influence upon the protonic mobility is in line with what has been suggested above, namely that anions and cations of the same charge have nearly the same influence on the mobility. Oxonium ion, H_3O^+, is unusual in that it appears to increase the conductivity slightly. Its presence may tend to facilitate proton jumps or it may take part in the conduction process itself, although to a much more limited degree than $H_4PO_4^+$ and $H_2PO_4^-$. A similar facilitation of proton conduction by the oxonium ion was found in sulfuric acid.[8]

(9) E. U. Franck, D. Hartmann, and F. Hensel, *Discussions Faraday Soc.*, **39**, 200 (1965).

Pure Quadrupole Resonance of Iodine in Ammonium, Rubidium, and Cesium Triiodides

by Akinobu Sasane, Daiyu Nakamura, and Masaji Kubo

Department of Chemistry, Nagoya University, Chikusa, Nagoya, Japan (*Received March 14, 1967*)

Pure quadrupole resonance studies have been made on iodine in ammonium, rubidium, and cesium triiodides at various temperatures. Three ν_1 and two ν_2 frequencies were observed indicating the existence of three kinds of nonequivalent iodine atoms in crystals. The observed frequencies were assigned to three kinds of nonequivalent iodine atoms as revealed by X-ray analysis. The charges on different iodine atoms in I_3^- were evaluated and interpreted in terms of resonance among various electronic structures. Slight anomalies found for ammonium triiodide are attributable to the formation of hydrogen bonds between ammonium ions and terminal iodine atoms carrying a negative fractional charge.

Introduction

Although it had been known for a long time that iodine dissolves in an aqueous solution of alkali iodides to form I_3^- ions, the geometric structure of the ions was determined for the first time in 1935 by Mooney, who carried out X-ray analysis on ammonium triiodide.[1] The I_3^- ion was found to be almost linear, the two I–I distances being different from each other by about 0.3 A. The electronic state of this ion has been a subject of considerable dispute. Since both a molecular iodine and an iodine ion have completed octets, the formation of an additional covalent bond requires at least one orbital of higher energy. Kimball[2] considered the 5d or the 6s orbital for the bivalency of the central iodine atom (sp or pd hybridization), while Pauling[3] and others[4] interpreted the linear structure of this ion in terms of the trigonal-bipyramidal orbitals of the central atom (sp^3d hybridization). On the other hand, Pimentel[5] carried out a simple molecular orbital calculation and explained the bonding in the triiodide ion in terms of the $p\sigma$ orbitals without introducing higher atomic orbitals. The present investigation has been undertaken in order to determine the charge distribution in an I_3^- ion by the observation of pure quadrupole resonance frequencies and to discuss the electronic structure of this ion.

Experimental Section

Apparatus. Two quadrupole resonance spectrometers already described[6] were employed for the determination of the pure quadrupole resonance frequencies of iodine. A self-quenching parallel-line superregenerative spectrometer was used for recording frequencies ranging over 70–300 Mc/sec, while the frequency range of 300–600 Mc/sec was covered by means of an externally quenched superregenerative spectrometer equipped with a Lecher line resonator. Resonance frequencies were determined at room, Dry Ice, and liquid nitrogen temperatures. Additional measurements were performed at intervals of a few degrees between −110 and 120° for ammonium triiodide showing an anomalous temperature dependence of resonance frequencies.

Materials. Equimolar amounts of ammonium iodide and iodine were dissolved in a small quantity of water. The solution was left to stand over phosphorus pentoxide in a desiccator. The crystals of ammonium triiodide were filtered off, washed with dilute hydriodic acid, and dried. Rubidium and cesium triiodides were prepared in a similar manner from rubidium and cesium iodides, respectively. For the identification of the samples, they were decomposed with

(1) R. C. L. Mooney, *Z. Krist.*, **90**, 143 (1935).

(2) G. E. Kimball, *J. Chem. Phys.*, **8**, 188 (1940).

(3) L. Pauling, "The Nature of the Chemical Bond," 2nd ed, Cornell University Press, Ithaca, N. Y., 1948, p 111.

(4) E. Cartmell and G. W. A. Fowles, "Valency and Molecular Structure," Butterworth and Co. Ltd., London, 1956, p 177.

(5) G. C. Pimentel, *J. Chem. Phys.*, **19**, 446 (1951).

(6) D. Nakamura, Y. Kurita, K. Ito, and M. Kubo, *J. Am. Chem. Soc.*, **82**, 5783 (1960).

sulfurous acid. The resulting solutions were neutralized with sodium hydroxide solution and subjected to the determination of iodine by the Volhard method. *Anal.* Calcd for NH_4I_3: I, 96.5. Found: I, 95.9. Calcd for RbI_3: I, 81.7. Found: I, 81.5. Calcd for CsI_3: I, 74.1. Found: I, 72.5.

Results

As shown in Table I, each compound gives rise to five absorption lines in the frequency range of 70–600 Mc/sec at all temperatures studied. The resonance frequencies of rubidium triiodide agree fairly well with the corresponding frequencies of cesium triiodide, whereas the observed frequencies of ammonium triiodide do not show even approximate agreement with those of the foregoing two compounds except for a line at 366–369 Mc/sec. This is discussed below in connection with the anomalous temperature variation of resonance frequencies of ammonium triiodide.

Discussion

Resonance Frequencies and Crystal Structure. Because ^{127}I has a nuclear spin equal to $^5/_2$ and yields ν_1 and ν_2, the appearance of five resonance lines indicates that at least three kinds of nonequivalent iodine atoms exist in each crystal and suggests that another line should appear in a frequency range outside the present observation. The fact that the five resonance lines are distributed over a fairly wide frequency range leads to a conclusion that the quadrupole coupling constants for the three sets of nonequivalent iodine atoms are different from one another to a considerable extent. Accordingly, it is presumed that the three kinds of iodine atoms are chemically nonequivalent[7] in agreement with the results derived from X-ray crystal analysis.[1,8]

Cesium triiodide forms orthorhombic crystals belonging to the space group Pmcn.[8] The crystals consist of cesium ions and I_3^- ions, all of which are crystallographically equivalent. Each I_3^- ion is almost linear, the valency angle $\angle$III being equal to 176.3°. Unlike an ICl_2^- ion,[9] an I_3^- ion is asymmetric, the two end iodine atoms, I_a and I_b, being separated from the central iodine atom, I_c, by 3.03 and 2.83 A, respectively. Ammonium triiodide crystals are known to be isomorphous with those of cesium triiodide and to have I_3^- ions similar to those in the cesium compound as crystal units.[1] Since no X-ray crystal analysis has been carried out on rubidium triiodide, X-ray powder patterns were taken in order to confirm the isomorphism of this compound with cesium and ammonium triiodides and to determine the lattice constants. Measurements were made by means of a self-recording X-ray diffractometer from Toshiba Co. (Model ADG 101) using the Cu Kα line. A goniometer was calibrated with a standard sample of silicon. Owing to the low symmetry of the crystal, diffraction through large angles gave rise to the overlap of two lines or more. Therefore, nine nonoverlapping lines were chosen below $2\theta = 34°$ to evaluate approximate lattice constants, the Miller indices of diffraction lines being determined with the aid of the diffraction patterns of cesium triiodide. The lattice constants thus obtained were refined by incorporating two additional nonoverlapping lines at $2\theta = 47.17$ and 55.27°. The refined values for the lattice constants, $a = 6.65$, $b = 9.71$, and $c = 10.88$ A, which are accurate within ±0.05 A, are of reasonable magnitude in comparison with those of cesium and ammonium triiodides.

Assignment of Resonance Frequencies. Five resonance frequencies observed for each compound at various

Table I: Pure Quadrupole Resonance Frequencies of ^{127}I in RI_3 (R = NH_4, Rb, Cs)

Compd		Temp, °C	Frequency, Mc/sec ν_1	Frequency, Mc/sec ν_2
NH_4I_3	a	23	87.34 ± 0.03	172.21 ± 0.06
		−80	76.86 ± 0.03	150.99 ± 0.06
		Liquid N_2	70.55 ± 0.01	138.07 ± 0.06
	b	21	239.2 ± 0.1	475.86 ± 0.03
		−79	252.0 ± 0.1	499.80 ± 0.03
		Liquid N_2	265.1 ± 0.1	515.10 ± 0.03
	c	29	366.21 ± 0.02	732.13 ± 0.02[a]
		−64	367.42 ± 0.02	
		Liquid N_2	368.81 ± 0.02	
RbI_3	a	29	113.99 ± 0.04	227.1 ± 0.1
		−65	115.19 ± 0.04	229.4 ± 0.1
		Liquid N_2	116.51 ± 0.04	232.1 ± 0.1
	b	23	217.08 ± 0.08	432.54 ± 0.02
		−65	217.71 ± 0.08	433.65 ± 0.02
		Liquid N_2	218.28 ± 0.08	434.66 ± 0.02
	c	29	367.60 ± 0.02	
		−67	368.94 ± 0.02	
		Liquid N_2	369.85 ± 0.02	
CsI_3	a	28	119.48 ± 0.04	238.8 ± 0.1
		−68	121.19 ± 0.04	241.9 ± 0.1
		Liquid N_2	122.90 ± 0.04	245.7 ± 0.1
	b	23	214.62 ± 0.08	428.63 ± 0.02
		−67	214.92 ± 0.08	429.46 ± 0.02
		Liquid N_2	215.89 ± 0.08	430.86 ± 0.02
	c	29	368.21 ± 0.02	
		−75	369.70 ± 0.02	
		Liquid N_2	371.63 ± 0.02	

[a] Observed at 25° by Kojima, *et al.*, ref 10.

(7) T. P. Das and E. L. Hahn, "Solid State Physics," Supplement 1, Academic Press, Inc., New York, N. Y., 1958, p 98.

(8) H. A. Tasman and K. H. Boswijk, *Acta Cryst.*, **8**, 59 (1955).

(9) R. C. L. Mooney, *Z. Krist.*, **100**, 519 (1939).

temperatures were assigned to two sets of ν_1 and ν_2 and an additional ν_1 frequency as shown in Table I for the following reasons.

Kojima, *et al.*,[10] have studied the pure quadrupole resonance of ammonium triiodide at 25° and observed two frequencies at 366.23 and 732.13 Mc/sec. The former coincides excellently with the second highest frequency detected by the present authors, whereas the latter is beyond the range of their investigation. Among the six lines, that of the lowest frequency is surely ν_1. The corresponding ν_2 is required to satisfy the theoretical relation, $2\nu_1 \geq \nu_2$. Accordingly, the line of the second-lowest frequency is unequivocally assigned to this ν_2. Then the third line must be interpreted as ν_1, while the line of the highest frequency surely represents ν_2. The fourth and the fifth lines were assigned, respectively, to ν_1 corresponding to the ν_2 frequency of the last line and ν_2 corresponding to the ν_1 frequency of the third line. Although an alternative assignment is possible on the basis of the aforementioned theoretical requirement alone, it can be ruled out for the following reason. In view of the almost linear structure of an I_3^- ion, the arrangement of four neighboring cations around each of the terminal iodine atoms, and a large field gradient q_z at the central iodine atom, it is unreasonable that the asymmetry parameter amounts to as high as 50.2–50.8% as it does if the alternative assignment is made.

The resonance lines of rubidium and cesium triiodides were interpreted in a similar manner. If one dares to make assignments different from those shown in Table I, the theoretical relation, $2\nu_1 \geq \nu_2$ is violated or the asymmetry parameters vary among different compounds in an inexplicable manner and become too large (for instance 37%) to be of reasonable magnitudes in view of the fact that even bridge iodine atoms in Al_2I_6[11,12] and Ga_2I_6[12] show asymmetry parameters ranging in 18–24%.

Since three ν_1 frequencies and the corresponding ν_2 frequencies have been determined, they should be correlated with three kinds of nonequivalent iodine atoms in crystals. The X-ray analysis[1,8] has shown that the I_b–I_c, distance (2.82 A in NH_4I_3 and 2.83 A in CsI_3) is fairly close to the internuclear distance 2.70 A of an iodine molecule in crystals,[13] whereas the I_a–I_c distance (3.10 A in NH_4I_3 and 3.03 A in CsI_3) is longer. As an approximation, let I_3^- ion be presumed to be formed of an iodine molecule and an iodine ion[14] approaching the molecule along the molecular axis, thereby polarizing the molecule to stabilize the system by electrostatic interactions.[15,16] Then it is expected that I_a bears the largest negative charge, I_b is charged to a lesser extent, and I_c has a positive fractional net charge. This qualitative prediction is supported by the fact that in the crystals of cesium triiodide, each I_a atom is surrounded by four cesium ions with a mean separation equal to 3.82 A, whereas each I_b atom has four neighboring cesium ions separated by 4.12 A on the average, the closer distance suggesting the presence of a stronger attractive center having a greater negative net charge. On the other hand, an I_c atom has only two cations in its vicinity at a distance of 4.10 A. Accordingly, the three ν_1 frequencies are attributable to I_a, I_b, and I_c in the order of increasing frequency.

Quadrupole Coupling Constant and Asymmetry Parameter. From ν_1 and ν_2, the quadrupole coupling con-

Table II: Quadrupole Coupling Constants and Asymmetry Parameters of ^{127}I in RI_3 (R = NH_4, Rb, Cs)

Compd		Temp, °C	eQq, Mc/sec	η
NH_4I_3	a	23	575.4 ± 0.4	0.105 ± 0.003
		−80	504.8 ± 0.2	0.118 ± 0.003
		Liquid N_2	466.8 ± 0.3	0.130 ± 0.003
	b	21	1587.5 ± 0.4	0.064 ± 0.003
		−79	1668.3 ± 0.3	0.080 ± 0.003
		Liquid N_2	1725.0 ± 0.3	0.151 ± 0.002
	c	29	2441.4 ± 0.2	0.018 (25°)
		−64	2449.5 ± 0.2	
		Liquid N_2	2458.7 ± 0.2	
RbI_3	a	29	757.5 ± 0.3	0.055 ± 0.006
		−65	765.1 ± 0.3	0.058 ± 0.006
		Liquid N_2	774.2 ± 0.3	0.056 ± 0.006
	b	23	1442.6 ± 0.2	0.054 ± 0.003
		−65	1446.5 ± 0.3	0.056 ± 0.003
		Liquid N_2	1449.8 ± 0.3	0.058 ± 0.003
	c	29	2450.7 ± 0.2	
		−67	2459.6 ± 0.2	
		Liquid N_2	2465.7 ± 0.2	
CsI_3	a	28	796.0 ± 0.4	0.02 ± 0.02
		−68	806.6 ± 0.4	0.037 ± 0.010
		Liquid N_2	819.0 ± 0.5	0.02 ± 0.02
	b	23	1429.5 ± 0.6	0.034 ± 0.005
		−67	1431.8 ± 0.6	0.026 ± 0.020
		Liquid N_2	1436.6 ± 0.4	0.041 ± 0.004
	c	29	2454.7 ± 0.2	
		−75	2464.7 ± 0.2	
		Liquid N_2	2477.5 ± 0.2	

(10) S. Kojima, A. Shimauchi, S. Hagiwara, and Y. Abe, *J. Phys. Soc. Japan*, **10**, 930 (1955).

(11) S. Hagiwara, K. Kato, Y. Abe, and M. Minematsu, *ibid.*, **12**, 1166 (1957).

(12) S. L. Segel and R. G. Barnes, *J. Chem. Phys.*, **25**, 578 (1956).

(13) P. M. Harris, E. Mack, and F. C. Blake, *J. Am. Chem. Soc.*, **50**, 1583 (1928).

(14) R. J. Hach and R. E. Rundle, *ibid.*, **73**, 4321 (1951).

(15) R. C. L. M. Slater, *Acta Cryst.*, **12**, 187 (1959).

(16) J. C. Slater, *ibid.*, **12**, 197 (1959).

stant eQq and the asymmetry parameter η were evaluated by use of Livingston and Zeldes' table.[17] Since ν_2^c was not observed for rubidium and cesium triiodides, the quadrupole coupling constants were calculated assuming that $\eta = 0$. This does not seem to cause any serious errors, because the asymmetry parameter observed for ammonium triiodide at room temperature is very small. The results are shown in Table II.

For both I_a and I_b (data are missing for I_c), the observed asymmetry parameter decreases progressively in the order of ammonium, rubidium, and cesium triiodides. This suggests that the field asymmetry originates from the field gradient[18] due to external ionic charges distributed in a crystal rather than to charge distribution inherent in an I_3^- ion such as due to the double-bond character of the I–I bond.

The quadrupole coupling constants of I_a and I_b of ammonium triiodide exhibit a marked temperature dependence, whereas that of I_c shows a small negative temperature coefficient characteristic of normal temperature dependence. This rather anomalous behavior is indicative of the existence of hydrogen bonding between ammonium ions and terminal iodine atoms. Accordingly, the quadrupole coupling constant of iodine in ammonium triiodide must be discussed with some reservation for the elucidation of the charge distribution in an isolated I_3^- ion.

Charge Distribution in an I_3^- Ion. The quadrupole coupling constants of I_a and I_b are smaller than the quadrupole coupling constant of atomic ^{127}I equal to 2292.7 Mc/sec,[19] indicating that the terminal iodine atoms are negatively charged.

According to Dailey and Townes,[20] the quadrupole coupling constant of a negatively charged halogen atom can be related to the ionic character i of the bond involving the atom by

$$eQq = (1 - s + d)(1 - i)eQq_{atom} \quad (1)$$

where s and d are the extents of s and d character, respectively, of the bonding orbital of the halogen and eQq_{atom} is the atomic quadrupole coupling constant of the halogen. Itoh and Kambe[21] have analyzed the line shape of quadrupole resonance line of iodine molecules and estimated the extents of s and d character as $s = 0.22$ and $d = 0.33$. In view of the lack of data for the I_3^- ion and in anticipation of the partial cancellation of d with s, let $s - d$ be ignored in comparison with unity. Then one has

$$|eQq| = (1 - i)|eQq_{atom}| \quad (2)$$

because the sign is immaterial in pure quadrupole spectroscopy.

From the observed quadrupole coupling constants at liquid nitrogen temperature, the ionic character i was calculated by use of eq 2 for I_a and I_b. Table III shows net charges on these iodine atoms.

Table III: Charge Distribution in I_3^-

Compd	Charge on iodine atoms, e		
	I_a	I_b	I_c
NH_4I_3	−0.80	−0.25	+0.05
RbI_3	−0.66	−0.37	+0.06
CsI_3	−0.64	−0.37	+0.06

The increase of the quadrupole coupling constant of I_c over $|eQq_{atom}|$ suggests that the central iodine atom carries a positive net charge. An alternative explanation that the net charge is negative but that the d character of the bonding orbitals of the central iodine atom is high and the ionic character is low so that $(1 - s + d)(1 - i) > 1$ (see eq 1) is ruled out, because the absolute value of the sum of negative net charges on I_a and I_b is greater than e.

For positively ionic halogens, Dailey and Townes[20] gave the following relation

$$eQq = [(1 - s + d)(1 - i) + 2(1 + \epsilon)i]eQq_{atom} \quad (3)$$

The second term in square brackets takes into account the contraction of p orbitals in partially positive halogen atoms, the empirical constant ϵ being 0.12 for iodine. Disregarding $s - d$, one is led to

$$|eQq| = (1 + i + 2\epsilon i)|eQq_{atom}| \quad (4)$$

The ionic character of the central iodine atom I_c was calculated by use of eq 4 and the net charge on I_c is shown in Table III. The positive fractional charge on the central iodine atom is contradictory with the electronic configuration in which the central iodine ion uses the trigonal-bipyramidal orbitals with three sets of lone pairs of electrons occupying the equatorial positions, because it is based on an electronic structure, $I–I^-–I$ having a negative charge on the central atom.

The sum of three charges on I_a, I_b, and I_c is $-1.00e$ for ammonium triiodide, $-0.97e$ for rubidium triiodide, and $-0.95e$ for cesium triiodide, in good agree-

(17) R. Livingston and H. Zeldes, "Table of Eigenvalues for Pure Quadrupole Spectra, Spin 5/2," ONRL Report 1913, Oak Ridge National Laboratory, Oak Ridge, Tenn., 1955.

(18) R. Ikeda, A. Sasane, D. Nakamura, and M. Kubo, *J. Phys. Chem.*, **70**, 2926 (1966).

(19) V. Jaccarino, J. G. King, R. A. Satten, and H. H. Stroke, *Phys. Rev.*, **94**, 1798 (1954).

(20) B. P. Dailey and C. H. Townes, *J. Chem. Phys.*, **23**, 118 (1955).

(21) T. Itoh and K. Kambe, *J. Phys. Soc. Japan*, **12**, 763 (1957).

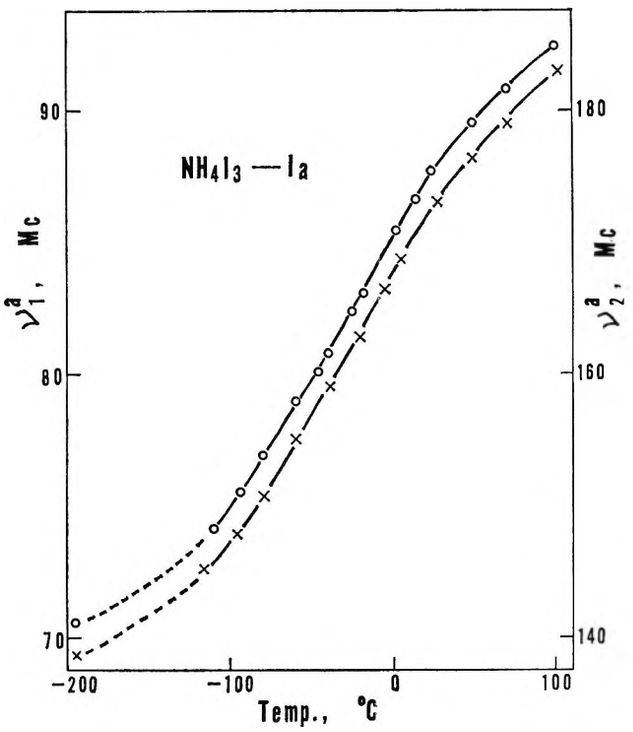

Figure 1. The temperature dependence of the ν_1^a (circles) and ν_2^a (crosses) resonance frequencies of ammonium triiodide.

ment with the theoretical value of $-e$, indicating the adequacy of the present calculations. However, the perfect agreement obtained for ammonium triiodide must be fortuitous, because this compound is rather exceptional owing to hydrogen bond formation as discussed in the next section.

The electronic structure of an I_3^- ion may be represented by resonance among structure A, charge-transfer structure B, and structure C, which takes into account the polarization of an iodine molecule by an approaching negative ion.

$I_a^- I_c$–I_b	I_a–$I_c I_b^-$	$I_a^- I_c^+ I_b^-$
A	B	C

In the last resonance structure, a double bond may be formed to some extent between I_c and I_b by making use of a d orbital of the terminal iodine atom in addition to those of the noble gas shell.[22,23] From the charge distribution of I_3^- ions in rubidium and cesium triiodides, it is concluded that the contribution of the resonance structures, A, B, and C, amounts to 59%, 31%, and 6%, respectively.

Anomalous Behavior of Ammonium Triiodide. Both ν_1^a and ν_2^a of ammonium triiodide show an extraordinary, large positive temperature coefficient (one order of magnitude greater than that of tungsten(VI) hexachloride[24,25] showing the greatest positive temperature coefficient among those ever reported for the quadrupole resonance frequencies of halogens) with its maximum at about $-40°$ as shown in Figure 1. The intensity of the resonance lines is weak above $-40°$ to about $-15°$. On the other hand, ν_1^b and ν_2^b show a normal negative temperature coefficient.[26,27] However, the absolute value of the temperature coefficient is much greater than those of rubidium and cesium triiodides. The determination of ν_1^b at small temperature intervals revealed that the temperature coefficient assumes its maximum value at $-40°$. Accordingly, it is concluded that ammonium triiodide undergoes some sort of transition at about $-40°$. Presumably, the rotation of ammonium ions takes place above this temperature affecting the field gradients at terminal iodine atoms through hydrogen bonding.[18,28] This might be related to another anomalous behavior of ammonium triiodide that ν_1^a and ν_2^a showed a marked saturation effect.

(22) R. S. Mulliken, *J. Am. Chem. Soc.*, **77**, 884 (1955).

(23) L. Pauling, "The Nature of the Chemical Bond," 3rd ed, Cornell University Press, Ithaca, N. Y., 1960, p 316.

(24) R. P. Hamlen and W. S. Koski, *J. Chem. Phys.*, **25**, 360 (1956).

(25) R. Ikeda, D. Nakamura, and M. Kubo, *J. Phys. Chem.*, **69**, 2101 (1965).

(26) H. Bayer, *Z. Physik*, **130**, 227 (1951).

(27) T. Kushida, *J. Sci. Hiroshima Univ.*, **A19**, 327 (1955).

(28) D. Nakamura and M. Kubo, *J. Phys. Chem.*, **68**, 2986 (1964)

The Viscosity of Molten Bismuth–Bismuth Triiodide Solutions[1]

by Jordan D. Kellner

Atomics International, Canoga Park, California 93140 *(Received March 20, 1967)*

The viscosity of the Bi–BiI_3 system was measured over the entire composition range. The values for the pure salt ranged from 1.59 cp at 500° to 1.86 cp at the melting point of 408°, with an apparent activation energy of 1.69 kcal/mole. Both the viscosity and the activation energy increase with added metal until a maximum is reached at about 55 mole % bismuth. At this composition the viscosity at 500° is 2.07 cp with an activation energy of 6.41 kcal/mole. The apparent Arrhenius behavior of these mixtures is explained by the fact that the liquids are free-volume limited and that the free volume is proportional to temperature. The maxima in the isotherms are then interpreted as a loss of free volume caused by the interstitial dissolution of bismuth in the salt.

Introduction

While the viscosity of many binary fused-salt systems has been measured, only one paper has been published on the viscosity of metal–salt systems.[2] Aten measured the viscosity of Bi–$BiCl_3$ solutions up to a concentration of 40 mole % Bi from 260 to 340°. In the present work, the viscosity of the Bi–BiI_3 system having a consolute temperature of 458° is measured across the entire composition range from pure salt to pure metal.

Experimental Section

Since it was necessary to keep the system closed owing to the high vapor pressure of the salt (about 340 mm at 500°), it was decided that a capillary technique for the determination of the viscosities of these solutions would be the most suitable. The cell design of Greenwood and Wade[3] was used in which a well around the lower end of the capillary maintained a constant lower liquid level. Thus, the average driving force was independent of the volume of liquid in the cell. This design has an advantage in that the system is completely enclosed with no cold spots to which the salt may distill. Repetitive runs were simple, involving just an inversion of the cell. In addition, there is no contamination from a manipulating gas. Two modifications of this design are incorporated into the cell shown in Figure 1. The well, D, was raised to reduce the effective head and thus lengthen the time of the flow of liquid through the capillary. Reasonable times for the flow were obtained in this manner without the use of narrow capillaries that clogged easily. Because the Bi–BiI_3 solutions form an opaque film on the wall, a second modification, the addition of three tungsten probes sealed through the cell at A, was used for remote sensing of the liquid level. One of the three probes terminates at the beginning of the reservoir, C, and the other two at the end of this reservoir. The two longer probes were insulated with a glass covering so as not to be shorted to the third probe by adhering solution. The time of flow was measured by an electronic clock (Hamner 803) that was turned on and off by positive pulses supplied by 1.5-v dry cells and UTC R74 transformers in the circuit shown in Figure 2. When the double-pole–single-throw switch, S, in Figure 2 is closed and the liquid level is covering all three probes (region a), about 15 ma flows through each circuit. When the liquid drops past probe 2 (region b), the current through this probe is suddenly reduced to zero. This produces a large (about +20 v) positive-going pulse from the secondary of the transformer T_1 that starts the clock. When the liquid level drops below probes 1 and 2 in Figure 2 (region c), the current, again dropping quickly to zero, produces another positive-going pulse at the secondary of transformer T_2. This pulse is used to stop the clock. The clock may be read in hundredths of seconds and was calibrated to be accurate to within 1 part in 10^6.

The cell was calibrated at room temperature with 5%

(1) This work was supported by the Research Division of the United States Atomic Energy Commission.

(2) A. H. W. Aten, *Z. Physik. Chem.*, **66**, 641 (1909).

(3) N. N. Greenwood and K. Wade, *J. Sci. Instr.*, **34**, 288 (1957).

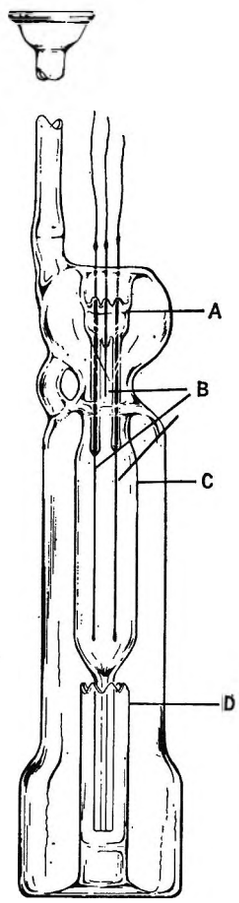

Figure 1. Pyrex viscosity cell: A, tungsten seals; B, tungsten probes; C, reservoir; D, well.

glycerine–water solution, double-distilled water, and acetone. Suitable corrections were applied to the calibration for the difference in temperature of unknown and standard liquid.

The BiI_3 used was obtained commercially and distilled twice *in vacuo*. The bismuth metal was filtered through glass wool *in vacuo* to remove oxide impurities. The powders were weighed in air and introduced into the cell *via* a long-fill tube. The cell was then evacuated and sealed at a pressure of 10^{-5} torr.

The cell was held in an Inconel 2.5-in. i.d. tube which was placed in a Marshall furnace mounted in a rocking frame. The Inconel tube was effective in limiting the temperature gradient along the cell to less than 1°. After the single-phase temperature was reached, the furnace was rocked for 10 min to assure the dissolution of the metal. The furnace was then inverted to charge the cell and the time of flow of the solution was noted. This process was repeated about 10 times at each of at least four different temperatures and about 20–30 times while the temperature was being changed. Data were

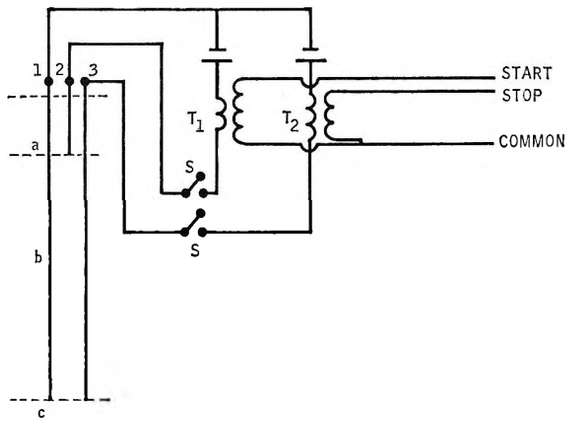

Figure 2. Remote level sensing circuit for determining time of flow: 1, 2, 3, tungsten probes; T_1, T_2, transformers; S, switch.

taken while increasing and decreasing temperature, in order to detect any change in viscosity caused by thermal deterioration of the solution. No such change was ever noted; the time of flow for runs with a given temperature agreed to within 0.2%.

Results

The viscosities of pure BiI_3 and of 15, 30, 45, 50, 55, 60, and 70 mole % bismuth solutions in BiI_3 were determined at temperatures ranging from 350 to 500°. The values for the pure salt ranged from 1.59 cp at 500° to 1.86 cp at the melting point of 408°.

Table I and Figure 3 show the variation of viscosity with temperature and composition. Some of the measurements were obtained while the liquid had probably separated into two phases, and those results are shown by dotted lines in Figure 3. While the data in the two-phase region may be of interest, they will not be discussed, since they are not amenable to interpretation. Therefore, only data on single-phase liquids are listed in Table I. The viscosity values were determined from the kinematic viscosity results and density data. Densities up to 40 mole % are known.[4] The densities of more concentrated solution were obtained by interpolation using a 70 mole % point of Topol and Ransom[5] and the value for pure bismuth.[6] An attempt was made to determine the viscosity of pure bismuth. However, the extremely low value for the kinematic viscosity of molten bismuth resulted in very short flow times and scatter in the data due to turbulent flow. Therefore, viscosity values for pure bismuth were taken from the literature.[7]

(4) F. J. Keneshea, Jr., and D. Cubicciotti, *J. Phys. Chem.*, **63**, 1472 (1959).

(5) L. E. Topol and L. D. Ransom, *J. Chem. Phys.*, **38**, 1663 (1963).

(6) E. Gebhardt and K. Kostlin, *Z. Metallk.*, **48**, 601 (1957).

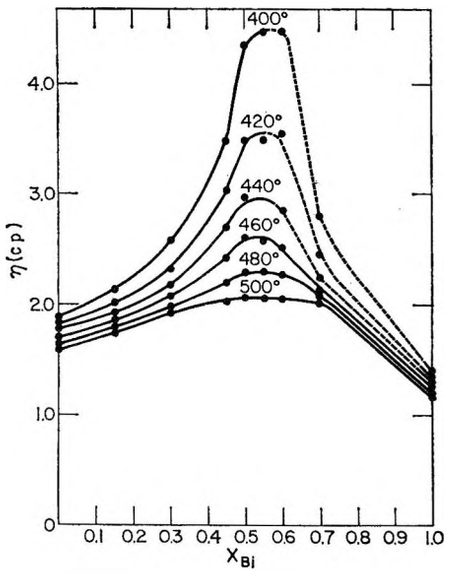

Figure 3. Viscosity isotherms *vs.* mole fraction of bismuth; the dotted portions denote two liquid phases.

Table I: Viscosities, η (in cp), of Bi–BiI_3 Solutions

Temp, °C	η	Temp, °C	η	Temp, °C	η	Temp, °C	η
—0% Bi—		—15% Bi—		—30% Bi—		—45% Bi—	
433	1.78	389	2.21	445	2.16	350	5.99
438	1.77	395	2.17	448	2.14	368	4.99
446	1.74	401	2.14	450	2.13	400	3.50
449	1.73	406	2.11	454	2.11	419	3.07
463	1.69	412	2.07	460	2.09	426	2.95
482	1.64	418	2.04	486	1.98	431	2.86
488	1.63	424	2.01			435	2.77
491	1.62	433	1.97			459	2.46
		455	1.88			461	2.42
		472	1.83			482	2.20
		493	1.76			494	2.09
						499	2.05
—50% Bi—		—55% Bi—		—60% Bi—		—70% Bi—	
366	5.71	415	3.71	438	2.93	448	2.21
370	5.57	426	3.33	441	2.86	452	2.19
375	5.39	432	3.12	445	2.77	455	2.17
381	5.13	440	2.94	450	2.69	458	2.16
385	4.97	450	2.76	455	2.61	472	2.11
395	4.60	456	2.68	470	2.42	476	2.10
400	4.40	464	2.52	491	2.16	481	2.09
418	3.74	496	2.11	499	2.08	485	2.08
443	3.02	500	2.07			495	2.06
476	2.41					498	2.05
494	2.16						

The isotherms of viscosity against molar composition shown in Figure 3 exhibit rather pronounced maxima at about 55–60 mole % metal. At 55% the viscosity at 500° is 2.07 cp compared with 1.59 cp for the pure salt at this temperature and 1.19 cp for the pure metal. The apparent activation energy for viscous flow for each composition was determined from the plots of ln η against $1/T$ in Figures 4 and 5 and is shown in Table II. In general, these E_{act} are fairly constant with temperature except for the more concentrated solutions at lower temperatures, where the two-phase liquid region of the phase diagram is approached. As was noted for the viscosity, the E_{act} also goes through a maximum at a composition of about 50 mole % Bi, varying from 1.69 kcal/mole for the pure salt to 7.71 kcal/mole at 50 mole % Bi.

Table II: The Constants a and b for Eq 1 for Each Composition and Apparent Energy of Activation

x_{Bi}	E_{act}, kcal/mole	10^3a	b	$[(V_s - b)/V_s] \times 100$ at 500°
0	1.69	1.132	0.1538	28
0.15	2.19	0.7832	0.1664	23
0.30	2.25	0.6760	0.1629	19
0.45	5.46	0.2125	0.1711	6
0.50	7.71	0.1737	0.1678	5.6
0.55	6.41	0.1440	0.1635	4.1
0.60	5.86	0.1377	0.1538	3.9
0.70	1.59	0.2859	0.1402	10

Discussion

According to the hole theories of viscous flow in liquids of Frenkel[8] and Eyring and associates[9] viscous flow can be thought of as consisting of two simultaneous events. (1) The flow unit must attain sufficient energy to break away from its neighbors and (2) a hole of sufficient size must form adjacent to the flow unit. This hole is formed from the free volume ordinarily present in the liquid. The free volume may be defined as the volume of a unit weight of liquid less the volume of the liquid in a rigid, closest packed structure. Thus maxima in viscosity isotherms may be interpreted in two ways. (1) A large flow unit or a change in binding occurs in the mixture (complex formation) or (2) there is a loss of free volume in the mixture.

When two events are involved, there is no theoretical reason to expect Arrhenius behavior as the tem-

(7) F. Sauerwald and K. Topler, *Z. Anorg. Allgem. Chem.*, **157**, 117 (1926).

(8) J. Frenkel, "Kinetic Theory of Liquids," Clarenden Press, Oxford, 1946.

(9) S. N. Glasstone, K. Laidler, and H. Eyring, "The Theory of Rate Processes," McGraw-Hill Book Co., Inc., New York, N. Y., 1941.

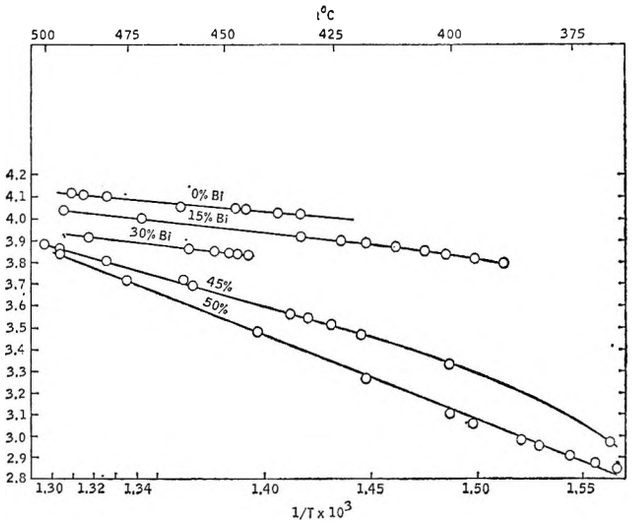

Figure 4. Negative natural logarithm of the viscosity ($-\ln \eta(\rho)$) *vs.* $1/T$ for x_{Bi} = 0–0.50.

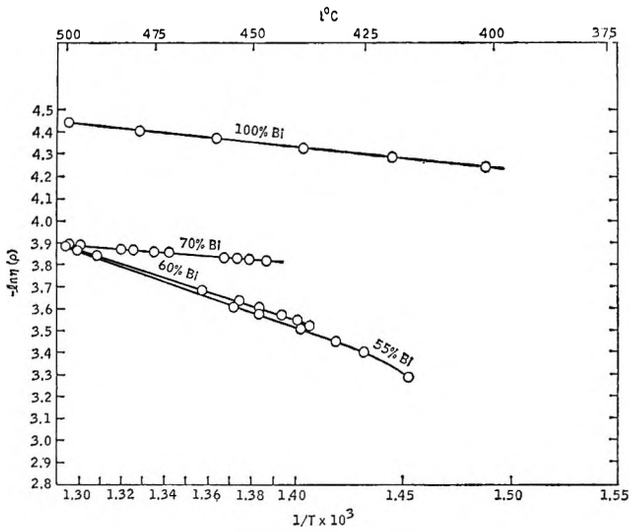

Figure 5. Negative natural logarithm of the viscosity *vs.* $1/T$ for x_{Bi} = 0.55–1.0.

perature is changed at constant pressure unless one of the above effects largely outweighs the other. As pointed out by Macedo and Litovitz,[10] in liquids whose thermal expansion is very small, the free volume is virtually temperature independent, and the apparent activation energy at constant pressure will be constant with temperature. Also, in liquids whose free volumes are proportional to the temperature, the liquid will again show Arrhenius behavior at constant pressure.[10] Since all of the compositions of Bi in BiI_3 show good Arrhenius behavior, one or the other condition applies. Evidently the free volume is the determining factor in the viscosity of these solutions, since it is well established that the solutions contain no complexes at the composition of the maxima.[11] That is, in salt-rich melts bismuth dissolves in its trihalides by the formation of the monomer subhalide BiI[12,13]

$$2Bi + BiI_3 \longrightarrow 3BiI$$

which does not polymerize, in contrast to the chloride and bromide in which the subhalide does undergo polymerization.[13] Therefore the mixture at low metal compositions (below 50 mole %) consists only of Bi^+, Bi^{+3}, and I^-. Evidence for the absence of complexes in the iodide system at concentrations of 35 mole % Bi and greater can be found in thermal diffusion studies.[11] These data show that at these concentrations the cations are exchanging electrons so rapidly that they are indistinguishable as far as mass transport is concerned. Any one cation is rapidly changing its valence from 1 to 3 and back again even though there is a definite bulk concentration of each cation at any given moment. Such a system may be denoted by BiI_x where x is between 1 and 3. Any autocomplexing or other complex formation would be detected by observing a separation of the solutions under the influence of a temperature gradient. Above a composition of 35 mole % Bi, no such thermal diffusion occurs. Therefore, no complexing of the solution takes place, and the positive deviations from additivity observed in the viscosity isotherms are not likely to be due to complex formation. It seems likely then that the apparent Arrhenius behavior of each composition is due to the free-volume effects outweighing any energy considerations since the melts are completely ionic. Also, the partial molar volumes of bismuth are actually negative at low metal concentrations and approach the value for pure bismuth only at large metal concentrations. This was thought[4] to be caused by the interstitial dissolution of bismuth metal or ions. In the light of subsequent knowledge[12,13] we can say that the bismuth species that eventually takes up interstitial positions in the quasi-lattice melt structure is the Bi^+ cation. Thus as bismuth is added, more and more free space is taken up and the viscosity increases because the space available for the movement of salt is reduced.

This view is further supported by the fact that the data can be given in terms of the Batchinski equation

(10) P. B. Macedo and T. A. Litovitz, *J. Chem. Phys.*, **42**, 245 (1965).

(11) J. D. Kellner, *J. Phys. Chem.*, **70**, 2341 (1966).

(12) S. J. Yosim, L. D. Ransom, R. A. Sallach, and L. E. Topol, *ibid.*, **66**, 28 (1962).

(13) L. E. Topol and L. D. Ransom, *J. Chem. Phys.*, **38**, 1663 (1963).

$$V_s = a\phi + b \quad (1)$$

where a and b are constants, V_s is the specific volume of the solution, and ϕ is the fluidity. Table II shows the values of a and b from a least-squares analysis. The data follow this linear expression to within 1%. As can be seen from eq 1, b is the specific volume when ϕ is zero or, in other words, when the liquid is completely rigid. Thus $V_s - b$ can be thought of as the free volume, or at least as a measure of it. The values of $(V_s - b)/V_s$ expressed as per cent are shown in Table II for each composition at 500°. These values, which should be at least qualitatively similar to the free volume, go through a minimum at the same composition that the viscosity goes through a maximum. This type of behavior is consistent with the idea that the species formed from the added bismuth takes up interstitial positions.

If the quasi-lattice salt structure is something approaching a closest packed arrangement of iodide ions, then in the pure salt one out of every three octahedral interstices would be occupied by a Bi^{3+} cation. At $^2/_3$ mole fraction, in a cubic closest packed arrangement, all of the octahedral spaces would be occupied by cations and one would expect the maximum in viscosity to occur at about this concentration. However, because of the increased coulombic forces, the anion structure would be expected to shrink somewhat when more cations are introduced, thereby taking up some free volume. This effect was thought[4] to be the reason for the negative values of the partial molar volume of bismuth at low concentrations of metal. The fact that the peak actually occurs at about 55% is possibly due to this contraction. Although there is some evidence[12] that bismuth atoms begin to appear at a concentration of 50 mole % metal, this species becomes predominant above 67 mole % bismuth, where the average cation charge is less than 1. At these concentrations, the melt properties approach those of the pure metal. The average flow unit size is decreasing as the large anions become more scarce, and the viscosity decreases until the value for the pure metal is reached.

The apparent activation energy at constant pressure in Table I is then largely the energy of formation of holes of flow unit size, since the viscosity of the system, as was pointed out above, is probably free-volume limited. The pure salt, having the largest free volume, has the smallest activation energy and, as the solution becomes more "condensed" with added bismuth cations, the energy of hole formation, and therefore the activation energy, increases.

Fluorocarbon Solutions at Low Temperatures. V. The Liquid Mixtures $C_2H_6 + C_2F_6$, $C_3H_8 + C_2F_6$, $CH_4 + C_3F_8$, $C_2H_6 + C_3F_8$, $C_3H_8 + C_3F_8$, n-$C_4H_{10} + C_3F_8$, i-$C_4H_{10} + C_3F_8$, $C_3H_8 + n$-C_4F_{10}, n-$C_6H_{14} + n$-C_4F_{10}, n-$C_7H_{16} + n$-C_4F_{10}, n-$C_9H_{20} + n$-C_4F_{10}, and n-$C_{10}H_{22} + n$-C_4F_{10}[1]

by John B. Gilmour, Judith O. Zwicker, Jeffrey Katz, and Robert L. Scott

Contribution No. 1997 from the Department of Chemistry, University of California, Los Angeles, California 90024 (*Received October 6, 1966*)

Total vapor pressures have been measured for three binary liquid mixtures and from these measurements equations for the molar excess Gibbs free energy have been derived, yielding the following values for $\tilde{G}^E$/cal at $x = 0.5$: $C_2H_6 + C_3F_8$ at 188°K, 165; $C_3H_8 + C_3F_8$ at 204°K, 212; at 214°, 204; at 224°K, 199; and n-$C_4H_{10} + C_3F_8$ at 228°K, 250. Liquid–liquid phase diagrams for 11 systems were determined, with critical solution temperatures as follows: $C_3H_8 + C_2F_6$, 190°K; $CH_4 + C_3F_8$, 127°K; $C_2H_6 + C_3F_8$, 166°K; $C_3H_8 + C_3F_8$, 196°K; n-$C_4H_{10} + C_3F_8$, 226°K; i-$C_4H_{10} + C_3F_8$, 208°K; $C_3H_8 + n$-C_4F_{10}, 204°K; n-$C_6H_{14} + n$-C_4F_{10}, 281°K; n-$C_7H_{16} + n$-C_4F_{10}, 303°K; n-$C_9H_{20} + n$-C_4F_{10}, 348°K; n-$C_{10}H_{22} + n$-C_4F_{10}, 378°K. The critical solution point for the system $C_2H_6 + C_2F_6$ is hidden by the melting curve, but is estimated to be 157°K. These results contain and extend earlier work on hydrocarbon + fluorocarbon systems. The anomalously large deviations from the predictions of solubility parameter theory are about the same for all systems, and show no significant dependence upon the differences in molar volume (or number of carbon atoms) between hydrocarbon and fluorocarbon. All of the critical solution temperatures fall on a simple grid which permits interpolation and (with caution) extrapolation. The critical composition shows a striking dependence upon the difference in molar volume and gives support to a volume-fraction or surface-fraction formulation of regular solution theory.

Introduction

The work reported in this paper is part of a continuing research program on fluorocarbon solutions; previously we have reported[2-5] low-temperature vapor pressures and phase diagrams for 13 systems involving fluorocarbons and fluorochemicals. In this paper we report similar measurements[5] on 12 more systems, with particular emphasis upon differences in molar volume (and differences in number of carbon atoms). Rowlinson and co-workers[6] have shown that large excess free energies persist even when the molar volumes of the pure components in a hydrocarbon + fluorocarbon mixture are nearly equal; an increase of 50% in the molar volume of the hydrocarbon had only a small effect on the magnitude of the large deviations from ideality. The present research, with hydrocarbons ranging in size from CH_4 to $C_{10}H_{22}$ (and those from C_3 to C_{10} mixed with a single fluorocarbon, n-C_4F_{10}), greatly extends the earlier work and arrives at generally similar conclusions.

(1) Based on part of a dissertation by J. B. Gilmour for the Ph.D. degree, University of California, Los Angeles, Calif., June 1965.

(2) N. Thorp and R. L. Scott, *J. Phys. Chem.*, **60**, 670 (1956).

(3) N. Thorp and R. L. Scott, *ibid.*, **60**, 1441 (1956).

(4) I. M. Croll and R. L. Scott, *ibid.*, **62**, 954 (1958).

(5) I. M. Croll and R. L. Scott, *ibid.*, **68**, 3858 (1964).

(6) J. S. Rowlinson, D. E. L. Dyke, and R. Thacker, *Trans. Faraday Soc.*, **55**, 903 (1959).

Experimental Section

Materials. The source and purity of the substances are outlined in Table I.

Table I: Materials Used

Compound	Source	Manufacturer's stated purity, %
C_2F_6	*a*	99.9
C_3F_8	*b*	98.0 (min)
n-C_4F_{10}	*c*	99.8
CH_4	*d*	99.5
C_2H_6	*b*	99.90
C_3H_8	*b*	99.9+
n-C_4H_{10}	*b*	~99.8
i-C_4H_{10}	*b*	100.00
n-C_6H_{14}	*e*	99.97
n-C_7H_{16}	*f*	99
n-$C_{10}H_{22}$	*f*	Bp 173–175°

[a] Dupont Organic Chemicals Department, Research and Development Division, Jackson Laboratory, Wilmington 99, Del. [b] Matheson Co., Newark, Calif. [c] Halocarbon Products Corp., Hackensack, N. J. [d] Matheson CP grade purified by Dr. Donald Davis, Chemistry Department, University of California, Los Angeles, Calif. [e] Phillips Petroleum Co., Bartlesville, Okla. [f] Matheson Coleman and Bell, East Rutherford, N. J.

All of the materials were degassed by alternate melting and freezing while pumping. With the exception of the C_3F_8 no further purification was attempted. The C_3F_8 gas was condensed at least three times onto a bed of activated charcoal and then allowed to boil off. The charcoal was activated by pumping and heating to 430–480°; it was reactivated between each condensation.

Apparatus and Experimental Procedure. Experimental mixtures were prepared by condensing successive measured quantities of gas from a gas buret into the vapor pressure or solubility apparatus at low temperatures. A conventional vacuum manifold arrangement was used to evacuate the apparatus before use and to transfer the gas from the storage bulbs into the gas buret. A liquid Freon low-temperature bath, similar to that described by Croll and Scott,[5] was used for both the solubility and vapor pressure measurements.

The bath temperature was measured and controlled using the output from a ten-junction copper–constantan thermopile which was immersed in the Freon. The thermopile was calibrated against the vapor pressures of the pure hydrocarbons as well as against the freezing point of pure xenon (161.3°K). A crushed-ice slush served as the reference temperature. The balancing and heater control circuit was essentially that of Croll and Scott[5] except that three times the earlier sensitivity was obtainable with the ten-junction thermopile and a more sensitive recorder. Under control conditions there were sinusoidal oscillations of temperature of ±0.02° about the average temperature. By adjusting the voltage across the heaters, the period of this oscillation could be varied from about 10 to 40 sec.

Vapor Pressure Measurement. The "click" gauge (Thorp and Scott[2]) used to measure vapor pressures is shown in Figure 1 together with the rest of the vapor pressure apparatus. The gauge is essentially a curved glass membrane which changes configuration (with a snap or click) where the difference in pressure between the two sides reaches a reproducible value; measurement of the nitrogen pressure on the far side of the membrane thus serves to determine the pressure inside the bulbs, *i.e.*, the total vapor pressure of the mixture.

Random fluctuations in the pressure of the order of 2–4 cm occurred unless the liquid mixture was sealed below the surface of the Freon. At first, the bulb was closed with a solenoid-operated valve which was used for vapor pressure measurements on $C_2H_6 + C_3F_8$ and C_3F_8. However, this valve proved difficult to operate and had a large vapor space necessitating difficult corrections, so it was later discarded. In all other measurements mercury from the gas buret was allowed to follow the gas into the mixture bulb through a capillary delivery line; the mercury would freeze there and plug the line.

After a measurement was made and before more

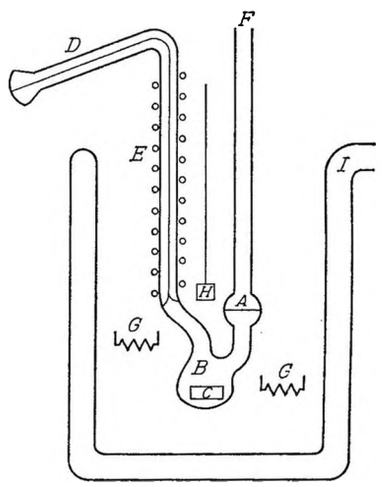

Figure 1. Schematic diagram of vapor pressure apparatus: A, click gauge; B, mixture bulb; C, stirring bar; D, delivery tube with 12/1 ball joint at end; E, delivery tube heater; F, glass tube to manometer; G, heaters, main and auxiliary; H, thermopile; I, dewar flask.

material was condensed into the vapor pressure bulb, a wire heater around the delivery tube was turned on and the inner dewar lowered so that the liquid Freon was below the frozen mercury. The mercury then melted and the vapor pressure of the mixture forced the mercury out of the delivery tube and into the gas buret which contained the new material to be added. Sometimes when the vapor pressure was low, the mixture had to be heated. This new method of isolating the mixture below the level of the Freon bath proved highly satisfactory; it was simple, reliable, fast, and involved much smaller uncertainties in the liquid composition.

Solubility Measurements. Liquid–liquid solubilities and solid–liquid solubilities were measured in an apparatus identical with that of the vapor pressure apparatus (Figure 1) except that a click gauge was not attached to the mixture bulb. A 60-w spotlight was placed behind the dewars, and critical solution temperatures and solid solubilities were directly observed through the two unsilvered dewars. Some observations of the unmixing temperatures T_u were made by observing the phase changes when one looked at an angle of 90° to a small focused illuminating beam which could be switched on as an alternative to the regular spotlight.

The conventional method of determining liquid–liquid miscibility is to raise or lower the bath temperature slowly and, when two phases appear (or disappear), the temperature T_u is recorded. However, in the present apparatus one could adjust the dials of the temperature control potentiometer to a point where the bath temperature varied sinusoidally within $\pm 0.02°$ of T_u and hold this temperature indefinitely. When the 90° beam was used, the phase change was well defined: as the temperature decreased and increased, passing each time through the unmixing temperature T_u, the mixture went from a transparent white to a very silky composition of two liquid phases which was churned by the smaller stirrer, and back again to a transparent white. The one-phase mixture was not colorless, but was white owing to critical opalescence. The passage of the system from one phase to two phases and back again occurred four times/min, or less, depending upon the setting of the heaters. At extremes of composition, this procedure was not feasible and the conventional method of varying the temperature had to be used.

Results[7]

Vapor Pressure Measurements. The results of the vapor pressure measurements are shown in Figures 2–4. The circles are the experimental data and the solid line is a least-squares fit of the data (see below). Only the total compositions were directly measured; however, since the vapor space is small, application of a small correction to the total composition yields an accurate estimate of the liquid composition (L). The vapor composition curve (V) is a calculated one.

The mole fractions x of the liquid are generally known to ± 0.01 for $C_3H_8 + C_3F_8$ and to ± 0.005 for n-$C_4H_{10} + C_3F_8$. The difference in the uncertainties in these two systems arises from the improvement obtained by using the frozen plug of mercury as explained above.

The uncertainties in the mole fractions for the system $C_2H_6 + C_3F_8$ are comparatively larger than in the other systems because of the large vapor space and the uncertainty in the composition of the vapor in the valve used for the system. Fortunately, the largest uncertainties (± 0.035 in the mole fraction) lie in the region $x = 0.0$–0.5, where the total vapor pressure is least sensitive to the liquid composition. The effect of this uncertainty upon the parameters used in the equation to fit the data was negligible. The liquid compositions for the remainder of the experimental points for this system are usually known to within 0.01 mole fraction.

The curve at $T = 203.5°K$ for the system $C_3H_8 + C_3F_8$ (Figure 3) is quite flat since the measurements of the vapor pressure were made 7.3°K above the critical solution temperature. Similarly, the vapor pressure of the system n-$C_4H_{10} + C_3F_8$ (Figure 4), measured only 2.2°K above its critical solution temperature, displays the same characteristic flatness. As can be seen from the figures, both systems form azeotropes.

These experimental vapor pressure data were processed by the computer program CH08B developed by Myers and Scott.[8] This program, a modification of the least-squares procedure proposed by Barker,[9] evaluates a set of coefficients α in an equation for the molar excess Gibbs free energy

$$\tilde{G}^E/RT = x_1x_2[\alpha_0 + \alpha_1(x_1 - x_2) + \alpha_2(x_1 - x_2)^2] \quad (1)$$

Table II gives the derived coefficients α_0, α_1, and α_2 for eq 1. W_1, W_2, and δ_{12} are corrections for nonideality of the vapors and the effect of applied pressure upon the vapor pressure

$$W_1 = (\tilde{V}_1 - B_{11})/RT \quad (2)$$

$$W_2 = (\tilde{V}_2 - B_{22})/RT \quad (3)$$

$$\delta_{12} = (2B_{12} - B_{11} - B_{22})/RT \quad (4)$$

(7) All of the experimental results reported here may be found in numerical form in the Ph.D. Dissertation of John B. Gilmour (UCLA, 1965), obtainable from the UCLA Library or from University Microfilms.

(8) D. B. Myers and R. L. Scott, *Ind. Eng. Chem.*, **55**, 43 (1963).

(9) J. A. Barker, *Australian J. Chem.*, **6**, 207 (1953).

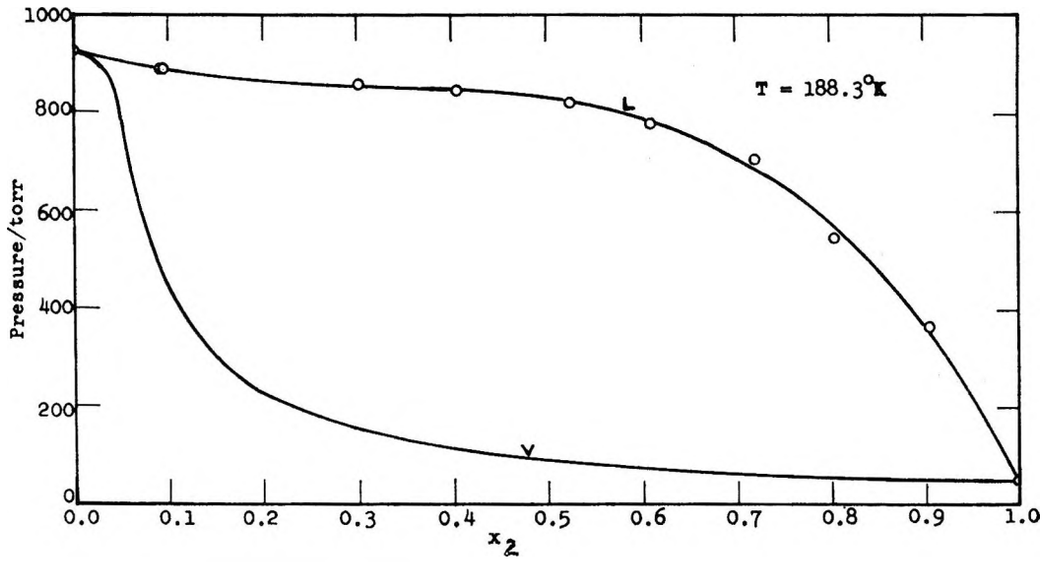

Figure 2. Pressure–composition diagram for the system $C_2H_6 + C_3F_8$ at 188.3°K: circles, experimental points; solid lines, computer curves.

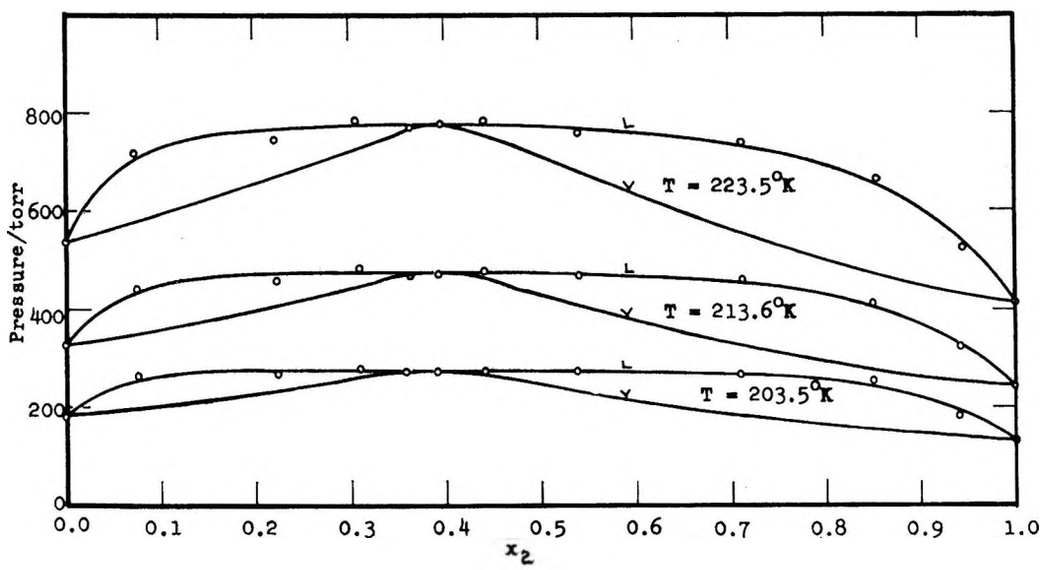

Figure 3. Pressure–composition diagrams for the system $C_3H_8 + C_3F_8$ at 203.5, 213.6, and 223.5°K: circles, experimental points; solid lines, computer curves.

where the subscripts refer to components 1 (hydrocarbon) and 2 (fluorocarbon).

The second virial coefficients, B_{11} and B_{22}, required for the program were obtained from a collection of virial data compiled by Dymond[10] or were estimated from the behavior of similar substances with the aid of the Berthelot-type equation proposed by Guggenheim.[11]

$$\frac{B}{\tilde{V}_c} = a - b\left(\frac{T_c}{T}\right)^2 \qquad (5)$$

where $\tilde{V}_c$ and T_c are the molar volume and temperature of the gas–liquid critical point. The parameters a and b ($^1/_4$ and $^3/_2$ in the Guggenheim equation) are not the same for all of the substances and have to be judiciously interpolated.

(10) J. A. Dymond, "A Compilation of Second and Third Virial Coefficients," Department of Chemistry, University of Oxford, 1964 (privately circulated).

(11) E. A. Guggenheim, *J. Imp. Coll. Chem. Eng. Soc.*, **32**, 13 (1953); *cf.* T. B. Tripp and R. D. Dunlap, *J. Phys. Chem.*, **66**, 635 (1962).

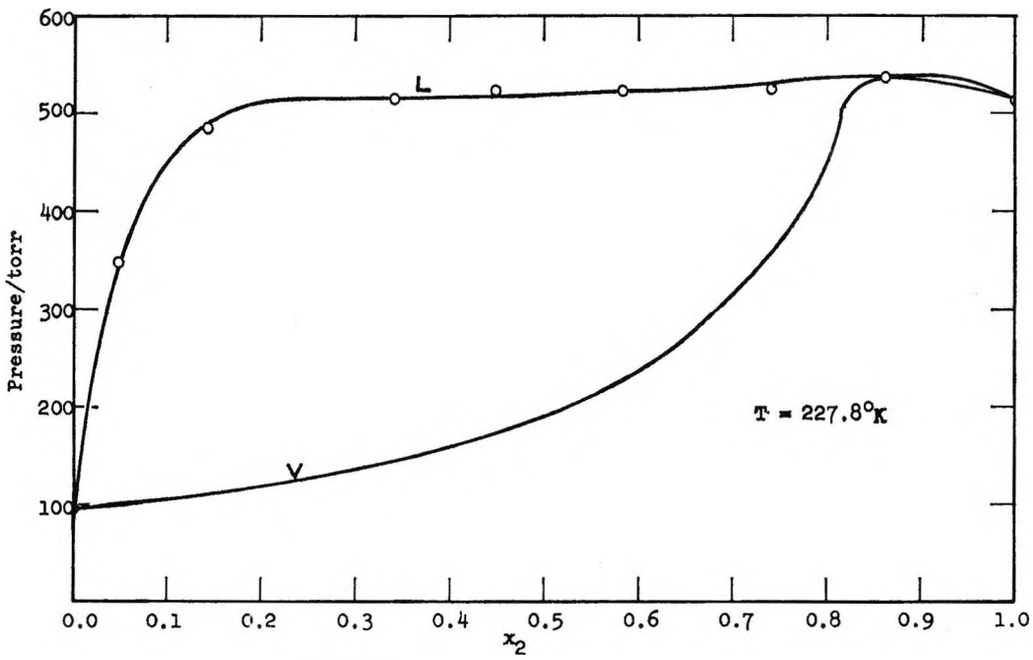

Figure 4. Pressure–composition diagram for the system n-C_4H_{10} + C_3F_8 at 227.8°K: circles, experimental points; solid lines computer curves.

Table II: Excess Free Energy Coefficients

	I C_2H_6 + C_3F_8	IIa C_3H_8 + C_3F_8	IIb C_3H_8 + C_3F_8	IIc C_3H_8 + C_3F_8	III n-C_4H_{10} + C_3F_8
T/K°	188.3	203.5	213.6	223.5	227.8
$W_1/10^{-5}$ torr^{-1}	4.91	7.74	6.74	5.90	10.8
$W_2/10^{-5}$ torr^{-1}	18.3	12.9	10.7	9.20	8.6
$\delta_{12}/10^{-5}$ torr^{-1}	1.4	0.01	0.01	0.01	0.91
α_0	1.77 ± 0.02	2.08 ± 0.04	1.93 ± 0.03	1.80 ± 0.02	2.21 ± 0.01
α_1	0.40 ± 0.03	0.24 ± 0.09	0.28 ± 0.06	0.29 ± 0.06	0.17 ± 0.02
α_2	0.13 ± 0.06	0.25 ± 0.17	0.24 ± 0.12	0.28 ± 0.11	0.33 ± 0.03
$\lim_{x_1 \to 0} \ln \gamma_1$	1.5	2.1	1.9	1.8	2.4
$\lim_{x_2 \to 0} \ln \gamma_2$	2.3	2.3	2.4	2.4	2.7
σ_P/torr	11.2	8.1	9.1	12.7	4.3
$100\sigma_P/P_{0.5}$	1.3	2.9	1.9	1.6	0.8

The correction δ_{12} (eq 4) involves the cross virial coefficient B_{12} and was estimated by using the law of corresponding states and the Lorentz–Berthelot combining rules for the intermolecular pair potential energy. For the dilute gas, the Scott[12] "three-liquid" formulation, combined with eq 2, yields

$$RT\delta_{12} = 6.0\tilde{V}_c[(T_c/T)^2(\eta^2 + \eta\xi - 0.17\xi^2) - 0.17\xi^2] \quad (6)$$

where $T_c = (T_{c1} + T_{c2})/2$, $\tilde{V}_c = (\tilde{V}_{c1} + \tilde{V}_{c2})/2$, $\xi = (\tilde{V}_{c2} - \tilde{V}_{c1})/(\tilde{V}_{c2} + \tilde{V}_{c1})$, and $\eta = (T_{c2} - T_{c1})/(T_{c2} + T_{c1})$. The subscripts 1 and 2 again refer to components 1 and 2. This equation and selected values of the critical volumes and temperatures were used to derive the values of δ_{12} tabulated in Table II. (Actually the Berthelot assumption—geometric mean of the energies—is a poor one for hydrocarbon + fluorocarbon mixtures, as these papers have shown. The

(12) R. L. Scott, *J. Chem. Phys.*, **25**, 193 (1953).

parameter δ_{12} is undoubtedly larger than that calculated from eq 6; however, the effect on the thermodynamic properties is entirely trivial.)

Also included in Table II is the standard deviation σ_P of the observed pressures from those calculated using eq 1 and the set of coefficients α.

An indication of the relative precision is given by the ratio $100\sigma_P/P_{0.5}$ where $P_{0.5}$ is the pressure of the system at $x = 0.5$. The relative precision is improved for system III (and other systems to be reported in a subsequent paper) which were measured on the final version of the vapor pressure apparatus. Some scatter in the vapor pressure may have been caused by condensation of a small amount of liquid in the delivery tube just below the valve on earlier versions of the vapor pressure apparatus. There was no possibility of this occurring with the mercury plug valve since the mercury usually filled the entire length of the delivery tube.

An auxiliary computer program was used to calculate vapor pressures for values of x other than these measured; this program also calculated the vapor compositions shown in Figures 2–4.

Solubility Measurements. No liquid–liquid immiscibility was observed for the system $C_2H_6 + C_2F_6$ shown in Figure 5. However, the slope of the solid solubility dx/dT is so very large that it is obvious that a metastable liquid–liquid miscibility curve lies just below. Such metastable curves have been observed in the systems phosphorus + carbon disulfide[13] and sulfur + quinoline.[14]

Figure 6 compares the solubility data for four systems in which the hydrocarbon (CH_4, C_2H_6, C_3H_8, or n-C_4H_{10}) is increased in size while the fluorocarbon, C_3F_8, remains the same. Also shown in Figure 6 is a branched hydrocarbon, i-C_4H_{10}, with C_3F_8. Figure 7 offers a similar comparison of the liquid–liquid phase diagrams for a single hydrocarbon, C_3H_8, with three fluorocarbons (C_2F_6, C_3F_8, and n-C_4F_{10}).

Following a suggestion of Munson,[15] we plot these data (and those in Figure 8 as well) in a reduced form as T/T_c *vs.* ϕ_2, where T_c is the critical solution temperature and $\phi_2 = x_2\tilde{V}_2/(x_1\tilde{V}_1 + x_2\tilde{V}_2)$ is the volume fraction of fluorocarbon. For convenience and consistency, we define the volume fraction in terms of the molar volumes of each pure liquid at its normal boiling point, a crude approximation to a corresponding state. No theoretical significance can be attached to any variation of the molar volumes in a volume fraction.

Critical opalescence was evident in the systems during solubility measurements. The transparent solutions immediately above T_u had a brown tint when viewed opposite a light which shone through them and, as mentioned earlier, were whitish when viewed 90° from the incident beam. As expected, this phenomenon was most pronounced for composition closest to the critical solution composition x_c.

Finally, Figure 8 shows miscibility curves for a wide

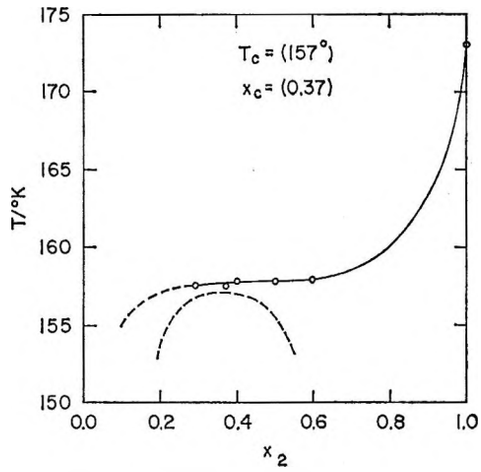

Figure 5. Phase diagram for the system $C_2H_6 + C_2F_6$. An estimated metastable liquid–liquid curve is sketched below the experimental solid–liquid curve.

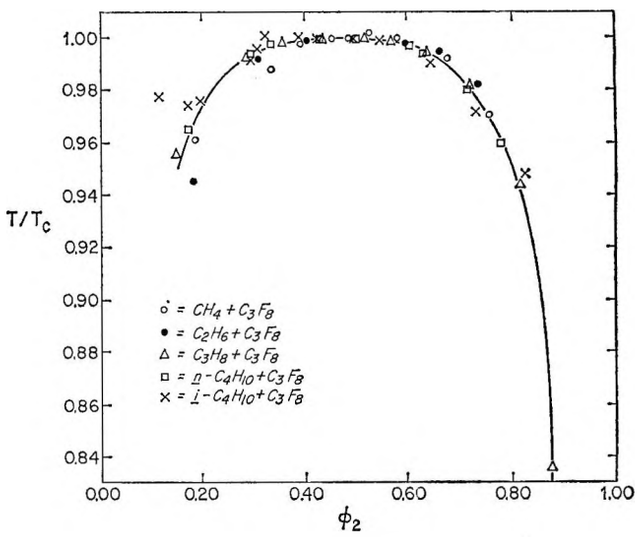

Figure 6. Liquid–liquid miscibilities for systems of five hydrocarbons (CH_4, C_2H_6, C_3H_8, n-C_4H_{10}, and i-C_4H_{10}) with C_3F_8. Temperatures are reduced by dividing by the critical solution temperature T_c. Compositions are volume fractions of fluorocarbon ϕ_2 (in terms of molar volumes at the normal boiling point).

(13) J. H. Hildebrand and T. F. Buehrer, *J. Am. Chem. Soc.*, **42**, 2213 (1920).

(14) D. L. Hammick and W. E. Holt, *J. Chem. Soc.*, 1995 (1926).

(15) M. S. B. Munson, *J. Phys. Chem.*, **68**, 796 (1964).

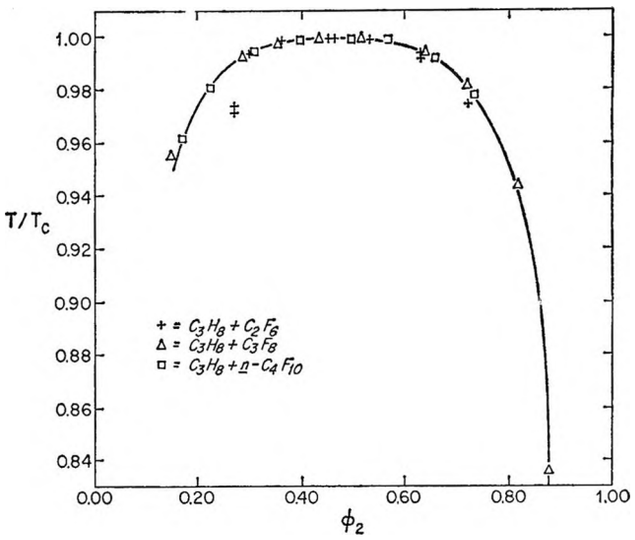

Figure 7. Liquid–liquid miscibilities in systems of C_3H_8 with three fluorocarbons (C_2F_6, C_3F_8, and n-C_4F_{10}. The coordinates and the smoothed curve are the same as in Figure 6.

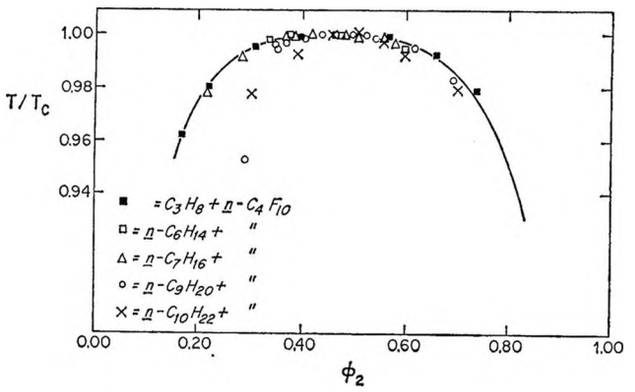

Figure 8. Liquid–liquid miscibilities in systems of five hydrocarbons (C_3H_8, n-C_6H_{14}, n-C_7H_{16}, n-C_9H_{20}, and n-$C_{10}H_{22}$) with n-C_4F_{10}. The coordinates and the smoothed curve are the same as in Figure 6.

range of hydrocarbons (C_3H_8, n-C_6H_{14}, n-C_7H_{16}, n-C_9H_{18}, and n-$C_{10}H_{22}$) with the fluorocarbon n-C_4F_{10}. Only the first of these systems could be studied in the low-temperature apparatus; the rest were measured in the conventional way: different amounts of the components were weighed into tubes which were then sealed; then T_u was determined in an ordinary water or oil bath.[16] These mole fractions were usually known to ± 0.005.

In general, these reduced solubilities fall roughly on the same curve. A possible explanation for the success of these Munson plots will be offered at the end of this paper. Numerical values of T_c and x_c are found in Table V.

Discussion

For many nonelectrolyte mixtures, a reasonable zeroth approximation for the molar excess Gibbs free energy is the regular-solution equation[17]

$$\tilde{G}^E = A_{12}\frac{x_1\tilde{V}_1 x_2\tilde{V}_2}{x_1\tilde{V}_1 + x_2\tilde{V}_2} = A_{12}(x_1V_1 + x_2V_2)\phi_1\phi_2 \quad (7)$$

where x_1 and x_2 are the mole fractions of the two components; φ_1 and φ_2, their volume fractions; $\tilde{V}_1$ and $\tilde{V}_2$, their molar volumes; and A_{12} is a measure of the interaction energy between unlike molecules relative to that between like molecules. According to solubility parameter theory[17]

$$A_{12} = (\delta_1 - \delta_2)^2 \quad (8)$$

where δ_1 and δ_2 are the "solubility parameters" of the components (the square roots of the cohesive energy density or energy of vaporization per unit volume).

Table III summarizes the physical properties of the pure liquids: the normal boiling point T_b, together with the molar heat of vaporization $\Delta\tilde{H}^v$, the molar volume $\tilde{V}$, and the solubility parameter δ at various relevant temperatures.

Table IV compares the values of the excess free

Table III: Physical Properties of the Pure Liquids

Substance	T_b/°K	T/°K	$\Delta\tilde{H}v$/ kcal	$\tilde{V}_T$/cm³	δ_T/ cal$^{-1/2}$ cm$^{3/2}$
CF_4	145.1	150	3.01	54.9	7.0
C_2F_6	194.9	195	3.86	86	6.4
C_3F_8	236.5	200	5.08	107	6.6
		210	4.99	110	6.4
		220	4.89	113	6.2
		230	4.77	115	6.1
		237	4.69	117	5.9
n-C_4F_{10}	271.2	271	5.48	149	5.7
CH_4	111.7	112	1.96	37.8	6.8
C_2H_6	184.5	185	3.51	55.0	7.6
C_3H_8	231.1	210	4.72	72.8	7.7
		220	4.60	73.9	7.5
		230	4.48	75.3	7.4
n-C_4H_{10}	272.7	273	5.35	96.4	7.1
i-C_4H_{10}	261.4	261	5.09	97.8	6.8
n-C_6H_{14}	341.9	342	6.94	140.9	6.7
n-C_7H_{16}	371.6	372	7.66	163.5	6.5
n-C_9H_{20}	423.9	424	9.03	210.6	6.3
n-$C_{10}H_{22}$	447.3	447	9.6	235.8	6.1

(16) Measurements on these systems (n-C_6H_{14} + n-C_4F_{10}, n-C_7H_{16} + n-C_4F_{10}, n-C_9H_{20} + n-C_4F_{10}, and n-$C_{10}H_{22}$ + n-C_4F_{10}) were made by J. O. Z. and J. K. while undergraduate chemistry majors at UCLA.

(17) J. H. Hildebrand and R. L. Scott, "Regular Solutions," Prentice-Hall Inc., Englewood Cliffs, N. J., 1962.

Table IV: Predicted and Observed Excess Free Energies and Enthalpies

	T/°K	$\tilde{G}^{E}_{0.5}$ (calcd)/cal	$\tilde{G}^{E}_{0.5}$ (obsd)/cal	$(\tilde{G}^{E}_{obsd} - \tilde{G}_{calcd})_{0.5}/RT$	$\tilde{H}^{E}_{0.5}$/cal	$\tilde{H}^{E}_{0.5}/\tilde{G}^{E}_{0.5}$
$C_2H_6 + C_3F_8$	188.3	12	165	0.41		
$C_3H_8 + C_3F_8$	203.5	35	212	0.44		
	213.6	34	204	0.41	338	1.7
	223.5	33	199	0.37		
n-$C_4H_{10} + C_3F_8$	227.8	57	250	0.43		
n-$C_4H_{10} + n$-C_4F_{10}	245		243		415	1.7
n-$C_5H_{12} + n$-C_5F_{12}	285		281		480	1.7
n-$C_6H_{14} + n$-C_6F_{14}	308		328		567	1.7
					516[a]	1.6

[a] Calorimetric value by A. G. Williamson and R. L. Scott, *J. Phys. Chem.*, **65**, 275 (1961).

Table V: Critical Solution Temperatures and Compositions

System[a] $C_mH_{2m+2} + C_nF_{2n+2}$ $m + n$	T_c/°K	$(x_2)_c$	$\xi = (\tilde{V}_2 - \tilde{V}_1)/(\tilde{V}_2 + \tilde{V}_1)^b$	$\frac{T_c/°K}{(\tilde{V}_1 + \tilde{V}_2)/cm^3}$	$\frac{T_c/°K}{(\tilde{V}_1^{2/3} + \tilde{V}_2^{2/3})/cm^2}$	Ref
1 + 1	94.5	0.43	0.19	1.02	3.52	*c*
2 + 1	150.1	0.50	0.00	1.37	5.18	*d*
2 + 2	(157)	(0.4)	0.22	1.12	4.62	
3 + 2	189.5	0.42	0.06	1.17	5.08	
1 + 3	127.0	0.25	0.51	0.82	3.50	
2 + 3	165.5	0.31	0.36	0.96	4.30	
3 + 3	196.2	0.37	0.22	1.02	4.69	
4 + 3	225.6	0.41	0.10	1.06	5.02	
i-4 + 3	207.7	0.42	0.09	0.97	4.58	
3 + 4	204.0	0.32	0.33	0.91	4.46	
4 + 4	232.2	0.37	0.21	0.95	4.74	*e*
6 + 4	280.7	0.44	0.03	0.97	5.10	
7 + 4	303.2	0.48	−0.05	0.97	5.23	
9 + 4	348.0	0.57	−0.17	1.00	5.48	
10 + 4	377.7	0.60	−0.23	0.99	5.72	
5 + 5	265.5	0.37	0.21	0.89	4.74	*f*
6 + 5	287.9	0.407	0.13	0.89	4.87	*g*
6 + 6	295.9	0.370	0.21	0.83	4.70	*h*
6 + 7	301.7	0.33	0.28	0.78	4.51	*i*
7 + 7	323.2	0.36	0.21	0.79	4.63	*j*
8 + 7	341	0.40	0.14	0.79	4.70	*k*
8 + 8	348.5	0.355	0.21	0.74	5.57	*l*

[a] Both components the formal isomer except as noted. [b] At normal boiling point. [c] Reference 4. [d] Reference 5. [e] J. H. Simons and J. W. Mausteller, *J. Chem. Phys.*, **20**, 1516 (1952). [f] J. H. Simons and R. D. Dunlap, *ibid.*, **18**, 335 (1950). [g] R. D. Dunlap, R. Digman, and J. Vreeland, Abstracts, 124th Meeting of the American Chemical Society, Chicago, Ill., Sept 1953. [h] R. G. Bedford and R. D. Dunlap, *J. Am. Chem. Soc.*, **80**, 282 (1958). [i] J. B. Hickman, *ibid.*, **77**, 6154 (1955). [j] J. H. Hildebrand, B. B. Fisher, and H. A. Benesi, *ibid.*, **72**, 4348 (1950). [k] D. N. Campbell and J. B. Hickman, *ibid.*, **75**, 2879 (1953). [l] A. Kreglewski, *Bull. Acad. Polon. Sci., Ser. Sci. Chim.*, **11**, 91 (1963).

energy at $x = 0.5$ (*i.e.*, $\tilde{G}^{E}_{0.5}$) predicted from eq 7 with those derived from the computer fit of the experimental data ($RT\alpha_0/4$ from Table I). In agreement with other studies[2-5,18] of hydrocarbon + fluorocarbon mixtures, the calculated values are consistently much too small. To give perspective to this comparison of the observed and predicted excess free energies, the ratio of the difference between these two to the thermal energy RT is given in column 5 of Table IV. This ratio shows no significant change as one changes the

(18) R. L. Scott, *J. Phys. Chem.*, **62**, 136 (1958).

molar volume of the hydrocarbon from 50 to 80% of the molar volume of the perfluoropropane.

For the system $C_3H_8 + C_3F_8$ it is possible to derive, from the excess free energies at three temperatures, an excess enthalpy $\tilde{H}^E = \tilde{G}^E - T(\partial\tilde{G}^E/\partial T)_P = 338 \pm 45$ cal mole^{-1}.

For comparison, Table IV also presents excess free energies and enthalpies for other similarly determined *n*-perfluoroalkane systems.[19] We see that $\tilde{G}^E$ increases regularly with the number of carbon atoms and that the ratio $\tilde{H}^E/\tilde{G}^E$ is virtually constant at 1.7.

Table V summarizes our data on critical solution temperature and compositions, augmented by similar data obtained by others. We can now examine critically the effect of molecular size (chain length or molar volume) upon the magnitude of the positive deviations from ideality.

Figure 9 shows a plot of the critical solution temperature against the total number of carbon atoms ($m + n$) in the normal hydrocarbon (m) + fluorocarbon (n) pair. It is immediately apparent that no special importance attaches to the case $m = n$, for these can be interpolated in an essentially linear manner (*cf.* 1 + 3, 2 + 3, 3 + 3, 4 + 3; or 3 + 2, 3 + 3, 3 + 4, etc.)

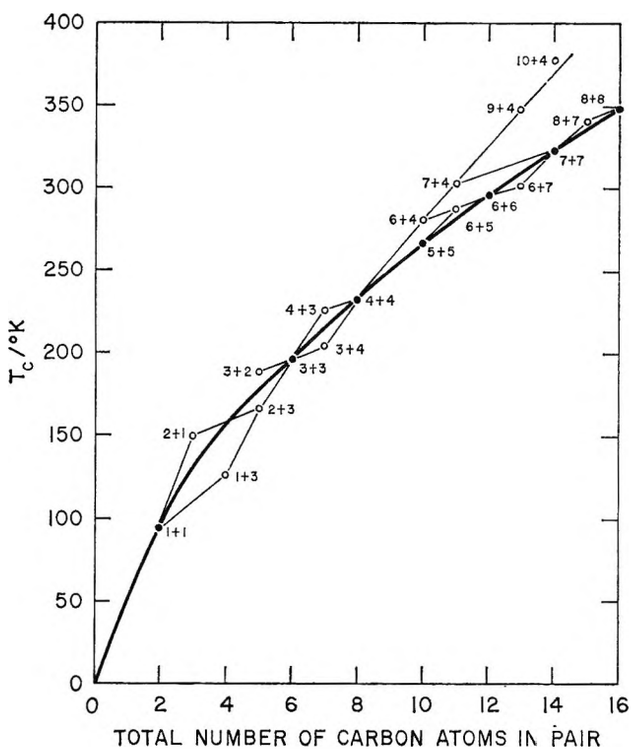

Figure 9. Critical solution temperatures of hydrocarbon + fluorocarbon mixtures. The abscissa is the total number of carbon atoms ($m + n$) in the normal hydrocarbon (m) and the normal fluorocarbon (n).

nor is there anything unique about those systems with approximately equal molar volumes (2 + 1, 7 + 4). All the systems lie on a self-consistent grid, on which one can certainly interpolate to get values for other systems; estimates by short extrapolations should also be reliable. Interpolation of the $C_2H_6 + C_2F_6$ system (2 + 2) yields $T_c = 157$°K; this value sketched in Figure 5 lies just below the nearly flat solid curve.

Volume-Dependent Interactions. Differentiation of eq 7 and of the analogous "Flory–Huggins" equation (FH), appropriate for solutions of long-chain polymers, yields[20] two sets of equations (RS for "regular solution"—eq 7—and FH) for the critical solution temperature and mole fraction in terms of $\tilde{V}_1$, $\tilde{V}_2$, and A_{12}. Writing $\langle\tilde{V}\rangle = (\tilde{V}_1 + \tilde{V}_2)/2$ and $\xi = (\tilde{V}_2 - \tilde{V}_1)/(\tilde{V}_2 + \tilde{V}_1)$, these are

$$\frac{2RT_c}{A_{12}\langle V\rangle} = \frac{2[(1+3\xi^2)^{3/2} - (1-9\xi^2)]}{27\xi^2} = 1 + \frac{\xi^2}{4} - \frac{\xi^4}{8} + \ldots \quad (9RS)$$

$$\frac{2RT_c}{A_{12}\langle V\rangle} = \frac{2(1-\xi^2)}{1+(1-\xi^2)^{1/2}} = 1 - \frac{3\xi^2}{4} - \frac{\xi^4}{8} + \ldots \quad (9FH)$$

$$2(x_2)_c = \frac{1+\xi-(1+3\xi^2)^{1/2}}{\xi} = 1 - \frac{3\xi}{2} + \frac{9\xi^3}{8} - \ldots \quad (10RS)$$

$$2(x_2)_c = \frac{2(1-\xi)^{3/2}}{(1-\xi)^{3/2} + (1+\xi)^{3/2}} = 1 - \frac{3\xi}{2} + \frac{5\xi^3}{8} - \ldots \quad (10FH)$$

A plot of $T_c/(\tilde{V}_1 + \tilde{V}_2)$ *vs.* ξ^2 is shown in Figure 10. A lack of close correlation between the experimental data and a constant A_{12} in either eq 9RS or 9FH is obvious. Of course, there is no reason to expect A_{12} to be exactly the same for all hydrocarbon + fluorocarbon systems; the differences between the interactions of $CH_3 + CH_2$ and $CF_3 + CF_2$ can easily account for marked differences in A_{12}.

The equations for the critical mole fraction, on the other hand, are independent of A_{12}, depending only upon the difference parameter ξ. Figure 11 shows a plot of $(x_2)_c$ *vs.* ξ for the systems listed in Table V.

(19) R. D. Dunlap, R. G. Bedford, J. C. Woodbrey, and S. D. Furrow, *J. Am. Chem. Soc.*, 81, 2927 (1959).

(20) Reference 17, p 143.

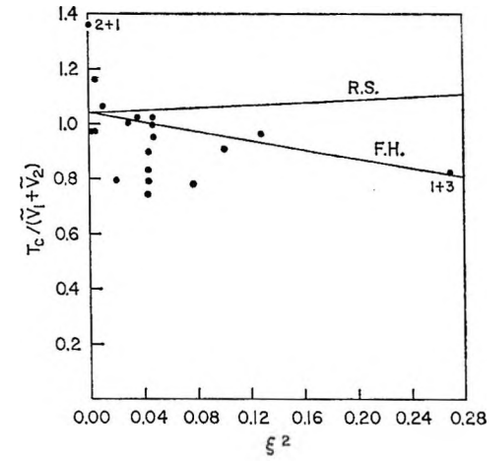

Figure 10. Critical solution temperature [plotted as $T_c/(\tilde{V}_1 + \tilde{V}_2)$] as a function of difference in molar volume [$\xi = (\tilde{V}_2 - \tilde{V}_1)/(\tilde{V}_2 + \xi_1)$] (see eq 9).

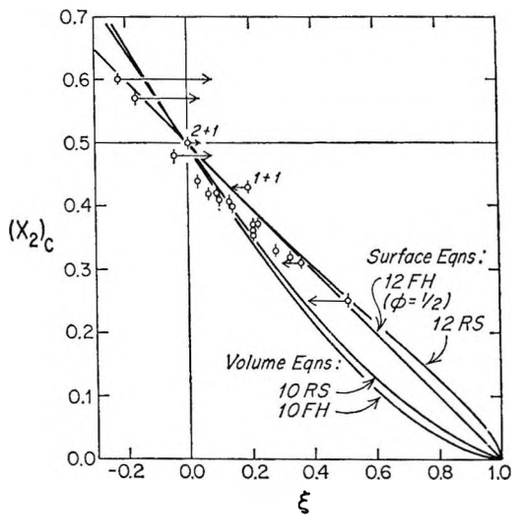

Figure 11. Critical composition $(x_2)_c$ as a function of difference in molar volume ($\xi = (\tilde{V}_2 - \tilde{V}_1)/(\tilde{V}_2 + \tilde{V}_1)$]. The solid lines are the predictions of volume interaction regular-solution theory (eq 10RS) and Flory–Huggins theory (eq 10FH) and the predictions of surface interaction regular-solution theory (eq 12RS) and Flory–Huggins theory (eq 12FH). The horizontal arrows indicate the change in the parameter ξ if it is estimated from the molar volumes of the liquids at the critical solution temperature rather than at their normal boiling points (see footnote 21).

Over the range of ξ represented, the differences between eq 10RS and 10FH (both of which have the same leading term in ξ) are almost trivial and certainly smaller than the differences between either and experiment. The consistency of the experimental points, except for the two systems involving CF_4 (1 + 1 and 2 + 1), is remarkable,[21] while the agreement with the simple volume fraction equation is far from perfect, it is clearly much better than the prediction $(x_2)_c = 1/2$ obtained from the "simple mixture" of Guggenheim,[22] with its excess free energy ($\tilde{G}^E = wx_1x_2$) symmetrical in mole fraction. These measurements (Figure 11) are probably the strongest evidence yet adduced[18] for the importance of molar volume differences in the thermodynamic properties of solutions,[23] and in particular for the superiority of the volume fraction in eq 7. For these systems, however, there is an alternative surface interaction formulation which fits even better.

Surface Interactions. For mixtures of large polyatomic molecules, one can argue that the interactions are between surface elements and that the molar volumes in eq 7 should be replaced by surface areas per mole. For mixtures of long-chain molecules with the same cross section (*e.g.*, two hydrocarbons), the surface area is roughly proportional to volume, and eq 7 can be retained or replaced by the q fractions of lattice theory.[24]

However, fluorocarbons and hydrocarbons do not have the same cross section, so we must fall back upon an even cruder formulation, the zeroth approximation that the surface area is proportional to the two-thirds power of the molar volume. To test this approach, we replace $\tilde{V}_1$ and $\tilde{V}_2$ in eq 7 by $\tilde{V}_1^{2/3}$ and $\tilde{V}_2^{2/3}$. The formalism of eq 9 and 10 remains unchanged if we

(21) One of the referees has questioned our use of molar volumes evaluated at the normal boiling point. He has pointed out that if one uses molar volumes estimated for the critical solution temperature, one obtains different values of ξ which, when used as the abscissa in Figure 11, yield for some systems better agreement with the theoretical volume fraction curves and reduce the discrepancies of the two CF_4 systems. Typical shifts produced by such a re-evaluation of ξ are shown by arrows in Figure 11.

We prefer to evaluate our molar volumes at the normal boiling point for the following reasons.

(1) Any theoretical justification for the volume fraction formulation of eq 7 rests on a model in which the molecules are reasonably close packed. The molar volume used should be a measure of intrinsic molecular size. Since it cannot be measured for the liquid at 0°K, the best alternative is measurement at some kind of corresponding temperature, for which the boiling point is one rough approximation.

(2) Some of the systems (especially those with n-C_4F_{10}) have critical solution temperatures far above the normal boiling point of one of the components. The molar volume of a greatly expanded pure liquid 100° above its normal boiling point (*e.g.*, n-C_4F_{10} at 378°K, only 6° below its gas–liquid critical point) is a very poor measure of the packing of its molecules in a mixture at that temperature. Moreover such "corrected" points (upper left of Figure 11) do not agree with the theoretical curves at all.

(3) An alternative explanation—that of surface interactions—accounts for at least part of the discrepancies observed.

(22) E. A. Guggenheim, "Thermodynamics," 3rd ed, Interscience Publishers, Inc., New York, N. Y., 1957, p 250 ff.

(23) See also ref 13, p 137–151, and J. A. Larkin, J. Katz, and R. L. Scott, *J. Phys. Chem.*, 71, 352 (1967).

(24) E. A. Guggenheim, "Mixtures," Oxford University Press, 1952, especially Chapters X and XI.

replace the variable $\xi = (\tilde{V}_2 - \tilde{V}_1)/(\tilde{V}_2 + \tilde{V}_1)$ by a new variable λ

$$\lambda = \frac{\tilde{V}_2^{2/3} - \tilde{V}_1^{2/3}}{\tilde{V}_2^{2/3} + \tilde{V}_1^{2/3}} = \frac{(1+\xi)^{2/3} - (1-\xi)^{2/3}}{(1+\xi)^{2/3} + (1-\xi)^{2/3}} = \frac{2}{3}\xi + \frac{10}{81}\xi^3 + \frac{38}{729}\xi^5 + \ldots \quad (11)$$

We then obtain as the analogs of eq 10RS and 10FH

$$2(x_2)_c = \frac{1 + \lambda - (1 + 3\lambda^2)^{1/2}}{2\lambda} = 1 - \xi + \frac{4}{27}\xi^3 - \ldots \quad \text{(12RS-surface)}$$

$$2(x_2)_c = \frac{(1-\lambda)^{3/2}}{(1-\lambda)^{3/2} + (1+\lambda)^{3/2}} = \frac{\tilde{V}_1}{\tilde{V}_1 + \tilde{V}_2} = 1 - \xi \quad \text{(12FH-surface)}$$

The result for the modified Flory–Huggins equation is especially simple, for it leads to the conclusion that the critical composition is always at a volume fraction $\phi_c = 1/2$. Unfortunately, this simple result does not appear to have any clear theoretical significance; we do not see any way to derive the surface fraction analog of the Flory entropy of athermal mixing, which would be essential to any consistent derivation of eq 12FH. On the other hand, the regular solution approach combines an ideal entropy of mixing (at constant volume) with an independent interaction energy, so eq 12RS (which is very similar to eq 12FH) is as self-consistent as eq 10RS.

The predictions of these "surface fraction" equations are also shown in Figure 11; we see that the agreement is markedly improved over that of the "volume fraction" equations. How far this result can be generalized is open to doubt, but for hydrocarbon + fluorocarbon mixtures, it should prove very useful. We note that the predicted symmetry of the phase diagram around $\phi_c = 1/2$ (a symmetry which necessarily fails as one approaches $\phi = 0$ and $\phi = 1$, unless $\tilde{V}_1 = \tilde{V}_2$) is a possible explanation of the success of the Munson reduced plot of ϕ *vs.* T/T_c (Figures 6–8).

The success of this surface formulation for the critical composition $(x_2)_c$ suggests that we reexamine the correlation of critical solution temperatures with differences in size. The analogs of eq 9 are

$$\frac{2RT_c}{A_{12}'V^{2/3}} = 1 + \frac{\xi^2}{9} + \frac{4\xi^4}{243} + \ldots \quad \text{(13RS-surface)}$$

$$\frac{2RT_c}{A_{12}'V^{2/3}} = 1 - \frac{\xi^2}{3} - \frac{4\xi^4}{27} + \ldots \quad \text{(13FH-surface)}$$

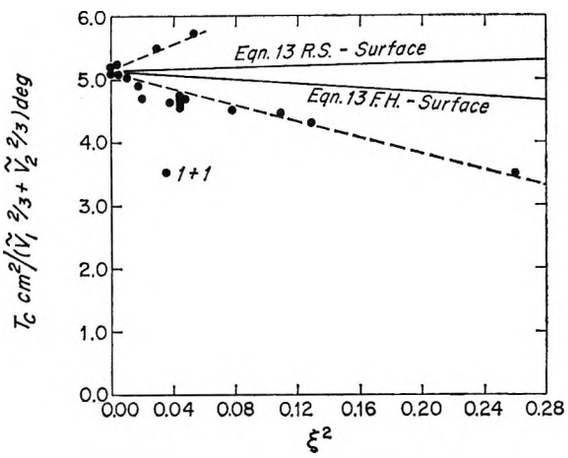

Figure 12. Critical solution temperature [plotted as $T_c/(\tilde{V}_1^{2/3} + \tilde{V}_1^{2/3})$] as a function of difference in molar volume [$\xi = (\tilde{V}_2 - \tilde{V}_1)/(\tilde{V}_2 + \tilde{V}_1)$] (see eq 13 and compare with Figure 10).

where A_{12}' is an interaction constant appropriate to a surface formulation.

A plot of $T_c/(\tilde{V}_1^{2/3} + \tilde{V}_2^{2/3})$ *vs.* ξ^2 is shown in Figure 12. The marked improvement over the scatter in Figure 10 is striking. Except for the system $CH_4 + CF_4$ a pattern emerges, although not that predicted by either eq 13. In spite of the predicted dependence upon ξ^2, an obvious dependence upon the sign of ξ is seen, for three points on the upper dashed curve correspond to negative ξ's.

We are reluctant to attach too much significance to Figure 10 for there is no reason to assume a constant A_{12}'. Since these are pairs in homologous series, there may be a hidden dependence of A_{12}' upon ξ.

It is important to distinguish what we call volume fraction or surface fraction formulations from the symmetry of phase diagrams or of thermodynamic functions. Thus an excess free energy given by eq 7 has a maximum value when

$$(x_2/x_1)_{max} = (\tilde{V}_2/\tilde{V}_1)^{1/2} \quad (14)$$

while at the critical solution point, the mole fraction ratio is entirely different and can be written approximately (exactly in FH) as

$$(x_2/x_1)_c = (\tilde{V}_1/\tilde{V}_2)^{3/2} \quad (15)$$

We see that the phase diagram is much more asymmetric (on a mole fraction scale). The corresponding surface fraction equations involve $\tilde{V}^{2/3}$ and can be written

$$(x_2/x_1)_{max} = (\tilde{V}_1^{2/3}/\tilde{V}_2^{2/3})^{1/2} = (\tilde{V}_1/\tilde{V}_2)^{1/2} \quad \text{(14-surface)}$$

$$(x_2/x_1)_c = (\tilde{V}^{2/3}/\tilde{V}_2^{2/3})^{3/2} = \tilde{V}_1/\tilde{V}_2 \quad \text{(15-surface)}$$

It is the *surface* interaction formulation which yields a

phase diagram which is at least roughly symmetrical in *volume* fraction. For a phase diagram to be symmetrical in surface fraction, one would need interactions proportional to $\bar{V}^{4/3}$.

Acknowledgments. This research was supported by the Atomic Energy Commission and by the National Science Foundation. We thank a referee for a number of very thought-provoking suggestions.

Isotope Effects on Vaporization from the Adsorbed State. The Methane System

by W. Alexander Van Hook

Chemistry Department, University of Tennessee, Knoxville, Tennessee 37916 *(Received May 1, 1967)*

It is pointed out that the statistical theory of isotope effects in condensed systems[1] is applicable to isotope effects on adsorption. The appropriate theoretical equations and approximations to them are discussed. Adsorption isotope effects for the methane "wet glass" system[2,3] are treated in detail as an example. Consistency with the theory is demonstrated and it is concluded that at least for this system rotation on the surface is strongly hindered and that it is not necessary to invoke different interaction potentials with the surface for different isotopically substituted molecules.

Introduction

In recent years, the statistical theory of isotope effects in condensed systems[1] has been successfully applied to processes involving vaporization from condensed liquids[4] and dilute solution.[5] The object of the present paper is to point out that this theory can also be used to treat the isotope effect on adsorption (AIE). After the appropriate formulas and approximations to them have been introduced, we shall proceed to treat the methane system as an example. The essential difference between this treatment and some earlier analyses of methane adsorption[6,7] is that the present approach takes explicit account of the effect of molecular structure on the AIE. It has been shown that structural considerations are essential in the analysis of the isotope effect on vaporization from pure liquids[4] or solution[5] and it is to be expected that they are also important in the AIE. In the second section of the paper, results of Bruner, Cartoni, and Liberti[2] and Bruner and Cartoni[3] are analyzed. These authors measured separation factors for all of the protio, deuterio and C^{13} isomers of methane, some as a function of temperature. Their extensive data including the AIE for the intermediate isotopic isomers afford a good test of the theory. In the paper which follows,[8] some new measurements on the CH_4–CD_4 system are

(1) J. Bigeleisen, *J. Chem. Phys.*, **34**, 1485 (1961).

(2) F. Bruner, G. P. Cartoni, and A. Liberti, *Anal. Chem.*, **38**, 298 (1966).

(3) F. Bruner and G. P. Cartoni, *J. Chromatog.*, **18**, 390 (1965).

(4) (a) J. Bigeleisen, S. V. Ribnikar, and W. A. Van Hook, *J. Chem. Phys.*, **38**, 489 (1963); J. Bigeleisen, M. J. Stern, and W. A. Van Hook, *ibid.*, **38**, 497 (1963); M. J. Stern, W. A. Van Hook, and M. Wolfsberg, *ibid.*, **39**, 3179 (1963); (b) W. A. Van Hook, *ibid.*, **44**, 234 (1966); (c) W. A. Van Hook, *ibid.*, **46**, 1907 (1967).

(5) W. A. Van Hook and J. T. Phillips, *J. Phys. Chem.*, **70**, 1515 (1966).

(6) S. Ross and J. P. Oliver, "On Physical Adsorption," Interscience Publishers, Inc., New York, N. Y , 1964, pp 236, 270.

(7) R. Yaris and J. R. Sams, *J. Chem. Phys.*, **37**, 571 (1962).

(8) J. T. Phillips and W. A. Van Hook, *J. Phys. Chem.*, **71**, 3276 (1967).

presented and these are discussed in the context of the material presented below and then compared with some other earlier measurements of the AIE for the CH_4–CD_4 system on various surfaces.

The Isotope Effect on Adsorption

The statistical theory of isotope effects in condensed systems leads on the basis of a cell model in the condensed phase and the assumption of harmonic frequencies to

$$\ln\left(\frac{P'}{P}\right) = \ln\left(\frac{\gamma' P^{0\prime}}{\gamma P^0}\right) = \sum_{\substack{\text{internal}\\ \text{frequencies}}}^{3N-6} \times \ln\left\{\frac{(u/u')_c}{(u/u')_g}\,\frac{e^{(u'-u)_c/2}}{e^{(u'-u)_g/2}}\,\frac{(1-e^{-u_c'})/(1-e^{-u_c})}{(1-e^{-u_g'})/(1-e^{-u_g})}\right\} + \sum_{\substack{\text{external}\\ \text{frequencies}}}^{6} \ln\left\{\left(\frac{u}{u'}\right)(e^{(u'-u)/2})\,\frac{(1-e^{-u'})}{(1-e^{-u})}\right\} + \frac{1}{RT}(P'V' - PV) + \left\{(B_0P + {}^1/_2C_0P^2) - (B_0P + {}^1/_2C_0P^2)'\right\} - G(\sigma,\sigma')_g \quad (1)$$

Here c and g refer to condensed and gaseous phases, $u = h\nu/kT$, the prime signifies the lighter isotope, γ is the activity coefficient, P^0 the vapor pressure of the pure liquid, and the last three terms are corrective and will be discussed later.

Equation 1 connects the force fields describing the motions of an isolated molecule in the gas phase and those of a condensed molecule in the cell defined by its neighbors with the vapor pressure ratio. These force fields are different owing to the intermolecular forces which become operative in the condensed phase. In the pure liquid they are exclusively "solute–solute" forces, in very dilute solution "solvent–solute," while in more concentrated solutions both types of forces must be considered. Similarly, for an adsorbed gas at low coverage, the origin of the forces is exclusively surface adsorbate in nature but at higher coverages lateral interactions must also be considered. The former case will be of interest later in this paper; it is nicely approximated in gas chromatography.

Now consider the corrective terms. The third term corrects for the isotope effect on molar volume. In the present context it must be rewritten in terms of the surface tension of the adsorbed film and the molar coverage. We expect the latter to be determined by the surface lattice constants and be isotopically invarient at low coverages and to approach $(V'/V)^{2/3}$ only as a limit at high coverages. For CH_4–CD_4 over the liquid range, $(V/V')^{2/3}$ amounts to only 1.007.[9] Similarly, the surface tension of the adsorbed film should be isotopically invarient at low coverages. The limit at high coverages is difficult to estimate. It is likely of the same order of magnitude as for the liquid, which for representative hydrocarbons is only about 0.1%/D atom.[10] The third term then is estimated as negligible even at high coverages.

The fourth term gives the correction for gas imperfection. B_0 and C_0 are the second and third virial coefficients. For pure samples around 1 atm pressure the correction amounts to about 1% of the vapor pressure isotope effect[4c,11] for the CH_4–CD_4 system. At lower pressures, such as were used in the study treated in the latter part of this paper, the corrections are, of course, smaller and may be neglected. (Additionally, it should be remembered that in chromatographic experiments, the sample S is in dilute solution of solvent carrier gas C. The appropriate virial coefficient is then B_{CS}. One might expect that for a helium or other inert nonpolarizable carrier that the isotope effect on B_{CS} would be less than that on B_{SS}. This would tend to make the fourth corrective term even smaller.)

The first two and the last terms in eq 1 then remain to be considered. The former have been derived on the assumption that the harmonic approximation is applicable to both the $3N - 6$ ($3N - 5$ for linear molecules) internal motions and the six (five) external modes which are assumed to be described by a harmonic hindering potential in the condensed phase. For the case where a two-dimensional lattice gas is assumed for the adsorbed system, the partition functions used in deriving[1] the form of eq 1 can be modified to include one or more free translations and/or rotations as needed. Alternatively, the force constants pertaining to these modes can be set equal to zero.

Experiments on the vapor pressure isotope effect[4b,c] have shown that the harmonic approximation is not appropriate for the lattice modes of at least liquid hydrocarbons but it has been found possible to describe these modes in terms of temperature-dependent "effective" harmonic frequencies. The approach is identical with that used in the pseudoharmonic theory which has been successfully applied to both monatomic and molecular solids.[12] For small or moderate temperature changes such effective frequencies might well be effectively constant for some systems at least to within the precision of the experimental measurements.[4a] We

(9) S. Fuks, J. C. Legros, and A. Bellemans, *Physica*, **31**, 606 (1965).

(10) L. S. Bartel and R. R. Roskos, *J. Chem. Phys.*, **44**, 457 (1966).

(11) G. Thomaes and R. van Steenwinkel, *Mol. Phys.*, **5**, 307 (1962).

(12) (a) T. H. K. Barron, *Discussions Faraday Soc.*, **40**, 69 (1965); (b) T. H. K. Barron in "Lattice Dynamics," R. F. Wallis, Ed., Pergamon Press, Ltd., London, 1965, p 247; (c) A. J. Leadbetter, *Proc. Roy. Soc.* (London), **A287**, 403 (1965).

might reasonably expect similar considerations to apply in dealing with adsorbed systems.

The last term in eq 1 is the correction for nonclassical rotation in the gas phase. This correction amounts to several per cent of the isotope effect on the vapor pressure for methane but is much smaller for more massive rotors. Any complete theoretical analysis of the methane system must include such a correction and also take proper account of the relative *ortho*, *meta*, and *para* spin isomers in both the gaseous and condensed phases for the symmetrically substituted isomers.[13] On the other hand, many applications of the theory will be made in an effort to illuminate specific experimental results which are themselves not of sufficient precision to demonstrate spin effects. One such example is the analysis of isotopic separation factors of methane which follows. In view of the fact that no effects due to spin isomerization were observed in the experiments, such small corrections will be ignored in both the gas and condensed phases in the analysis below. This will have the effect of slightly shifting the force constants used to describe the effective harmonic frequencies. Since the corrections would in any event be small, this will not change the force of our arguments. We are then led to

$$\frac{P'}{P} = \prod_{\text{internals}}^{3N-6}\left[\frac{(u/u')_c}{(u/u')_g}\right]\left[\frac{e^{(u'-u)_c/2}}{e^{(u'-u)_g/2}}\right]\times \left[\frac{(1-e^{-u_c'})/(1-e^{-u_c})}{(1-e^{-u_g'})/(1-e^{-u_g})}\right]\times \prod_{\text{externals}}^{6}\left[\frac{u}{u'}\right]_c \times [e^{(u'-u)_c/2}]\left[\frac{1-e^{-u_c'}}{1-e^{-u_c}}\right] \quad (2)$$

We choose to call this result derived on the basis of a cell model, neglect of anharmonicities, gas imperfection, isotope effects on surface coverage, etc., the "complete equation."

If the $3N$ frequencies of the system can be factored into two distinct sets, eq 2 reduces to

$$\ln\frac{P'}{P} = \frac{A}{T^2} - \frac{B}{T} \quad (3)$$

The A term is interpreted as a first-order quantum correction for modes $u \ll 2\pi$. It takes the form

$$A = \frac{1}{24}\left(\frac{h}{k}\right)^2\left\{\sum_{\text{ext}}(\nu'_i{}^2 - \nu_i^2)\right\} \quad (4)$$

where the sum is over the external frequencies. The equation is written here in terms of an Einstein distribution of lattice frequencies but can be easily expressed in terms of the Debye or other distributions. Alternatively suitable averages may be taken over an assumed distribution and substituted into eq 4. The B term accounts for the contribution of the change in zero point energy of the higher ($u > 2\pi$) frequencies on condensation. It is given by

$$B = \frac{h}{2k}\{(\sum\nu_g' - \sum\nu_c') - (\sum\nu_g - \sum\nu_c)\} \quad (5)$$

where the sums are over all internal frequencies.

Methane Adsorption on Wet Glass

In this section we make an application of the theoretical formulas discussed above. Bruner, Cartoni, and Liberti[2] and Bruner and Cartoni[3] have made careful measurements of the isotope effects on adsorption for the systems $^{12}CH_4$–$^{12}CD_4$, $^{12}CH_4$–$^{12}CHD_3$, $^{12}CH_4$–$^{12}CH_2D_2$, $^{12}CH_4$–$^{12}CH_3D$, and $^{12}CH_4$–$^{13}CH_4$. The first pair was measured over the range 84–153°K and the others were measured around 85°K. A capillary chromatographic technique was used. The columns were prepared[2] by drawing soft glass capillary, etching the inner surface at 100° with 20% NaOH solution, washing, drying, and then treating to constant activity by passing nitrogen saturated with water vapor through the column. This last part of the treatment has prompted us to label the columns as "wet glass."

The ratio of corrected chromatographic retention volumes is readily identified with the inverse ratio of thermodynamic activities[5] which in turn is given following the arguments above by the complete equation (eq 2) or the approximation to it (eq 3). The frequencies

$$\frac{V_R}{V_R'} = \frac{\gamma' P^{0\prime}}{\gamma P^0} = \frac{P'}{P} = \text{right-hand side of eq 2} \quad (6)$$

$$\ln\frac{V_R}{V_R'} = \ln\frac{P'}{P} = \frac{A}{T^2} - \frac{B}{T} \quad (7)$$

which enter the equations must of course have been calculated from proper gas and condensed phase force fields. In the calculations which are reported in this paper, eq 6 will be employed exclusively, but we will find it convenient in the discussion to speak of lattice (A) and zero point energy (B) terms and thus to orient much of our discussion about eq 7. (In the temperature region of interest (80–150°K), eq 7 is not a particularly good approximation to eq 6 for the force fields which we employ. The difference is on the order of 10% of the isotope effect itself.)

Ideally, one would have independent spectroscopic data for the gas and condensed phases of ordinary

(13) See R. F. Curl, Jr., J. V. Kasper, K. S. Pitzer, and K. Sathianandan, *J. Chem. Phys.*, **44**, 4636 (1966), for a discussion of the methane case; J. King, Jr., and S. W. Benson, *ibid.*, **44**, 1007 (1966); A. Katorski and D. White, *ibid.*, **40**, 3183 (1964), for treatments of the hydrogen case.

methane. These would enable force fields for the two phases to be determined, the frequencies for all isotopic species to be calculated, and the B terms thus defined. Unfortunately, no spectroscopic data for methane adsorbed on wet glass is available. We, therefore, in our first calculation, I (Table I), assume a B term such as would be deduced from the normal mode frequency shifts on condensation to the liquid. These shifts together with literature references are shown in Table I. The values for the gas-phase frequencies are those calculated from the force field of Jones[14] which is shown in valence coordinates in Table II. The condensed phase fields used in the calculations are also shown. In a second calculation, II (Table I), we have employed the B term which Bruner, *et al.*, deduced[2] by fitting their data for the CH_4–CD_4 system from 85 to 150°K to an equation of type 7. They quote $\ln [V_R(CH_4)/V_R(CD_4)] = (1766/T^2) - (13.8/T)$. We have multiplied the force constant changes employed in calculation I by the ratio B_{II}/B_I to deduce a force field for calculation II which is also listed in Tables I and II.

Table I: Gas and Condensed Phase Internal Frequencies of CH_4 (cm^{-1})

	ν_{gas}[a]	$\Delta\nu_{(gas-liq)}$	(Gas-conc)$_{calcd}$ Field I	(Gas-conc)$_{calcd}$ Field II
$_1$(A)	3143.9	8[b]	8.3	12.8
$_2$(E)	1573.7	1.5[c]	1.5	2.3
$_3$(F)	3154.3	10[d]	10.0	15.5
$_4$(F)	1358.1	1.5[c]	1.5	2.3

[a] Calculated from force field of ref 14. [b] M. F. Crawford, H. L. Welsh, and J. H. Harrold, *Can. J. Phys.*, **30**, 81 (1952). [c] N. Shepard and D. J. C. Yates, *Proc. Roy. Soc.* (London), **A238**, 69 (1956). These authors report $\Delta(\nu_2 + \nu_4) = 3$ cm^{-1}. [d] See ref 15.

It is now necessary to evaluate the A contribution. For methane, the lattice term A can be written[4b]

$$A = \frac{1}{24}\left(\frac{h}{k}\right)^2\left\{3\nu_{tr}'^2\left(1 - \frac{M'}{M}\right) + \sum_{i=1}^{3}\nu_R'^2\left(1 - \frac{I_i'}{I_i}\right)\right\} \quad (8)$$

where ν_{tr}' and ν_R' signify the hindered translational and rotational frequencies of ordinary methane and M, M' and I, I' the masses and moments of inertia of the substituted molecules. One of the most interesting points about the Italian experiments is that the $^{13}CH_4$ measurement enables the relative contributions of the translational and rotational terms to be assessed because the moments of inertia of $^{13}CH_4$ and $^{12}CH_4$ are equal. The term $A(^{13}CH_4)$ is then a direct experimental measure of the translational contribution. Once known, A_{trans} for any other isotopic isomer can be calculated and the A_{rotn} contribution for that isotopic isomer determined by difference. In this fashion the importance of hindered rotation in the adsorbed phase can be assessed. Finally, the separation factors can be calculated for the other isomers using the parameters defined above and the results compared with experiment, thus testing the theory. Such a calculation will be outlined below.

Table II: Force Fields

	Gas[a]	Condensed I	Condensed II
F_r	5.49500[b]	5.46203	5.44403
F_{rr}	0.12400	0.12467	0.12504
F_α	0.54935	0.54821	0.54759
$F_{\alpha\alpha'}$	−0.01855	−0.01855	−0.01855
$F_{\alpha r'}$	0.16519	0.16519	0.16519
$F_{\alpha\alpha''} = F_{\alpha r''}$	0	0	0
		a b	
$(CH_4)_{trans}$[c]		80.75 77.36	81.47
$(CH_4)_{rotn}$		94.51 90.55	106.03

[a] Field and notation of Jones.[14] This author quotes five independent constants which we have expressed as above purely for convenience in using our computational technique. [b] Units are millidynes per angstrom for stretches and millidyne angstroms per square radian for bends. Not all figures are significant; they are reported only for computational accuracy. [c] Lattice force field is reported in terms of the frequencies calculated for the unsubstituted species.

The available data are shown in Table III. It is evident that columns a and b are similar but not identical. A 15–20% difference in the effect is observed between the columns for CH_3D and CD_4. This is not unexpected. Phillips and Van Hook[8] have shown that the separation factor is a function of the water content on glass columns and it is possible that slight differences in column preparation could account for the observed difference. Unfortunately, data for the ^{13}C effect are only available for the b column, whereas we should like to know the ^{13}C effect for both sets of data to facilitate cross-comparisons. In order to procede, we shall directly apply the ^{13}C-b result to calculations on the a column without making a 20% correction because, to anticipate, most of the deuterium isotope effect is due to hindered rotation (an effect which cannot be present in the ^{13}C case). Secondly, even a 20% correction would be only slightly larger than the bounds on

(14) L. H. Jones, *Mol. Spectry.*, **3**, 632 (1959).

Table III: Observed and Calculated Separation Factors for Isotopic Methanes in Units of $10^2[\ln (P_{CH_4}/P_X)]$

X	Temp, °K	Obsd[a] col a	Calcd Ia	Obsd[d] col b	Calcd Ib	Temp fit[f] b	Calcd II
$^{13}CH_4$	84			1.2	(1.2)		(1.2)
	85	1.2[b]	(1.2)[c]				
$^{12}CH_3D$	84			3.3	2.1		3.5
	85	3.9	3.5		3.0		3.3
$^{12}CH_2D_2$	84						
	85	6.3	6.2		5.2		6.2
$^{12}CHD_3$	84						
	85	8.2	8.1		6.8		7.1
$^{12}CD_4$	84		9.8	8.1	(8.1)	8.6	(8.1)
	85	9.4	(9.4)		7.8	8.2	7.8
	100		5.6		4.4	3.8	3.7
	125		2.2		1.5	0.3	0.3
	150		0.6	−1.6[e]	0.0	−1.4, −1.5[e]	−1.3
	200		−0.8		−1.1	−2.5	−2.4

[a] See ref 3. Calculated from reproduction of chromatogram using 4.5 min as correction for residence time in the gas phase (this amounts to a 2% correction on retention times). [b] Transferred from column b. [c] Parentheses denote values used in the fitting process. [d] See ref 2. [e] 152°K. [f] Predicted by the smoothed fit to CH_4–CD_4 data in ref 2; $\ln (P_{CH_4}/P_{CD_4}) = (-13.82/T) + (1766/T^2)$.

the experimental precision and would not materially affect the development below or the conclusions drawn from it.

An outline of the calculation based on field I follows. Substitution of $B_I(^{13}CH_4)$ and the experimental $^{13}CH_4/^{12}CH_4$ ratio (1.012 at 84°K) into eq 3 gave $A_{^{13}C} = 94(°K)^2$. The translational contribution of the CD_4 term is then $321(°K)^2$ since

$$A_{CD_4,trans} = \left(\frac{1 - (M_{CH_4}/M_{CD_4})}{1 - (M_{^{12}CH_4}/M_{^{13}CH_4})}\right) A_{^{13}CH_4}$$

Substitution into eq 7 together with the experimental CD_4/CH_4 ratio, $\ln (P_{CH_4}/P_{CD_4}) = 0.094$ at 85°K (column a), allows the rotational contribution to be estimated as $1094(°K)^2$. The equivalent lattice frequencies and force constants are deduced from eq 8 assuming three isotopic translations and three isotropic librations. Other assumed frequency distributions would not change the force of our arguments. The deduced force constants were employed as initial guesses for lattice constants in a calculation using the complete equation which itself was fit to the experimental CD_4 ratio at 85°K. The final values of the lattice frequencies differed from the initial guesses by only some 2 cm^{-1} out of 90 cm^{-1} at 85°K. The difference is due to the failure of approximation 7 in this temperature range. The final values for the lattice frequencies of condensed CH_4 are reported in lieu of the force constants describing these modes in Table II. It is interesting to compare the result for hindered rotation with the 63 cm^{-1} suggested by Ewing[15] for the liquid. Clearly a significant increase in the barrier hindering rotation occurs in going from the liquid to the wet glass surface.

We have thus employed the $^{13}CH_4$ and the CD_4 data together with an internal field assumed to be equivalent to the liquid to fix a condensed phase force field for adsorbed methane. Isotope effects for the intermediate isomers are easily calculated using the complete equation. The results at 85° are compared with experiment in Table III. The predicted intermediate separation factors at 85° (Table III) are in striking agreement with experiment. They unequivocally demonstrate that hindered rotation is occurring on the surface. (In the absence of hindered rotation, the effects would go 2.35, 4.7, 7.0, and 9.4% for CH_3D, CH_2D_2, CHD_3, and CD_4 instead of the observed 3.9, 6.3, 8.2, and 9.4%.)

In a second calculation (Ib), internal field I was fit to the CD_4 data on column b at 84°K by the procedure outlined above. The calculated isotope effects for the other isomers are shown in Table III. The agreement with the available experimental data (CH_3D at 84°K) is again satisfactory. The results calculated at other temperatures from field Ib are also shown. These can be compared with the values calculated from Bruner, *et al.*, smoothed fit to the data. The tail off from the calculated values at the higher temperatures reflects the choice of a B term significantly lower than the experimental best fit.

In a final calculation, field II was fit to the CD_4 data at 84°K on column b. The results of calculations with this field are shown in the last column of Table III.

(15) G. E. Ewing, *J. Chem. Phys.*, **40**, 179 (1964).

Agreement is again satisfactory. In particular, the temperature coefficient is better than that for field Ib. This is to be expected from the relative starting points of the two calculations; even so, calculation Ib reproduces the observed temperature variation of the CD_4/CH_4 data remarkably well and there is actually very little reason to choose between the two fields from this criterion alone.

In summation, we should like to reemphasize that our object has been not to deduce a unique force field which describes the molecular motions of adsorbed methane but rather to demonstrate that the isotope effects displayed by this system are consistent with the theory of isotope effects in condensed systems. To do so we employed two different but plausible condensed phase internal force fields and deduced the translational and librational contributions from the data on two isotopes at one temperature. The data on the temperature coefficient and on the intermediate isomers served as a test for the theory. The results indicate that rotation on the surface is strongly hindered. They also show in a broader sense that isotope effects on adsorption can be understood in terms of the adsorbed layer surface interaction and that such interpretation must include the effect of the details of the molecular structure.

The present approach is then to be contrasted with calculations which are based on virial expansion techniques.[7,16] A proper virial calculation is in principle exact, at least in the low-coverage limit. The details of surface–molecule and molecule–molecule interactions can be treated using effective pair potentials which for polyatomic molecules are angle dependent. Proper inclusion of the angular dependency should lead to treatment of the effects we have labeled as "due to hindered rotation." In actual fact, however, the gas surface interaction for structured molecules is so complicated that it becomes necessary to spheracalize the potential. In that event, the angularly dependent (hindered rotational) properties are hidden under the new spheracalized effective potential which is now, in general, isotope dependent.[17] Such effective potentials are not able to explain details of the interaction due to molecular geometry such as the large deviations from the rule of the mean discussed in the present paper. The point is that details of molecular structure are important and should be considered and that the Bigeleisen approach which is employed here offers a convenient formalism for making such considerations.

Acknowledgment. This research was supported by The Petroleum Research Fund administered by the American Chemical Society. Conversations with Dr. Max Wolfsberg of Brookhaven National Laboratory were helpful in the formulation of this paper.

(16) (a) P. L. Gant and K. Yang, *J. Am. Chem. Soc.*, **86**, 5063 (1964); (b) G. Constabaris, J. R. Sams, and G. D. Halsey, Jr., *J. Phys. Chem.*, **65**, 367 (1961).

(17) A reference which also gives many citations to work developing this point of view is R. Wolfe and J. R. Sams, *J. Chem. Phys.*, **44**, 2181 (1966).

Gas Chromatography of Perdeuteriomethane. Isotope Effect on Adsorption on Porous Glass

by James T. Phillips and W. Alexander Van Hook

Chemistry Department, University of Tennessee, Knoxville, Tennessee 37916 *(Received May 1, 1967)*

The separation factor for CH_4–CD_4 on dry porous glass was measured between room temperature and −170°. The isotope effect is inverse and approximately linear in $1/T$. A significant lowering of the isotope effect is observed when the surface is poisoned with water. The results are discussed in the context of the statistical theory of isotope effects in condensed systems and consistency with the theory is demonstrated.

Introduction

The gas chromatographic fractionation of compounds isotopically substituted with deuterium (and/or tritium) is a topic of current interest. References to the current literature are given by Van Hook and Phillips.[1] They summarized some recent gas–liquid chromatographic results and demonstrated consistency with the statistical theory of isotope effects in condensed systems as formulated by Bigeleisen.[2]

The problem of the isotope effect on physical adsorption is also amenable to treatment by the theory.[3] The case of CH_4–CD_4–surface is of interest. A number of authors have reported values for the CD_4/CH_4 isotope effect as a function of temperature on various surfaces.[4] Unfortunately, the zero point energy shift on condensation has not been independently determined in any of these systems and thus an independent check on the predictions of the theory is precluded.

On the other hand, Shepard and Yates[5] have made a careful determination of the zero point energy shifts on adsorption for the methane–porous glass (Vycor) system by an infrared technique. Their data are shown in Table I. The adsorbed phase measurements were made at about 90°K. The results may be employed to determine a condensed phase force field which, together with the gaseous field,[6] may be used to evaluate the zero point energy (B) term discussed in the preceding paper. If an independent assessment of the lattice (A) term can be made, the isotope effect itself can be estimated. We therefore decided to measure separation factors for the CH_4–CD_4 system on a glass surface prepared in a fashion as identical as possible with that of Shepard and Yates. Comparison between the measured isotope effects and those calculated from the spectroscopic data would then provide a test of the theory. It should be emphasized at the outset that our study was not directed toward elucidating the nature of the glass surface or of the energetics of the glass–methane interaction. We rather selected this particular surface because the vibrational spectrum of the adsorbed species had been measured and these results could be employed to make a straightforward prediction of the isotope effects by a calculation based only on the properties of the gas phase and sorbed molecules. The nature of the adsorptive surface does not directly enter.

It was our original idea when planning the experiments described below that the A term would be relatively small and easy to estimate. Studies on vapor pressure ratios of various hydrocarbons[7] with B terms of the order of magnitude of that shown in Table I give

(1) W. A. Van Hook and James T. Phillips, *J. Phys. Chem.*, **70**, 1515 (1966).

(2) J. Bigeleisen, *J. Chem. Phys.*, **34**, 1485 (1961).

(3) W. A. Van Hook, *J. Phys. Chem.*, **71**, 3270 (1967).

(4) (a) P. L. Gant and K. Yang, *J. Am. Chem. Soc.*, **86**, 5063 (1964); (b) F. Bruner, G. P. Cartoni, and A. Liberti, *Anal. Chem.*, **38**, 298 (1966); (c) F. Bruner and G. P. Cartoni, *J. Chromatog.*, **18**, 390 (1965); (d) G. Constabaris, J. R. Sams, Jr., and G. D. Halsey, Jr., *J. Phys. Chem.*, **65**, 367 (1961).

(5) N. Shepard and D. J. C. Yates, *Proc. Roy. Soc.* (London), **A238**, 69 (1956).

(6) L. H. Jones, *Mol. Spectry.*, **3**, 632 (1959).

(7) (a) J. Bigeleisen, S. V. Ribnikar, and W. A. Van Hook, *J. Chem. Phys.*, **38**, 489 (1963); (b) J. Bigeleisen, M. J. Stern, and W. A. Van Hook, *ibid.*, **38**, 497 (1963); (c) W. A. Van Hook, *ibid.*, **44**, 234 (1966); (d) W. A. Van Hook, *ibid.*, **46**, 1907 (1967).

Table I: Observed Frequencies of Gas Phase and Adsorbed Methane

Frequency	Species	ν_{gas}[a]	ν_{ads}[a]	$\nu_{gas} - \nu_{ads}$[a] (calcd)
ν_3	F	3018.8	3006 ± 2	12.8 (12.8)
ν_1	A	2916.5	2899 ± 2	17.5 (17.5)
$\nu_2 + \nu_4$	F + E	2823	2819 ± 10	4.0 (2.0 + 2.0)

[a] See ref 5.

A/T^2 contributions usually much less than 50% of B/T. In such an event, the A contribution would not need to be precisely known in order to test the outlines of the theory. Since the experiments were completed, the results of Liberti and his co-workers[4b] have become available. They indicate that at least on wet glass the A/T^2 contribution in fact predominates.[3] This observation makes the analysis of the results which follow less straightforward.

Experimental Section

We chose to measure the isotope effect by a chromatographic technique. The sample of porous (Vycor) glass was essentially identical with the glass employed by Shepard and Yates.[5] It consisted of small pieces of cullet which were further crushed and screened. A 60/100 mesh cut was used. The glass was heated in air to 400° to remove any organic deposit by oxidation and then packed into 0.06–0.08-in. i.d. glass or copper tubes which were compactly coiled and fixed to a previously described[8] "homemade" gas chromatograph apparatus employing a helium carrier and thermal conductivity detection. Precautions were taken to dry the helium carrier by passing it through a charcoal trap immersed in liquid nitrogen before entering the column. The columns were baked overnight at 400° in a stream of dry helium (or sometimes oxygen followed by dry helium for columns with glass walls) to remove any water adsorbed during the packing procedure. After treatment they were carefully protected from water vapor and, as a final precaution, were periodically baked to ensure dryness. In this fashion, we hoped to ensure a surface nearly approximating that used by Shepard and Yates. We choose to call a surface prepared in this fashion "dry" even though we are aware that additional water can be removed by heating to higher temperatures. However, the point of interest was not to investigate separation factors as a function of the water content of the surface but rather to measure them on any surface where an independent spectroscopic study had been made. It was observed that the chromatographic properties of the surface are affected by the water content (see below).

The adsorption of methane on dry porous glass columns is marked and highly nonideal chromatographic peaks are observed. (These were of the shape which Keulemans[9] categorizes as type IV.) Even at high temperatures, inordinate tailing prevented the possibility of actually resolving separate and well-defined chromatographic peaks for CH_4 and CD_4. It was therefore necessary to determine the retention times of the two species in separate runs. To do so, the system was allowed to equilibrate thoroughly at the experimental temperature with the flow rate and column length selected so the observed retention time was on the order of 1–20 min. (Longer times were inconvenient because of the difficulty of maintaining constant bath temperatures over long periods while for shorter times the relative error in time measurement becomes important.) The appreciable temperature coefficient of adsorption forced the use of a wide variety of column lengths. These varied from 50 ft used at the highest (23°) temperatures to the 1.5-in. column used at −166°. Alternate injections of CH_4 and CD_4 were made. The reproducibility of these alternate CH_4 (or CD_4) injections served as criteria of the experimental technique.

A point of further complication is that for this highly nonideal system the peak shape and position are functions of the sample size as well as of the temperature. A somewhat exaggerated example is shown in Figure 1.

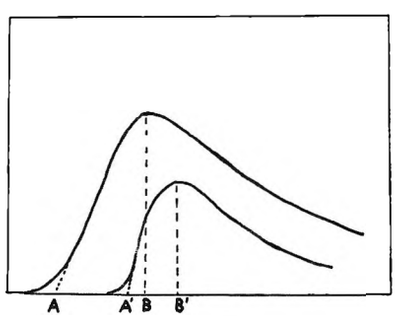

Figure 1. Chromatographic peak shapes.

The skewed shape of the peaks might well indicate that a single activity coefficient will not serve to describe adequately the gas–surface interaction at all concentrations mapped by the peak. Even so, it was our working hypothesis that equivalent parts of the curves could be compared to determine a ratio (*i.e.*, the isotope effect). To do so, the corrected retention times of the peak maxima (B, B′) or of first appearance (AA′) were

(8) W. A. Van Hook and M. E. Kelly, *Anal. Chem.*, **37**, 508 (1965).

(9) A. I. M. Keulemans, "Gas Chromatography," Reinhold Publishing Corp., New York, N. Y., 1957, p 101.

plotted *vs.* peak area (sample size) for both isotopes. The plots were linear to within experimental error for our range of sample sizes (0.05–0.3 cc of NTP). They were extrapolated to zero sample size and the ratios of these corrected retention times defined the experimental isotope effect. The measured ratio was the same to within experimental error for either the peak maxima or position of first deflection.

One possible origin for the extreme nonideality of the chromatographic peaks is that the surface is nonuniform and contains sites of varying adsorption energy. The relative occupancy of such sites could depend strongly on temperature and this should be reflected in the thermodynamics of the adsorption process and thus in the isotope effect. It would also be reflected in a significant temperature coefficient for the spectroscopic frequencies of the adsorbed species. In that case, the observed separation factors and those calculated from the spectroscopic data could only be meaningfully compared near the temperature at which the spectroscopic measurements were made. The frequency shifts on condensation are not available as a function of temperature for methane, but it is interesting to note that for acetylene sorbed on porous glass, $\Delta\nu_3$ decreases by about 30% on warming from 90 to 300°K. If a similar temperature coefficient on the zero point energy shift of methane was operative, it would tend to improve the agreement between the observed and calculated isotope effects (see below).

The porous glass used in these columns retained oxygen, nitrogen, and even hydrogen strongly. It was therefore necessary to estimate the dead volume from the column dimensions rather than to measure the retention volume of an inert gas in order to determine the corrections to the observed retention times. These were very small except for the longest (50 ft) column.

Results and Discussion

The results are shown plotted *vs.* reciprocal temperature in Figure 2 as the natural logarithms of the corrected retention volume ratios. The bars indicate our assessment of the experimental error. Within the experimental precision, which is not good, the effect is approximately linear in $1/T$. This indicates a small A term in an equation of the type $\ln(P/P') = (A/T^2) - (B/T)$.[3] The results of Gant and Yang[4a] on charcoal and of Liberti[4b] on wet glass are also indicated for purposes of comparison.

We wish to consider first the effect on the dry glass. It is unfortunate that methane was so strongly adsorbed that it was impossible to measure the isotope effects down to 90°K and thereby make a direct comparison with the effect calculated from the data of Shepard and Yates[5] at their experimental temperature. Nonetheless, it is interesting to make comparisons at higher temperatures.

The spectroscopic data are shown in Table I. Jones[6] gives a gas phase (harmonic) force field which is convenient for our purposes. We have used the data in Table I to define the condensed phase internal field quoted in column 2 of Table II. The predicted phase shifts are given in the last column of Table I. These correspond to a predicted zero point energy term of $12.7/T$. It is interesting at this point to consider some calculations using the complete equation (eq 6 of the preceeding paper). In the first calculation (A), the lattice constants were selected such that the perpendicular hindered translation for CH_4 was 73 cm^{-1} (a value deduced from Oliver and Ross[10] for methane adsorbed on charcoal) and the other lattice frequencies were set equal to zero. In a second calculation (B), we set $T_x = T_y = 50$ cm^{-1}, $T_z = 73$ cm^{-1}, $R_x = R_y = 25$ cm^{-1}, and $R_z = 0$. The results are shown as the dotted lines in Figure 1. Agreement with the experimental values is evidenced at the lower temperatures but it worsens as the temperature is raised. This is because the calculations are in the harmonic approximation and an intercept near 0, 0 is demanded. For the real system anharmonicities, changes in condensed phase force constants, etc., are to be expected. The result is a marked deviation from the harmonic temperature dependence. Therefore, comparisons between the spectroscopically based calculations and the experiments should be made only in the low-temperature region.

Table II: Internal Force Fields for Gas Phase and Adsorbed Methane

	Gas[a]	Adsorbed
F_r	5.4950	5.4467
F_α	0.5493	0.5478
F_{rr}	0.1240	0.1184
$F_{\alpha r'}$	0.1652	0.1652
$F_{\alpha r''}$	0.0000	0.0000
$F_{\alpha\alpha'}$	−0.0186	−0.0186
$F_{\alpha\alpha''}$	0.0000	0.0000

[a] Field of Jones[6] transformed to valence coordinates.

The most significant point concerning these data are that they suggest a very small A term. This is surprising in view of the analysis[3] of the Italian data on wetted glass where the lattice contribution was demonstrated to be large. It dominates the total effect and produces the negative slope of the lowermost line of

(10) S. Ross and J. P. Oliver, "On Physical Adsorption," Interscience Publishers, Inc., New York, N. Y., 1964, p 236.

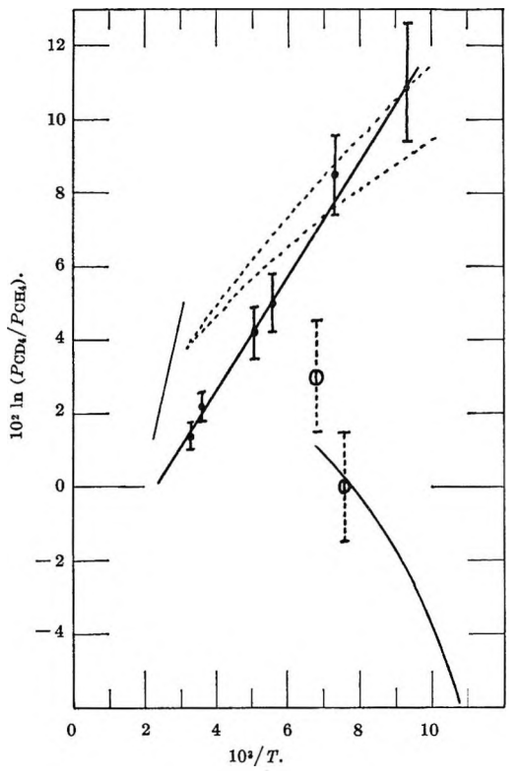

Figure 2. Chromatographic separation factors for CD_4–CH_4: ●, present data on dry porous (Vycor) glass; ○, present data on wet porous (Vycor) glass; lower solid curve, smoothed data of Bruner, Cartoni, and Liberti[4b] on wet glass capillary; uppermost solid line, smoothed data of Gant and Yang[4a] on charcoal; upper dotted lines, calculated from complete equation (eq 6, ref 3). (Top, field A; bottom, field B.)

Figure 2. Even so, the temperature dependency of their data indicates a large B term of 13.8°K,[4b] even larger than the 12.7°K calculated here for dry Vycor. The basic difference between the two surfaces then must lie in the relative lattice contributions. In a final experiment, a dry porous glass column at room temperature was wet by equilibrating it for about 12 hr with a stream of helium which had been bubbled through water also at room temperature. Separation factors were then measured at two temperatures. The results are shown in Figure 2 with the other data. It is clear that the isotope effect is significantly lowered from the values found on the dry column. (The absolute retention times were also lowered.) Note also that the sign of the temperature coefficient has changed and that these wet glass results are in satisfactory agreement with the data of Liberti, *et al.*, on their wetted columns. We conclude that the essential difference between the two columns is the presence of the water. This makes the surfaces markedly different. Evidently on the wet glass (which is probably completely covered with water), the external lattice modes are strongly hindered, while on the dry surface they are not. The zero point energy terms are of comparable magnitude for both surfaces. The difference could well lie in the rotational contribution. The idea that rotation is not strongly hindered on dry porous glass agrees with the analysis of the band shape of ν_3 for adsorbed methane given by Shepard and Yates.[5] They state that at least one, but not as many as three, degrees of rotational freedom are consistent with the observed band shape. However, they give no estimate of the size of any of the remaining barriers to rotation on the surface. (Clearly this point could be settled experimentally by comparing the retention times of CH_3D and $^{13}CH_4$ on the dry surface.[3] Unfortunately, however, experimental difficulties prohibited these measurements on our columns at the necessary level of precision.)

A final comparison of the separation factors can be made with the data of Gant and Yang[4a] taken on charcoal. These data are also shown in Figure 2. The slope is positive and almost twice the value for that on the porous glass. Accordingly, a significantly larger B term and total frequency phase shift are to be expected with this system. Unfortunately, we know of no infrared data on the methane–charcoal system which could be used to test this prediction.

We conclude that the data presented in this paper for the CH_4–CD_4–dry Vycor porous glass surface system demonstrate consistency with the theory of isotope effects in condensed systems and with the earlier spectroscopic data on this system. In a broader sense, it strengthens the point of view that isotope effects on adsorption can only be understood in terms of the adsorbed layer–surface interaction itself. Obviously, any interpretation must include not only the molecule surface interaction itself but also the effect of the details of molecular structure. The reason that different surfaces exhibit different effects is simply because the parameters describing the molecule–surface interaction are different.

Unfortunately, the system which we selected for study exhibits such a large adsorbate–surface interaction that it is useless in any practical sense for chromatographic separations.

Acknowledgment. This work was supported by the Petroleum Research Fund administered by the American Chemical Society. We wish to express our thanks to the donors of said fund. We also wish to thank Dr. D. J. C. Yates of Esso Research for the donation of the porous glass.

Ultraviolet Absorption of Ammonia at High Temperatures behind Shock Waves

by P. G. Menon[1] and K. W. Michel[2]

Institute of Physical Chemistry, University of Göttingen, Göttingen, West Germany *(Received November 29, 1966)*

Ultraviolet absorption of ammonia heated to 2600°K behind shock waves has been studied at 2225, 2300, and 2400 A. The values of E in the Boltzmann factor obtained from a plot of log ϵ *vs.* $1/T$ of the shock-tube data agree fairly well with the energies above $v_2'' = 0$ in the $2p_z$–3s transition obtained from spectroscopic measurements by Walsh and Warsop. Absorption is also observed at 3360 A, indicating the formation of NH radicals in the shock-tube decomposition of ammonia.

Ultraviolet absorption data for ammonia at room temperature have been recently reported by Walsh and Warsop,[3] who have tried to give an interpretation of the spectrum using the older as well as their new results. Dixon[4] studied the absorption of ammonia heated to 900°K and was able to obtain bands up to 2431 A. At higher temperatures complications arise owing to the heterogeneous decomposition of ammonia on the walls of the container. Shock-tube heating of ammonia and the measurement of absorption by the gas, heated by the incident and reflected shock waves, seemed to be a way out of the above difficulty. Temperatures up to 2600°K for ammonia–argon mixtures could be reached in this way. At still higher temperatures the decomposition of ammonia is too rapid to measure the initial absorption spectrophotometrically.[5]

The use of shock-tube techniques for the study of physicochemical problems has been dealt with in detail in three recent monographs.[6-8] The kinetics of the shock-tube decomposition of ammonia has been studied by Jacobs[9] and Mathews, Gibbs, and Holsen.[5] Since ammonia is one of the products in the pyrolysis of hydrazine, its behavior at high temperatures is of particular interest in the study of hydrazine.[10] The results obtained for the ultraviolet absorption of ammonia in the shock tube up to about 2600°K are given in this paper.

Experimental Section

The Shock Tube. An eloxized square aluminum pipe, 3.2 cm on a side inside, is used as the shock tube. The high-pressure driver section is 180 cm long so that the reflected rarefaction wave cannot interfere with the reaction at the observation window for at least 1 msec. This section can be filled with hydrogen as driver gas up to 16 atm pressure. It is equipped with a turnable knife near the flange for cutting an aluminum diaphragm of thickness 0.15–0.20 mm. The low-pressure section is 250 cm long and is provided with a gas inlet and a vacuum connection at opposite ends as shown in Figure 1. At 90 and 190 cm from the middle flange, glass windows are fixed flush with the wall. At 240 cm from the flange, *i.e.*, 10 cm from the end plate, quartz windows (Ultrasil from Heraeus, 91% transmission at 2300 A) are used for transmitting ultraviolet light.

Electronic Setup. A simple schlieren arrangement with two RCA 931 photomultipliers at the first two windows furnishes the time signals for measuring the initial speed of the incident shock. The first signal

(1) Regional Research Laboratory, Hyderabad-9, India.

(2) Institut fuer extraterrestrische Physik, 8064 Garching bei Muenchen, West Germany.

(3) A. D. Walsh and P. A. Warsop, *Trans. Faraday Soc.*, **57**, 345 (1961).

(4) J. K. Dixon, *Phys. Rev.*, **43**, 711 (1933).

(5) J. C. Mathews, M. E. Gibbs, and J. N. Holsen, presented at the 139th National Meeting of the American Chemical Society, St. Louis, Mo., 1961.

(6) E. F. Greene and J. P. Toennies, "Chemische Reaktionen in Stosswellen," Dietrich Steinkopff Verlag, Darmstadt, 1959.

(7) A. Ferri, Ed., "Fundamental Data Obtained from Shock-Tube Experiments," AGARDograph No. 41, Pergamon Press Inc., New York, N. Y., 1961.

(8) A. G. Gaydon and I. R. Hurle, "The Shock Tube in High Temperature Chemical Physics," Reinhold Publishing Corp., New York, N. Y., 1963.

(9) T. A. Jacobs, PB Report 149, 140, U. S. Department of Commerce, Office of Technical Services, Washington, D. C., 1960; *J. Phys. Chem.*, **67**, 665 (1963).

(10) K. W. Michel and H. G. Wagner, *Z. Physik. Chem.*, **68**, 3318 (1964).

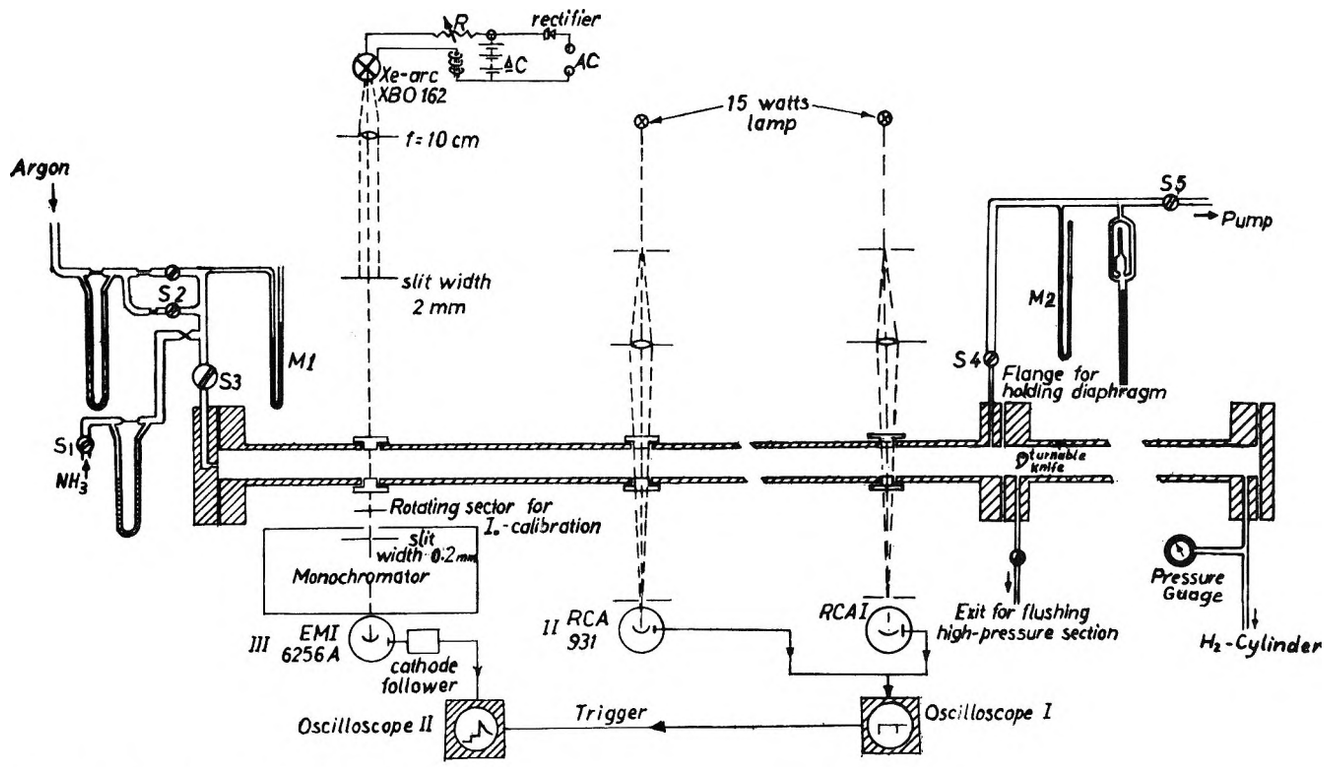

Figure 1. Experimental setup for shock-tube studies.

serves as a trigger for oscilloscope I (Tektronix 545, 53/54K plug-in unit). The plus gate pulse at the end of the sweep serves as a trigger for oscilloscope II (same type as the first) which exhibits the photoelectric current from an EMI6256A photomultiplier at the third station. The third signal of the incident shock at station III is recorded, and not only shock velocity but also shock attenuation can be determined. For calculating instantaneous shock speeds, it is assumed that the attenuation is linear with respect to distance. The instantaneous Mach number can be calculated correct to 0.5%. Since the arrival of the reflected shock wave at station III is indicated by a further signal, the reflected shock velocity can also be calculated. Owing to the short distance (10.2 cm) from the end plate, however, this velocity may have an error of 1.4%. Hence its determination serves only as a check for the consistency of the data; the parameters of the incident shock are all calculated from the Mach number M_s of the incident wave.

Absorption Measurements. A xenon high-pressure arc (Osram XBO 162, feed current 10-amp dc) emits the ultraviolet light which passes through the quartz windows of the shock tube. It is focused far behind the first slit of the monochromator (Zeiss M4 QII, dispersion $d\lambda/ds$ = 27 A/mm). The light intensity is measured before and after each run by using a rotating sector of 2.8 kc/sec.

Absorption measurements for ammonia at 2175, 2225, 2300, and 2400 A have been made. The occurrence of NH radicals during the decomposition of ammonia has been investigated by measurements at 3360 A.

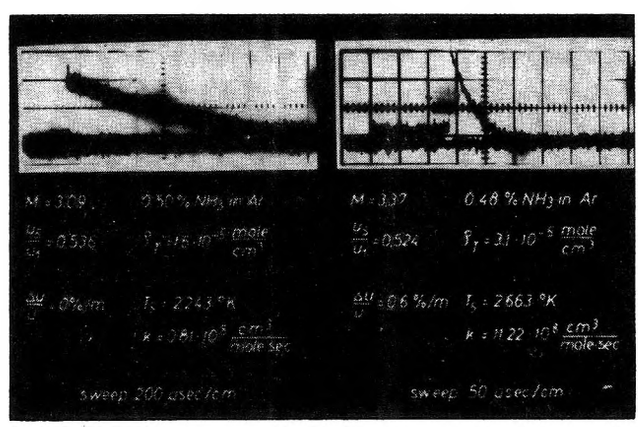

Figure 2. Typical example of traces from oscilloscope II. Absorption of ultraviolet light by ammonia heated by the incident and by the reflected shock waves. The latter is followed by a marked decomposition of ammonia, as indicated by the falling off of the trace from maximum absorption.

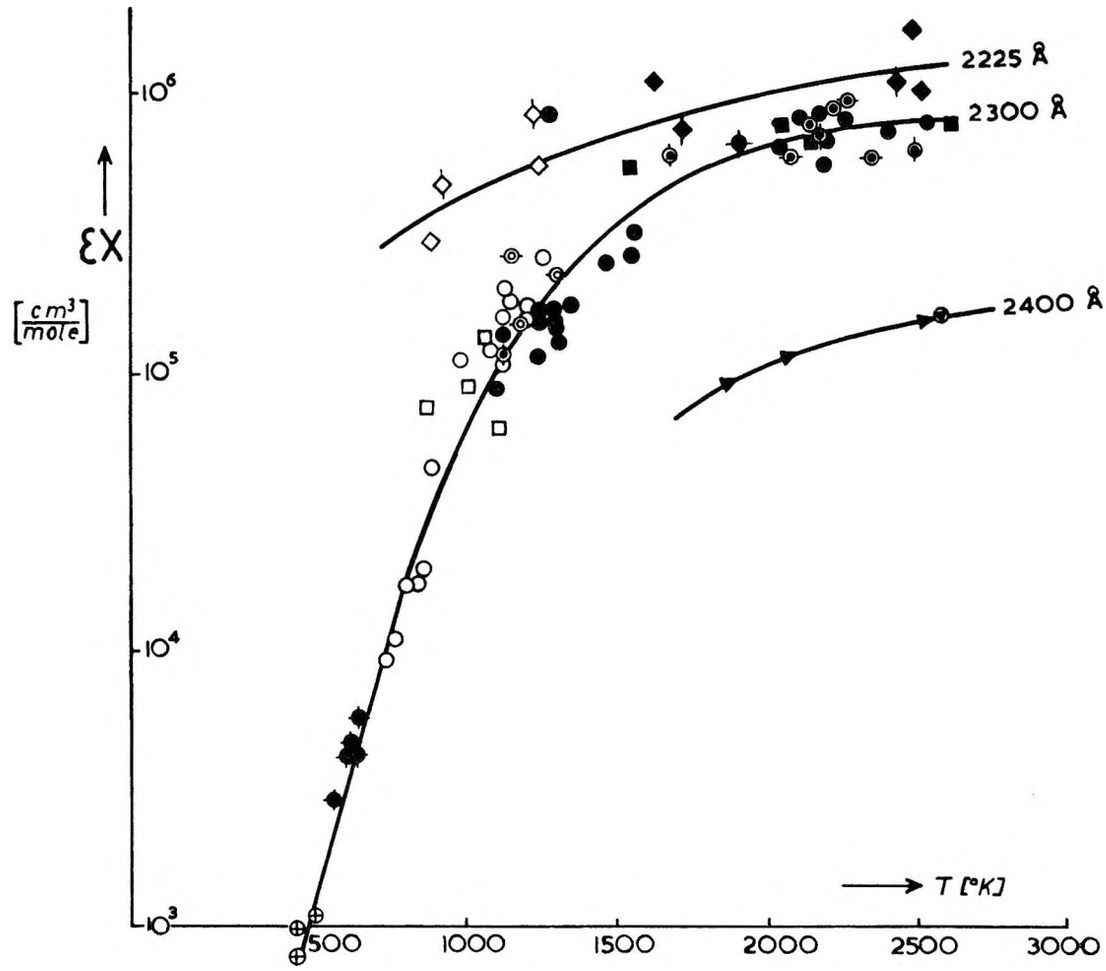

Figure 3. Extinction coefficient of ammonia as a function of temperature. Open points indicate incident shock data and closed points, reflected shock data. A cross on a point indicates shocks in 100% ammonia; a vertical stripe, 0.8% ammonia in argon; a horizontal stripe, 0.4%; and no stripe, the most general case of 1.8–2.5%. An encircled point indicates a driver gas pressure of 13 atm, an incident shock pressure of about 3 atm, and a reflected shock pressure of about 15 atm; for other points these pressures are 4, 1.2–2.0, and 5.5–7.0 atm, respectively. The shock reflection is usually at 10.2 cm from the observation window except for the square points for which it is at 0.8 cm.

Materials. Ammonia and hydrogen are taken directly from cylinders without further purification. Tank argon for welding is used as the diluent for ammonia. A mass spectrometric check of the argon shows that it contains 40 ppm of nitrogen.

Procedure. The low-pressure side of the shock tube is evacuated and a stream of the mixture of argon with ammonia of the desired composition (0.4–2.5% NH_3) is passed through it, maintaining the final pressure (8–25 cm) for at least 15 min before the inlet and vacuum-line stopcocks are closed simultaneously. This is necessary to ensure that the concentration of ammonia in the stream, indicated by the flowmeters, is not altered owing to a subsequent attainment of adsorption equilibrium of ammonia on the inner walls of the eloxized aluminum shock tube. The rest of the procedure is standard shock-tube practice.[6-8]

Results

In deducing extinction coefficients (ϵ) from oscilloscope traces, it is assumed that there is a homogeneous distribution of ammonia across the entire shock-tube diameter (light path through hot gas). This was substantiated by varying the ammonia concentration by a factor of 20, whence the value of ϵ was still found to be the same within the accuracy of the measurements. The other assumption is that the absorption band does not have any fine structure. This was shown by the fact that slight variations of the wave length on the monochromator caused no serious alteration in ϵ.

From this one may conclude that the rotational structure has been blurred out.

Two typical examples of traces from oscilloscope II are shown in Figure 2. The extinction coefficient of ammonia at the temperature and density of the gas behind the incident wave (T_2, ρ_2) and the reflected wave (T_5, ρ_5) can be evaluated from these oscillograms. The values of ϵx are given in cm³/mole (x is the geometric path length of 3.2 cm). A plot of ϵx *vs.* T for various ammonia concentrations yields distinct curves for the three wavelengths used (Figure 3). Good agreement is seen with the results from runs where the driver gas pressure is 13 atm instead of the usual 4 atm, or when the reflection of the shock is at 0.8 cm from the third window instead of the usual distance of 10.2 cm. (For this run a dummy aluminum block of length 9.4 cm is placed in front of the end flange.) The data from reflected shock waves also tally well with those from the incident shock waves.

Light absorption by ammonia in the initial gas at room temperature is quite negligible at the wavelengths used. Corrections to account for stray light in the monochromator have to be applied to the light intensity at 2225 A (3.5–4.3% depending on the slit opening); no correction is found to be necessary at wavelengths above 2300 A.

Discussion

In light of the spectroscopic data for ammonia given by Walsh and Warsop,[3] the present absorption measurements are carried out within the band whose vibrational origin, $v_2'' = 0$, lies at 2168 A. This band corresponds to the $2p_z$–3s transition of ammonia. Since the extinction coefficient values increase with temperature, they must arise from ground-state vibrational levels with quantum numbers v_2'' greater than zero. Bands at 2212, 2245, 2287, 2335, and 2390 A have been assigned[3] to the vibrational transitions $v_2'' = 1$, 2, 3, 4, and 5, respectively, all going to $v_2'' = 0$. The energies above $v_2'' = 0$ in the $2p_z$–3s transition obtained from spectroscopic measurements[3] are compared in Table I with the values of E in the Boltzmann factor, obtained from a plot of log ϵ *vs.* $1/T$ of the shock-tube data (Figure 4).

Table I: Comparison of Spectroscopic Results with Shock-Tube Results

Spectroscopic results			Shock-tube results	
Energy levels	λ, A	Energy above $v_2'' = 0$, cm⁻¹	λ, A	E, cm⁻¹
			2225	1310
2⁺	2245	1597		
3⁺	2287	2380		
			2300	2620
4⁺	2335	3330		
5⁺	2390	4315		
			2400	3200

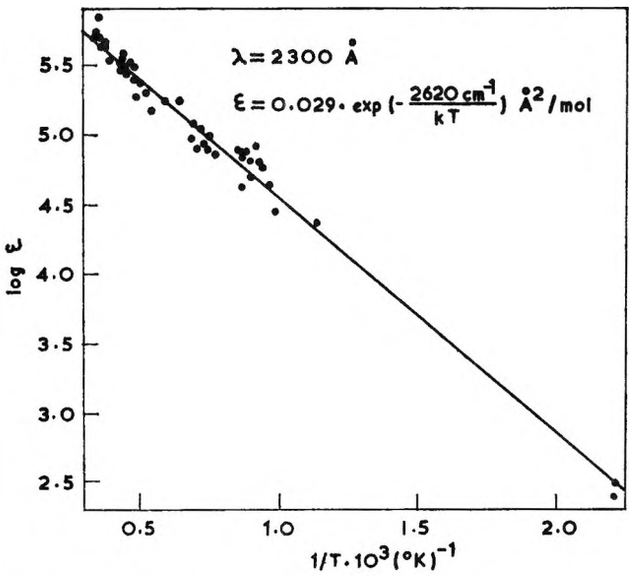

Figure 4. Plot of log ϵ *vs.* $1/T$ at 2300 A.

The results are fairly satisfactory, especially when one remembers that the shock-tube data are all calculated on the basis of ideal one-dimensional shock theory.

Appreciable light absorption has been observed at 3360 A. This may be an indication of the occurrence of NH radicals in the shock-tube decomposition of ammonia. No absorption is seen at 3000 A. The occurrence of NH radicals in the catalytic decomposition of ammonia at about 1000° and pressures of 10^{-4} to 1 mm has quite recently been reported by Melton and Emmett.[11]

Kinetic studies of the decomposition of ammonia in the shock tube have been reported elsewhere.[12] Similar spectroscopic and kinetic investigations of the decomposition of nitrous oxide in a shock tube, carried out in this institute, have also been published recently.[13–15]

(11) C. E. Melton and P. H. Emmett, *J. Phys. Chem.*, **68**, 3318 (1964).

(12) K. W. Michel and H. G. Wagner, 10th Symposium on Combustion, University of Cambridge, Cambridge, 1964, p 354.

(13) A. Jost, K. W. Michel, J. Troe, and H. G. Wagner, NASA Document N63-22347, Wright-Patterson Air Force Base, Ohio, 1963.

(14) W. Jost, K. W. Michel, J. Troe, and H. G Wagner, *Z. Naturforsch.*, **19a**, 59 (1964).

(15) H. A. Olschewski, J. Troe, and H. G. Wagner, *Nachr. Akad. Wiss. Goettingen, II, Math. Physik. Kl.*, No. 8, 115 (1965).

Acknowledgment. The authors express their thanks to Professor W. Jost and Dr. H. G. Wagner for their keen interest in this work and for many valuable discussions. This work was done in 1961–1962 when P. G. M. was the recipient of a fellowship from the Alexander von Humboldt Foundation.

Proton Relaxation Rates in Aqueous Solutions Containing Cupric Ion Chelated with Various Alkyl-Substituted Ethylenediamines

by Maurice Griffel

Johnson Research Foundation, University of Pennsylvania, Philadelphia, Pennsylvania 19104
(Received January 10, 1967)

Longitudinal and transverse proton magnetic resonance relaxation times were measured in 0.05 *M* copper solutions containing ethylenediamine and progressively substituted N-alkylethylenediamines. In agreement with earlier work, the results may be explained as due to dipole–dipole interaction up to the point where sufficient amine has been added to form the bis chelate. Beyond this point a scalar coupling mechanism plays an important role in the relaxation of nitrogen-bound protons. Exchange of such protons with those of bulk water occurs after chemical exchange of the amine molecules. The complete replacement of the amine protons by alkyl groups makes this mechanism inoperative and T_1 and T_2 do not deviate from their values for the bis complex.

Proton magnetic resonance relaxation times in dilute aqueous solutions containing a paramagnetic ion are those of the bulk water and are determined both by the various mechanisms through which the ion is effective and by the length of time that an individual proton remains in the immediate environment of the ion.[1–6] When there are no added ligands, the only exchange is that of protons between the coordination sphere of the ion and the bulk water. The presence of an additional ligand containing replaceable protons requires the consideration of (a) the extent to which the added ligand displaces water from the coordination sphere, (b) the inherent effectiveness of the paramagnetic ion in relaxing the protons of the ligand, and (c) the mechanisms (and associated kinetics) by which the protons of the ligand exchange with those of bulk water.

There have been a number of investigations[4,7–12] of proton relaxation in solutions containing copper. In particular, Morgan and co-workers[8,9] have used spin-echo techniques to measure both the longitudinal (T_1) and transverse (T_2) relaxation times in dilute solutions

(1) N. Bloembergen, E. M. Purcell, and R. V. Pound, *Phys. Rev.*, **73**, 679 (1948).

(2) N. Bloembergen, *J. Chem. Phys.*, **27**, 572 (1957).

(3) I. Solomon, *Phys. Rev.*, **99**, 559 (1955).

(4) R. A. Bernheim, T. H. Brown, H. S. Gutowsky, and D. E. Woessner, *J. Chem. Phys.*, **30**, 590 (1959).

(5) R. G. Shulman, H. Sternlicht, and B. J. Wyluda, *ibid.*, **43**, 3116 (1965).

(6) T. J. Swift and R. E. Connick, *ibid.*, **37**, 307 (1962).

(7) L. O. Morgan and A. W. Nolle, *ibid.*, **31**, 365 (1959).

(8) L. O. Morgan, J. Murphy, and P. F. Cox, *J. Am. Chem. Soc.*, **81**, 5043 (1959).

(9) P. F. Cox and L. O. Morgan, *ibid.*, **81**, 6409 (1959).

(10) J. P. Hunt and H. W. Dodgen, *J. Chem. Phys.*, **35**, 2261 (1961).

(11) R. G. Pearson and R. D. Lanier, *J. Am. Chem. Soc.*, **86**, 705 (1964).

(12) Z. Luz and R. G. Shulman, *J. Chem. Phys.*, **43**, 3750 (1965).

containing complexes of cupric ion with ethylenediamine and with 2,2′-bipyridine. They found that up to a mole ratio of ligand/Cu^{2+} = 2 (region I), the behavior of the relaxation times was very similar for both ligands. This finding appears to rule out exchange of protons between bulk water and the firmly ligated ethylenediamine. Additional evidence could be adduced by using various N-alkyl-substituted ethylenediamines. Here the number of replaceable protons can be changed from 4 to 0. If no corresponding change occurs in T_1 and T_2, it would indicate that the N protons of the chelated amine indeed do not exchange to any appreciable extent with those in the bulk of the water. The same compounds could also serve to illumine the role of the N protons when ligand/Cu^{2+} is greater than 2 (region II). Here the various ethylenediamines are only weakly bound and chemical exchange occurs between bound and free amine.

Experimental Section

The chelating agents used were 2,2′-bipyridine, ethylenediamine, N-methylethylenediamine, N,N-dimethylethylenediamine, N,N′-dimethylethylenediamine, N,N-dimethyl-N′-ethylethylenediamine, and N,N,N′,N′-tetramethylethylenediamine. All compounds were obtained from K & K Chemical Co. and were redistilled before use. The 0.1 *M* cupric nitrate stock solution was prepared from AR chemicals and was standardized against KIO_3 with sodium thiosulfate. With the exception of bipyridine which was added by weight, the various amines were dissolved in water to form 0.5 *M* solutions. The solutions used in the relaxation measurements had a total copper concentration of 0.05 *M*, the ratio of organic compound to copper being varied from 0 to 4 by dilution with water. All measurements were made at 25° using spin-echo techniques as described by Carr and Purcell[13] with modifications of Meiboom and Gill.[14] The radiofrequency used was 25 Mc/sec.

Results

For both 2,2′-bipyridine and ethylenediamine, the findings of Morgan, Murphy, and Cox[8] were essentially confirmed. Despite the difficulties in spin-echo measurements, the results are numerically in good agreement. However, as shown in Figure 1, the decrease in T_1 in region II is less precipitous than found by Morgan and does not become flat in the same way.

The results for the substituted ethylenediamines are shown in Figures 1 and 2. Qualitatively, the behavior in region I is the same as for ethylenediamine itself, although the highest relaxation times occur when the ethylenediamine/Cu^{2+} ratio is about 2.2. However,

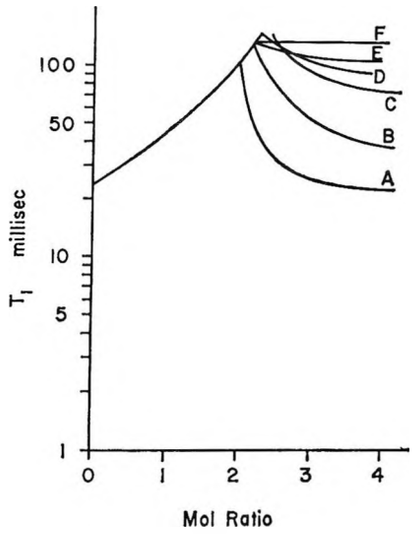

Figure 1. Longitudinal relaxation times *vs.* mole ratio for cupric ion complexed with various ethylenediamines: A, ethylenediamine; B, N-methylethylenediamine; C, N,N-dimethylethylenediamine; D, N,N′-dimethylethylenediamine; E, N,N-dimethyl-N′-ethylethylenediamine; F, N,N,N′,N′-tetramethylethylenediamine.

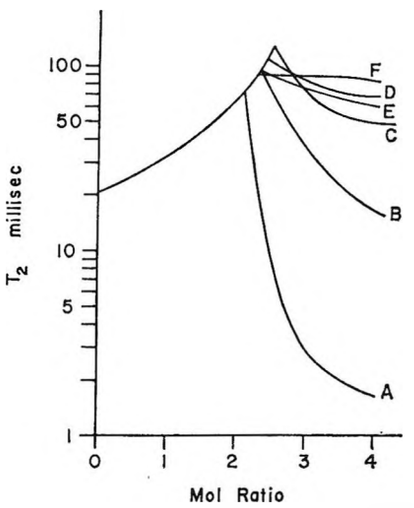

Figure 2. Transverse relaxation times *vs.* mole ratio for cupric ion complexed with various ethylenediamines.

the decrease of T_1 and T_2 in region II becomes progressively less as substitution increases. Moreover, the difference between T_1 and T_2 is less marked. For the fully substituted tetramethylethylenediamine, the values of T_1 and T_2 in region II remain essentially constant.

(13) H. Y. Carr and E. M. Purcell, *Phys. Rev.*, **94**, 630 (1954).
(14) S. Meiboom and D. Gill, *Rev. Sci. Instr.*, **29**, 688 (1958).

Discussion

Two types of interaction[15] are primarily responsible for the relaxation of the protons within the coordination sphere of the metal. The first of these is a dipole–dipole interaction and the second is an isotropic hyperfine coupling. They lead to well-known expressions for the reciprocals of T_{1M} and T_{2M}, the relaxation times of protons in the coordination sphere.

In the absence of chemical exchange, it is possible to consider the nuclear moment as being present in one or more discrete environments, each associated with a relaxation rate. The intervention of chemical exchange results in an alteration of the observed relaxation times in a manner given by Bloembergen and Morgen[16] and by Swift and Connick.[6]

Within the confines of region I, the relaxation rate is directly proportional to the number of available sites (*i.e.*, those occupied by water molecules), and it is not necessary to consider the relaxation of axial and equatorial water separately. As shown by Bernheim and co-workers,[4] only the dipole–dipole interaction makes an effective contribution to T_{1M} and T_{2M} which we calculate to be 9.7×10^{-5} sec. Since chemical exchange of water is rapid, the contributions of the paramagnetic ion to the observed proton relaxation times is likewise controlled by the dipole–dipole interaction.

The relaxation behavior in region II is best considered in terms of the results found for ethylenediamine and for the completely substituted tetramethylethylenediamine. The former was previously investigated and discussed by Cox and Morgan.[9] The two main features exhibited by ethylenediamine are the wide divergence of T_2 from T_1 and the rapid decrease of both from the values found for the bis complex. The decrease in T_1 was attributed to the rapid molecular exchange of ethylenediamine between the coordination sphere and the bulk of the solution made possible by the presence of uncoordinated ligand in the solution. When the concentration of the latter is sufficiently high, the exchange becomes rapid enough to make the number of protons in the coordination sphere effectively the same as in the hexaaquo ion. However, the fact that the asymptotic value of T_1 is (within experimental error) the same as that for the hexaaquo ion is fortuitous since T_{1M} in this region is an average of those for oxygen-bonded and nitrogen-bonded protons. These considerations would lead to the prediction that addition of ethylenediamine to a solution containing copper fully complexed with bipyridine would result in a marked decrease in T_1. Such an effect was indeed found; the presence of 0.05 M ethylenediamine in solution which is 0.05 M in copper and 0.15 M in 2,2′-bipyridine results in a threefold decrease in T_1 and incidently proves the lability of bipyridine in the complex.

To account for the difference between T_1 and T_2 for ethylenediamine in region II, Morgan proposed that isotropic hyperfine coupling is the main mechanism of the transverse relaxation. In order to calculate the contribution, it would be necessary to know the interaction constant A and this quantity is not available. While A might be obtained from the frequency shift,[17] such a measurement would require a very high concentration of paramagnetic ion with resultant broadening of the line. There are additional complications which have to do with the uncertainty regarding the species present. For example, Bjerrum and Nielsen[18] suggest that a third ethylenediamine molecule coordinates to copper by only one of the amino groups. Copper would then either have a coordination number of 5 or retain one molecule of water. In any case, the value of A so obtained would represent an average. Whatever the details of the species present, it seems clear that the isotropic hyperfine coupling contributes to T_2. Proton relaxation is complete within the residence time of the ligands and the rate of chemical exchange is now the factor controlling the contribution of the N-bonded protons to the relaxation rate. The fact that these protons are active mediators in region II is proven by the results with tetramethylethylenediamine which exchanges in and out of the coordination sphere of copper but cannot participate in proton exchange. Both T_1 and T_2 thus remain at the values they have for the bis complex and relaxation proceeds only *via* the coordinated water molecules.

Between the two extremes represented by ethylenediamine and tetramethylethylenediamine the relaxation rates and the number of exchangeable protons may be arranged in the same sequence. However, the contribution of the N-bonded protons is not a linear function of the number of such protons. This is shown in Table I which pertains to solutions for which the ratio ligand/Cu^{2+} is 4. The relaxation rate in the case of the tetramethylamine is associated with all mechanisms not involving N-proton exchange. Under the assumption that these mechanisms operate to the same extent with the other amines, the data in column 4 of Table I are "adjusted" values of T_1^{-1} and represent the relative longitudinal relaxation rates due to the N-bonded pro-

(15) A. Abragam, "The Principles of Nuclear Magnetism," Oxford University Press, London, 1961.

(16) N. Bloembergen and L. O. Morgan, *J. Chem. Phys.*, **34**, 842 (1961).

(17) N. Bloembergen, *ibid.*, **27**, 595 (1957).

(18) J. Bjerrum and E. J. Nielsen, *Acta Chem. Scand.*, **2**, 297 (1948).

Table I: Longitudinal Relaxation Times at the Mole Ratio Amine/Cu^{2+} = 4

Solution[a]	T_1, msec	$1/T_1$, sec^{-1}	$(1/T_1) - (1/T_1(a))$[b]
A	23	44	36
B	40	25	17
C	76	13	5
D	90	11	3
E	110	9.1	1.4
F	130	7.7	0

[a] For key to designation of solutions see Figure 1. [b] $T_1(a)$ = 130 msec.

Table II: Transverse Relaxation Times at the Mole Ratio Amine/Cu^{2+} = 4

Solution[a]	T_2, msec	$1/T_2$, sec^{-1}	$(1/T_2) - (1/T_2(a))$[b]
A	1.3	770	759
B	16	62	51
C	54	18	7
D	75	13	2
E	70	14	3
F	90	11	0

[a] For key to designation of solutions see Figure 1. [b] $T_2(a)$ = 90 msec.

tons. It is seen that the adjusted rate in the case of ethylenediamine is over 20 times the rate for the amine containing only one replaceable proton. The disparity is even greater for the "adjusted" values of T_2^{-1} given in Table II.

These results lead to several observations. If T_{1M} and T_{2M} were sufficiently small so that only the lifetime of the protons in the coordination sphere determined the two relaxation rates, then we would expect that the latter would be directly proportional to the number of N-bonded protons, and, further, they would be equal. For all the amines, T_1 is determined both by T_{1M} and τ_M, the lifetime of a proton in the coordination sphere. In the case of ethylenediamine, T_{2M} is sufficiently small so that T_2 is determined by τ_M and, indeed, $(1/T_2) - (1/T_2(a)) = 1/\tau_M = k$ (Swift and Connick's Case C).[19] From a knowledge of concentrations of the various species one may then calculate[8] the second-order rate constant for the exchange between free amine and the bis complex. Such a calculation is not possible for the other amines since T_{2M} is not negligible with respect to τ_M, and the situation does not resolve into a simple limiting case.

Acknowledgment. This work has been done during the tenure of NIH Special Fellowship 5-F3-CA-28, 137-02 for which the author is very grateful. I thank Professor Mildred Cohn for her hospitality in making available the facilities of her laboratory. It is a pleasure to record the benefit derived from conversations with Mr. John S. Leigh, who constructed the apparatus and initiated me into its use.

(19) $T_2(a)$ is the relaxation time of protons in the solution for which amine/Cu^{2+} = 2

Thermodynamic Properties and Ultraviolet Spectra of Cyanogen Iodide Complexes with Some n Donors

by Hari D. Bist[1] and Willis B. Person[2]

Department of Chemistry, University of Florida, Gainesville, Florida *(Received January 27, 1967)*

The ultraviolet absorption spectrum of ICN in *n*-heptane and of its complexes with diethyl ether, ethanol, and tetrahydrofuran has been investigated in *n*-heptane solution. From the "blue-shifted" ICN band at 240 mμ, the thermodynamic properties K, $\Delta H°$, and $\Delta S°$ and the characteristics of this absorption band (ϵ_{max}, $\Delta\nu_{1/2}$, f, and D) were determined for the complexes. Comparison of these properties with the corresponding values for I_2 complexes establishes the similarity in both thermodynamic and spectroscopic behavior. The failure to observe the charge-transfer absorption is discussed. It is concluded that this failure is due to a shift of $h\nu_{CT}$ to about 1–2 ev of higher energy (as compared to I_2 complexes) because of a smaller vertical electron affinity (estimated to be only 0.9 ev for ICN) and a more negative value of G_0 for the ICN complexes.

Introduction

In spite of its potential interest as an electron acceptor to be compared with I_2, ICl, and other halogens, very little information exists about electron-donor–acceptor complexes with ICN. Fairbrother[3] measured the apparent dipole moments of ICN in different solvents, noting an appreciable increase for μ in solutions with electron donors as solvents, similar to that which he had found earlier for I_2.[4] In that paper[3] he commented on and reported experiments confirming the frequency shifts in the ultraviolet spectrum of ICN observed earlier by Gillam.[5] Further studies of the changes in the ultraviolet spectra in complexing solvents are reported by Haszeldine,[6] and changes in the infrared spectra were reported by Haszeldine,[6] by Glusker and Thompson,[7] and by Person, Humphrey, and Popov.[8] Formation constants for a few complexes have been reported from measurements made in the infrared region.[9] However, only a relatively few complexes have been studied even that quantitatively.

One question arising from these studies concerns the frequency of the charge-transfer absorption band which presumably exists for these complexes. Haszeldine[6] reports some changes in the ultraviolet spectrum near the limit of transmission of his spectrometer—*i.e.*, around 200 mμ. Badger and Woo[10] and Yakovleva[11] have reported the spectrum of ICN vapor in this region. Badger and Woo[10] assign the broad absorption found here (with peak at 247 mμ) to a transition to an electronic upper state which dissociates to give the products $I(^2P_{3/2}) + CN^*(^2\Pi)$. This transition then corresponds roughly to the transition for the visible absorption band of I_2 (mostly to the upper state, which dissociates to give $I(^2P_{3/2}) + I^*(^2P_{1/2})$. Hence, one might expect the absorption in this region for the σ acceptor, ICN, to exhibit a change on complexing similar to that found for the visible I_2 band—*i.e.*, a "blue shift" and intensification.[12] The possibility that the charge-transfer ab-

(1) Fulbright Exchange Fellow, 1963–1965.

(2) Visiting Associate Professor of Chemistry and National Science Foundation Senior Postdoctoral Fellow, Laboratory of Molecular Structure and Spectra, Department of Physics, University of Chicago, Chicago, Ill., 1965–1966. The experimental work was done at the University of Iowa.

(3) F. Fairbrother, *J. Chem. Soc.*, 180 (1950).

(4) F. Fairbrother, *ibid.*, 1051 (1948).

(5) A. E. Gillam, *Trans. Faraday Soc.*, **29**, 1132 (1933).

(6) R. N. Haszeldine, *J. Chem. Soc.*, 4145 (1954).

(7) D. L. Glusker and H. W. Thompson, *ibid.*, 471 (1955).

(8) W. B. Person, R. E. Humphrey, and A. I. Popov, *J. Am. Chem. Soc.*, **81**, 273 (1959).

(9) A. I. Popov, R. E. Humphrey, and W. B. Person, *ibid.*, **82**, 1850 (1960).

(10) R. M. Badger and S. Woo, *ibid.*, **53**, 2572 (1931).

(11) A. V. Yakovleva, *Izv. Akad. Nauk SSSR, Ser. Fiz.*, **14**, 517 (1950); *Chem. Abstr.*, **45**, 3239*b* (1951).

sorption band of complexed ICN is superimposed on the absorption in this region by the free ICN should not be overlooked, however.

Because the changes in the ultraviolet region of the spectrum of complexed ICN do occur in the region below 250 mμ, the choice of donors which can be studied is limited. The requirement of transparency rules out aromatic π donors, such as benzene, as well as many interesting n donors—*e.g.*, sulfides. The requirement of stability rules out the stronger n donors—*e.g.*, trimethylamine—which react further with ICN. Hence, only the ethers and alcohols, among the usual kinds of donors, form complexes which can be studied in the ultraviolet region. We report a study of the complexes of ICN with diethyl ether and with ethyl alcohol, in an attempt to obtain the thermodynamic properties K, ΔH, and ΔS for complex formation, and to obtain further information about the spectral changes of ICN near 250 mμ. In an attempt to provide some information about the interaction of ICN with a stronger n donor, we report also some much less complete results of a study of the complex with tetrahydrofuran.

Experimental Section

Chemicals. Iodine cyanide was prepared by the method of Bak and Hillebert[13] and was purified by recrystallizations from chloroform.

Solvents and donors were purified according to standard procedures.[14-16] *n*-Heptane (Phillips Petroleum Co., pure grade) was shaken with a mixture of concentrated HNO_3 and H_2SO_4 and again repeatedly with concentrated H_2SO_4, washed, and distilled under nitrogen over sodium. Ethyl alcohol (95%) was refluxed over freshly burnt quicklime and then distilled. "Superdry" alcohol was prepared from this by distilling it again from magnesium activated with I_2. Ether was stored over sodium and fractionally distilled. The tetrahydrofuran was purified by removing peroxides and dried well, immediately before use.

The solutions were freshly prepared on the day of use. The donor and ICN were weighed into a 25-ml volumetric flask, with a semimicro Mettler balance, and the volume was adjusted with *n*-heptane. For reference in the double-beam spectrometer, solutions containing solvent and donor at the same concentration as in the ICN sample solution were also prepared.

Spectra. The spectra were recorded in the region 360–170 mμ (or over portions of this region) with a Beckman DK-2A far-ultraviolet spectrophotometer. A matched pair of Beckman far-ultraviolet silica cells (1 cm) was used. These cells were mounted in the Beckman temperature-regulated cell holder, whose temperature was controlled by circulating a glycol–water mixture from a Haake thermostat and, for low temperatures, from a Sargent water bath cooler. The temperature in the cells could be controlled to ±0.2° in the range from −12 to 60°.

Oxygen and other undesirable vapors were removed by purging the instrument with Linde high-purity dry nitrogen. A slow purge was maintained continuously, and the purge rate was increased during the study, especially for the low-temperature studies in order to prevent condensation of H_2O.

The cells containing the ICN solution and the reference solution were placed in the spectrometer and the spectra were recorded at 28°. Then the temperature was adjusted in steps and the spectra were recorded at each temperature, after allowing 30 min or more for the cell compartment to reach equilibrium. Spectra were recorded in the order: 28, 19, 5, −10° (45 and 60°, in the case of the alcohol complex). Actually, the temperature of the cells was adjusted only approximately to these values. The spectra were read, and the absorbance was plotted as a function of temperature for each solution. The absorbances at each of the temperatures above were read from the graph by interpolation. In order to check that possible irreversible reactions did not occur during the time needed to go through this cycle, the spectrum of the solution at 28° was usually recorded at the end of the cycle as well.

Dissolved oxygen in *n*-heptane shows considerable absorption in this region of the ultraviolet spectrum—especially below 2100 A. Stringent precautions were taken to avoid it including: (i) distilling all chemicals under nitrogen atmosphere just before use; (ii) purging both the donor and the solvent with extra dry high-purity nitrogen just before preparing the solutions under N_2 atmosphere in a drybox; (iii) filling the Beckman stoppered quartz cells in the drybox; and (iv) keeping the spectrometer, and especially the cell compartment, purged continuously with dry nitrogen. We did not detect any complications due to the contact charge-transfer absorption of O_2.

A further small error (about 3%) occurred in the molar concentrations of the solutions owing to the changes in volume as a result of the temperature changes. This effect was ignored, since it was small

(12) For example, see R. S. Mulliken, *J. Chim. Phys.*, 20 (1964); R. S. Mulliken, *Rec. Trav. Chim.*, 75, 845 (1956).

(13) B. Bak and A. Hillebert, *Org. Syn.*, 32, 29 (1952).

(14) K. B. Wiberg, "Laboratory Technique in Organic Chemistry," McGraw-Hill Book Co., Inc., New York, N. Y., 1960.

(15) A. Weissberger, Ed., "Technique of Organic Chemistry," Vol. VII, Interscience Publishers, Inc., New York, N. Y., 1955.

(16) A. I. Vogel, "Elementary Practical Organic Chemistry. Part I. Small Scale Preparations," Longmans, Green and Co., Ltd., London, 1957.

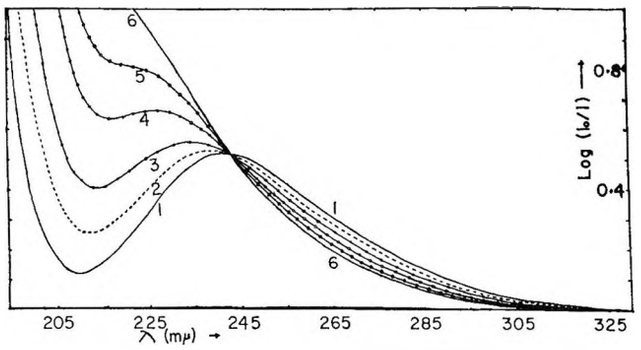

Figure 1. The ultraviolet absorption spectra of Et_2O·ICN solutions; solvent, *n*-heptane; 23°; 1.00-cm cell. The ICN and Et_2O concentrations in millimoles per liter are: (1) 3.368 and 0.000; (2) 3.368 and 39.75; (3) 3.466 and 107.99; (4) 3.499 and 338.3; (5) 3.629 and 1297.3; (6) 3.695 and 9626.3.

and since quantitative information about the density changes in our solvent system was not readily available.

Results

Figure 1 presents representative spectra of solutions in *n*-heptane of approximately constant ICN concentration with increasing concentrations of ether. It illustrates the decrease in the intensity of the free ICN band at 241 mμ (in *n*-heptane) as the complex is formed, with the resulting increase in the band due to the complexed ICN at 225 mμ. The isosbestic point indicates that only two species exist in these solutions. We note that the absorption by this shifted ICN band at 225 mμ in the complex is overlapped by the stronger absorption near 200 mμ. It is still not *absolutely* clear whether this strong band results from a shift of the absorption band already seen near 200 mμ, for ICN in *n*-heptane, or whether a charge-transfer absorption band for the complex is superimposed on the ICN absorption in this region. However, we believe the arguments in favor of the former interpretation of our spectra are reasonably convincing.

From a set of absorption curves such as those shown in Figure 1 for the solution at a given temperature, the formation constant and molar absorptivities can be determined in the usual way.[17] Since the absorption of the complex overlaps that of the free ICN, a correction must be made for the latter. The concentration of free ICN is given by

$$[\mathrm{ICN}] = (\mathrm{ICN})_0 - \frac{K(\mathrm{ICN})_0 D_0}{1 + KD_0} \qquad (1)$$

Here the zero subscript denotes the total concentration of the species, determined from the weight. The absorbance at λ due to free ICN is

$$A_{\lambda f} = \epsilon_{\lambda f} l [\mathrm{ICN}] \qquad (2)$$

The value of $\epsilon_{\lambda f}$ in the solutions containing donor is assumed to be the same as that found for ICN alone in *n*-heptane. Hence, we may compute the absorbance of the complex corrected for that due to free ICN

$$A_{C\lambda} = A_\lambda - A_{\lambda f} \qquad (3)$$

Here A_λ is the total observed absorbance at λ in the solution, and $A_{C\lambda}$ is that due to complex alone.

We may now use $A_{C\lambda}$, measured in a series of solutions with differing donor concentrations, in the Benesi–Hildebrand[18] or Scott[19] equations to obtain the value of $\epsilon_{C\lambda}$ and K. (Or, better, we may use the Liptay[20] procedure to treat these data.) However, in order to make the corrections of eq 1–3, we must estimate K. We have done this using Nagakura's equation[21]

$$K = \frac{D_0(A_0 - A') + D_0'(A - A_0)}{D_0 D_0'(A' - A)} \qquad (4)$$

Here A_0, A, and A' are the absorbances of solutions whose total donor concentrations are 0, D_0, and D_0' moles/l., respectively. After making this estimate for K, the corrected absorbance is computed by eq 1–3 and then treated by the Liptay procedure[20,22] to obtain K and $\epsilon_{C\lambda}$ values, cycling until K does not change.

The Liptay analysis of the data was programmed[22] in FORTRAN IV for the IBM 7040/7044 computer. Absorbance data from five solutions with different donor concentrations were read at eleven wavelengths from 210 to 235 mμ (at 2.5-mμ intervals) for the ether complex, and at four wavelengths from 210 to 225 mμ (at 5-mμ intervals) for the alcohol complex. The resulting K values, together with ϵ_{max} values (at λ 225 mμ for the ether complex and at λ 217 mμ for the alcohol complex) are tabulated in Table I. No trends were noticed in the ζ matrix or in the D_m matrix in the Liptay analysis,[20] suggesting that there is little noticeable effect owing to failure of either the assumption that $\epsilon_{\lambda f}$ is constant or that only 1:1 complexes are present.

This analysis was carried out at each of four temperatures from data obtained above and illustrated for a typical solution in Figure 2. This figure again illustrates the increase in absorption of the complex near

(17) G. Briegleb, "Elektronen-Donator-Acceptor-Komplexe," Springer-Verlag, Berlin, 1961, Chapter XII.

(18) H. A. Benesi and J. H. Hildebrand, *J. Am. Chem. Soc.*, **71**, 2703 (1949).

(19) R. L. Scott, *Rec. Trav. Chim.*, **75**, 787 (1956).

(20) See ref 17; W. Liptay, *Z. Elektrochem.*, **65**, 375 (1961).

(21) S. Nagakura, *J. Am. Chem. Soc.*, **80**, 520 (1958), and other references cited there.

(22) L. Julien, Ph.D. Thesis, University of Iowa, 1966.

Table I: Equilibrium Constants, K, for Complex Formation, and ϵ_{max} Values for ICN Complexes with Tetrahydrofuran and with Diethyl Ether and Ethanol at Different Temperatures

Donor							
THF			Diethyl ether		Ethanol		
Temp, °C	K, l./mole	ϵ_c(220)	K, l./mole	ϵ_c(225)	Temp, °C	K, l./mole	ϵ_c(217)
−9.5			17.1 ± 1.9	255 ± 7	−12.0	10.90 ± 0.7	266 ± 3
5.0			8.3 ± 1.0	260 ± 14	4.0	6.8 ± 0.7	264 ± 8
18.0			6.2 ± 0.7	241 ± 15	19.0	4.3 ± 0.2	270 ± 6
27.0	13 ± 4	236 ± 21	3.8 ± 0.3	257 ± 9	28.0	3.5 ± 0.4	255 ± 16

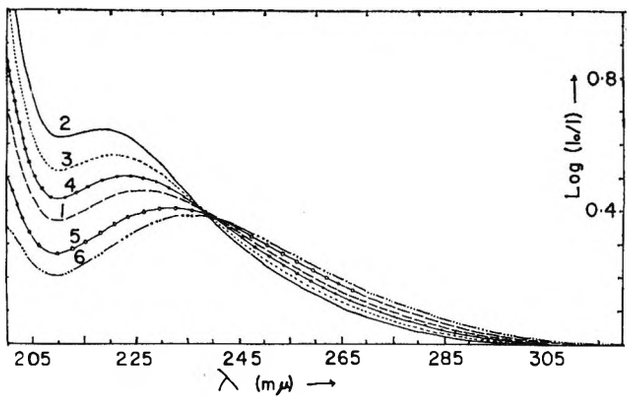

Figure 2. Temperature dependence of the ultraviolet absorption spectra of an EtOH·ICN solution; solvent, n-heptane; 1.00-cm. cell. Concentrations for ICN and EtOH are 3.335 and 201.3 mM, respectively. The temperatures for the curves are: (1) 30.6, (2) −12.2, (3) 5.8, (4) 19.2, (5) 46.8, (6) 59.8°.

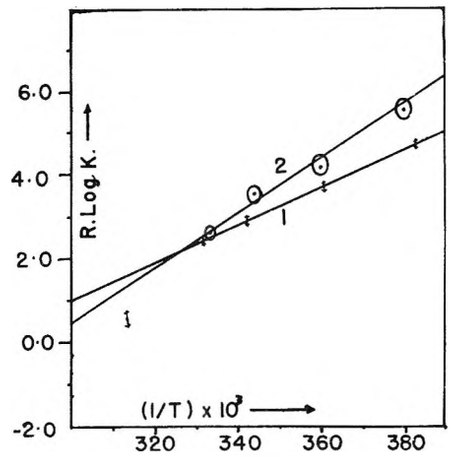

Figure 3. The relationship between R ln K and $1/T$. Straight lines 1 and 2 correspond to EtOH·ICN and Et_2O·ICN, respectively.

220 mμ and decrease in absorption by the free ICN at 240 mμ as more complex forms at the lower temperatures. Again, we note the presence of an isosbestic point.[23] Note that ϵ_{max} in Table I is independent of temperature within experimental error, as expected over this small range of temperature. We note also that the experimental uncertainty in K is rather high (±10%). However, we believe this uncertainty is acceptable for such weak complexes.

We note that the results for C_2H_5OH–ICN confirm the somewhat more qualitative results reported by Haszeldine.[6]

The tetrahydrofuran–cyanogen iodide complex was studied only at 27°, using the same technique as for the the others. The results are given in Table I.

The value of $\Delta H°$ for the formation of the complex is obtained from the temperature dependence of K by plotting R ln K *vs.* $1/T$, as shown in Figure 3. The resulting values of $\Delta H°$ and $\Delta S°_{298}$ (based on a standard state of 1 M concentrations) are listed in Table II, together with values from other I_2 complexes for comparison.

Discussion

On the basis of the results shown in Table II, we conclude that ICN and I_2 have similar acceptor strengths. The enthalpies for the ICN complexes with alcohol and ether and $\Delta G°$ for the THF complex are perhaps slightly more negative than for the corresponding I_2 complexes, as might be expected from the additional energy contribution due to the dipole–induced-dipole term for the polar ICN complexes ($\mu_{ICN} \simeq 3.76$ in benzene solution[3]). However, the best interpretation of the results in Table II is apparently that I_2 and ICN possess almost identical acceptor strengths.

It is of interest to note there that the points for $\Delta H°$ and $\Delta S°$ for the ICN complexes (after conversion to the same standard state) fit quite well on the line

(23) The isosbestic point shifts at higher temperatures for the C_2H_5OH–ICN solutions. When these solutions are cooled again to 28°, the spectrum is identical with that observed at the start of the experiment, indicating that the higher temperature changes responsible for the loss of isosbestic point are reversible. We do not understand this observation, but we have obtained the thermodynamic properties reported here from studies below 45°, where the isosbestic point in Figure 2 remains constant.

Table II: Thermodynamic Properties for Some Complexes of ICN and of I_2 with Some n Donors (Based on 1 *M* Solutions as the Standard State)

Acceptor	Donor	Solvent	K_{298}, l./mole	$-\Delta G°$, kcal/mole	$-\Delta H°$, kcal/mole	$-\Delta S°$, cal/deg mole
ICN[a]	Et_2O	*n*-Heptane	3.8	0.79	6.5 ± 0.5	19.1
ICN[a]	EtOH	*n*-Heptane	3.5	0.74	4.5 ± 0.5	12.7
ICN[a]	THF	*n*-Heptane	13	1.54	...	...
ICN[b]	Dioxane	$CHCl_3$	1.2	0.11	...	...
ICN[b]	Pyridine	C_6H_6	51	2.34	...	...
I_2[c]	Et_2O	*n*-Heptane	0.87	−0.08	4.2	14.4
I_2[d]	EtOH	*n*-Heptane	0.86	−0.09	4.6 ± 0.4	15.6
I_2[c]	THF	*n*-Heptane	3.0	0.65	5.3	15.9
I_2[e]	Dioxane	*n*-Heptane	1.2	0.11	3.5	11.4
I_2[e]	Pyridine	*n*-Heptane	290	3.37	8.0	15.5

[a] This research. [b] From Popov, Humphrey, and Person.[9] [c] From M. Brandon, M. Tamres, and S. Searles, Jr., *J. Am. Chem. Soc.*, **82**, 2129 (1960); M. Tamres and M. Brandon, *ibid.*, **82**, 2134 (1960). [d] From Julien.[22] [e] Recomputed from the summary by G. Briegleb, ref 17, pp 124–125.

found empirically for I_2 complexes[24] when $-\Delta S°$ is plotted against $-\Delta H°$.

We might also note here that the monomer–dimer equilibrium for ethanol in *n*-heptane[25] may complicate the interpretation both of the ICN and of the I_2 data for this donor. The concentration ranges of ethanol used to obtain K in both studies are roughly comparable, however, so that the comparison between I_2 and ICN in Table II is probably relatively valid.

It is of some interest to investigate quantitatively the changes in the 247-mμ ICN band on complexing and to compare them with those for the corresponding changes in the visible band of I_2. The intensity of the absorption of this band in the complex reported in Table I may be too high, since the increased overlap with the stronger band around 200 mμ in the complex makes it difficult to obtain an accurate intensity for the 247-mμ band above. However, examination of Figures 1 and 2 suggests that the overlap is not too great on the long-wavelength side of λ_{max}. Hence, we have estimated the f number and transition dipole, D, by the approximate formulas[26]

$$f = 4.32 \times 10^{-9}[\epsilon_{max}\Delta\nu_{1/2}]$$

$$D = 0.0958[\epsilon_{max}\Delta\nu_{1/2}/\nu_{max}] \quad (5)$$

Here, we have estimated that $\Delta\nu_{1/2}$ is two times the difference in reciprocal centimeters from the half-intensity point on the right-hand side of the band to the wavenumber of maximum absorption, ν_{max}. This estimate may be in error by about 5% or so, owing to the asymmetry of the band. However, the overlap by the absorption around 200 mμ prevents us from measuring $\Delta\nu_{1/2}$ directly. The final results are given in Table III.

We see there that the "blue shift" and intensification of this band in complexes of ICN are indeed quite similar to those observed for the complexes of I_2. The band for free ICN is intrinsically much weaker than the corresponding band in free I_2 and may be more susceptible to "inert solvent" effects. Hence, the ratio of intensities for ICN (complex/vapor) is greater than for I_2, but we see that D increases by about 0.2–0.3 debye/A for both I_2 and ICN complexes.

Finally, we may examine the reason for the failure to observe the charge-transfer band. We believe that the intensification observed for the complexed ICN in the region around 200 mμ (Figures 1 and 2) is probably not great enough for it to be due to the charge-transfer absorption. Hence, λ_{CT} is probably less than 190 mμ. If so, the charge-transfer frequency must come more than 12,000 cm^{-1} higher (or $h\nu_{CT}$ is more than 1.5 ev greater) than the corresponding transition for I_2 complexes. Such a large difference from I_2 is not obviously to be expected. The charge-transfer frequency is determined by:[26-28] (1) the ionization potential of the donor, which is the same for ether complexes with I_2 and with ICN, for example; (2) G_1, the stabilization of the dative-state energy, W_1; G_1 should be roughly the same for I_2 and for ICN complexes, assuming the configuration in the latter to be D- - -I–

(24) M. Tamres and M. Brandon, *J. Am. Chem. Soc.*, **82**, 2134 (1960).

(25) U. Liddel and E. D. Becker, *Spectrochim. Acta*, **10**, 70 (1957); E. D. Becker, *ibid.*, **17**, 436 (1961).

(26) See ref 17; also *cf.* R. S. Mulliken and W. B. Person, *Ann. Rev. Phys. Chem.*, **13**, 107 (1962).

(27) R. S. Mulliken, *J. Am. Chem. Soc.*, **74**, 811 (1952).

(28) W. B. Person, *J. Chem. Phys.*, **38**, 109 (1963).

Table III: Changes in the Frequency and Intensity of the 247-mμ Band and of the Visible I_2 Band on Complexing

	Iodine[a]						ICN[b]					
	λ_{max}, mμ	$\Delta\nu_{1/2}$, cm^{-1}	ϵ_{max}	f	D	$(\nu_C - \nu_0)$,[c] cm^{-1}	λ_{max}, mμ	$\Delta\nu_{1/2}$[d] cm^{-1}	ϵ_{max}	f	D	$(\nu_C - \nu_0)$,[c] cm^{-1}
Vapor	520	3300	832	0.012	1.15	...	249	8400 ± 100	72	0.0026	0.35	...
n-Heptane	520	3200	918	0.013	1.19	0	241	8200 ± 200	160	0.0056	0.56	1300
EtOH (CCl_4)	443	4500	1082	0.021	1.41	3300	217	9000	268	0.010	0.71	5900
Et_2O (*n*-heptane)	462	4100	950	0.017	1.29	2300	220	9000	263	0.010	0.73	5300
THF (*n*-heptane)	455	(4500)[e]	950	0.018	1.40	2800	225	9000	250	0.010	0.68	4200

[a] From H. Tsubomura and R. P. Lang, *J. Am. Chem. Soc.*, **83**, 2085 (1961), except for I_2 vapor, which is estimated from E. Rabinowitch and W. C. Wood, *Trans. Faraday Soc.*, **32**, 540 (1936); see also E. A. Ogryzlo and G. E. Thomas, *J. Mol. Spectry.*, **17**, 198 (1965); and for the THF complex which is estimated from Brandon, Tamres, and Searles (footnote c of Table II). [b] This research. All solutions were in *n*-heptane. [c] ν_0 = wavenumber of maximum absorption in the vapor; ν_C = wavenumber of maximum absorption in the solution, or of the complex in solution. This difference is probably accurate to about ±500 cm^{-1}, with the larger uncertainty applying in particular to the overlapping band in the complexes. [d] $\Delta\nu_{1/2}$ was measured for ICN vapor and in *n*-heptane solution; for the complexes, where the overlap with the 200-mμ band was a problem, we estimated $\Delta\nu_{1/2}$ as described in the text. The uncertainty in these estimated values is believed to be ±500 cm^{-1}. [e] Estimated.

CN; (3) the resonance energies, X_1 and X_0 ($=\beta^2_1/W_1 - W_0$); (4) the electron affinity of the acceptor; and (5) G_0 the stabilization (or repulsion) energy of the no-bond state, W_0. The latter three terms must contain the clue to the large difference in charge-transfer frequencies of ICN complexes, compared to the I_2 complexes.

The electron affinity of CN is about 3.2 ev;[29] the dissociation energy of the I–C bond is expected to be about 2.5 ev,[30] and the IC bond length about 2.00 A.[30] Following the reasoning given for the halogens,[28] we predict the dissociation energy for the IC bond in $(ICN)^-$ to form I + CN^- to be about 1.25 ev, with r_{IC} about 2.3 A and ν_{IC} about 240 cm^{-1}. With these estimated parameters, the vertical electron affinity of ICN is predicted by the methods of ref 28 to be about 0.9 ev, or about 0.8 ev less than for I_2.

In order to account for the remaining difference observed in the charge-transfer energies, consider G_0. For I_2 complexes with ethers, we should expect G_0 to be about +0.5–1.0 ev, by analogy with the values for amine–iodine complexes,[28] together with the knowledge that the O–I distance in ether–iodine complexes is relatively longer.[31] If the O–I distance in ether–cyanogen iodide complexes is similar, we may still expect G_0 to be more negative than for the I_2 complexes because of the increased electrostatic attraction between the polar ICN and the donor. This effect may be partially canceled, however, by the decreased resonance energy for ICN compared to I_2 resulting from the increased separation between W_1 and W_0 (see ref 28). However, this latter effect may also result in a longer O–I distance in the complexes with ICN, so that G_0 may be reduced essentially to zero.

Hence, it would seem reasonable that the lower vertical electron affinity of ICN compared to I_2 (0.9 ev, instead of 1.7 ev), together with a more negative G_0 (0 instead of +0.5 ev) resulting from the increased electrostatic attractive energy in the ICN complexes, may indeed account successfully for a shift of the charge-transfer frequency in ICN complexes toward higher energies by 1–2 ev, when compared to I_2 complexes.

Acknowledgments. Financial support from Public Health Service Research Grants No. GM-10168 and GM-14648 from the Division of General Medicine, PHS, is gratefully acknowledged. We are grateful to Dr. Larry Julien for the program for the Liptay calculation and for his cooperation elsewhere. It is a pleasure to acknowledge assistance from the University of Iowa Computer Center.

(29) J. T. Herren and V. H. Dibeler, *J. Am. Chem. Soc.*, **82**, 1555 (1960).

(30) (a) L. Pauling, "The Nature of the Chemical Bond," 3rd ed, Cornell University Press, Ithaca, N. Y., 1960; (b) L. E. Sutton, Ed., "Tables of Interatomic Distances and Configuration in Molecules and Ions," Special Publication No. 11, The Chemical Society, London, 1958.

(31) O. Hassel and C. Romming, *Quart. Rev.* (London), **16**, 1 (1962).

Activity Coefficient Measurements in Aqueous NaCl–LiCl and NaCl–KCl Electrolytes Using Sodium Amalgam Electrodes

by James N. Butler, Rima Huston, and Philomena T. Hsu

Tyco Laboratories, Inc., Waltham, Massachusetts 02154 *(Received February 21, 1967)*

Measurements have been made of the potential of the cell $Na,Hg|Na^+,M^+,Cl^-|AgCl|Ag$ where M^+ is either Li^+ or K^+. In the case of LiCl–NaCl electrolytes, activity coefficients can be calculated from these measurements, which agree with results obtained by the isopiestic method. Attempts to measure activity coefficients in KCl–NaCl electrolytes using the same cell were unsuccessful because of the reaction $Na(Hg) + K^+ \rightleftharpoons K(Hg) + Na^+$. This interference mechanism is discussed and the potentials observed in KCl electrolytes are explained quantitatively.

Introduction

In a previous publication,[1] we presented the results of activity coefficient measurements in aqueous NaCl–Na_2SO_4 solutions using sodium amalgam electrodes in the cell

$$Na,Hg|Na^+,Cl^-,SO_4^{2-}|AgCl|Ag$$

which obeyed Harned's rule and agreed within experimental error with two independent measurements on the same system using cation-sensitive glass electrodes.[2,3] The only other measurements of activity coefficients using sodium amalgam electrodes have been concerned with the system NaCl–NaOH[4-7] and no studies have been made by this method in systems where another cation was present in addition to sodium.

This paper presents some activity coefficient measurements made with the cell

$$Na,Hg|Na^+,Li^+,Cl^-|AgCl|Ag$$

and the results of some unsuccessful attempts to apply the same method to NaCl–KCl electrolytes.

Experimental Section

The experimental method used was the same as previously described.[1] Solutions were prepared from reagent grade salts and triply distilled conductivity water, and analyzed for chloride by titration with $AgNO_3$. The reproducibility of measurements was less satisfactory than in the NaCl–Na_2SO_4 system, typical errors being ± 0.5 mv or greater, and the capillaries of the dropping amalgam electrode became plugged much more frequently.

Theoretical Considerations

Systems which contain a single common cation (such as NaCl–Na_2SO_4 or NaCl–NaOH) require only that the amalgam electrode be reversible to the cation. In systems containing more than one cation, however, a further requirement is that the electrode be reversible to one cation *only*. This limits the number of systems that can be measured with, say, a sodium amalgam electrode to mixtures with cations whose reduction potentials are considerably more negative than that of Na^+.

Although the standard potential (Table I) of pure sodium is 212 mv more positive than that of potassium and 320 mv more positive than that of lithium,[8] these values cannot be used to predict quantitatively the behavior of amalgams of these metals, as has sometimes been done. The solid phases in equilibrium with dilute

(1) J. N. Butler, P. T. Hsu, and J. C. Synnott, *J. Phys. Chem.*, **71**, 910 (1967).

(2) R. D. Lanier, *ibid.*, **69**, 3992 (1965).

(3) J. M. T. M. Gieskes, *Z. Physik. Chem.* (Frankfurt), **50**, 78 (1966).

(4) H. S. Harned, *J. Am. Chem. Soc.*, **47**, 684 (1925).

(5) H. S. Harned and J. M. Harris, *ibid.*, **50**, 2633 (1928).

(6) H. S. Harned and M. A. Cook, *ibid.*, **59**, 1890 (1937).

(7) A. Ferse, *Z. Physik. Chem.* (Leipzig), **229**, 51 (1965).

(8) G. Charlot, "Selected Constants, Oxidation-Reduction Potentials, IUPAC Tables," Pergamon Press, Inc., New York, N. Y., 1958.

alkali metal amalgams are not the alkali metals themselves, but compounds of the alkali metals with mercury: $NaHg_4$, KHg_{11}, and $LiHg_3$. The activity of alkali metal in these solid phases may be as much as a factor of 10^{14} less than that of the pure metals. Calculations of relative activities of metals in the amalgams at different potentials must thus be based on amalgam standard potentials rather than the standard potentials of the pure metals.[9,10]

Table I: Standard Potentials of Alkali Metals and Their Amalgams at 25°

Metal	Metal std potentl,[b] v	Amalgam std potentl,[a] v	Amalgam ref
Na	−2.713	−1.9575 ± 0.0005	10
		−1.958 ± 0.001	11
		−1.9574 ± 0.001	12
K	−2.925	−1.971	10, 14
Li	−3.03	−2.188	10, 15

[a] Amalgam ref state: infinite dilution, mole fraction scale. [b] See ref 8.

For the dilute amalgams the most convenient standard state of activity is that of unit mole fraction in the ideal solution. To obtain activity, the experimental values for the emf of amalgam concentration cells are extrapolated to infinite dilution, where the activity coefficient is assumed to be unity.

In the cells we consider, the reference electrode is reversible to chloride ion, so we may formulate the Nernst equation for a sodium amalgam electrode as

$$E = E^0 - \frac{RT}{F} \ln \frac{X_{Na}\gamma_{Na}}{m_{Na^+}\gamma_{\pm}} \tag{1}$$

where X_{Na} is the mole fraction in the amalgam, γ_{Na} is the activity coefficient in the amalgam; m_{Na^+} is the molality of Na^+ in the electrolyte, and $\gamma_{\pm}$ is the mean activity coefficient of NaCl in the electrolyte.

The standard potentials of the amalgams of Na, K, and Li are given in Table I. Note that the standard potentials of Na and K amalgams differ by only 13 mv, whereas the standard potentials of Na and Li amalgams differ by 230 mv. The activity coefficients of the various amalgams have been calculated by Davies, *et al.*,[9] based on the experimental results of Dietrick, *et al.*,[11] Bent and Swift,[12] and Richards and Conant[13] for sodium amalgams, Armbruster and Crenshaw[14] for potassium amalgams, and Spiegel and Ulich[15] for lithium amalgams. For 0.1 mole % amalgams, such as we have used, the activity coefficients are between 1.00 and 1.05.

As an example, consider now a sodium amalgam electrode in contact with an electrolyte containing sodium and potassium ions. Although the equations are written for two specific ions, the treatment applies quite generally to any amalgam electrode in a solution containing two or more cations. The amalgam will quickly acquire some finite concentration of potassium, so that the electrode reactions occurring may be summarized as in eq a–e.

$$Na(Hg) \longrightarrow Na^+ + e^- \tag{a}$$

$$Na^+ + e^- \longrightarrow Na(Hg) \tag{b}$$

$$H_2O + e^- \longrightarrow {}^1/_2H_2 + OH^- \tag{c}$$

$$K(Hg) \longrightarrow K^+ + e^- \tag{d}$$

$$K^+ + e^- \longrightarrow K(Hg) \tag{e}$$

The total current (anodic = positive) flowing at a given potential is given by

$$i = i_a - i_b - i_c + i_d - i_e \tag{2}$$

where the partial currents are given by Tafel equations of the type

$$\begin{aligned}
i_a &= i_0^{(Na)} \exp\left[\frac{F}{RT}(1 - \alpha^{(Na)})(E - E_e^{(Na)})\right] \\
i_b &= i_0^{(Na)} \exp\left[-\frac{F}{RT}\alpha^{(Na)}(E - E_e^{(Na)})\right] \\
i_c &= i_0^{(H)} \exp\left[-\frac{F}{RT}\alpha^{(H)}(E - E_e^{(H)})\right] \\
i_d &= i_0^{(K)} \exp\left[\frac{F}{RT}(1 - \alpha^{(K)})(E - E_e^{(K)})\right] \\
i_e &= i_0^{(K)} \exp\left[-\frac{F}{RT}\alpha^{(K)}(E - E_e^{(K)})\right]
\end{aligned} \tag{3}$$

where E_e is the equilibrium potential (see Table I), i_0 is the exchange current, and α is the cathodic transfer coefficient for the reaction indicated by the superscript

(9) M. O. Davies, E. Schwartz, E. Yeager, and F. Hovorka, "The Physical and Chemical Properties of Dilute Alkali Amalgams," Part I, Technical Report No. 7, Contract Nonr 581(00), June 1957, AD 138 849.

(10) See ref 9, Part II, Technical Report No. 20, Contract Nonr 2391(00), July 1963, AD 609 294.

(11) H. Dietrick, E. Yeager, and F. Hovorka, "The Electrochemical Properties of Dilute Sodium Amalgams," Technical Report No. 3, Contract Nonr 581(00), April 1953, AD 7 512.

(12) H. E. Bent and E. Swift, *J. Am. Chem. Soc.*, **58**, 2216 (1936).

(13) T. W. Richards and J. B. Conant, *ibid.*, **44**, 601 (1922).

(14) M. H. Armbruster and J. L. Crenshaw, *ibid.*, **56**, 2525 (1934).

(15) G. Spiegel and H. Ulich, *Z. Physik. Chem.* (Leipzig), **A178**, 187 (1937).

(see Table II). The dependence of i_0 on composition is given approximately by[16]

$$i_0 = nFk_a^0 C_{M^+}^{(1-\alpha)} C_M^{(\alpha)} \quad (4)$$

For the alkali metal, $n = 1$. The units of Fk_a^0 given in Table II are such that C_{M^+} and C_M are both in moles per liter and i_0 is in amps per cm². Reasonable values for the kinetic parameters of hydrogen evolution on dilute amalgams under the conditions of our experiments are $i_0^{(H)} = 3 \times 10^{-13}$ amp/cm² and $\alpha^{(H)} = 0.50$, independent of pH.[17-19]

Table II: Kinetic Parameters for the Alkali Metal Amalgams[16]

Metal	α	Fk_a^0, amp l. cm^{-2} mole^{-1}
Na	0.61	17.4
K	0.59	5.0
Li	0.65	8.9

The effect of the hydrogen evolution reaction can be diminished by making the solution more alkaline, which shifts the reversible potential of the hydrogen reaction to more negative values and decreases i_c. For example, at a potential of −1.795 v with pH 12.0, the current i_c is 4.5×10^{-4} amp/cm², which is only about 0.01% of the current due to the sodium reaction. This produces a negligible shift in potential, less than 0.005 mv. It is important that traces of oxygen and organic matter, which increase i_c, be absent from the experimental system.[17-19]

Potassium ions, on the other hand, produce an effect which cannot be made negligible. Consider what happens when a 0.1 mole % sodium amalgam is introduced into a solution containing 0.5 *m* NaCl and 0.5 *m* KCl. Initially, the concentration of potassium in the amalgam is very small and the equilibrium potential for potassium, according to eq 1, is very positive. From eq 3 we see that the predominant reactions initially will be eq a, b, and c, but even in this initial stage the potential measured at the amalgam electrode is not the equilibrium potential of the Na–Na$^+$ couple. The zero current potential is more positive than the true equilibrium potential of sodium in that solution, because reaction a must compensate for the additional cathodic current of reaction e. This is shown in Figure 1. The partial currents at a sodium amalgam electrode containing a small amount of potassium, in a solution containing both Na$^+$ and K$^+$, were calculated using eq 1–4 and the data in Tables I and II. Note that the zero current

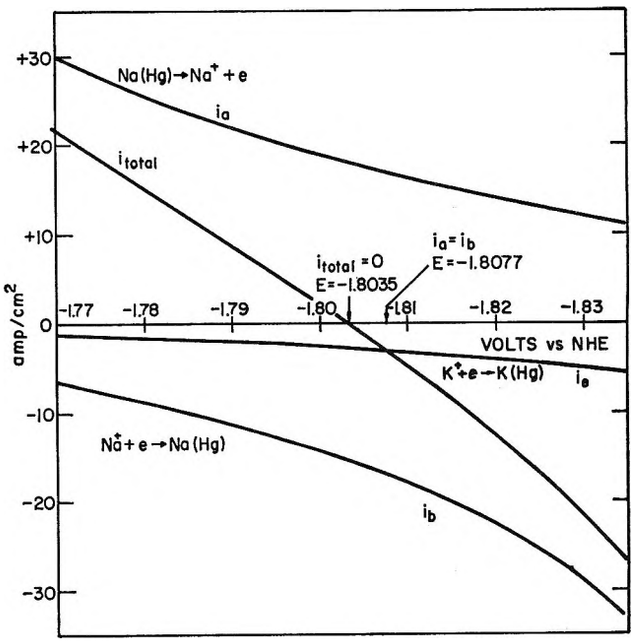

Figure 1. Initial partial currents at a sodium amalgam electrode (0.1 mole %) in contact with an electrolyte containing 0.5 *m* Na$^+$ and 0.5 *m* K$^+$, pH 12. The partial currents for hydrogen evolution and potassium dissolution are less than 10^{-3} amp/cm². Note that the zero current potential (−1.8035 v) is 4.2 mv more positive than the equilibrium potential (−1.8077 v) expected for the Na(Hg)/Na$^+$ couple if there were no influence from potassium ion.

potential is shifted by 4.2 mv in the presence of potassium.

The concentration of potassium in the amalgam grows with time and the potential $E_e^{(K)}$ becomes more negative. Since the anodic reaction of sodium dissolution (eq a) is required (at zero net current) to balance not only the sodium deposition (eq b) but also the potassium deposition (eq e), the sodium content of the amalgam is depleted and the potential $E_e^{(Na)}$ becomes more positive. Eventually, an equilibrium potential is reached which is defined by eq 2, with $i = 0$, and with the various partial currents given by eq 3. This potential is neither the equilibrium potential for sodium nor the equilibrium potential for potassium. In the limit where $i_0^{(K)}$ is very small compared to $i_0^{(Na)}$, or $E_e^{(K)}$ is much more negative than $E_e^{(Na)}$, the equilibrium value reached will be essentially $E_e^{(Na)}$; but in the case we are considering, such an assumption is not valid.

(16) H. Imai and P. Delahay, *J. Phys. Chem.*, **66**, 1683 (1962).

(17) A. N. Frumkin, *Advan. Electrochem. Electrochem. Eng.*, **1**, 65 (1961).

(18) V. N. Korshunov and Z. A. Iofa, *Dokl. Akad. Nauk SSSR*, **141**, 143 (1961).

(19) A. Frumkin, V. Korshunov, and Z. A. Iofa, *ibid.*, **141**, 413 (1961).

A simplified solution to this rather complex problem can be obtained by considering an infinite reservoir of electrolyte and a limited amount of sodium amalgam and permitting the reaction

$$Na(Hg) + K^+ \rightleftharpoons K(Hg) + Na^+$$

to go to equilibrium. Because the electrolyte supply is infinite, the concentrations of the ions will not change, but because the amount of the amalgam is finite, its concentrations are subject to the restriction

$$X_K + X_{Na} = X_{Na}^0 \qquad (5)$$

where X_{Na}^0 is the initial mole fraction of sodium in the amalgam and X_K and X_{Na} are the concentrations at equilibrium. The concentration ratio in the amalgam can be estimated from the standard potentials of the amalgams. Applying eq 1 to the cell

$$Na(Hg)|Na^+,K^+|K(Hg)$$

with $E = 0$, using known activity coefficients for the electrolytes[20] and amalgams,[9] and combining with eq 5, we obtain $X_{Na}^\circ/X_{Na} = 1.565$. By eq 1 this corresponds to a shift of the sodium amalgam electrode potential to a value 11.5 mv more positive than if K^+ had not been present. Figure 2 shows the partial currents at equilibrium, calculated using eq 1–5. Experimental evidence in support of this scheme is presented in the next section.

Of course, the real situation is much more complicated, as we have indicated, but this shift probably represents a reasonable upper limit. If the ratio of Na^+ to K^+ in the electrolyte is larger or if the measurements are made before the full equilibrium is established, then the potential shift may be smaller; if the ratio of Na^+ to K^+ is smaller, the potential shift may be even larger. In the limit where $X_{Na^+} \rightarrow 0$, the potential at equilibrium is that of the potassium amalgam electrode, which corresponds to a negative shift in potential. Thus it does not seem possible to make accurate activity coefficient measurements with sodium amalgam electrodes in solutions containing K^+. A totally analogous argument may be made for solutions containing Na^+ and Li^+, but the conclusion is more favorable.

From Table I, we can see that the standard potential of Li amalgam is 230 mv more negative than that of Na amalgam and from Table II that the exchange current is smaller than that for sodium. Using eq 1 and 5, with K replaced by Li, we find that for Li^+/Na^+ ratios less than 30, the error due to the reaction

$$Na(Hg) + Li^+ \rightleftharpoons Li(Hg) + Na^+$$

is less than 0.1 mv. Thus we predict that no appreciable systematic errors may be observed in Li^+–Na^+ mixtures (using sodium amalgam electrodes) if more than 3% of the cations present are Na^+. Because of the lower exchange current of the lithium reaction (Table II), we expect that the effect will be even smaller than predicted. This is borne out by our experimental measurements, which are presented in the next section.

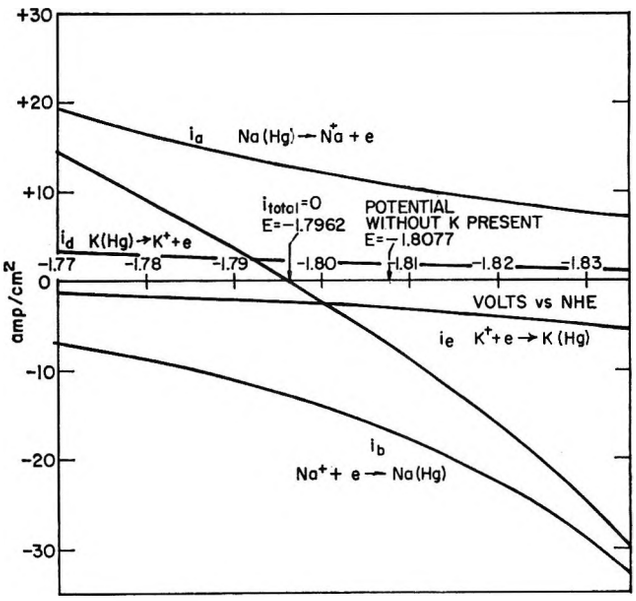

Figure 2. Equilibrium partial currents at a sodium amalgam electrode (0.1 mole %) in contact with a large excess of electrolyte containing 0.5 *m* Na^+ and 0.5 *m* K^+, pH 12. The partial current for hydrogen evolution is less than 10^{-3} amp/cm². The equilibrium composition of the amalgam is 0.064 mole % Na and 0.036 mole % K. The zero current potential (−1.7962 v) is 11.5 mv more positive than the equilibrium potential (−1.8077 v) expected for the Na(Hg)/Na^+ couple if there were no influence from potassium ion.

Results and Discussion

NaCl–LiCl Electrolyte. The mean activity coefficient γ_{12} of NaCl in the mixed electrolyte was calculated from the known emf and concentration values using the equation

$$E = -\frac{RT}{F} \ln \left[\frac{(m_{Na^+})(m_{Cl^-})(\gamma_{12})^2}{(m_{Na^+}{}^0)(m_{Cl^-}{}^0)(\gamma_{10})^2} \right] \qquad (6)$$

where m_{Na^+} and m_{Cl^-} are the molalities of Na^+ and Cl^- in the mixed electrolyte, $m_{Na^+}{}^0$ and $m_{Cl^-}{}^0$ are the molalities in the reference solution, and γ_{10} is the mean activity coefficient of NaCl in the reference solution. The electrolyte in the reference cell was in each case the solution listed as "100% ionic strength NaCl,"

(20) R. A. Robinson and R. H. Stokes, "Electrolyte Solutions," 2nd ed, Butterworth and Co. Ltd., London, 1959.

the first entry in each part of the data tables. The other electrolytes were made by mixing accurately weighed amounts of this solution with a LiCl stock solution of approximately the same ionic strength.

To minimize the possible interference from hydrogen evolution at the amalgam electrodes, the solutions were made alkaline with NaOH. The ionic strength listed in the data tables includes a contribution from the NaOH present; but since this was a constant amount, it was not included in calculating the ionic strength fraction present as NaCl. For example, one stock solution (designated "100% NaCl") really was 0.010 m in NaOH and 1.005 m in NaCl, making a total ionic strength of 1.015.

The activity coefficients of the stock solutions were calculated using the activity coefficient values for pure NaCl solutions given by Robinson and Stokes,[20] together with values of the Harned's rule constants for NaOH–NaCl mixtures obtained by Harned and Cook.[6] The correction for the presence of NaOH was in every case less than 0.002 in log $\gamma_{\pm}$, which is of the same order of magnitude as the uncertainty in the literature values for γ_{NaCl}. For most of the solutions measured, the correction for the NaOH added was much smaller.

The effect of NaOH on the activity coefficient of NaCl in solutions containing large fractions of other salts may be somewhat different than in solutions containing only NaCl and NaOH, but since the corrections were small and no data yet exist for activity coefficients in these quaternary systems, no further corrections were attempted.

The results of our experiments on NaCl–LiCl electrolytes are given in Table III, as are the activity coefficient values corrected to round values of ionic strength: 0.1, 0.5, 1.0, 2.0, and 3.0 m. The experimental data were fitted to Harned's rule[20,21]

$$\log \gamma_{12} = \log \gamma_{10} - \alpha_{12} X_2 I \qquad (7)$$

using the corrected activity coefficient values, and the results are summarized in Table IV. The Harned rule coefficient α_{12} should depend to some extent on the total ionic strength I but not on the fraction of the second component X_2.

Values of α_{12} were obtained by two different statistical methods. In the first method, $-\log \gamma_{10}$ was held constant at the value (second column of Table IV) obtained from the literature data for pure NaCl solutions,[20] with the small corrections for the presence of NaOH.[6] A value of α_{12} was calculated from eq 7 for each NaCl–LiCl mixture and the mean values of α_{12} for each ionic strength, together with the 95% confidence intervals (obtained from Student's t-distribution), are listed in the third column of Table IV. This method gives heavier weight to points of high LiCl/NaCl ratio.

Table III: Mean Activity Coefficients of NaCl in NaCl–LiCl Electrolytes at 25°

Total ionic strength[a]	Ionic strength fraction NaCl[b]	E, mv	$-\text{Log } \gamma_{\pm}$	$-\text{Log } \gamma_{\pm}$ cor[f]
0.1137	1.0000	0	0.1130[c]	0.1090
0.1135	0.6999	8.4	0.1094	0.1056
0.1134	0.4800	19.0	0.1118	0.1081
0.1133	0.4251	20.4	0.1092	0.1055
0.1133	0.2956	26.0	0.0854	0.0818
0.1132	0.1640	39.5	0.0899	0.0864
0.5094	1.0000	0	0.1665[c]	0.1658
0.5082	0.8615	1.5	0.1628	0.1623
0.5070	0.7219	6.2	0.1630	0.1626
0.5060	0.5599	12.7	0.1618	0.1615
0.5048	0.4573	18.7	0.1550	0.1547
0.5030	0.2520	31.9	0.1391	0.1390
0.5019	0.1133	52.9	0.1440	0.1439
1.015	1.0000	0	0.1857[c]	0.1856
1.012	0.8996	2.3	0.1794	0.1794
1.008	0.7501	7.3	0.1820	0.1820
1.002	0.4999	15.6	0.1640	0.1640
0.996	0.2500	32.5	0.1597	0.1598
0.992	0.1014	52.2	0.1436	0.1434
0.991	0.0500	68.4	0.1472	0.1470
0.991	0.0101	91.8	0.1108	0.1105
2.0142	1.0000	0	0.1746[c]	0.1749
1.9741	0.7736	4.1	0.1445	0.1438
1.9628	0.4938	10.8	0.1044	0.1030
1.9600	0.4226	9.4	0.0586	0.0570
1.9582	0.3804	17.6	0.1019	0.1002
1.9563	0.3315	19.3	0.0852	0.0844
1.9513	0.2065	33.3	0.1013	0.0990
1.9485	0.1379	42.7	0.0928	0.0902
3.014	1.0000	0	0.1463[c]	0.1468
3.005	0.9001	2.7	0.1461	0.1463
3.010[d]	0.500[d]	−29.2[e]	0.088[d]	0.088[d]
2.943	0.1002	54.6	0.1098	0.1062

[a] Containing 0.004 m NaOH to adjust pH of 0.1, 0.5, and 2 m solutions, 0.010 m NaOH for others. [b] Based on total of NaCl and LiCl, but excluding NaOH·$(1 - X_2)$ in eq 7. [c] Activity coefficient of NaCl in stock solution, calculated using values from ref 20 for pure NaCl and Harned rule coefficients for NaCl–NaOH mixtures from ref 6. [d] Solutions were not analyzed and concentrations may be in error by as much as 1%, leading to errors in $-\log \gamma_{\pm}$ of as much as 0.02. [e] Reference solution 1.50 m NaCl. [f] To 0.100, 0.500, 1.000, 2.000, and 3.000 m using data from ref 20, Appendix 8.3, and α_{12} values interpolated from ref 22.

(21) H. S. Harned and B. B. Owen, "The Physical Chemisty of Electrolytic Solutions," 3rd ed, Reinhold Publishing Corp., New York, N. Y., 1958.

Table IV: Harned Rule Coefficients for NaCl–LiCl Electrolytes at 25°

(Errors Are 95% Confidence Limits)

Total ionic strength	$-\text{Log } \gamma_{10}$[a]	$-\alpha_{12}$[b]	$-\text{Log } \gamma_{10}$[c]	$-\alpha_{12}$[c]	$-\alpha_{12}$[d]
0.10	0.1090	0.17 ± 0.16	0.114 ± 0.018	0.30 ± 0.30	...
0.50	0.1658	0.042 ± 0.018	0.168 ± 0.009	0.058 ± 0.028	...
1.00	0.1856	0.045 ± 0.017	0.190 ± 0.016	0.056 ± 0.027	...
2.00	0.1749	0.067 ± 0.016	0.162 ± 0.037	0.052 ± 0.034	0.037
3.00	0.1468	0.019 ± 0.025	0.143 ± 0.063	0.019 ± 0.029	0.035

[a] Reference solution, value calculated from data in ref 20 and 6 (uncertainty approximately ±0.002). [b] Mean value with γ_{10} fixed at the value in the second column. [c] Least-squares fit with both γ_{10} and α_{12} adjustable. [d] Isopiestic method[22] (random error approximately ±0.001).

In the second method, the experimental values of γ_{12} and X_2 were fitted to eq 7 by the least-squares method and best values of α_{12} and γ_{10} were obtained from the slope and intercept of the straight line. These parameters, together with their confidence limits, are listed in columns 4 and 5 of Table IV.

The values of α_{12} obtained by the isopiestic method[22] are given in the last column of Table IV. Within the confidence limits, our data agree with $\alpha_{12} = 0.035$ for all points except 2.00 m, using the first method. The least-squares value of γ_{10} agrees with the literature value to better than 99% confidence.

Although our experiments have shown general agreement, we have not been able to attain the precision afforded by the isopiestic method. At higher ionic strengths the potential measurements were irreproducible. At lower ionic strengths, although the measurements were reproducible, α_{12} is uncertain because the error in α_{12} for a given error in slope varies inversely with the ionic strength. Nevertheless, these results are useful because they provide a completely independent check on the isopiestic method. A good approximation for NaCl–LiCl electrolytes appears to be to use $\alpha_{12} = -0.035$ independent of ionic strength below 4 m, decreasing to -0.033 at 6 m.

From the osmotic coefficients[20] of NaCl and LiCl solutions, we can obtain a value of α_{21}, which will give the activity coefficients of LiCl in the mixed electrolytes. For 1–1 electrolytes, if Harned's rule is obeyed by both components, the Gibbs–Duhem relation becomes[20,21]

$$\alpha_{21} = \alpha_{12} + \frac{2}{2.303\,I}(\phi_2^0 - \phi_1^0) \qquad (8)$$

The second term in this equation is 0.070 for ionic strengths between 1 and 3 m, increases to 0.073 at 0.5 m, and increases to 0.075 at 6 m. Taking $\alpha_{12} = -0.035$ as a representative value, we obtain $\alpha_{21} = +0.035$ for ionic strengths below 3 m, increasing to +0.040 at ionic strength 6 m. Since α_{12} and α_{21} are both virtually independent of ionic strength, their sum is also independent of ionic strength and the thermodynamic cross-differentiation consistency test[20,21] is satisfied. The isopiestic data[22] show small deviations from Harned's rule at high ionic strengths, but these are negligible below 4 m.

Thus, as we saw for the NaCl–Na_2SO_4 system, a single value for α_{12} and a single value of α_{21} suffice to calculate the activity coefficients of NaCl–LiCl electrolytes, at all ionic strengths, for any requirements but the most exacting.

NaCl–KCl Electrolytes. Our experiments using the cell

$$\text{Na,Hg}|\text{Na}^+,\text{K}^+,\text{Cl}^-|\text{AgCl}|\text{Ag}$$

have confirmed the conclusion reached theoretically in the first part of the paper—activity coefficient measurements cannot be made with sufficient accuracy in NaCl–KCl electrolytes using sodium amalgam elec-

Table V: Measurements in NaCl–KCl Electrolytes

m_{NaCl}	m_{KCl}	Measured	Potential calcd from isopiestic data,[a] mv: Including amalgam effect	Potential calcd from isopiestic data,[a] mv: Neglecting amalgam effect
0.50	0.50	9.2 ± 0.3	7.3	18.79
0.200	0.200	26.6 ± 0.2	25.6	14.13
		28.0 ± 0.5		

[a] Reference cell for the first set contained 1.00 m NaCl; reference cell for the second set contained 0.200 m NaCl. Solutions contained 5×10^{-4} m NaOH.

(22) R. A. Robinson and C. K. Lim, *Trans. Faraday Soc.*, 49, 1144 (1953).

trodes. The general scheme proposed in our theoretical discussion has also been confirmed, although extensive experiments were not made. The results of three experiments made with NaCl–KCl electrolytes are summarized in Table V. Our experimental potential values are listed in the third column. The potential calculated on the assumption that the sodium amalgam electrode reached equilibrium with the NaCl–KCl electrolyte is listed in the fourth column and the potential calculated from the isopiestic data[23–25] on the assumption that the sodium amalgam electrode was reversible to Na^+, with no effect of K^+, is listed in the fifth column.

The observed potential fluctuated irregularly as the amalgam drops fell from the capillaries and not smoothly as in solutions containing only Na^+. Note that the experimental values agree to within a few millivolts with those calculated assuming that the analgam electrode reached equilibrium with the solution. However, the uncertainty in this correction is in most cases larger than the activity coefficient variation described by Harned's rule and it is clear that accurate measurements on the activity coefficients of sodium salts in the presence of potassium salts (or *vice versa*) cannot be made by the amalgam electrode method.

Acknowledgments. This work was supported by the U. S. Department of the Interior, Office of Saline Water. The authors thank Dr. R. A. Robinson for his encouragement on this project, Mr. Andrew Menna for assisting in apparatus construction, and Mr. Marcel Fajnzylber for assistance with some of the analytical work.

(23) R. A. Robinson, *Trans. Faraday Soc.*, **49**, 1411 (1953).

(24) R. A. Robinson, "Electrochemical Constants," National Bureau of Standards Circular 524, U. S. Government Printing Office, Washington, D. C., 1953, pp 171–184.

(25) R. A. Robinson, *J. Phys. Chem.*, **65**, 662 (1961).

Scavenger Kinetics in the Radiolysis of Cyclohexane Solutions. II. Cyclohexane–Methyl Iodide Mixtures

by Inder Mani and Robert J. Hanrahan

Chemistry Department, University of Florida, Gainesville, Florida *(Received March 8, 1967)*

The scavenging effects of added HI and I_2 in the radiolysis of cyclohexane–methyl iodide solutions have been investigated. An interpretation of the results which is similar to those made earlier for pure alkyl iodides and for pure hydrocarbons has been found to be applicable also to mixtures of these compounds. It is shown from a simple mechanism that total iodine yields, total free-radical yields, and yields for HI produced and consumed can be calculated from a knowledge of the limiting rates of iodine production (or consumption) at zero dose with added I_2, HI, and no additives. Differential rate expressions for HI and I_2 concentrations are readily obtained, but they cannot be integrated analytically. However, it was possible to integrate them numerically by the second-order Runge–Kutta method, using an IBM 709 computer. The computer program allows evaluation of the role of various parameters in determining the shape of experimental iodine concentration *vs.* dose graphs. Initial G values for production of iodine, hydrogen iodide, and free radicals are tabulated for various concentrations of the cyclohexane–methyl iodide mixtures, and trends are discussed in terms of mechanisms for energy localization in solution radiolysis.

Introduction

Several years ago it was reported by this laboratory[1] that solutions of methyl iodide and cyclohexane produce iodine under radiolysis, and that the resulting graphs of iodine concentration *vs.* dose are nearly linear. In the course of that work it was found, rather surprisingly, that solutions with concentrations of cyclohexane between about 80 and 95% by volume, which produce iodine if irradiated without additives, nevertheless consume iodine initially if iodine is added before radiolysis. As radiolysis proceeds the iodine concentration reaches a minimum and then increases. Although it was suspected at the time that this behavior was due to HI produced in the reaction and then competing with I_2 for radicals, the data were not published awaiting a quantitative interpretation. A plausible mechanism could be written, but it appeared impractical to solve the associated kinetic expressions. For a study of this type, differential rate expressions, relating G values to concentrations and rate constants, are not adequate. The experimental variables, I_2 concentration *vs.* dose, are related to integrated rate equations.

Although a set of integrated rate expressions was presented earlier[2] for the rather similar kinetic problem in irradiated ethyl iodide, the results are not directly applicable in the present case. The over-all stoichiometry of the radiation-induced reaction in methyl iodide–cyclohexane solutions is somewhat more complicated than in ethyl iodide. In addition, the analytical integration done for ethyl iodide radiolysis kinetics requires that the rate constant ratio for reaction of radicals with HI and I_2, respectively, be unity. This is not a sufficiently good approximation in the present case. More recently, Perner and Schuler[3] have presented an ingenious indirect analytical solution for HI–I_2 scavenger kinetics in irradiated hydrocarbons. Again, it appears impossible to extend the mathematical treatment to hydrocarbon–alkyl iodide solutions. A further approach to the same problem of HI and I_2 in irradiated

(1) T. S. Croft and R. J. Hanrahan, *J. Phys. Chem.*, **66**, 2188 (1962).

(2) R. J. Hanrahan and J. E. Willard, *J. Am. Chem. Soc.*, **79**, 2434 (1957).

(3) D. Perner and R. H. Schuler, *J. Phys. Chem.*, **70**, 2224 (1966).

cyclohexane was recently suggested by this laboratory.[4] Since the integration of the kinetic expressions was performed numerically using an IBM 709 computer, there were no serious mathematical barriers to extending this treatment to the analysis of radiolysis kinetics in cyclohexane–methyl iodide solutions. In the present paper, data taken in the radiolysis of solutions of methyl iodide in cyclohexane over the concentration range from 20 to 99.9% cyclohexane are presented and interpreted by the numerical integration technique. G values for various primary processes are tabulated, and trends in these values as a function of composition of the mixtures are discussed from the viewpoint of possible mechanisms for energy localization.

Experimental Section

Phillips "pure grade" cyclohexane was purified by passing it through silica gel. Iodine and hydriodic acid were Baker Analyzed reagents. Hydrogen iodide was produced by dehydrating hydriodic acid. Methyl iodide (Eastman Organic Chemicals) was passed through alumina, distilled on a Todd still, and passed through alumina again. Individual 4-ml samples of the solutions were prepared volumetrically, dried over P_2O_5, degassed, transferred under vacuum to the irradiation vessels, and sealed off. Irradiations were done with a Co^{60} γ irradiator.[5] The dose rate in the Fricke dosimeter [$G(Fe^{3+}) = 15.6$] was found to be 0.631×10^{18} ev/ml min. For methyl iodide the value of μ(sample)/μ(dosimeter) was calculated to be 1.950 based on absorption by Compton effect and photoelectric effect. For cyclohexane, the value 0.780 was obtained on the basis of electron density ratios. Relative absorption figures for the intermediate solutions were obtained by assuming an interpolation linear in volume fractions. Iodine was analyzed spectrophotometrically using a Beckman DU spectrophotometer. The positions of λ_{max} and the extinction coefficients for the various solutions were used as given by Croft and Hanrahan.[1]

Results

All of the experimental data consist of measurements of iodine concentration *vs.* dose, for various solutions. Yields of iodine production for pure, degassed solutions of cyclohexane in methyl iodide with no added scavengers were reported by Croft and Hanrahan.[1] The general character of the results reported by them is that all solutions containing 5% or more methyl iodide by volume produced iodine nearly linearly with dose; the G value for iodine production decreased with increasing cyclohexane concentration. The slopes of the graphs of iodine concentration *vs.* dose are designated "normal rate" in this paper, given in the units of micromoles per minute.[6]

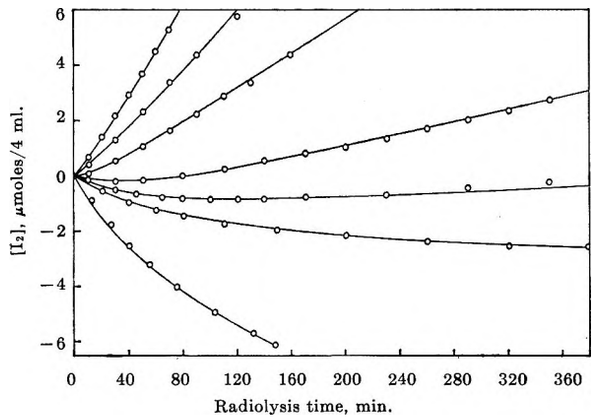

Figure 1. Net iodine production or consumption in the radiolysis of cyclohexane–methyl iodide solutions, with added I_2, as a function of radiation time: circles, experimental values; smooth curves, computed values. Volume per cent cyclohexane, reading downward, is 20, 40, 60, 80, 90, 95, and 99.9.

Production of iodine in the radiolysis of solutions of cyclohexane and methyl iodide in which I_2 was present initially as a free-radical scavenger are shown in Figure 1. In all experiments the initial concentration of I_2 was about 1.5×10^{-3} M. Note that the graph shows net iodine production or consumption; that is, the initial iodine concentration has been subtracted from the total measured iodine concentration in plotting the ordinate points. It can be seen that all of the curves are concave upward. In the case of solutions from 80 to 95 vol. % cyclohexane, the iodine concentration actually decreases at first and then increases. The minimum in the 95% graph occurs off the scale of the figure, at 2400 min. In the case of solution with 99.9% cyclohexane by volume, iodine is regularly consumed until no iodine is left after 148 min. The initial slopes of the lines in Figure 1, whether positive or negative, are designated as the "minimum rates."

Results for iodine production with added HI are shown in Figure 2. These graphs are all concave downward. For 99.9 vol. % cyclohexane solution, only a portion of the graph has been shown. The complete graph is given in Figure 3. The slopes at zero dose will be referred to as the "maximum rates."

The G values for the normal rate of iodine production without additives, the maximum rate with added HI,

(4) I. Mani and R. J. Hanrahan, *J. Phys. Chem.*, **70**, 2233 (1966).

(5) R. J. Hanrahan, *Intern. J. Appl. Radiation Isotopes*, **13**, 254 (1962).

(6) As in our previous paper,[2] the units micromoles/4 ml and radiolysis time in minutes are used for convenience in programming the digital computer.

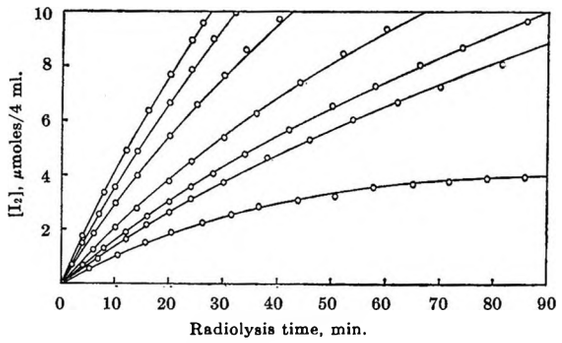

Figure 2. Iodine production in the radiolysis of cyclohexane–methyl iodide solutions, with added HI, as a function of radiation time: circles, experimental values; smooth curves, computed values. Volume per cent cyclohexane, reading downward, is 20, 40, 60, 80, 90, 95, and 99.9. Initial HI concentration is 6.1×10^{-3} *M*.

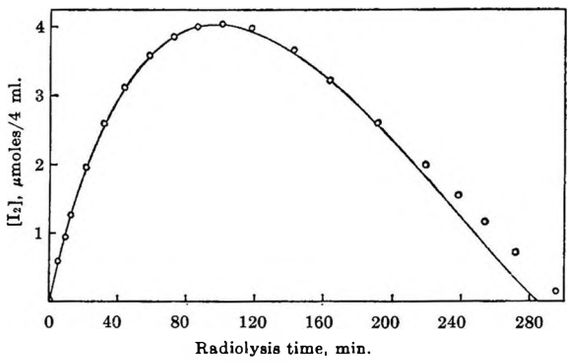

Figure 3. Iodine production in the radiolysis of cyclohexane–methyl iodide solution, for 99.9 vol. % cyclohexane, with added HI, as a function of radiation time: circles, experimental values; smooth curves, computed values. Initial HI concentration is 3.4×10^{-3} *M*.

and the minimum rate with added I_2 are listed in Table I.

Table I: Experimental *G* Values for the Radiolysis of Cyclohexane–Methyl Iodide Solutions

Cyclohexane, vol. %	$G(I_2)$ Normal[a]	$G(I_2)$ Maximum (with HI added)	$G(I_2)$ Minimum (with I_2 added)
0	1.41	6.51[b]	1.20[b]
20	1.23 (1.11)	6.18	0.84
40	1.10 (0.85)	6.25	0.56
60	0.79 (0.60)	6.18	0.09
80	0.45 (0.25)	5.24	−0.28
90	0.18 (0.053)	4.37	−0.64
95	0.05 (0.004)	4.09	−0.94
99.9	0	3.45	−2.62
100	0	2.96	−3.08

[a] For solutions without adding HI or I_2 prior to irradiation. These values have been taken from ref 1. The values in the parentheses are obtained after extended periods of irradiation and were measured in the present work. [b] Iodine yields in pure methyl iodide with added HI and I_2 are taken from ref 2.

Discussion

Kinetic Model. It is clear from previous work[1,7,8] that primary processes in the radiolysis of cyclohexane–methyl iodide solutions involve several complex interactions such as charge exchange, electron capture, and transfer of electronic excitation energy, with the result that energy originally deposited in one component of the mixtures may ultimately lead to decomposition of the other. Such interactions must be considered when one attempts to rationalize the relative magnitudes of the yields of various primary processes as a function of cyclohexane and methyl iodide concentrations; this is done in a later section of this paper. For any given solution, however, the net result of the primary processes is the production of I_2, HI, and alkyl radicals, which then take part in competitive reactions under steady-state kinetic conditions. Therefore, for the present purposes, a somewhat simplified kinetic scheme is adequate.

Reactions in spurs[9]

$$c\text{-}C_6H_{12} \text{---}\rightsquigarrow (c\text{-}C_6H_{12}^+ + e^-) \longrightarrow c\text{-}C_6H_{12}^* \quad (1a)$$

$$c\text{-}C_6H_{12} \text{---}\rightsquigarrow c\text{-}C_6H_{12}^* \quad (1b)$$

$$c\text{-}C_6H_{12}^* \longrightarrow c\text{-}C_6H_{10} + H_2 \quad (2)$$

$$c\text{-}C_6H_{12}^* \longrightarrow c\text{-}C_6H_{11}\cdot + H\cdot \quad (3)$$

$$CH_3I \text{---}\rightsquigarrow (CH_3I^+ + e^-) \longrightarrow CH_3I^* \quad (4a)$$

$$CH_3I \text{---}\rightsquigarrow CH_3I^* \quad (4b)$$

$$c\text{-}C_6H_{12}^* + CH_3I \longrightarrow c\text{-}C_6H_{12} + CH_3I^* \quad (5)$$

$$CH_3I^* \longrightarrow CH_3\cdot + I\cdot \quad (6)$$

$$CH_3I^* + CH_3I \longrightarrow C_2H_6 + I_2 \quad (7a)$$

$$CH_3I^* + CH_3I \longrightarrow C_2H_4 + 2HI \quad (7b)$$

$$H\cdot + CH_3I \longrightarrow HI + CH_3\cdot \quad (8)$$

Thermal radical reactions

$$I\cdot + I\cdot \longrightarrow I_2 \quad (9)$$

$$R\cdot + I_2 \longrightarrow RI + I\cdot \quad (10)$$

$$R\cdot + HI \longrightarrow RH + I\cdot \quad (11)$$

(7) L. J. Forrestal and W. H. Hamill, *J. Am. Chem. Soc.*, **83**, 1535 (1961).

(8) R. H. Schuler, *J. Phys. Chem.*, **61**, 1472 (1957).

(9) Asterisks represent electronically excited species.

$$H\cdot + I_2 \longrightarrow HI + I\cdot \quad (12)$$

$$H\cdot + HI \longrightarrow H_2 + I\cdot \quad (13)$$

This scheme allows for production of hydrogen atoms, alkyl radicals, cyclohexene, and molecular hydrogen from cyclohexane as well as methyl radicals, stable hydrocarbons (*e.g.*, C_2H_6), hydrogen iodide, and iodine from methyl iodide. The distinction between atomic and molecular iodine formally indicated in eq 6 and 7 is of minor significance, since iodine atoms combine to form I_2 in any event (eq 9). The distinction which we attempt to suggest in eq 6 and 7 is that *net* iodine is produced only if the corresponding methyl radicals are stabilized as hydrocarbons. Some of the steps in the sequence are intended to represent net processes rather than actual mechanisms. In particular, energy redistribution between cyclohexane and methyl iodide (eq 5) could involve electron capture or charge exchange as well as transfer of excitation energy. Furthermore, there is evidence that net iodine production from methyl iodide (eq 7) occurs by an ionic route.[10] It is important to the quantitative treatment given below that, for a fixed ratio of methyl iodide to cyclohexane in the solutions, the rate of each of the processes listed under "reactions in spurs" is taken as a constant, unaffected by scavengers at low concentrations. Reaction 8 is not a "spur reaction" in the usual sense but is included in this group because methyl iodide, which is a good radical scavenger, was present at much higher concentration than any other scavenger in most of our experiments. Under these circumstances, all hydrogen atoms are converted to HI by reaction 8.

Because of the complexity of the situation, further approximations are required before mathematical analysis is attempted. In considering the thermal radical reactions, the distinction between methyl and cyclohexyl radicals is ignored, and it is assumed that the same rate constant can represent reactions of either with a scavenger. It is also assumed that the ratio of rate constants for reactions 11 and 10 (alkyl radicals with HI and I_2) is the same as the ratio for reactions 13 and 12 (hydrogen atoms with HI and I_2); this ratio is designated k_{HI}/k_{I_2}.

In treating the above reaction scheme kinetically, two parallel sets of equations are obtained. One set applies to all solutions with sufficient added methyl iodide to convert all H atoms to HI, so that the effective yield of H atoms available to take part in competitive reactions between HI and I_2 is zero. This regime applies at least to the range from 0 to 95 vol. % cyclohexane, and probably higher. The second set of equations is applicable if some hydrogen atoms escape reactions with methyl iodide and fall prey to the I_2–HI competition. Our results for 99.9% cyclohexane solutions represent this situation.

Mathematical Analysis. The reaction scheme presented above is treated by conventional kinetics. It is assumed that I_2, HI, and alkyl radicals (and H atoms, in the appropriate concentration range) are produced by the radiation and that HI and I_2 then compete for the radicals (and hydrogen atoms) according to eq 10–13. The steady-state assumption is applied to alkyl radical (and hydrogen atom) concentrations. Expressions for the net rates of change of iodine and HI concentrations can be derived in a manner similar to the pure cyclohexane case.[4] They are

$$\frac{d[I_2]}{dt} = B + ((A + D)/2) - (A + D)\left(\frac{[I_2]}{[I_2] + ([HI]k_{HI}/k_{I_2})}\right) \quad (14)$$

$$\frac{d[HI]}{dt} = C - (A + D) + (A + 2D)\left(\frac{[I_2]}{[I_2] + ([HI]k_{HI}/k_{I_2})}\right) \quad (15)$$

where A = thermal aklyl radical production rate, B = production of I_2 from spurs, C = production of HI from spurs or by reaction 8, and D = net rate of production of H atoms escaping reaction 8. Since the net yield of thermal hydrogen atoms is zero for solutions ranging from 0 to 95 vol. % cyclohexane, the D factor is zero and the corresponding rate expressions are

$$\frac{d[I_2]}{dt} = B + (A/2) - \{A[I_2]/([I_2] + ([HI]k_{HI}/k_{I_2}))\} \quad (16)$$

$$\frac{d[HI]}{dt} = C - A + \{A[I_2]/([I_2] + ([HI]k_{HI}/k_{I_2}))\} \quad (17)$$

In order to obtain equations giving I_2 and HI concentrations as a function of time, it is necessary to solve eq 14 and 15 or 16 and 17. As in the case of pure cyclohexane,[4] integration of the equations was accomplished numerically using the Runge–Kutta method on an IBM 709 computer.

Assignment of Parameters. To solve the rate expressions it is necessary to provide values for the quantities A, B, C, and D and for the ratio of the rate constants k_{HI}/k_{I_2}. The parameters A and B can be evaluated in a manner similar to that for pure cyclo-

(10) H. A. Gillis, R. R. Williams, and W. H. Hamill, *J. Am. Chem. Soc.*, **83**, 17 (1961).

hexane.[4] For the initial maximum rate of iodine production with added HI and the initial minimum rate of production of iodine with added I_2, eq 14 becomes

$$\left(\frac{d[I_2]}{dt}\right)_{max} = (\text{max rate}) = B + ((A + D)/2) \quad (18)$$

$$\left(\frac{d[I_2]}{dt}\right)_{min} = (\text{min rate}) = B - ((A + D)/2) \quad (19)$$

which can be added and subtracted to give

$$B = (\text{max rate} + \text{min rate})/2 \quad (20)$$

$$A + D = (\text{max rate} - \text{min rate}) \quad (21)$$

The corresponding equations for 0–95 vol. % cyclohexane solutions are (20) and (22)

$$A = (\text{max rate} - \text{min rate}) \quad (22)$$

It will be noted that both A and B can be computed unambiguously from experimental data for solutions with 0–95% cyclohexane. For solutions very dilute in methyl iodide, B is given directly and the sum of A and D is established but not their separate values. Resolution of the values of A and D is discussed below.

To evaluate the quantity C, which gives the rate of HI production from spurs, the expression derived by Hanrahan and Willard can be used[2,11]

$$\left(\frac{[HI]}{[I_2]}\right)_{norm} = (k_{I_2}/k_{HI})\left(\frac{\text{norm rate} - \text{min rate}}{\text{max rate} - \text{norm rate}}\right) \quad (23)$$

Since HI and I_2 are produced at a constant rate in radiolysis experiments with no additives, we can write

$$\left(\frac{d[HI]}{dt}\Big/\frac{d[I_2]}{dt}\right)_{norm} = \left(\frac{[HI]}{[I_2]}\right)_{norm} \quad (24)$$

$$\left(\frac{d[HI]}{dt}\right)_{norm} = \left(\frac{[HI]}{[I_2]}\right)_{norm}(\text{norm rate}) \quad (25)$$

by adding (14) and (15) we get

$$\frac{d[HI]}{dt} = C + B - (A/2) - \frac{d[I_2]}{dt} + \{D[I_2]/([I_2] + ([HI]k_{HI}/k_{I_2}))\} \quad (26)$$

After substituting (19) and (25) and rearranging, one obtains

$$C = \left(\frac{[HI]}{[I_2]}\right)_{norm}(\text{norm rate}) + (\text{norm rate} - \text{min rate}) - \{D[I_2]/([I_2] + ([HI]k_{HI}/k_{I_2}))\} \quad (27)$$

The corresponding expression for 20–25% solutions is

$$C = \left(\frac{[HI]}{[I_2]}\right)_{norm}(\text{norm rate}) + (\text{norm rate} - \text{min rate}) \quad (28)$$

The quantity C could be found experimentally if HI yields were measured. However, the HI yield is difficult to measure accurately. If the ratio k_{HI}/k_{I_2} can be established, then the HI production rate C can be found by substitution of the value of $[HI]/[I_2]$ now found by eq 23 into eq 28.

Since experimental values of the ratios k_{HI}/k_{I_2} for the series of solutions studied were not available, k_{HI}/k_{I_2} was treated as an adjustable parameter in the calculations. The computed effect of varying the ratio k_{HI}/k_{I_2} for the various solutions with added I_2 is shown

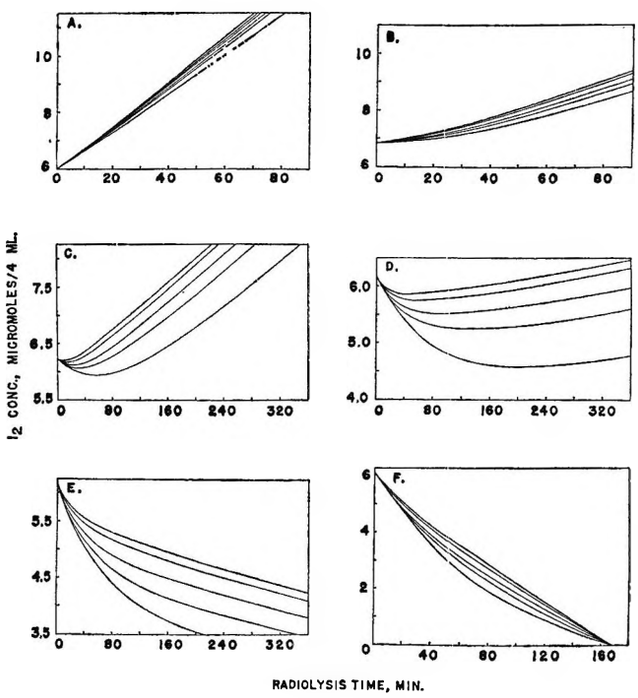

Figure 4. Role of k_{HI}/k_{I_2} as an adjustable parameter; I_2 production in the radiolysis of cyclohexane–methyl iodide solutions with added I_2. (A) 20 vol. % cyclohexane, 1.5×10^{-3} M initial I_2; values of k_{HI}/k_{I_2} reading downward are 2.0, 1.5, 1.0, 0.6, 0.4, and 0.1. (B) 60 vol. % cyclohexane, 1.7×10^{-3} M initial I_2; values of k_{HI}/k_{I_2} reading downward are 2.0, 1.5, 1.0, 0.7, and 0.4. (C) 80 vol. % cyclohexane, 1.55×10^{-3} M initial I_2; values of k_{HI}/k_{I_2} reading downward are 2.0, 1.5, 0.9, 0.6, and 0.3. (D) 90 vol. % cyclohexane, 1.55×10^{-3} M initial I_2; values of k_{HI}/k_{I_2} reading downward are 2.0, 1.5, 0.9, 0.6, and 0.3. (E) 95 vol. % cyclohexane, 1.55×10^{-3} M initial I_2; values of k_{HI}/k_{I_2} reading downward are 2.0, 1.5, 0.9, 0.6, and 0.4. (F) 99.9 vol. % cyclohexane, 1.5×10^{-3} M initial I_2; values of k_{HI}/k_{I_2} reading downward are 2.0, 1.5, 0.9, 0.7, and 0.4.

(11) There is a misprint in the equation as given originally in ref 2.

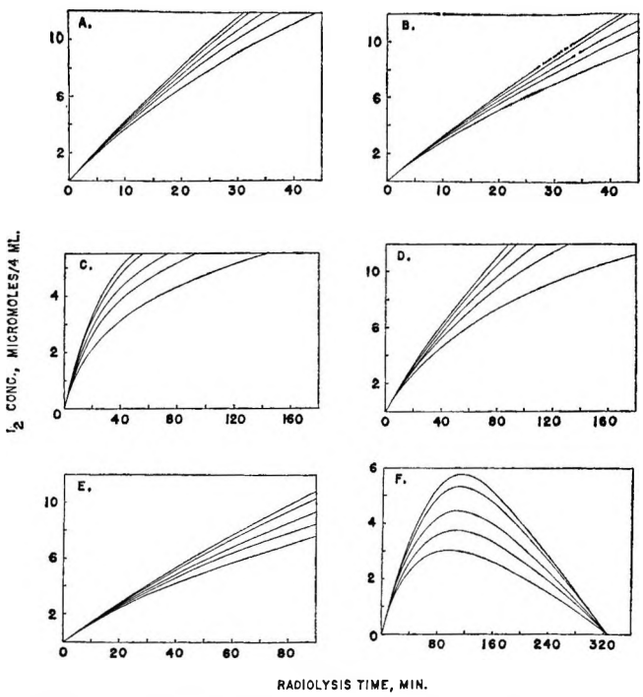

Figure 5. Role of k_{HI}/k_{I_2} as an adjustable parameter; I_2 production in the radiolysis of cyclohexane–methyl iodide solutions with added HI. (A) 20 vol. % cyclohexane, 6.1×10^{-3} M initial HI; values of k_{HI}/k_{I_2} reading downward are 2.0, 1.5, 1.0, 0.7, and 0.4. (B) 60 vol. % cyclohexane, 5.2×10^{-3} M initial HI; values of k_{HI}/k_{I_2} reading downward are 2.0, 1.5, 1.0, 0.7, and 0.4. (C) 80 vol. % cyclohexane, 1.5×10^{-3} M initial HI; values of k_{HI}/k_{I_2} reading downward are 2.0, 1.5, 0.9, 0.6, and 0.3. (D) 90 vol. % cyclohexane, 6.1×10^{-3} M initial HI; values of k_{HI}/k_{I_2} reading downward are 2.0, 1.5, 0.9, 0.6, and 0.3. (E) 95 vol. % cyclohexane, 6.1×10^{-3} M initial HI; values of k_{HI}/k_{I_2} reading downward are 2.0, 1.5, 0.9, 0.6, and 0.4. (F) 99.9 vol. % cyclohexane, 3.4×10^{-3} M initial HI; values of k_{HI}/k_{I_2} reading downward are 2.0, 1.5, 0.9, 0.6, and 0.4.

in Figure 4. For the entire range of cyclohexane–methyl iodide solutions, it is found that increasing the rate constant ratio increases the iodine concentration achieved at a given radiolysis time. This effect becomes more pronounced as the per cent cyclohexane in the solution is increased. However, the initial slope of the graphs is the same in all cases and approaches that for which k_{HI}/k_{I_2} is zero. Similar effects of varying the rate constant ratio are observed for experiments with added HI and are shown in Figure 5. The effect of varying the ratio in the case of 99.9% solutions is quite similar to that observed for pure cyclohexane.[2]

For solutions from 0 to about 95% cyclohexane, that is, for all cases in which there is a nonzero "normal rate" of iodine production, the arbitrary assignment of the single parameter k_{HI}/k_{I_2} should suffice to fit the equations to experimental data. Under these circumstances A and B come directly from experimental data, and C can be calculated if k_{HI}/k_{I_2} is fixed. It has been found that adjusting only k_{HI}/k_{I_2} gave a good fit of experimental data for solutions with 20–90% cyclohexane. However, this procedure gave a rather poor fit for 95% solution. It was found that the difficulty was due to the parameter C for HI production. Results of calculations using C as an adjustable parameter are shown in Figure 6 for an experiment with added I_2. It can be seen that the results are very sensitive to this parameter. (Curves for the experiment with added HI are now shown, since they are only slightly sensitive to changes in the HI production rate.) The value of C predicted from eq 23 and 28 is 0.033 μmole/min; the best fit of experimental data was obtained when C was adjusted to 0.029. Since the calculation of C from eq 23 and 28 is somewhat indirect and requires several mathematical manipulations of the experimental data, the difference between 0.029 and 0.033 is within experimental error. Hence, the scheme can be considered to fit directly to all solutions through 95% cyclohexane.

However, determination of the various parameters for solutions with more than 95% cyclohexane involves some difficulties. For these solutions, the normal rate of iodine production is zero. This indicates that the yield of radicals exceeds that of iodine, but does not tell by how much. For the 0–95% concentration range, four parameters—A, B, C, and k_{HI}/k_{I_2}—are needed and three experimental data—maximum, minimum, and normal rates of iodine production—are available. Hence, only one parameter needs to be adjusted arbitrarily. Above 95% cyclohexane, only two useful pieces of data, maximum and minimum rates of iodine production, are available and only two of the four

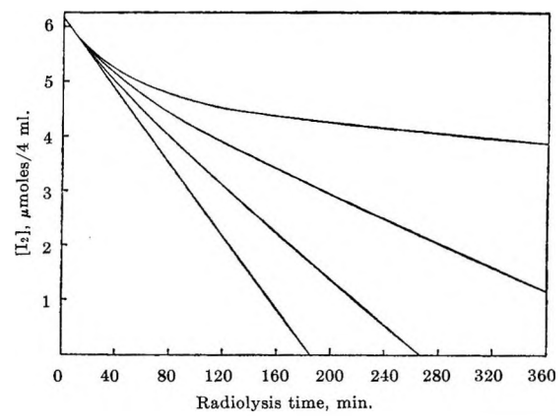

Figure 6. Role of HI production from spurs as an adjustable parameter; I_2 production in the radiolysis of cyclohexane–methyl iodide solution, for 95 vol. % cyclohexane with added I_2 (1.5×10^{-3} M), as a function of radiation time. G(HI) values, reading downward, are 0.85, 0.57, 0.28, and 0.0.

parameters, A and B, are fixed. Hence the values of both C and k_{HI}/k_{I_2} must be established. The situation is somewhat simplified because k_{HI}/k_{I_2} was found to have the same value of 0.71 for 90–95% solutions and for pure cyclohexane, and it can reasonably be assumed to have the same value between 95 and 100% cyclohexane solutions. This still leaves C to be determined.

However, another complication develops in solutions approaching pure cyclohexane, exemplified by the 99.9% case. For such solutions, it can no longer be assumed that the effective yield of thermal H atoms is zero. For these solutions, B is determined from eq 32; k_{HI}/k_{I_2} can be taken as 0.71. The sum of A and D is determined from eq 33, and C is undetermined. Thus, it is necessary to vary two quantities, C and D, to fit the equations to experimental data. After several computer calculations, it has been concluded that the sum of C and D was rather well defined as 0.041 ± 0.003 μmole/min. Considerably more variation is possible in the individual values. An adequate fit of the experimental data could be obtained with values of D in the range of 0.012–0.024 with C adjusted to maintain the sum of C and D as constant. The effects of varying D for experiments with added I_2 and HI are shown in Figures 7 and 8, respectively. Similar effects of varying C are shown in Figures 9 and 10. The combination $C = 0.023$ and $D = 0.020$ was used to calculate the curves for 99.9% solution in Figures 1–3. This set of values, with a rather high H atom yield and low HI yield, gave a better fit at longer radiolysis times than the reverse combination. However, this is probably somewhat fortuitous. A lower H atom yield ($G \simeq 0.5$) and higher HI yield ($G \simeq 0.9$) are more consistent with other work and the trends in the present data. The major difficulty for the 99.9% solution is probably due to the depletion of CH_3I during radiolysis; its initial concentration is only about 1.6×10^{-2} M. Complete consumption of HI (and I_2) as shown in Figure 3 required 5 hr of radiolysis at an absorbed dose rate of about 0.5 Mrad/hr, which would consume 25% of the methyl iodide present if $G(-CH_3I) \simeq 2$.

Comparison with Experiments. Input data for a computation on a given cyclohexane–methyl iodide solution are maximum, minimum, and normal rates of iodine production. An initial concentration of I_2 or HI is given to the computer, matching an actual experiment. The ratio k_{HI}/k_{I_2} is used as an adjustable parameter. The results of such calculations are shown by smooth curves in Figures 1–3; circles represent experimental data. It can be seen that the theoretical curves fit the experimental points quite satisfactorily. From these curve fittings, different k_{HI}/k_{I_2} values have been obtained for the various solutions.[12,13] These values are listed in Table II. Initial I_2 concentrations in the solutions were 1.4×10^{-3} to 1.7×10^{-3} M and the initial HI concentration was 6.1×10^{-3} M in the experiments shown in Figure 2.

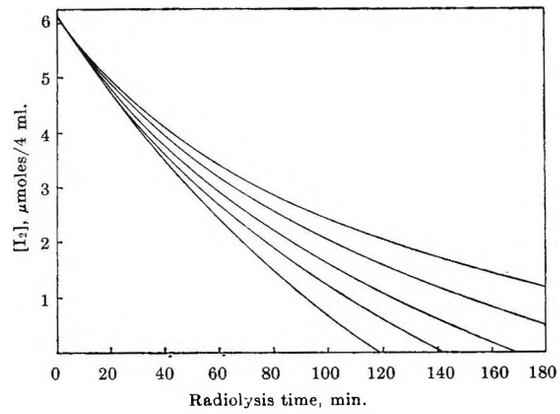

Figure 7. Role of H atom yield as an adjustable parameter; I_2 consumption in the radiolysis of cyclohexane–methyl iodide solution, for 99.9 vol. % cyclohexane with added I_2 (1.51×10^{-3} M), as a function of radiation time. $G(H\cdot)$ values, reading downward, are 1.40, 1.05, 0.70, 0.35, and 0.0.

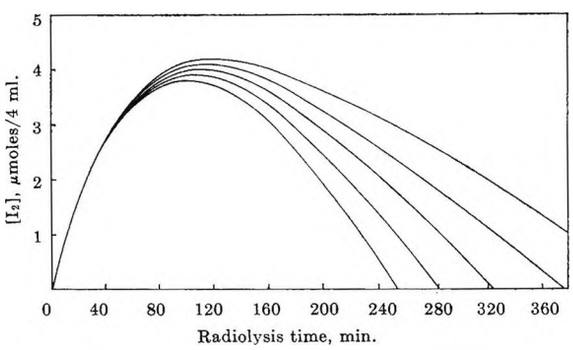

Figure 8. Role of H atom yield as an adjustable parameter; I_2 production in the radiolysis of cyclohexane–methyl iodide solution, for 99.9 vol. % cyclohexane with added HI (3.4×10^{-3} M), as a function of radiation time. $G(H\cdot)$ values, reading downward, are 1.40, 1.05, 0.70, 0.35, and 0.0.

A difficulty which was encountered in fitting theoretical curves to iodine production and consumption data requires comment. Some of the iodine concentration *vs.* dose graphs for radiolysis of HI or I_2 in cyclohexane–methyl iodide solutions cover several hours of radiolysis.

(12) One factor which can account at least partially for the observed moderate variation of the ratio k_{HI}/k_{I_2} is the effect of solvent polarity on the rates of the respective reactions.[13] Perhaps more important is the fact that the ratio is actually an average value weighted according to the proportions of the various radicals (mainly methyl and cyclopropyl) which are involved in the reactions with HI and I_2.

(13) K. J. Laidler, "Chemical Kinetics," 2nd ed, McGraw-Hill Book Co., Inc., New York, N. Y., 1965, p 207.

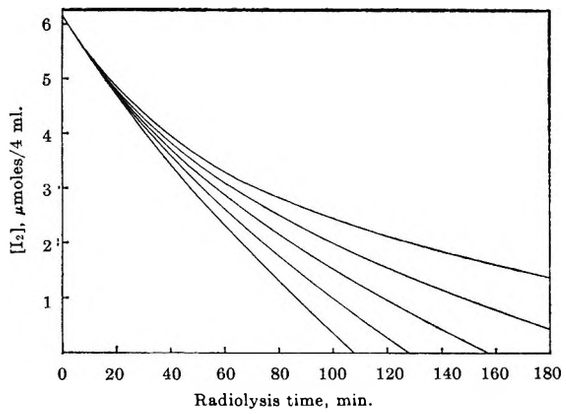

Figure 9. Role of HI production from spurs as an adjustable parameter; I_2 consumption in the radiolysis of cyclohexane–methyl iodide solution, for 99.9 vol. % cyclohexane with added I_2 (1.5×10^{-3} M), as a function of radiation time. G(HI) values, reading downward, are 1.40, 1.05, 0.70, 0.35, and 0.0.

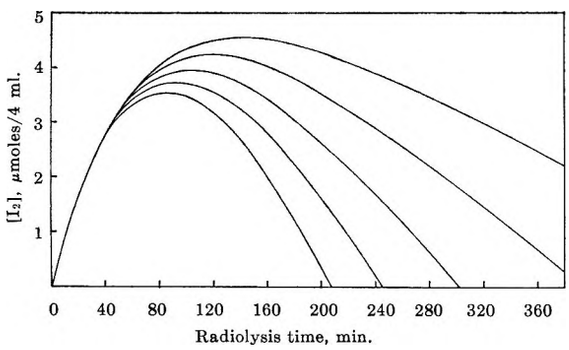

Figure 10. Role of HI production from spurs as an adjustable parameter; I_2 production in the radiolysis of cyclohexane–methyl iodide solution, for 99.9 vol. % cyclohexane with added HI (3.4×10^{-3} M), as a function of radiation time. G(HI) values, reading downward, are 1.40, 1.05, 0.70, 0.35, and 0.0.

As mentioned above, Croft and Hanrahan[1] reported that the rates of iodine production in cyclohexane–methyl iodide solutions without additives were nearly linear at low doses. For the longer radiolysis times used in the present work, changes in the normal rates become significant. The decrease in $G(I_2)$ from its initial value to the value obtained after several hours of radiolysis was of the order of 0.15–0.25 molecule/100 ev (Table I). This is a relatively small effect considering that total G values of I_2 production in spurs were in the range of 1.5–3.5 (Table II). This falloff cannot be due to HI–I_2 competition kinetics as described above. Equations 14 and 15 unambiguously predict constant rates of formation of I_2 and HI for the radiolysis with no additives, provided only that the yields of primary processes (A, B, C, and D) are constant. It is probable that HI and I_2 are actually formed at constant rates but react with olefins produced during extended periods of radiolysis.

Table II: Calculated $G(R\cdot)$, $G(I_2)$, and G(HI), and Rate Constant Ratios

(1) Cyclohexane vol. %	(2) G for thermal free-radical production[a]	(3) G for I_2 production in spurs[b]	(4) G for HI production in spurs[c]	(5) k_{HI}/k_{I_2}[d]
0	5.31	3.855	0.27	...
20	5.34	3.510	0.31	0.98
40	5.69	3.405	0.37	0.94
60	6.09	3.135	0.55	0.90
80	5.52	2.48	0.59	0.55
90	5.01	1.87	0.69	0.71
95	5.03	1.57	0.94[e]	0.71
99.9	6.07	0.41	0.81	0.71
100	6.04	...	...	0.71

[a] (Max rate − min rate). [b] (Max rate + min rate)/2. [c] Calculated from eq 28. [d] Values obtained by adjusting k_{HI}/k_{I_2} as a parameter for curve fitting. [e] This value is predicted by eq 28. As explained in the text, a slightly lower value gives the best fit of theoretical curves to experimental data, but the difference is within experimental error.

Although the falloff in normal rates was not considered decisive in interpreting the role of HI–I_2 competition kinetics in cyclohexane–methyl iodide solutions, it did pose problems in several respects. If the true initial values of the normal rates of iodine production are used in eq 14 and 15, then the equations will predict rates for solutions with added HI and I_2 which will approach these values at large doses. In the actual radiolyzed solutions, however, lower rates are found at large doses, as in the case of radiolysis with no additives. As a result, the predicted yields from the integrated equations would not match the experimental results. It was possible to avoid this difficulty by utilizing the large-dose values of the normal rates in the equations, rather than the initial values, when calculating the smooth curves in Figures 1–3.

Although use of the long-term normal rates permitted more satisfactory fitting of curves to experimental data, is is clear that the initial values are more significant in establishing true yields of primary processes. Accordingly, it was decided that the initial values of the rates should be used in preparing Tables II and III. It can easily be verified that the G values for the thermal free radical yields and for the yields of I_2 from spurs are not affected by this correction (see eq 20 and 22). However, the yields of HI from spurs as given in Tables II and III are increased by 0.1–0.25 molecule/100 ev for

Table III: Cyclohexane–Methyl Iodide Solutions: Comparison between Observed and Calculated Yields

(1) Cyclohexane vol. %	(2) $G(I\cdot)$ normal[a]	(3) HI reacting with free radicals[b]	(4) Net HI produced[c]	(5) Total scavenger equivalents[d]	(6) $G(R\cdot)$[e]	(7) G for excess scav equiv over $G(R\cdot)$[f]
0	2.82	0.21	0.06	8.25	5.31	2.94
20	2.46 (2.22)	0.27	0.04	7.64	5.34	2.30
40	2.20 (1.70)	0.29	0.08	7.55	5.69	1.86
60	1.58 (1.20)	0.51	0.04	7.37	6.09	1.28
80	0.90 (0.50)	0.53	0.06	6.14	5.52	0.62
90	0.36 (0.11)	0.69	0	5.12	5.01	0.11
95	0.10 (0.01)	0.94	0	4.78	5.03	(−0.25)
99.9	0			2.44	6.07	(−3.63)
100	0				6.04	

[a] For solutions with no I_2 or HI added prior to irradiation. [b] $G(I_2)$ for the radiolysis without additives minus $G(I_2)$ with added I_2. [c] (Column 4, Table II) − (column 3, Table III). [d] 2(column 3, Table II) + 2(column 4, Table II). [e] G for thermal free-radical production in spurs. [f] (Column 5 − column 6).

solutions with 20–90 vol. % cyclohexane, and the total yields of scavenger equivalents are increased about 0.2–0.5 molecule/100 ev, compared to the values which would be found if the large-dose value for $G(I_2$, no additives) was used.

Concentration Dependence of Primary Yields. For the entire range of solutions of cyclohexane–methyl iodide, the present calculations provided data for the yield of thermal alkyl radicals, I_2, and HI from spurs. These data are listed in Table II. As the cyclohexane concentration is increased, $G(I_2)$ decreases and $G(HI)$ increases fairly smoothly. However, $G(R\cdot)$ does not show a clear trend as a function of composition of the mixtures; it is approximately constant at 5.5 ± 0.5. The fluctuations which are observed are probably due to the fact that this is a composite quantity which includes the yields of both cyclohexyl and methyl radicals. The net yields of each of them and their sum are determined by numerous reactions, some competitive and others additive, resulting in an approximately constant combined yield.

Table III shows a number of additional derived yields for processes which affect net iodine production in the radiolysis of cyclohexane–methyl iodide solutions. It can be seen that the net, observed yield of iodine (column 2, Table III) is much less than that produced from spurs (column 3, Table II). The difference, of course, is due to reactions of cyclohexyl and methyl radicals with I_2. There is also a thermal process producing I_2, namely, the reaction of radicals with HI, but this is a relatively small effect. The same situation occurs in the radiolysis of pure alkyl iodides; it has been shown previously[2,10] that in such systems the observed I_2 yield is the sum of the excess of iodine production over alkyl radical production in spurs plus the contribution due to the reaction of thermal free radicals with HI.

A discussion of trends in primary yields in the radiolysis of cyclohexane–methyl iodide solutions was presented several years ago by Croft and Hanrahan.[1] Their remarks were of necessity hypothetical, since detailed yield data were not available at that time. They investigated the postulate that the various intermediates, reacting in a simple free-radical scheme similar to that used here, might be formed in yields determined directly by the electron per cent of the parent compound in the mixture. A graph was presented showing the concentration dependence of total radical yields and total iodine yields predicted by such a model. The graph predicts that net iodine production should fall to zero for solutions richer in cyclohexane than about 30 electron %. Since their experimental results showed that net iodine production persists until methyl iodide is diluted with about 93 electron % cyclohexane, they concluded that there was evidence of substantial sensitized decomposition of the methyl iodide. This conclusion has been confirmed during the course of the present work. Taking into account the role of HI, G values for total scavenger equivalents for the entire range of solutions have been calculated and are plotted as a function of electron % cyclohexane; see Figure 11. It will be noted that the yields of HI and I_2 from methyl iodide in the mixture and markedly greater than would be predicted by an "ideal solution" law. There is only a small gradual diminution in the total scavenger yields up to about 80 electron % solutions; the yields fall sharply in solutions richer in cyclohexane than 80 electron %. Although the figure indicates that there should be no net iodine production for solutions with

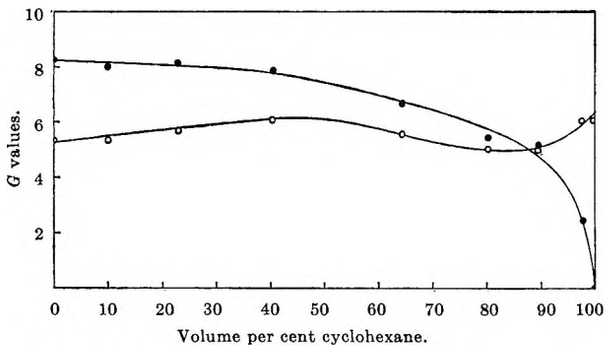

Figure 11. G values as a function of composition for cyclohexane–methyl iodide solutions: ●, total scavenger yield in equivalents; ○, thermal free-radical production.

more than 85 electron % cyclohexane, difference between this value and the experimentally observed value is probably due to small errors in determining the various parameters.

In considering the relationship of the various HI rates given in Tables II and III, it should be recalled that the HI which is produced from spurs has two possible fates. Most of it reacts with alkyl radicals giving a complementary yield of iodine atoms. Therefore, the rate at which HI plays the role of a scavenger for R· is given by (norm rate − min rate), where norm and min rates are the rates of iodine production without additives and with I_2 added, respectively. These values are listed in column 3, Table III. The remaining HI appears as net HI accumulating in the solutions; see column 4, Table III. The sum of these figures is the total rate of HI production, given in column 4, Table II.

Since, on reaction with alkyl radicals, HI furnishes a hydrogen atom to the radical and releases an iodine atom, the reaction capacity of HI is equal to two scavenger equivalents. Hence, the total scavenger capacity in equivalents is the yield of iodine atoms produced from spurs plus twice the yield of HI from spurs. Column 5, Table III, shows the total scavenger activity in equivalents. Column 7 shows the scavenger equivalents which are in excess of the free radicals produced and is obtained by subtracting column 6 from column 5. The figures given are just the sum of the I_2 yield, which is measurable, and the HI yield, which is inferred. The negative values for total scavenger yields for 95 and 99.9 vol. % cyclohexane solutions simply indicate that there is no net HI or I_2 present in the irradiated solutions over this concentration range.

It has been proposed by Gillis, Williams, and Hamill[10] that the production of iodine in the radiolysis of pure CH_3I is due to the ion–molecule mechanism

$$CH_3I^+ + CH_3I \longrightarrow (CH_3)_2I^+ + I\cdot \qquad (29)$$

The product ion, upon neutralization, gives a net yield of C_2H_6 and I_2. Croft and Hanrahan suggested that the efficient production of iodine in dilute solutions in cyclohexane is due to the same mechanism and that it is able to occur with considerable efficiency because of charge transfer from cyclohexane

$$C_6H_{12}^+ + CH_3I \longrightarrow C_6H_{12} + CH_3I^+ \qquad (30)$$

The present results are compatible with these suggestions. The postulate that charge-exchange process 30 occurs appears necessary to account for net iodine production in solutions in which methyl iodide is the minor constituent. However, the possibility that electron capture also occurs, as suggested by Forrestal and Hamill,[7] cannot be excluded.[14] It is likely that electron capture and charge exchange both occur efficiently in solutions with several per cent or more of methyl iodide.

Acknowledgment. This work was supported by the University of Florida Nuclear Science Program and by Atomic Energy Commission Contract AT-(40-1)-3106. Services of the IBM 709 computer were provided by the University of Florida Computing Center. This is Document No. ORO-3106-22.

(14) The suggestion that electron capture is important in related studies of the radiolysis of alkyl iodide–*n*-pentane solutions has been made by P. R. Geissler and J. E. Willard, *J. Am. Chem. Soc.*, 84, 4627 (1962).

A Pulse-Radiolysis Study of the Dependence of the Reaction of Atomic Oxygen with Oxygen on the Nature of the Third Body[1]

by Myran C. Sauer, Jr.

Chemistry Division, Argonne National Laboratory, Argonne, Illinois 60439 *(Received April 10, 1967)*

The rate constant of the third-body (Ar)-controlled reaction of oxygen atoms with molecular oxygen is found to be independent of whether the oxygen atom originates from O_2, CO_2, or N_2O. The third-body efficiencies of He, CO_2, and N_2O relative to an Ar efficiency of 1.0 have been determined as 0.8, 5, and 5, respectively.

Introduction

Measurement of the formation rate of ozone and the rate constant for the reaction

$$O + O_2 + Ar \longrightarrow O_3 + Ar \qquad (1)$$

by the pulse radiolysis of gaseous mixtures of argon and oxygen has been previously described.[2] The present paper describes similar experiments in which different molecules were used as sources of oxygen atoms and in which the effect of different third bodies was determined.

Experimental Section

General Information. The experimental techniques of preparing and irradiating the high-pressure gas samples were similar to those used previously.[2] The spectrophotometric method of obtaining the ozone formation curves after the electron pulse was the same as has been previously described.[2] Analysis of the Polaroid photographs of the oscilloscope traces was carried out essentially as has been described,[2] but some of the later photographs were analyzed by an automatic, computerized method.[3]

Materials. The Ar and O_2 have been previously described.[2] The CO_2 was Airco, the listed maximum impurities being 10 ppm of O_2, 50 ppm of CO, 50 ppm of N_2, and 10 ppm of H_2. The results did not depend upon whether the CO_2 was used directly from the tank or first subjected to several cycles of freezing and pumping. The He was Grade A from U. S. Bureau of Mines, the listed impurities being less than 50 ppm total, of which less than 1 ppm was O_2. The N_2O was Matheson, 98% minimum purity. Mass spectral analysis showed less than 200 ppm of O_2. In experiments where N_2O was not the main gas, it was purified by several cycles of freezing and pumping. Where N_2O was the main gas, it was purified by passing it through a 6 in. long column of Ascarite, followed by several cycles of freezing and pumping. (Ozone formation curves could not be obtained when the N_2O was used without the Ascarite treatment.)

Samples. The ranges of concentration over which the components in the various systems studied were varied are given as follows in parentheses: I: Ar (0.5–4.3 M), CO_2 (0.015–0.06 M), O_2 (7×10^{-4}–28×10^{-4} M); II: Ar (1.1–2.5 M), N_2O (0.01–0.034 M), O_2 (7×10^{-4}–28×10^{-4} M); III: He (1.1–3.1 M), O_2 (8×10^{-4}–26×10^{-4} M); IV: CO_2 (0.5–2.7 M), O_2 (3×10^{-4}–16×10^{-4} M); V: N_2O (1.5 M), O_2 (5×10^{-4} M).

The spectrum of the absorbing species formed was checked for all of these systems and found to correspond to the spectrum of ozone. Samples similar to those listed above, but *without* O_2, were pulse irradiated, and the results showed that there was no significant amount of oxygen impurity in the gases used and that negligible amounts of species absorbing in the region around 260 mμ were produced.

Results and Discussion

The production of oxygen atoms in irradiated systems where CO_2 or N_2O is present at concentrations

(1) Based on work performed under the auspices of the U. S. Atomic Energy Commission.

(2) M. C. Sauer, Jr., and L. M. Dorfman, *J. Am. Chem. Soc.*, 87, 3801 (1965).

(3) M. C. Sauer, Jr., Argonne National Laboratory Report, ANL-7113, Oct 1965.

small compared with the Ar but about 20 times greater than the O_2 concentration is likely to result mainly from interactions between excited or ionized argon and the CO_2 or N_2O, followed by subsequent decomposition of the excited or ionized CO_2 or N_2O, either directly or in neutralization processes. However, the O_2 may contribute more to oxygen atom formation than one would predict on the basis of its ratio to CO_2 or N_2O. In the case of CO_2, electrons with energy below 4.6 ev will not undergo dissociative attachment[4] with CO_2 but will attach[5] to the O_2. The O_2^- could then yield oxygen atoms upon neutralization. In the case of N_2O, the situation is less favorable for production of O_2^-, since electrons of energy above 0.5 ev undergo dissociative attachment[4] with the N_2O.

The sequence of reactions producing oxygen atoms is completed[2] in a time period comparable in length to the 1-μsec electron pulse. This allows us conveniently to study reactions of the oxygen atoms which have half-times of *ca.* 5 μsec or greater. The gas concentrations were such that the half-times for the ozone formation reaction were in the range of 10 μsec. The ozone formation curves yielded good linear plots when first-order-formation test plots were made in the manner previously described.[2] For a given set of O_2 and M concentrations, the rate constant, k_1, of the over-all reaction was calculated from the slope of the first-order-formation test plot by

$$k_1 = (-\text{slope})/[O_2][M] \qquad \text{(I)}$$

The results are given in Table I, and are expressed in terms of the reaction scheme

$$O + O_2 \underset{k_{2r}}{\overset{k_2}{\rightleftharpoons}} O_3^* \qquad (2)$$

$$O_3^* + M \xrightarrow{k_3} O_3 + M \qquad (3)$$

which describes, in detail, the course of reaction 1. As has been shown,[2] k_1 is given by

$$k_1 = \frac{k_2 k_3}{k_{2r} + k_3[M]} \qquad \text{(II)}$$

Therefore, the experimental values of k_1, determined from (I), were plotted as $1/k_1$ *vs.* [M], and the values of k_2k_3/k_{2r} and k_2 were determined from the intercept and slope, respectively. Because of the fact that the value of $1/k_1$ did not change much over the pressure range examined, the slope was not obtained with sufficient accuracy for some of the systems examined, and the values of k_2 are therefore not listed in Table I. However, the intercept was more accurately known because of the low value of the slope.

Table I: Summary of Results

Sample compn			
Main gas	Other gases	$10^{-8}k_2k_3/k_{2r}$, M^{-2} sec^{-1}	$10^{-8}k_2$, M^{-1} sec^{-1}
Ar[a]	O_2	0.83 ± 0.08	7 ± 5
Ar[b]	CO_2, O_2[c]	1.0 ± 0.2	5 ± 2
Ar	N_2O, O_2[c]	0.8 ± 0.2	...
CO_2	O_2	4.2 ± 0.5	11 ± 3
N_2O[d]	O_2	3.5 ± 0.7	...
He	O_2	0.7 ± 0.1	...

[a] Reference 2. [b] The error limit on k_2k_3/k_{2r} determined from these experiments is to a large extent due to an unexplained difference in results between two sets of irradiation vessels. The same phenomenon was not apparent in experiments on the other systems where the same two sets of vessels were used. [c] The concentration of CO_2 or N_2O was typically a few per cent of the concentration of Ar; in calculating the values of k_1, the CO_2 and N_2O were taken to have five times the third-body efficiency of Ar. [d] This value is the result of the only sample (out of three), using purified N_2O, from which usable curves were obtained. The difficulties may be due to impurities, and the result should be considered with some caution.

The values of k_2k_3/k_{2r} for M $\equiv$ Ar given for the first three systems listed in Table I are in fair agreement, although slightly lower, with values of k_1 determined (for M $\equiv$ Ar) by other workers. A discussion of previous determinations of k_1 in relation to the result for high-pressure Ar–O_2 systems has already been given.[2] The values of k_2 are in reasonable agreement with a mass spectrometric study[6] of the rate of the reaction $O^{18} + O^{16}O^{16} \rightarrow O^{16} + O^{18}O^{16}$.

The relative efficiencies of the various third bodies used can be obtained directly from the ratios of the appropriate values of k_2k_3/k_{2r} in Table I. Helium is apparently only slightly less efficient than Ar, and CO_2 and N_2O are about five times more efficient than Ar.

The data of Table I are of interest with respect to the question of what electronic state the oxygen atom is in during reaction 2. Looking at the first three systems listed, we see that the value of k_2k_3/k_{2r} is independent (within a 20% range) of whether the source of oxygen atoms is O_2, CO_2, or N_2O (Ar is the third body in all three cases). This favors the argument that reaction 2 proceeds mainly *via* ground-state (^3P) oxygen atoms in all three systems and that initially excited oxygen atoms are predominantly deactivated to the ground state before taking part in the ozone formation reaction. (The problems involved in ascertaining the electronic

(4) D. Rapp and D. D. Briglia, *J. Chem. Phys.*, **43**, 1480 (1965).

(5) E. W. McDaniel, "Collision Phenomena in Ionized Gases," John Wiley and Sons, Inc., New York, N. Y., 1964, p 404.

(6) J. T. Herron and F. S. Klein, *J. Chem. Phys.*, **40**, 2731 (1964).

state of the oxygen atoms produced by pulse radiolysis of Ar–O_2 systems have been discussed.[2]) However, an alternative explanation is that the rate constant (k_1) for excited oxygen atoms is not much different from that for ground-state atoms. This explanation is not supported by a recent estimate[7] of the value of k_2k_3/k_{2r} for ^1D oxygen atoms of $0.72 \times 10^8\ M^{-2}\ sec^{-1}$, where O_2 is the third body, because, if the third-body efficiency of Ar is only 0.6 that of O_2 as it is for the reaction of $O(^3P)$,[8] then k_2k_3/k_{2r} for $O(^1D)$ is about $0.43 \times 10^8\ M^{-2}\ sec^{-1}$, where Ar is the third body. Of course, if the proportion of excited oxygen atoms is minor, their effect would not be noticed.[2]

In the systems containing N_2O, reaction of excited oxygen atoms with N_2O to form $N_2 + O_2$ is estimated to occur quite rapidly,[9] and therefore all excited oxygen atoms should be removed before the ozone formation occurs. The reaction $O(^1D) + CO_2 \rightarrow CO + O_2$ is not important,[10] and $O(^1D)$ is probably deactivated to $O(^3P)$ in the presence of CO_2, as will be discussed. The reactions of $O(^3P)$ with N_2O[11] and CO_2 are very slow and will not interfere at all with the ozone formation reaction. If such reactions did occur, the ozone production would be reduced markedly, and the ozone formation rate constant would be markedly increased when higher pressures of N_2O or CO_2 were used; this effect was not observed.

Incidentally, the possibility of NO being produced from the N_2O and influencing the ozone formation curves by reacting with oxygen atoms or with the ozone was ruled out experimentally by noting the lack of effect of pulse intensity ($O + NO$ and $O + O_3$ would be more important relative to $O + O_2$, the higher the pulse intensity, since the former are second order while the latter is pseudo first order) and the lack of a change with repeated pulsing (such a change might be expected if ozone were reacting with a species produced by the pulse, since ozone concentration builds up in the irradiation vessel). The same conclusions were reached in the case of CO_2-containing samples.

Concerning the effect of CO_2 on atomic oxygen, there is no evidence that $O(^3P)$ reacts with CO_2 to form a CO_3 complex, and the experimental data presented here argue strongly against such a complex being important in the ozone formation reaction sequence. However, the formation of CO_3 from the reaction of $O(^1D)$ with CO_2 has been postulated in several studies,[10,12-19] although there is disagreement as to the lifetime of the complex and also as to whether the $O(^1D)$ is deactivated to $O(^3P)$ when and if the complex dissociates. The infrared absorption spectrum of CO_3 in a matrix of solid CO_2 has been thoroughly studied, but an absorption spectrum in the visible and ultraviolet regions was too weak to be determined.[19] A recent work[18] gives experimental evidence that the gas-phase reaction of $O(^1D)$ with CO_2 to form CO_3 has a rate constant greater than $6 \times 10^8\ M^{-1}\ sec^{-1}$ and is at least five times as fast as the deactivation to $O(^3P)$. The rate constant for deactivation predicted from the preceding is in the same range as that arrived at on the basis of the estimate[7] of $9 \times 10^5\ M^{-1}\ sec^{-1}$ for deactivation of $O(^1D)$ by He and the finding that CO_2 is 50 times as efficient.[16] Therefore, even if we neglect the CO_3 formation, all $O(^1D)$ would be deactivated in about 1 μsec at the lowest CO_2 concentration used in the present work. Concerning $O(^1S)$, the statement has been made[18] that $O(^1S)$ is strongly quenched by CO_2. This seems to be contrary to the hypothesis that $O(^1S)$ causes a chain-exchange reaction[14] in the radiolysis of CO_2.

The experimental results presented here on the systems containing CO_2 show no evidence that CO_3 is important in the formation of ozone. Variations of the concentrations of the components of the systems can all be explained on the basis of reactions 2 and 3, and no mechanism involving CO_3 can be devised which fits the experimental observations. The most plausible explanation of these results is that excited oxygen atoms either are rapidly deactivated to $O(^3P)$ or react with CO_2 to form CO_3, which would be required to have no effect on the ozone formation reaction, the ozone being formed entirely from the reaction of $O(^3P)$ with O_2.[20]

(7) J. O. Sullivan and P. Warneck, *J. Chem. Phys.*, **46**, 953 (1967).

(8) See discussion of this in ref 2.

(9) A reaction efficiency approaching collisional frequency is implied by H. Yamazaki and R. J. Cvetanovic, *J. Chem. Phys.*, **39**, 1902 (1963). Even if the rate constant were as low as $10^8\ M^{-1}\ sec^{-1}$, the excited oxygen atoms would be consumed in about 1 μsec, and there would be no effect on the ozone formation curves.

(10) D. Katakis and H. Taube, *ibid.*, **36**, 416 (1962).

(11) F. Kaufman, *Progr. Reaction Kinetics*, **1**, 1 (1961).

(12) R. J. Cvetanovic, *J. Chem. Phys.*, **43**, 1850 (1965).

(13) P. Warneck, *ibid.*, **43**, 1849 (1965); see also references listed in this paper.

(14) M. Anbar and P. Perlstein, *Trans. Faraday Soc.*, **62**, 1803 (1966).

(15) D. L. Baulch and W. H. Breckenridge, *ibid.*, **62**, 2768 (1966).

(16) K. F. Preston and R. J. Cvetanovic, *J. Chem. Phys.*, **45**, 2888 (1966).

(17) T. G. Slanger, *ibid.*, **45**, 4127 (1966).

(18) R. A. Young and A. Y. M. Ung, *ibid.*, **44**, 3038 (1966).

(19) N. G. Noll, D. R. Clutter, and W. E. Thompson, *ibid.*, **45**, 4469 (1966).

(20) NOTE ADDED IN PROOF. The third-body efficiencies reported here are in agreement (±20%) with those recently reported by F. Kaufman and J. R. Kelso, *ibid.*, **46**, 4541 (1967).

The Kinetics of the Hydrogenation of Benzene over Supported Cobalt

by William F. Taylor[1] and H. Kenneth Staffin

Stevens Institute of Technology, Hoboken, New Jersey *(Received May 15, 1967)*

A detailed study of the kinetics of the hydrogenation of benzene to cyclohexane over supported cobalt has been made. The specific activity, *i.e.*, the reaction rate per unit area of cobalt, apparent activation energy, and reaction orders were measured at 65–205° in a differential flow reactor. Three typical oxides, *i.e.*, silica, alumina, and silica–alumina, and a nonoxide, *i.e.*, carbon, were used as substrates for the cobalt. At low temperatures the rate of benzene hydrogenation exhibited a near-zero-order dependence on benzene partial pressure and an approximate first-order dependence on hydrogen partial pressure. At higher temperatures the order in hydrogen rose to approximately 2, and the order in benzene increased to low positive values. Cyclohexene was not detected in the effluent gases. The results are consistent with a mechanism in which a strongly bound benzene molecule is hydrogenated in a kinetically slow step to cyclohexene, followed by a rapid hydrogenation to cyclohexane. The specific activity, apparent activation energy, and preexponential factor for cobalt supported on the various oxide substrates were essentially the same. However, cobalt supported on carbon exhibited a different apparent activation energy and preexponential factor.

I. Introduction

As pointed out previously,[2] studies of catalysis over cobalt surfaces have received less attention than corresponding studies over metals such as nickel or platinum. This is probably the case because cobalt is less extensively used as a catalyst. However, to elucidate the factors involved in catalysis by metals, knowledge of the catalytic properties of metals other than those most commonly used as catalysts is of interest.

Although benzene has been hydrogenated over cobalt by a number of investigators,[3,4] no detailed kinetics were obtained. Recently a number of authors[5–7] have postulated that the hydrogenation of benzene over transition metals involves the formation of π-bonded intermediates. Thus, as part of an extended study of catalysis over supported metals, it was decided to investigate the kinetics of the hydrogenation of benzene over supported cobalt. The cobalt catalysts used were the identical catalysts employed in previous work[2] involving ethane hydrogenolysis kinetics and hydrogen chemisorption studies which established the degree of dispersion of the cobalt on the various supports. Thus, the specific catalytic activity, *i.e.*, the activity per unit surface area of cobalt, could be calculated for the hydrogenation of benzene, which is essential for any fundamental comparison of the activity of cobalt for benzene hydrogenation over a series of catalysts supported on differing substrates. In the past the role of the support has often been ignored, but a number of recent studies[8,9] have shown that marked effects can exist. In the present study, three different oxide supports, *i.e.*, silica, alumina, and silica–alumina, and a nonoxide support, *i.e.*, carbon, were employed.

II. Experimental Section

A. Apparatus and Procedure. The benzene hy-

(1) Government Research Laboratory, Esso Research and Engineering Co., Linden, N. J.

(2) D. J. C. Yates, J. H. Sinfelt, and W. F. Taylor, *Trans. Faraday Soc.*, **61**, 2044 (1965).

(3) (a) P. H. Emmett and N. Skau, *J. Am. Chem. Soc.*, **65**, 1029 (1943); (b) G. C. A. Schuit and L. L. VanReijen, *Advan. Catalysis*, **10**, 242 (1958).

(4) A. Juliard and C. Herbo, *Bull. Soc. Chim. Belges*, **47**, 718 (1938).

(5) J. J. Rooney, *J. Catalysis*, **2**, 53 (1963).

(6) V. Völter, *ibid.*, **3**, 297 (1964).

(7) D. Shopov and A. Andreev, *ibid.*, **6**, 316 (1966).

(8) W. F. Taylor, D. J. C. Yates, and J. H. Sinfelt, *J. Phys. Chem.*, **68**, 2962 (1964).

(9) W. F. Taylor, J. H. Sinfelt, and D. J. C. Yates, *ibid.*, **69**, 3857 (1965).

drogenation data were obtained in a flow reactor system at atmospheric pressure using a vertically mounted stainless steel reactor tube 1.0 cm in diameter and 8.0 cm in length. The general features of this type of unit have been described previously.[10] The benzene was metered to the unit by means of a calibrated constant-rate syringe drive pump obtained from the Ace Scientific Co., Linden, N. J. The benzene was vaporized in a preheater tube and then mixed with the helium and hydrogen and passed downflow through the catalyst bed. The helium and hydrogen flow rates were measured in a monometer system using dibutyl phthalate as the monometer fluid, which was chosen because of its low vapor pressure.[11] The temperature of the catalyst bed was measured by an iron–constantan thermocouple. The thermocouples were individually calibrated by their manufacturer, the Thermo-Electric Co., Saddle Brook, N. J. The products from the reactor were analyzed by a gas chromatographic unit coupled directly to the outlet of the reactor. The column used was 10 ft long and contained 7,8-benzoquinoline (20% on 45–60 mesh firebrick).

The reactants, benzene and hydrogen, were passed over the catalyst in the presence of helium diluent. A total gas flow rate of 1 l./min was used throughout. The run procedure consisted of passing the reactants over the catalyst for a period of 5 min, at which time a sample of the product was taken for chromatographic analysis. The benzene flow was then shut off and the hydrogen and helium flow continued for a period of 15 min at the reaction temperature prior to another run. In this way, it was possible to minimize variation in catalyst activity from period to period. In each run the catalyst was diluted with 0.5 g of ground Vycor beads of the same particle size as the catalyst. The catalyst charge varied from 95 to 110 mg, and quartz wool was packed on top of the catalyst to hold it in place. A preliminary experiment indicated that the ground Vycor and quartz wool was inactive for benzene hydrogenation over the range of conditions encountered in this work. The catalyst was reduced overnight at 370° with flowing H_2 using a procedure previously described.[2]

B. Materials. The gases employed in this work were ultrahigh-purity helium (ionization grade) and ultrahigh-purity hydrogen obtained from the Matheson Co., East Rutherford, N. J. The hydrogen was further purified by passing it through a Deoxo unit containing a palladium catalyst to remove traces of oxygen as water prior to passage through a molecular sieve drier. The benzene employed was high-purity chromatoquality benzene obtained from Matheson Coleman and Bell, East Rutherford, N. J. Chromatographic analyses indicated it to be 99.9% benzene. An analysis for sulfur indicated it to contain 1.2 ppm. The benzene was dried before use with 13X molecular sieve.

The cobalt catalysts contained 10 wt % cobalt and were prepared by impregnating the supports with a solution of $Co(NO_3)_2 \cdot 6H_2O$ dissolved in deionized water. The material was dried at 105°, after which it was pressed into wafers which were subsequently crushed and screened to between 45 and 60 mesh. The Co on Al_2O_3 and Co on carbon catalysts were screened directly after drying. The silica used was Cabosil HS5 (340 m^2/g surface area), obtained from the Cabot Corp., Boston, Mass. The alumina was prepared by heating β-alumina trihydrate, obtained from Davison Chemical Co., for 4 hr at 600°, and had a surface area of 295 m^2/g. The silica–alumina was DA-1 cracking catalyst (nominally 13% Al_2O_3–87% SiO_2) with a surface area of 450 m^2/g, also obtained from Davison Chemical Co. The carbon was Darco G-60 activated charcoal (410 m^2/g surface area), obtained from Ace Scientific Co., Linden, N. J.

III. Results

The reaction of benzene with hydrogen to form cyclohexane was studied over the various catalysts at temperatures from 65 to 205° at low conversion levels. The degree of conversion ranged from about 0.3 to 1.1%, most of the data having been obtained at conversion levels below 1%. Consequently, the partial pressures of the reactants (benzene and hydrogen) do not vary much through the reaction zone, and the system approaches that of a differential reactor. The reaction rates per gram of catalyst were determined from the relation

$$r = \frac{F}{W}X \qquad (1)$$

where F represents the feed rate of benzene to the reactor in moles per hour, W represents the weight in grams of the catalyst charged to the reactor, and X represents the fraction of benzene converted to cyclohexane. The operating parameters of the gas chromatograph used for the analyses were adjusted so that benzene, cyclohexane, and cyclohexene could be determined with ease. No cyclohexene was detected in the effluent gas stream.

In an actual run to determine reaction rates, the catalyst was first prereduced with flowing hydrogen,

(10) D. J. C. Yates, W. F. Taylor, and J. H. Sinfelt, *J. Am. Chem. Soc.*, 86, 2996 (1964).

(11) S. Dushman and J. M. Lafferty, "Scientific Foundations of Vacuum Technique," 2nd ed, John Wiley and Sons, Inc., New York, N. Y., 1962, p 214.

after which the reactor was cooled in flowing hydrogen to a convenient reaction temperature. At a standard set of conditions of hydrogen and benzene partial pressures, P_H and P_B, respectively, the activity of the freshly reduced catalyst was determined. Following this, reaction rates were measured at a series of temperatures in a rising-temperature sequence. The data are shown in the Arrhenius plots in Figures 1 and 2.

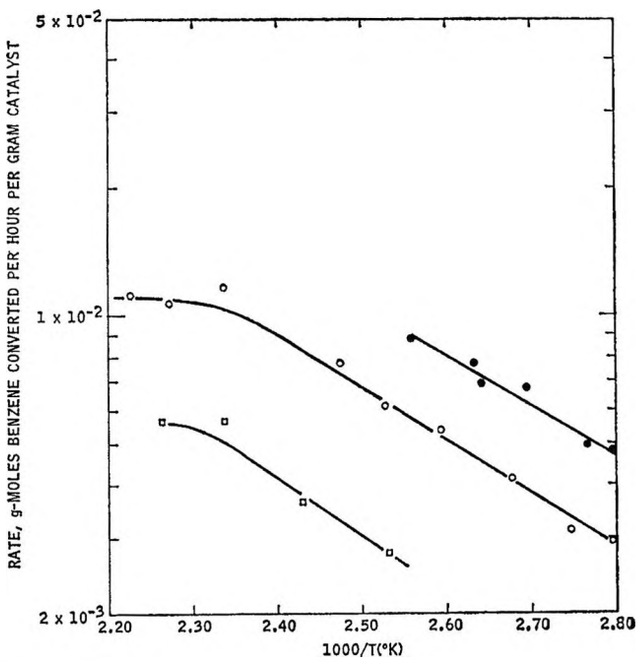

Figure 1. Effect of temperature on the rate of benzene hydrogenation over supported cobalt catalysts at P_B = 0.040 atm and P_H = 0.500 atm: ●, Co on Al_2O_3; ○, Co on SiO_2; □, Co on SiO_2–Al_2O_3.

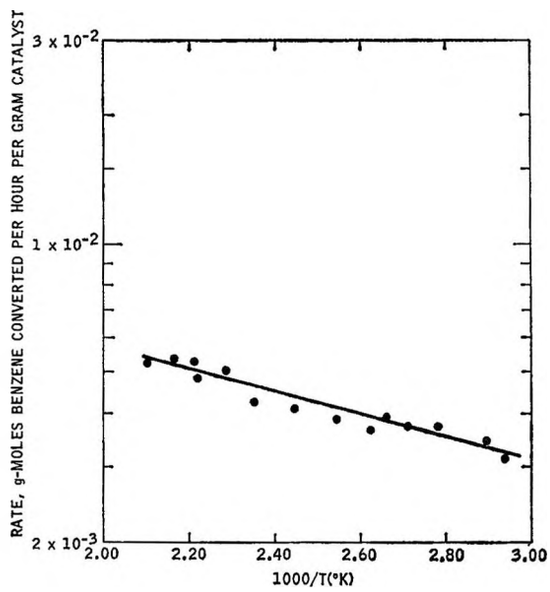

Figure 2. Effect of temperature on the rate of benzene hydrogenation over cobalt supported on carbon at P_B = 0.040 atm and P_H = 0.500 atm.

Table I: Relative Rates of Benzene Hydrogenation as a Function of Benzene and Hydrogen Partial Pressures

Catalyst	Temp, °C	P_B, atm	P_H, atm	r/r_0[a]
10% Co–SiO_2	123	0.040	0.300	0.74
		0.040	0.500	1.00
		0.040	0.600	1.36
		0.013	0.500	0.82
		0.040	0.500	1.00
		0.080	0.500	1.25
	179	0.040	0.300	0.50
		0.040	0.500	1.00
		0.040	0.600	1.57
		0.013	0.500	0.55
		0.040	0.500	1.00
		0.080	0.500	1.48
	127	0.013	0.500	0.86
		0.040	0.500	1.00
		0.080	0.500	1.26
10% Co–Al_2O_3	118	0.040	0.300	0.67
		0.040	0.500	1.00
		0.040	0.600	1.12
		0.040	0.500	1.00
		0.080	0.500	1.20
10% Co–SiO_2–Al_2O_3	178	0.040	0.300	0.32
		0.040	0.500	1.00
		0.040	0.600	1.53
		0.013	0.500	0.68
		0.040	0.500	1.00
		0.080	0.500	1.30
10% Co–C	95	0.040	0.300	0.53
		0.040	0.500	1.00
		0.040	0.600	1.31
		0.013	0.500	0.98
		0.040	0.500	1.00
		0.080	0.500	1.11
	179	0.040	0.300	0.35
		0.040	0.500	1.00
		0.040	0.600	1.51
		0.013	0.500	0.76
		0.040	0.500	1.00
		0.080	0.500	1.30

[a] Rate relative to the rate at the given standard conditions of P_B and P_H for the particular catalyst and temperature in question; the r/r_0 values cannot be used by themselves to compare the activities of the catalysts.

Table II: Summary of Reaction Orders[a]

Catalyst	P_B, atm	P_H, atm	Temp, °C	Order in benzene, n	Order in hydrogen, m
10% Co–SiO_2	0.0130–0.080	0.500	123	0.2	...
	0.040	0.300–0.600	123	...	1.0
	0.013–0.080	0.500	179	0.5	...
	0.040	0.300–0.600	179	...	1.7
10% Co–Al_2O_3	0.040–0.080	0.500	118	0.3	...
	0.040	0.300–0.600	118	...	1.0
10% Co–SiO_2–Al_2O_3	0.0130–0.080	0.500	178	0.4	...
	0.040	0.300–0.600	178	...	2.0
10% Co–C	0.0130–0.080	0.500	95	0.1	...
	0.040	0.300–0.500	95	...	1.2
	0.0130–0.080	0.500	179	0.3	...
	0.040	0.300–0.500	179	...	2.1

[a] Orders with respect to benzene and hydrogen in the power rate law $r = kP_B^nP_H^m$.

After determining the effect of temperature on rates over the freshly reduced catalyst, the temperature was lowered to an intermediate value in the range studied, and a series of measurements was made to determine the effects of the partial pressures of hydrogen and benzene on the rates. Since it had been observed from preliminary experiments that a series of such measurements over an extended period of time resulted in some loss of activity, it was decided to bracket all of the rate measurements with measurements at a standard set of conditions. In this way it was possible to detect variations in catalyst activity during the series of measurements. This procedure has been discussed in detail elsewhere.[10] The effect of a kinetic variable such as hydrogen or benzene partial pressure was then determined by comparing the rate at a given set of conditions with the average of the rates at the standard conditions immediately before and after the period in question. For each set of conditions the rate r relative to the rate r_0 at the standard conditions can be expressed by the ratio r/r_0, which should be reasonably independent of moderate variations in catalyst activity. The value for r/r_0 is unity by definition at the standard conditions chosen. Values of the relative rates r/r_0 as a function of benzene and hydrogen pressures and the standard conditions chosen for each catalyst are given in Table I.

The data show that the rate of benzene hydrogenation increases with increasing hydrogen partial pressure, but is relatively less dependent on benzene partial pressure. The dependence of the rate on the partial pressures of benzene and hydrogen can be expressed in the form of a simple power law, $r = kP_B^nP_H^m$. Approximate values of the exponents n and m as derived from the experimental data are summarized in Table II. It can be seen that the effect of benzene and hydrogen pressure is directionally the same for all of the catalysts. For those catalysts whose reaction orders were measured at two different temperature levels, it can be seen that both the order in benzene, n, and the order in hydrogen m, increased with increasing temperature. Apparent activation energies, derived from the slopes of the linear, low-temperature portion of the Arrhenius plots in Figures 1 and 2 are shown in Table III. A comparison of the activity per gram of catalyst of the various cobalt catalysts at a given set of conditions is shown in Table IV. The conditions arbitrarily chosen for this comparison were 105°, P_B = 0.040 atm, and P_H = 0.500 atm. The specific activities of the various cobalt catalysts were compared by dividing the reaction rate per gram of catalyst, shown in Table IV, by the known corresponding cobalt surface area per gram of catalyst.

Table III: Summary of Apparent Activation Energies

Catalyst	Temp, range, °C[a]	Apparent activation energy, kcal/mole
10% Co–Al_2O_3	83–116	5.4
10% Co–SiO_2	83–133	5.8
10% Co–SiO_2–Al_2O_3	105–133	6.1
10% Co–C	65–205	1.2

[a] Other conditions: P_B = 0.040 atm and P_H = 0.500 atm.

Table IV: Comparison of the Activities and Specific Activities of the Catalysts

Catalyst	Rate at 105°, mole converted/hr g[a]	Cobalt surface area,[b] m²/g	Specific rate, r, at 105°, mole converted/hr m² of cobalt[a]	Preexponential factor, r',[d] moles converted/hr m² of cobalt[a]
10% Co-Al_2O_3	7.00×10^{-3}	7.8	0.90×10^{-3}	1.19
10% Co-SiO_2	4.40×10^{-3}	5.6	0.79×10^{-3}	1.73
10% Co-SiO_2-Al_2O_3[c]	1.75×10^{-3}	1.7	1.03×10^{-3}	3.49
10% Co-C	3.90×10^{-3}	3.9	1.00×10^{-3}	4.92×10^{-3}

[a] Other conditions: $P_B = 0.040$ atm and $P_H = 0.500$ atm. [b] From ref 2. [c] Extrapolated. [d] Determined from the relationship $r = r' \exp(-E/RT)$, where r is the specific rate shown above and E is the apparent activation energy measured at the conditions shown in Table III.

IV. Discussion

Although benzene has been catalytically hydrogenated over cobalt by a number of investigators,[3,4] no detailed kinetics were reported. As pointed out by Bond[12] there is no unanimous agreement on a mechanism for the catalytic hydrogenation of benzene, even for extensively studied catalysts such as nickel and platinum. Recently, however, a number of investigations have been reported which shed considerable light on the mechanism of aromatic ring hydrogenation over transition metals. Hartog and Zwietering[13] confirmed the presence of cyclohexene derivatives as an intermediate in the low-temperature (25–60°), liquid-phase hydrogenation of alkyl aromatics over nickel, ruthenium, and rhodium. The highest levels of cyclohexene derivatives were observed with ruthenium and rhodium, much lower levels were observed with nickel, and no cyclohexene derivatives were observed with platinum and palladium. However, Haensel[14] observed cyclohexene as a reaction intermediate when dehydrogenating cyclohexane to benzene over a supported platinum catalyst at 520° in a vapor-phase flow system at extremely high space velocities. These results suggest that cyclohexene is an intermediate in the conversion of benzene to cyclohexane, and its concentration away from the surface of the catalyst depends greatly on how fast it is converted to benzene. No cyclohexane was observed in the vapor phase in the present work with supported cobalt. This suggests that, over cobalt, cyclohexene is rapidly coverted to benzene. In this respect, Madden and Kemball[15] have demonstrated that cyclohexene is hydrogenated much more rapidly than benzene over nickel films.

The rate of benzene hydrogenation over supported cobalt exhibited a near-zero-order dependence on benzene partial pressure and a first-order dependence on hydrogen partial pressure at low temperatures. At higher temperatures, the order in hydrogen rose to an approximate value of 2, the order in benzene increasing to low positive values. A number of authors[5–7] have proposed that the hydrogenation of benzene over transition metals involves the formation of π-bonded intermediates, suggesting that benzene is strongly bound to the metal surface. This agrees well with the observed low reaction order in benzene. The observed limiting order in hydrogen of approximately 2, considered in light of the evidence in the literature, suggests that a strongly bound benzene molecule is hydrogenated in a kinetically slow step to cyclohexene, followed by a rapid hydrogenation to cyclohexane

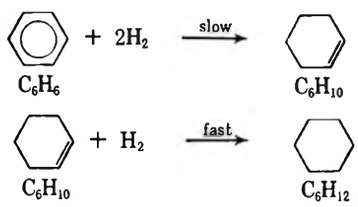

The specific activity, *i.e.*, activity per unit area of cobalt, apparent activation energy, and preexponential factors for cobalt supported on three different oxide substrates were the same. Boudart[16] has pointed out the importance of distinguishing between "facile" and "demanding" reactions and reaction conditions when probing the effect of the support on the specific activity of a metal, with a "facile" reaction and reaction conditions being defined as those for which the specific activity of the metal catalyst is independent of its mode of preparation. Thus, the hydrogenation of benzene over 10% cobalt supported on typical oxide substrates would be classified as a "facile" system. In this respect, Dorling

(12) G. C. Bond, "Catalysis by Metals," Academic Press Inc., New York, N. Y., 1962, p 316.

(13) F. Hartog and P. Zwietering, *J. Catalysis*, **2**, 79 (1963).

(14) V. Haensel, G. R. Donaldson, and F. J. Riedl, *Proc. Intern. Congr. Catalysis, 3rd, Amsterdam, 1964*, **1**, 294 (1965).

(15) W. F. Madden and C. Kemball, *J. Chem. Soc.*, 302 (1961).

(16) M. Boudart, A. Aldag, J. E. Benson, N. A. Dougharty, and C. G. Harkins, *J. Catalysis*, **6**, 92 (1966).

and Moss[17] reported a similar observation for the hydrogenation of benzene over a series of platinum on silica catalysts. However, when 10% cobalt is supported on carbon, a nonoxide, the apparent activation energy and preexponential factor were lower. A similar charge in kinetic parameters, when cobalt is supported on carbon *vs.* typical oxide substrates, was reported for the hydrogenolysis of ethane.[2] Although the cause of this carbon-substrate effect has not been elucidated in detail, it may very well reflect, as suggested by Völter,[6] an influence of the substrate on the stability of the benzene–metal complex formed during the catalytic hydrogenation.

(17) T. A. Dorling and R. L. Moss, *J. Catalysis*, **5**, 111 (1966).

The Hydrophobic Bond in Micellar Systems. Effects of Various Additives on the Stability of Micelles of Sodium Dodecyl Sulfate and of *n*-Dodecyltrimethylammonium Bromide[1]

by Marilyn F. Emerson and Alfred Holtzer

Department of Chemistry, Washington University, St. Louis, Missouri 63130 *(Received March 6, 1967)*

The results of measurements of the (conductivity) critical micelle concentrations (cmc) of sodium dodecyl sulfate (SDS) and *n*-dodecyltrimethylammonium bromide (DTAB) at several temperatures in a wide variety of aqueous media containing protein denaturants or closely related compounds and in D_2O are presented. The observed temperature dependence of the cmc in a given medium has been shown to provide the standard enthalpy and entropy changes accompanying addition of a detergent molecule to a micelle of the most probable size in that medium: the relative contributions of these over-all enthalpic and entropic terms to the micelle stability are discussed. It is also shown that present experimental techniques are inadequate to allow assessment of the electrical and hydrophobic contributions to these thermodynamic parameters. Qualitatively, correlations are observed between the hydrophobic nature of the additive and its micelle-breaking power, but only by confining the comparisons within a group of similar compounds and by allowing for the possibility that some compounds may penetrate the micelle. Simple experimental criteria are developed for distinguishing such penetrating additives from nonpenetrating ones. Application of even these limited, qualitative correlations to the case of hydrophobic bonds in proteins, it is made clear, will have to be done with considerable caution.

Introduction

That hydrophobic bonds play an important role in stabilizing the native structures of proteins in aqueous solutions is well established.[2,3] Unfortunately, attempts to describe these forces molecularly and analyze how they are influenced by additives or temperature[4,5] have not proved to be of very great predictive value. To choose a specific case, there is much evidence that substances like urea disrupt protein structures,[2,6] at least in part, by breaking hydrophobic bonds; in spite of claims to the contrary,[5] however, the mechanism of this action is not understood sufficiently to allow a firm prediction, even a qualitative one, to be made of how the effectiveness of urea compares with, say, tetramethylurea.[7]

It is also evident that hydrophobic bonds cannot be the *only* important source of stabilization of native protein conformations. That most proteins denature when heated immediately implies (although many authors, but not all,[8] have been content to ignore the implication) that forces other than hydrophobic bonds

(1) This investigation was supported by Research Grant RG-5488 from the Division of General Medical Sciences, Public Health Service.

(2) W. Kauzmann, *Advan. Protein Chem.*, 14, 1 (1959).

(3) J. A. Schellman and C. Schellman in "The Proteins," Vol. II, H. Neurath, Ed., Academic Press Inc., New York, N. Y., 1964, Chapter 7, p 1.

(4) G. Némethy and H. A. Scheraga, *J. Phys. Chem.*, 66, 1773 (1962).

(5) M. Abu-Hamdiyyah, *ibid.*, 69, 2720 (1965).

(6) D. F. Waugh, *Advan. Protein Chem.*, 9, 325 (1954).

(7) M. F. Emerson, Ph.D. Thesis, Washington University, St. Louis, Mo., 1966.

(8) H. A. Scheraga, G. Némethy, and I. Z. Steinberg, *J. Biol. Chem.*, 237, 2506 (1962).

dominate the enthalpy of unfolding; disruption of hydrophobic bonds, as far as we know, is either slightly exothermic or athermal, at least near room temperature.[9,10] Furthermore, there is experimental evidence that substances such as urea can lower the free energy of an exposed peptide group in aqueous solution relative to a group that is hydrogen bonded to another peptide group;[11] thus, the action of this denaturant is not exclusively confined to hydrophobic bond breakage.

In view of these ambiguities concerning the role of additives and temperature in protein denaturation, it seemed desirable to carry out an extensive investigation of the effect of temperature, urea, and other organic additives ("denaturants") on a "simple" model system containing hydrophobic bonds—aqueous solutions of detergent micelles. Detergent systems are attractive as models, not only for their simplicity, but because the hydrophobic bonding can be assessed relatively easily through measurement of the critical micelle concentration (cmc). The particular detergents chosen in this investigation were sodium dodecyl sulfate (SDS) and *n*-dodecyltrimethylammonium bromide (DTAB), and their cmc's were measured over a wide range of conditions of solvent and temperature.

As will be seen, the results allow qualitative conclusions to be drawn about hydrophobic bonds in micelles, a system of considerable intrinsic interest, but the extension of these conclusions to include hydrophobic bonds in proteins will have to be made with considerable circumspection; indeed, the results indicate that interpretation of protein denaturation experiments may be even more equivocal than has been suspected.

Experimental Section

Unless otherwise specified, all chemicals used were reagent grade and were used without further purification.

Tetramethylurea (boiling range, 176.5–177.5°; obtained from John Deere Chemical Co., Pryor, Okla.) was used without further purification.

N,N'-Dimethylurea (Matheson Coleman and Bell; Practical grade) was recrystallized twice from hot ethanol. The recrystallized product had a melting range of 107–108°, as compared to the reported value of 107°.

Deuterium Oxide (99.8% D) was obtained from Stohler Isotope Chemicals, Montreal, Quebec, Canada.

The preparative procedures for the detergents used in this study have been described elsewhere.[7,12] These references also contain a description of the conductivity apparatus used for determination of critical micelle concentrations.

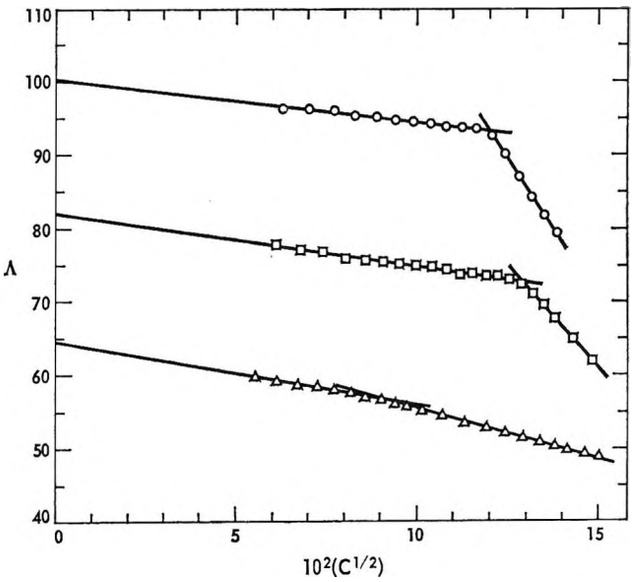

Figure 1. Conductometric titration curves for DTAB at 25°; concentration (C) is in moles per liter: O, H_2O; □, 2.51 M methanol; Δ, 2.00 M 1-propanol.

Results

The conductivity critical micelle concentrations (cmc) of DTAB and SDS in a wide variety of aqueous media were measured at several temperatures. The temperature dependence of the cmc of DTAB in D_2O was also determined. Some typical plots of the conductance data from which the cmc's were derived are presented in Figure 1. The numerical values of all the measured cmc's, along with estimates of the uncertainties involved in determining them from the data, are catalogued elsewhere.[7] To conserve space, we present here only enough of the data to illuminate the points in question.

It was found that, in general, the change in slope of the equivalent conductivity at the cmc becomes more and more gradual with increasing concentration and hydrophobic character of the additive, and, usually, with increasing temperature. In extreme cases, the break in the curve is sufficiently gradual that the cmc is very difficult to assess. Thus, for example, the cmc can be determined with reasonable accuracy for a 6.00 M urea solution at 25°, but not for a 1.00 M tetra-

(9) (a) J. A. V. Butler, *Trans. Faraday Soc.*, **33**, 229 (1937); (b) D. D. Eley, *ibid.*, **35**, 1281, 1421 (1939).

(10) J. T. Edsall and G. Scatchard in "Proteins, Amino Acids and Peptides as Ions and Dipolar Ions," E. J. Cohn and J. T. Edsall, Ed., Reinhold Publishing Corp., New York, N. Y., 1943, p 183.

(11) D. P. Robinson and W. P. Jencks, *J. Biol. Chem.*, **238**, PC1558 (1963).

(12) M. F. Emerson and A. Holtzer, *J. Phys. Chem.*, **71**, 1898 (1967).

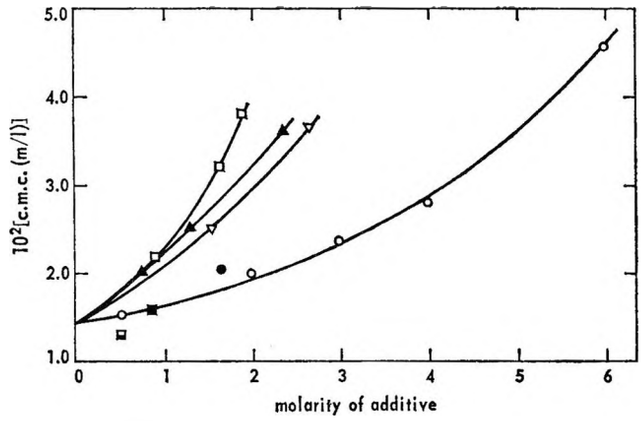

Figure 2. Cmc's for DTAB in aqueous organic solvents at 25°: O, urea; ●, N-methylurea; ▲, N,N′-dimethylurea; ■, thiourea; □, sucrose.

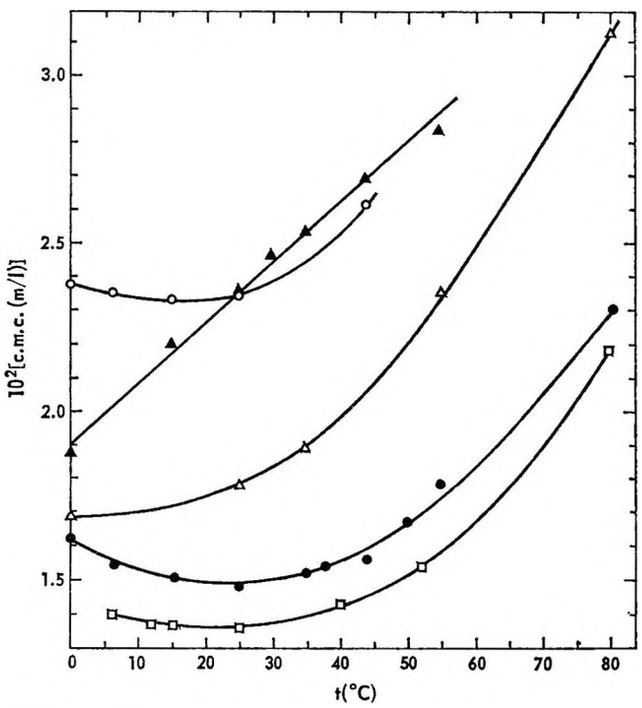

Figure 3. Dependence of cmc on temperature for DTAB in: ●, H_2O: □, D_2O; △, 1.00 *M* dioxane; ▲, 2.00 *M* dioxane; O, 3.00 *M* urea.

methylurea solution at the same temperature. This result, somewhat surprisingly, is independent of the micelle-breaking power of the solutions. Thus, a 2 *M* methanol solution destroys micelles (compared to water), whereas 2 *M* 1-propanol stabilizes them; nevertheless, the observed slope change is considerably sharper in the case of methanol (Figure 1).

A few typical plots of the experimental cmc's are

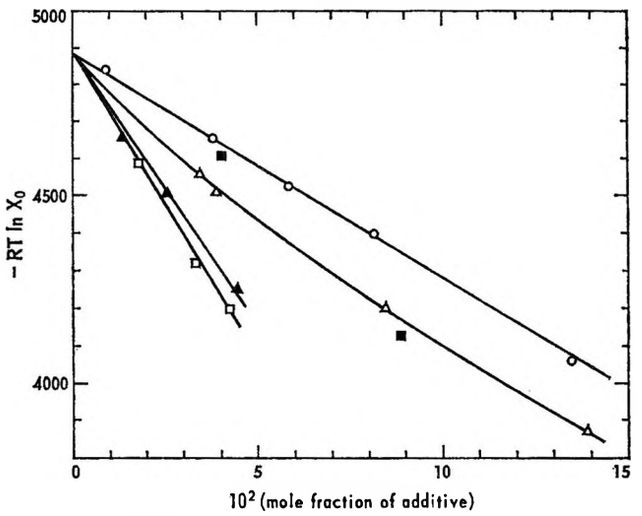

Figure 4. Stability of DTAB micelles in aqueous organic solvents at 25°: O, urea; ▲, N,N′-dimethylurea; □, tetramethylurea; △, acetamide; ■, acetone.

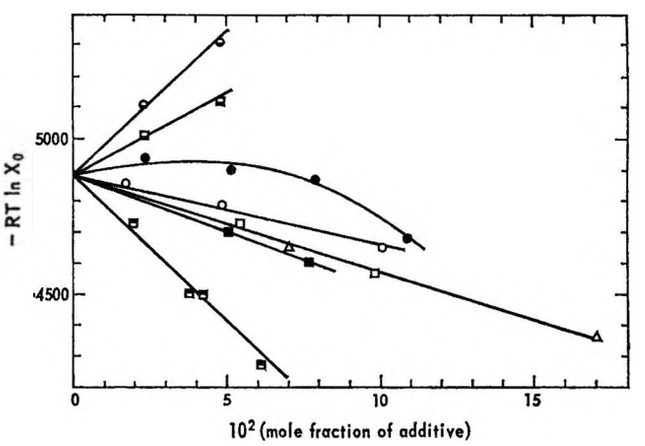

Figure 5. Stability of DTAB micelles in aqueous organic solvents at 25°: O, methanol; □, ethylene glycol; △, glycerol; ■, 1,3-propanediol; ◘, 2-propanol; ◒, 1-propanol; ●, ethanol; ◓, dioxane.

presented directly in Figure 2, which shows the molar cmc for DTAB at 25° as a function of the molarity of the organic additive, and in Figure 3, which shows the variation with temperature of the molar cmc of DTAB in several solvent media. Although the results for SDS show the same general trends as for DTAB, some differences do exist between the two detergents. In general, the organic additives are not as effective in breaking up SDS micelles as they are in breaking up DTAB micelles. Urea at 25° presents a striking case of this—2.00 *M* urea raises the cmc of DTAB by 46%, and 6.00 *M* urea raises it by 306%; the corresponding values for SDS are 16 and 104%. Most of the sub-

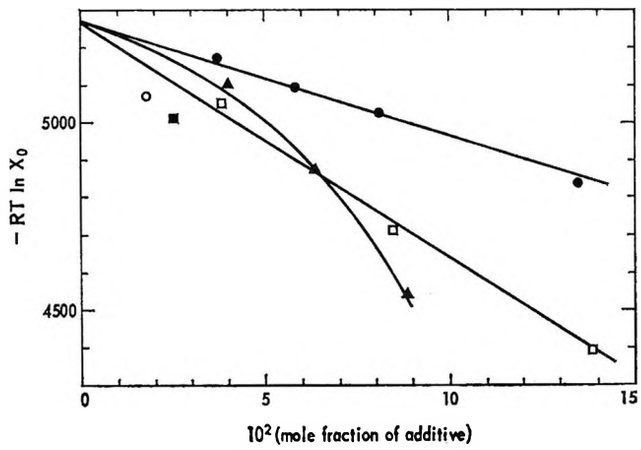

Figure 6. Stability of SDS micelles in aqueous organic solvents at 25°: ●, urea; □, acetamide; ▲, acetone; O, tetramethylurea; ■, N,N′-dimethylurea.

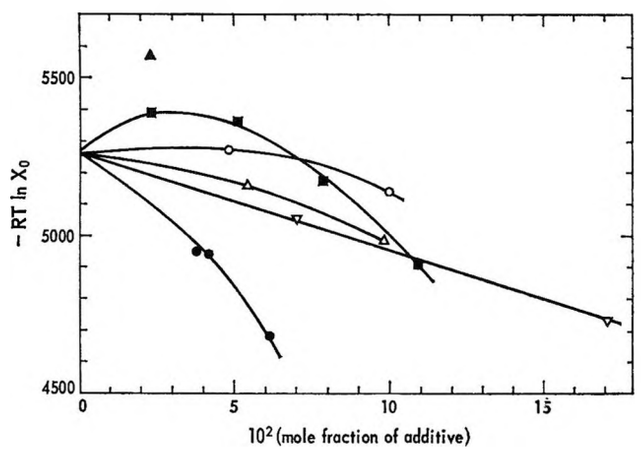

Figure 7. Stability of SDS micelles in aqueous organic solvents at 25°: O, methanol; Δ, ethylene glycol; ▽, glycerol; ■, ethanol; ●, dioxane; ▲, 1- and 2-propanol.

stances which increase the cmc's of both detergents at 25° are not only less effective with both detergents at low temperatures, but actually *decrease* the cmc of SDS at 0°.

The effects of various additives on the cmc at 25° are displayed in a somewhat different manner in Figures 4 and 5 (DTAB) and in Figures 6 and 7 (SDS), *i.e.*, as RT (ln X_0) *vs.* mole fraction of additive, where X_0 represents the cmc in base mole fraction units. The temperature dependence of the cmc is presented in Figures 8–10 (DTAB) and in Figure 11 (SDS) as $-RT(\ln X_0)$ *vs.* T(°K) and $-R(\ln X_0)$ *vs.* $1/T$, respectively. The reasons for plotting the data in these various ways will be made clear in the next section, where it will be shown that the slope of the $-RT(\ln X_0)$ *vs.* T plot is the standard entropy change and that

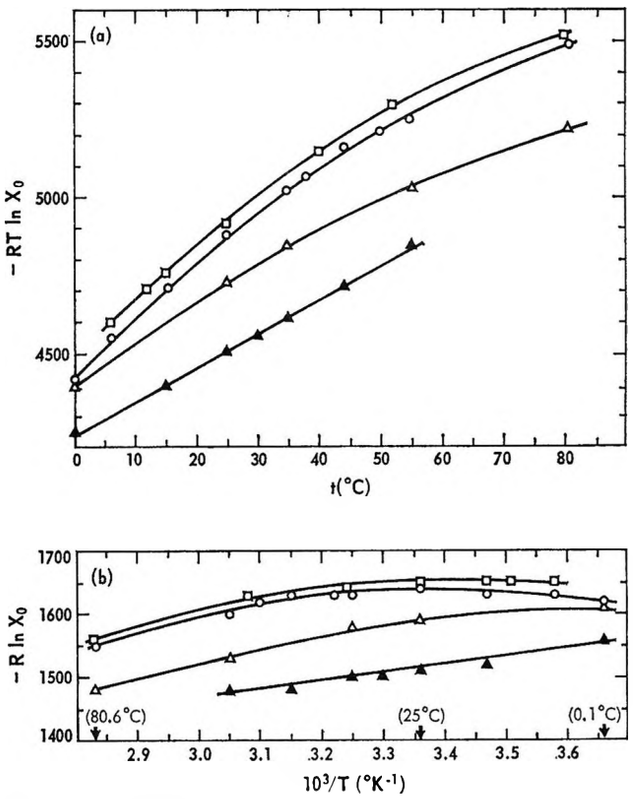

Figure 8. Dependence of cmc on temperature for DTAB in: O, H_2O; □, D_2O; Δ, 1.00 M dioxane; ▲, 2.00 M dioxane.

of the $-R(\ln X_0)$ *vs.* $1/T$ plot is the negative of the standard enthalpy change for the addition of one more monomer to a micelle having the number of monomers most probable at the cmc.

One point of disagreement with earlier work is noteworthy. Corrin and Harkins[13] have found that dioxane and the alcohols have effects on the cmc's of two cationic detergents—dodecylammonium chloride and decyltrimethylammonium bromide—which are qualitatively similar to those found here; at low concentrations of methanol and dioxane, however, they report a *decrease* in the cmc relative to water. Since no such behavior was observed here, we have assumed it to be an artifact of the method (colorimetric titration) used by the earlier workers, which involves inclusion of a dye in the system. Indeed, we have found this method to be less satisfactory than conductivity.[7]

Discussion

1. Thermodynamic Quantities from Experimental Data. It has been shown that the quantity $RT(\ln X_0)$, where X_0 is the cmc in mole fraction units, is the stand-

(13) M. L. Corrin and W. D. Harkins, *J. Chem. Phys.*, **14**, 640 (1946).

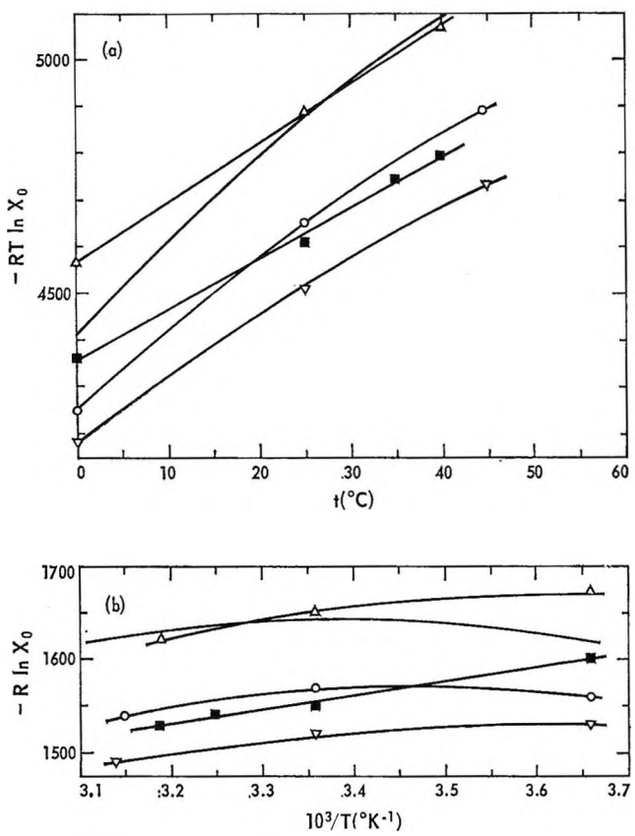

Figure 9. Dependence of cmc on temperature for DTAB in: △, 2.50 *M* ethanol; ○, 2.00 *M* urea; ■, 2.00 *M* acetone; ▽, 2.00 *M* acetamide. The solid line without data points refers to pure water (see Figure 8).

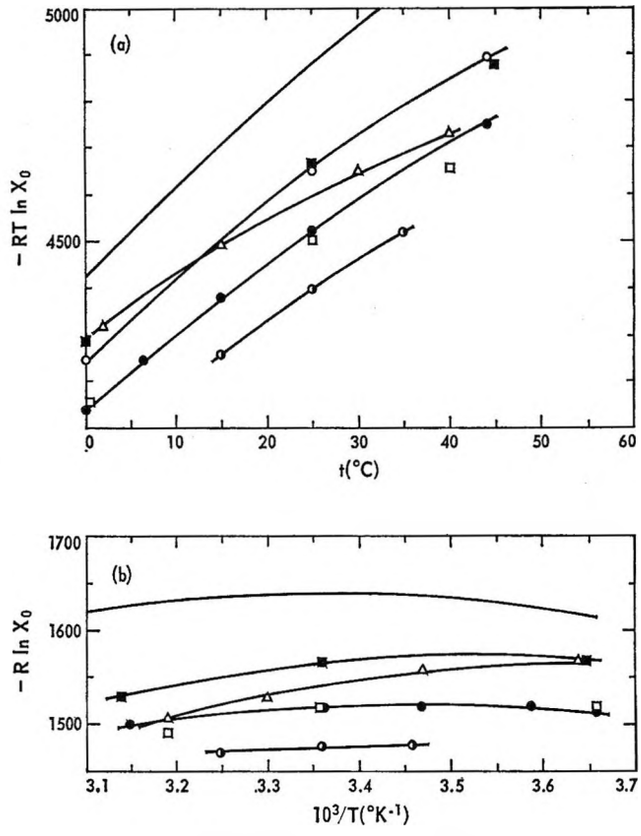

Figure 10. Dependence of cmc on temperature for DTAB in: ○, 2.00 *M* urea; ●, 3.00 *M* urea; ◑, 4.00 *M* urea; ■, 0.73 *M* N,N′-dimethylurea; □, 1.32 *M* N,N′-dimethylurea; ▲, 1.00 *M* tetramethylurea. The solid line without data points refers to pure water (see Figure 8).

ard free energy change ($\Delta G_{\hat{N}}^{\infty}$) for the addition of one more monomer to an aggregate which already contains the number of monomers most probable at the cmc ($\hat{N}$).[14] Thus, the lower the cmc, the more negative will be $\Delta G_{\hat{N}}^{\infty}$ and the more stable the micelle at any particular temperature.

The relative stability of the micelles under various sets of conditions is clearly depicted, of course, by giving the value of the equilibrium constant (or of its logarithm) for the addition reaction described above. This is given by $-\Delta G^{\infty}_{\hat{N}}/T$ ($=R \ln K$) which is, in turn, given by the experimental quantity $-R(\ln X_0)$. It is this latter experimental quantity, therefore, that most clearly represents the relative micelle stability in systems at different temperatures.

Furthermore, since $\Delta H^{\infty}_{\hat{N}} = (\partial(\Delta G_{\hat{N}}/T)/\partial(1/T))_p$, we can obtain the standard differential heat of micelle formation in various solvent media by plotting $-R(\ln X_0)$ *vs.* $1/T$ for the various experimental conditions; the slopes of these curves (as in Figures 8b, 9b, 10b, and 11b) are thus equal to the negative of the standard enthalpy changes. Moreover, since $\Delta S^{\infty}_{\hat{N}} = -(\partial \Delta G^{\infty}_{\hat{N}}/\partial T)_p$, we can obtain the corresponding standard entropy changes directly from slopes of $-RT(\ln X_0)$ *vs.* T plots (Figures 8a, 9a, 10a, and 11a). Alternatively, of course, the entropy could be obtained from the relation $\Delta G^{\infty}_{\hat{N}} = \Delta H^{\infty}_{\hat{N}} - T\Delta S^{\infty}_{\hat{N}}$.

The results (Figures 8–11) show that the process of (ionic) micelle formation is not, in general, driven entirely by the positive standard entropy change; except in H_2O, D_2O, and aqueous urea solutions at temperatures below 25° (where $\Delta H^{\infty}_{\hat{N}} > 0$), the standard enthalpy changes are *also* favorable to micelle formation and at high temperatures contribute, in some cases, as much to $\Delta G^{\infty}_{\hat{N}}$ as the entropy changes. For example, for DTAB in water at 55° $\Delta H^{\infty}_{\hat{N}} = -2600$ cal and $T\Delta S^{\infty}_{\hat{N}} = +2600$ cal. Although $\Delta S^{\infty}_{\hat{N}}$ is positive over the temperature range considered here, it becomes less positive as the temperature is increased. For example, $\Delta S^{\infty}_{\hat{N}}$ is equal to 19 eu for DTAB in water at 15° but at 55° is equal to 8 eu.

(14) M. F. Emerson and A. Holtzer, *J. Phys. Chem.*, 69, 3718 (1965).

The values of $\Delta H^{\infty}_{\hat{N}}$ (and $T\Delta S^{\infty}_{\hat{N}}$) determined in this matter are only approximate and may have a probable error of as much as ±500 cal/mole. We must keep in mind, also, that the cmc's involved here are much higher than in the case of solutions containing added electrolytes, so that the activity coefficients may no longer be close to unity; this introduces an additional uncertainty in that $RT(\ln X_0)$ is not exactly the standard free energy change (X_0 should be replaced by the activity of monomer). Thus, the results are only semiquantitative.

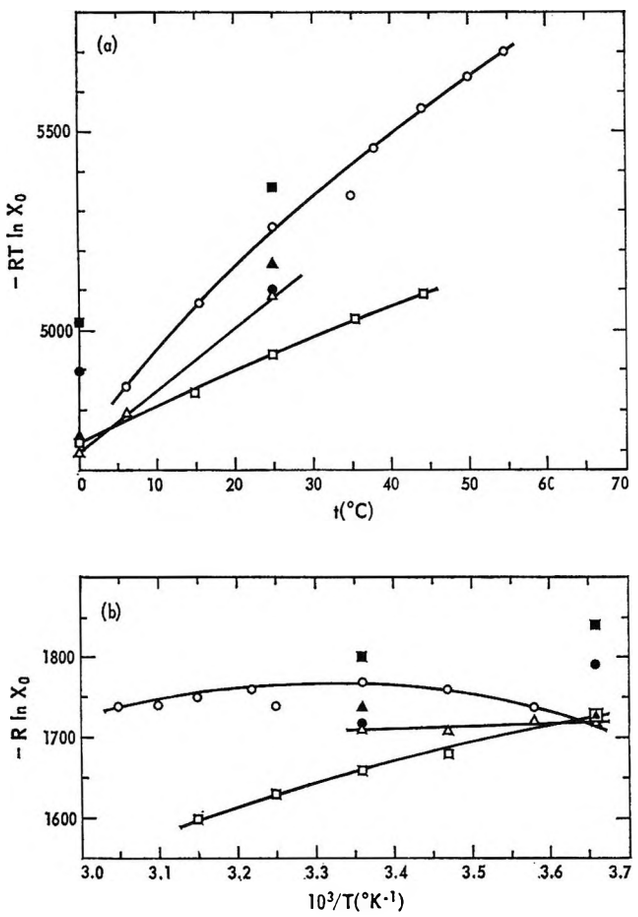

Figure 11. Dependence of cmc on temperature for SDS in: O, H_2O; ▲, 2.00 *M* urea; △, 3.00 *M* urea; □, 2.00 *M* dioxane; ●, 2.00 *M* acetone; ■, 2.50 *M* ethanol.

There is an additional difficulty in using these thermodynamic results to compare micelle stabilities in various media: values of $\Delta G^{\infty}_{\hat{N}}$ should, in general, not be compared directly, since the electrostatic contribution to this total free energy change depends on $\hat{N}$ (as well as on the dielectric properties of the medium), whereas the hydrophobic contribution, to first approximation, does not. Thus, for different additives, the micelles may contain very different numbers of monomers, and attempted direct correlation of the cmc with the hydrophobic properties cannot be expected to be meaningful even if the dielectric effect of the medium can be estimated. We shall confine our comparisons, therefore, to groups of closely related compounds, where the micelle size is not expected to change appreciably.

2. Factors Contributing to Micelle Stability in Pure Water and in Deuterium Oxide. First, we consider the process of micelle formation in pure water and inquire how the cmc is expected to change with changing temperature. Since the transfer of hydrocarbon groups from an aqueous to a nonpolar environment is normally endothermic, we expect hydrophobic bonds, and thus micelles, to become more stable as the temperature is increased; *i.e.*, the cmc should decrease with increasing temperature. From Figures 3, 8b, and 11b we see that this is indeed the case for both DTAB and SDS in water at temperatures below 25°; however, as the temperature is increased *above* 25°, the stability *decreases*. Thus, we cannot explain the observed behavior in terms of hydrophobic bonds alone. However, these are ionic detergents, and we therefore expect the macroscopic dielectric properties of the medium to play a role in determining the stability; lowering the dielectric constant of the medium (by increasing the temperature) should tend to break up the micelles, *i.e.*, to raise the cmc, by increasing the repulsive force between the ionic heads of the detergent molecules. There are thus two opposing effects to consider, and a postulated predominance of the hydrophobic over the dielectric effect at low temperatures and of the dielectric over the hydrophobic at high temperatures would be sufficient to explain the observed maximum in the stability. This requires, then, that the electrical part of the free energy change for the addition of one more monomer to a micelle that already contains the most probable number of monomers at the cmc, *i.e.*, the process of adding one more charge to the surface of a sphere which already contains the most probable number of charges at the cmc, be exothermic.

Let us see if we can *predict*, not merely rationalize, the sign of this electrical part of the enthalpy change. In the absence of added electrolyte and assuming that the concentration of monomers is sufficiently low so that the ionic strength may be approximated as zero

$$\Delta G^{\infty}_{\hat{N},\mathrm{el}} = \frac{\hat{N}\epsilon^2}{Db} \qquad (1)$$

where D is the dielectric constant of the medium, b the micellar radius, and ϵ the magnitude of the protonic charge. The corresponding entropy change is

$$\Delta S^{\infty}_{\hat{N},\mathrm{el}} = -\left[\frac{\partial(\Delta G^{\infty}_{\hat{N},\mathrm{el}})}{\partial T}\right]_{\mathrm{p}} = \frac{-\hat{N}\epsilon^2}{b}\left[\frac{\partial(1/D)}{\partial T}\right]_{\mathrm{p}} - \frac{\epsilon^2}{Db}\left(\frac{\partial \hat{N}}{\partial T}\right)_{\mathrm{p}} \quad (2)$$

Thus

$$\Delta H^{\infty}_{\hat{N},\mathrm{el}} = \frac{\hat{N}\epsilon^2}{Db} + \frac{\hat{N}\epsilon^2 T}{D^2 b}\left(\frac{\partial D}{\partial T}\right)_{\mathrm{p}} - \frac{\epsilon^2 T}{Db}\left(\frac{\partial \hat{N}}{\partial T}\right)_{\mathrm{p}} \quad (3)$$

If we insert the empirical relationship $D = D_0\epsilon^{-T/\theta}$ [where θ is a constant for a given medium and D_0 is the dielectric constant at $T = \theta$[15]] into the above expression, we obtain

$$\Delta H^{\infty}_{\hat{N},\mathrm{el}} = \frac{\hat{N}\epsilon^2}{Db}\left[1 - \frac{T}{\theta} - \frac{T}{\hat{N}}\left(\frac{\partial \hat{N}}{\partial T}\right)_{\mathrm{p}}\right] \quad (4)$$

Thus, the sign of the enthalpy change depends on θ, $\hat{N}$, and $\partial\hat{N}/\partial T$. For water, $\theta = 219$,[15] so that if $\partial\hat{N}/\partial T$ is sufficiently small, the process will indeed be exothermic. However, Debye's[16] light-scattering results (DTAB in 0.034 *M* KCl) give a value of -0.4 ± 0.3 for $\partial\hat{N}/\partial T$ between 30 and 60°; and, for the detergents considered here, $\hat{N}$ probably lies somewhere between 50 and 100. Using $\hat{N} = 100$ and $\partial\hat{N}/\partial T = -0.4$, then, we find that $\Delta H^{\infty}_{\hat{N},\mathrm{el}} = (0.72)\hat{N}\epsilon^2/Db$ at 45°; *i.e.*, the reaction is *endothermic*. However, using $\hat{N} = 100$ and $\partial\hat{N}/\partial T = -0.1$, we find that $\Delta H^{\infty}_{\hat{N},\mathrm{el}} = (-0.13)\cdot\hat{N}\epsilon^2/Db$ at 45°, *i.e.*, the reaction is exothermic. Thus, the sign of the enthalpy change can be reversed by using different values of $\partial\hat{N}/\partial T$ within the narrow range allowed by the experimental data; the only available value of this quantity (Debye's) is thus not precise enough to allow *even the sign* of the enthalpy change to be determined *a priori*. Indeed, extensive and very precise measurements would be required to better the situation, since a change in the temperature of 25° would produce (if $\partial\hat{N}/\partial T = -0.4$) a change in $\hat{N}$ of only 10; for a micelle containing 100 monomers, this is smaller than the limits of precision of the measurement.

That no minimum is observed in the plot of the cmc *vs.* temperature for nonionic micelles[17] would seem to indicate that the decreasing dielectric constant does contribute a negative quantity to the enthalpy in the ionic case. More precise determinations of $\partial\hat{N}/\partial T$ thus should reveal that this quantity is actually rather small. However, there is also the possibility that the hydrocarbon part of the free energy change depends on temperature in a different manner for ionic and nonionic detergents.

Let us now try to predict the effect on the cmc of substituting D_2O for H_2O; first, we consider the electrical part of the free energy change and then the hydrocarbon part. Since the dielectric constant of D_2O is only very slightly lower (a fraction of 1%) than that of H_2O[18] over the entire temperature range, the electrical contribution should tend to make the micelles only negligibly less stable in D_2O at any particular temperature.

Discussion of the hydrocarbon part of the free energy is considerably more equivocal. In fact, if, as seems clear, the influence of such solutes on water structure is involved,[19,20] a definite prediction becomes impossible. Immersion of a hydrocarbon chain in water allegedly results in formation of an ordered region of solvent molecules (an iceberg) about the hydrocarbon molecule. This formation of the iceberg presumably mitigates (free energetically) the unfavorable effects of inserting a hydrocarbon into a liquid (water) of much greater cohesive energy density. Iceberg formation *must* be free energetically mitigating, or icebergs would not form. Consideration of the effect of substitution of D_2O for H_2O produces immediate ambiguity; since D_2O is of higher energy density, insertion of a hydrocarbon is more unfavorable. However, since D_2O is the more structured solvent, the icebergs that form should be the better able to mitigate the situation. Thus, in D_2O, insertion might cost more (in negative free energy), but subsequent iceberg formation might succeed in gaining back more than the difference. Therefore, although the iceberg argument may very well describe the situation correctly, it is at present indeterminate. It is, of course, possible that the icebergs are not of the same structure as the solid water, a possibility that only increases the ambiguities. Needless to say, by emphasizing either the insertion cost or the iceberg profit, an investigator can obtain a "satisfactory explanation" of *any* experimental result, which explains the popularity of the iceberg concept; there is no doubt of its seductive power.

From Figures 3 and 8, we see that DTAB micelles are, in fact, more stable in D_2O than in H_2O; *i.e.*, hydrophobic bonds are stronger in D_2O, at all temperatures considered. However, the two curves get progressively closer as the temperature is increased.

Thus, it is not possible to make an *a priori* prediction of the dependence of the cmc on temperature or on the nature of the aqueous isotopic species even in the

(15) R. W. Gurney, "Ionic Processes in Solution," McGraw-Hill Book Co., Inc., New York, N. Y., 1931, p 16.

(16) P. J. Debye, *Ann. N. Y. Acad. Sci.*, **51**, 575 (1949).

(17) M. J. Schick, *J. Phys. Chem.*, **68**, 3585 (1964).

(18) J. Wyman and E. N. Ingalls, *J. Am. Chem. Soc.*, **60**, 1184 (1938).

(19) H. S. Frank and M. W. Evans, *J. Chem. Phys.*, **13**, 507 (1945).

(20) G. Némethy and H. A. Scheraga, *ibid.*, **36**, 3382 (1962); **36**, 3401 (1962).

simplest cases where no organic additives are present. The transfer of the hydrocarbon chain of any detergent from H_2O or D_2O into the micelle will, in general, be endothermic; however, the electrical part of the enthalpy change may be positive or negative, depending rather sensitively on $\hat{N}$ and $\partial\hat{N}/\partial T$, and these quantities will, in general, depend on the particular detergent used. The influence of D_2O, as opposed to H_2O, depends on the thermodynamic details of iceberg formation; these cannot be evaluated at present, not even qualitatively.

3. Factors Contributing to Micelle Stability in Solutions Containing Nonpenetrating Additives. There is evidence that some substances such as the alcohols (with the probable exception of methanol) penetrate the interior of the micelle and form mixed micelles.[21] This situation is more complex than the case where the additives cannot penetrate the micelle, and its discussion will be reserved for the next section.

We do not, on the other hand, expect substances such as urea, glycerol, etc. to be capable of penetrating the micelle (since these are not very soluble in hydrocarbon substances) although there are no definitive data on the point.

Consider, then, the effect of, say, urea on the cmc at some given temperature. Although urea raises the dielectric constant of water ($\Delta D/\Delta c = 3$ at 25°),[22] which, if $\hat{N}$ does not change too much, should tend to stabilize the micelles (relative to water) by decreasing the repulsive force between the ionic heads of the detergent molecules, it nevertheless *breaks up* micelles at 25°[23] and increases the solubility of amino acids containing nonpolar side chains.[24] Consequently, its effect on the hydrocarbon part of the free energy must predominate although we have no *a priori* way of deciding that this is the case. This effect can be seen in Figures 2, 4, and 6, where it is shown that both DTAB and SDS micelles are broken up (relative to water) in aqueous urea solutions at 25°.

The change in the cmc with temperature in aqueous solutions of urea (Figures 9–11) is very similar to that observed in pure water. These results indicate that the transfer of a hydrocarbon group to the interior of the micelle is probably endothermic in aqueous urea solutions as well as in water, since the stability increases with increasing temperature up to 25°. Above 25°, the stability decreases again, probably because of the dielectric effect—but, we cannot even estimate the magnitude of this effect for urea solutions. Again, Schick[17] finds no minimum in the cmc *vs.* T curve for nonionic micelles in aqueous urea solutions, indicating that it is indeed the opposite temperature dependence of the hydrocarbon and electrical effects that gives rise to the minima for ionic detergents.

What do we expect to be the effect of changing the hydrophobic character of the nonpenetrating denaturant? Predictions based on the idea of water structure have been shown to be unsatisfactory; such arguments become indeterminate when pursued in depth.[7] Thus, we are forced to take a much more semiempirical approach; increasing the size of the hydrophobic group of an organic additive (at constant temperature and concentration) should make the solvent less "water-like" and more "hydrocarbon-like," and thus we expect, on the basis that "like dissolves like," that this factor would make the molecularly dispersed system more stable. At any particular temperature, then, we must consider two factors: first, we expect compounds with a larger hydrophobic surface to break up micelles more (through ΔG^{∞}_{HC}), and, second, we expect compounds which lower the dielectric constant of water more to break up the micelles more (through ΔG^{∞}_{el}). However, we must confine our attention to substances which are closely related, in the hope that values of $\hat{N}$ will then not be too different.

Let us first consider a series of selected alcohols at 25°; the order of effectiveness in breaking up micelles is glycerol $\geq$ ethylene glycol $\geq$ methanol (Figures 5 and 7). Since neither glycerol nor ethylene glycol is very soluble in hydrocarbons, their partition between water and hydrocarbons greatly favors water and we do not expect any of these substances to penetrate the micelle interior appreciably. Methanol has the least lowering effect on the dielectric properties of the medium[25] and would be expected to have little hydrophobic interaction with hydrocarbon chains; as expected, then, methanol is the least effective denaturant (*i.e.*, micelle breaker). Glycerol lowers the dielectric constant of water most effectively of the three,[25] and, although the hydrophobic part of the molecule is increased compared to methanol, so is the hydrophilic part. Nevertheless, owing to van der Waals type of interactions, glycerol may be expected to have slightly more effective hydrophobic contacts with the detergent hydrocarbon chains than methanol and is the best denaturant, as expected. Thus, although the differences in the demicellizing

(21) W. D. Harkins, R. W. Mattoon, and R. Mittelman, *J. Chem. Phys.*, **15**, 763 (1947).

(22) J. Wyman, *Chem. Rev.*, **19**, 213 (1936).

(23) W. Bruning and A. Holtzer, *J. Am. Chem. Soc.*, **83**, 4865 (1961).

(24) P. L. Whitney and C. Tanford, *J. Biol. Chem.*, **237**, PC1735 (1962).

(25) G. Åkerlof, *J. Am. Chem. Soc.*, **54**, 4125 (1932).

abilities of these substances are quite small, they seem to make some sense.

The results for 1,3-propanediol (Figure 11) support this view: we would expect this substance to have dielectric properties similar to glycerol but to have greater hydrophobic interaction with the hydrocarbon chains of the micelles and thus be the better denaturant, which is the case.

For urea and some closely related substances (Figures 4 and 6) the order of effectiveness in breaking up micelles at 25° is *N,N'*-dimethylurea > acetamide > urea. Urea and *N,N'*-dimethylurea both raise the dielectric constant of water[22] to about the same extent (~10% for a 3 *M* solution) and acetamide[22] lowers it slightly (~3% for a 3 *M* solution). On this basis, then, we expect both urea and *N,N'*-dimethylurea to be less effective than acetamide in breaking up micelles; however, this effect should be small because of the rather small changes in the dielectric constant. The hydrophobic effects of these additives should be dominant, therefore, and, indeed, the order of increasing hydrophobic character is the same as the order of demicellizing effectiveness. Thus, as long as only closely related series of nonpenetrating compounds are considered, the qualitative influence of these additives on micelles can be predicted from very simple considerations.

We note here also that the temperature dependence of the cmc in solutions of urea, acetamide, and *N,N'*-dimethylurea is very similar to that in pure water. The micelle stability increases or decreases only slightly between 0 and 25° and then decreases above 25°, the order of effectiveness of the three substances being the same over the whole temperature range.

The caution which must be exercised in placing substances in the various groups should be emphasized; we might, for example, have expected acetone and tetramethylurea to be included in the urea series since they are certainly structurally related. If this is done, however, the simple consideration used above produces results in disagreement with experiment. Acetone[22] and probably tetramethylurea lower the dielectric constant of water, which would tend to increase the cmc. Furthermore, the hydrophobic properties of these substances would certainly lead us to expect acetone to be more effective than acetamide and tetramethylurea to be more effective than *N,N'*-dimethylurea. From Figures 4 and 6, however, we see that at 25° tetramethylurea is only slightly more effective than N,N'-dimethylurea and that, at low concentrations, acetone is even *less* effective than acetamide. Furthermore, the temperature dependence for the two additional additives is quite different from that for water and for aqueous solutions of the original three related substances—the micelles in acetone or tetramethylurea solutions are quite stable at low temperatures. Thus, although 1.00 *M* tetramethylurea breaks up DTAB micelles better than 2.00 *M* at 25°, it *stabilizes* them relative to 2.00 *M* urea at 5° (Figure 9). A more striking example of this behavior is shown in Figure 11; 2.00 *M* acetone breaks up SDS micelles (relative to water) at 25°, yet actually stabilizes them at 5°. Anyone in need of a sobering view of predictability in this field might well contemplate that the answer to the question of whether acetone breaks hydrophobic bonds is, apparently, that it depends on the temperature.

These last two substances (acetone and tetramethylurea), unlike urea, acetamide, and *N,N'*-dimethylurea, are very soluble in hydrocarbons and may be able to penetrate the micelles; this more complicated situation will now be considered.

4. Factors Contributing to Micelle Stability in Solutions Containing Penetrating Additives. Let us consider, on the same basis as before, the homologous series of alcohols—methanol, ethanol, and 1-propanol—at 25°. 1-Propanol not only has the largest hydrophobic surface but also lowers the dielectric constant of water the most, ethanol falls in between on both counts, and methanol has the smallest hydrophobic surface as well as the least effect in lowering the dielectric constant.[25] We would predict, then, that 1-propanol should be the most effective, and methanol the least, in breaking up micelles. The results for both DTAB (Figure 5) and SDS (Figure 7) show, in general, the opposite order: methanol increases the cmc slightly, ethanol decreases the cmc at low concentration and then raises it slightly at 5.00 *M*, and 1-propanol (as well as 2-propanol and *t*-butyl alcohol) decreases the cmc more effectively than ethanol.

Thus, when substances such as these alcohols are present, we cannot explain the results even qualitatively in terms of the changes—hydrophobic and dielectric—produced in the solvent media; we must take into account the changes produced in the micelles themselves. X-Ray diffraction studies indicate that the hydrocarbon chains of the alcohols penetrate the micelle interior while the polar groups remain on the micelle surface; thus, without appreciably changing the micellar volume, mixed micelles are formed.[21] We would expect these mixed micelles to be more stable than ordinary micelles (at low concentrations of alcohol, at least), since the electrical (repulsive) properties should not have been changed too much by inclusion of a neutral alcohol molecule, but the hydrophobic (attractive) interactions between the hydrocarbon chains near the micelle surface where there is ample room[26] should have been en-

hanced. We expect this stabilization to be roughly dictated by the amount of alcohol which enters the micelle in this manner. The partition coefficients for these alcohols between water and long-chain hydrocarbon oils have been measured and are, for methanol $\cong$100, ethanol $\cong$30, and 1-propanol $\cong$10.[27,28] Thus, hardly any methanol but a considerable amount of 1-propanol may be inside the micelle "phase" and we would expect the micelle stability to be enhanced by its presence.

Looking back now at the results for acetone and tetramethylurea (Figures 9 and 11), we see that, for both, the temperature dependence is very much like that for ethanol. Since both substances are infinitely miscible with both water and hydrocarbons, since the partition coefficient of acetone between water and hexane is roughly 10, and since, although we do not know the partition coefficient for tetramethylurea, we would not expect it to favor water overwhelmingly, they may provide some stabilization due to solubilization of the hydrophobic parts into the micelle. Thus, even though the net effect is an increase in the cmc, the substances are not as effective at breaking up micelles as they would be if they could not get inside the micelle. That the cmc increases very sharply above a certain concentration of these additives indicates that this is the case—thus, acetone is less effective than acetamide at low concentrations but becomes so much more effective at higher concentrations (once the micelles are acetone saturated) that micelles are no longer detected in acetone, though still present in solutions with the same concentration of acetamide.

Dioxane (Figures 5, 7, 8, and 11) is a good denaturant for micelles at 25° and above, perhaps because of its low dielectric constant,[29] but is not as effective at low temperatures. It shows the same type of temperature and concentration dependence as the penetrating substances already mentioned and is very soluble in both water and hydrocarbons (although the partition coefficient is not known).

We would expect this penetration effect to be sharply concentration dependent; a certain amount of, say, alcohol can enter the micelle without changing the micellar volume, but upon further addition of alcohol, no more favorable contacts near the micelle surface can be made, and deeper penetration only disrupts contact of the long chains; hence the hydrophobic and dielectric effects alone dictate the micelle stability. Thus, at 25°, 5.00 M ethanol becomes a more effective demicellizer than water, and for SDS even more effective than methanol.

We would also expect this effect to be temperature dependent and the change in cmc with temperature to depend on the change in partition of the hydrocarbon part of the additive between the micelle and water, as well as on the change in the dielectric properties of the media. Such partition coefficient data apparently do not exist, but from the results (Figures 9 and 11) we would guess that the nonpolar part of ethanol may be relatively more soluble in hydrocarbons (compared to water) at low temperatures than at high.

Thus, an additive, in addition to changing the dielectric and hydrophobic properties of the solvent medium, may also be incorporated into the micelle and increase the stability through direct hydrophobic interactions. All of these effects will be both concentration and temperature dependent and, in different substances, will depend on these variables in different ways. It must be emphasized that we have no direct experiments that enable the three factors to be sorted out quantitatively.

However, we may have found here indirect means of distinguishing penetrating from nonpenetrating additives. First, at 25° and at low concentrations, the penetrating additives are not as effective as we would expect them to be (from data on related compounds) on the basis of their dielectric and hydrophobic properties. Second, at higher concentrations, they become increasingly more effective, and at still higher concentrations, where micelles can still be detected in solutions of related nonpenetrating additives, no micelles can be detected. Third, at a particular concentration, the effect of a particular penetrating additive on the cmc is very temperature dependent—the micelles being quite stable at low temperatures and quite unstable at high—and the temperature dependence no longer shows a minimum (cmc *vs.* T) as in the case of the nonpenetrating additives. These three experimental criteria can thus be used to distinguish the two cases; of course, data on partition of the additive between water and hydrocarbons are also helpful.

5. Conclusions and Implications for Proteins. In general, then, it is not possible to take the numerical value of the cmc as a single criterion for the hydrophobic bond strength in micelles; the cmc is directly related to the standard free energy change for the addition of one more monomer to the micelle which already contains the number of monomers most probable at the cmc, and this most probable number of monomers is expected to be quite different, at least for each different class of additive. Within each of the various classes of com-

(26) See ref 7, Appendix II.

(27) B. B. Wroth, *Expt. Sta. Record*, **38**, 616 (1918); *Chem. Abstr.*, **12**, 2153 (1918).

(28) R. Macy, *J. Ind. Hyg. Toxicol.*, **30**, 140 (1948); *Chem. Abstr.*, **42**, 6619 (1948).

(29) G. Åkerlof and O. A. Short, *J. Am. Chem. Soc.*, **58**, 1241 (1936).

pounds, however, and as long as a particular member is not soluble in the micelle, the effects of the different additives can be roughly correlated with their hydrophobic and dielectric properties.

If we could determine ΔG^{∞}_{HC} in every case (instead of just the cmc), we might be able to correlate it with the properties of all the nonpenetrating additives, in general, instead of just within certain classes of compounds. Unfortunately, the addition of the denaturant changes the electrostatic as well as the hydrophobic properties of the micelles and we would expect $\hat{N}$ (the most probable number of monomers per micelle) to be quite different for the different classes of compounds. Furthermore, the usual methods for determining $\hat{N}$, *e.g.*, light scattering, equilibrium ultracentrifugation, etc., cannot be used because there is no known way to interpret the data for a highly charged macromolecule in these multicomponent systems.

The effects of additives are very difficult to predict because of the possibility of penetrability. The presence of more methyl groups in an additive does not ensure in all cases (*e.g.*, alcohols) that it will be a better hydrophobic bond breaker at a particular temperature, nor does the fact that a substance is a good hydrophobic bond breaker at one temperature ensure in all cases (*e.g.*, acetone) that it will be as effective at all temperatures. The results can be explained in a very qualitative manner in terms of hydrophobic bonds if the effect of the additives on the micelles themselves (*i.e.*, penetration) is considered. Simple experimental criteria have been described here that enable one to determine when such penetration exists.

The analogous problem in the protein case—that of possible participation of an additive in the protein structure itself—may very well also exist. The assumption that additives do *not* affect the nonpolar contributions to the free energy of the native form of protein molecules is often quite explicitly made in investigations bearing on protein denaturation. It is ordinarily assumed that, insofar as the hydrophobically bonded regions of the molecule are concerned, the native molecule has the same structure in the medium containing additives as it does in water. Ironically enough, one group of investigators,[30] while making this assumption for the protein case, insists, quite correctly, that the analogous assumption for micelles is of dubious validity. In our view, there is little reason to believe that native protein structures would not be as susceptible to alteration by the presence of such additives as micelles are. Indeed, this idea is supported by the recent finding (from X-ray determinations of the three-dimensional structure of several protein molecules) that many nonpolar amino acid residues are located on the molecular surface.[31] If so, many protein denaturation studies may represent *creation* of a structural problem that is not directly related to that posed by the native protein structure, rather than a step toward a solution.

Acknowledgment. The authors wish to thank Dr. Martin Schick of Lever Brothers for expert advice on the synthesis of SDS samples and Professor Joseph Kurz of Washington University for stimulating and informative discussions and for his helpful criticisms of the manuscript.

(30) D. B. Wetlaufer, S. K. Malik, L. Stoller, and R. L. Coffin, *J. Am. Chem. Soc.*, **86**, 508 (1964).

(31) J. C. Kendrew, G. Bodo, H. M. Dintzis, R. G. Parrish, H. Wykhoff, and D. C. Phillips, *Nature*, **181**, 662 (1958).

The Heat of Formation and Entropy of Aluminum(II) Chloride(g) and Its Dimer, $Al_2Cl_4(g)$[1]

by B. J. Chai, H. C. Ko, M. A. Greenbaum, and M. Farber

Rocket Power, Inc., Pasadena, California 91107 *(Received January 12, 1967)*

A transpiration study of the reaction between solid and liquid aluminum and the vapor species of aluminum chloride has been carried out in the temperature range of 800–1000°K. The heats and entropies of reaction yielded thermal functions for $AlCl_2(g)$ and its dimer $Al_2Cl_4(g)$. Employing estimated thermal functions, values for $\Delta H_f^\circ{}_{298}$ for $AlCl_2(g)$ and $Al_2Cl_4(g)$ are -66.0 ± 3 and -194.0 ± 5 kcal/mole, respectively. The corresponding entropy for $Al_2Cl_4(g)$ at 900°K is 116 ± 1 cal/deg mole.

Introduction

Several investigations[2-6] involving the reaction of aluminum chloride vapor and aluminum, both liquid and solid

$$AlCl_3(g) + 2Al(l, s) = 3AlCl(g) \quad (1)$$

have yielded a value for the heat of formation of AlCl(g). These experiments were of the atmospheric pressure transpiration type. A recent study of this reaction in this laboratory[7] by means of moleculer flow effusion is in good agreement with these values.

Although the previous studies showed only the formation of AlCl as a product of reaction 1, the possibility exists that the vapor product from the Al–$AlCl_3$ equilibrium is a complex one and contains the following five vapor species: AlCl, $AlCl_2$, $AlCl_3$, Al_2Cl_4, and Al_2Cl_6.

Bond energy considerations indicate the probable formation of $AlCl_2$ and its dimer as a result of the reactions

$$AlCl_3(g) + AlCl(g) = 2AlCl_2(g) \quad (2)$$

$$2AlCl_2(g) = Al_2Cl_4(g) \quad (3)$$

However, the literature does not report any thermal data for either $AlCl_2$ or its dimer.

Therefore, in order to obtain thermal data for $AlCl_2$ and its dimer Al_2Cl_4, a number of transpiration experiments were performed at atmospheric pressure in the temperature range 800–1000°K. These experiments involved the use of argon as a carrier gas for the aluminum chloride vapor species. This gaseous mixture was passed over a boat containing pure aluminum.

Experimental Section

Apparatus. The experimental apparatus employed in this study consisted of a dual heating system for (1) generating aluminum chloride vapor and (2) heating the cell containing aluminum to the desired transpiration temperature.

The gaseous aluminum chloride was generated by heating the highly purified $AlCl_3(c)$ in a 250-ml glass flask by means of a heating mantle. A saturable-core reactor–recorder combination was used to monitor and control the temperature of the flask. The flow rate of the gaseous $AlCl_3$ was controlled by controlling the temperature of the $AlCl_3$ generator. Argon was employed as the carrier gas and its flow rate was measured by means of an accurately calibrated flowmeter. The

(1) This work was sponsored by the Air Force Rocket Propulsion Laboratory, Research and Technology Division, Air Force Systems Command, United States Air Force, Edwards Air Force Base, Calif., under Contract AF 04(611)-10929.

(2) (a) P. Gross, C. S. Campbell, P. J. C. Kent, and D. L. Levi, *Discussions Faraday Soc.*, **4**, 206 (1948); (b) A. S. Russell, K. E. Martin, and C. N. Cochran, *J. Am. Chem. Soc.*, **73**, 1466 (1951).

(3) R. F. Barrow, *Trans. Faraday Soc.*, **56**, 952 (1960).

(4) A. G. Gaydon, "Dissociation Energies and Spectra of Diatomic Molecules," Chapman and Hall, Ltd., London, 1953.

(5) R. Heimgartner, *Schweiz. Arch. Angew. Wiss. Tech.*, **18**, 241 (1952).

(6) S. A. Semenkovich, *Zh. Prikl. Khim.*, **33**, 1281 (1966).

(7) M. A. Frisch, M. A. Greenbaum, and M. Farber, *J. Phys. Chem.*, **69**, 3001 (1965).

argon was introduced into the aluminum chloride generator flask and the resulting mixture was transpired into the reaction zone containing the solid and liquid aluminum.

The furnace was a heavily insulated nichrome resistance type, 12 in. long by 1.25-in. diameter. The furnace tube was constructed of aluminum oxide and measured 1-in. i.d. Each end of the furnace tube was closed by a Monel flange, which also provided the openings for the gas delivery and exit tubes, as well as for the chromel–alumel thermocouple. The temperature of the cell was held constant by means of a silicon-controlled rectifier–recorder combination.

The aluminum was contained in an aluminum oxide boat which was placed inside an aluminum oxide reaction cell having a 10-mm i.d. The reaction cell was restricted to a diameter of 1.5 mm on each side of the boat to prevent back-diffusional losses. The tube admitting the $AlCl_3$–Ar mixture to the cell was also constructed of aluminum oxide.

The aluminum chloride in the argon–aluminum chloride vapor mixture was collected in a 250-ml flask after leaving the reaction zone. The aluminum chloride generator and collection flasks were connected to the transpiration apparatus with Teflon and Monel fittings. These fittings were heated with heating tapes, and four immersion heaters were attached to the flanges in the ends of the furnace tube to prevent condensation of the aluminum chloride vapor entering or leaving the reaction zone. The temperature of these heating tapes and immersion heaters was maintained at approximately 230° by the use of variable rheostats.

Procedure. The commercially obtained aluminum chloride (anhydrous) of 99.5% purity was further purified by sublimation prior to its use. The sublimation procedure also converted traces of moisture into HCl(g) which would be driven off as a vapor. As a further precaution against impurities, prior to each run approximately 1 g of 99.9%, 200 mesh aluminum powder was added to the sublimated aluminum chloride and thoroughly mixed by vigorous agitation for use in the generator flask.

Weight loss of the Al samples was established by weighing before and after each run. The amount of $AlCl_3$ passed over the sample was determined by weighing the generator before and after each run. After leaving the reaction, the $AlCl_3$ in the gas mixture was collected in a second flask and weighed. (This weight gain was essentially equal to the weight loss in the first flask.)

The weight loss of aluminum due to vaporization by passing argon alone over the aluminum sample was found to be insignificant and in agreement with that predicted from the published vapor pressure of aluminum. To further check that no HCl or water vapor was present in the aluminum chloride generator flask, argon gas was passed through the generator, which was heated to 50°, and then passed over a sample of aluminum in the reaction cell, which was heated to 900°K. At this low generator temperature the quantity of $AlCl_3$ in the vapor state is very small and therefore the resulting quantity of aluminum lost due to the reaction with $AlCl_3$ would also be insignificant. Thus any large losses of aluminum would have to be attributed to the entrained HCl(g) which reacts quantitatively with aluminum at the experimental temperatures. Since no reaction was observed, it can be concluded that the reaction taking place was due to $AlCl_3$ and not to impurities.

Results and Discussion

The obtaining of the requisite thermal data required an analysis of a series of 31 transpiration experiments in the temperature range of 800–1000°K and at 25° temperature intervals (Table I). The flow rates were in the range 15–25 cc/min which were sufficient to establish equilibrium of the vapor species above the aluminum. Since there were no apparent differences in the equilibrium values obtained in this flow rate region, they were assumed to have established equilibrium.[8,9] The orifice in the cell prevented any appreciable back diffusion. The experimental data including $AlCl_3$ and Al weight losses and flow rates are presented in Table I.

Four transpiration studies[2,6,10] and a spectrographic study[4] gave results for the heat of reaction 1 in good agreement with those of the effusion experiments previously performed in this laboratory[7] for the reaction in the temperature range 930–1034°K. The equilibrium constants obtained from the effusion data were chosen as the basis of correcting the total weight loss for Al for this reaction. Also, the equilibrium for the dissociation of the dimer

$$Al_2Cl_6(g) = 2AlCl_3(g) \qquad (4)$$

was employed in correcting the $AlCl_3$ flow data.

The remainder of the Al weight loss could then be distributed between $AlCl_2$ and its dimer Al_2Cl_4. The appropriate reactions would be

$$2AlCl_3(g) + Al(l, s) = 3AlCl_2(g) \qquad (5)$$

(8) H. C. Ko, M. A. Greenbaum, and M. Farber, *J. Phys. Chem.*, **71**, 254 (1967).

(9) M. Farber, *J. Chem. Phys.*, **36**, 661 (1962).

(10) D. B. Rao and V. V. Dadape, *J. Phys. Chem.*, **70**, 1349 (1966).

Table I: Experimental Data for the Reaction of $AlCl_3$ Vapor and Al(s, l)

Temp, °K	Time, hr	Wt loss of $AlCl_3$, g	Wt loss of Al, mg	Flow of Ar, cc/hr	G-atoms of Ar/hr $(N_{Ar}) \times 10^2$	G-atoms of Al/hr (wt loss) $(N_{Al}) \times 10^5$
800	6.0	28.85	5.9	1338	5.48	3.643
800	6.0	47.95	8.7	1338	5.48	5.370
800	5.0	54.41	6.3	1440	5.91	4.670
800	5.0	34.10	4.0	1482	6.07	2.960
800	3.0	29.08	3.9	1030	4.22	4.820
800	0.67	11.00	1.7	1026	4.20	9.450
800	5.0	16.99	2.3	938	3.85	1.705
825	5.0	38.20	5.7	1338	5.48	4.220
825	5.0	28.05	4.6	1338	5.48	3.410
851	5.0	47.05	8.9	1060	4.34	6.590
851	4.5	36.33	6.0	1020	4.18	4.930
851	3.5	23.70	4.8	1092	4.47	5.070
875	4.0	36.90	7.8	1194	4.90	7.225
875	3.0	25.80	5.6	1194	4.90	6.910
875	5.0	29.05	6.2	912	3.74	4.600
901	4.0	24.22	7.3	1020	4.18	6.780
901	4.0	26.55	7.5	956	3.92	6.960
901	4.5	26.10	7.7	913	3.74	6.330
925	4.0	23.02	10.6	1194	4.90	9.82
925	4.0	19.66	9.2	1133	4.57	8.52
925	4.0	30.90	17.2	1338	5.48	15.94
949	5.0	11.07	7.7	1290	5.29	5.71
949	2.5	24.09	11.0	780	3.20	16.30
949	2.5	21.47	10.2	942	3.86	15.10
949	1.25	13.41	5.1	942	3.86	15.10
975	3.0	29.40	21.4	1338	5.48	26.42
975	4.0	22.33	15.5	1250	5.12	14.38
975	3.5	39.00	26.3	1338	5.48	27.85
975	3.0	26.80	19.7	1338	5.48	24.35
1000	4.0	30.65	29.9	1338	5.48	27.65
1000	4.0	39.45	38.9	1338	5.48	36.00

and

$$4AlCl_3(g) + 2Al(l, s) = 3Al_2Cl_4(g) \quad (6)$$

The partial pressures involved for the necessary equilibria were calculated from the weight loss data by means of the gas law equation

$$P = \frac{nRT_0}{V_0} \quad (7)$$

where n is the number of g-atoms of liquid or solid Al reacting in unit time with a given volume V_0 of transpiring gas at a pressure of 1 atm. This gas includes all species, *i.e.*, Ar, $AlCl_3(g)$, $Al_2Cl_6(g)$, and the products formed. T_0 is the ambient temperature. Thus the partial pressure of AlCl in atmospheres would be

$$P_{AlCl} = \frac{n_{AlCl}}{n_T} \quad (8)$$

where n_T is the total moles of gas in the transpiration mixture. A preliminary plot of the equilibrium constant for reaction 6 *vs.* $1/T$ based on the assumption that reaction 5 was negligible showed extreme curvature indicating a possible mixture of the two species $AlCl_2$ and Al_2Cl_4. Therefore, an iterative process was adopted for the solution of eq 5 and 6.

Combining equations 1, 4, 5, and 6, and their respective equilibrium constants, the equations were obtained

$$N_{Al_2Cl_6} = \frac{[(4 + K_4)N^T_{AlCl_3} + K_4N_{Ar}] \pm \sqrt{[(4 + K_4)N^T_{AlCl_3} + K_4N_{Ar}]^2 - 4(4 + K_4)(N^T_{AlCl_3})^2}}{2(4 + K_4)} \quad (9)$$

$$N_{AlCl_3} = N^T_{AlCl_3} - 2N_{Al_2Cl_6} \quad (10)$$

$$(N_{Al_{(l)}})^3 = \frac{(K_1)(N_{AlCl_3} - N_{Ar} + N_{Al_2Cl_6})^2(N_{AlCl_3})}{3.375} \quad (11)$$

$$(N_{Al_{(s)}})^3 = \frac{(K_5)(N_{AlCl_3} + N_{Ar} + N_{Al_2Cl_6})(N_{AlCl_3})^2}{27} \quad (12)$$

$$N_{Al_{(s)}} = N_{Al} - N_{Al_{(l)}} - N_{Al_{(s)}} \quad (13)$$

$$K_6 = \frac{3.375(N_{Al_{(s)}})^3(N_{AlCl_3} + N_{Ar} + N_{Al_2Cl_6})}{(N_{AlCl_3})^4} \quad (14)$$

where N_{Ar} = number of g-atoms of argon passed over sample in 1 hr; $N^T_{AlCl_3}$ = number of moles of $AlCl_3$ passed over sample in 1 hr; N_{Al} = total number of g-atoms of Al lost from sample in 1 hr; N_{AlCl_3}, $N_{Al_2Cl_6}$ = number of moles of respective gases formed as a result of the equilibrium and passed over the sample in 1 hr; $N_{Al_{(l)}}$ = number of g-atoms of Al lost per hour due to reaction 1. $N_{Al_{(s)}}$, $N_{Al_{(s)}}$ = number of g-atoms of Al lost per hour due to reactions 5 and 6, respectively. N_{AlCl}, N_{AlCl_2}, and $N_{Al_2Cl_4}$ had been omitted from the total number of moles of gas in the mixture because they were negligibly small compared to N_{AlCl_3}, $N_{Al_2Cl_6}$, and N_{Ar}.

The iteration was based on the assumption that for the proper distribution of weight loss between the two species straight lines would occur for the slopes representing the ΔH_r for the reactions represented by eq 5 and 6.

The first iteration assumed the estimated value in the JANAF tables[11] for $\Delta H_f°_{298}(AlCl_2(g))$ (-75.0 ± 20 kcal/mole). It was assumed that the estimated entropy for the triatomic molecule $AlCl_2$ was sufficiently accurate (within 3 eu) to allow free energy calculations for reaction 5, based on assumed values for the heat of formation of $AlCl_2(g)$. However, calculations showed that, choosing -75 kcal/mole for $\Delta H_f°_{298}(AlCl_2(g))$, the amount of Al required for reaction 5 under the temperature and pressure conditions in this study would be much greater than the actual weight loss of Al. For example, at 800°K reaction 5 would have consumed $\sim 3.4 \times 10^{-4}$ g-atom of Al while the actual loss of Al was only $\sim 3.6 \times 10^{-5}$ g-atom. Finally, only a value of -66 kcal/mole for $\Delta H_f°_{298}(AlCl_2(g))$ would make the proper corrections for the weight loss of Al which would result in a fairly straight slope when log K_6 was plotted against $1/T$. This value of -66 kcal/mole is very critical in that even a difference of 1 kcal would make the plot of log K_6 *vs.* $1/T$ have a pronounced curvature. For example, at 825°K a value of -66 kcal/mole for $\Delta H_f°_{298}(AlCl_2(g))$ yields 6.57×10^{-8} for K_6 where values of -65 and -67 yield 7.36×10^{-8} and 5.26×10^{-8} for K_6, respectively. This small difference could be within the uncertainty of the experimental data. However, at the other end of the temperature range, 975°K, a value of -66 kcal/mole yields 7.68×10^{-9} for K_6 while a value of -65 kcal/mole gives 2.31×10^{-8} for K_6 and a value of -67 kcal/mole gives 1.30×10^{-10} for K_6.

Thus at the low end of the temperature range investigated a change from -65 to -67 kcal/mole for the value of $\Delta H_f°_{298}(AlCl_2(g))$ produces only a change of approximately 1.3-fold in K_6. At the high end of the temperature range, however, the same change in $\Delta H_f°_{298}(AlCl_2(g))$ produces a 60-fold change in K_6. On this basis it can be concluded that well within the scatter of the data points the value of -66 ± 1 kcal for $\Delta H_f°_{298}(AlCl_2(g))$ is the only one which will satisfactorily explain the experimental data.

Table II presents the partial pressures and weight losses calculated for the species involved in the various equilibria. The equilibrium constants K_1 for reaction 1 are from the effusion experiments.[7] K_4 represents the equilibrium constant for reaction 4 and is calculated from free energy values of the JANAF tables.[11] K_5 is the equilibrium constant for reaction 5 based on a value of -66 kcal/mole for $\Delta H_f°_{298}(AlCl_2(g))$, specific heats, entropy of $AlCl_2(g)$, and the free energy of $AlCl_3(g)$. Finally, K_6 is the equilibrium constant for reaction 6 after corrections were completed for reac-

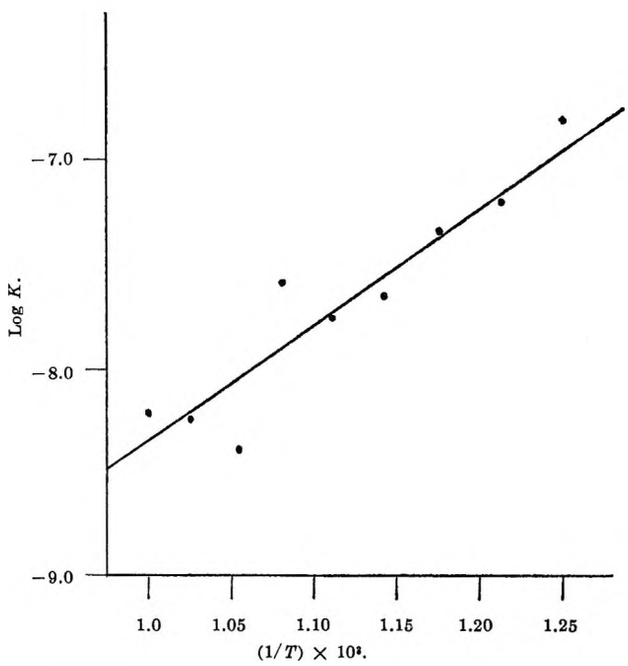

Figure 1. The logarithm of the equilibrium constant for the reaction $2Al(l, s) + 4AlCl_3(g) = 3Al_2Cl_4(g)$, as a function of the reciprocal temperature.

(11) "JANAF Thermochemical Tables," The Dow Chemical Co., Midland, Mich.

Table II: Equilibrium Data for the Reaction of $AlCl_3$ and Al

Temp, °K	K_4	$10^2 N_{AlCl_3}$ (per hr)	$10^3 N_{Al_2Cl_6}$ (per hr)	K_1	$10^6 N_{Al}$ (per hr due to reaction 1)	K_6	$10^6 N_{Al}$ (per hr due to reaction 5)	$10^6 N_{Al}$ (per hr due to reaction 6)	$10^8 K_6$	Av log K_6
800	0.199	1.335	11.40	4.37×10^{-14}	0.098	3.2×10^{-12}	0.119	3.433	34.20	
800	0.199	1.950	20.30	4.37×10^{-14}	0.131	3.2×10^{-12}	0.162	5.077	28.90	
800	0.199	2.490	28.45	4.37×10^{-14}	0.160	3.2×10^{-12}	0.205	4.306	7.89	
800	0.199	1.780	16.75	4.37×10^{-14}	0.128	3.2×10^{-12}	0.153	2.679	6.16	−6.84
800	0.199	2.120	25.80	4.37×10^{-14}	0.216	3.2×10^{-12}	0.168	4.436	12.98	
800	0.199	3.320	45.40	4.37×10^{-14}	0.184	3.2×10^{-12}	0.251	9.016	24.55	
800	0.199	0.937	8.09	4.37×10^{-14}	0.072	3.2×10^{-12}	0.084	1.550	9.12	
825	0.323	2.310	17.20	3.90×10^{-13}	0.289	1.446×10^{-11}	0.301	3.630	5.39	−7.23
825	0.323	1.814	12.03	3.90×10^{-13}	0.247	1.446×10^{-11}	0.246	2.917	6.57	
851	0.523	3.110	19.80	2.82×10^{-12}	0.613	6.31×10^{-11}	0.597	5.380	5.40	
851	0.523	2.740	16.60	2.82×10^{-12}	0.553	6.31×10^{-11}	0.532	3.845	2.92	−7.35
851	0.523	2.388	13.21	2.82×10^{-12}	0.511	6.31×10^{-11}	0.478	4.081	5.77	
875	0.845	3.690	16.25	1.70×10^{-11}	1.247	2.28×10^{-10}	1.055	4.923	2.22	
875	0.845	3.500	14.85	1.70×10^{-11}	1.197	2.28×10^{-10}	1.008	4.705	2.32	−7.66
875	0.845	2.418	9.76	1.70×10^{-11}	0.852	2.28×10^{-10}	0.706	3.042	1.98	
901	1.370	2.925	8.13	9.34×10^{-11}	1.720	8.42×10^{-10}	1.293	3.767	1.95	
901	1.370	3.154	9.23	9.34×10^{-11}	1.774	8.42×10^{-10}	1.352	3.861	1.57	−7.76
901	1.370	2.800	7.80	9.34×10^{-11}	1.608	8.42×10^{-10}	1.214	3.508	1.74	
925	2.000	3.168	5.76	4.57×10^{-10}	3.170	2.57×10^{-9}	2.020	4.630	2.88	
925	2.000	2.726	4.87	4.57×10^{-10}	2.820	2.57×10^{-9}	1.766	3.934	2.90	−7.59
925	2.000	4.144	8.33	4.57×10^{-10}	7.830	2.57×10^{-9}	2.580	5.530	2.02	
949	2.920	1.450	1.08	1.78×10^{-9}	3.345	7.4×10^{-9}	1.580	0.785	0.25	
949	2.920	5.254	9.98	1.78×10^{-9}	6.175	7.4×10^{-9}	4.150	5.980	0.90	−8.40
949	2.920	4.806	8.32	1.78×10^{-9}	6.210	7.4×10^{-9}	3.920	5.170	0.83	
949	2.920	5.892	10.94	1.78×10^{-9}	6.850	7.4×10^{-9}	4.690	3.560	0.14	
975	4.270	5.990	6.90	6.31×10^{-9}	11.830	2.2×10^{-8}	7.090	7.970	1.61	
975	4.270	3.534	3.33	6.31×10^{-9}	8.120	2.2×10^{-8}	4.505	1.745	0.10	−8.23
975	4.270	6.743	8.16	6.31×10^{-9}	12.880	2.2×10^{-8}	7.850	7.120	0.77	
975	4.270	5.494	6.13	6.31×10^{-9}	11.730	2.2×10^{-8}	6.580	6.040	0.95	
1000	6.250	5.028	3.66	2.0×10^{-8}	15.330	5.92×10^{-8}	8.450	3.870	0.33	−8.21
1000	6.250	6.365	5.23	2.0×10^{-8}	17.940	5.92×10^{-8}	10.310	7.750	1.18	

tions 1 and 5. Figure 1 presents a plot of the log of K_6 *vs.* $1/T$.

The ΔH_r and ΔS_r of reaction 6 were found to be -25.9 ± 3.7 kcal and -64.2 ± 4.2 cal/deg mole, respectively, at 900°K. This set of values is obtained from analysis of the average points. An analysis of all of the individual data points yields -28.0 ± 3.0 kcal and -66.5 ± 3.4 cal/deg for ΔH_r and ΔS_r of reaction 6, respectively. Analysis of the average data points yields values of -194.8 ± 1.2 kcal/mole and 116 ± 1.4 cal/deg mole for $\Delta H_f°_{900}$ and $S°_{900}$ for $Al_2Cl_4(g)$. A corresponding third-law heat of reaction could not be calculated since no value for the entropy of $Al_2Cl_4(g)$ is reported. However, the second-law entropy of 116 cal/deg mole is a reasonable value for a molecule of this size and structure.

It should be pointed out that the uncertainties quoted are statistical ones only and do not include those involved in other thermodynamic values that have been employed for the present calculations. The calculation of the heat of formation and entropy of $Al_2Cl_4(g)$ at 298°K is speculative since there are no reported heat capacities or spectroscopic data for this molecule. Employing rough estimates[12] for these functions, values for $\Delta H_f°_{298}$ of -194 ± 5 kcal/mole and $S°_{298}$ of 90 ± 5 cal/deg mole are obtained. Also, these estimates allow the calculation of heats and entropy of

(12) The estimated heat capacities of $Al_2Cl_4(g)$ at 298 and 900°K are 24 and 32 cal/deg mole, respectively. These estimates are based on an analogy of the similarity of the $Al_2Cl_4(g)$ to $B_2Cl_4(g)$ molecule. The heat capacity of $B_2Cl_4(g)$ at 298 and 900°K is reported as 22.7 and 29.2 cal/deg mole, respectively.[11]

dimerization for reaction 3 of −62 kcal and −47 cal/deg mole at 298°K, respectively. Comparison may be made to dimerization values for B_2Cl_4 of −77 kcal and −44 cal/deg mole for the heat and entropy, respectively. The thermodynamic functions for $AlCl_2(g)$ and $Al_2Cl_4(g)$ are presented in Table III.

Table III: Thermodynamic Data for $AlCl_2(g)$ and $Al_2Cl_4(g)$

$\Delta H_f°_{900}(Al_2Cl_4(g))$	−194.8 ± 1.2 kcal/mole
$S°_{900}(Al_2Cl_4(g))$	116 ± 1.4 cal/deg mole
$\Delta H_f°_{298}(Al_2Cl_4(g))$	−194 ± 5 kcal/mole[a]
$S°_{298}(Al_2Cl_4(g))$	90 ± 5 cal/deg mole[a]
$\Delta H_f°_{298}(AlCl_2(g))$	−66 ± 3 kcal/mole

[a] Estimated values.

Having obtained a fairly accurate value for $\Delta H_f°$ of $AlCl_2$, it was possible to obtain a check on the assumption of eq 1 for the effusion data. In the temperature range of the effusion experiments[7] for reaction 1 a ΔH_r of 95 kcal/mole was obtained. Employing a value of −66 kcal/mole for $\Delta H_f°_{298}$ of $AlCl_2(g)$, a ΔH_r at an average temperature of 900°K for reaction 5 of 86 kcal is calculated. Since the slopes for eq 1 and 5 differ by only 9 kcal, or 10%, curvature in reaction 1 would not be readily seen unless reaction 5 were contributing more than 10% to the Al weight loss. Therefore, in order to check the validity of the effusion experiments in the temperature range 850–1000°K, free energies (extrapolated from previous results at this laboratory)[7] were calculated for eq 2 at the highest and lowest temperatures, 850 and 1000°K. Since the amounts of $AlCl_2(g)$ in equilibrium with AlCl and $AlCl_3$ range from only 5 to 8% over this temperature range, the validity of the effusion experiments is further established. However, it would appear that at atmospheric pressure transpiration experiments would involve considerable quantities of both AlCl and $AlCl_2$.

Summary

The experimental transpiration studies together with the analytical treatment present an attempt to define the vapor species in the complex equilibrium system formed as a result of the reaction of $AlCl_3(g)$ and Al(l, s). This analysis allows the calculation of thermodynamic data for the previously unreported species $AlCl_2(g)$ and $Al_2Cl_4(g)$. The data obtained are consistent with the previously reported transpiration and effusion data for AlCl(g).

NOTES

Crystalline Transition of Cyclohexanesulfamic Acid

by S. D. Bruck[1] and N. R. Stemple

Thomas J. Watson Research Center, International Business Machines Corporation, Yorktown Heights, New York 10598
(Received August 19, 1966)

The object of this note is to report the existence of a monoclinic–orthorhombic transition occurring at about room temperature in the well-known sweetening agent cyclohexanesulfamic acid, $C_6H_{11}NHSO_3H$. This observation is supported by X-ray diffraction and calorimetric data.

Experimental Section

Oscillation and Weissenberg photographs using Cu Kα radiation were taken at ~20 and ~40° to determine the lattice parameters and symmetry of each phase. Cooling was accomplished by blowing a stream of cooled nitrogen gas on the crystal during the X-ray exposures. Heating was done with an infrared heat lamp with approximate temperatures measured by a thermometer.

Calorimetric studies were carried out with a Perkin-Elmer differential scanning calorimeter, DSC-1B. The operational principles of this instrument in comparison to classical adiabatic calorimetry have already been

(1) Chemical Engineering Department, The Catholic University of America, Washington, D. C. 20017.

described.[2] Recently, several investigators reported dsc data of high a degree of accuracy and reproducibility with organic,[3] polymeric,[4,5] and inorganic materials.[6] The 10–15-mg samples of cyclohexanesulfamic acid (K & K Laboratories, Inc., Plainview, N. Y.) were weighed on a Cahn electronic microbalance, enclosed in aluminum pens, and blanketed with dry nitrogen at constant flow rate. The instrument was first calibrated with pure standards at the same heating rate that was used with the test samples. The area under the endotherm is proportional to the number of calories involved in the transition. As is the common practice in differential thermal analysis (dta), a straight line was constructed between the onset (269°K) and conclusion (308°K) of the endotherm, and the area under the curve was measured by a planimeter. Since in this treatment the instrumental base line is ignored, the small heat capacity effects which may remain have been estimated to be less than the instrumental and integrating errors.[3]

Result and Discussion

Table I summarizes the crystallographic data at ~20° and at ~40° as obtained from X-ray diffraction measurements. The results indicate that a monoclinic–orthorhombic transition has occurred. The monoclinic form exhibits systematic absences for (*h*0*l*) reflections with *h* odd, and therefore is assigned to the space group P2/a-C_{2h}^4 or Pa-C_s^2, whereas the orthorhombic structure has additional systematic absences for (0*kl*) with *l* odd, and therefore belongs to the space group Pca2_1-C_{2v}^5 or Pcam-D_{2h}^{11}. The space group Pcam requires a disordered arrangement of the molecules. X-ray diffraction photographs indicate that single crystals of cyclohexanesulfamic acid cooled below the transition temperature show a strong tendency to twin on the (100) plane with a common *b* axis. This is observed for all crystals on an (*h*0*l*) Weissenberg photograph by a doubling of all (*h*0*l*) reflections, except (*h*00), representing the two twin orientations. The separation of the (00*l*) reflection, being twice the deviation of β from 90°, allows an accurate measurement of β to be made. Since diffraction from each twin orientation was separable, the systematic extinctions could easily be determined for the monoclinic form.

The monoclinic–orthorhombic transition of cyclohexanesulfamic acid is also supported by thermodynamic data obtained by differential scanning calorimetry. An anomalous absorption of heat is observed over the temperature range 269–380°K which is characterized by a peak at 300.5 ± 1°K. The area under the endotherm between 269 and 308°K represents an energy of 300 ± 15 cal/mole with an entropy increment of 1.00 ± 0.05 cal deg^{-1} mole^{-1}.

Table I: Crystallographic Data on Cyclohexanesulfamic Acid

Crystallographic parameters	Temp, °C ~20° (monoclinic)	~40° (orthorhombic)
Unit cell edge, *a*	9.517 ± 0.002 A	9.496 ± 0.002 A
Unit cell edge, *b*	11.210 ± 0.002 A	11.272 ± 0.002 A
Unit cell edge, *c*	8.201 ± 0.002 A	8.202 ± 0.002 A
Unit cell angle, β	90.9° ± 0.1	90.0°
Unit cell volume, *V*	874.9 A^3	877.9 A^3
Space group	P2/a-C_{2h}^4 or Pa-C_s^2	Pca2_1-C_{2v}^5 or Pcam-D_{2h}^{11}
No. of molecules per unit cell, *Z*	4	4

Acknowledgments. The authors appreciate the discussions with Dr. Y. Okaya and the technical assistance of Mr. A. R. Taranko.

(2) (a) M. J. O'Neill, *Anal. Chem.*, **36**, 1238 (1964); (b) E. S. Watson, M. J. O'Neill, J. Justin, and N. Brenner, *ibid.*, **36**, 1233 (1964).

(3) E. M. Barrall, II, R. S. Porter, and J. F. Johnson, *J. Phys. Chem.*, **71**, 1224 (1966).

(4) F. E. Karasz and J. M. O'Reilly, *J. Polymer Sci.*, **B3**, 561 (1965).

(5) L. Mandelkern, J. G. Fatou, R. Denison, and J. Justin, *ibid.*, **B3**, 803 (1965).

(6) J. Block and A. P. Gray, *Inorg. Chem.*, **4**, 304 (1965).

Association in Vapor of Ionic Salts. Vapor Density of Rubidium Bromide and Cesium Bromide

by K. Hagemark and D. Hengstenberg

North American Aviation Science Center, Thousand Oaks, California 91360 *(Received February 8, 1967)*

Previously, Datz, Smith, and Taylor[1] have published vapor density data for NaCl, KCl, and RbCl, CsCl, NaBr, NaI, and KI. More recently, vapor density data for KBr have been reported.[2] The deviation from ideal gas behavior could be accounted for by assuming monomers and dimers in the vapor phase. Blander[3]

(1) (a) S. Datz, W. T. Smith, Jr., and E. H. Taylor, *J. Chem. Phys.*, **34**, 558 (1961); (b) S. Datz and W. T. Smith, Jr., *J. Phys. Chem.*, **63**, 938 (1959).

(2) K. Hagemark, M. Blander, and E. B. Luchsinger, *ibid.*, **70**, 276 (1966).

(3) M. Blander, *J. Chem. Phys.*, **41**, 170 (1964).

Table I: Experimental Data for Pressure–Temperature Relation for RbBr and CsBr

Density, mole/l.	Temp, °K	Pressure, mm
	RbBr	
3.680×10^{-4}	1366	28.60
	1410	30.49
	1376	28.91
	1339	27.48
	1310	26.74
	1397	29.71
5.049×10^{-4}	1352	37.43
	1421	41.55
	1392	40.15
	1336	36.74
	1307	34.97
	1375	39.10
	CsBr	
3.726×10^{-4}	1384	30.71
	1421	32.02
	1313	28.27
	1347	29.28
5.752×10^{-4}	1419	47.86
	1364	45.51
	1317	43.06
4.188×10^{-4}	1373	33.96
	1421	35.72
	1406	35.10
	1348	33.05
	1298	31.32

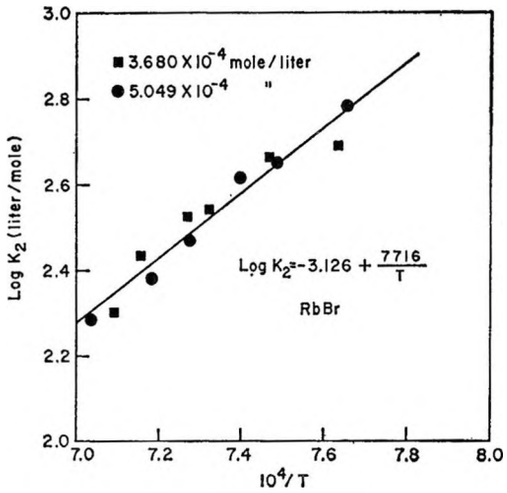

Figure 1. Dimerization constant, K_2, for the equilibrium $2RbBr \rightleftarrows Rb_2Br_2$.

desiccator over P_2O_5. Single crystals of RbBr and CsBr were prepared in an argon atmosphere from fused crystalline material from Electronic Space Products, Inc. All RbBr experiments were carried out with the single crystal material, whereas the CsBr single crystal material was used only as a check of the results from the 99.99% powder.

The dimerization constant is calculated from the equation

$$K_2 = R^*T\frac{p_2}{p_1^2}$$

Table II: Predicted and Measured Values of the Thermodynamic Properties of RbBr and CsBr

	d[a]	Log K_2 (1300°K)		ΔE_2, kcal/mole		ΔS_p,[b] eu	
		Exptl	Calcd	Exptl	Calcd	Exptl	Calcd
RbBr	2.9447	2.82	2.95	−35	−37.0	−26	−26.6
CsBr	3.0722	2.45	2.68	−28	−35.5	−22	−26.4

[a] S. H. Bauer and R. F. Porter in "Molten Salt Chemistry," M. Blander, Ed., Interscience Publishers, Inc., New York, N. Y., 1964, p 642. [b] The standard states for ΔS_p are the ideal gas at 1 atm.

has found the calculated dimerization constants to be in excellent agreement with a dimensional theory of association in ionic vapors.

In the present work, measurements of the pressure–temperature relation at constant density were made for the vapor phase of RbBr and CsBr. The apparatus was a modification of the liquid gold isotensoscope of Datz, *et al.*[1] Both the apparatus and the experimental procedure are described in a previous paper.[2] The cesium bromide was 99.99% pure reagent grade, crystalline powder from Matheson Coleman and Bell. It was heated at 130° for 2 hr and then stored in a vacuum

where R^* is in l. atm deg^{-1} mole^{-1}, and T is the absolute temperature. p_1 and p_2 are the partial pressures of monomer and dimer, respectively, and are calculated from

$$p_1 = 2p_T - p_{id}$$

$$p_2 = p_{id} - p_T$$

where p_T is the observed pressure and p_{id} is the pressure one would find if there were no association.

The experimental data are given in Table I, and the calculated dimerization constants are shown as a func-

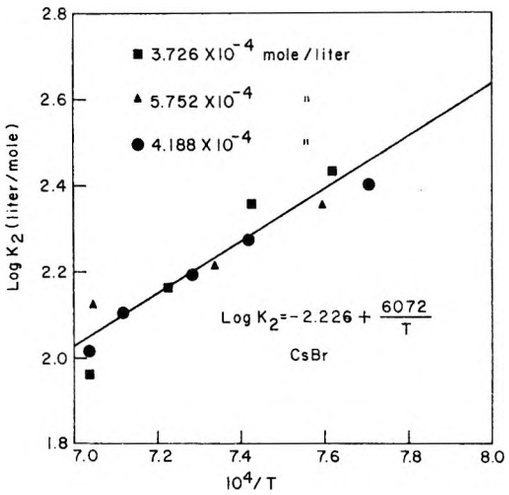

Figure 2. Dimerization constant, K_2, for the equilibrium $2CsBr \rightleftarrows Cs_2Br_2$.

tion of temperature in Figures 1 and 2. The measured and predicted values for the association constant as well as the energy, ΔE_2, and entropy, ΔS_p (standard state is the ideal gas at 1 atm), of association are given in Table II. The agreement between theoretical[3] and experimental values for the dimerization constant is very good. The dimensional theory correctly predicts the dimerization constant to decrease with increasing internuclear distance, d. Because of the narrow temperature range of the measurements, the experimental values for the energy and entropy of dimerization are less precise than the corresponding association constant.

Acknowledgments. The authors wish to thank Dr. M. Blander for his valuable suggestions, Mr. J. Mohl for supplying the single crystals of RbBr and CsBr, and Mr. E. Eisel for constructing the fused silica apparatus.

Xenon Dioxide Difluoride: Isolation and Some Properties

by J. L. Huston

Department of Chemistry, Loyola University, Chicago, Illinois 60626 *(Received March 13, 1967)*

During the early development of xenon chemistry, mass spectra[1] were observed of two oxyfluorides, $XeOF_4$ and XeO_2F_2, which had been made by mixing water with XeF_6. Their formation was ascribed to stepwise hydrolysis of XeF_6. Since then $XeOF_4$ has been isolated[2] and its properties have been studied, but attempts to prepare and isolate XeO_2F_2 in substantial quantity by partial hydrolysis of XeF_6 or by partial reaction of XeF_6 with glass have not been successful.[3] (In both cases the ultimate reaction product is XeO_3.)

It has now been found, during a mass spectrographic study of the chemical properties of xenon compounds, that the reaction of XeO_3 and $XeOF_4$ provides a convenient method for preparation of xenon dioxide difluoride, permitting the compound to be isolated and some of its properties to be observed. It has also been found that the reaction of XeO_3 and XeF_6 produces $XeOF_4$.

An aqueous solution of XeO_3 is placed in a Kel-F tube fitted with a valve and, after pumping to remove water, the solid is gently warmed with a portable air blower. $XeOF_4$ (or XeF_6) in excess is distilled onto the XeO_3, using Dry Ice rather than liquid nitrogen to effect the distillation in order to minimize the chance of detonating the XeO_3 by thermal shock. The valve is closed and the tube is allowed to remain overnight for dissolution of the solid XeO_3 to occur. The result is a homogeneous liquid mixture of XeO_2F_2, $XeOF_4$, and XeF_2 which is subjected to fractional distillation in a Kel-F line, purification of the XeO_2F_2 being followed mass spectrographically with a Bendix time-of-flight instrument. $XeOF_4$ is readily removed because of its volatility. XeF_2 is removed with greater difficulty from the less volatile XeO_2F_2; as it is removed, those portions of the mass spectrum due to XeO_2F_2 alone are enhanced relative to those portions due to both

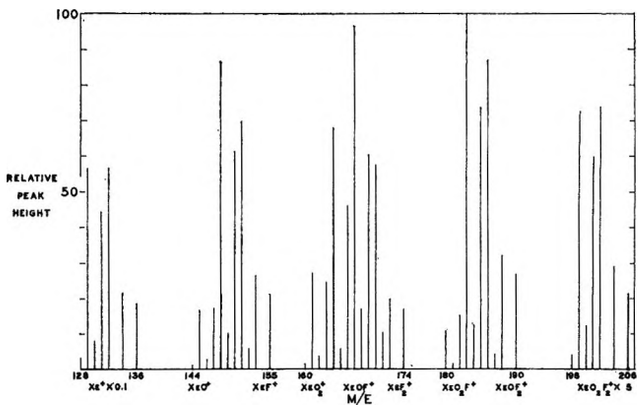

Figure 1. Positive ion mass spectrum of XeO_2F_2. Electron energy 70 ev, pulsed electron beam. Source pressure *ca.* 5×10^{-6} torr.

(1) M. H. Studier and E. N. Sloth, "Noble-Gas Compounds," H. Hyman, Ed., University of Chicago Press, Chicago, Ill., 1963, p 47.

(2) C. L. Chernick, H. H. Claassen, J. G. Malm, and P. L. Plurien, ref 1, p 106.

(3) *E.g.*, M. H. Studier and J. L. Huston, unpublished results.

XeO_2F_2 and XeF_2. In particular, the ratio of the peak at m/e 164 ($Xe^{132}O_2^+$ and $Xe^{129}OF^+$) to the peak at m/e 170 ($Xe^{132}F_2^+$) rises to a limiting value of 1.2 and at the same time the ratio of the peak at m/e 183 ($Xe^{129}OF_2^+$ and $Xe^{132}O_2F^+$) to the peak at m/e 170 ($Xe^{132}F_2^+$) rises to a limiting value of 1.7. These ratios are believed to be characteristic of pure XeO_2F_2.

Figure 1 shows the quantitative positive ion mass spectrum, presented in the form of a bar graph derived from spectral scans and normalized to a peak height of 100 for m/e 183. From this can be derived the following fragmentation pattern where the intensity of the XeO^+ is set equal to 1.0.

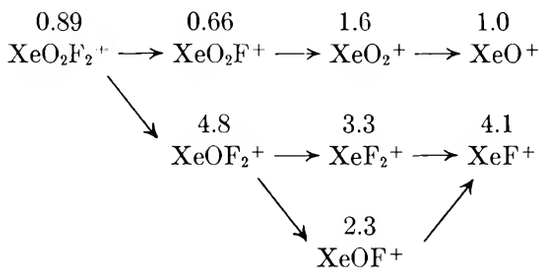

A number of scans have been examined for any significant fluctuations in the intensities of XeO^+, XeO_2^+, and $XeOF_2^+$ relative to the rest of the spectrum which would indicate the presence of XeO, XeO_2, or $XeOF_2$ in the XeO_2F_2 or their formation in the mass spectrometer. No such evidence for their independent existence has been found.

Intensity of Xe^+ relative to the rest of the spectrum is not reproducible, depending on xenon background in the line and in the mass spectrometer.

The negative ion mass spectrum of XeO_2F_2 was observed qualitatively as shown (Figure 2) in a photograph of an oscilloscope display; it consists of XeF^-, XeF_2^- and $XeOF^-$. No heavier ions could be observed even though a Studier blanking circuit[4] was used to eliminate XeF_2^- and lighter ions, thereby preventing saturation of the electron multiplier of the mass spectrometer and maximizing the chance of observing any heavier ions. Similarity of the negative ion mass spectrum of $XeOF_4$ should be noted where Studier and Sloth[1] observed XeF^-, XeF_2^-, XeF_3^-, XeF_4^-, and $XeOF_3^-$. The spectra of these oxyfluorides appear to emphasize the electronegativity of fluorine.

Xenon dioxide difluoride at room temperature forms colorless crystals (Figure 3) which have a vapor pressure between that of XeO_3 and $XeOF_4$ and which grow by sublimation. A purified sample melts at 30.8° to give a colorless liquid: no color change like that observed in XeF_6 occurs.[5] Gillespie has suggested[6] that XeO_2F_2 may polymerize by formation of Xe–O–Xe bridges, but no higher melting low volatility material has yet been observed. The melting point is lowered by the presence of XeF_2 impurity, *e.g.*, a sample whose 183/170 ratio was only 1.25 melted over the range 29.5–30.5°.

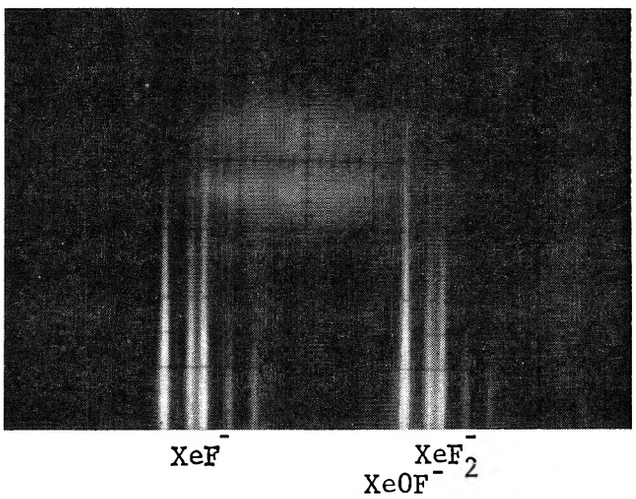

Figure 2. Negative ion mass spectrum of XeO_2F_2. Electron energy 70 ev, continuous electron beam. Source pressure *ca.* 1×10^{-5} torr (value fully open between sample and source.)

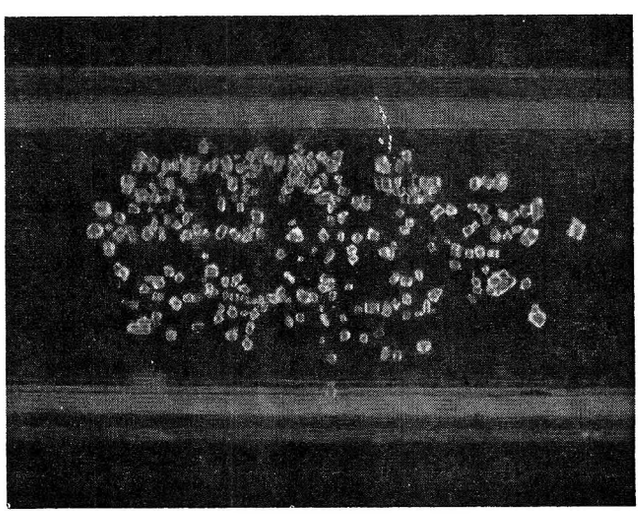

Figure 3. Crystals of XeO_2F_2 deposited by sublimation on the inside of a Kel-F tube.

XeO_2F_2 can decompose to XeF_2 and O_2, the rate de-

(4) M. H. Studier, Argonne National Laboratory, unpublished results. Presented at the Bendix Symposium on Time of Flight Mass Spectrometry, Cincinnati, Ohio, 1965.

(5) J. G. Malm, H. Selig, J. Jortner, and S. A. Rice, *Chem. Rev.*, **65**, 207 (1965).

(6) J. R. Gillespie, "Noble-Gas Compounds," H. Hyman, Ed., University of Chicago Press, Chicago, Ill., 1963, p 333.

pending on previous conditioning of the containing apparatus. A sample kept in a Kel-F tube well conditioned by $XeOF_4$ showed no appreciable decomposition in 2 days at room temperature, but other samples have shown marked production of XeF_2 in less well-conditioned apparatus. It reacts with XeF_6, with liquefaction, to produce $XeOF_4$, the reaction being rather slow. Production of $XeOF_4$ has also been observed in Kel-F apparatus overly conditioned by XeF_6.

XeO_2F_2 exposed to moist air rapidly hydrolyzes to XeO_3, but a faint ozone-like odor can be discerned, somewhat reminiscent of the odor of xenon tetroxide.

Chemical analysis confirming the identity of the compound was effected by distilling it into a silica container and decomposing it by heating to 300°. The stoichiometry of such decomposition of a xenon fluoride, oxide, or oxyfluoride in silica will fix the oxidation state of the xenon and the fluorine content of the compound in terms of the relative amounts of xenon, oxygen, and silicon tetrafluoride produced. The validity of the procedure was verified by similarly decomposing a sample of carefully purified $XeOF_4$.

$$XeOF_4 \xrightarrow{SiO_2} 1.0Xe + 1.5O_2 + 1.0SiF_4 \quad \text{(calculated)}$$
$$\longrightarrow 1.0Xe + 1.5O_2 + 0.9SiF_4 \quad \text{(found)}$$
$$XeO_2F_2 \xrightarrow{SiO_2} 1.0Xe + 1.5O_2 + 0.5SiF_4 \quad \text{(calculated)}$$
$$\longrightarrow 1.0Xe + 1.5O_2 + 0.45SiF_4 \quad \text{(found)}$$

The mixtures of Xe, O_2, and SiF_4 were analyzed mass spectrographically, with relative sensitivities to the three gases calibrated by means of a known mixture.

Further confirmation has been provided by a preliminary study of the Raman and infrared spectra of the solid[7] which are consistent with the pseudo-trigonal bipyramidal structure predicted by Gillespie,[6] a molecule of symmetry C_{2v}. One strong Raman band at 537 cm^{-1} and an infrared band at 610 cm^{-1} can be assigned, respectively, to symmetrical and unsymmetrical stretching of a linear or near-linear F–Xe–F, and strong Raman bands at 851 and 882 cm^{-1} can be assigned to Xe–O stretching.[8]

Acknowledgment. The author wishes to thank Mr. John Schmieg for technical assistance.

(7) H. H. Claassen and J. L. Huston. Further details will be published.

(8) NOTE ADDED IN PROOF. Since submission of this note, one sample of XeO_2F_2 has exploded. It was contained in a Kel-F tube fitted with a Kel-F needle valve, and exploded while the valve was being closed. The sample contained a small amount of XeO_3 which may have acted as a detonator, but the force of the explosion was too great to have been due to the XeO_3 alone. Evidently, while XeO_2F_2 is more stable than XeO_3, it should be handled with the same precautions.

^{17}O Hyperfine Splitting in a μ-Amido-μ-peroxodicobalt Complex[1]

by John A. Weil and Judith K. Kinnaird

Argonne National Laboratory, Argonne, Illinois
(Received March 20, 1967)

We have prepared a sample of μ-amido-μ-peroxobis(tetraamminecobalt)tetranitrate, enriched to contain 11.7% of its bridging oxygen as ^{17}O, and have obtained its solution esr spectrum (Figure 1), taken at X-band and room temperature. In addition to the primary 15 lines arising from the hyperfine contribution of the two equivalent ^{59}Co nuclei (g = 2.0341, $|A_{Co}|$ = 12.43 oersteds),[2,3] weak secondary lines from molecules containing one ^{17}O atom in the bridge are visible in the wings; no further peaks lying beyond these lines were observable either in ordinary spectra or in spectra taken with use of a CAT. We conclude that the outer two secondary lines arise from $m_{^{17}O} = \pm {}^5/_2$ transitions split due to hyperfine interaction with the cobalt nuclei, whereas the other observed secondary lines result from superpositions of $m_{^{17}O} = \pm {}^5/_2$ and $\pm {}^3/_2$ lines. The measured spacings of the outer two lines were 12.3 and 12.9 oersteds at the low-field and high-field ends, respectively, and thus are equal to $|A_{Co}|$ within experimental error (±0.5 oersted). This assignment of lines gave the oxygen coupling constant as $|A_O|$ = 22.5 ± 0.3 oersteds. A computer-calculated spectrum using g, $|A_{Co}|$ and $|A_O|$ and a Lorentzian first derivative line width of 5.8 oersteds gave good agreement with the observed spectrum.

Comparison of the heights of the lowest-field secondary peak and primary peak yielded the ratio 0.039, in exact agreement with the value calculated from the nominal ^{17}O abundance.

Observation of the large ^{17}O splitting affords the first direct evidence that the unpaired electron is actually shared by the cobalt atoms *via* the oxygen bridge, rather than through direct overlap of cobalt orbitals or *via* the amido bridge. The latter mechanisms have seemed less probable because of the large Co–Co distance (3.24 A) and lack of resolved ^{14}N hyperfine structure in the esr spectrum, as well as on theoretical grounds.

It is of particular interest to compare our results

(1) Based on work performed under the auspices of the U. S. Atomic Energy Commission.

(2) E. A. V. Ebsworth and J. A. Weil, *J. Phys. Chem.*, **63**, 1890 (1959).

(3) M. Mori, J. A. Weil, and J. K. Kinnaird, *ibid.*, **71**, 103 (1967).

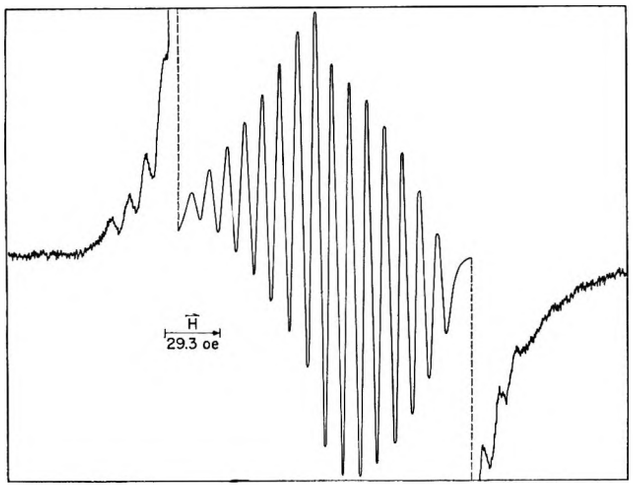

Figure 1. The esr spectrum (9516 Mc/sec) of μ-amido-μ-peroxobis(tetraammmecobalt) (4+) ions containing 11.7% ^{17}O, taken at room temperature in very dilute HNO_3. The detection sensitivity was decreased by a factor of 32 when scanning the central portion to display the primary 15-line cobalt hfs from the unlabeled ions.

with those for the O_2^- ion. From a single crystal determination of the g tensor,[4,5] we note that the deviations from the free-electron g are considerably smaller than those of O_2^- in alkali halides,[6] and that the principal values are far from uniaxial. If the electron could be considered to be situated primarily on the peroxo bridge in our ion, this would imply that the splitting $\Delta = E(2p\pi_{gy}) - E(2p\pi_{gz})$ ($x \parallel$ O–O, see ref 6) is much larger than the effective spin-orbit splitting λ. This is reasonable for the known[7,8] planar configuration

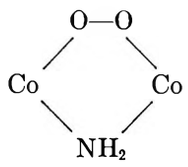

of our ion (we taken $x \parallel$ O–O and $z \perp$ ring plane). The O–O bond distance here is 1.32_0 A,[7] whereas it is in the range 1.32–1.35 A in O_2^-.[9] For $|\Delta/\lambda| >> 1$, we assume the relation $|A_{^{17}O}| = |8\pi/3\ \beta_N g_N\ \Psi^2(O)|$ to be meaningful and thus estimate $|\Psi(O)|^2 = 0.7 \times 10^{-24}$ cm^{-3}.[10] This approximation is not tenable for O_2^-, for which a more elaborate analysis[11] of the ^{17}O splittings has been carried through and has led to the value $|\Psi(O)|^2 = 0.64 \times 10^{-24}$ cm^{-3}. Comparison of these values suggests that the peroxo bridge can reasonably be thought of as a modified superoxide ion. It is of interest also to note that splitting of the states $2p\pi_{gy}$ and $2p\pi_{gz}$ (which are degenerate for free O_2^-) occurring as a result of asymmetric positioning of neighboring atoms will cause increased stability in this three-electron system (*cf.* ref 9).

No correct and detailed quantum-chemical model for any dicobalt peroxo ion has yet been published. Since the CoO_2Co system is planar, a first approximation to a ground-state molecular orbital can reasonably be taken as

$$(3d_t)_{Co(a)} + (2p\pi z)_{O(a)} - (2p\pi z)_{O(b)} - (3d_t)_{Co(b)}$$

However, this wave function has a nodal plane at the nuclei and can thus yield only vanishing values of $|\Psi(O)|^2$. Thus, just as in O_2 and in several nitrogen oxides,[12] it will be necessary to invoke configuration interaction, mixing in excited states containing unpaired σ electrons, to estimate the ^{17}O (and ^{59}Co) coupling constants.

The marked stability of the dicobalt peroxo complexes may well be explained if the energies of the oxygen $2p\pi z$ orbitals and the cobalt $3d_t$ orbitals happen to be very close.

The preparation of the dibridged complex was carried out in a closed reaction vessel from 1.7 g of $Co(NO_3)_2$ in ammoniacal solution, treated with labeled O_2 (100 cc at STP) at room temperature, to form μ-peroxobis(pentaamminecobalt)tetranitrate. Subsequently, after treatment at 35° with a mixture of NH_4OH and KOH to cause amido bridging, oxidation at ~0° with $(NH_4)_2Ce(NO_3)_6$, and separation of the products, recrystallization yielded 0.03 g of the desired dibridged complex. The synthesis is essentially a scaled-down version of

(4) J. A. Weil and G. L. Goodman, *Bull. Am. Phys. Soc.*, [2] **6**, 152 (1961); the principal g values reported for the closely analogous ethylenediamine complex ion are 2.079 (x), 2.023 (y), and 2.010 (z).

(5) J. A. Weil, G. L. Goodman, and H. G. Hecht, "Proceedings of the 1st International Conference on Paramagnetic Resonance, Jerusalem, July 1962," Vol. II, Academic Press Inc., New York, N. Y., 1963, p 880.

(6) W. Känzig and M. H. Cohen, *Phys. Rev. Letters*, **3**, 509 (1959); the principal g values reported are 2.4350 (x), 1.9512 (y), and 1.9551 (z).

(7) G. G. Christoph, R. E. Marsh, and W. P. Schaefer, private communication. In work already published (W. P. Schaefer and R. E. Marsh, *J. Am. Chem. Soc.*, **88**, 178 (1966)), it was shown that the CoO_2Co system in single-bridged complexes is also planar.

(8) Because the X-ray studies have now shown the ring to be planar, it appears likely that the postulate of cocking of the O–O bridge out of the Co–N–Co plane discussed in ref 5 is not correct, since this was based merely on the observation of small deviations from uniaxial behavior of the two cobalt hyperfine tensors, obtained from a rather difficult analysis of the complex epr spectra.

(9) F. Halverson, *Phys. Chem. Solids*, **23**, 207 (1962).

(10) Similarly, $|\Psi(O)|^2 = 0.22 \times 10^{-24}$ cm^{-3} at each cobalt nucleus.

(11) H. R. Zeller, R. T. Shuey, and W. Känzig, "Colloque sur les Centres Colorés dans les Cristaux Ioniques, Paris, March 1967," to be published. The present authors thank H. R. Z., *et al.*, for several helpful private communications and use of the results on O_2^- in advance of publication.

(12) J. C. Baird, *J. Chem. Phys.*, **37**, 1879 (1962), and references therein.

the one to be described in a future publication.[13] The esr spectra were taken in saturated solutions of the complex in dilute acid (1 drop of HNO_3/150 cc of H_2O).

Observation of ^{17}O hyperfine structure in μ-peroxo-bis(pentaamminecobalt) (5+) ions is much more difficult than for the dibridged (4+) ion discussed herein, as a result of the much smaller solubility and broader epr lines of the former. However, attempts to carry out such measurements are in progress.

(13) M. Mori, J. A. Weil, and M. Ishiguro, submitted for publication.

The Reactions of Hydrogen Atoms with Simple Thiols

by Robert R. Kuntz

Department of Chemistry, University of Missouri, Columbia, Missouri 65201 *(Received January 30, 1967)*

The photolysis of simple thiols in the gas phase results in the production of H atoms and thiyl radicals.[1] Several investigators[2,3] have studied reaction of these H atoms with the parent compound by the competition technique involving reactions 1–3. A steady-state

$$RSH + h\nu \longrightarrow RS + H \quad (1)$$

$$H + RSH \longrightarrow H_2 + RS \quad (2)$$

$$H + C_2H_4 \longrightarrow C_2H_5 \quad (3)$$

derivation involving H atom reactions leads to eq I,[2,3] where $R_{H_2}^0$ and $R_{H_2}^s$ are the rates of hydrogen production in the absence and presence of scavenger ethylene. Rate constant ratio values of 1.6[2] and 1.7[3] have been obtained for H_2S and methyl mercaptan, respectively. The present study uses a similar technique to measure this rate constant ratio for ethyl, *n*-propyl, and *n*-butyl mercaptans in order to determine the effect of substituents on the rate of H-atom removal from the thiol group.

$$\frac{R_{H_2}^s}{R_{H_2}^0 - R_{H_2}^s} = \frac{k_2[RSH]}{k_3[C_2H_4]} \quad (I)$$

Experimental Section

Hydrogen sulfide (>99.5%), ethane (>99.0%), ethylene (>99.5%), and methyl mercaptan were obtained from Matheson and used without purification except for bulb-to-bulb distillation. Gas chromatographic analysis of the ethane showed 0.1% ethylene present. Ethyl, *n*-propyl, and *n*-butyl mercaptans (Eastman) were used without further purification. Care was taken to exclude mercury vapor from the reaction during transfer and analysis by use of a series of liquid air traps. Pressure measurements were made with a mechanical diaphragm gauge. The reaction cell, low-pressure mercury light source providing 2537-A light, and analysis system have been described previously.[4] Sample decomposition was usually restricted to less than 1% to avoid complications from secondary products. All photolyses were performed at 24°.

Results and Discussion

Table I summarizes the results of this study. For H_2S, the ratio k_2/k_3 is seen to be pressure independent over the range of 8–35 cm total pressure and 5–10 cm H_2S pressure with an average value of 2.1 ± 0.1. Darwent and Roberts[2] reported a value of 1.6 and also noted the pressure independence.

The apparent rate constant ratios for the mercaptans all show a strong dependence on total pressure with the value remaining constant within experimental error over the low-pressure range, then decreasing rapidly after a few centimeters of pressure (depending on the particular mercaptan used). In order to investigate this effect, several runs were made in which the pure mercaptan or a constant mercaptan–ethylene mixture was photolyzed over a pressure range effected by the addition of ethane to the system. Ethane is relatively inert to H atom attack in the presence of the more reactive H atom donor mercaptans. These results are shown in Table II. A comparison of the relative rates of hydrogen evolution in the photolysis of methyl mercaptan with and without added ethylene is shown in Figure 1. It is seen that the apparent decrease in the rate constant ratio is due to the pressure-induced decrease in hydrogen production. Pressure effects have not been noticed in the previous studies of methyl mercaptan photolysis using the full mercury arc and pressure up to 30 cm.[3] Several reasonable possibilities for this effect seem to be excluded from the data presented. These are as follows.

(i) There are H atom scavenging impurities in the ethane used for pressurization. To explain the entire decrease in hydrogen yield exhibited in Figure 1, one can calculate, using reasonable rate constants, that 2.4%

(1) J. G. Calvert and J. N. Pitts, Jr., "Photochemistry," John Wiley and Sons, Inc., New York, N. Y., 1966, pp 490, 491.

(2) B. deB. Darwent and R. Roberts, *Proc. Roy. Soc.* (London), **A216**, 344 (1953).

(3) T. Inabe and B. deB. Darwent, *J. Phys. Chem.*, **64**, 1431 (1960).

(4) R. R. Kuntz, *ibid.*, **69**, 2291 (1965).

Table I

P_{RSH}, cm	$P_{C_2H_4}$, cm	$10^9 R_{H_2}$, moles/sec	k_2/k_3
	H_2S		
5.05	0	1.41	...
5.05	3.55	1.04	1.98
5.05	5.68	0.93	2.18
5.05	9.30	0.77	2.26
5.05	14.90	0.60	2.18
5.05	22.00	0.46	2.11
10.1	0	2.84	...
10.1	8.67	1.91	1.77
10.1	12.35	1.80	2.11
10.1	17.47	1.52	1.98
10.1	24.6	1.40	2.36
		Av = 2.1 ± 0.1	
	CH_3SH		
5.05	0	22.6	...
5.05	2.70	18.7	2.47
5.05	4.83	14.0	1.58
5.05	7.30	12.2	1.75
5.05	11.0	9.37	1.58
5.05	16.2	6.77	1.38
5.05	24.1	5.15	1.41
	C_2H_5SH		
4.97	0	21.1	...
4.97	3.90	15.0	1.94
4.97	6.60	12.2	1.83
4.97	8.65	11.0	1.91
4.97	11.9	9.0	1.76
4.97	17.9	6.4	1.57
	n-C_3H_7SH		
3.98	0	16.5	...
3.98	2.34	13.6	2.75
3.98	3.98	11.5	2.30
3.98	5.7	9.8	2.09
3.98	7.9	8.3	1.98
3.98	10.2	6.1	1.51
3.98	13.3	5.35	1.60
5.1	0	18.7	...
5.1	3.7	14.2	2.30
5.1	5.25	13.1	2.42
5.1	6.75	11.0	1.92
5.1	9.7	9.0	1.79
5.1	14.4	7.0	1.71
2.06	0	8.90	...
2.06	1.35	7.32	3.03
2.06	2.06	6.84	3.32
2.06	2.70	6.28	3.14
2.06	4.05	5.20	2.75
2.06	6.17	3.96	2.42
	n-C_4H_9SH		
0.78	0	4.68	...
0.78	0.69	3.76	3.54
0.78	0.86	3.64	3.85
0.78	1.10	3.36	3.58
0.78	1.46	3.14	3.76
0.78	2.09	2.80	3.92
2.8	0	1.68	...
2.8	1.13	1.51	3.62
2.8	2.34	1.26	2.50

olefin (C_2H_4) or 0.02% oxygen would be required. Actual analysis of the ethane by H-flame chromatography using a Porapak Q column shows only 0.1% C_2H_4. Even though each sample was thoroughly degassed before use, this small amount of oxygen might be present. The lack of an effect of added ethane on the H_2 yields in H_2S photolysis, however, and the dependence of k_2/k_3 on total pressure only, independent of pressurizer, seems to indicate that impurities are not responsible for the observed effect.

(ii) "Hot" H atoms or vibrationally excited C_2H_5 from reaction 3 cannot cause the observed decrease in H_2 production since ethylene is not present in one of the CH_3SH systems presented in Figure 1 and the decrease still occurs. In the absence of any reasonable alternative, "hot" H atoms may become thermalized, but should still produce hydrogen by reaction 2.

(iii) Third-body combinations are usually unimportant in this pressure region. If one assumes the mechanism given is the only one of importance and that thiyl radicals disappear only by recombination,[5] then the [H] and [RS] may be approximated from eq II and III using the measured value of k_2[6] and $k_t = 10^{13}$

$$R_{H_2} = k_2[H][RSH] \quad \text{(II)}$$

$$R_{RSSR} \sim R_{H_2} \sim k_t[RS]^2 \quad \text{(III)}$$

cc/mole sec. To account for the observed decrease in H_2 production

$$H + RS + M \longrightarrow RSH + M \quad (4)$$

k_4 must be *ca.* 10^{-26} cc^2/molecule^2 sec. This is six orders of magnitude larger than the generally observed values of $k_4 \sim 10^{-32}$ cc^2/molecule^2 sec.[7] Thus, third-body effects would seem to be unimportant.

(iv) Quenching of excited RSH molecules does not seem plausible since the mercaptans show a predissociation-type absorption spectrum which is consistent with the high quantum yield of H_2 production ($\phi \sim 0.9$).[1] Collisional frequencies at these pressures are such that the lifetime of the dissociating species must be $>10^{-10}$ sec, assuming unit efficiency in deactivation. Again, this seems unreasonable.

Table II: Pressure Effect on k_2/k_3

RSH/C_2H_4	P_T,[a] cm	$10^6 R_{H_2}$, moles/sec	k_2/k_3
	H_2S		
...	0.79	0.20	...
0.59	2.3	0.109	2.03
0.59	3.4	0.111	2.11
0.59	4.8	0.112	2.17
0.59	9.7	0.109	2.03
0.59	20.1	0.109	2.03
0.59	30.4	0.097	1.59
	CH_3SH		
...	1.06	4.37	...
0.75	2.5	2.63	2.01
0.75	13.0	2.64	2.04
0.75	17.2	2.56	1.89
0.75	25.2	2.21	1.36
0.75	39.2	1.94	1.07
...	0.99	4.26	...
0.70	2.4	2.45	1.93
0.70	4.6	2.34	1.74
0.70	8.9	2.40	1.84
0.70	20.3	2.12	1.41
0.70	31.2	1.82	1.07
0.70	42.2	1.73	0.98
0.70	54.8	1.81	1.05
	C_2H_5SH		
...	1.10	3.40	...
0.84	2.4	2.20	2.18
0.84	10.2	2.09	1.91

[a] $P_T = P_{H_2S} + P_{C_2H_4} + P_{C_2H_6}$ in centimeters of mercury.

The pressure effect cannot, then, be explained with the available data. The rate constant ratio for the low-pressure region is consistent with the previous measurements[3] for methyl mercaptan. These pressure-independent ratios for the other mercaptans are collected in Table III.

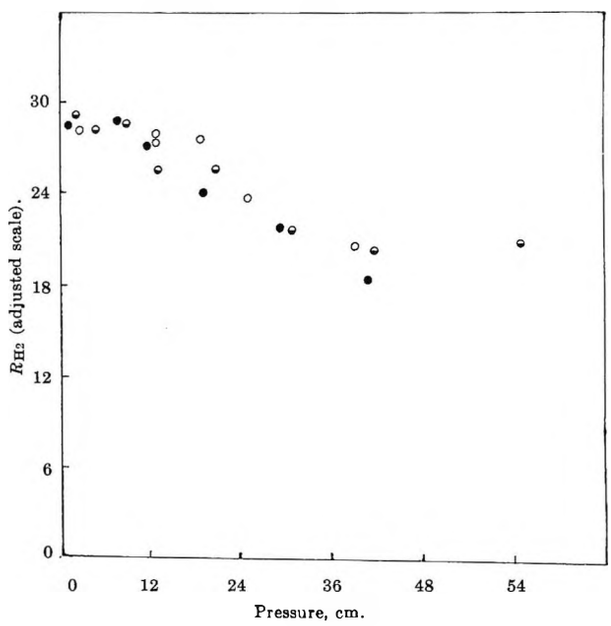

Figure 1. Hydrogen yields in the photolysis of methanethiol: ●, 1 cm CH_3SH; ○, $RSH/C_2H_4 = 0.75$, 1 cm CH_3SH; ⊖, $RSH/C_2H_4 = 0.70$, 1 cm CH_3SH. Scale adjusted to give equal amounts of hydrogen at low pressures.

Table III: Summary of k_2/k_3 Values for the Mercaptans in the Pressure-Independent Region

Mercaptan	k_2/k_3[a]	Lit. values
H_2S	2.1 ± 0.1	1.6[2]
CH_3SH	1.7 ± 0.2 (9 values)	1.7[3] (50°)
C_2H_5SH	1.9 ± 0.1 (5 values)	
n-C_3H_7SH	3.2 ± 0.1 (3 values)	
n-C_4H_9SH	3.7 ± 0.1 (6 values)	

[a] Reported errors are average fluctuations from the mean. The methanethiol fluctuations are larger owing to interference of the methane and hydrogen peaks in the chromatographic analysis of the product.

Acknowledgment. This investigation was supported by U. S. Public Health Research Grant RH-00321, Division of Radiological Health.

(5) R. P. Steer, B. L. Kalra, and A. R. Knight, *J. Phys. Chem.*, 71, 783 (1967).

(6) Based on $k_3 = 1.6 \times 10^{11}$ cc/mole sec: K. Yang, *J. Am. Chem. Soc.*, 84, 3795 (1962).

(7) O. K. Rice, "Proceedings of IXth International Astronautical Congress," Amsterdam, 1958, p 9.

Photolysis of Gaseous Benzene at 1470 A

by W. M. Jackson, J. L. Faris, and B. Donn

National Aeronautics and Space Administration, Goddard Space Flight Center, Greenbelt, Maryland
(Received April 3, 1967)

Although a great deal of work has been done on the photolysis of aliphatic hydrocarbons[1] in the vacuum ultraviolet region, very little work has been reported on the photolysis of aromatic hydrocarbons in this region. Benzene, which is the simplest aromatic hydrocarbon, has recently been photolyzed in the 1600–2000-A region[2] and at the 1849-A Hg line.[3-5] They have shown that the primary photochemical processes are the production of polymeric material along with the formation of acetylene and fulvene. In the absorption spectra of benzene there exists another sharply banded region below 1650 A.[6] It is possible that the mechanism for the photolysis of benzene might be different in this region of the spectrum and could consist of the molecular formation of hydrogen which is characteristic of saturated hydrocarbons[1] or the elimination of an H atom and the formation of a benzyl radical. With this idea in mind, we have photolyzed benzene vapor at 1470 A and analyzed the gaseous products by gas chromatography and mass spectrometry.

The apparatus consisted of a xenon resonance lamp with a sapphire window, a 50-cc reaction cell, and a grease-free gas handling system. The output of the lamp, as measured by CO_2 actinometry, was 6×10^{14} quanta/cm^2 sec. The C_6H_6 was obtained from Phillips Petroleum Co. and the C_6D_6 from Bio Rad Laboratories. The benzenes were then degassed under vacuum after H_2O and CO_2 had been removed by Na and an ascarite column. Gas chromatographic analyses were performed using an 18-ft, 1/8-inch o.d. stainless steel column packed with 15% DMS on 60–80 mesh chromosorb P, a 12-ft, 1/4-in. aluminum column packed with 15% Squalane on 60–80 mesh diatoport P, and a 6-ft, 1/8-in. stainless steel column packed with 10% silicone rubber SE-30 on 80–100 mesh diatoport S. Chromatographic analysis of the benzenes did not indicate any detectable impurities. Hydrogen and deuterium were analyzed on a C.E.C. 620 mass spectrometer.

The reaction was carried out at benzene pressures of 200×10^{-3} and 10 torr for times ranging from 3 to 60 min. After the reaction was stopped, the condensable products were frozen into a stainless steel sample flask at liquid nitrogen temperature, and the gas above the frozen condensate was analyzed by mass spectrometry. These analyses showed that neither hydrogen nor deuterium was formed during the photolysis. From the known sensitivities of the mass spectrometer for H_2 and D_2 it was estimated that samples as small as 10^{-9} mole of hydrogen or deuterium could have been detected by this method.

The frozen sample was then warmed up and a 500-μl gas syringe sample was taken and analyzed by gas chromatography. A few experiments were done in which the sample was only warmed to $-90°$ and the volatile gas was analyzed by mass spectrometry.

The chromatographic and mass spectrometric analysis showed that the gaseous products formed in the reaction were acetylene, ethylene, methylacetylene, vinylacetylene and, at high benzene pressures, butene. No evidence was found for the formation of biphenyl, confirming the observation that hydrogen was not formed in the reaction. The amount of volatile products formed is much less than the number of quanta

Table I: Products Formed in the Photolysis of C_6H_6 at 1470 A (Benzene Pressure 10 torr)

Time, min	H_2[a]	C_2H_2[b]	C_2H_4[b]	CH_3C_2H[b]	C_4H_8[b]	$C_2H_3C_2H$[b]	$(C_6H_5)_2$[c]
10	N.d.	1	0.03	0.16	0.07	0.24	N.d.
30	N.d.	1	0.03	0.17	0.07	0.24	N.d.
60	N.d.	1	0.03	0.17	0.09	0.22	N.d.

[a] Not detected on the mass spectrometer. [b] These relative peak areas were determined on a Squalane column and are not corrected for relative sensitivities. [c] Not detected on the SE-30 column.

(1) J. R. McNesby and H. Okabe, *Advan. Photochem.*, **3**, 157 (1964).

(2) H. Ward, J. Wishnok, and P. D. Sherman, Jr., *J. Am. Chem. Soc.*, **89**, 162 (1967).

(3) J. K. Foote, M. H. Mallon, and J. N. Pitts, Jr., *ibid.*, **88**, 3698 (1966).

(4) K. Shindo and S. Lipsky, *J. Chem. Phys.*, **45**, 2292 (1966).

(5) L. Kaplan and K. E. Wilzbach, *J. Am. Chem. Soc.*, **89**, 1031 (1967).

(6) M. E. A. El Sayed, M. Kasha, and Y. Tanaka, *J. Chem. Phys.*, **34**, 334 (1961).

absorbed, indicating the major product is polymer formation. The polymer was observed under all reaction conditions as evidenced by the decreased transmission of the cell after each run.

Quantitative results were difficult to obtain, except at high benzene pressures, because of the small amount of gaseous products formed. At these pressures of benzene, most of the light is absorbed in a region near the window of the reaction vessel and some of the observed products may represent secondary photolysis. Except for butene, the products formed at high pressure, shown in Table I, are identical with the products formed at low pressures. The higher acetylenes have been observed in the photolysis of acetylene[1] and are probably the result of secondary photolysis of this compound.

The present work shows that reactions 1 and 2 are not major reactions in the photolysis of benzene at 1470 A.

$$C_6H_6 + h\nu \longrightarrow C_6H_5 + H \quad (1)$$

$$C_6H_6 + h\nu \longrightarrow C_6H_4 + H_2 \quad (2)$$

Changes in the Absorption Spectrum of Methylene Blue with pH[1]

by G. S. Singhal and E. Rabinowitch

Department of Botany, University of Illinois, Urbana, Illinois
(Received March 7, 1967)

Knowledge of the variations in the absorption spectrum of methylene blue (MB) in different solvents and at different pH is important in view of applications of this pigment in biology, clay mineralogy, and some basic photochemical experiments.[2]

The effects of pH, time, and temperature on the methylene blue spectrum in aqueous solutions had been studied before.[3-7] Demethylation of tetramethyl thionine (methylene blue) to trimethyl thionine (TMT, or "methylene azure B") and to asymmetric dimethyl thionine ("methylene azure A") had been shown to occur.[3] Suggestion that TMT might exist in two tautomeric forms was made by Holmes and Snyder.[4b] TMT is present as a positive ion in acidic solution and as a neutral molecule in alkaline solution.[8] The dimer MB_2^+ is formed in aqueous solution at pH 3.4 at concentrations above 2.5×10^{-6}.[9] Palit and Saxena[10] have found, at pH 11.2, an increase in the shoulder-to-peak ratio in the MB absorption band, suggesting that more dimer is formed in alkaline solution. They suggested that the red form of the dye, extracted into benzene at pH 11.2, is a dimer of MB. These observations contradict those of Lewis, *et al.*,[11] who had found that MB does not dimerize in solvents of low dielectric constant (*cf.* also Rabinowitch and Epstein[9]).

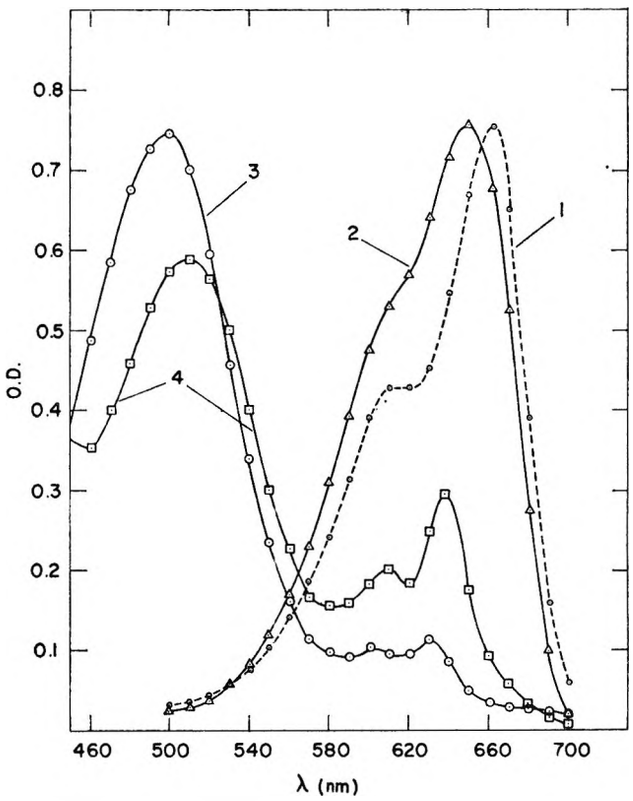

Figure 1. Absorption spectra: 1, methylene blue in water; 2, TMT in water; 3, TMT in ether; 4, TMT in benzene.

(1) This research was supported by grants from the National Science Foundation (GB 3305) and the U. S. Atomic Energy Commission (AT(11-1)-1502).

(2) D. Frackowiak and E. Rabinowitch, *J. Phys. Chem.*, **70**, 3012 (1966).

(3) W. J. MacNeal and J. A. Killian, *J. Am. Chem. Soc.*, **48**, 740 (1926).

(4) (a) W. C. Holmes, *Stain Techn.*, **3**, 45 (1928); (b) W. C. Holmes and E. F. Snyder, *ibid.*, **4**, 7 (1929).

(5) R. D. Lillie, *ibid.*, **18**, 1 (1943).

(6) Y. Koyama, M. Masuda, and M. Yoshikawa, *Osaka Daigaku Igaku Zasshi*, **10**, 1193 (1958).

(7) L. Michaelis, H. P. Schubert, and S. Granick, *J. Am. Chem. Soc.*, **62**, 204 (1940).

(8) K. Bergmann and C. T. O'Konski, *J. Phys. Chem.*, **67**, 2169 (1963).

(9) E. Rabinowitch and L. P. Epstein, *J. Am. Chem. Soc.*, **63**, 69 (1941).

(10) S. R. Palit and G. K. Saxena, *Nature*, **209**, 1127 (1966).

(11) G. N. Lewis, O. Goldschmid, T. T. Magel, and J. Bigeleisen, *J. Am. Chem. Soc.*, **65**, 1150 (1943).

In the above-mentioned studies, spectrophotometric identification of the different forms of the dye was obtained either by visual examination of the spectrum, or by measuring the optical density in the absorption maximum, or the peak-to-shoulder ratio in the absorption band in MB solutions of different pH, and comparing it with the corresponding values in pure water. We thought it might be of interest to know more about the different stages in the change of the absorption spectrum of MB with growing pH and to check whether the "red" form of MB extracted into benzene, at pH 11.2, really is a dimer. For this purpose, we extracted MB into ether or benzene at different pH's and measured the absorption spectrum after transfer of the dye from the organic solvent back into water.

The MB of Merck and Co. was purified by crystallizing it once from 0.1 N HCl and then twice from water. The resulting product had an absorption peak at 663–664 nm (Figure 1), and a molar extinction coefficient in this peak equal to 9.0×10^4. In the concentration used, its aqueous solution had a pH of 4.5. Concentrations used were below 1×10^{-5} M. All of the absorption spectra were measured with a Bausch and Lomb spectrophotometer (Spectronic 505).

Results and Discussion

When a buffered aqueous solution of the dye (pH 8.5) was shaken with ether, the ether layer became slightly pinkish. The absorption spectrum of the ether solution and that of the residue from evaporation of the ether extract, dissolved in water, are given in Figure 1. Also given in this figure is the spectrum of the same residue dissolved in benzene. Shaking under argon instead of air did not make any difference. The position of the absorption maximum (650 nm) in water suggests that this product is trimethyl thionine (TMT).[8] The addition of oxalic acid to the ethereal solution turned the red color into pinkish blue. When this solution was shaken with water, the ether layer gradually turned from pinkish to colorless and the water layer became increasingly blue in color. Even without the addition of any oxalic acid, when the ethereal solution of TMT was shaken with water, the water layer became bluish. The absorption maximum of aqueous solution was in both cases at 650 nm. This observation indicates that, presumably, TMT (red form) is extracted into ether or benzene as a neutral molecule, while the blue form of TMT, present in neutral or acidic aqueous medium, is an ion. A break in the E_0 *vs.* pH curve at pH 12.2 confirms the existence of two forms of TMT. A similar transition point could not be observed in MB in the same pH range. These observations are in agreement with those of Bergmann and O'Konski[8] referred to earlier.

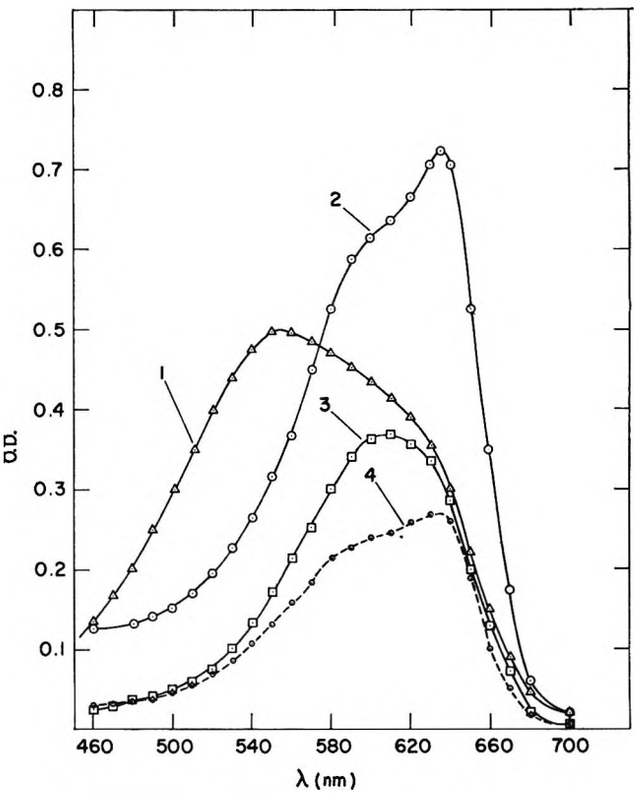

Figure 2. Absorption spectra: 1, TMT in water at pH 13.0; 2, TMT solution (pH 13.0) adjusted to pH 3.0; 3, ether extract of TMT solution (pH 13.0) dissolved in water (pH ~6.5); 4, ether extract of TMT solution (pH 13.0) dissolved in water (pH ~4.0).

To check the reversibility of the acid–base conversion, the following two TMT spectra in aqueous solution were compared; one was measured with TMT solution having pH 13.0 (Figure 2) and the other with TMT first dissolved in an aqueous solution of pH 13.0 and then adjusted to pH 3.0 (Figure 2). The blue shift of the band (λ_{max} ~635 nm) in the second case suggests that the acid–base equilibrium of TMT is not completely reversible. This contention is further supported by spectra of the aqueous solution, prepared from TMT extract in ether (obtained from aqueous TMT solution at pH 13.0), adjusted to pH 4.0 and pH 6.5 (Figure 2). This incomplete reversibility probably indicates a further demethylation of TMT, which seems to be base-catalyzed, and also suggests that it may be difficult to obtain pure TMT because of further demethylations.

Following the observations[5] that the absorbancy changes of alkaline solutions are time dependent, the time course of these changes was studied. The absorption in the region of 610 nm, in an alkaline solution of

Table I: OD at 610 nm/OD at 663 nm as a Function of Time at pH 10.7 and as a Function of pH (after 30 min)

	Time, hr						pH		
	0	0.83	2.5	18	70	90	6.7	11.0	13.0
OD at 610 nm / OD at 663 nm	0.705	0.748	0.768	0.785	0.878	0.905	0.695	0.732	1.19

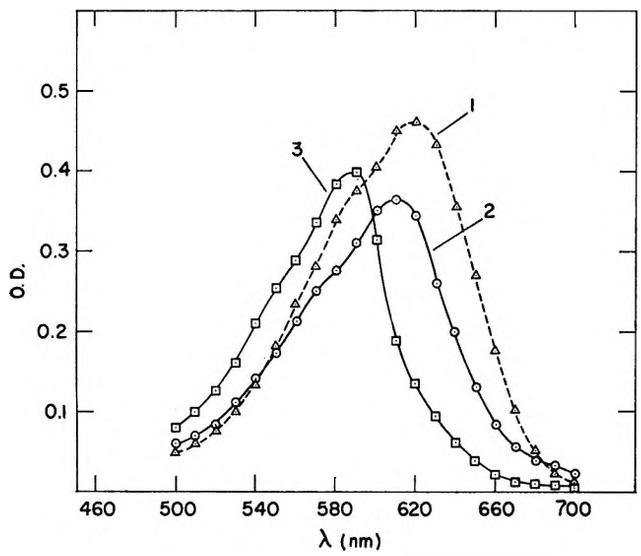

Figure 3. Absorption spectra of differently demethylated methylene blue: 1, dimethyl thionine, obtained from MB solution (pH ~12.0) within 1 hr; 2, monomethyl thionine, obtained from a MB solution (pH ~10.7) after about 60 hr; 3, completely demethylated MB–MB solution (pH ~12.0) measured after 1 week.

MB (pH 10.7) when measured within 1 hr, was comparatively stronger than in pure water. With time, the over-all absorption decreased and the relative absorption around 610 nm increased (Table I). Also included in the table is the pH effect on the ratio of OD at 610 and 663 nm. After about 60 hr, the pink form was extracted from MB solution (pH ~10.7) into benzene and dried under vacuum. Its aqueous solution had λ_{max} 610 nm and a shoulder at ~570 nm (Figure 3, curve 2).

In another series of experiments, extraction into benzene from an aqueous solution at pH 12 was completed within 1 hr. Aqueous solution of the extracted material had its λ_{max} at 619 nm, with a shoulder at ~578 nm (Figure 2, curve 1).

Formanek[12] found the absorption maxima of mono-, di-, tri-, and tetramethyl thionines at 610, 622 (symmetrical), 652, and 667 nm, respectively. As reported above, we have observed the absorption maxima for the red forms, obtained at different pH values and at different times, at 610, 619, and 650 nm. These are in good agreement with Formanek's values for mono-, di-(symmetrical) and trimethyl thionines. This suggests that the red or pink forms, which we observed in alkaline solutions under different pH conditions and at different times, were the different demethylated products of MB. Comparison of absorption maxima at 589 nm (Figure 3, curve 3) of the solution (pH 12) measured after a week with that of thionin (λ_{max} 595 nm) leads to the conclusion that ultimately MB may be completely demethylated, *i.e.*, converted to thionine.

Our results do not support the conclusion of Palit and Saxena[10] that the red extract of MB contains a dimer. The spectrum of all red forms observed had the shoulder attributable to a vibrational sub-band (Figure 3) in the same relative position in which the absorption band of the dimer usually appears in dye. It seems that the red form is not an MB dimer, which has been reported to have two absorption peaks, at 610 nm and at 700 nm.[8] The spectrum of TMT in benzene or ether (Figure 1) gives support to this conclusion. The two forms of the demethylated dye can be expressed as

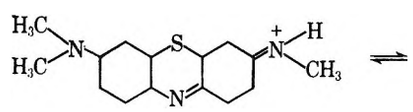

blue form of TMT present in acidic or neutral aqueous solution

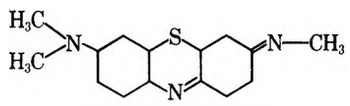

red or pink form of TMT present in basic solutions, readily soluble in ether or benzene

Bergmann and O'Konski also suggested a similar acid–base transition in TMT.[8]

Summarizing the above results, it seems that in basic solutions methylene blue is stepwise demethylated, depending upon pH and time. The red form, observed in basic solutions, probably is the neutral form of the demethylated product.

(12) J. Formanek, "Untersuchung und Nachweis organischer Farbstoffe aud spektroskopischem Wege," 2nd ed, Part 1, J. Springer, Berlin, 1908, pp 142–164.

Product Inventory of the Radiolysis of Crystalline Choline Chloride[1]

by Margaret Ackerman and Richard M. Lemmon

Laboratory of Chemical Biodynamics, Lawrence Radiation Laboratory, University of California, Berkeley, California
(Received March 17, 1967)

The earliest report of the unique radiation sensitivity of crystalline choline chloride indicated that the identified radiolysis products, trimethylamine and acetaldehyde, accounted for essentially all the decomposed choline.[2] However, that indication was provided principally by paper chromatographic studies of nonvolatile products. The present study, which includes quantitative measurements of all detectable products, was undertaken in the hope that a full product inventory would shed further light on this unique radiolysis mechanism.

Experimental Section

Sample Preparation and Irradiation. The unlabeled choline chloride used was the Eastman Organic Chemicals White Label product. The ^{14}C-methyl-labeled compound was prepared by allowing $^{14}CH_3I$ to react with dimethylaminoethanol; the resultant iodide was converted to chloride by treatment with Ag_2O followed by HCl. The labeled chloride was recrystallized from ethanol–ether. By means of a 3000-curie ^{60}Co source, the crystalline samples (133 mg each) were given a total dose of 28–192 Mrads at a rate of 11.6×10^5 rads/hr. In order to look for a dose rate effect, in one experiment (5) the dose rate was increased to 116×10^5 rads/hr.

Determination of Hydrogen, Methane, and Acetaldehyde. The irradiated samples were connected (through break-seals) to a vacuum system of known volume fitted with a Zimmerli pressure gauge and two traps. The first trap served both as a collector of volatile products and as a reservoir for the ethanol that was used to dissolve the sample. The second trap contained 4-A Molecular Sieve (Linde) onto which methane was quantitatively absorbed at −196° and quantitatively released when the trap was subsequently heated to 150° for a few minutes.

After the seals were broken and ethanol distilled into the sample tubes to dissolve the crystals, all volatile materials were distilled into the first trap (held at −196°). Hydrogen and methane passed through, the methane to be absorbed in the sieve trap (also at −196°). The amount of H_2 was determined by its pressure in a known volume. The methane was determined by gas chromatography (glpc) (Varian Aerograph Model A-350, 5-A molecular sieve column, 4 ft × 0.25 in., 80°, flow rate (He) 30 cc/min, CH_4 retention time 16 min).

The compounds in the first trap were determined by glpc (A-350, 20-ft × 0.38-in. column of 30% "UCON Polar" on acid- and dimethylchlorosilane-treated 45/60 Chromosorb W, 70°, flow rate 30 cc/min). The following compounds (identified by mass spectrometry) were found at the indicated retention times (minutes): 20, CH_3Cl; 32, acetaldehyde; 70, ethanol (solvent); 88, acetal; 110, crotonaldehyde; and 140, paraldehyde. The yields of these products were determined by peak-area comparisons with known amounts of these compounds.

Methyl Chloride as a Radiolysis Product. During the course of earlier work on the radiolysis of choline chloride, traces of methyl chloride had been observed (but not reported) on gas chromatograms used to purify deuterated acetaldehyde and trimethylamine products.[3] In the present study, at a total dose of 30 Mrads, only barely detectable amounts of methyl chloride were formed. In the earlier work, higher total doses at higher dose rates were usually employed. Suspecting that either or both of these factors could be responsible for the production of methyl chloride, we prepared four 0.5-g samples of crystalline choline chloride. Sample 1 received 30 Mrads at 11.6×10^5 rads/hr (the same dose rate and approximately the same total dose as given to all other samples in the present work). Sample 2 received 30 Mrads at 116×10^5 rads/hr. Sample 3 received 192 Mrads at 116×10^5 rads/hr (the dose rate and total dose used in the previous work[3]). Sample 4 received 192 Mrads at 11.6×10^5 rads/hr. The volatile products from all samples were chromatographed on "UCON Polar," as described above. Only samples 3 and 4, those receiving a total dose of 192 Mrads, contained a detectable amount (about 0.2% of the decomposed choline) of methyl chloride.

Determination of Trimethylamine and Polymer. Current and past work have shown that the trimethylamine produced in the radiolysis appears as the hydrochloride salt. No detectable amounts of trimethylamine had ever been observed until base was added to an irradiated sample. Past work had also indicated that no other amines were being formed in appreciable quantity since radioautographs of paper chromatograms of irradiated

(1) The work described in this paper was sponsored by the U. S. Atomic Energy Commission.

(2) B. M. Tolbert, *et al.*, *J. Am. Chem. Soc.*, **75**, 1867 (1953).

(3) R. M. Lemmon and M. A. Smith, **85**, 1395 (1963).

Table I: Products Appearing in the γ Radiolysis of Crystalline Choline Chloride

Expt no.	Dose, Mrads (at 11.6×10^5 rads/hr)	Time of storage at 25°, days[a]	Choline decomposed, mmoles	Product formation: Compd	Amount, mmole	% decompd choline
1	37.2	143	0.372[b]	H_2	0.014	3.8
				CH_4	0.008	2.1
				CH_3CHO	0.351[d]	94.4
2	34.9	232	0.358[c]	H_2	0.008	2.2
3	28.2	15	0.311[b]	H_2	0.007	2.3
				CH_4	0.008	2.6
				CH_3CHO	0.296[e]	95.2
4	192	1	0.88[g]	CH_3Cl	0.002[h]	0.2
5	192[f]	1	1.79[g]	CH_3Cl	0.004[h]	0.2
6	32.6	422	0.284[i]	$(CH_3)_3N$	0.288	100
				Polymer	<0.002	<1
7	29.3	15	0.252[i]	CH_3CHO	0.242[j]	96.5
				$(CH_3)_3N$	0.252	100
				Polymer	<0.002	<1
8	28.2	181	0.311	Cl_2	<0.003	<1

[a] Between irradiation and analysis. Earlier work has shown that, for a given radiation dose, the per cent decomposition is dependent upon this time: R. O. Lindblom, R. M. Lemmon, and M. Calvin, *J. Am. Chem. Soc.*, **83**, 2484 (1961). [b] Sum of products found on gas–liquid partition chromatograms. [c] Estimated from decompositions measured in similar samples. [d] Sum of (in mmoles): CH_3CHO (0.022), acetal (0.133), crotonaldehyde (0.023; equivalent to 0.046 CH_3CHO), paraldehyde (0.050; equivalent to 0.150 CH_3CHO). [e] Sum of (in mmoles): CH_3CHO (0.011), acetal (0.076), crotonaldehyde (0.004; equivalent to 0.008 CH_3CHO), paraldehyde (0.067; equivalent to 0.201 CH_3CHO). [f] Dose rate 116×10^5 rads/hr. [g] Based on amount of CH_3CHO observed from the irradiation of 500 mg (3.53 mmoles) of choline chloride. [h] At lower total doses there was no detectable CH_3Cl. [i] Determined by counting undecomposed choline-^{14}C on paper chromatogram. [j] Sum of (in mmoles): CH_3CHO (0.04), acetal (0.091), crotonaldehyde (0.003; equivalent to 0.006 CH_3CHO), paraldehyde (0.047; equivalent to 0.141 CH_3CHO).

^{14}C-methyl-labeled choline chloride revealed only two active spots: one was undecomposed choline chloride and the other was trimethylamine hydrochloride. In order to confirm this observation by gas chromatography, the volatile products from a 1-g sample of irradiated choline chloride were observed directly by glpc (10-ft × 0.25-in. column of 15% THEED 5% TEP on 60/80 Chromosorb W, 65°, He flow rate 40 cc/min—a column that will cleanly separate NH_3, methylamine, dimethylamine, and trimethylamine). Only trimethylamine (t_R 2.7 min) was observed on this chromatogram.

Because the amounts of undecomposed choline chloride and of polymer formed could be learned at the same time, paper (rather than gas) chromatography was chosen as the means of determining the amount of trimethylamine formed. Consequently, two 100-mg samples of the ^{14}C-methyl-labeled compound, containing a total activity of 9.2×10^4 dpm, were prepared and irradiated (30 Mrads). The samples were stored 422 days; then the tube was opened and the crystals were dissolved in 1 ml of methanol. An aliquot (10 μl) was withdrawn from each sample and chromatographed (one direction) on Whatman No. 1 paper using 1-butanol–water–12 *N* HCl (4:1:1) as a developing solvent. Radioautographs of these chromatograms were used to locate the radioactive spots so that the amount of activity could be measured by a Geiger tube. Trimethylamine hydrochloride and undecomposed choline chloride were the only detectable radioactive spots. Polymeric material, which had been observed previously on the origin of chromatograms from samples given 192 Mrads, was not produced in detectable amounts by the 30-Mrad dose given these samples (under conditions when as little as 1% could have been observed). The percentages of trimethylamine hydrochloride are essentially equivalent to the percentages of choline decomposed.

Search for Cl_2 as a Possible Radiolysis Product. The search for Cl_2 was made by chromatographing all the volatile products from the irradiated crystals; the crystals were dissolved in absolute ethanol and the volatiles (including EtOH) vacuum-line transferred into a trap from which they could be directly injected into a gas chromatograph (Varian Aerograph Model A-350, 5-ft × 0.25-in. column of "Poropak Q," 50°,

He flow rate 40 cc/min). Under these conditions the retention time for Cl_2 is 2.3 min.

Results and Discussion

The quantitative data on the radiolysis products are presented in Table I and may be summarized as follows.

(1) Experiments 1–3 show that H_2 and CH_4 are only very minor products at doses of about 30 Mrads and postirradiation storage times of 15–232 days. The average per cent of decomposed choline appearing as H_2 is 2.7%. This corresponds to a $G(H_2)$ from choline chloride of 1.1. The corresponding average figure for $G(CH_4)$ is 0.9. These are representative G values for the production of H_2 and CH_4 from, for example, saturated hydrocarbons.[4] Since the radiolysis of crystalline choline chloride has been observed with $G(-M)$ values as high as 55,000,[5] it is reasonable to conclude that the H_2 and CH_4 come from ordinary, random, radiolytic processes that are unrelated to the unique, chain-decomposition mechanism.

(2) Experiments 4 and 5 demonstrate that CH_3Cl is also a very minor product. We were unable to detect this compound in 30-Mrad irradiations. At 192 Mrads we did find detectable CH_3Cl–about 0.2% of the total decomposition products and independent of the dose rate. The corresponding $G(CH_3Cl)$ is 0.06.

(3) Experiments 6 and 7 show that there is very little polymer formed at 30 Mrads. We know from previous unpublished observations that extensive radiation decomposition leads to more polymer; here, however, at about 30% decomposition, the polymer formation is negligible. What this polymer may be is suggested by the appearance of crotonaldehyde and paraldehyde (see footnotes *d*, *e*, and *j* in Table I). It is well known that aldehydes tend to polymerize on irradiation.[6]

(4) Experiment 7 relates the appearance of acetaldehyde (determined by gas chromatography) to that of trimethylamine (determined by paper chromatography). An exact duplicate of this experiment was performed and led to almost identical results; that experiment, in the interests of space saving, is not recorded in the table. This work further indicates that acetaldehyde and trimethylamine account for nearly all of the radiation decomposition of choline. The 96.5% value for acetaldehyde (last column) is a minimal figure; small mechanical losses are expected during transfer operations.

(5) Experiment 8 was a direct search for molecular chlorine as a possible radiolysis product. (Again, a separate experiment, with very similar results, was performed.) This search was made because of the possibility that Cl atoms could be involved in the radiolysis mechanism, a possibility suggested by the appearance of CH_3Cl at higher doses. However, the results of this work indicate that if any Cl_2 is formed, it is less than 1% of the decomposed choline (we are unable to set a smaller upper limit because water and Cl_2 have the same retention time on our "Poropak" columns).

(6) Other compounds sought, but not found on our chromatograms, were ethylene glycol, ethylene chlorohydrin, methylaminoethanol, and dimethylaminoethanol.

The present work clearly indicates that the decomposition mechanism is very clean. The chain mechanism leads very specifically to a scission of the choline cation between the nitrogen atom and the adjacent methylene carbon, leading to the production of trimethylamine and acetaldehyde. For doses up to about 3×10^7 rads and approximately 30% choline decomposition, all other products comprise, at most, only 5% of the total radiolysis yield.

(4) A. J. Swallow, "Radiation Chemistry or Organic Compounds," Pergamon Press Inc., New York, N. Y., 1960, pp 61–75.

(5) R. O. Lindblom, R. M. Lemmon, and M. Calvin, *J. Am. Chem. Soc.*, **83**, 2484 (1961).

(6) J. C. McLennan and W. L. Patrick, *Can. J. Res.*, **5**, 470 (1931).

Second-Order Spectra of Symmetric Cyanine Dyes

by Robert A. Berg, Gloria Moyano, and Richard A. Pierce

Department of Chemistry, Washington University, St. Louis, Missouri 63130 *(Received March 30, 1967)*

The analysis by Kuhn[1] of the spectra of cyanine dyes is one of the outstanding successes of the particle-in-a-box model applied to the interpretation of molecular spectra. That work was concerned entirely with the first, allowed transition corresponding to $\Delta n = 1$ and was based largely on the data reported previously by Brooker, *et al.*,[2] on the transitions of longest wavelength. We report here on the second-order absorption spectra of a particular set of cyanine dyes, of which one of the primary resonance structures is

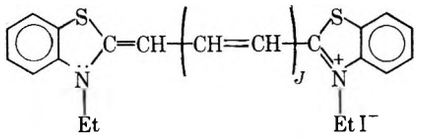

$J = 0, 1, 2, 3$

(1) H. Kuhn, *Helv. Chim. Acta*, **31**, 1441 (1948).

The dyes were obtained from the Pierce Chemical Co. Spectra were taken in methanol solution with a Perkin-Elmer 202 spectrophotometer. Extinctions measured in the visible transitions agreed with the values reported by Brooker, *et al.*[2] The second-order spectra in the near-ultraviolet region are shown in Figure 1.

We have assigned these spectra to the transitions $\Delta n = 2$. Two transitions of this type are possible: one from the next to last filled electronic level to the first unfilled level and another, of higher energy, from the last filled level to the second unfilled level. The spectra of Figure 1 show two resolved peaks in two cases and a single, broad absorption in the other two cases; the shoulder on the short-wavelength side of $J = 1$ may correspond to the second transition. The designations a and b are made accordingly. In the particle-in-a-box model there are no adjustable parameters in the prediction of wavelengths of the second-order transitions. The calculations require only the experimental wavelength of the visible transition λ_1 and the number of units in the conjugated chain. The results for our series of dyes are $\lambda_{2a} = (2J + 7)/(4J + 12)\lambda_1$ and $\lambda_{2b} = (2J + 7)/(4J + 16)\lambda_1$. The calculations and observations are presented in Table I. The agreement is about as good as for the visible transitions.[1]

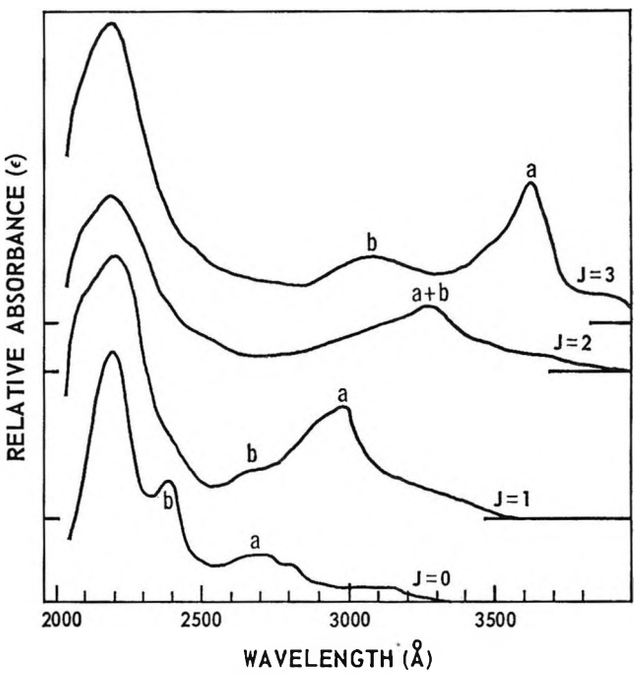

Figure 1. Second-order spectra. The relative absorbance scale for each dye is independent; however, for each dye a base line is given and the extinction coefficient ϵ of the peak at 2200 A is nearly constant in the series at 3.5×10^4 l./mole-cm, so absolute values of ϵ can be obtained.

Table I: Wavelengths (A) of Second-Order Transitions

J	λ_1	λ_{2a}, calcd	λ_{2b}, calcd	λ_2, obsd
0	4230	2470	1850	2665, 2385
1	5590	3140	2510	2975, 2650
2	6540	3590	3000	3270
3	7580	4110	3530	3620, 3080

All of the second-order bands obey Beer's law for the monomeric species. Integrated intensities have been measured as $\int \epsilon d \ln \tilde{\nu}$, where ϵ is the molar extinction coefficient and $\tilde{\nu}$ is frequency in reciprocal centimeters. The second-order bands are only $^1/_8$–$^1/_{10}$ as intense as the visible transition. For example, with $J = 3$ the integrated intensity is 2.58×10^4 l./mole-cm in the visible and only 0.29×10^4 l./mole-cm in the sum of the two second-order transitions. It is known[3] that the particle-in-a-box model accounts very well for the relative intensities of the visible transitions in a series of dyes; for $J = 0$, 1, 2, and 3 the calculated[3] relative integrated intensities are 0.28, 0.47, 0.71, and 1.00, respectively, and our observed relative intensities are 0.28, 0.50, 0.78, and 1.00. There is no simple way to calculate the intensities of the second-order transitions since they are forbidden in the particle-in-a-box model. However, we expect that as these transitions become symmetry allowed (see discussion below), the relative intensities would be the same as the relative intensities of the $\Delta n = 1$ transitions, this being determined only by the "box" length.[3] The observed relative intensities in the second-order transitions are 0.60, 0.82, 0.76, and 1.00; in these bands there is an irregular increase of intensity with "box" length.

Cyanine dyes oriented in stretched polyvinyl alcohol (PVA) film show directional absorption[4] and fluorescence[5] of the visible transition, with the electric vector of the light parallel to the strain direction. We have prepared oriented PVA films containing some of the cyanine dyes reported above. These show a preferential absorption of the second-order transitions in the same direction as for the visible, allowed transitions. However, the degree of linear dichroism is much less than in the visible bands; for example, the $J = 1$ dye in an oriented film gave a dichroic ratio of 4.9 in the

(2) L. G. S. Brooker, H. R. Sprague, C. P. Smyth, and G. L. Lewis, *J. Am. Chem. Soc.*, **62**, 1116 (1940).

(3) C. Sandorfy, "Electronic Spectra and Quantum Chemistry," Prentice-Hall, Inc., Englewood Cliffs, N. J., 1964, Chapter 14.

(4) E. H. Land and C. D. West, *Colloid Chem.*, **6**, 176 (1946).

(5) H. Kuhn, *J. Chem. Phys.*, **17**, 1198 (1949).

visible transition and only 1.6 in the second-order transition.

Simpson[6] has identified second-order peaks in the spectra of a series of two polymethine dyes. We have presented here a more extensive series; furthermore, the second-order bands are very well isolated in all but the first member of this series. The transitions $\Delta n = 2$ are forbidden in molecules with a center of symmetry. It seems that in the ground and excited electronic states there is sufficient rotation about double bonds, or asymmetric vibration, so that the symmetry restriction is lifted and the "forbidden" transitions appear. This explanation is consistent with the reduced linear dichroism in the second-order spectra, as well as the poor fit of relative intensities to calculations based on the particle-in-a-box model. However, that model can still be used as a good first approximation in predicting the wavelengths of the second-order spectra of symmetric cyanine dyes.

Acknowledgment. This work was supported in part by a grant to Washington University from the National Aeronautics and Space Administration and by a grant from the Research Corporation.

(6) W. T. Simpson, *J. Chem. Phys.*, 16, 1124 (1948).

The Vaporization of Cadmium Phosphide[1]

by Richard Schoonmaker and Kenneth Rubinson

Department of Chemistry, Oberlin College, Oberlin, Ohio
(Received April 19, 1967)

Metal phosphides are attractive compounds for studies of the kinetics of retarded vaporization since they vaporize by decomposition to relatively simple gaseous species with well-known structures and thermodynamic properties. As a class, they have been the object of increasing interest in recent years as a result of their semiconducting properties. At the present time there is remarkably little available information about the thermal stabilities of phosphides.

Shchukarev and co-workers[2] reported a heat of formation for $Zn_3P_2(c)$ of -98 kcal/mole while in subsequent work[3] a heat of formation of -27 kcal/mole was reported for $Cd_3P_2(c)$. The large difference between Shchukarev's heats of formation for zinc and cadmium phosphides, which have the same crystal structure,[4] is unexpected since a drastic change in bonding would not be predicted when zinc is replaced by cadmium in the crystal. Schoonmaker, Venkitaraman, and Lee,[5] hereafter referred to as SVL, have reported $\Delta H_f^\circ{}_{298}[Zn_3P_2(c)] = -39.5$ kcal/mole. In addition, they found evidence for a low coefficient for vaporization from $Zn_3P_2(c)$ and concluded that an enthalpy barrier to activation for vaporization was at least partially responsible for deviation of the vaporization coefficient from unity. The present work was undertaken to determine the thermal stability of cadmium phosphide and to investigate the extent of analogy between the processes of vaporization from crystalline zinc and cadmium phosphides.

Experimental Section

The torsion effusion and mass spectrometric apparatus and experimental techniques used in this work are similar to those previously described.[5,6] Finely divided, polycrystalline Cd_3P_2 was prepared by direct union of the elements at 450–500° in an evacuated, sealed tube. A sample of the product was analyzed for cadmium by electrodeposition and gave 84.48% compared to a theoretical value of 84.49. X-Ray diffraction spectra of the phosphide provided no evidence for uncombined cadmium metal. On solution of the finely powdered phosphide in dilute acid there was either no residue or only a faint trace of undissolved phosphorus.

Three conventional, double-orifice torsion effusion cells were machined from high-density graphite. The torque cells were identical except for effective orifice areas which were in the ratio 9.1:2.7:1 for cells 1, 2, and 3, respectively. For each cell, several runs were made with torsion fibers of 0.0025- and 0.0051-cm diameters. Mass spectrometric analyses were made on a molecular beam generated by vaporization of $Cd_3P_2(c)$ in a Knudsen cell with an orifice diameter of 0.140 cm.

Theory

Detailed theory applicable to this work has been described by SVL.[5] A linear equation (1) has been

$$1/p_t = M(\overline{Wa}) + (1/p_e) \qquad (1)$$

(1) This work was supported by grants from the U. S. Army Research Office (Durham) and the National Science Foundation.

(2) S. A. Shchukarev, M. P. Morozova, and G. Grossman, *Zh. Obshch. Khim.*, 25, 633 (1955).

(3) S. A. Shchukarev, M. P. Morozova, and M. M. Bortnikova, *ibid.*, 28, 3289 (1958).

(4) W. B. Pearson, "A Handbook of Lattice Spacings and Structures of Metals and Alloys," Pergamon Press Ltd., London, 1958.

(5) R. C. Schoonmaker, A. R. Venkitaraman, and P. K. Lee, *J. Phys. Chem.*, 71, 2676 (1967).

(6) P. K. Lee and R. C. Schoonmaker, "Condensation and Evaporation of Solids," Gordon & Breach Publishing Co., New York, N. Y., 1965, p 379.

used to extrapolate pressure in the effusion cells, p_t, to zero effective orifice area, $\overline{Wa}$, to obtain the total pressure, p_e, of all gaseous species in equilibrium with solid cadmium phosphide. If the vaporization occurs by congruent decomposition according to (2) and if the

$$Cd_3P_2(c) \rightleftharpoons 3Cd(g) + {}^1/_2P_4(g) \qquad (2)$$

$$\downarrow\uparrow$$

$$P_2(g)$$

partial pressure of $P_2(g)$ is neglible compared to that of $P_4(g)$, the equilibrium constant for (3) and the partial pressures of $P_4(g)$ and Cd(g) may be related to the total equilibrium pressure by the equations: $K_p = 0.238p_e^{7/2}$; $p_{P_4} = 0.143p_e$; $p_{Cd} = 0.857p_e$.

$$Cd_3P_2(c) \rightleftharpoons 3Cd(g) + {}^1/_2P_4(g) \qquad (3)$$

Results

At the beginning of runs with fresh samples, torque cell deflection was larger than the steady-state value to which it declined after a period of time. The steady state was constant and reproducible for several hours.

In the earliest runs sample weights were recorded, but no precaution was taken to use identical quantities for different runs with a given cell with the consequence that while the data for any single run were reproducible, pressures with a given cell were not consistent when different runs were compared. When a large number of pressure measurements was available it was apparent that pressure in the torque cell varied with sample weight and it was concluded that sample surface area effects were important. This conclusion was verified by use of a differential torque cell[7] which is, in effect, two identical conventional, double-orifice torque cells arranged in such a way that effusion from a set of orifices in one cell produces a torque couple which acts in opposition to the couple produced by effusion from he other cell. When one set of chambers contained approximately twice as much sample as the other set, the differential torque cell deflected in the direction which would be expected if the effusion rate was greater in the set which contained the larger weight of $Cd_3P_2(c)$. In all subsequent runs exactly the same weight of samples was used.

Figure 1 shows the temperature and orifice area dependences of total pressure over $Cd_3P_2(c)$ in three different torque cells. The line for each cell is a composite of data from several runs with both 0.0025- and 0.0051-cm diameter torsion fibers. The data for each cell were smoothed by a least-squares procedure and total pressures were calculated for each cell at 10° intervals over the temperature range 530–650°K. Figure 2 illustrates a typical linear extrapolation, eq 1, from

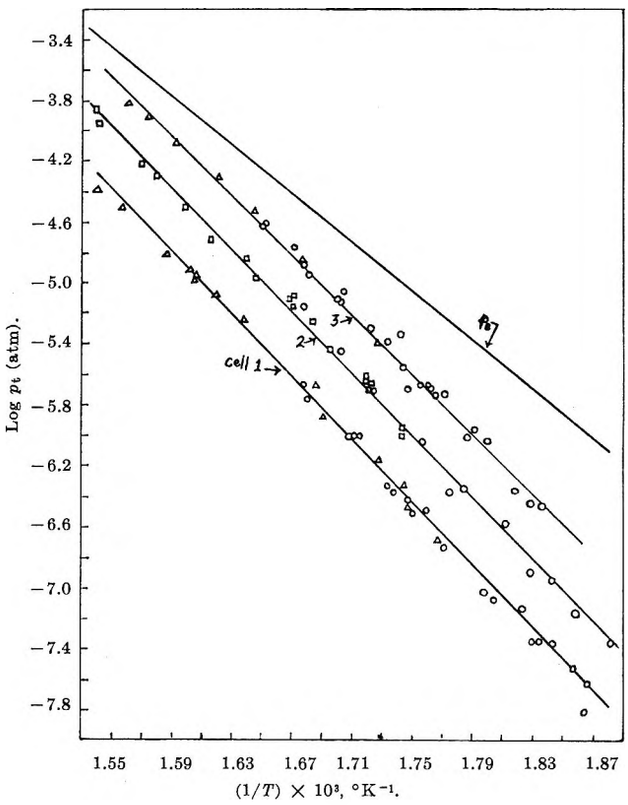

Figure 1. Logarithm of the total pressure in torsion effusion cells *vs.* reciprocal temperature: O, 0.0025-cm diameter torsion fiber; △ and □, 0.0051-cm diameter torsion fibers.

which the total pressure of all gaseous species in equilibrium with crystalline cadmium phosphide may be determined. The temperature dependence of the vapor pressure is well represented by log p_e (atm) = $(-7725.2/T) + 8.4933$.

Visual observation, mass spectrometric analyses of effusing vapors, and comparison of X-ray diffraction spectra of fresh samples and residues after vaporization all provided strong evidence for vaporization of cadmium phosphide by congruent decomposition. The detailed reasoning is very similar to that previously presented for zinc phosphide.[5] For example, in the mass spectrometric studies no ions were detected which contained both cadmium and phosphorus, but, over a temperature range of 130°, the Cd^+/P_4^+ ratio remained essentially constant while the Cd^+ intensity changed by a factor of more than 10^3. In the interest of brevity we do not reproduce further details of the argument. In the congruent decomposition, equilibrium total pressures may be used to calculate the partial pressures and equilibrium constants listed in Table I. Even for

(7) R. C. Schoonmaker, A. Buhl, and J. Lemley, *J. Phys. Chem.*, 69, 3455 (1965).

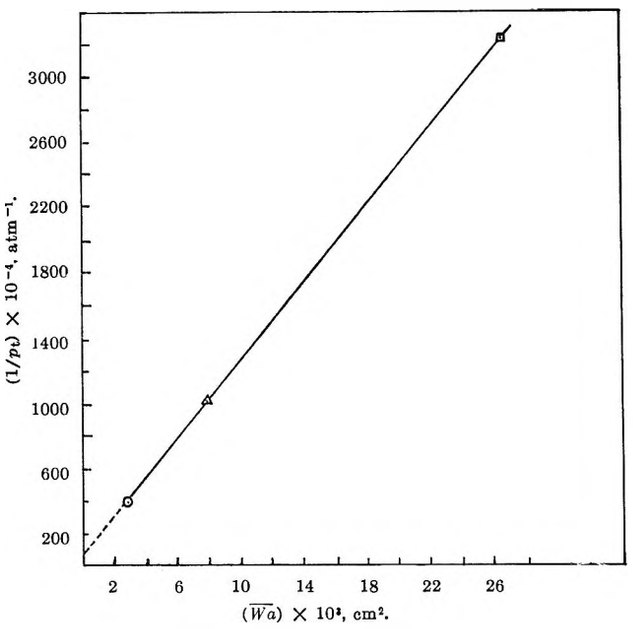

Figure 2. Linear extrapolation of $1/p_o$ to zero effective orifice area at 540°K: □, △, ○, cells 1, 2, 3, respectively.

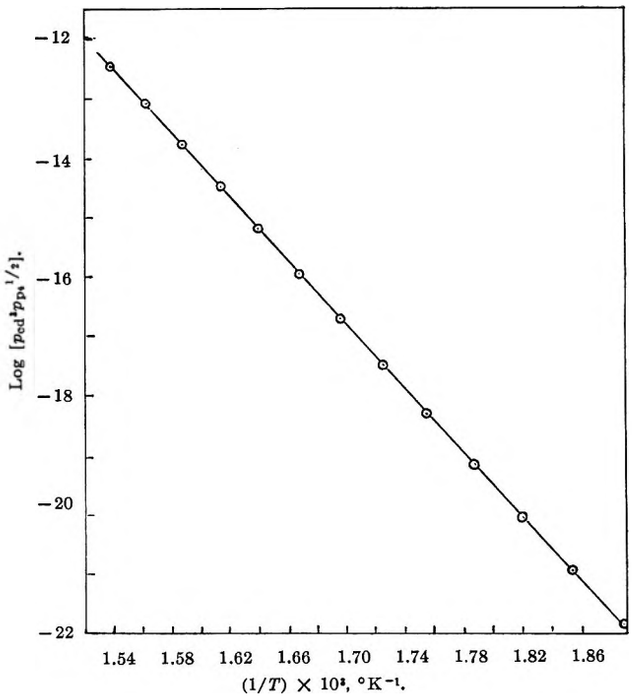

Figure 3. Logarithm of K_p *vs.* reciprocal temperature for $Cd_3P_2(c) \rightleftharpoons 3Cd(g) + {}^1/_2P_4(g)$.

the torque cell with the largest orifice, $P_2(g)$ is a neglible species in the analysis since the ratio $p_{P_2}/p_{P_4} \approx 10^{-3}$ over the temperature interval of this work.

Table I: Thermodynamic Data for the Decomposition of $Cd_3P_2(c)$[a]

Temp, °K	p_{Cd}	p_{P_4}	$K_p = p_{Cd}{}^3 p_{P_4}{}^{1/2}$
530	7.06×10^{-7}	1.18×10^{-7}	1.20×10^{-22}
540	1.32×10^{-6}	2.20	1.07×10^{-21}
550	2.41	4.01	8.86×10^{-21}
560	4.26	7.10	6.50×10^{-20}
570	7.52	1.26×10^{-6}	4.77×10^{-19}
580	1.29×10^{-5}	2.14	3.08×10^{-18}
590	2.15	3.58	1.88×10^{-17}
600	3.54	5.90	1.07×10^{-16}
610	5.82	9.96	6.13×10^{-16}
620	9.25	1.54×10^{-5}	3.09×10^{-15}
630	1.47×10^{-4}	2.44	1.56×10^{-14}
640	2.29	3.81	7.40×10^{-14}
650	3.51	5.84	3.30×10^{-13}

[a] All pressures are in atmospheres.

Figure 3 is a plot of log K_p *vs.* reciprocal temperature from the slope of which $\Delta H°_{600} = 124 \pm 4$ kcal/mole may be determined for the decomposition represented by eq 3. Temperature dependences of ion intensities corresponding to Cd^+ and $P_4{}^+$ from mass spectrometric measurements on vapors effusing from a Knudsen cell gave values of 128 and 133 kcal/mole from the slopes of plots of log $[T^{7/2} I_{Cd^+} {}^3 I_{P_4{}^+}{}^{1/2}]$ *vs.* reciprocal temperature. The torsion effusion value of 124 kcal/mole for (3) may be combined with thermochemical data from standard references[8,9] for phosphorus and cadmium and $[H°_{600} - H°_{298}] = 9.1$ kcal/mole for $Cd_3P_2(c)$, estimated from the classical harmonic oscillator approximation, to give a value of -29.5 ± 5 kcal/mole for the enthalpy of formation of $Cd_3P_2(c)$ from crystalline red phosphorus and cadmium.

From the relation $\alpha \leq (1/Mp_eA')$, where M is the slope in eq 1 and A' is the cross-sectional area of the torque cell sample chamber, upper limits to the gross coefficient for condensation or vaporization of cadmium phosphide may be calculated which vary with temperature from 6.1×10^{-4} at 530°K to 5.6×10^{-3} at 650°K.

Discussion

Zinc and cadmium phosphides both vaporize by congruent decomposition in the temperature range around 600°K and both compounds have low gross coefficients for condensation on or vaporization from the M_3P_2 crystal surface. The heat of formation of

(8) K. K. Kelley, Bureau of Mines Bulletin 584, U. S. Government Printing Office, Washington, D. C., 1960.

(9) "JANAF Thermodynamic Data," Dow Chemical Co., Midland, Mich., 1961.

$Cd_3P_2(c)$ determined by the torsion effusion method employed in this work is in good agreement with Shchukarev's value[2] which was obtained by calorimetry in a KBr–Br_2 solution.

The results for Cd_3P_2, like those of SVL[5] for Zn_3P_2, suggest that α is temperature dependent and that the deviation from unity may be caused, in part at least, by an enthalpy barrier to activation for vaporization which exceeds the equilibrium enthalpy change. The foregoing implies that the torsion effusion value for ΔH°_T for the vaporization process should be smaller than the mass spectrometrically determined values since the latter were determined by measurement of ion intensities in a steady-state system in which the vapor pressure was below saturation. The dependence of pressure on sample surface area which was observed in this work is consistent with a prediction[10] which was based on a theoretical model for vaporization from porous solids of substances with low vaporization coefficients. Motzfeld[11] and Rosenblatt[10] have discussed the derivation and limitations of equations of type (1); and, in particular, they have directed attention to the assumptions which are necessary to obtain a simple relationship between α and M. If eq 1 is more than an empirical relation which is useful for extrapolation purposes and if the limiting values for α are meaningful, comparison of values of α from the present work with those of SVL[5] suggests that the gross coefficient for vaporization for cadmium phosphide may be considerably smaller than for zinc phosphide. There is some evidence to suggest that in both cases as well as for the vaporization of red phosphorus[12] and arsenic[13] the low vaporization coefficient may be the result of an excess enthalpy of activation associated with rearrangement of bond distances and angles in the formation of X_4 units which do not exist in the crystal. Cd_3P_2 has a tetragonal $D5_9$ structure[4] in which each phosphorus atom has 12 near neighbors, 4 at 4.26 A, 4 at 4.34 A, and 4 at 4.45 A. The P–P distance in $P_4(g)$ is 2.21 A.[14] Although Zn_3P_2 and Cd_3P_2 have similar crystal structures, the nearest neighbor phosphorus distances are considerably larger in the latter, and it is possible that the additional separation of phosphorus atoms is responsible for the lower coefficient for vaporization of the cadmium compound. Unfortunately, a test of this hypothesis cannot be extended to mercuric phosphide since apparently there is no well-defined Hg_3P_2 phase[15] in the mercury–phosphorus system in the temperature range of interest.

The abnormally high initial rate of vaporization from fresh samples of Cd_3P_2 found in this work is reminiscent of a result previously observed in the vaporization of $P_4(g)$ from red phosphorus.[12] We can offer no explanation which is preferable to Brewer and Kane's suggestion that the phenomenon may have been the result of distorted or defective crystals in which the atoms were not so rigidly fixed as in a perfect crystal.

Acknowledgment. R. C. Schoonmaker wishes to thank the National Science Foundation for a fellowship and Professor C. A. Coulson, Mathematical Institute, Oxford University, for providing facilities and generous hospitality during a sabbatical leave when this note was prepared.

(10) G. M. Rosenblatt, *J. Electrochem. Soc.*, **110**, 563 (1963).

(11) K. Motzfeld, *J. Phys. Chem.*, **59**, 139 (1955).

(12) L. Brewer and J. S. Kane, *ibid.*, **59**, 105 (1955).

(13) G. M. Rosenblatt, P. K. Lee, and M. B. Dowell, *J. Chem. Phys.*, **45**, 3454 (1966).

(14) C. R. Maxwell, S. B. Hendricks, and V. M. Mosley, *ibid.*, **3**, 699 (1935).

(15) B. Aronson, T. Lunström, and S. Rundquist, "Borides, Silicides, and Phosphides, a Critical Review of their Preparation, Properties, and Crystal Structure," Methuen & Co. Ltd., London, 1965.

A Posteriori Separation of Faradaic and Double-Layer Charging Processes: Analysis of the Transient Equivalent Network for Electrode Reactions

by W. D. Weir

Department of Chemistry, Harvard University, Cambridge, Massachusetts 02138 *(Received February 24, 1967)*

In a recent critique of the assumptions upon which several treatments of nonstationary-state electrochemical processes have been based, Delahay has shown that *a priori* separation of faradaic and double-layer charging processes is without operational justification.[1] The coordinate conclusion that *a posteriori* separation can have only formal and not operational significance[2] seems unwarranted, however. This communication suggests an operational justification for *a posteriori* separation under appropriate conditions through an analysis of the transient equivalent network proposed by Weir and Enke.[3]

(1) P. Delahay, *J. Phys. Chem.*, **70**, 2373 (1966).

(2) P. Delahay and G. Susbielles, *ibid.*, **70**, 3150 (1966).

(3) W. D. Weir and C. G. Enke, *ibid.*, **71**, 280 (1967).

The central assertion of the Delahay critique is that local charge separation or recombination can occur under appropriate circumstances without external current flow, and this idea was developed for the case of an expanding electrode which is potentiostatically poised at equilibrium with a solution of fixed concentration of a cation M^{-z} to which the electrode is reversible. As the electrode area is increased, the relative surface excess Γ_+ of M^{+z} can remain constant only by an increase in the absolute surface quantity of M^{+z} through (i) ionic transport from solution to the double layer, enforced by the potentiostat, and (ii) local charge separation, without external current, the result of an increase in the rate of the charge separation process, $M \rightarrow M_{surface}{}^{+z} + ze_{metal}{}^{-}$, relative to the charge recombination process, $M_{surface}{}^{+z} + ze_{metal}{}^{-} \rightarrow M$, with which it would be in equilibrium were the area of the electrode to remain constant. The relative contributions of processes i and ii to the charging response depend upon the relative rates of the potentiostatically enforced mass-transport process and the charge-transfer reaction. Based upon this analysis of ionic transport and charge-separation–recombination processes, three equations of general validity were developed by Delahay. These equations, upon solution for appropriate boundary conditions, describe the nonstationary-state electrode response. The set of general equations and the physical interpretation given by Delahay to the response of the expanding electrode as it charges toward equilibrium both show unequivocally the inappropriateness of *a priori* separation.

Direct extension of the physical argument given for this problem by Delahay to the problem of the response of a constant area electrode which is displaced from equilibrium by a coulombic perturbation is not without difficulty, however.[4] In the *expanding* electrode problem, with charging *toward* equilibrium, a supplementary contribution to double-layer charging through charge separation is a consequence both of instantaneous deficiency of surface excess Γ_+ and instantaneous anodic overpotential, which the potentiostat acts to reduce; for a *constant-area* electrode, with charging *away from* equilibrium, such a supplementary contribution to double-layer charging through spontaneous charge separation (in the case of cathodic charging) or recombination (for anodic charging) would require a displacement of the charge-transfer equilibrium in the sense opposite to that dictated by the prevailing surface excesses and the overpotential. For example, in the case of cathodic charging from equilibrium, Γ_+ increases as a consequence of ionic transport to the double layer, and this increase is reflected in a transient cathodic overpotential. A supplementary contribution to double-layer charging would require further enhancement of Γ_+ through an increase in the rate of charge separation, $M \rightarrow M^{+z} + ze_{metal}{}^{-}$, relative to the rate of charge recombination, $M^{+z} + ze_{metal}{}^{-} \rightarrow M$, despite the greater-than-equilibrium surface excess of M^{+z} and the cathodic overpotential, an unreasonable result. Displacement of the charge-transfer equilibrium during charging, if it occurs at all, must correspond, for this case, to net recombination of charges and, in general, to a faradaic process in the usual sense of that term.

For the case of coulombic perturbation of a constant-area electrode, then, it would appear that formal separation of ionic transport and charge-separation–recombination processes corresponds directly to the intuitive separation of double-layer charging and faradaic processes. It is necessary to qualify this conclusion through more detailed consideration of the kinetic discharge process over the time interval of charging, however.

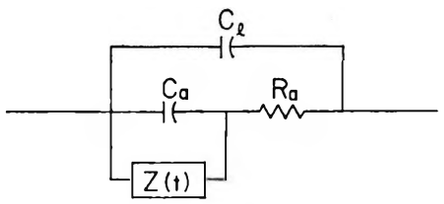

Figure 1. Transient network equivalent to the metal–electrolyte interface for a charge-transfer process which is time-resolved from coupled mass-transport and other prior processes.

Consider that a charge increment $(dq)_c$ is applied through an external circuit to an electrode of constant area which is initially at equilibrium with a fixed concentration of an ion M^{+z} to which it is reversible, and that a displacement of electrode potential $d\varphi$ is observed.[5] If, over the time interval to which this displacement of electrode potential corresponds, a change in electrode charge $(dq)_d$ occurs through the faradaic discharge process, then the net charge increment for the electrode over this potential interval is $dq = (dq)_c - (dq)_d$. The differential quotient $dq/d\varphi$ has the dimensions of capacitance, and for the case where the charge increment is totally nonfaradaic, *i.e.*, $(dq)_d = 0$, the customary differential capacitance

(4) Discussion by F. C. Anson and by H. Gerischer of a presentation of the physical ideas of P. Delahay [*J. Electrochem. Soc.*, **113**, 967 (1966)] (see pp 972, 973) reflects this difficulty.

(5) Equilibrium between the diffuse layer and the bulk concentration of M^{+z} is assumed; removal of this restriction has been treated by G. C. Barker, *J. Electroanal. Chem.*, **12**, 495 (1966).

is defined $dq/d\varphi = (dq)_c/d\varphi = C_l$. If, on the other hand, $(dq)_c = 0$ (corresponding to open-circuit relaxation) a discharge capacitance can be defined $dq/d\varphi = -(dq)_d/d\varphi = C_a$. Then, because the two contributions are defined over the same potential interval $d\varphi$, the total capacitance of the interface is $C = dq/d\varphi = (dq)_c/d\varphi - (dq)_d/d\varphi = C_l + C_a$.[6] If the discharge process is assumed to be formally decoupled from ionic transport, the discharge must involve changes only of surface concentrations, expressed as relative surface excesses; then $(dq)_d = -zF \cdot d\Gamma_+$ if $(dq)_d$ is the change in electrode charge due to a z-electron faradaic process which changes the surface excess of M^{+z} by $d\Gamma_+$ over the potential interval $d\varphi$, and the discharge capacitance takes on the form $C_a = -zF \cdot (d\Gamma_+/d\varphi)$. Subject to the restriction required to give C_a this form, the total capacitance is $C = C_l + C_a = (dq)_c - zF \cdot (d\Gamma_+/d\varphi)$, which is customarily identified with the capacitance of an ideal reversible electrode; C_l is that capacitance associated with an ideal polarizable electrode. To accord with intuition, at $t = 0$ the observed charging behavior must be that of an ideal polarizable electrode, while for $t \to \infty$, charging as an ideal reversible electrode must prevail. In his analysis, Delahay noted that the transition between these two classes of behavior must depend upon the exchange current of the charge-transfer process, but no quantitative interpretation of a transition time constant was given.

A deterministic model for relaxation processes which embodies these ideas has been proposed.[3] The transient equivalent network, shown in Figure 1, illustrates clearly the relationship between the double-layer charging path (through C_l) and the capacitive discharge path (through C_a and the charge-transfer resistance R_a). The impedance $Z(t)$ represents the kinetic contributions of mass transport and any other coupled processes (adsorption, partial or total desolvation, orientation, surface or volume chemical reaction, preceding charge-transfer step(s), or any combination of these), which can be resolved in time from the charge-transfer process represented by R_a.[7] Over the time interval in a transient charging measurement where the admittance of C_a is very large relative to $1/Z(t)$, the surface discharge occurs while the coupled steps, which with it comprise the series mechanism for the over-all reaction, can be neglected. A transition between the charging of C_l alone and parallel charging of C_l and C_a over this interval can be directly observed and related to the network time constant $R_aC_aC_l/(C_a + C_l)$. The magnitudes of C_l and $C_a + C_l$ can be determined by direct measurement of charging slopes at constant current.[8] The transient equivalent thus gives quantitative significance to the transition which has been discussed qualitatively by Delahay, and it provides operational justification for the definition of the two capacitances, C_l and C_a.

The identification in the transient equivalent network of two current paths and their associated capacitances lends credibility to an *a posteriori* separation of double-layer charging (referring only to the current path through C_l) and faradaic (referring to the current path through C_a and R_a) processes for nonstationary-state electrochemical reactions. It must be recognized, however, that the charge-transfer reaction associated with the faradaic process does make a contribution to the total charging response of the metal–electrolyte interface.

Acknowledgment. Support from the Research Corporation and from the William F. Milton Fund of Harvard University is gratefully acknowledged.

(6) In this discussion, formal separation of nonfaradaic and discharge contributions to the total charge increment has been made only to define C_l and C_a, and it corresponds for this case to the separation of ionic transport and charge separation–recombination processes, as shown above, not to an *a priori* separation of these variables without justification.

(7) The assumption of formal separation of mass transport and other coupled processes from charge transfer is operationally justified only when these processes can be experimentally resolved in time by the technique applied to the study of a specific electrochemical reaction.

(8) Charging measurements at very short times may be required. The transition has been observed for constant-current charging at the mercury–electrolyte interface in solutions of mercurous perchlorate for times up to 400 nsec.[3]

COMMUNICATIONS TO THE EDITOR

Comments on Weir's Note on "*A Posteriori* Separation of Faradaic and Double-Layer Charging Processes: Analysis of the Transient Equivalent Network for Electrode Reactions"

Sir: These comments on Weir's note[1] pertain to the following points: (1) coupling between faradaic and double-layer charging processes in general and more particularly for electrodes of constant area; (2) the three previously proposed[2] general equations in relation to charge separation or recombination; (3) *a posteriori* separation of faradaic and charging processes.

(1) The difficulty in extending intuitive analysis, based on charge separation or recombination, to electrodes of constant area can be avoided by considering the *general* forms of the equations for faradaic and charging processes.[3] The faradaic current i_f for an electrode of constant area, in general, depends on the departure from the equilibrium values of the potential E_e, the concentrations a_e, b_e... of reactants and products, and the concentrations u_e, v_e... of other ions present in solution (supporting electrolyte). If a, b... and u, v... are the nonequilibrium concentrations just outside the double layer and E the potential corresponding to i_f, one has $i_f = f(\delta E, \delta a..., \delta u...)$ where $\delta E = E - E_e$, $\delta a = a - a_e$..., $\delta u = u - u_e$ and f represents some general function whose explicit form is not needed. (In many instances $\delta u...$ can be neglected for a small perturbation.) Likewise, the perturbation δq of the charge density q on the electrode is some general function $\delta q = g(\delta E, \delta a..., \delta u...)$.

The classical treatment of nonsteady-state or periodic electrode processes involves the sole consideration of i_f in the analysis of mass transfer, the charging current depending only on a *constant* differential capacity of the double layer. It follows from the general forms of i_f and δq that this *a priori* separation of faradaic and charging processes is not justified, in all rigor, since both i_f and δq depend on the same variables δE, $\delta a...$, $\delta u...$. It is only when the changes of concentration δa, $\delta b...$ do not practically affect δq that the classical approach is satisfactory for all practical purposes. When this simplification is not justified, the mass transfer problem must be solved by considering *simultaneously* its effect on i_f and δq. Analysis can be extended to an electrode of varying area by including the change of area δA in i_f and δq. Thus, coupling between faradaic and charging processes results from the dependence of i_f and δq on variables which are determined in part by another process, namely mass transfer. Charge separation or recombination is not introduced in this reasoning, but the conclusion previously reached[2] about the major defect of the classical approach is confirmed. The idea of charge separation or recombination arose in the chronological development, *i.e.*, in the analysis of double-layer charging of an electrode of varying area.

(2) Weir states:[1] "Based upon this analysis of ionic transport and charge separation–recombination, three equations of general validity were developed by Delahay." It should be emphasized that these three equations do not involve the concept of charge separation or recombination as they are based on the balance of transport through the electrode–solution interface and the rates of storage at this interface.[2] The first equation equates the faradaic current, as given by any suitable expression, to the sum of the reactant flux and the rate of reactant storage (multiplied by the charge zF involved per mole of reactant). The second equation balances the fluxes of reactant and product and the storage rates of these species. These two equations are the boundary conditions for which the mass transfer problem must be solved. The third general equation equates the current being measured to the sum of the flux of reactant and the storage rates of all other ions (flux and rates being multiplied by zF). These equations involve a model, which hopefully has been correctly described,[2] but they do not require the introduction of charge separation or recombination. (*Cf.* also a recent note.[4]) The introduction of this concept showed the need for some general equations, but the concept is not contained in these equations.

(3) Weir writes[1] in his initial paragraph, "The coordinate conclusion that *a posteriori* separation can have only formal and not operational significance seems unwarranted, however" (see also his further discussion). We examine the general forms of i_f and δq, and we suppose that the mass-transfer problem is solved as indicated above. The changes δE, $\delta a...$, $\delta u...$ are then functions of time for a nonsteady-state perturbation and of frequency for a periodic perturbation (steady-state solution in the latter case). The measured current i is some function $i = h(\delta E, \delta a...,$

(1) W. D. Weir, *J. Phys. Chem.*, **71**, 3357 (1967).

(2) P. Delahay, *ibid.*, **70**, 2067, 2373 (1966).

(3) P. Delahay and K. Holub, submitted for publication.

(4) P. Delahay, K. Holub, G. Susbielles, and G. Tessari, *J. Phys. Chem.*, **71**, 779 (1967).

$\delta u \ldots$). In principle, it does not seem possible to devise a measurement at any finite time, different from zero, which would separate the current i into two components attributed to the faradaic and charging processes, respectively. This seems impossible because both processes are coupled as indicated before. It is perhaps possible to isolate the charging process by measurement at time zero if one neglects the finite rate of double layer relaxation. This was already discussed before.[2,5] It should be noted that this operation seems possible provided one assumes that charging is instantaneous, whereas the faradaic process proceeds at a finite rate for a finite exchange current. Thus one *isolates* one process, but one does not separate one process from the other when both processes occur simultaneously.

Finally, one should remember that the description of the electrode response involves a large number of parameters. For instance, for an amalgam electrode one must consider three variables (E, $c_{M^{+z}}$, and c_M) and four functions (i_f, q and the surface excesses of M^{+z} and M). Description of a perturbation of small amplitude thus requires 12 partial derivatives in the most general case (ten partial derivatives if one introduces the exchange current instead of the derivatives of i_f with respect to the three variables). These coefficients must somehow appear in the equivalent circuit, and unambiguous analysis of experimental data appears very difficult except when some of the partial derivatives can be dropped.[6]

(5) P. Delahay and G. Susbielles, *J. Phys. Chem.*, **70**, 3150 (1966).
(6) K. Holub, G. Tessari, and P. Delahay, *ibid.*, **70**, 2612 (1967).

DEPARTMENT OF CHEMISTRY PAUL DELAHAY
NEW YORK UNIVERSITY
NEW YORK, NEW YORK 10003

RECEIVED MAY 22, 1967

Carbon-13 Satellite Interference with Chemical Shift Measurements in Cyclohexane–Diethylamine Solutions[1]

Sir: A recent publication of a study of diethylamine hydrogen bonding by nmr by Springer and Meek[2] reports a constant chemical shift for the NH proton at concentrations of less than 0.1109 mole fraction amine (X) in cyclohexane. They have taken this constant chemical shift to be that of the nonhydrogen-bonded proton of the amine, by the assumption that only the nonassociated form of diethylamine exists in cyclohexane over this range of concentrations. We have also observed the chemical shift of the NH proton of this amine as a function of concentration in cyclohexane. Samples were distilled from CaO through a Hempel column and stored in dry nitrogen or a desiccator. Sample tubes were oven dried and similarly stored until use. The data, obtained at 31°, are shown in Table I alongside those obtained at 40° by Springer and Meek. The Varian A-60 nmr spectrometer was used in both studies. At values of X of 0.11 and less, practically the same chemical shifts of the NH proton were obtained, despite the different temperatures.

An alternative explanation for the constant chemical shift obtained at low amine concentrations follows from consideration of the 60-Mc/sec spectrum of cyclohexane, which includes not only the characteristic, sharp signal 87 cps to the low-field side of the tetramethylsilane signal, but also two signals arising from ^{13}C–proton coupling, *i.e.*, ^{13}C satellites, approximately 9 cps broad at half-height, occurring about 62 cps to the high- and low-field sides of the main solvent signal. In a $0.117X$ diethylamine solution in cyclohexane the number of amine protons bonded to nitrogen atoms

Table I: Chemical Shift of Diethylamine NH Proton as a Function of Concentration in Cyclohexane

X of amine	NH chemical shift, cps[a]	X of amine	NH chemical shift, cps[b]
		1.000	44
		0.6710	47
		0.4815	52
0.1864	59		
0.1618	60		
0.1286	61		
0.1142	62		
		0.1109	63
0.1082	63		
0.1008	63		
		0.09204	63
0.0858	64		
		0.05986	64
		0.02606	63

[a] Relative to cyclohexane signal. [b] Data of Springer and Meek,[1] converted from units to cps from cyclohexane signal.

(1) This work was supported in part by the National Science Foundation and the Office of Saline Water, U. S. Department of the Interior.
(2) C. S. Springer, Jr., and D. W. Meek, *J. Phys. Chem.*, **70**, 481 (1966).

equals the number of solvent protons bonded to ^{13}C atoms. Further, the amine concentration at which each satallite arises from the same number of protons as does the NH signal is $0.062X$. Thus, at this amine concentration each satellite signal would be expected to be as large as the NH proton signal, and at somewhat higher amine concentrations one of the satellite signals, due to its broadness, could obscure the resonance position of the NH proton if it should overlap it. This does occur, as can be seen from Table I, in which all chemical shifts for X less than 0.19 are within 3 cps of 62 cps. Our findings have recently been confirmed by Springer and Meek.[3]

We have also observed the variation of chemical shift of the NH proton of piperidine as a function of concentration in cyclohexane.[4] As the piperidine NH signal is at lower field strength than that of diethylamine at all concentrations studied, both the piperidine NH proton signal and the ^{13}C satellite were easily observed and differentiated in the more dilute piperidine solutions studied. In these solutions there is still a linear variation of the NH chemical shift with concentration.

Therefore, we suggest that diethylamine does hydrogen bond at concentrations less than $0.11X$, although a change of NH chemical shift cannot be observed due to the position of the ^{13}C satellite. A linear variation below $0.1618X$ would imply a monomer–dimer equilibrium at very low concentrations in addition to any higher polymers formed at higher concentrations.[5]

(3) C. S. Springer, Jr., and D. W. Meek, private communication.

(4) R. A. Murphy and J. C. Davis, Jr., to be published.

(5) C. M. Huggins, G. C. Pimentel, and J. N. Schoolery, *J. Phys. Chem.*, **60**, 1311 (1956).

DEPARTMENT OF CHEMISTRY
UNIVERSITY OF TEXAS
AUSTIN, TEXAS 78712
RUTH ANN MURPHY

DEPARTMENT OF CHEMISTRY
UNIVERSITY OF SOUTH FLORIDA
TAMPA, FLORIDA 33620
JEFF C. DAVIS, JR.

RECEIVED MAY 4, 1967

A Correlation between Nitrogen Chemisorption and the Rate of Anodic Oxidation of Propane on Platinum Black

Sir: Surface areas of Pt black catalysts used for the anodic oxidation of propane have been determined in our laboratory by the BET method. An unusual feature of the results, presented in Table I, is the larger value for the surface area when nitrogen is used in place of argon as the adsorbing gas. This effect was not related to the experimental technique as shown by measurements on silica and titania (Table I). A volume of nitrogen approximately equal to the difference in the BET surface areas could not be pumped off the platinum catalyst at the temperature of adsorption (−195°). Irreversible adsorption is commonly interpreted as chemisorption. In this case, the behavior is consistent with the infrared spectroscopic evidence for low-temperature chemisorption of molecular nitrogen on nickel, palladium, and platinum presented by Van Hardeveld and Van Montfoort.[1] The heat of adsorption computed from measurements at two temperatures was 6.5 kcal/mole. More details of this work are presented in another publication.[2]

Table I

Sample	Surface area,[a] m²/g: N_2	Surface area,[a] m²/g: Ar	Ratio, N_2:Ar	Corrected ratio[b]	θ	Activity,[c] ma/cm²
TiO_2	5.28	4.83	1.076	1.00	...	...
SiO_2	24.3	22.6	1.074	1.00	...	...
Pt Black[d]						
Commercial	30.1	21.0	1.43	1.34	0.34	80
73-48	29.0	26.2	1.11	1.045	0.045	24
73-51	21.0	14.9	1.39	1.30	0.30	70
73-45	32.7	25.0	1.28	1.19	0.19	32
73-57	20.8	14.9	1.38	1.28	0.28	45
73-57	21.1	15.0	1.39	1.29	0.29	45

[a] Cross-sectional areas used for N_2 and Ar were 16.2 and 14.6 A², respectively. [b] Assuming ratio for SiO_2 and TiO_2 should be 1.00. [c] Given by the current density at 400 mv *vs.* rhe, see ref 3. [d] For details of preparation, see J. Giner, J. M. Parry, and S. M. Smith, paper presented at the 154th National Meeting of the American Chemical Society, Chicago, Ill., Sept 1967.

The amount of chemisorbed nitrogen (Table I) depends on the conditions of preparation of the catalyst, probably because chemisorption of nitrogen occurs on specific Pt sites whose number changes with crystallite size.[1]

The intrinsic activity of several platinum catalysts toward the anodic oxidation of propane is compared

(1) R. Van Hardeveld and A. Van Montfoort, *Surface Sci.*, **4**, 396 (1966).

(2) R. Jasinski, J. M. Parry, and E. F. Rissmann, to be published.

with the extent of nitrogen chemisorption in Figure 1. Nitrogen chemisorption (θ) is given in terms of the ratio of the difference between the N_2 and Ar values to the Ar value of the surface area. A small correction was first made to the nitrogen values so that the N_2 to Ar ratio of surface areas for TiO_2 and SiO_2 equaled 1. The measurement of the intrinsic activity of the platinum black catalysts is described elsewhere.[3]

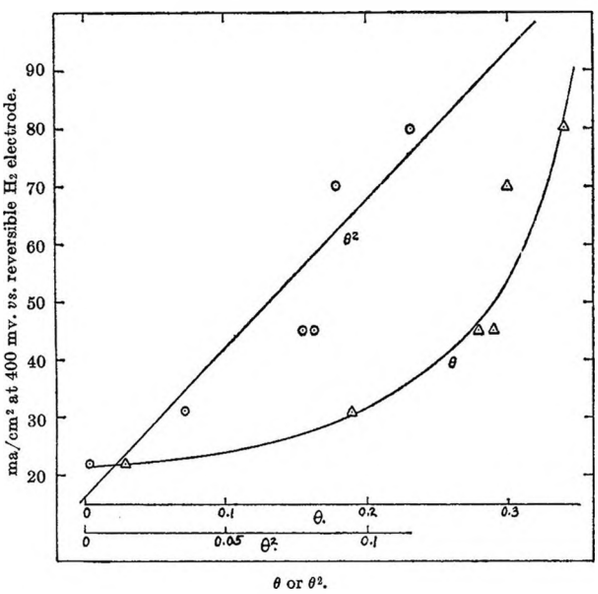

Figure 1. Rate of anodic oxidation of propane at 400 mv *vs.* rhe as a function of the fractional coverage of chemisorbed N_2, θ, and θ^2.

The correlation between electrocatalytic activity and nitrogen chemisorption suggests that the same sites are involved in both processes. It should be noted that there is no direct relation between activity and surface area measured with Ar; that is, we are not measuring a secondary surface area effect.

It might seem that the definition of θ given above violates one of the assumptions of the BET equation, namely that the heat of adsorption is uniform over the surface. However, as discussed by Emmett,[4] if the chemisorption is essentially complete at low relative pressures, it does not seriously interfere with the determination of surface area. This implies that physical adsorption of N_2 on chemisorbed N_2 proceeds with approximately the same heat of adsorption as on the free surface of the metal. In our case, BET plots based on the total volume of N_2 adsorbed gave excellent straight lines.

Van Hardeveld and Van Montfoort identify the active sites for N_2 adsorption as the B_5 sites that occur in linear arrays in 110 and higher index surfaces. At a B_5 site the adsorbate is equidistant from five platinum atoms, four in the surface layer and one in the layer immediately below the surface. The mechanism of anodic oxidation of propane may involve adsorption of the C_1 and C_3 atoms on adjacent B_5 sites with subsequent cleavage of one of the C–C bonds to form relatively reactive radicals. The B_5 sites in the linear array are separated by a distance (2.76 A) just greater than that of the alternate carbon atoms in a paraffin chain (2.52 A). This stereochemical factor may provide an explanation for the more rapid anodic oxidation of the linear paraffins compared with branched-chain and unsaturated molecules, and may also account for the relative ease of oxidation of propane and butane compared with ethane or methane.

Acknowledgement. This work was supported by U. S. Army Engineer Research and Development Laboratories, Fort Belvoir, Virginia, under Contract No. DAAE 15-67-C-0048.

(3) J. Giner, J. M. Parry, and S. M. Smith, Extended Abstracts, Vol. III, ECS Meeting, Dallas, Texas, May 1967, p 40.

(4) P. H. Emmett, "Catalysis," Vol. I, Reinhold Publishing Corp., New York, N. Y., 1954, p 51.

TYCO LABORATORIES, INC.
WALTHAM, MASSACHUSETTS 02154
JOHN M. PARRY
E. F. RISSMANN

RECEIVED JUNE 6, 1967

Chlorine-35 Nuclear Quadrupole Resonance and the Structure of the Bichloride Ion in Tetramethylammonium Bichloride[1]

Sir: There has been considerable interest recently in the structure of the bichloride anion, particularly with respect to the symmetry of the hydrogen position. Waddington,[2] on the basis of infrared spectra, originally assigned a symmetrical structure to the bichloride ion in tetramethylammonium bichloride. Chang and Westrum[3] performed low-temperature heat capacity measurements on that compound and interpreted their

(1) This work was supported by the Directorate of Chemical Sciences, Air Force Office of Scientific Research, under Grant No. AF-AFOSR-859-65. Contribution No. 356 from Tufts University Department of Chemistry.

(2) T. C. Waddington, *J. Chem. Soc.*, 1708 (1958).

(3) S. Chang and E. F. Westrum, *J. Chem. Phys.*, **36**, 2571 (1962).

results as being most consistent with the symmetrical structure. Recently, Evans and Lo[4] have performed more extensive infrared studies and have proposed that in the tetramethylammonium salt the bichloride anion is unsymmetrical, although they consider it symmetrical in other tetraalkylammonium salts. They further reported[5] on a study of the chlorine-35 nuclear quadrupole resonance which they also interpreted on the basis of an unsymmetrical structure. We had previously measured these coupling constants[6] and wish to confirm the results of Evans and Lo and to provide an additional indication that their interpretation is correct.

For a symmetrical structure, one expects to observe a single resonance line for the two equivalent chlorines, and two lines well separated for an unsymmetrical structure. A single line is observed for tetramethylammonium bichloride, at 20.21 Mc/sec at liquid nitrogen temperature. We were also able to observe the chlorine-35 resonance in the deuterated compound $[(CH_3)_4N]ClDCl$ at 21.12 Mc/sec (also at liquid nitrogen temperature), which Evans and Lo were unable to find. Although our scans were made to somewhat lower frequencies than Evans and Lo could reach (*ca.* 5.5 Mc/sec as opposed to their 10 Mc/sec), we still observed no further resonances.

The most straightforward interpretation of these results would be that the ion has a symmetrical structure. On the other hand, the observed frequency is rather higher than one might expect on the basis of very simple arguments comparing the observed frequency for bichloride with that for HCl, and one must allow for the possibility that the second resonance is lower than the lowest frequency searched.[5]

In an attempt to assess more accurately the implications of these measurements for the interpretation of the structure, we have carried out a simple calculation of the field gradient at the chlorine nucleus using a method recently described by Cotton and Harris.[7] This method makes no prior assumptions about hybridization and thus disposes of one difficulty of the Townes and Dailey approach. Basically, it amounts to carrying out a Wolfsberg–Helmholz-type molecular orbital calculation and a Mulliken analysis[8] of the population in the chlorine 3p orbitals, and attributing the total observed field gradient to imbalance in p-electron densities. In order to judge the reliability of the calculation, it was applied to HCl as well as bichloride.

The results of the calculation are shown in Figure 1. The calculations were performed as a function of the hydrogen–chlorine distance in HCl and in the bichloride ion, at a fixed Cl–Cl distance in the latter of 3.2 A. The calculation gives a coupling constant for HCl at the

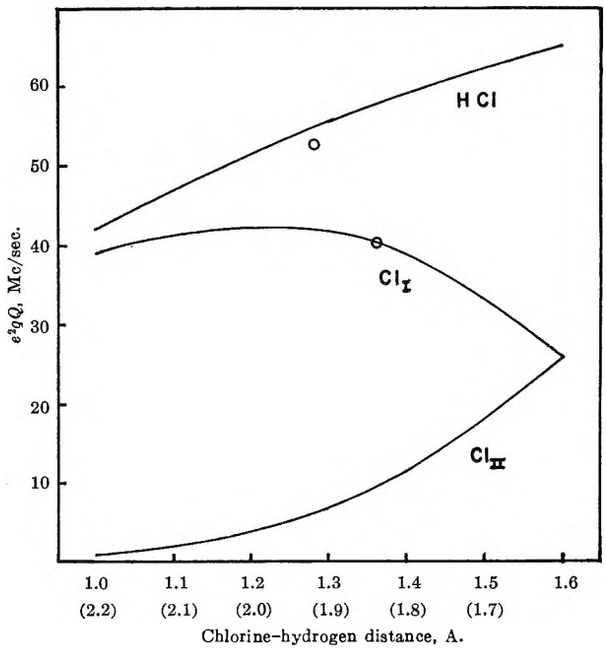

Figure 1. Quadrupole coupling constant *vs.* chlorine–hydrogen internuclear distance. Solid lines are results of the calculation. Cl_I and Cl_{II} refer to the chlorines nearest and farthest from the hydrogen in bichloride, respectively. The circle near the HCl line is the observed e^2qQ at the known internuclear distance. The circle on the Cl_I line is the observed e^2qQ for $[(CH_3)_4N]ClHCl$. Numbers in parentheses on the abscissa are distances for Cl_{II}–H.

equilibrium internuclear distance of 1.25 A of 54.1 Mc/sec. which agrees very well with the observed value of 52.94 Mc/sec.[9] For the bichloride ion with a symmetrical structure, the predicted coupling constant is 25.7 Mc/sec (at a chlorine–chlorine distance of 3.2 A) corresponding to a frequency of 12.8 Mc/sec. The observed coupling constant (assuming $\eta = 0$) of 40.42 Mc/sec corresponds to a shorter Cl–H distance of 1.36 A, *i.e.*, a very asymmetric structure. The smaller coupling constant is then predicted to fall below 10 Mc/sec, which is lower than Evans and Lo predicted and lower than we were able to search. As the calculation proved quite successful in predicting the correct HCl coupling constant, we feel it deserves to

(4) J. C. Evans and G. Y-S. Lo, *J. Phys. Chem.*, **70**, 11 (1966).

(5) J. C. Evans and G. Y-S. Lo, *ibid.*, **70**, 2702 (1966).

(6) S. M. Welsh, M.S. Thesis, Tufts University, June 1966.

(7) F. A. Cotton and C. B. Harris, *Proc. Natl. Acad. Sci. U. S.*, **56**, 12 (1966).

(8) For a treatment of this type of calculation, see C. J. Ballhausen and H. B. Gray, "Molecular Orbital Theory," W. A. Benjamin, Inc., New York, N. Y., 1965, especially Chapter 8.

(9) H. C. Allen, *J. Phys. Chem.*, **57**, 501 (1953).

be taken as significant evidence in support of an unsymmetrical structure for the bichloride ion in tetramethylammonium bichloride.

DEPARTMENT OF CHEMISTRY
TUFTS UNIVERSITY
MEDFORD, MASSACHUSETTS 02155

T. E. HAAS
S. M. WELSH

RECEIVED JUNE 30, 1967

The Effect of Water on Hydrogen Yields in the γ Radiolysis of 1,4-Dioxane[1]

Sir: In continuation of our work on radiation-induced processes in solutions of 1,4-dioxane,[2] it proved necessary to make a careful study of the method of purification with special attention to the exclusion of water. As a result of such a study, the following purification procedure was developed. For removal of peroxides, 1,4-dioxane (Matheson Coleman and Bell spectroquality reagent) was passed through a column of activated alumina. Then, always under an atmosphere of dry nitrogen, the dioxane was refluxed over sodium for ~16 hr and subsequently distilled from sodium on a Nester–Faust spinning-band column. The middle portion was retained and stored in a drybox under dry nitrogen. No impurity was detectable by gas chromatography with a flame-ionization detector. No ultraviolet absorption was detectable with a Cary Model 14-R at wavelengths longer than 290 nm; at wavelengths of 280, 260, 240, and 220 nm, the optical densities for a 1-cm path were 0.01, 0.03, 0.05, and 0.10, respectively, with a sharp increase in optical density near 212 nm.

Degassed samples of the purified dioxane were γ-irradiated (^{60}Co) at a dose rate of 1.8×10^{18} ev ml^{-1} min^{-1}. A value of $G(H_2) = 1.4$ was obtained in contrast with $G(H_2) = 2.1$ reported previously.[2,3] $G(H_2)$ was constant over the dose range 3.6×10^{18} to 4.9×10^{20} ev ml^{-1} and was relatively insensitive to the presence of 10^{-2} M iodine or ~10^{-2} M N_2O. However, as shown in Figure 1, a progressive increase in $G(H_2)$ occurs with increasing concentration of water added to the dioxane prior to irradiation. Qualitatively similar results were obtained on addition of methanol or ammonia in place of water.

In the previous studies of dioxane radiolysis,[2,3] precautions for exclusion of water were apparently inadequate. In view of the sensitivity of $G(H_2)$ to water content of the dioxane, it must be concluded that the higher reported value[2,3] of $G(H_2)$ is not for pure dioxane.

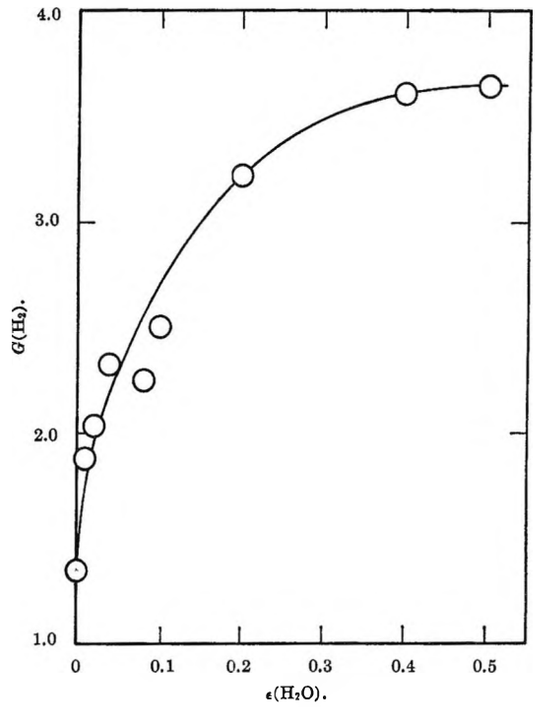

Figure 1. Effect of water on the γ radiolysis of 1,4-dioxane for a dose of 1.1×10^{20} ev ml^{-1}. Electron fraction, ϵ, is used in conformity with convention; values of $\epsilon = 0.01$ (the lowest concentration point on the graph) and $\epsilon = 0.5$ correspond to 0.56 and 23 M and to mole fractions of 0.046 and 0.80, respectively.

Such a value was reproduced in the present study with ~1 M solutions of water or methanol in dioxane.

It is possible to interpret the enhancement of $G(H_2)$ by water in terms of a proton-transfer mechanism. Absence of an effect of 10^{-2} M iodine on $G(H_2)$ from pure dioxane indicates a negligible contribution of thermal H. Thus, in the absence of water, neutralization of a primary dioxane cation, RH^+, by an electron does not produce thermal H. Although ~10^{-2} M N_2O solution gives $G(N_2) = 1.2$, which indicates appreciable electron scavenging, $G(H_2)$ is suppressed by only 0.2. Thus, neutralization of RH^+ by an electron yields H_2 with only ~16% efficiency. In the presence of water, the proton-transfer reaction 1 competes with neutralization of RH^+ by an electron. With increase

$$RH^+ + H_2O \longrightarrow R\cdot + H_3O^+ \qquad (1)$$

in water concentration, then, electrons are increasingly neutralized by H_3O^+, rather than by RH^+, and H_2 or

(1) This is U. S. Atomic Energy Commission Document COO-38-560.

(2) E. A. Rojo and R. R. Hentz, *J. Phys. Chem.*, 69, 3024 (1965).

(3) Y. Llabador and J. P. Adloff, *J. Chim. Phys.*, 61, 681 (1964).

H (which forms H_2 by abstraction from dioxane) is produced in each such neutralization process. In conformity with the proposed mechanism, it is found that N_2O considerably diminishes $G(H_2)$ in dioxane containing water. It should also be noted that the dependence of $G(H_2)$ on water concentration (*cf.* Figure 1) is characteristic of cation-scavenging reactions[4,5] rather than the considerably more efficient electron-scavenging reactions.[6]

A complete study of product yields in the radiolysis of pure dioxane and its mixtures with water is in progress. Dioxane–water mixtures permit study of the effects of γ irradiation as a function of a continuous change in dielectric constant from that characteristic of a hydrocarbon to that of water.

(4) F. Williams, *J. Am. Chem. Soc.*, **86**, 3954 (1964).

(5) A. A. Scala, S. G. Lias, and P. Ausloos, *ibid.*, **88**, 5701 (1966).

(6) See, *e.g.*, Table VII in R. R. Hentz, D. B. Peterson, S. B. Srivastava, H. F. Barzynski, and M. Burton, *J. Phys. Chem.*, **70**, 2362 (1966).

DEPARTMENT OF CHEMISTRY AND THE RADIATION LABORATORY
UNIVERSITY OF NOTRE DAME
NOTRE DAME, INDIANA 46556

ROBERT R. HENTZ
FRANK W. MELLOWS
WARREN V. SHERMAN

RECEIVED JULY 24, 1967